Insertion of Olefins into Nickel Alkyl Complexes: Mechanistic Studies and Polymerization Catalysis

Thesis by

Shuoyan Xiong

In Partial Fulfillment of the Requirements for the Degree of

Doctor of Philosophy

CALIFORNIA INSTITUTE OF TECHNOLOGY

Pasadena, California

2023

(Defended on January 10, 2023)

Shuoyan Xiong
ORCID: 0000-0002-2579-4260

To my family

for their unconditional support and love

ACKNOWLEDGEMENTS

Looking back, nearly at the end of my graduate career, I really, really appreciate many people who have contributed to my development as an academic, an experimental chemist, and as a person. Without them, associates, coworkers, collaborators, mentors, and friends, I wouldn't have been able to accomplish this work.

First and foremost I would like to thank my advisor, Professor Theodor Agapie. Since I arrived at Caltech for my visit weekend, I have been thrilled by Theo's enthusiasm for all kinds of chemistry, which first drew me to Caltech and later has been representative of most of my interaction with him. We have discussed numerous scientific ideas at various places: conference room, office, lab, after a random seminar, or even during a walk. Thank you, Theo, for always constructively criticizing my ideas in ways I haven't thought about before, and, in many cases, still supporting me to try them even though I couldn't convince you of the merit after discussion. Thank you also for always reminding me to focus on fundamental and important questions and to find answers in extremely thorough ways. In addition, Theo has also given me ample opportunities to present my research and always providing detailed feedbacks so that I eventually feel confident of my results and the way I share them. Another indelible influence by Theo is teaching. Theo immediately became my role model of teaching since I attended Ch112. Later I had the fortune to work as a TA for Theo in two different classes. I am very much impressed by Theo's enthusiasm in class and attention in detail. Theo's outlook, methods, and mannerisms have left a persisting influence on my scientific psyche, in both research and teaching. I wouldn’t be the researcher and scientist I am without his mentorship. Thank you, Theo!

I would also like to thank my thesis committee: Professor Robert Grubbs, Professor Harry Gray, Professor Jonas Peters, and Professor Maxwell Robb. Bob had been the chair of my committee for the first three years. He had always been generous with compliments and encouragements during my interaction with him. Thank you, Bob! I deeply mourn the loss of you, but we are all remembering you in a variety of ways. Harry became the chair of my committee in my last year. Harry always asked tough questions in an encouraging way and brought a little bit of comic relief afterwards. Thank you, Harry! Your altitude to science, with a strong sense of responsibility and faith as a fellow scientist, has really been a motivation for me to conduct challenging research. Jonas, thank you for criticizing me hard but constructively in my proposal defense, and instructing me about "realistic ambitions". I hope you can see my progress in the future. Max, thank you for your continuous support over these five years and your in-depth, professional feedback from the side of organic and polymer chemistry.

Other faculty at Caltech have also been influential in my scientific development. Professor John Bercaw, thank you for showing me your elaborate high-pressure setup on the second floor, troubleshooting hand in hand with me, and allowing me to use it. Though I was not able to obtain expected results, this experience was still valuable to me. Your continued passion for pursuing chemistry by yourself is also inspiring. Teaching is an important part of the PhD training. In addition to Theo, I also have to thank professors who I had worked with during first few terms of my PhD as they taught me fundamentals of being a TA: Professor Nathan Lewis and Professor Sarah Reisman. Thank you! I also had the fortune to work as a GLA for NMR facility for over three years. I am extremely grateful to Dr. David Vander Velde for giving me this chance, and

for providing constant support and detailed assistance in instrument maintenance, user training, and numerous VT and kinetic experiments for my own research projects.

In the Agapie group, I have been privileged to work with many creative and amiable colleagues with unique personalities. I would like to acknowledge them all. Jessica, Marcus, Josh, and Nate, thanks for your patience in putting up with my endless stream of questions and helping me become familiar with lab facilities and setting up complicated experiments. Manar, working with you closely, on the same project and in the same box, is really a memorable experience for me. Thank you for all your help in setting up experiments, refining crystals and editing papers, and for many other affairs beyond research. Gwen, it's extremely lucky for me to work with you and Manar in "Cohort C" during pandemic. Thank you both for your company and support as fellow lab members. Chris, I really enjoyed playing board games with you and Marcus on Saturday once in a while. Priyo, I am grateful for working with you on the same project during my last year. The POP system is all yours now! I would also like to acknowledge Alex, Angela, Anna and Meaghan, who joined the Agapie lab with me at the same time, and Gavin, Linh, Mike, Fernando, Matthew, younger members of the Agapie group. Y'all are a lively group that have made graduate school that much better with your company. Angela, I am so excited that you are taking over the polymer project in your last few months. Mike, thank you for great conversations and organizing group parties in your apartment. Matt and Linh, thanks so much for helping me mounting crystals. Fernando, thank you for taking over the SPS group job. Alex, it has been a real pleasure getting to be a (small) part of your development as a synthetic organometallic chemist since your fresh year. I look forward to seeing how your projects (in our lab and in your

graduate school) evolve. To every graduate student, postdoc, and undergraduate student in the group who I have overlapped with, I am so glad you were part of my graduate school experience. Thank you and good luck!

Outside the Agapie Lab, I must thank our fantastic collaborators, whose contributions have been invaluable not only to this thesis, but also to my personal developments. My thesis is centered on searching for new, high-performance catalysts for polar polyolefin synthesis, for which I would like to thank our collaborators from Dow, Dr. Brad Bailey, Dr. Heather Spinney, Dr. Alex Nett, Dr. Todd Senecal, and Dr. Jerzy Klosin. Thank you for providing an industry perspective on my chemistry during monthly meetings and manuscript preparations, and for your efficiency and patience in setting up numerous high-throughput polymerizations. Also, I would like to thank Hannah Bailey, Steve Marshall, Heidi Clements for running polymerizations and FT-IR and GPC analysis of copolymer samples. This thesis could not have been as detailed, thorough, and impactful without the experimental contributions and intellectual engagement from Dow colleagues. I also want to acknowledge our collaborators from the computational side, Prof. Thomas Miller, Dr. Xinglong Zhang, and Dr. James Lawniczak. We had been working on mechanistic studies together over two years. Thank you for contributing your time, expertise, and resources to this project!

Many thanks also go to the people that run the facilities and administrative staff at Caltech. Larry Henling, I relied heavily on you for my crystallographic studies. I had hoped for a long time that one day I could bring a brilliant crystalline sample meeting all your standards. Thanks a lot for your help! Dr. Mike Takase, thanks for teaching us to always be independent! Margarita Davis, thank you very much for all the scheduling and

reimbursement stuffs. Your constantly immediate (more than prompt) email responses are very touched. Joe Drew and Nate Siladke, thank you both for helping us to be able to conduct research smoothly and safely. Alison Ross, thanks for your help in paperwork and administration. Rick Gerhart and Nathan Hart, thanks for all your glassblowing works.

I would also like to acknowledge several other people who have been involved in my early development as a synthetic chemist. Professor Changle Chen allowed me to start original research in his group during my second year. Jiesheng and Chen, as my mentors in the Chen group, have guided me into the world of organic and polymer chemistry hand in hand. Thank you all! Professor Tobin Marks, thank you so much for accepting me as a visiting undergrad, providing feedback on my research and presentation, and supporting me in my PhD applications. Tracy, Yanshan, and Jiazhen, thank you for your mentoring in the Marks group. Jiazhen, I always recall your patience with me while doing cannula transfer.

I also want to thank many friends and colleagues that have provided support over the years. Thank you Jiajun, Quan, and Zhihao, for being my roommates over the last four/five years. Your company really means a lot to me. I hope we still have a few more chances to continue our "Wondering night" on Saturdays. Chen and Jianjun, I am so glad to have you both as groomsmen at my wedding. Mengshan, Gen, Weiting, Haotian, Xinyu, Lin, Chen and Danqi, we have some incredible trips over the past five years, and I hope also in the future. Many friends and colleagues at Caltech have influenced me in many ways scientifically and beyond. Thank you all! Xiaoran, thank you for all your suggestions when I had a hard time choosing, from joining a lab at Caltech school to

postdoc applications. I also want to thank Kurtis, Jen, Mengshan, Kaipeng, and Ziting for their support during my postdoc application. To all my friends from high school, undergraduate, and graduate school, you all have taught me so much about life, the universe, and everything. Thank you and good luck!

Last, but certainly not least, I would like to thank my family. Mom and Dad, thank you for helping me, supporting me, caring for me, and brightening my days unyieldingly since the start. I know that would never change. Thank you for encouraging me to follow my dreams, which is only possible because of you, and everything you have taught me. Yu, my wife, I am so incredibly blessed to have you in my life. Thank you for joining me for my graduate school adventure. It's certain that I couldn't have made it through so many times without your company, support, and encouragement. I hope I can give back to you similarly. You are the love of my life. I am so excited to see what adventures we will have and what memories we will create. Huihui, thank you for providing us your company and laugh. Your creativity is really inspiring!

ABSTRACT

Polyolefins account for over half of global plastic production. The incorporation of polar functionalities can provide value-added polyolefins with desirable material properties and potential degradability. To achieve this, coordination copolymerization of ethylene and fundamental polar comonomers by transition-metal catalysts is the most direct, economical, and environmentally friendly method. Though it has been pursued for decades, the catalyst performance (*e.g.* activity, thermal stability) is still far below practical thresholds. The major issue is the "polar monomer problem": coordination of the polar group in the comonomer to the metal center competes with vinyl coordination, a prerequisite for the monomer enchainment (chain propagation).

This thesis describes mechanism-driven developments of industrially applicable molecular catalysts toward addressing the "polar monomer problem", with a focus on nickel catalysts for ethylene/acrylate copolymerization. A general introduction is provided in Chapter 1.

Chapters 2~3 present the systematic studies of olefin insertion reactions, elementary steps of this copolymerization, with newly developed and high-performing nickel phosphine phenoxide catalysts. Nickel alkyl complexes generated after tBA insertion that are key intermediates representing the catalyst resting states were identified, isolated, and for the first time, crystallographically characterized, including a novel four-membered chelate, one elusive intermediate that has been pursued for decades. Further, isolation of these intermediates allowed the establishment of kinetic profiles of olefin insertion reactions involved in catalyst initiation and chain propagation, and further

investigations of elementary steps of chain propagation, such as olefin coordination and complex isomerization.

A major issue of current Ni catalysts is their low thermal stability. Most of them are operated at temperatures < 70 ºC. However, thermally robust catalysts are preferred in industry as they do not require precise temperature control during polymerization that is highly exothermic. In addition, chain propagation is faster at higher temperatures, potentially leading to higher activity. Based on knowledge obtained from aforementioned mechanistic studies, a new type of highly active, thermally robust Ni enolate catalyst for ethylene/acrylate copolymerization was rationally designed and developed (Chapter 4). Specifically, they remain highly active at 110 ºC, notable for this preparation. Chapter 5 describes subsequent catalyst modifications that led to significant enhancements in catalyst initiation and chain propagation, and consequent improvements of catalyst activity by nearly one order of magnitude.

While nickel enolate catalysts described in Chapter 5 feature remarkably high activity and thermal stability, the molecular weight (Mw) of resulting copolymers are too low for material applications. Chapter 6 presents an iterative catalyst design that applies strategies demostrated in Chapters 4 and 5 to nickel phosphine phenoxide catalysts studied in Chapters 2 and 3. Resulting nickel complexes are extremely active (~37000 kg/(mol*h)) and producing high Mw (~50000) ethylene/acrylate copolymers. In addition, fully blocking axial positions from the "top" of the nickel center also allows the isolation of a novel Ni alkyl complex directly relevant to β-H elimination, as well as mechanistic investigations of related reactions. These elementary steps have been little

explored but are key to control the polymer Mw, chain-end structure, and chain walking behavior in polar polyolefin synthesis.

Partially inspired by multiple metal centers in enzymes, multinuclear transition-metal catalysts have been developed and showed promise in copolymerization of non-polar monomers. However, unexpected challenges appeared while applying similar strategies in solving the "polar monomer problem". Chapter 7 examines potential effects of secondary metal additives that are proximal to the nickel and reveals how ligands binding to the secondary metal center could also significantly affect catalysis. Chapter 8 presents a systematic mechanistic study of cation shuttling and monomer insertion with a dinickel-based multimetallic system and proposes a "cation shuttling polymerization" strategy for addressing the "polar monomer problem".

Overall, Chapters 1 through 8 present: 1) detailed mechanistic profiles of elementary steps of nickel-catalyzed ethylene/acrylate copolymerization including catalyst initiation, chain propagation (monomer insertion) and chain elimination, as well as elementary transformations for monomer insertions such as olefin coordination and complex isomerization, with both mono-nickel and nickel-based multimetallic catalysts; 2) consequent iterative catalyst developments that have enabled the efficient synthesis of polar-functionalized polyolefins with significantly improved catalyst activity and stability, polar monomer incorporation, and control over copolymer structures.

PUBLISHED CONTENT AND CONTRIBUTIONS

Several published articles and manuscripts in preparation were reproduced as a part of this thesis or will be adopted from parts of this thesis. Parts of this thesis are results of scientific collaborations, without which, the reported studies would not be possible.

Chapter 1

Shuoyan Xiong, Priyabrata Ghana, and Theodor Agapie*. "Synthesis of Ethylene/Acrylate Copolymers via Transition-Metal Catalysis." *In preparation.*

S.X. and T.A. conceived the presented idea.
S.X. conducted literature collection and review.
S.X. drafted the manuscript and all authors contributed to manuscript editing.

Chapter 2

Shuoyan Xiong†, Manar M. Shoshani†, Xinglong Zhang†, Heather A. Spinney, Alex J. Nett, Briana S. Henderson, Thomas F. Miller III*, Theodor Agapie*. "Efficient Copolymerization of Acrylate and Ethylene with Neutral P,O-Chelated Nickel Catalysts: Mechanistic Investigations of Monomer Insertion and Chelate Formation." *J. Am. Chem. Soc.*, **2021**, 143, 6516-6527.

S.X. and T.A. conceived the presented idea.
S.X. performed synthesis and mechanistic studies and polymer characterization and analyzed the catalysis data.
M.M.S. performed synthesis and mechanistic studies.
X.Z. performed DFT calculations.
H.A.S., A.J.N., and B.S.H. performed polymerization studies and polymer characterization.
S.X., M.M.S and X.Z. drafted the manuscript and all authors contributed to manuscript editing.

Chapter 3

Manar M. Shoshani†, **Shuoyan Xiong†**, James Lawniczak, Xinglong Zhang, Thomas F. Miller III*, Theodor Agapie*. "Phosphine-Phenoxide Nickel Catalysts for Ethylene/Acrylate Copolymerization: Olefin Coordination and Complex Isomerization Studies Relevant to the Mechanism of Catalysis." *Organometallics*, **2022**, 41, 2119-2131.

M.M.S., **S.X.** and T.A. conceived the presented idea.
M.M.S. and **S.X.** performed synthetic and mechanistic studies.
J.L. and X.Z. performed DFT calculations.
M.M.S. and **S.X.** drafted the manuscript and all authors contributed to manuscript editing.

Chapter 4

Shuoyan Xiong, Alexandria Hong, Brad C. Bailey, Heather A. Spinney, Todd D. Senecal, Hanah Bailey, Theodor Agapie*. "Highly Active and Thermally Robust Nickel Enolate Catalysts for the Synthesis of Ethylene-Acrylate Copolymers." *Angew. Chem. Int. Ed*, **2022**, 61, e202206637.

S.X. and T.A. conceived the presented idea.
S.X. performed synthesis experiments and polymer characterization and analyzed the catalysis data.
A.H. performed synthesis experiments.
B.C.B, H.A.S., T.D.S. and H.B. performed polymerization studies and polymer characterization.
S.X. drafted the manuscript and all authors contributed to manuscript editing.

Chapter 5

Shuoyan Xiong, Priyabrata Ghana, Brad C. Bailey, Heather A. Spinney, Briana S. Henderson, Matthew R. Espinosa, Theodor Agapie* "Impacts of Labile Ligands on Catalyst Initiation and Chain Propagation in Ni-Catalyzed Ethylene/Acrylate Copolymerization" *ACS Catalysis*, **2023**, 13, 5000-5006.

S.X. and T.A. conceived the presented idea.
S.X. performed synthesis experiments and polymer characterization and analyzed the catalysis data.
P.G. performed synthesis experiments.
B.C.B, H.A.S., and B.S.H performed polymerization studies and polymer characterization.
M.R.E. performed single-crystal X-ray diffraction (scXRD) studies.
S.X. drafted the manuscript and all authors contributed to manuscript editing.

Chapter 6

Shuoyan Xiong, Alexandria Hong, Brad C. Bailey, Heather S. Spinney, Briana S. Henderson, Steve Marshall, Theodor Agapie* "Acrylate-Induced β-H Elimination in Insertion Polymerization" *In Preparation.*

S.X. and T.A. conceived the presented idea.
S.X. performed synthetic and mechanistic studies and polymer characterization and analyzed the catalysis data.
A.H. performed mechanistic studies.
B.C.B, H.A.S., B.S.H and S.M. performed polymerization studies and polymer characterization.
S.X. drafted the manuscript.

Chapter 7

Shuoyan Xiong, Manar M. Shoshani, Alex J. Nett, Heather S. Spinney, Briana S. Henderson, Theodor Agapie* "Nickel-Based Heterometallic Catalysts in Functional Polar Polyolefin Synthesis: Interrogating Effects of Secondary Metal Additives" *In Preparation.*

S.X. and T.A. conceived the presented idea.
S.X. performed synthetic and mechanistic studies, polymerization studies and polymer characterization, and analyzed the catalysis data.
M.M.S. performed single-crystal X-ray diffraction (scXRD) studies.
A.J.N, H.A.S., and B.S.H performed polymerization studies and polymer characterization.
S.X. drafted the manuscript and all authors contributed to manuscript editing..

Chapter 8

Shuoyan Xiong, Brad C. Bailey, Heather S. Spinney, Briana S. Henderson, Theodor Agapie* "Dynamically Controlled Ethylene/Acrylate Copolymerization by A Dinickel Catalyst System via Cation Shuttling" *In Preparation.*

S.X. and T.A. conceived the presented idea.
S.X. performed synthetic and mechanistic studies and polymer characterization and analyzed the catalysis data.
B.C.B., H.A.S., and B.S.H performed polymerization studies and polymer characterization.
S.X. drafted the manuscript and all authors contributed to manuscript editing..

TABLE OF CONTENTS

LIST OF FIGURES

Chapter 3

Chapter 4

LIST OF TABLES

CHAPTER 1

GENERAL INTRODUCTION

1 Background

Polyolefins account for over half of global plastic production, partly due to their low cost and desirable properties such as innocuousness, chemical stability, and resistance to corrosion.[1-5] However, the non-polar nature of hydrocarbon chains limits the applications of this indispensable class of materials.[6] Incorporation of polar functionalities can significantly improve polyolefins' physical and material properties such as wettability, adhesion, and printability, and potential degradability, thus expanding the range of potential applications.[7-13]

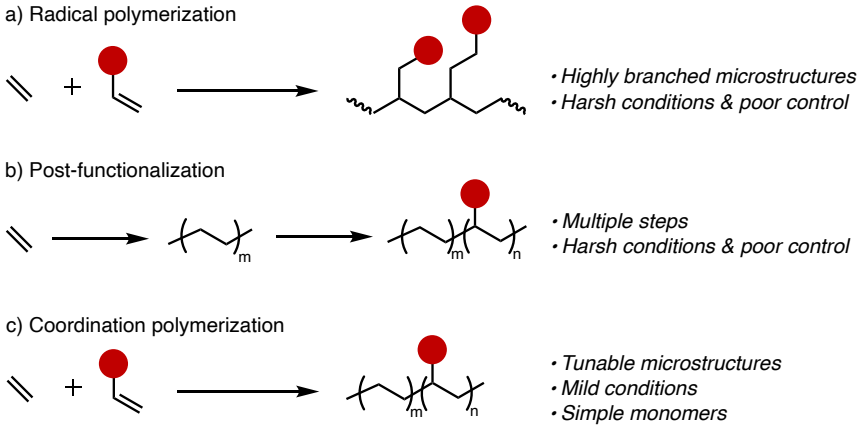

Figure 1.1. Methods for synthesis of functional polyolefins.

Industrially, polar-functionalized polyolefins are produced via post-polymerization or radical copolymerization (Figure 1.1a,b).[14-16] Both methods are poorly controllable and energy intensive as they require high temperature and high ethylene pressure. In contrary, metal-catalyzed coordination copolymerization of polar and non-polar olefins (Figure 1.1c) is performed under relatively mild conditions and via machinery and process compatible with current industrialized preparation of non-polar

polyolefins (polyethylene, polypropylene, etc), thus being of high interest as an alternative method.[17-20]

Among functional polyolefins, ethylene-acrylate copolymers (EAcP) are of special interest as they combine excellent filler acceptance, toughness, thermal stability, flexibility, and adhesion across a wide temperature range.[8, 16, 21-28] EAcP by industrial radical preparations have been widely used as commodity materials in food and medical packaging, composite films, wires/cables/hoses, and toys.[8, 16, 21-24, 29-30] They are also potential precursors for ethylene/acid ionomers, another type of well-known commercial products (e.g. Surlyn@ from DuPont, Primacor™ from SK). Transition-metal-catalyzed coordination copolymerization of ethylene and acrylates is not only a controlled, atom- and energy-efficient alternative for the preparation of aforementioned polymer products, but also provides new possibilities regarding copolymer structures and properties.[31-34] For example, it can provide linear high Mw EAcP as the next generation of high-density-polyethylene (HDPE) that is not accessible by industrial radical preparations.[15, 35-36]

In this regard, metal-catalyzed ethylene/acrylate copolymerization has been extensively studied.[1, 11, 21, 37-39] Further, catalysts showing promise in this copolymerization have also been widely employed in copolymerization of ethylene and other types of polar comonomers.[8, 11, 21, 37-41] However, the low catalyst performance (typically <100 kg/(mol*h)) prevented any potential industrial applications for a long period of time.[36, 38, 41] It is notable that the last 5 years have seen emerging new, high-performance Pd and Ni catalysts that show significantly improved activity or ability to

produce EAcP with novel, controlled microstructures.[38, 40, 42] Such encouraging results are also triggering revisiting mechanistic details of this copolymerization process, as well as investigations of material properties of resulting copolymers.[12, 43-44] In this chapter, we first discuss mechanistic pathways of metal-catalyzed ethylene/acrylate copolymerization, challenges of this catalysis, and catalyst design strategies (Section 2). Recent advances in catalyst developments are discussed subsequently, with emphasis on single-component catalysts and mechanistic understanding of this copolymerization that promotes iterative catalyst design (Section 3~5). The next session is focused on material properties of EAcP and EAcP-based polymers (Section 6). Introduction to the following chapters is included throughout the discussion and at the end.

2 Copolymerization Mechanism and Catalyst Design Strategies

In olefin polymerization, a single-component catalyst typically features a metal center supported by a multidentate ligand and at least one initiating alkyl and one labile ligand L (Figure 1.2, A).[20, 45] Replacing the ligand L by olefinic monomers (B) allows subsequent migratory insertion (C). β-H elimination (D) may happen after insertion of several monomers, and subsequent replacement of the long-chain olefin by an olefinic monomer (E) results in chain termination. Insertion of ethylene into metal hydride species is generally fast, which initiates propagation of another polymer chain.

The complexity of ethylene/acrylate copolymerization mechanism includes several aspects.[33, 46-47] First, the presence of a large amount of the ester group that can

coordinate to the metal center can significantly suppress catalytic activity. Second, cross polymerization happens (Figure 1.2, blue steps), and one monomer insertion can affect subsequent monomer insertion. For example, polar group coordination may happen after acrylate insertion, inhibiting subsequent insertion. Overall, the existence of multiple cases of monomer enchainment and activity suppression makes it hard to generalize the rate-determining step or catalyst design strategies. Moreover, mechanistic details of different catalyst systems may differ, as changes in nature of the metal and the supporting ligands can significantly alter the catalyst behavior. Notably, a detailed mechanistic profile has been established for ethylene/acrylate copolymerization by P,O-Ni catalysts (Section 4, and Chapter 2-3, 5~6).

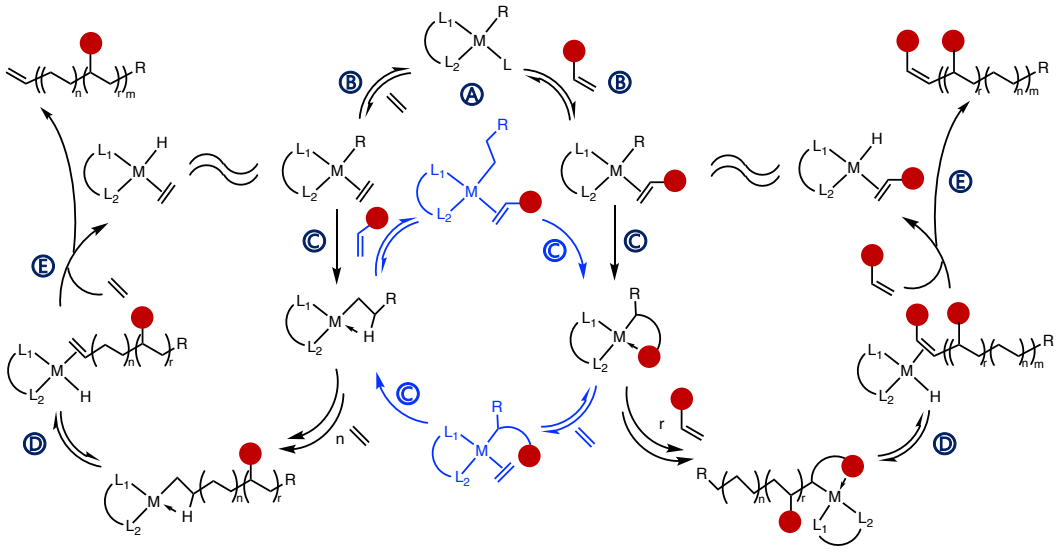

Figure 1.2. Mechanism of copolymerization of ethylene and polar monomers (red sphere: polar group).

Despite these challenges, several aspects that are important for catalyst design have been identified after trial and error.[1, 33, 46] First, late transition metals are less oxophilic and thus are more tolerant toward polar group coordination. To date, late-transition-

metal catalysts are the only catalysts that are capable of copolymerizing ethylene and fundamental polar monomers with polar groups directly attached to vinyl, including acrylate).[38] In addition, strategies such as proximal steric hindrance,[48-51] ligand asymmetry,[36, 40] secondary coordination sphere[52-54] have shown promise in many examples, which is also discussed in chapters 2, 4, 6. Inspired by nature, it has been proposed that introducing a secondary Lewis acidic metal may prevent the polar group's inhibitory coordination to the active metal center. However, it is challenging to develop multimetallic catalysts with tailored proximity. More details are included in Chapters 7 and 8.

3 Palladium Catalysts

In the field of functional polyolefin synthesis via transition-metal catalysis, acrylates are among those polar comonomers attempted first, with literature dated back to the 1980s.[55] Brookhart's α-diimine Pd catalysts (Figure 1.3, i) are the first literature example that produce ethylene/acrylate copolymers (EAcP).[31] Resulting copolymers are highly branched and acrylate units are primarily located at the end of branches. Mechanistic studies revealed that acrylate inserts in a 2,1-mode and fast isomerization happens to generate a six-membered chelate.[56-57] Corresponding rearrangement is thought to account for the branch-end "insertion" of acrylates. It is notable that chain-walking is a characteristic behavior for such symmetric α-diimine catalysts in olefin polymerization.[17, 39, 58] Detailed mechanistic profiles have been established for this phenomenon.[56, 59-61]

A major limitation of the original Brookhart catalysts is low copolymerization activities. In addition, the highly branched microstructures limit many applications that require high-density-polyethylene (HDPE) type copolymers. Extensive structure-performance studies have thus been conducted to improve catalyst performance, with a focus on steric hindrance proximal to Pd center.[48, 60, 62-78] Initially employed for tuning catalytic behavior in ethylene homopolymerization, this approach has also shown promise in ethylene/acrylate copolymerization over the last few years. Chen and coworkers have shown that extremely bulky substituents enable the synthesis of EAcP with high molecular weight (Mw) and low branching (Figure 1.3, ii).[27-28, 48] Jian and Mecking reported catalysts with Cs-symmetry that produce branched EAcP with main-chain insertion of acrylates (iii).[79] In addition to modifying substituents on α-diimine ligands, analogous ligands have also been developed (iv-v),[80-81] but they mainly show similar or lower performance in ethylene/acrylate copolymerization compared to classical Brookhart catalysts.

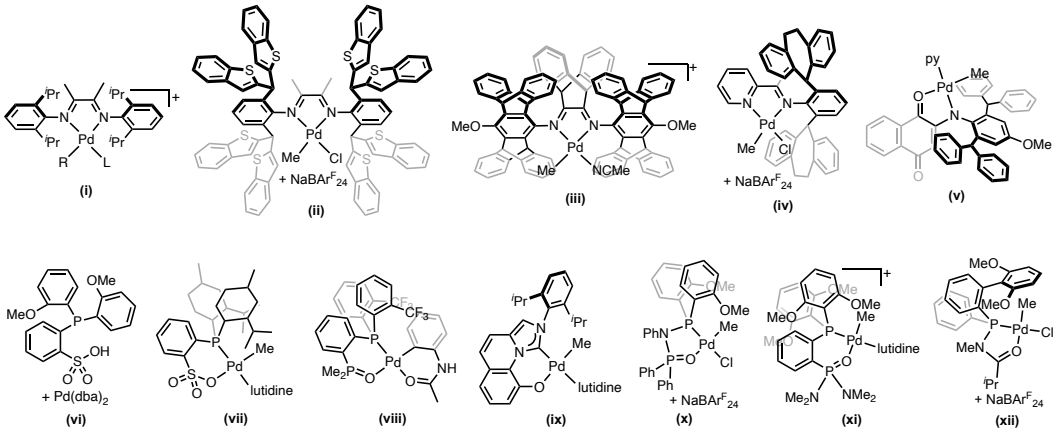

Figure 1.3. Representative Pd catalysts for ethylene/acrylate copolymerization.

Drent-type phosphine-sulfonate (PSO) Pd catalysts represent another important class. They produces linear EAcP with in-chain insertion of acrylate units (Figure 1.3, vi), which is potentially originated from the neutral net charge and ligand asymmetry as revealed by mechanistic studies by Nozaki, Mecking, and others.[35-36, 46-47, 82-91] Acrylate oligomerization is also feasible with this type of catalysts.[33] It is also notable that they are also capable of copolymerizing ethylene and a variety of other monomers.[9, 34-35, 47, 88, 92-105]

The major limitations of PSO-Pd catalysts are their low activities and low copolymer Mw. Nozaki has quantified the steric influence of PSO ligands and found that the copolymer Mw can be significantly increased using a menthyl substituent on phosphine (Figure 1.3, vii).[89, 106] Other substituents have also been extensively investigated by several groups.[53, 107-115] In addition, replacing either the phosphine or sulfonate moieties by other ligand donors has also shown promise.[13] Recent advances in this direction include bisphoshpine monoxide (BPMO),[116-118] IzQO-type ligands,[119-120] diphosphazane monoxide,[108, 121-123] phosphonic diamide-phosphine (PDAP) ligands,[124] and N-bridged phosphine carbonyl ligands[125-127] (Figure 1.3, viii-xii). Notably, cationic PDAP-Pd catalysts reported by Carrow and coworkers can produce EAcP with Mw up to $220*10^3$ kg/mol.[124] Until now, catalyst performance of PSO-Pd and analogous catalysts is still too low for commercial viability, however the knowledge of PSO ligand design has inspired the development of a variety of novel ligands including PO ligands for Ni catalysts, which is discussed in the following sections.

4 Nickel Catalysts

Despite aforementioned progresses, Pd catalysts hold little industrial interest due to the high cost of palladium and the low activities of reported catalysts.[38, 60] In this regard, Ni catalysts are potential alternatives as nickel is electronically similar to palladium but more earth abundant.[40-41] Ni catalysts supported by ligands that were previously employed in active Pd catalysts were developed first.[52-53, 66, 109-110, 113, 128-133] However, they are generally only capable of copolymerizing ethylene and comonomers with the polar group not directly attached to the vinyl. Notably, a few examples reported in the last few years showed promise in ethylene/acrylate copolymerization (Figure 1.4, i-iv), though with limited activity (<30 kg/(mol*h)).[121-122, 126-127, 134-136] Separately, a few Ni complexes also show activity in this copolymerization upon addition of a large excess of MAO or AlR_3 (c.a. 500 equiv.), which is included in Section 5.

Ni phosphine-phenoxide catalysts represent a major advance in this field. Initially reported by Shimizu in 2017, metalation of phosphine-phenol proligands and $Ni(COD)_2$ generates single-component catalysts showing an activity of 390 kg/(mol*h) in producing EAcP with a acrylate incorporation of 1.1% (Figure 1.4, v).[50] Introduction of bulkier substituents on phosphine leads to higher activity but lower acrylate incorporation. Later, Li and coworkers significantly expanded the catalyst scope to Ni(py)Me type complexes based on air-stable proligands (vi).[137-138] It is also notable that many of these proligands were synthesized from bisaryl phosphine chlorides that have previously been employed in synthesis of PSO ligands. Also similar

to PSO-Pd catalysts, these asymmetric Ni catalysts generally produce highly linear copolymers (Branching <1/1000C).[50] As most other neutral Ni catalysts, these catalysts suffer from relatively low thermal stability and are typically operated at 10-70 °C. However, thermally robust catalysts are preferred in industry as they do not require precise temperature control during polymerization that is highly exothermic. In addition, chain propagation is faster at higher temperatures, potentially leading to higher activity. Toward this, we reported Ni(py)CH_2SiMe_3 catalysts with steric shielding on the O side that remain highly active at temperatures ~100 °C (vii-viii).[43-44, 51] Higher acrylate incorporation (up to 12%) was also observed with a Ni bisphosphine phenoxide catalyst (Chapter 2).

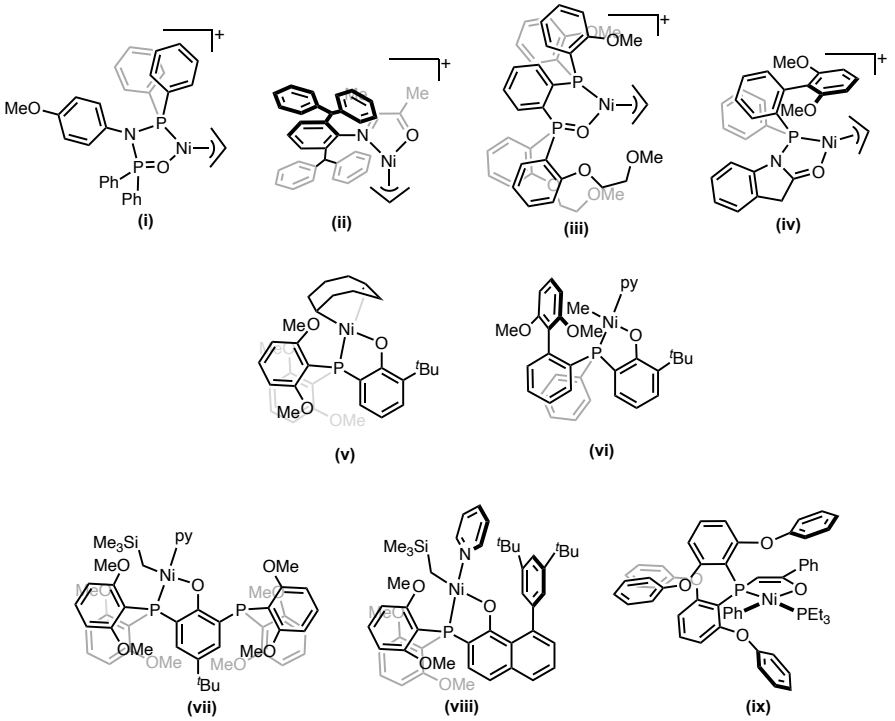

Figure 1.4. Representative Ni catalysts for ethylene/acrylate copolymerization.

Very recently, we reported bulky Ni phosphine-enolate complexes that are high-performance catalysts for EAcP synthesis (Chapter 4).[51] The key is the extremely bulky bisphenoxyphenyl group on phosphine, which provides steric shielding from the phosphine (P) side extending to the enolate (O) side (Figure 1.4, ix). In batch reactors, activity up to 5000 kg/(mol*h) (efficiency up to 35000 g copolymer/(g Ni*h)) was achieved at 110 °C, representing a new level of activity and thermal stability. Slightly higher amount of branching (1~3/1000C) was observed in resulting copolymers than that by Ni phenoxide catalysts mentioned above, highlighting the impact of chelating frameworks.

The aforementioned remarkable performance of P,O-Ni catalysts leads to significant efforts in mechanistic studies. Though acrylate insertion reactions have been studied with NO-Ni catalysts,[139] for a long-time mechanistic studies of Ni-catalyzed ethylene/acrylate copolymerization have been hindered by the lack of efficient catalysts and difficulties in isolation of key intermediates. In this regard, the first isolation and characterization of pyridine-coordinated and four-membered chelated species generated after acrylate insertion are remarkable (Figure 1.5, also included in Chapter 2).[43-44] It is also notable that these intermediates are also highly active catalysts by themselves. Based on these compounds, combination of experimental and DFT studies (Chapters 2, 3) reveals that: 1) catalyst initiation starts with ethylene; 2) ethylene insertion after acrylate insertion is the overall limiting step for copolymerization; 3) back-to-back acrylate insertion is unlikely to happen; 4) a cis-trans isomerization via a five-coordinate transition state occurs prior to migratory

insertion; and 5) olefin's coordination is >6 orders of magnitude weaker than ligand L (e.g. PEt_3, pyridine) coordination (Figure 1.5).

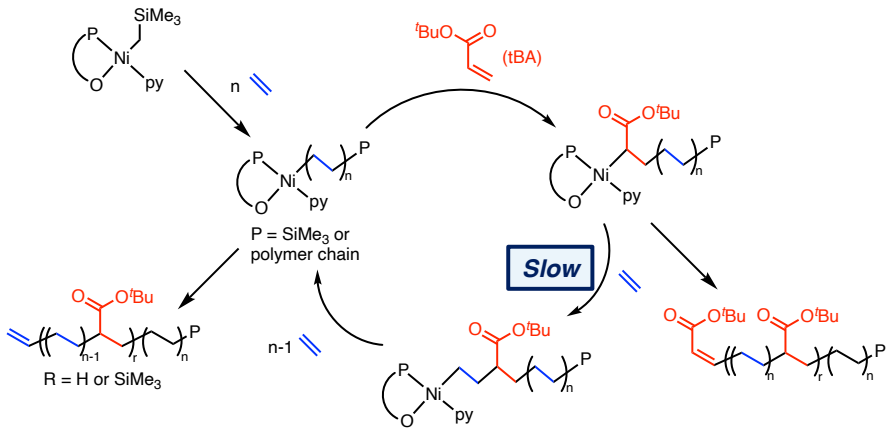

Figure 1.5. A mechanism profile of EAcP synthesis by PO-Ni catalysts.

Notably, the above mechanistic details indeed provide insights in subsequent catalyst design. For example, the weak olefin coordination observed with P,O-Ni system implies that ligand L (e.g. PEt_3) may also be involved in chain propagation. Indeed, faster catalyst initiation and higher rates of chain propagation were observed with pyridine-coordinated species than PEt_3 coordinated species, which leads to significant increase in activity for Ni enolate catalysts. Consequently, an activity reaching 24000 kg/(mol*h) was achieved (Chapter 5).

Overall, recent advances on Ni catalysts have rapidly revolutionized the field of metal-catalyzed EAcP synthesis that were dominated by Pd catalysts and brought up possibilities of practical applications in the near future. With these catalysts that are thermally stable, extremely active, and/or produce copolymers with a wide range of acrylate incorporation, the upcoming tasks are to develop a catalyst system having all three above features, implement copolymerization under more industrially relevant

conditions, and investigate material properties of EAcP produced by these catalysts.

5 Other Catalyst Systems

The above two sections mainly focused on single-component, homogenous Pd and Ni catalysts. They represent state-of-art performance in EAcP synthesis, and their single-component nature allows detailed mechanistic studies and structural-performance benchmarking those are vital for iterative catalyst developments. Notably, knowledge obtained from these studies may also be applied in designing *in-situ* generated or heterogenized catalysts, which is the focus of this section.

For Fe or Ni-based systems, single-component active species is highly oxygen sensitive, and thus *in-situ* activation of MX_2 type precatalysts (M: metal, X: halide) by alkylation reagents has been a common protocol.[76, 140-142] Several Ni precatalysts have shown activity in ethylene/acrylate copolymerization upon activation of a large excess of MAO or AlR_3 (c.a. 500 equiv. to Ni).[52, 143-144] On the contrary, Fe-based systems to date only produce polyethylene/polyacrylate blends under copolymerization conditions.[142] Separately, Stibrany have reported a Cu/MAO system that produces acrylate-based EAP with 55~72% acrylate incorporation.[145] It is notable that the amount of MAO or AlR_3 used in these systems is comparable to the amount of polar monomer (typically 500~2000 equiv. to Ni). Utilizing these reagents compromises atom efficiency and increases cost. It's well established that these Lewis acidic Al alkyl/alkoxide can act as masking reagent for polar monomers.[146-148] They may also promote chain transfer, which compromises copolymer Mw and inhibits mechanistic

studies.[149-151]

Heterogeneous olefin polymerization catalysts have dominated industrial polyolefin production.[152] Immobilization of high-performance homogeneous Pd or Ni catalysts potentially provides heterogeneous catalysts suitable for EAcP synthesis and thus became an emerging area recently.[38] Several supported Pd catalysts have shown promise in EAcP synthesis (Figure 1.6), such as polystyrene supported PSO-Pd catalysts by Mecking (i),[153] sulfated zirconia supported α-diimine Pd catalysts by Conely (ii),[154-155] and SiO_2-supported anilinonaphthoquinone Pd catalysts by Chen and Cai (iii).[156] However, these catalysts suffer from low catalyst activity (<50 kg/(mol*h)) and limitations in acrylate incorporation (typically <0.5%). These issues have been resolved in a recent example by Chen, in which P,O-Ni catalysts were heterogenized via an ionic anchoring strategy.[157] Resulting supported catalysts show showed performance superior to their homogenous counterparts (Figure 1.6, iv).

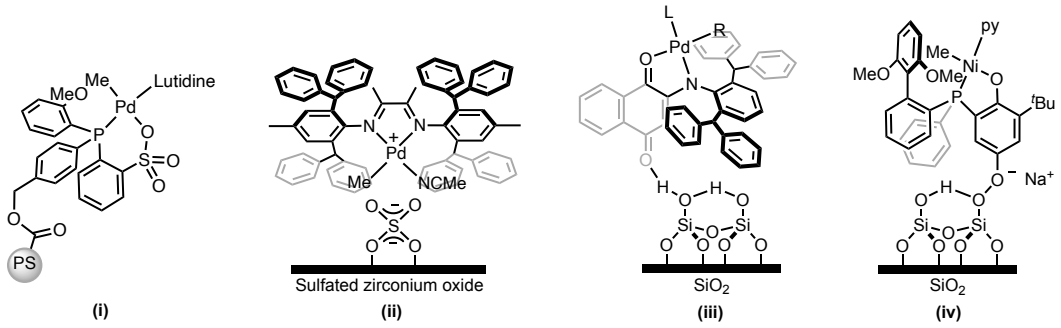

Figure 1.6. Heterogenous catalyst system for EAP synthesis.

6 Material Properties of EAcP and EAcP-Based Polymers

Compared to their non-polar analogues, ethylene/acrylate copolymers (EAcP) have shown improved physical and material properties.[12, 105] Moreover, such properties are

derived from intrinsic properties of the functional groups in the polymer chain instead of additives. Therefore, additive-induced poisoning effects on mechanical properties and environmental and health concerns related to additive release can be prevented.[158]

Among all properties, hydrophilicity, typically estimated by the water contact angle (WCA), is one of the most commonly studied properties for EAcP produced by transition metal catalysis. Acrylate incorporation can significantly decrease the WCA and potentially increase adhesion properties. For example, WCA of ethylene/MA copolymers produced by α-dimine Pd catalysts decreases from 104° to 54° as the MA incorporation increases from 0% to ~7%.[27-28, 159] Converting the ester functionalities to carboxylic acids leads to further decrease in WCA to ~40°.[28] Carboxylic acid-functionalized polyolefins also showed significantly improved dyeability.[159]

It is also notable that these properties can be precisely controlled by tuning catalyst structure and polymerization conditions, and moreover, the tunability of transition metal catalysis provides possibilities of introducing custom-made properties in EAcP or EAcP-based polymers. For example, Mecking reported vitrimer synthesis starting from Pd-catalyzed copolymerization of ethylene and ketal-functionalized acrylates.[99] Subsequent reaction of copolymers with phenyl-oxoborolanes and diboronic esters leads to molecularly defined functional polyolefin vitrimers that combines the advantageous properties of cross-linked materials with thermoplastic processability.[160] Another desired property for next generation polyolefins is degradability. Towards this, Mecking reported synthesis of photodegradable EAcP via terpolymerization of ethylene, CO and acrylate by Ni phosphine phenoxide catalysts.[161]

7 Summary

Controlled functional polyolefin synthesis by coordination copolymerization of ethylene and polar monomers have been one of the most significant and profound challenge for in the field of polyolefin catalysis for decades. Catalytic synthesis of EAcP is one specific target that have been intensively studied, with numerous efforts from both academia and industry. However, its applications have been hampered by low catalyst performance. Over last 5~6 years, significant advances have been made in both aspects. EAcP with more diverse, but controlled and custom-made microstructures and material properties have been rationally synthesized. Further, recently developed highly active, thermally stable Ni catalysts have rapidly revolutionized this field that were dominated by Pd catalysts and brought up possibilities of practical applications in the near future.

This thesis is focused on mechanistic studies and catalyst development of Ni-catalyzed EAcP synthesis, with a specific emphasis on insertion of olefins into Ni alkyl complexes, the elementary organometallic transformation in olefin (co)polymerization. Chapter 2 outlines a catalyst design strategy that leads to thermally stable Ni catalysts with significant improved acrylate incorporation or resistance to acrylate induced chain transfer. This chapter also provides mechanistic details of chelate formation, as well as a kinetic profile of catalyst initiation and chain propagation. Chapter 3 elucidates specific mechanistic details related to olefin coordination and ligand isomerization. Chapter 4 demonstrates how knowledge from these studies can promote development of a new

type of EAcP catalyst, while Chapter 5 is an example of how such knowledge can promote iterative catalyst design. Chapter 6 is focused on β-H elimination, one step controls chain-termination but has been little explored. Inspired by nature, it have been proposed that introducing a secondary Lewis acidic metal may prevent polar group's inhibitory coordination to active metal center. Toward this, Chapters 7 and 8 include two types of multimetallic catalysts for EAcP synthesis.

REFERENCES

(1) Chen, C., Designing catalysts for olefin polymerization and copolymerization: beyond electronic and steric tuning. *Nat. Rev. Chem.* **2018,** *2* (5), 6-14.

(2) Hustad, P. D., Frontiers in olefin polymerization: Reinventing the world's most common synthetic polymers. *Science* **2009,** *325* (5941), 704-707.

(3) Sauter, D. W.; Taoufik, M.; Boisson, C., Polyolefins, a success story. *Polymers* **2017,** *9* (6), 185.

(4) AlMa'adeed, M. A.-A.; Krupa, I., *Polyolefin Compounds and Materials*. Springer: 2016.

(5) Kaminsky, W., Polyolefins: 50 years after Ziegler and Natta II. *Adv. Polym. Sci.* **2013**.

(6) Chung, T. M., *Functionalization of polyolefins*. Elsevier: 2002.

(7) Boffa, L. S.; Novak, B. M., Copolymerization of polar monomers with olefins using transition-metal complexes. *Chem. Rev.* **2000,** *100* (4), 1479-1494.

(8) Franssen, N. M.; Reek, J. N.; de Bruin, B., Synthesis of functional 'polyolefins': state of the art and remaining challenges. *Chem. Soc. Rev.* **2013,** *42* (13), 5809-5832.

(9) Zou, C.; Chen, C., Polar-functionalized, crosslinkable, self-healing, and photoresponsive polyolefins. *Angew. Chem. Int. Ed* **2020,** *59* (1), 395-402.

(10) Baur, M.; Lin, F.; Morgen, T. O.; Odenwald, L.; Mecking, S., Polyethylene materials with in-chain ketones from nonalternating catalytic copolymerization. *Science* **2021,** *374* (6567), 604-607.

(11) Nakamura, A.; Ito, S.; Nozaki, K., Coordination− insertion copolymerization of fundamental polar monomers. *Chem. Rev.* **2009,** *109* (11), 5215-5244.

(12) Tan, C.; Zou, C.; Chen, C., Material Properties of Functional Polyethylenes from Transition-Metal-Catalyzed Ethylene–Polar Monomer Copolymerization. *Macromolecules* **2022**.

(13) Carrow, B. P.; Nozaki, K., Transition-metal-catalyzed functional polyolefin synthesis: effecting control through chelating ancillary ligand design and mechanistic insights. *Macromolecules* **2014,** *47* (8), 2541-2555.

(14) Boaen, N. K.; Hillmyer, M. A., Post-polymerization functionalization of polyolefins. *Chem. Soc. Rev.* **2005,** *34* (3), 267-275.

(15) Ehrlich, P.; Mortimer, G. A., Fundamentals of the free-radical polymerization of ethylene. In *Fortschritte der Hochpolymeren-Forschung*, Springer: 1970; pp 386-448.

(16) Venkatesh, R.; Harrisson, S.; Haddleton, D. M.; Klumperman, B., Olefin copolymerization via controlled radical polymerization: copolymerization of acrylate and 1-octene. *Macromolecules* **2004,** *37* (12), 4406-4416.

(17) Guan, Z.; Cotts, P.; McCord, E.; McLain, S., Chain walking: a new strategy to control polymer topology. *Science* **1999,** *283* (5410), 2059-2062.

(18) Arriola, D. J.; Carnahan, E. M.; Hustad, P. D.; Kuhlman, R. L.; Wenzel, T. T., Catalytic production of olefin block copolymers via chain shuttling polymerization. *Science* **2006,** *312* (5774), 714-719.

(19) Delferro, M.; Marks, T. J., Multinuclear olefin polymerization catalysts. *Chem. Rev.* **2011,** *111* (3), 2450-2485.

(20) Makio, H.; Terao, H.; Iwashita, A.; Fujita, T., FI Catalysts for olefin polymerization□ A comprehensive treatment. *Chem. Rev.* **2011,** *111* (3), 2363-2449.

(21) Ittel, S. D.; Johnson, L. K.; Brookhart, M., Late-metal catalysts for ethylene homo-and copolymerization. *Chem. Rev.* **2000,** *100* (4), 1169-1204.

(22) Bombaugh, K.; Cook, C.; Clampitt, B., Investigation of Comonomer Distribution in Ethylene-Acrylate Copolymers with Thermal Methods. *Analytical Chemistry* **1963,** *35* (12), 1834-1837.

(23) Bonotto, S., Mechanical properties of crosslinked polyethylene and crosslinked ethylene–ethyl acrylate copolymers. *Journal of Applied Polymer Science* **1965,** *9* (12), 3819-3835.

(24) Hausmann, K.; Chou, R. T.; Lee, C. Y., Novel functionalised ethylene acrylate copolymers as polymer

modifiers. *Polymers and Polymer Composites* **2004,** *12* (2), 119-125.

(25) Afrifah, K. A.; Matuana, L. M., Fracture toughness of poly (lactic acid)/ethylene acrylate copolymer/wood-flour composite ternary blends. *Polymer international* **2013,** *62* (7), 1053-1058.

(26) Su, Y.; Yin, H.; Wang, X.; Ma, Y.; Vupputuri, S.; Guo, Z.; Song, G., Preparation and properties of ethylene-acrylate salt ionomer/polypropylene antistatic alloy. *Advanced Composites and Hybrid Materials* **2021,** *4* (1), 104-113.

(27) Dai, S.; Chen, C., Direct synthesis of functionalized high-molecular-weight polyethylene by copolymerization of ethylene with polar monomers. *Angew. Chem. Int. Ed.* **2016,** *55* (42), 13281-13285.

(28) Dai, S.; Zhou, S.; Zhang, W.; Chen, C., Systematic investigations of ligand steric effects on α-diimine palladium catalyzed olefin polymerization and copolymerization. *Macromolecules* **2016,** *49* (23), 8855-8862.

(29) Otey, F. H.; Westhoff, R. P.; Russell, C. R., Biodegradable films from starch and ethylene-acrylic acid copolymer. *Industrial & Engineering Chemistry Product Research and Development* **1977,** *16* (4), 305-308.

(30) Sullivan, M. J.; Melvin, T.; Nesbitt, R. D., Golf ball cover of neutralized poly (ethylene-acrylic acid) copolymer. Google Patents: 1990.

(31) Johnson, L. K.; Mecking, S.; Brookhart, M., Copolymerization of ethylene and propylene with functionalized vinyl monomers by palladium (II) catalysts. *J. Am. Chem. Soc.* **1996,** *118* (1), 267-268.

(32) Younkin, T. R.; Connor, E. F.; Henderson, J. I.; Friedrich, S. K.; Grubbs, R. H.; Bansleben, D. A., Neutral, single-component nickel (II) polyolefin catalysts that tolerate heteroatoms. *Science* **2000,** *287* (5452), 460-462.

(33) Guironnet, D.; Roesle, P.; Rünzi, T.; Göttker-Schnetmann, I.; Mecking, S., Insertion polymerization of acrylate. *J. Am. Chem. Soc.* **2009,** *131* (2), 422-423.

(34) Weng, W.; Shen, Z.; Jordan, R. F., Copolymerization of ethylene and vinyl fluoride by (phosphine-sulfonate) Pd (Me)(py) catalysts. *J. Am. Chem. Soc.* **2007,** *129* (50), 15450-15451.

(35) Drent, E.; van Dijk, R.; van Ginkel, R.; van Oort, B.; Pugh, R. I., Palladium catalysed copolymerisation of ethene with alkylacrylates: polar comonomer built into the linear polymer chain. *Chem. Commun.* **2002,** (7), 744-745.

(36) Nakamura, A.; Anselment, T. M.; Claverie, J.; Goodall, B.; Jordan, R. F.; Mecking, S.; Rieger, B.; Sen, A.; Van Leeuwen, P. W.; Nozaki, K., Ortho-phosphinobenzenesulfonate: A superb ligand for palladium-catalyzed coordination–insertion copolymerization of polar vinyl monomers. *Acc. Chem. Res.* **2013,** *46* (7), 1438-1449.

(37) Chen, E. Y.-X., Coordination polymerization of polar vinyl monomers by single-site metal catalysts. *Chem. Rev.* **2009,** *109* (11), 5157-5214.

(38) Tan, C.; Chen, C., Emerging palladium and nickel catalysts for copolymerization of olefins with polar monomers. *Angew. Chem.* **2019,** *131* (22), 7268-7276.

(39) Wang, F.; Chen, C., A continuing legend: the Brookhart-type α-diimine nickel and palladium catalysts. *Polym. Chem* **2019,** *10* (19), 2354-2369.

(40) Mu, H.; Zhou, G.; Hu, X.; Jian, Z., Recent advances in nickel mediated copolymerization of olefin with polar monomers. *Coord. Chem. Rev.* **2021,** *435*, 213802.

(41) Mu, H.; Pan, L.; Song, D.; Li, Y., Neutral nickel catalysts for olefin homo-and copolymerization: relationships between catalyst structures and catalytic properties. *Chem. Rev.* **2015,** *115* (22), 12091-12137.

(42) Zhou, G.; Mu, H.; Jian, Z., A comprehensive picture on catalyst structure construction in palladium catalyzed ethylene (co) polymerizations. *J. Catal.* **2020,** *383*, 215-220.

(43) Xiong, S.; Shoshani, M. M.; Zhang, X.; Spinney, H. A.; Nett, A. J.; Henderson, B. S.; Miller III, T. F.; Agapie, T., Efficient Copolymerization of Acrylate and Ethylene with Neutral P, O-Chelated Nickel Catalysts: Mechanistic Investigations of Monomer Insertion and Chelate Formation. *J. Am. Chem. Soc.* **2021,** *143* (17), 6516-6527.

(44) Shoshani, M. M.; Xiong, S.; Lawniczak, J. J.; Zhang, X.; Miller, T. F.; Agapie, T., Phosphine-Phenoxide Nickel Catalysts for Ethylene/Acrylate Copolymerization: Olefin Coordination and Complex Isomerization Studies Relevant to the Mechanism of Catalysis. *Organometallics* **2022**.

(45) Guo, L.; Liu, W.; Chen, C., Late transition metal catalyzed α-olefin polymerization and copolymerization with polar monomers. *Mater. Chem. Front.* **2017,** *1* (12), 2487-2494.

(46) Guironnet, D.; Caporaso, L.; Neuwald, B.; Göttker-Schnetmann, I.; Cavallo, L.; Mecking, S., Mechanistic

insights on acrylate insertion polymerization. *J. Am. Chem. Soc.* **2010,** *132* (12), 4418-4426.

(47) Nakamura, A.; Munakata, K.; Ito, S.; Kochi, T.; Chung, L. W.; Morokuma, K.; Nozaki, K., Pd-catalyzed copolymerization of methyl acrylate with carbon monoxide: structures, properties and mechanistic aspects toward ligand design. *J. Am. Chem. Soc.* **2011,** *133* (17), 6761-6779.

(48) Dai, S.; Sui, X.; Chen, C., Highly Robust Palladium (II) α-Diimine Catalysts for Slow-Chain-Walking Polymerization of Ethylene and Copolymerization with Methyl Acrylate. *Angew. Chem. Int. Ed.* **2015,** *54* (34), 9948-9953.

(49) Zhang, Y.; Wang, C.; Mecking, S.; Jian, Z., Ultrahigh branching of main-chain-functionalized polyethylenes by inverted insertion selectivity. *Angew. Chem.* **2020,** *132* (34), 14402-14408.

(50) Xin, B. S.; Sato, N.; Tanna, A.; Oishi, Y.; Konishi, Y.; Shimizu, F., Nickel catalyzed copolymerization of ethylene and alkyl acrylates. *J. Am. Chem. Soc.* **2017,** *139* (10), 3611-3614.

(51) Xiong, S.; Hong, A.; Bailey, B. C.; Spinney, H. A.; Senecal, T. D.; Bailey, H.; Agapie, T., Highly Active and Thermally Robust Nickel Enolate Catalysts for the Synthesis of Ethylene-Acrylate Copolymers. *Angew. Chem. Int. Ed.* **2022**.

(52) Li, M.; Wang, X.; Luo, Y.; Chen, C., A Second-Coordination-Sphere Strategy to Modulate Nickel-and Palladium-Catalyzed Olefin Polymerization and Copolymerization. *Angew. Chem. Int. Ed.* **2017,** *56* (38), 11604-11609.

(53) Tan, C.; Qasim, M.; Pang, W.; Chen, C., Ligand–metal secondary interactions in phosphine–sulfonate palladium and nickel catalyzed ethylene (co) polymerization. *Polym. Chem* **2020,** *11* (2), 411-416.

(54) Wang, G.; Peng, D.; Sun, Y.; Chen, C., Interplay of supramolecular chemistry and photochemistry with palladium-catalyzed ethylene polymerization. *CCS Chemistry* **2021,** *3* (7), 2025-2034.

(55) Klabunde, U.; Itten, S. D., Nickel catalysis for ethylene homo-and co-polymerization. *Journal of Molecular Catalysis* **1987,** *41* (1-2), 123-134.

(56) Mecking, S.; Johnson, L. K.; Wang, L.; Brookhart, M., Mechanistic studies of the palladium-catalyzed copolymerization of ethylene and α-olefins with methyl acrylate. *J. Am. Chem. Soc.* **1998,** *120* (5), 888-899.

(57) Deng, L.; Woo, T. K.; Cavallo, L.; Margl, P. M.; Ziegler, T., The role of bulky substituents in Brookhart-type Ni (II) diimine catalyzed olefin polymerization: a combined density functional theory and molecular mechanics study. *J. Am. Chem. Soc.* **1997,** *119* (26), 6177-6186.

(58) Guo, L.; Dai, S.; Sui, X.; Chen, C., Palladium and nickel catalyzed chain walking olefin polymerization and copolymerization. *ACS Catal.* **2016,** *6* (1), 428-441.

(59) Leatherman, M. D.; Svejda, S. A.; Johnson, L. K.; Brookhart, M., Mechanistic studies of nickel (II) alkyl agostic cations and alkyl ethylene complexes: investigations of chain propagation and isomerization in (α-diimine) Ni (II)-catalyzed ethylene polymerization. *J. Am. Chem. Soc.* **2003,** *125* (10), 3068-3081.

(60) Chen, Z.; Liu, W.; Daugulis, O.; Brookhart, M., Mechanistic studies of Pd (II)-catalyzed copolymerization of ethylene and vinylalkoxysilanes: Evidence for a β-silyl elimination chain transfer mechanism. *J. Am. Chem. Soc.* **2016,** *138* (49), 16120-16129.

(61) Chapleski, R. C.; Kern, J. L.; Anderson, W. C.; Long, B. K.; Roy, S., A mechanistic study of microstructure modulation in olefin polymerizations using a redox-active Ni (II) α-diimine catalyst. *Catal. Sci. Technol.* **2020,** *10* (7), 2029-2039.

(62) Liu, Y. S.; Harth, E., Distorted Sandwich α-Diimine PdII Catalyst: Linear Polyethylene and Synthesis of Ethylene/Acrylate Elastomers. *Angew. Chem. Int. Ed.* **2021**.

(63) Hai, Z.; Lu, Z.; Li, S.; Cao, Z.-Y.; Dai, S., The synergistic effect of rigid and flexible substituents on insertion polymerization with α-diimine nickel and palladium catalysts. *Polym. Chem* **2021,** *12* (32), 4643-4653.

(64) Ma, X.; Zhang, Y.; Jian, Z., Tunable branching and living character in ethylene polymerization using "polyethylene glycol sandwich" α-diimine nickel catalysts. *Polym. Chem* **2021,** *12* (9), 1236-1243.

(65) Ge, Y.; Li, S.; Fan, W.; Dai, S., Flexible "Sandwich"(8-Alkylnaphthyl α-Diimine) Catalysts in Insertion Polymerization. *Inorg. Chem.* **2021,** *60* (8), 5673-5681.

(66) Zhong, L.; Zheng, H.; Du, C.; Du, W.; Liao, G.; Cheung, C. S.; Gao, H., Thermally robust α-diimine nickel and palladium catalysts with constrained space for ethylene (co) polymerizations. *J. Catal.* **2020,** *384*, 208-217.

(67) Li, S.; Dai, S., 8-Arylnaphthyl substituent retarding chain transfer in insertion polymerization with unsymmetrical α-diimine systems. *Polym. Chem* **2020,** *11* (45), 7199-7206.

(68) Sui, X.; Hong, C.; Pang, W.; Chen, C., Unsymmetrical α-diimine palladium catalysts and their properties in olefin (co) polymerization. *Mater. Chem. Front.* **2017,** *1* (5), 967-972.

(69) Zou, W.; Chen, C., Influence of backbone substituents on the ethylene (co) polymerization properties of α-diimine Pd (II) and Ni (II) catalysts. *Organometallics* **2016,** *35* (11), 1794-1801.

(70) Camacho, D. H.; Salo, E. V.; Ziller, J. W.; Guan, Z., Cyclophane-based highly active late-transition-metal catalysts for ethylene polymerization. *Angew. Chem. Int. Ed.* **2004,** *43* (14), 1821-1825.

(71) Allen, K. E.; Campos, J. s.; Daugulis, O.; Brookhart, M., Living polymerization of ethylene and copolymerization of ethylene/methyl acrylate using "sandwich" diimine palladium catalysts. *ACS Catal.* **2015,** *5* (1), 456-464.

(72) Jones, G. R.; Basbug Alhan, H. E.; Karas, L. J.; Wu, J. I.; Harth, E., Switching the Reactivity of Palladium Diimines with "Ancillary" Ligand to Select between Olefin Polymerization, Branching Regulation, or Olefin Isomerization. *Angew. Chem.* **2021,** *133* (3), 1659-1664.

(73) Tran, Q. H.; Wang, X.; Brookhart, M.; Daugulis, O., Cationic α-Diimine Nickel and Palladium Complexes Incorporating Phenanthrene Substituents: Highly Active Ethylene Polymerization Catalysts and Mechanistic Studies of syn/anti Isomerization. *Organometallics* **2020**.

(74) Zhu, L.; Fu, Z.-S.; Pan, H.-J.; Feng, W.; Chen, C.; Fan, Z.-Q., Synthesis and application of binuclear α-diimine nickel/palladium catalysts with a conjugated backbone. *Dalton Trans* **2014,** *43* (7), 2900-2906.

(75) Chen, S.-Y.; Pan, R.-C.; Liu, Y.; Lu, X.-B., Bulky o-Phenylene-Bridged Bimetallic α-Diimine Ni (II) and Pd (II) Catalysts in Ethylene (Co) polymerization. *Organometallics* **2021,** *40* (22), 3703-3711.

(76) Johnson, L. K.; Killian, C. M.; Brookhart, M., New Pd (II)-and Ni (II)-based catalysts for polymerization of ethylene and. alpha.-olefins. *J. Am. Chem. Soc.* **1995,** *117* (23), 6414-6415.

(77) Williams, B. S.; Leatherman, M. D.; White, P. S.; Brookhart, M., Reactions of vinyl acetate and vinyl trifluoroacetate with cationic diimine Pd (II) and Ni (II) alkyl complexes: identification of problems connected with copolymerizations of these monomers with ethylene. *J. Am. Chem. Soc.* **2005,** *127* (14), 5132-5146.

(78) Long, B. K.; Eagan, J. M.; Mulzer, M.; Coates, G. W., Semi-Crystalline Polar Polyethylene: Ester-Functionalized Linear Polyolefins Enabled by a Functional-Group-Tolerant, Cationic Nickel Catalyst. *Angew. Chem. Int. Ed.* **2016,** *55* (25), 7106-7110.

(79) Zhang, Y.; Wang, C.; Mecking, S.; Jian, Z., Ultrahigh branching of main-chain-functionalized polyethylenes by inverted insertion selectivity. *Angew. Chem. Int. Ed.* **2020,** *59* (34), 14296-14302.

(80) Li, S.; Dai, S., Highly efficient incorporation of polar comonomers in copolymerizations with ethylene using iminopyridyl palladium system. *J. Catal.* **2021,** *393*, 51-59.

(81) Li, K.; Mu, H.; Kang, X.; Jian, Z., Suppression of Chain Transfer and Promotion of Chain Propagation in Neutral Anilinotropone Nickel Polymerization Catalysis. *Macromolecules* **2022**.

(82) Neuwald, B.; Olscher, F.; Göttker-Schnetmann, I.; Mecking, S., Limits of activity: weakly coordinating ligands in arylphosphinesulfonato palladium (II) polymerization catalysts. *Organometallics* **2012,** *31* (8), 3128-3137.

(83) Wucher, P.; Roesle, P.; Falivene, L.; Cavallo, L.; Caporaso, L.; Göttker-Schnetmann, I.; Mecking, S., Controlled acrylate insertion regioselectivity in diazaphospholidine-sulfonato palladium (II) complexes. *Organometallics* **2012,** *31* (24), 8505-8515.

(84) Wucher, P.; Goldbach, V.; Mecking, S., Electronic influences in phosphinesulfonato palladium (II) polymerization catalysts. *Organometallics* **2013,** *32* (16), 4516-4522.

(85) Neuwald, B.; Falivene, L.; Caporaso, L.; Cavallo, L.; Mecking, S., Exploring electronic and steric effects on the insertion and polymerization reactivity of phosphinesulfonato pdii catalysts. *Chem. - Eur. J.* **2013,** *19* (52), 17773-17788.

(86) Noda, S.; Nakamura, A.; Kochi, T.; Chung, L. W.; Morokuma, K.; Nozaki, K., Mechanistic studies on the formation of linear polyethylene chain catalyzed by palladium phosphine− sulfonate complexes: experiment and theoretical studies. *J. Am. Chem. Soc.* **2009,** *131* (39), 14088-14100.

(87) Kanazawa, M.; Ito, S.; Nozaki, K., Ethylene polymerization by palladium/phosphine–sulfonate catalysts in the presence and absence of protic solvents: structural and mechanistic differences. *Organometallics* **2011,** *30* (21), 6049-6052.

(88) Nozaki, K.; Kusumoto, S.; Noda, S.; Kochi, T.; Chung, L. W.; Morokuma, K., Why did incorporation of acrylonitrile to a linear polyethylene become possible? Comparison of phosphine− sulfonate ligand with diphosphine and imine− phenolate ligands in the Pd-catalyzed ethylene/acrylonitrile copolymerization. *J. Am. Chem. Soc.* **2010,** *132* (45), 16030-16042.

(89) Nakano, R.; Chung, L. W.; Watanabe, Y.; Okuno, Y.; Okumura, Y.; Ito, S.; Morokuma, K.; Nozaki, K., Elucidating the key role of phosphine− sulfonate ligands in palladium-catalyzed ethylene polymerization: Effect of ligand structure on the molecular weight and linearity of polyethylene. *ACS Catal.* **2016,** *6* (9), 6101-6113.

(90) Zhou, X.; Lau, K.-C.; Petro, B. J.; Jordan, R. F., cis/trans Isomerization of o-Phosphino-Arenesulfonate Palladium Methyl Complexes. *Organometallics* **2014,** *33* (24), 7209-7214.

(91) Conley, M. P.; Jordan, R. F., cis/trans isomerization of phosphinesulfonate palladium (II) complexes. *Angew. Chem. Int. Ed.* **2011,** *50* (16), 3744-3746.

(92) Ito, S.; Munakata, K.; Nakamura, A.; Nozaki, K., Copolymerization of vinyl acetate with ethylene by palladium/alkylphosphine− sulfonate catalysts. *J. Am. Chem. Soc.* **2009,** *131* (41), 14606-14607.

(93) Ito, S.; Kanazawa, M.; Munakata, K.; Kuroda, J.-i.; Okumura, Y.; Nozaki, K., Coordination− insertion copolymerization of allyl monomers with ethylene. *J. Am. Chem. Soc.* **2011,** *133* (5), 1232-1235.

(94) Leicht, H.; Göttker-Schnetmann, I.; Mecking, S., Incorporation of vinyl chloride in insertion polymerization. *Angew. Chem. Int. Ed.* **2013,** *52* (14), 3963-3966.

(95) Jian, Z.; Baier, M. C.; Mecking, S., Suppression of chain transfer in catalytic acrylate polymerization via rapid and selective secondary insertion. *J. Am. Chem. Soc.* **2015,** *137* (8), 2836-2839.

(96) Ota, Y.; Ito, S.; Kobayashi, M.; Kitade, S.; Sakata, K.; Tayano, T.; Nozaki, K., Crystalline Isotactic Polar Polypropylene from the Palladium-Catalyzed Copolymerization of Propylene and Polar Monomers. *Angew. Chem. Int. Ed.* **2016,** *55* (26), 7505-7509.

(97) Jian, Z.; Falivene, L.; Boffa, G.; Sánchez, S. O.; Caporaso, L.; Grassi, A.; Mecking, S., Direct synthesis of telechelic polyethylene by selective insertion polymerization. *Angew. Chem. Int. Ed.* **2016,** *55* (46), 14378-14383.

(98) Na, Y.; Chen, C., Catechol Functionalized Polyolefins. *Angew. Chem. Int. Ed.* **2020**.

(99) Odenwald, L.; Wimmer, F. P.; Mast, N. K.; Schußmann, M. G.; Wilhelm, M.; Mecking, S., Molecularly Defined Polyolefin Vitrimers from Catalytic Insertion Polymerization. *J. Am. Chem. Soc.* **2022,** *144* (29), 13226-13233.

(100) Leicht, H.; Göttker-Schnetmann, I.; Mecking, S., Synergetic effect of monomer functional group coordination in catalytic insertion polymerization. *J. Am. Chem. Soc.* **2017,** *139* (20), 6823-6826.

(101) Schuster, N.; Rünzi, T.; Mecking, S., Reactivity of functionalized vinyl monomers in insertion copolymerization. *Macromolecules* **2016,** *49* (4), 1172-1179.

(102) Borkar, S.; Newsham, D. K.; Sen, A., Copolymerization of Ethene with Styrene Derivatives, Vinyl Ketone, and Vinylcyclohexane Using a (Phosphine− sulfonate) palladium (II) System: Unusual Functionality and Solvent Tolerance. *Organometallics* **2008,** *27* (14), 3331-3334.

(103) Luo, S.; Vela, J.; Lief, G. R.; Jordan, R. F., Copolymerization of ethylene and alkyl vinyl ethers by a (phosphine-sulfonate) PdMe catalyst. *J. Am. Chem. Soc.* **2007,** *129* (29), 8946-8947.

(104) Kochi, T.; Noda, S.; Yoshimura, K.; Nozaki, K., Formation of linear copolymers of ethylene and acrylonitrile catalyzed by phosphine sulfonate palladium complexes. *J. Am. Chem. Soc.* **2007,** *129* (29), 8948-8949.

(105) Zhou, G.; Cui, L.; Mu, H.; Jian, Z., Custom-made polar monomers utilized in nickel and palladium promoted olefin copolymerization. *Polym. Chem* **2021,** *12* (27), 3878-3892.

(106) Ota, Y.; Ito, S.; Kuroda, J.-i.; Okumura, Y.; Nozaki, K., Quantification of the steric influence of alkylphosphine–sulfonate ligands on polymerization, leading to high-molecular-weight copolymers of ethylene and polar monomers. *J. Am. Chem. Soc.* **2014,** *136* (34), 11898-11901.

(107) Xia, J.; Zhang, Y.; Hu, X.; Ma, X.; Cui, L.; Zhang, J.; Jian, Z., Sterically very bulky aliphatic/aromatic

phosphine-sulfonate palladium catalysts for ethylene polymerization and copolymerization with polar monomers. *Polym. Chem* **2019,** *10* (4), 546-554.

(108) Sun, J.; Chen, M.; Luo, G.; Chen, C.; Luo, Y., Diphosphazane-monoxide and Phosphine-sulfonate Palladium Catalyzed Ethylene Copolymerization with Polar Monomers: A Computational Study. *Organometallics* **2019,** *38* (3), 638-646.

(109) Chen, M.; Chen, C., Rational design of high-performance phosphine sulfonate nickel catalysts for ethylene polymerization and copolymerization with polar monomers. *ACS Catal.* **2017,** *7* (2), 1308-1312.

(110) Liang, T.; Chen, C., Side-arm control in phosphine-sulfonate palladium-and nickel-catalyzed ethylene polymerization and copolymerization. *Organometallics* **2017,** *36* (12), 2338-2344.

(111) Yang, B.; Xiong, S.; Chen, C., Manipulation of polymer branching density in phosphine-sulfonate palladium and nickel catalyzed ethylene polymerization. *Polym. Chem* **2017,** *8* (40), 6272-6276.

(112) Wu, Z.; Hong, C.; Du, H.; Pang, W.; Chen, C., Influence of ligand backbone structure and connectivity on the properties of phosphine-sulfonate Pd (II)/Ni (II) catalysts. *Polymers* **2017,** *9* (5), 168.

(113) Wu, Z.; Chen, M.; Chen, C., Ethylene polymerization and copolymerization by palladium and nickel catalysts containing naphthalene-bridged phosphine–sulfonate ligands. *Organometallics* **2016,** *35* (10), 1472-1479.

(114) Chen, M.; Yang, B.; Chen, C., Redox-Controlled Olefin (Co) Polymerization Catalyzed by Ferrocene-Bridged Phosphine-Sulfonate Palladium Complexes. *Angew. Chem. Int. Ed.* **2015,** *54* (51), 15520-15524.

(115) Jian, Z.; Wucher, P.; Mecking, S., Heterocycle-substituted phosphinesulfonato palladium (II) complexes for insertion copolymerization of methyl acrylate. *Organometallics* **2014,** *33* (11), 2879-2888.

(116) Mitsushige, Y.; Carrow, B. P.; Ito, S.; Nozaki, K., Ligand-controlled insertion regioselectivity accelerates copolymerisation of ethylene with methyl acrylate by cationic bisphosphine monoxide–palladium catalysts. *Chem. Sci.* **2016,** *7* (1), 737-744.

(117) Mitsushige, Y.; Yasuda, H.; Carrow, B. P.; Ito, S.; Kobayashi, M.; Tayano, T.; Watanabe, Y.; Okuno, Y.; Hayashi, S.; Kuroda, J., Methylene-bridged bisphosphine monoxide ligands for palladium-catalyzed copolymerization of ethylene and polar monomers. *ACS Macro Lett.* **2018,** *7* (3), 305-311.

(118) Carrow, B. P.; Nozaki, K., Synthesis of functional polyolefins using cationic bisphosphine monoxide–palladium complexes. *J. Am. Chem. Soc.* **2012,** *134* (21), 8802-8805.

(119) Nakano, R.; Nozaki, K., Copolymerization of propylene and polar monomers using Pd/IzQO catalysts. *J. Am. Chem. Soc.* **2015,** *137* (34), 10934-10937.

(120) Akita, S.; Nozaki, K., Copolymerization of ethylene and methyl acrylate by palladium catalysts bearing IzQO ligands containing methoxyethyl ether moieties and salt effects for polymerization. *Polymer Journal* **2021,** *53* (9), 1057-1060.

(121) Chen, M.; Chen, C., A Versatile Ligand Platform for Palladium-and Nickel-Catalyzed Ethylene Copolymerization with Polar Monomers. *Angew. Chem. Int. Ed.* **2018,** *57* (12), 3094-3098.

(122) Zou, C.; Liao, D.; Pang, W.; Chen, M.; Tan, C., Versatile PNPO ligands for palladium and nickel catalyzed ethylene polymerization and copolymerization with polar monomers. *J. Catal.* **2021,** *393*, 281-289.

(123) Cai, Z.; Do, L. H., Thermally Robust Heterobimetallic Palladium–Alkali Catalysts for Ethylene and Alkyl Acrylate Copolymerization. *Organometallics* **2018,** *37* (21), 3874-3882.

(124) Zhang, W.; Waddell, P. M.; Tiedemann, M. A.; Padilla, C. E.; Mei, J.; Chen, L.; Carrow, B. P., Electron-rich metal cations enable synthesis of high molecular weight, linear functional polyethylenes. *J. Am. Chem. Soc.* **2018,** *140* (28), 8841-8850.

(125) Zhang, Y.; Jian, Z., 2-Phosphine-pyridine-N-oxide palladium and nickel catalysts for ethylene polymerization and copolymerization with polar monomers. *Polymer* **2020**, 122410.

(126) Cui, L.; Jian, Z., A N-bridged strategy enables hemilabile phosphine–carbonyl palladium and nickel catalysts to mediate ethylene polymerization and copolymerization with polar vinyl monomers. *Polym. Chem* **2020,** *11* (38), 6187-6193.

(127) Zhu, N.; Liang, T.; Huang, Y.; Pang, W.; Chen, M.; Tan, C., Influences of ligand backbone substituents on phosphinecarbonylpalladium and-nickel catalysts for ethylene polymerization and copolymerization with polar

monomers. *Inorg. Chem.* **2021,** *60* (17), 13080-13090.

(128) Ito, S.; Ota, Y.; Nozaki, K., Ethylene/allyl monomer cooligomerization by nickel/phosphine–sulfonate catalysts. *Dalton Trans* **2012,** *41* (45), 13807-13809.

(129) Xia, J.; Zhang, Y.; Zhang, J.; Jian, Z., High-performance neutral phosphine-sulfonate nickel (II) catalysts for efficient ethylene polymerization and copolymerization with polar monomers. *Organometallics* **2019,** *38* (5), 1118-1126.

(130) Si, G.; Na, Y.; Chen, C., Ethylene (co) Oligomerization by Phosphine-Pyridine Based Palladium and Nickel Catalysts. *ChemCatChem* **2018,** *10* (22), 5135-5140.

(131) Fu, X.; Zhang, L.; Tanaka, R.; Shiono, T.; Cai, Z., Highly robust nickel catalysts containing anilinonaphthoquinone ligand for copolymerization of ethylene and polar monomers. *Macromolecules* **2017,** *50* (23), 9216-9221.

(132) Zou, C.; Dai, S.; Chen, C., Ethylene polymerization and copolymerization using nickel 2-iminopyridine-N-oxide catalysts: modulation of polymer molecular weights and molecular-weight distributions. *Macromolecules* **2018,** *51* (1), 49-56.

(133) Tao, W. j.; Nakano, R.; Ito, S.; Nozaki, K., Copolymerization of ethylene and polar monomers by using Ni/IzQO catalysts. *Angew. Chem. Int. Ed.* **2016,** *55* (8), 2835-2839.

(134) Liang, T.; Goudari, S. B.; Chen, C., A simple and versatile nickel platform for the generation of branched high molecular weight polyolefins. *Nat. Commun.* **2020,** *11* (1), 1-8.

(135) Xu, M.; Yu, F.; Li, P.; Xu, G.; Zhang, S.; Wang, F., Enhancing chain initiation efficiency in the cationic allyl-nickel catalyzed (co) polymerization of ethylene and methyl acrylate. *Inorg. Chem.* **2020,** *59* (7), 4475-4482.

(136) Tahmouresilerd, B.; Xiao, D.; Do, L. H., Rigidifying Cation-Tunable Nickel Catalysts Increases Activity and Polar Monomer Incorporation in Ethylene and Methyl Acrylate Copolymerization. *Inorg. Chem.* **2021**.

(137) Zhang, Y.; Mu, H.; Wang, X.; Pan, L.; Li, Y., Elaborate tuning in ligand makes a big difference in catalytic performance: bulky nickel catalysts for (co) polymerization of ethylene with promising vinyl polar monomers. *ChemCatChem* **2019,** *11* (9), 2329-2340.

(138) Zhang, Y.; Mu, H.; Pan, L.; Wang, X.; Li, Y., Robust bulky [P, O] neutral nickel catalysts for copolymerization of ethylene with polar vinyl monomers. *ACS Catal.* **2018,** *8* (7), 5963-5976.

(139) Berkefeld, A.; Drexler, M.; Möller, H. M.; Mecking, S., Mechanistic insights on the copolymerization of polar vinyl monomers with neutral Ni (II) catalysts. *J. Am. Chem. Soc.* **2009,** *131* (35), 12613-12622.

(140) Zaccaria, F.; Zuccaccia, C.; Cipullo, R.; Budzelaar, P. H.; Vittoria, A.; Macchioni, A.; Busico, V.; Ehm, C., Methylaluminoxane's molecular cousin: A well-defined and "complete" al-activator for molecular olefin polymerization catalysts. *ACS Catal.* **2021,** *11* (8), 4464-4475.

(141) Chen, E. Y.-X.; Marks, T. J., Cocatalysts for metal-catalyzed olefin polymerization: activators, activation processes, and structure− activity relationships. *Chem. Rev.* **2000,** *100* (4), 1391-1434.

(142) R. Kumar, K.; Sivaram, S., Ethylene polymerization using iron (II) bis (imino) pyridyl and nickel (diimine) catalysts: effect of cocatalysts and reaction parameters. *Macromolecular Chemistry and Physics* **2000,** *201* (13), 1513-1520.

(143) Saki, Z.; D'Auria, I.; Dall'Anese, A.; Milani, B.; Pellecchia, C., Copolymerization of Ethylene and Methyl Acrylate by Pyridylimino Ni (II) Catalysts Affording Hyperbranched Poly (ethylene-co-methyl acrylate) s with Tunable Structures of the Ester Groups. *Macromolecules* **2020,** *53* (21), 9294-9305.

(144) Cao, L.; Cai, Z.; Li, M., Phosphinobenzenamine Nickel Catalyzed Efficient Copolymerization of Methyl Acrylate with Ethylene and Norbornene. *Macromolecules* **2022,** *55* (9), 3513-3521.

(145) Stibrany, R. T.; Schulz, D. N.; Kacker, S.; Patil, A. O.; Baugh, L. S.; Rucker, S. P.; Zushma, S.; Berluche, E.; Sissano, J. A., Polymerization and copolymerization of olefins and acrylates by Bis (benzimidazole) copper catalysts. *Macromolecules* **2003,** *36* (23), 8584-8586.

(146) Dong, J.; Wang, Z.; Hong, H.; Chung, T., Synthesis of isotactic polypropylene containing a terminal Cl, OH, or NH2 group via metallocene-mediated polymerization/chain transfer reaction. *Macromolecules* **2002,** *35* (25), 9352-9359.

(147) Marks, T. J.; Chen, J.; Gao, Y., Early Transition Metal Catalysis for Olefin-Polar Monomer Copolymerization. *Angew. Chem. Int. Ed.* **2020**.

(148) Mariott, W. R.; Rodriguez-Delgado, A.; Chen, E. Y.-X., Chain termination and transfer reactions in the acrylate polymerization by a monometallic chiral zirconocenium catalyst system. *Macromolecules* **2006,** *39* (4), 1318-1327.

(149) Quevedo-Sanchez, B.; Nimmons, J. F.; Coughlin, E. B.; Henson, M. A., Kinetic modeling of the effect of MAO/Zr ratio and chain transfer to aluminum in zirconocene catalyzed propylene polymerization. *Macromolecules* **2006,** *39* (13), 4306-4316.

(150) Quintanilla, E.; di Lena, F.; Chen, P., Chain transfer to aluminium in MAO-activated metallocene-catalyzed polymerization reactions. *Chem. Commun.* **2006,** (41), 4309-4311.

(151) Santoro, O.; Piola, L.; Cabe, K. M.; Lhost, O.; Den Dauw, K.; Vantomme, A.; Welle, A.; Maron, L.; Carpentier, J.-F.; Kirillov, E., Long-Chain Branched Polyethylene via Coordinative Tandem Insertion and Chain-Transfer Polymerization Using rac-{EBTHI} ZrCl2/MAO/Al–alkenyl Combinations: An Experimental and Theoretical Study. *Macromolecules* **2020,** *53* (20), 8847-8857.

(152) Baier, M. C.; Zuideveld, M. A.; Mecking, S., Post-metallocenes in the industrial production of polyolefins. *Angew. Chem. Int. Ed.* **2014,** *53* (37), 9722-9744.

(153) Wucher, P.; Schwaderer, J. B.; Mecking, S., Solid-supported single-component Pd (II) catalysts for polar monomer insertion copolymerization. *ACS Catal.* **2014,** *4* (8), 2672-2679.

(154) Tafazolian, H.; Culver, D. B.; Conley, M. P., A well-defined Ni (II) α-diimine catalyst supported on sulfated zirconia for polymerization catalysis. *Organometallics* **2017,** *36* (13), 2385-2388.

(155) Culver, D. B.; Tafazolian, H.; Conley, M. P., A bulky Pd (II) α-diimine catalyst supported on sulfated zirconia for the polymerization of ethylene and copolymerization of ethylene and methyl acrylate. *Organometallics* **2018,** *37* (6), 1001-1006.

(156) Zhang, H.; Zou, C.; Zhao, H.; Cai, Z.; Chen, C., Hydrogen-Bonding-Induced Heterogenization of Nickel and Palladium Catalysts for Copolymerization of Ethylene with Polar Monomers. *Angew. Chem.* **2021,** *133* (32), 17586-17591.

(157) Zou, C.; Si, G.; Chen, C., A general strategy for heterogenizing olefin polymerization catalysts and the synthesis of polyolefins and composites. *Nat. Commun.* **2022,** *13* (1), 1-12.

(158) Ljungberg, N.; Wesslen, B., Tributyl citrate oligomers as plasticizers for poly (lactic acid): thermo-mechanical film properties and aging. *Polymer* **2003,** *44* (25), 7679-7688.

(159) Dai, S.; Chen, C., Palladium-catalyzed direct synthesis of various branched, carboxylic acid-functionalized polyolefins: Characterization, derivatization, and properties. *Macromolecules* **2018,** *51* (17), 6818-6824.

(160) Röttger, M.; Domenech, T.; van der Weegen, R.; Breuillac, A.; Nicolaÿ, R.; Leibler, L., High-performance vitrimers from commodity thermoplastics through dioxaborolane metathesis. *Science* **2017,** *356* (6333), 62-65.

(161) Baur, M.; Mecking, S., Polyethylenes with Combined In-Chain and Side-Chain Functional Groups from Catalytic Terpolymerization of Carbon Monoxide and Acrylate. *ACS Macro Lett.* **2022,** *11* (10), 1207-1211.

CHAPTER 2

Efficient Ethylene/Acrylate Copolymerization by P,O-Ni Catalysts and Investigations of Monomer Insertion and Chelate Formation

This work was published in part as:

J. Am. Chem. Soc., **2021**, 143, 6516-6527.

Chapter 2

CONTRIBUTIONS AND ACKNOWLEDGEMENTS

Shuoyan Xiong and Theodor Agapie conceived the presented idea. S.X. performed synthesis and mechanistic studies and polymer characterization and analyzed the catalysis data. Manar M. Shoshani performed synthesis and mechanistic studies. Xinglong Zhang and Thomas F. Miller III performed DFT calculations and result analysis. Heather A. Spinney, Alex J. Nett, and Briana S Henderson performed polymerization studies and polymer characterization. S.X., M.M.S., and X.Z. drafted the manuscript that is reproduced as this chapter. H.A.S., A.J.N., B.S.H., T.F.M., and T.A. contributed to manuscript editing.

We are grateful to Dow (T.A.) and the Natural Sciences and Engineering Research Counsel of Canada (M.M.S.) for funding. We thank Brad C. Bailey and Jerzy Klosin (Dow) for insightful discussions. X.Z. acknowledges the Agency for Science, Technology and Research (A*STAR), Singapore, for a National Science Scholarship. We thank Michael K. Takase and Lawrence Henling for assistance with X-ray crystallography and David VanderVelde for assistance with NMR spectroscopy. We thank Heidi Clements, Hannah Bailey, and Joshua Castleman (Dow) for assistance in collecting polymer characterization data (GPC, DSC, FT-IR). We thank Todd D. Senecal and Steve Marshall (Dow) for assistance in collecting batch reactor data. Support has been provided for the X-ray diffraction and NMR instrumentation via the Dow Next Generation Educator Fund. X.Z. and T.F.M. acknowledge the computational resources from the Extreme Science and Engineering Discovery Environment

(XSEDE) Bridges computer at the Pittsburgh Supercomputing Center through allocation TG-MCB160013.

ABSTRACT

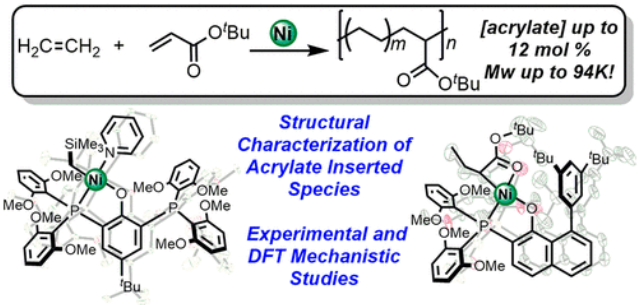

The efficient copolymerization of acrylates with ethylene using Ni catalysts remains a challenge. Herein, we report two neutral Ni(II) catalysts (POP-Ni-py (**1**) and PONap-Ni-py (**2**)) that exhibit high thermal stability, significantly higher incorporation of polar monomer (for **1**) or improved resistance to tBA-induced chain transfer (for **2**), compared to previously reported catalysts. Nickel alkyl complexes generated after tBA insertion, POP-Ni-CCO(py) (**3**) and PONap-Ni-CCO(py) (**4**), were isolated and for the first time, characterized by crystallography. Weakened lutidine vs pyridine coordination in **2**-lut facilitated the isolation of a N-donor-free adduct after acrylate insertion PONap-Ni-CCO (**5**) which represents a novel example of a four-membered chelate relevant to acrylate polymerization catalysis. Experimental kinetic studies of six cases of monomer insertion with aforementioned nickel complexes indicate that pyridine dissociation and monomer coordination are fast relative to monomer migratory insertion and that monomer enchainment after tBA insertion is the rate limiting step of copolymerization. Further evaluation of monomer insertion using density functional theory studies identified a cis-trans isomerization via Berry-pseudorotation involving one of the pendant ether groups as the rate-limiting step for propagation, in the absence of a polar

group at the chain end. The energy profiles for ethylene and tBA enchainments are in qualitative agreement with experimental measurements.

Chapter 2

GENERAL INTRODUCTION

Polyolefins account for over half of global plastic production.[1] Incorporation of polar groups can improve desirable properties such as wettability, adhesion, and printability, expanding the potential applications of polyolefins.[2-4] Coordination copolymerization circumvents limitations of industrially practiced free radical preparations and provides a high degree of control of the polymer microstructure under mild conditions, as demonstrated for non-polar polyolefins. [5-8] Late transition metal catalysts have demonstrated promise in the coordination polymerization of non-polar and polar olefins, due to lower inhibition by heteroatoms.[2, 9-11] Early developments with cationic α-diimine Pd complexes highlighted the promise of group 10 metals for the copolymerization of ethylene and polar olefins, in particular monomers with polar groups not directly attached to the olefinic carbons. [12-16] More recently, phosphine-sulfonate Pd catalysts were reported to generate linear copolymers/cooligomers with significant in-chain incorporation of various vinyl monomers.[17-23] Mechanistic studies indicate that the improved reactivity of the phosphine-sulfonate system is derived from the less electrophilic Pd center and the electronic asymmetry of the ligand.[19, 24-26] Other [P,O]-type Pd complexes have since been developed generating copolymers with higher molecular weights, tunable branching density, and enhanced functional group incorporation.[27-34]

Despite their tunability and tolerance of various functional groups, these Pd catalysts are not suitable for industrial applications due to the high cost of palladium and their

relatively low performance. Implementation of Ni-based catalysts can potentially offer a significant economic and environmental advantage; however, nickel polymerization catalysts typically suffer from poor thermal stability (operation temperature < 70 ºC), severe activity suppression by polar groups and either produce copolymers with low molecular weights or limited polar group incorporation.[2, 29, 35-38] Therefore, the development of thermally robust nickel catalysts for the production of high Mw polyolefins with higher levels of polar group incorporation, remains a significant challenge.

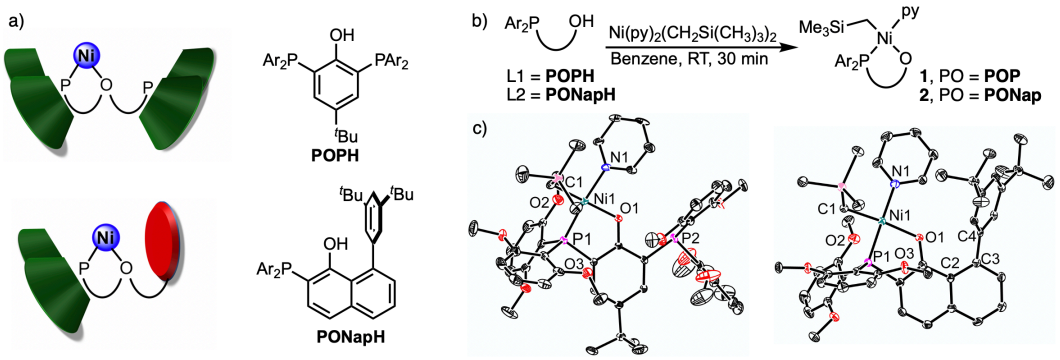

Figure 2.1. Design and development of nickel catalysts with bulky phosphine-phenoxide ligands: a) rationale of ligand design; b) preparation of nickel complexes; c) solid-state structures of **1** (left) and **2** (right).

Increasing steric bulk close to the metal center has been hypothesized to inhibit chain transfer, polar groups' coordination, and potential catalyst decomposition during copolymerization.[14, 25-26, 39] However, this strategy can also hinder polar olefin coordination to the metal center in copolymerization. For example, bulky, electron-rich phosphine substituents are important for the high activity of SHOP (Shell Higher Olefin Process) type [P,O]-Ni catalysts, but also detrimental for polar monomer incorporation.[37, 40] In contrast, a strategy less explored focuses on tuning steric bulk

from the "O"-side rather than from the "P"-side (Figure 2.1a). Based on previous reports with [P,O]-Pd complexes[32] and limited studies with [P,O]-Ni complexes[37, 40] we hypothesized that pendant steric hindrance from the "O"-side of SHOP-type nickel catalysts may also be sufficient to prevent bulky polar groups' inhibitory coordination, but not significantly hinder coordination of the smaller olefin group. To this end, we report nickel catalysts supported by [P,O] ligands featuring an additional bulky phosphorus (III) substituents *ortho* to the phenoxide (**POP**) and with a rigid aryl substituent (**PONap**) (Figure 2.1a). Nickel catalysts (**1** and **2**) supported by these ligands show high thermal stability (highly active under temperatures up to 100 ºC). Furthermore, enhanced tBA incorporation (for **1**) and better resistance to tBA-induced chain transfer (for **2**) was observed.

Despite the recent success of SHOP-type nickel catalysts in ethylene/acrylate copolymerization, detailed mechanistic studies are lacking. We present here mechanistic insights of ethylene/acrylate copolymerization with **1** and **2**. A combination of bulk copolymerization data, spectroscopic and crystallographic characterization of isolated intermediates, experimental kinetics studies of monomer insertions, and DFT calculations provide a detailed profile of the chain initiation/propagation processes. This includes the structural characterization of the first isolated intermediates relevant to nickel catalyzed copolymerization in these systems. Additionally, an associative isomerization process involving the pendant ether groups is identified as a required step prior to monomer migratory insertion via the lowest energy pathway. These investigations highlight how ligand structure affects

catalytic activity and polar group incorporation, and thereby provide insight towards future catalyst design.

RESULTS AND DISCUSSION

Synthesis and Characterization of Nickel (Trimethylsilyl)methyl Pyridine Complexes Supported by POP and PONap

The phenol proligands (**POPH** and **ONapH**) were synthesized in a fashion similar to known diarylphosphine phenols (see SI).[40-42] Metalation of **POPH** and **PONapH** with 1 equiv. of nickel bis(pyridine) bis((trimethylsilyl)methyl) in benzene allowed for the isolation of the corresponding nickel (trimethylsilyl)methyl complexes (**1** and **2**, Figure 2.1b). The ^{1}H NMR spectra of the isolated nickel complexes each display a doublet near -0.6 ppm, diagnostic for the Ni-CH_2-Si moiety. Additionally, peaks in the aromatic region are indicative of a bound pyridine.

Single crystal X-ray diffraction (XRD) studies provided structural confirmation of the identity of these complexes (Figure 2.1c).[40, 42-43] Notably, the Ni(1)-N(1) distance of **2** (1.997(2) Å) is significantly longer than that of **1** (1.938(3) Å), suggesting a weakly bound pyridine in **2**, likely due to the rigidity of the bulky aryl group on the phenoxide side of the ancillary ligand. In addition, the C(2)-C(3)-C(4) angle in **2** (125.0(2)°) is considerably larger than expected (120°), indicating a distortion due to the steric repulsion between the 3,5-di-tertbutylphenyl and the pyridine. The ether groups pendant to the bound phosphine ligand are close to Ni, with a Ni(1)-O(2) distance of

2.837(3) Å for **1** and 2.691(1) Å for **2**, both of which are shorter than the sum of van der Waals radii of Ni and O and thus indicating potential interactions.

Catalytic Production of Ethylene/tBA Copolymers

To evaluate the catalytic performance of the new ligand designs, efforts were focused on the production of ethylene/tBA copolymers with **1** or **2**. Copolymerization trials were carried out in toluene at 400 psig of ethylene under different temperature and tBA concentration to examine their effects on catalytic activity and properties of the copolymers (Tables 1, S5.1-S5.4). High activity (321 kg/(mol·h), 70 ºC, entry 1, Table 2.1) was observed even with in-situ formation of **1**, using proligand (**POPH**) and 1 equiv. of the nickel precursor ($Nipy_2(CH_2SiMe_3)_2$). The molecular weight, M_w, of copolymer produced reached 94,200 g/mol and the incorporation of tBA was 2.52 mol%. Compared to the reported monophosphine [P,O] catalyst, under similar conditions, more than a two-fold increase in tBA incorporation was observed for **1**, a significant increase while maintaining similar catalytic activity (Act.=390 kg/(mol·h), M_w=185,000 g/mol, incorp.(tBA)=1.1 mol%, entry 2, Table 2.1 in ref 81).[37]

Notably, higher activity was observed upon increasing the temperature to above 90 ºC (entry 1 vs 2, Table 2.1). Previously reported nickel catalysts typically display significantly decreased activity in copolymerization of ethylene and polar monomers at temperatures higher than 50 ºC, with few exceptions exhibiting high activity up to 70 ºC.[40, 44] Both **1** and **2** are highly active at temperature up to 100 ºC (Table 2.1, entry 5 and 14), representing a record level of thermal stability of nickel catalysts for ethylene/acrylate copolymerization. This unique behavior may result from cumulative

stabilizing effects of the proximal methoxy groups and bulky substituents ortho to the phenoxide. While **1** shows similar activity at 90 ºC and 100 ºC, a ~40% increase of activity is observed for **2**, suggesting the substituent rigidity in **2** serving a role for better thermal stability.

Table 2.1. Ethylene/tBA copolymerization.

Entry	Cat.	[tBA]/M	T (°C)	A.[b]	M_w[c]	PDI	%Mol tBA	T_m/°C
1	**POPH** + Ni[b]	0.05	70	321	94.2	2.3	2.5	108
2	**POPH** + Ni[b]	0.05	90	598	59.4	2.2	2.2	111
3	**POPH** + Ni[b]	0.1	90	245	40.8	2.3	5.1	95
4	**POPH** + Ni[b]	0.15	90	118	28.9	2.3	8.2	82
5	**POPH** + Ni[b]	0.15	100	113	22.7	2.2	7.8	82
6	**POPH** + Ni[b]	0.2	100	82	19.1	2.2	12.0	68
7	1	0.05	90	661	55.1	2.2	2.1	111
8[c]	1	0.12	90	460	44.9	2.4	3.7	106
9[c]	1	0.23	90	290	31.1	2.2	8.7	82
10	2	0.05	70	206	16.5	2.3	0.75	121
11	2	0.05	90	481	10.1	2.2	0.73	121
12[d]	2	0.1	90	262	9.0	2.0	1.4	115
13[d]	2	0.15	90	205	7.6	2.2	2.0	111
14	2	0.05	100	637	8.1	2.1	0.70	121

[a] Unless specified, V=5 mL, [catalyst]=0.25 μmol, ethylene pressure=400 psi, toluene solvent, each entry represents multiply replicated runs (see section S5 for detailed procedures and original data). [b] Two stock solution (1mM in toluene) of proligand **POPH** and the nickel precursor Ni ($py_2Ni(CH_2SiMe_3)_2$) were mixed in situ and stirred for 30 min prior to polymerization. [c] V(total)=640 mL, [Ni]=59.2 μmol, ethylene pressure=400 psi, time=75 min, toluene solvent. [d] [**2**]=0.5 μmol.

Increasing the tBA concentration leads to a proportional increase of tBA incorporation (Table 2.1, entries 2-4), but results in lower catalytic activity. At the same time, the M_w of the copolymers decreased substantially with increased polar monomer concentration (Table 2.1, entries 2-4). The decrease in activity is likely a consequence of slower subsequent insertions after the incorporation of a polar olefin.[37] The decreased molecular weight may result from slower propagation due to higher level of polar olefin insertion or a higher propensity for chain transfer or termination. [26, 40, 45]

Access to similarly active precatalysts, **1** and **2,** provides an opportunity to evaluate the impact of catalyst structure on catalytic performance. Higher Mw copolymers featuring high tBA incorporation are produced by **1** compared to **2**, for example, comparing entry 7 (2.11 mol% incorporation, Mw 55,100 g/mol, act.=661 kg/(mol·h)) to entry 11 (0.73 mol% incorporation, Mw 10100 g/mol, act.=481 kg/(mol·h)). Though lower molecular weights are observed for all copolymers produced by **2**, only a small effect of tBA concentration on copolymers' molecular weights is observed. For example, doubling the concentration of tBA leads to ~30 % decrease in the molecular weight of copolymers produced by **1** (Table 2.1: entry 2 vs 3) while only a 10% decrease in the molecular weight was observed for copolymers produced by **2** (Table 2.1: entry 11 vs 12). These differences suggest factors not simply related to tBA, such as the ancillary ligand rigidity or size, may have a more significant effect in controlling M_w of the copolymer produced by **2** than by **1**.

The analysis of the copolymers as a function of comonomer concertation provides insight into the relative overall rates of insertion of the two monomers.

Concentrations of tBA from 0.05 M to 0.23 M have been tested, while the ethylene concentration in solution is roughly 2 M.[46-47] For **1**, the mol percent incorporation of tBA varies from 2.1% to 12% as the ratio of the concentration of tBA to ethylene varies from 1:40 to 1:10, respectively. These results indicate that overall propagation rates of ethylene and tBA are roughly within the same order of magnitude. Under the same conditions, the incorporation ratio of tBA with **1** is 3 to 4 times higher than with **2**. Additional mechanistic studies were conducted to determine the reaction steps that control the differences in performance between **1** and **2** (vide infra).

Isolation and Characterization of tBA Insertion Products

The notably high tBA incorporation observed with **1** along with the differences in catalytic performance when comparing **1** and **2** led us to investigate the mechanistic basis of these observations. Microstructure analysis and/or tBA insertion studies have revealed that tBA insertion proceeds in a 2,1 fashion for both Pd[48-49] and Ni[50] catalysts. One of the postulated deactivation pathways in acrylate and ethylene copolymerization is coordination of the carbonyl moiety of the inserted acrylate to the metal center forming a 4-membered chelate;[51] however, direct evidence supporting this claim is lacking. Structurally characterized acrylate insertion species with Pd exhibit a six-membered or eight membered chelate.[48-49] To date, examples of structurally characterized products of acrylate insertion with Ni are lacking in the literature. One report outlines an NMR characterized example of 2,1 insertion of methyl acrylate into a Ni-alkyl with the product showing no interaction between the ester group and the Ni center.[50] Though extensive NMR and DFT studies were conducted on this species,

no solid-state structure was reported. Structures resembling the chelated 2,1 insertion products of acrylates have been generated through oxidative addition by Ni(0) sources, though not in the context of olefin polymerization.[52-54]

Given the dearth of examples of Ni promoted acrylate insertion, the reactivity of **1** and **2** with tBA was studied. Addition of excess tBA to **1** or **2** causes a color change from light orange to red. Analysis of the $^{31}P\{^{1}H\}$ and ^{1}H NMR spectra confirms the disappearance of the starting complexes and the appearance of a single new species with broad peaks in each case. Addition of excess pyridine results in sharpening of resonances not assigned to pyridine. The growth of a new ^{t}Bu resonance in ^{1}H NMR and the absence of a signal in the upfield region corresponding to Ni-CH_2 suggest insertion of acrylate into the Ni-CH_2SiMe_3 bond. Resonances in the aromatic region are indicative of pyridine coordination and suggest the generation of species similar to the previously reported acrylate insertion product,[49-50] **POP-Ni-CCO-py** (**3**) and **PONap- Ni-CCO-py** (**4**), respectively (Figure 2.2a). The broad peaks in both ^{1}H and $^{31}P\{^{1}H\}$ NMR spectra of **3** and **4** and the effect of excess pyridine in the NMR spectra are indicative of a fluctional process that involves pyridine dissociation. The bulkier alkyl group resulting upon insertion may weaken the metal-pyridine interaction and lead to significant dissociation on the NMR time scale. Either a 3-coordinate species or a chelate through binding of the carbonyl group to the metal could be generated in solution.

High quality single XRD data was obtained for **4**, while moderate quality data was obtained for **3** (Figure 2.2b). Both confirmed the assignment of **3** and **4** as the products

of 2,1-insertion of tBA. Pyridine coordination is observed in both compounds consistent with solution NMR data. The long metal-oxygen distance of the carbonyl group from the inserted tBA (3.733(2) Å) indicates no bonding interaction in the solid-state, in contrast with the calculated structure of the previously reported acrylate insertion product supported by a phenoxyimine ligand that has a Ni-O distance of 3.18 Å suggestive of a weak interaction.[50]

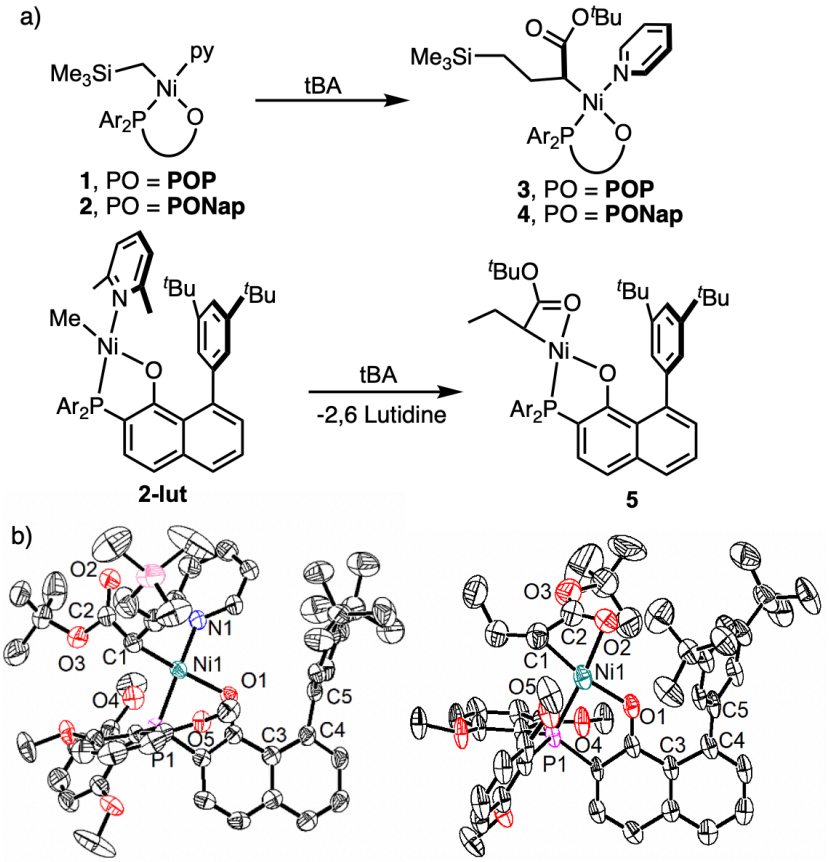

Figure 2.2. a) Preparation of **3**~**5** and b) solid-state structures of **4** (left) and **5** (right).

Toward accessing a pyridine-free version of **2** to determine the propensity for four-membered chelate formation, a variant with the weaker binding lutidine ligand (**2-lut**) was synthesized from the reaction of **PONapH** and $NiMe_2$(TMEDA) in the presence

of excess of 2,6-lutidine. Upon in situ generation of this species, 25 equivalents of tBA were added. After 0.5 h, a color change from light orange to red was observed. Upon removal of volatile materials, both ^{1}H and $^{31}P\{^{1}H\}$ NMR spectra indicate consumption of **2-lut** and the formation of a new species. Though many resonances are similar to those of **4**, lutidine resonances are not observed upon workup, indicating loss of this ligand to generate compound **5**. The NMR resonances in the ^{1}H and $^{31}P\{^{1}H\}$ NMR spectra are broad, suggesting a fluxional process independent of pyridine. Interconversion between two isomers such as a three-coordinate and a chelated species is consistent with these data.

Single crystal X-ray diffraction studies determined the identity of **5** as the chelate in the solid-state. Notably, this is first structural characterization of the chelate resulting from a single insertion of acrylate in systems competent in catalysis. The carbonyl oxygen's distance to the Ni center of 1.940(5) Å indicates a bonding interaction, slightly elongated when compared to reported nickel complexes featuring "$NiCR_2C(OR)O$" chelates (1.900-1.905 Å).[52-54] The C(2)-O(2) distance (1.285(9) Å) in **5** is elongated in comparison to **4** (1.227(4)Å) due to coordination to Ni.[54-57] Other structural parameters in the coordination sphere of Ni are similar to **4**. A suite of NMR experiments was performed to determine the solution structure of **5**. Although these data do not rule out a solution structure with the carbonyl dissociating, they provide conclusive support for the Ni-alkyl group connectivity observed in the solid-state (see SI, section S3 for detailed NMR analysis).

Kinetics of Monomer Enchainment

In the ethylene/tBA copolymerization, chain initiation and propagation occur via ethylene or tBA enchainment (as a combination of ligand substitution and olefin migratory insertion) each from three distinct precursors (Figure 2.3; left): Ni-alkyl of catalyst precursor, Ni-alkyl after ethylene insertion and Ni-alkyl after acrylate insertion. Further differentiation in behavior is possible if two monomer insertions are considered (e.g. ethylene insertion after ethylene insertion vs tBA insertion after ethylene insertion). To elucidate kinetic details of monomer enchainment, kinetics experiments monitored by NMR have been conducted as discussed below.

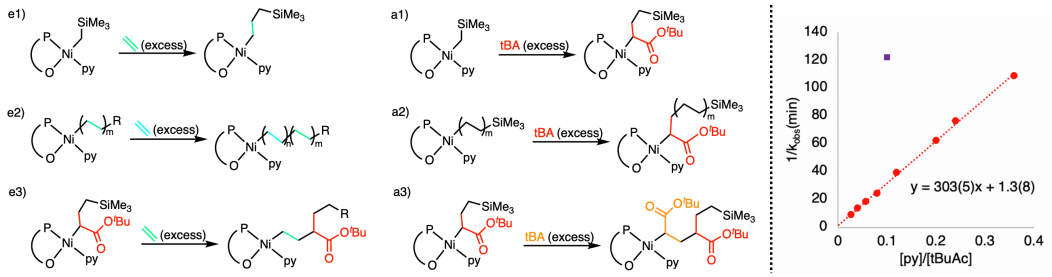

Figure 2.3. Six cases of ethylene and tBA insertion (left) and double reciprocal plot ($1/k_{obs-1}$ vs [py]/[tBA]) of case a1 (right, Measurements for **1** are shown in red and for **2** in purple. Conditions: [Ni] = 0.0157 M, Solvent PhCl, T = 50 ºC).

Enchainment of tBA with Nickel (Trimethylsilyl)methyl Species (a1). As discussed above, the addition of excess tBA to **1** or **2** at room temperature results in consumption of **1** and **2** and quantitative formation of the corresponding insertion products (Figure 2.2a). Kinetic measurements under pseudo-1st order conditions of excess tBA were employed to experimentally evaluate mechanistic possibilities for tBA enchainment. The decrease of the concentration of the nickel (trimethylsilyl)methyl complexes over time was monitored by $^{31}P\{^{1}H\}$ NMR spectroscopy. Decay of **1** and **2** in the tBA enchainment corresponds to the initiation of the precatalyst and may not

be representative of propagation through tBA enchainment. The use of excess pyridine (2 equiv. for **1** and 10 equiv for **2**) was necessary for linear pseudo-1st order behavior (see SI section S8.2).

To investigate the influence of the leaving pyridine (denoted as "L") and incoming tBA, the rate of monomer enchainment (overall rate of ligand substitution and migratory insertion) for **1** was measured at varying tBA and pyridine concentrations (10~75 equiv. of tBA, 2~6 equiv. of pyridine). NMR monitoring was conducted at 50 ºC in chlorobenzene, for better solubility compared to C_6D_6. Data is summarized in a double reciprocal plot (Figure 2.3; right). The linear dependence indicates that pseudo-1st order rate constant (k_{obs1}, where rate=k_{obs1}[Ni] and k_{obs1} = k_{a1}[tBA]/[py]) is proportional to the concentration of tBA and inversely proportional to the concentration of pyridine in the range of concentrations studied. The fitted linear relationship between $1/k_{obs1}$ and [py]/[tBA] has a slope of 303(5) min and an intercept near zero (1.3(6) min). This scenario indicates that migratory insertion of tBA is slower than ligand substitution (Detailed discussion: SI S11.1). Notably, a tBA bound species has not been observed with **1** or **2** under a wide range of temperatures from -80 ℃ to 50 ℃, indicating the potential pre-equilibrium between pyridine- and tBA-bound species is shifted far to the left. Nevertheless, more information is necessary to distinguish mechanistic pathways for the substitution of pyridine by tBA.

Based on aforementioned linear relationship, an observed rate constant for the a1 process (k_{a1}, rate=k_{a1}[Ni][tBA]/[py]) can be derived, k_{a1}=0.0033 min^{-1} for **1**. Analogous measurements with **2** with 100 equiv. of tBA and 10 equiv. of pyridine results in

k_{a1}=0.00082 min^{-1}. This indicates that tBA enchainment into **1** is roughly four times faster than tBA enchainment into **2**. Notably this difference is comparable to the difference of tBA incorporation in copolymerization (3.1 times, entry 7 vs entry 11, Table 2.1). This may suggest that other processes involved in the copolymer generation, such as the rates of ethylene enchainment, are similar. Indeed, the catalytic activities are roughly equivalent.

Enchainment of Ethylene: Rate of Initiation and Propagation with Ethylene (e1&e2). The addition of excess ethylene to **1** or **2** results in more rapid consumption of the Ni (trimethylsilyl)methyl complex compared to tBA. In contrast with ***a1***, decay of [**1**] or [**2**] over time upon exposure to ethylene does not fit a *pseudo*-1st order approximation. For example, under a set of conditions tried (See SI section S8.3), only 75% of **1** or **2** is converted by the time 90% of ethylene is consumed, indicating a competition between ethylene insertion into **1** or **2**, as catalyst initiation, vs insertion into the products of ethylene insertion **1-$C_{2n}H_{4n}$** or **2-$C_{2n}H_{4n}$** (where n is the number of ethylene molecules inserted), as propagation. This behavior is distinct from reported cases of "slow-initiation" or "slow-propagation".[15, 45, 58] Additionally, a linear dependence of ln[C_2H_4] vs time is observed, as determined by the decay of ethylene in solution over time, starting with 15 equiv. of C_2H_4 relative to the Ni complex, in the presence of excess pyridine. This scenario indicates that initiation (***e1***) and propagation (***e2***) have similar overall rates. It is worth noting that the similar enchainment rates could arise from appropriately matched ligand substitution and ethylene insertion

(larger and smaller, respectively, for example), not necessarily from the same rates for the elementary step of ethylene insertion.

The measured values for the observed rate constants ($k_{obs1'}$, rate=$k_{obs1'}$[ethylene], where $k_{obs1'}$=k_{e1}[Ni]/[py])) for ethylene consumption are 0.0194(2) min^{-1} for **1** and 0.0214(2) min^{-1} for **2**. Notably, **1/1-$C_{2n}H_{4n}$** and **2/2-$C_{2n}H_{4n}$** feature similar rates of ethylene enchainment, which is consistent with their similar copolymerization activity. This is also in agreement with the similar rates of ethylene insertion implicated by the finding that the relative rates of acrylate insertion match the polar monomer incorporation (*vide supra*). Assuming the rate law of ethylene insertion is similar to that of tBA insertion (rate=k_{a1}[Ni][tBA]/[py]), the rates of initiation can be compared (k_{e1} vs k_{a1}) as a direct comparison between ethylene and acrylate enchainment (Table 2.2 case *e1/e2* vs *a1*). For both **1** (k_{e1}=0.194 min^{-1} vs k_{a1}=0.0033 min^{-1}) and **2** (k_{e1}=0.21 min^{-1} vs k_{a1}=0.00082 min^{-1}), the enchainment of ethylene is roughly two orders of magnitude faster than acrylate. This is significantly different from the relative rates estimated from copolymerization data, indicating that the measured rates of incorporation into the Ni (trimethylsilyl)methyl complexes cannot be used as models for propagation. To address this issue, attempts were made to measure the rate of tBA insertion after ethylene insertion.

Rate of tBA Enchainment into Ethylene Inserted Species (a2). As shown above, consecutive ethylene insertion limits the possibility of isolation of single ethylene inserted species; however, all the ethylene inserted species overlap in $^{31}P\{^{1}H\}$ NMR. Therefore, experiments monitoring the decay of the resonance corresponding to all

ethylene inserted species (**1-$C_{2n}H_{4n}$**) in $^{31}P\{^1H\}$ NMR were designed and employed to measure the rate of tBA enchainment after ethylene. Excess ethylene (25 equiv.) was added to a solution of **1** and pyridine (10 equiv.) of in chlorobenzene. Residual ethylene was removed after ~55% of **1** was converted to **1-$C_{2n}H_{4n}$**. Subsequently, 15 equiv. of tBA were added and the consumption of **1-$C_{2n}H_{4n}$** over time was monitored by $^{31}P\{^1H\}$ NMR. First order kinetics were observed. The rate constant (k_{a2}, rate=k_{a2}[Ni][tBA]/[py]) for the decay of **1-$C_{2n}H_{4n}$** is roughly 200 times faster than initiation (Table 2.2 case *a1* vs *a2*, both for **1**). This corresponds to acrylate enchainment after ethylene, therefore being a model of propagation. Such a change of insertion rates indicates that tBA enchainment is significantly faster when a smaller alkyl chain is bound to nickel, which is in contrast with the ethylene behavior. This difference in reactivity may be a consequence of the significant difference in size between the two olefins, the binding and insertion of the larger acrylate being more drastically disfavored when the alkyl group on Ni is larger. Comparing to the copolymerization data, k_{a2} is similar to k_{e2}, in agreement with the measured ratio of tBA and ethylene in the polymer being proportional to the ratio of their concentration in solution.

Ethylene and tBA Enchainment into tBA Inserted Species: A Shift of Rate-Determining Step (e3&a3). The species generated after polar monomer insertion are typically implicated in the propagation limiting step because of the deactivating effect of the chelates.[37, 50] To gain mechanistic insight into the behavior of these species with the present catalysts, we performed kinetics studies starting with **3**.

Ethylene insertion after tBA insertion (***e3***) was explored by monitoring consumption of **3** and ethylene over time. Ethylene insertion occurs competitively into **3** and its insertion product. Decay of **3** over a first half time corresponds to only 15 % consumption of ethylene, therefore pseudo-1st order conditions were assumed. Indeed, the plot of ln[**3**] vs time is linear, and the enchainment rate constant (k_{e3}, excluding the concentration of pyridine and ethylene, rate=k_{e3}[Ni][ethylene]/[py]) equals 0.0108(5) min^{-1}, though only partial monitoring of decay was possible under these conditions. Notably, k_{e3} is smaller than k_{e1}, k_{e2} and k_{a2} (Table 2.2 for complex **1**), indicating that ethylene enchainment after tBA insertion is the rate-determining step for propagation during copolymerization.

To investigate back-to-back tBA insertion (***a3***), the kinetics of the reaction of tBA with **1** were further analyzed. Over extended periods, an additional peak was observed in the $^{31}P\{^{1}H\}$ NMR spectrum at ~-7.4 ppm. This peak is close to that of **3** (-6.8 ppm) and is assigned to the double insertion product. Since the $SiMe_3$ group is three carbons away from nickel in **3**, we propose that the nickel alkyl chain in **3** is sterically and electronically similar to that in the tBA inserted species that features a long alkyl chain. At the same time, additional low-intensity peaks are observed in the same region and are assigned to the products of subsequent insertion. The presence of these species has hindered the isolation of the double inserted species. The rate of the formation of the double-inserted product was extracted based on a non-linear approximation of the change of [**1**] and [**3**] over time. Comparing k_{a3} to k_{e3} under similar concentrations of pyridine (Table 2.2 case *e3* vs *a3*) indicates that double

insertion of tBA is unlikely under the copolymerization conditions. This is consistent with microstructural analysis of the ethylene/tBA copolymers produced by **1** and **2** (Figure S2.6.1~6.4).[37] Additionally, >99% of tBA units are located at the internal positions of the polymer chain consistent with ethylene rather than tBA inducing chain initiation.

Table 2.2. Comparison of rate constants. These correspond to the overall olefin enchainment process involving ligand substitution to bind the olefin and olefin insertion.

Case (xi)	Ni complex	k_{xi} (min^{-1})[a]
e1/e2	**1/1-$C_{2n}H_{4n}$**	0.19
e1/e2	**2/2-$C_{2n}H_{4n}$**	0.21
e3[c]	**1 (3)**	0.011
a1	**1**	0.0033
a1	**2**	0.00082
a2	**1 (1-$C_{2n}H_{4n}$)**	0.6
a3[d]	**1 (3)**	0.0004

[a]Unless specified, [py]=0.157 M. [b]k_{xi}: rate constant excluding the concentration of pyridine and the monomer, *xi*: *e1/e2/e3/a1/a2/a3*, rate=k_{xi}[Ni][Monomer]/[py]. [c][py]=0.099 M. [d][py]=0.033 M.

In summary, the following mechanistic aspects of monomer enchainment were elucidated experimentally: (1) ligand substitution is relatively fast comparing to olefin insertion, though further investigation is necessary to understand the energetics and mechanistic pathways for this process. (2) Enchainments of acrylate and ethylene have similar rate constants, consistent with the polymerization data; this is the basis of the high level of incorporation with catalyst **1**. (3) The propagation limiting step of ethylene-tBA copolymerization with this catalyst system is monomer insertion after tBA insertion. Ethylene incorporation after tBA is about one order of magnitude slower than after ethylene. (4) tBA induced chain initiation and back-to-back tBA insertion are significantly slower than the other four cases of monomer enchainment, therefore less favorable during copolymerization, consistent with reported

microstructure analysis of copolymers generated by P,O-nickel catalysts.[37](5) The relative rate constants of ethylene and tBA enchainment with **1** and **2** are in agreement with copolymerization data.

DFT Calculations

Density functional theory (DFT) calculations were performed to understand the energetics and mechanism of the present Ni-catalyzed co-polymerization of ethylene and tBA. Geometry optimizations were performed with M06 functional[59] with Karlsruhe-family basis set of double-ζ valence def2-SVP[60-61] for all atoms. Single-point (SP) corrections were carried out at M06/def2-TZVP[60] level with SMD model[62] to account for the solvent effect of chlorobenzene (see SI for full details).

Ethylene and tBA Enchainment into Nickel (Trimethylsilyl)methyl Species (e1 & a1)

We first investigated the first insertion of ethylene vs tBA into catalyst **1**. Two geometric isomers of the square planar Ni catalyst were considered, with the alkyl group trans to O, as experimentally observed, and with the alkyl trans to P (**1'**). The reaction paths and the associated energy profile are shown in Figure 2.4 (see SI section 9.4 and 9.9 for full profiles). Starting from isomer **1** (reaction path 1), the 2,1-insertion of tBA has the lowest activation barrier (**ts1-ac**) at 30.5 kcal mol^{-1}; the regioisomeric 1,2-insertion of tBA (**ts1-ac-r**) has a significantly higher barrier at 41.5 kcal mol^{-1}. This is in agreement with the observation that the migratory insertion occurs at the β-carbon site of an α,β-unsaturated carbonyl, akin to conjugate addition as the growing polymer chain adds into the conjugated C=C double bond.[10, 18, 24, 26, 63] The insertion of

ethylene (**ts1-et**) has a barrier of 33.1 kcal mol^{-1}. This implies that reaction proceeding through path 1 favors the insertion of tBA over ethylene by roughly 60 times, which is contradictory to the experimental observation that the first insertion of ethylene proceeds *ca.* 2 orders of magnitude faster than the tBA insertion.

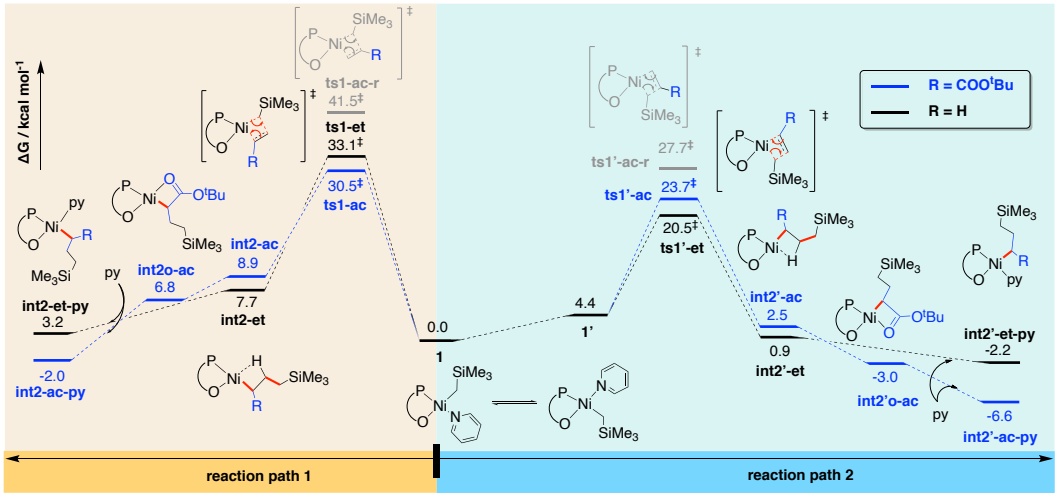

Figure 2.4. Gibbs energy profile computed at SMD(chlorobenzene)-M06/def2-TZVP//M06/def2-SVP level of theory for the first insertion of ethylene vs tBA into two geometric isomeric forms of POPNi-py catalyst, **1** and **1'**.

It is known that cis/trans isomerization of coordinatively asymmetric catalysts (Pd[24, 26, 64-65] and Ni[65]) play crucial roles in polymerization. The geometric isomer **1'** is less stable (by 4.4 kcal mol^{-1}) than isomer **1** but has lower barriers for the first insertion of monomers (reaction path 2, Figure 2.4). Specifically, the insertion of ethylene into the isomeric Ni-catalyst **1'** has the lowest activation barrier (**ts1'-et**) at 20.5 kcal mol^{-1}. The insertion of tBA in either regioselective ways (**ts1'-ac**, at 23.7 kcal mol^{-1} and **ts1'-ac-r**, at 27.7 kcal mol^{-1}) are both less favorable. In particular, the insertion of ethylene is 3.2 kcal mol^{-1} more favorable than the 2,1-insertion of tBA, translating to a selectivity in favor of ethylene insertion by about 150-fold using simple TST. This chemical

selectivity of monomer insertion is in agreement with the experimental observation that the first insertion of ethylene occurs roughly two orders of magnitude faster than that of tBA when concentration of these two monomers are similar. Despite a better second-order perturbative stabilization energy ($\Delta E^{(2)}$) from the forming C–C bond to Ni d-orbital in **ts1'-ac** than in **ts1'-et**, by 12.3 kcal mol^{-1} (Figure S2.9.15), poorer steric interactions in **ts1'-ac** due to the additional ester group of tBA than in **ts1'-et** (NCI plot, Figure S2.9.14) give rise to a greater barrier for insertion of tBA as opposed to ethylene. Comparing reaction paths 1 and 2, the insertion TSs in reaction path 2 benefit from the *trans effect* where the growing polymer chain trans to the more electron-donating P-atom (more diffuse electron cloud) undergoes migratory insertion more kinetically favorably, by *ca.* 10 kcal mol^{-1}. Comparing to TSs in path 2 (favored path), the Ni-centers in TSs in path 1 are more electrophilic (NBO charge of 0.450 in **ts1-et** and 0.498 in **ts1-ac**, compared to 0.036 in **ts1'-et** and 0.427 in **ts1'-ac**) and have less stable $\Delta E^{(2)}$ vales (by ~20 kcal mol^{-1}), making migratory insertion slower in path 1 than in path 2 (Figure S2.9.14-15).

The mechanism for the isomerization of the two geometric isomeric forms of the **1** was investigated (see SI section S10). Of the dissociative, intermolecular associative, and pendant ether associative paths evaluated, the last one has the lowest energy via a penta-coordinate structure followed by a pseudorotational TS (**ts-5coord** shown in Figure S2.9.13) at 27.1 kcal mol^{-1}. This TS is higher than the olefin insertion TS, which is in contrast to previous studies of isomerization in square planar complexes.[24] While the overall energy profile of chain enchainment with isomerization via a penta-

coordinate species is consistent with experimental kinetic analysis (SI section 11.2), we cannot rule out an alternate mechanism for isomerization that has a lower barrier.

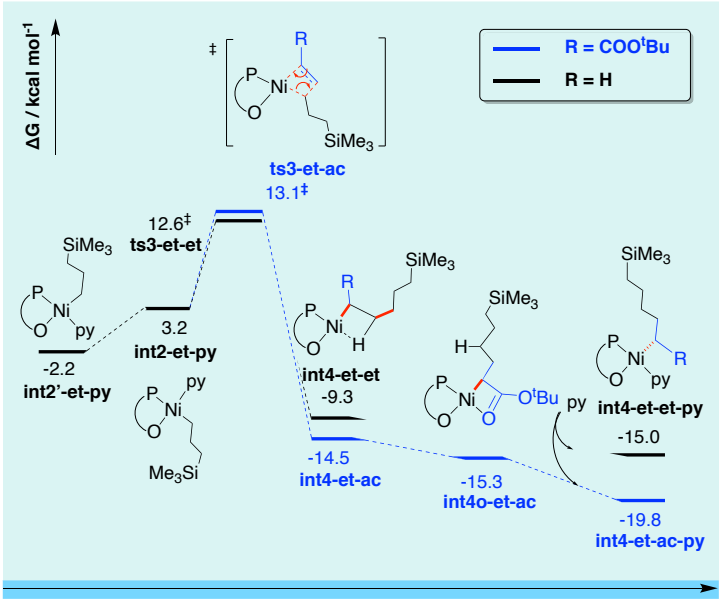

Figure 2.5. Gibbs energy profile computed at SMD(chlorobenzene)-M06/def2-TZVP//M06/def2-SVP level of theory for the second insertion of ethylene vs tBA into first ethylene inserted product **int2'-et-py** from Figure 2.1.

Ethylene and tBA Enchainment into Ethylene Inserted Species (e2 & a2)

The second insertion step was similarly investigated. The Gibbs energy profiles for the second insertion of ethylene vs tBA into the first ethylene inserted products are shown in Figure 2.5. Similar to the first insertion, the second insertion steps, where the growing polymer chain is trans to P-atom (paths 3), have lower activation barriers (again by *ca.* 10 kcal mol^{-1}) than their geometric isomers (not shown). Therefore, isomerization is again required to access the lowest energy reaction path, placing the growing polymer chain trans to P-atom, so that the insertion step can benefit from the trans effect. The enchainment of ethylene (**ts3-et-et**, at 12.6 kcal mol^{-1}) has a lower

barrier, by 0.5 kcal mol^{-1}, than that of tBA (**ts3-et-ac**, at 13.1 kcal mol^{-1}). This energetic difference is rather small and typically falls within the numerical accuracy of DFT, implying that the rate of second insertion of ethylene into first ethylene-inserted product is comparable to that of tBA into first ethylene-inserted product, consistent with experimental measurements. *The similarity of the tBA and ethylene enchainment barriers here is a significant aspect of* ***1*** *that drives the high levels of acrylate incorporation.*

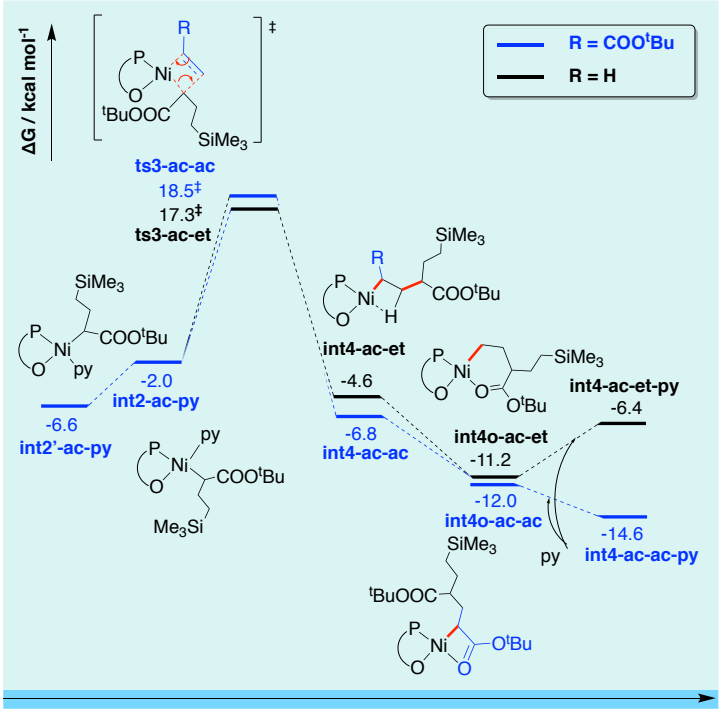

Figure 2.6. Gibbs energy profile computed at SMD(chlorobenzene)-M06/def2-TZVP//M06/def2-SVP level of theory for the second insertion of ethylene vs tBA into first acrylate inserted product **int2'-ac-py**.

Ethylene and tBA Enchainment into tBA Inserted Species (e3 & a3)

The second insertion into first tBA-inserted product (Figure 2.6) shows again a lower energy path going through isomerization. The insertion of ethylene into first tBA-inserted product (**ts3-ac-et**) has a barrier of 19.3 kcal mol^{-1} which is 1.2 kcal mol^{-1}

lower than the insertion of tBA (**ts3-ac-ac**, barrier of 20.5 kcal mol^{-1}), suggesting that ethylene incorporation into tBA-insertion product occurs ~6x faster than tBA incorporation into tBA-insertion product when concentrations of these two monomers are similar. The relative rates of insertion can be further influenced by the relative ratios of olefins in a linear dependency (Equation G and H in SI 11.2).[66] Although the barriers of insertion of ethylene vs tBA after tBA insertion are closer than observed experimentally and inferred from microstructures of ethylene/tBA copolymers, computations reproduce qualitatively the relative rates of insertion of either olefin after ethylene vs after acrylate. Both monomers have a higher barrier of insertion after acrylate (19.3–22.3 kcal mol^{-1}) than after ethylene (9.4–9.9 kcal mol^{-1}), by *ca.* 10 kcal mol^{-1}.

DFT results: Discussion

We can similarly compare the rates of enchainment of either olefin after the first enchainment of ethylene vs tBA. There are barrier differences in the first incorporation of ethylene vs tBA due to i) the first enchainment barrier, which is lower for ethylene than for tBA by 3.2 kcal mol^{-1} (**ts1'-et** vs **ts1'-ac**, barriers of 16.1 kcal mol^{-1} vs 19.3 kcal mol^{-1}, Figure 2.4); ii) relative concentrations of olefins and ethylene/tBA-inserted products; iii) the isomerization barrier for the first insertion product vs for first tBA-insertion product. Comparing the enchainment of ethylene into first ethylene-inserted product vs first tBA-inserted product, there is a barrier difference of 9.9 kcal mol^{-1} disfavoring the later (**ts3-et-et**, with a barrier of 9.4 kcal mol^{-1} vs **ts3-ac-et**, with a barrier of 19.3 kcal mol^{-1}). In actual copolymerization, the concentration

of ethylene-insertion products will be much higher than that of tBA-insertion products considering that the barrier of first ethylene is 3.2 kcal mol^{-1} lower than first tBA insertion (approximately by 150x) and the concentration of ethylene is higher than that of tBA (by 10 - 40 times). Taken together, this implies that the enchainment of ethylene into ethylene-inserted product is orders of magnitude faster than into tBA-inserted product.

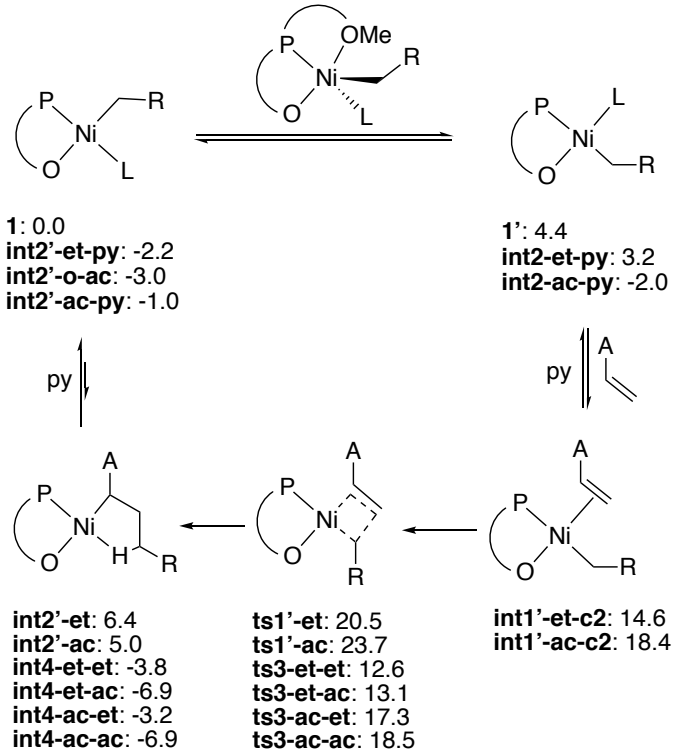

Figure 2.7. Overall Gibbs energy profile computed at SMD(chlorobenzene)-M06/def2-TZVP//M06/def2-SVP level of theory. Note: 1) Ethylene: A=H, tBA: A=C(O)O^{t}Bu; 2) L: pyridine or oxygen of tBA; 3) R: $SiMe_3$ or polymer chains.

Similarly, we compare the enchainment of tBA into the first ethylene-inserted product vs the first tBA-inserted product, yielding the same picture: the insertion of tBA into ethylene-inserted product (**ts3-et-ac**, Figure 2.5) has a barrier of 9.9 kcal mol^{-1} whereas the enchainment of tBA into tBA-inserted product (**ts3-ac-ac**, Figure 2.6)

has a much higher barrier of 20.5 kcal mol^{-1}. This difference of 10.6 kcal mol^{-1} is very similar to the difference in the second enchainment of ethylene into first ethylene vs tBA insertion product above (9.9 kcal mol^{-1}). This implies that the enchainment of either olefin into ethylene-inserted product occurs much more rapidly than into tBA-inserted product.

DFT computations thus suggest that isomerization is essential in accessing the reaction pathway with lower insertion barriers by placing the growing polymer chain trans to the P-atom (*trans effect*). Reaction kinetics are in agreement with experimental observations that insertion of tBA or ethylene after an acrylate insertion is much slower than after ethylene. Therefore, the resting state of the catalyst is the species generated after acrylate insertion. In terms of rates of insertion, the first enchainment of ethylene is computed to be about 150 times faster than the first insertion of tBA, in quantitative agreement with experimental measurements. *After the first ethylene insertion, the enchainment of either ethylene and tBA have approximately equal barriers, making this catalyst an attractive candidate for polar olefin copolymerization*. Comparing these relevant TSs (**ts3-et-et** and **ts3-et-ac**), we envision that this property is likely a feature of the phosphine phenoxide ligand where the flexible, albeit bulky O-side allows the ethylene-inserted growing polymer chain to extend without steric hinderance while the P-side allows for efficient interactions with either olefin. On the other hand, the enchainment of either olefin after tBA insertion (**ts3-ac-et**, **ts3-ac-ac**) is orders of magnitude slower than after ethylene insertion (**ts3-et-et** and **ts3-et-ac**), likely due to

the unfavorable sterics between the tBA-inserted growing polymer chain and the bulky O-side groups of the ligand.

CONCLUSION

Complexes **1** and **2** serve as thermally robust, high-performance catalysts for the copolymerization of ethylene and tBA. The two catalysts display steric bulk on the oxygen side of the phosphinophenoxide ligand as a rotationally flexible phosphine substituent (**POP** ligand) and a rigid aryl derivative (**PONap** ligand). Complex **1** produce high molecular weight copolymers (M_w>40000) with record levels of tBA incorporation (5.05 mol %) and high activity. Complex **2**, though similarly active, produces lower molecular weight polymer with lower incorporation of tBA (0.75 %), under the same conditions, potentially due to the rigid steric profile adjacent to the phenoxide donor, hindering tBA coordination, and therefore enchainment. Both catalysts are highly active at elevated temperatures. These studies clearly demonstrate that the substituents on the oxygen side of the phosphinophenoxide ligand can tune catalytic behavior to achieve state-of-the-art performance.

Detailed mechanistic studies were performed to gain mechanistic insight into this class of catalysts. Upon exposure to an excess of tBA, complexes **1** and **2** produced the single insertion products, in 2,1 fashion, both with pyridine bound to the Ni center. Furthermore, using a derivative of **2** with a weaker lutidine donor, **2-lut**, the acrylate insertion product was isolated as a four-membered chelate, **5**. These complexes

represent intermediates of copolymerization and demonstrate the regioselectivity of insertion and the propensity to form chelates.

Kinetics were performed with a focus on the best performing catalyst, **1**. Important for the high levels of acrylate incorporation, enchainment of acrylate and ethylene have similar rate constants. tBA induced chain initiation and back-to-back tBA insertion are significantly slower than the other four cases of monomer enchainment, therefore less favorable during copolymerization. The propagation limiting step of ethylene-tBA copolymerization with this catalyst system is ethylene incorporation after tBA, which is about one order of magnitude slower than after ethylene.

DFT calculations support the finding that the enchainment after acrylate is slower than after ethylene. Moreover, computations reveal that migratory insertion is substantially more facile if the alkyl group is trans to the phosphine donor. However, computations also reveal that isomerization within the coordination sphere of Ni, to transfer the alkyl substituents from trans to O to trans to P has the highest transition state energy in the entire reaction profile. The isomerization process is facilitated by the methoxy-O moieties. Taking into account the experimental and computational data, the mechanism of monomer enchainment involves catalyst isomerization to move the alkyl chain trans to phosphine, ligand substitution to coordinate olefin, and migratory insertion in 2,1-fashion (Figure 7).

In conclusion, this study reports a Ni catalyst for ethylene-acrylate copolymerization that shows increased amounts of acrylate incorporation while maintaining high levels of activity as compared to state-of-the-art Ni based catalysts. Synthetic, mechanistic

and DFT studies provide insights into the structural features that affect the behavior of this catalyst. Large and flexible steric bulk at the phenoxide substituent and ether groups capable to transiently coordinate is beneficial. Further structure-reactivity studies are in progress.

Chapter 2

EXPERIMENTAL SECTION

1. General Considerations

All air- and water-sensitive compounds were manipulated under N_2 or Ar using standard Schlenk or glovebox techniques. The solvents for air- and moisture-sensitive reactions were dried over sodium benzophenone ketyl or calcium hydride or by the method of Grubbs.[67] Deuterated solvents were purchased from Cambridge Isotopes Lab, Inc.; C_6D_6, and C_7D_8 was dried over a purple suspension with Na/benzophenone ketyl and vacuum transferred; C_6D_5Cl was dried over CaH_2 for greater than 24 h, vacuum transferred, and passed over an activated alumina plug. Ethylene (99.999%) for kinetic experiments was purchased from Matheson Tri-Gas and used without further purification. 2,6-lutidine was dried with sieves and distilled over $AlCl_3$ to remove 3-picoline and 4-picolline. t-Butyl acrylate were dried over 4 Å sieves for greater than 72h, vacuum transferred, and passed over an activated alumina plug. Acrylates used in kinetic studies contain 200~300 ppm of monomethyl ether hydroquinone as inhibitor. Dimethoxybenzene, 1-methoxynaphthalene, and pyridine were dried over calcium hydride and vacuum-transferred or distilled prior to use. 3,5-ditertbutylbromobenzene was dried by heating at 70 °C under vacuum for 16 hours. 2.5 M ^{n}BuLi, BBr_3, Br_2, $ZnCl_2$, and palladium-tetrakistriphenylphosphine were purchased from Sigma-Aldrich and used without further purification. Bis(dimethoxyphenyl)phosphine chloride,[68] 1,3-dibromo-5-(tert-butyl)-2-(methoxymethoxy)benzene,[69] $NiMe_2TMEDA$,[70] and $Nipy_2(CH_2Si(CH_3)_3$[71] were synthesized according to literature procedures. All ^{1}H, ^{13}C, and ^{31}P spectra of organic and organometallic compounds were recorded on Varian Mercury 300, Varian INOVA-400, or 500, or Bruker Cryoprobe 400 spectrometers. ^{1}H and ^{13}C chemical shifts are reported relative to residual solvent resonances.

2. Synthesis of ligands and metal complexes

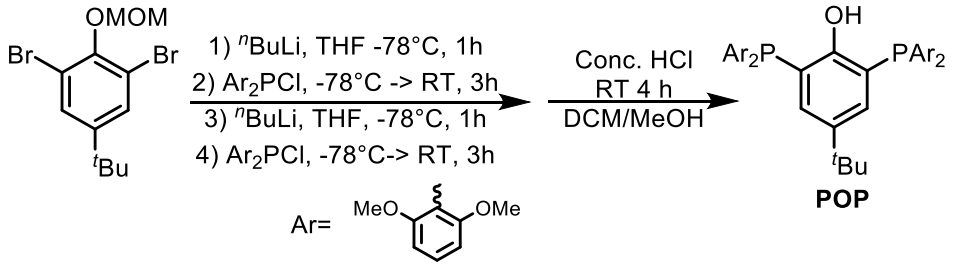

POPH: A Schlenk flask fitted with a screw-in Teflon stopper was charged with a solution of 1,3-dibromo-5-(tert-butyl)-2-(methoxymethoxy)benzene (3.52 g, 10.0 mmol) in THF (40 mL) and cooled to -78 °C under nitrogen. A hexane solution of *n*-butyllithium (4 mL, 2.5 M, 10.0 mmol) was added dropwise via syringe. After stirring for an additional 30 min at -78 °C, a solution of bis(2,6-dimethoxyphenyl)phosphine chloride (3.41 g, 10.0 mmol) in THF (20 mL) was added dropwise via cannula. After complete addition, the reaction was allowed to warm up to room temperature and stirred for an additional 3 h, yielding a yellow solution. The reaction was then cooled to -78 °C and a hexane solution of *n*-butyllithium (4 mL, 2.5 M, 10.0 mmol) was added dropwise via syringe. After stirring for an additional 30 min at -78 °C, a solution of bis(2,6-dimethoxyphenyl)phosphine chloride (3.41 g, 10.0 mmol) in THF (20 mL) was added dropwise via cannula. After complete addition, the reaction was allowed to warm up to room temperature and stirred for an additional 3 h, yielding a bright orange solution. The volatiles were then removed under vacuum. The pale yellow residue was dissolved in degassed CH_2Cl_2 (20 mL) and degassed MeOH (10 mL) followed by the addition of concentrated aqueous HCl (5 mL). The resulting mixture was degassed immediately via three freeze-pump-thaw cycle with a liquid nitrogen bath. After stirring for 4 h under room temperature, volatiles were removed under vacuum. In a N_2-filled glovebox (no exclusion of water), the resulting pale-yellow residue was taken up in CH_2Cl_2 (40 mL), washed with saturated aqueous solutions of K_2CO_3 (3 x 10 mL)

and NH_4Cl (3 x 10 mL), dried over $MgSO_4$, and filtered through Celite. The volatiles were removed under reduced pressure. In a glovebox (exclusion of water and oxygen), the resulting pale-yellow solid was dissolved in ether and filtered through Celite. The volatile materials were removed once more under vacuum and the resulting mixture was washed by hexanes (10 mL) and the solid was collected via vacuum filtration, yielding 2,6-bis(bis(2',6'-dimethoxyphenyl)phosphino)-4-tert-butylphenol (**POPH**) (1.68g, 22% yield) as a white powder. ^{1}H NMR (400 MHz, C_6D_6): δ 7.56−7.54 (d, $^3J_{HH}$ = 8.4 Hz, 2H, PhH), 7.50 (s, 1H, OH), 7.03−6.99 (t, $^4J_{HH}$ = 8.4 Hz, 4H, PhH), 6.26-6.23 (dd, $^3J_{HH}$ = 8.4 Hz, $^3J_{HH}$ = 2.6 Hz, 8H, PhH), 3.13 (s, 24H, OCH_3), 1.17 (s, 9H, $C(CH_3)_3$); $^{13}C\{^1H\}$ NMR (101 MHz, C_7D_8): δ 162.88 (d, $^2J_{CP}$ = 8.7 Hz, 8C, aryl-C), 159.45 (t, $^2J_{CP}$ = 13.1 Hz, 2C, aryl-C), 139.30 (t, $^3J_{CP}$ = 6.1 Hz, 2C, aryl-C), 131.18 (d, J_{CP} = 21.7 Hz, 2C, aryl-C), 129.27 (s, 4C, aryl-C), 122.32 (d, $^2J_{CP}$ = 13.1 Hz, 2C, aryl-C), 115.57 (d, J_{CP} = 27.3 Hz, 4C, aryl-C), 104.55 (s, 8C, aryl-C), 55.48 (s, 24C, OCH_3), 34.31 (s, 1C, $C(CH_3)_3$), 32.01 (s, 9C, $C(CH_3)_3$); $^{31}P\{^1H\}$ NMR (121 MHz, C_6D_6): δ -55.61 (s).

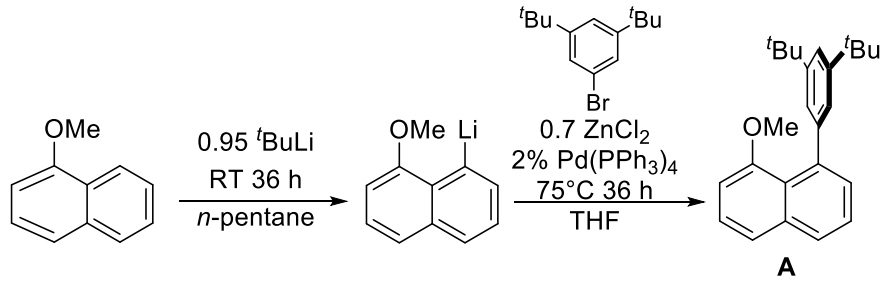

8-(3,5-di(tert-butyl)phenyl)-1-methoxynaphthalane: To a solution of 1-methoxy-naphthalene (7.21 g, 45.60 mmol) in *n*-pentane (75 ml) in a Teflon-fitted Schlenk tube was added tert-butyl lithium (2.87 g, 45.30 mmol). The solution was stirred in the glovebox for 36 h and the resulting yellow suspension was passed through a frit. The collected yellow solid was washed with *n*-pentane (2 x 50 mL) and dried under vacuum. The lithium salt was then collected (7.20 g, 96.2% yield) and used without further purification. The lithium salt (5.25 g, 32.0 mmol) was

dissolved in THF (100mL). $ZnCl_2$ (3.04 g, 22.4 mmol) was then added as a solid to the stirring solution over the course of 15 minutes. The resultant cloudy pale-yellow solution was stirred for an additional 0.5 h. Palladium-tetrakistriphenylphosphine (740 mg, 0.64 mmol) and 3,5 di-tertbutyl-bromobenzene (8.61 g, 32.0 mmol) were then added as solids to the stirring solution. The Schlenk tube was then sealed and transferred to the Schlenk line and equipped with a reflux condenser. The solution was heated at 75 °C for 36 hours, under an N_2 atmosphere, and then cooled to room-temperature at which point distilled water (25 mL) was added. The suspension was transferred to a round bottom flask and the THF was evaporated on a rotary evaporator. The crude material was then extracted with dichloromethane (3 x 100 mL), washed with H_2O (3 x 40 mL), and then dried with $MgSO_4$. After filtering, the volatiles were removed and the crude pale-yellow oil (9.65g, 87.1 % yield) was used without further purification. Confirmation of product assignment was determined by ^{1}H NMR spectroscopy. ^{1}H NMR (400 MHz, $CDCl_3$): δ 7.80 (dd, $^3J_{HH}$ = 8. Hz, $^4J_{HH}$ = 1.3 Hz, 1H, PhH), 7.50 (d, $^3J_{HH}$ = 8.3 Hz, 1H, PhH), 7.47 (dd, $^3J_{HH}$ = 8.3 Hz, $^3J_{HH}$ = 7.3 Hz, 1H, PhH), 7.38 (apparent t, $^3J_{HH}$ = 8.0 Hz, 1H, PhH), 7.36 (t, $^4J_{HH}$ = 1.9 Hz, 1H, PhH), 7.33 (dd, $^3J_{HH}$ = 7.2 Hz, $^4J_{HH}$ = 1.3 Hz, 1H, PhH), 7.17 (d, $^4J_{HH}$ = 1.9 Hz, 2H, PhH), 6.77 (d, $^3J_{HH}$ = 7.8 Hz, 1H, PhH), 3.45 (s, 3H, OCH_3), 1.36 (s, 18H, ^{t}Bu).

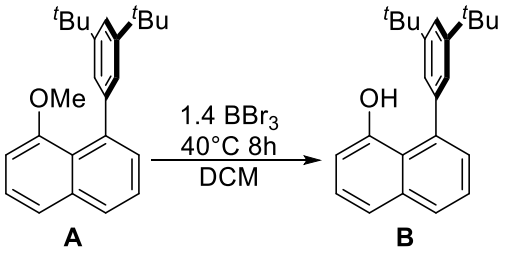

8-(3,5-di(tert-butyl)phenyl)-1-naphthol: To a two-neck round bottom flask equipped with a reflux-condenser, and solid **A** (9.65 g, 27.9 mmol) was added anhydrous dichloromethane (200 mL) via cannula transfer. The round bottom was then cooled to – 78 °C and BBr_3 (3.43 mL,

36.3 mmol) was added to the stirring solution using two separate syringes. The solution was then warmed to room temperature and then heated to 40 °C and stirred for an additional 8 hours. The light brown solution was then cooled to 0 °C and distilled water was carefully added to quench the excess BBr_3. The organic fraction was then separated, and the aqueous fraction was further extracted with dichloromethane (2 x 50 mL). The organic fractions were combined and washed with water (3 x 30 mL), and then dried with $MgSO_4$. After filtration, the solution was filtered through a plug of silica and washed with additional dichloromethane. All volatiles were then removed and the crude pale-yellow solid E (8.50 g, 91.5 % yield) was used without further purification. Confirmation of product assignment was determined by ^{1}H NMR spectroscopy. ^{1}H NMR (400 MHz, $CDCl_3$): δ 7.86 (dd, $^3J_{HH}$ = 8.2 Hz, $^4J_{HH}$ = 1.3 Hz, 1H, PhH), 7.56 (t, $^4J_{HH}$ = 1.9 Hz, 1H, PhH), 7.35-7.52 (overlapping multiplets, 3H, PhH), 7.34 (d, $^4J_{HH}$ = 1.9 Hz, 2H, PhH), 7.24 (dd, $^3J_{HH}$ = 7.0 Hz, $^3J_{HH}$ = 1.3 Hz, 1H, PhH), 6.91 (dd, $^3J_{HH}$ = 7.5 Hz, $^4J_{HH}$ = 1.3 Hz, 1H, PhH), 5.90 (s, 1H, O*H*), 1.37 (s, 18H, ^{t}Bu).

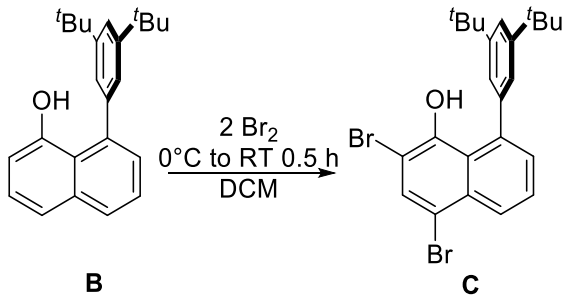

8-(3,5-di(tert-butyl)phenyl)-2,4-dibromo-1-mnaphthol: A solution of **B** (8.50 g, 25.5 mmol) in dichloromethane (250 mL) and transferred to a two-neck round bottom flask equipped with a pressure equalizing dropping funnel. To the dropping funnel was added 2 equivalents of bromine (2.62 mL, 50.9 mmol) as a solution in dichloromethane (10 mL). Connected through tubing, is an oil bubbler and a saturated aqueous solution of NaOH. Compressed air was pushed through the apparatus to allow for efficient quenching of the formed HBr. The reaction vessel

was cooled to 0 °C and the solution of bromine was slowly added via dropping funnel over the course of 0.5 hours. After complete addition of bromine, the cooling bath was removed, and the reaction was stirred at room temperature for an additional 0.5 hours. A saturated solution of sodium thiosulfate was then added to the stirring solution and the organic layer was separated. The aqueous layer was further extracted with dichloromethane (2 x 150 mL) and the organic layers were combined and washed with water (3 x 100 mL). After collecting the organic layer, the solution was filtered through a plug of silica which was washed with additional dichloromethane. All volatiles were then removed from the solution and the pale-yellow solid **C** (9.06 g, 70.5 % yield) was used without further purification. Confirmation of product assignment was determined by ^{1}H NMR spectroscopy. ^{1}H NMR (400 MHz, $CDCl_3$): δ 8.28 (d, $^3J_{HH}$ = 8.5 Hz, 1H, PhH), 7.95 (s, 1H, PhH), 7.59 (dd, $^3J_{HH}$ = 8.5 Hz, $^3J_{HH}$ = 8.0 Hz, 1H, PhH), 7.57 (t, $^4J_{HH}$= 1.9 Hz, 1H, PhH), 7.34 (d, $^3J_{HH}$ = 7.0 Hz, 1H, PhH), 7.28 (d, $^4J_{HH}$ = 1.9 Hz, 2H, PhH), 6.34 (s, 1H, O*H*), 1.36 (s, 18H, ^{t}Bu).

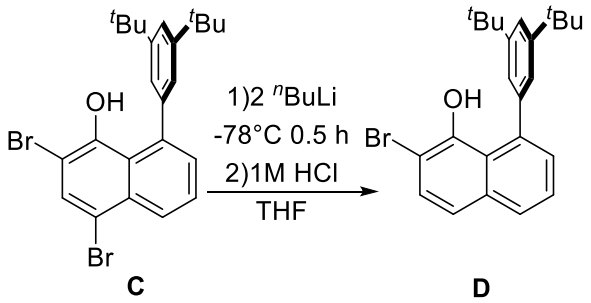

8-(3,5-di(tert-butyl)phenyl)-2-bromo-1-naphthol: A solution of **C** (9.06g, 18.5 mmol) in anhydrous THF (150 mL) in a two-neck round bottom equipped with a stir bar is cooled to -78 °C. To this stirring solution is added 2 equivalents of *n*-butyl-lithium (13.3 mL, 2.5 M. 37.0 mmol) dropwise, via syringe. The solution was left stirring at -78 °C for 0.5 h, at which point the solution was quickly transferred to a stirring solution of 1M HCl (50 mL). The resulting solution was allowed to warm to room temperature and was stirred for an additional 0.5 hours. The

solution was extracted with dichloromethane (3 x 200 mL), and the combined organics were washed with water (3 x 100 mL). The combined organics were then dried with $MgSO_4$, filtered, and evaporated to afford the crude product **D** which was further purified by column chromatography in hexanes (5.3 g, 69.7 % yield) to obtain a white solid. ^{1}H NMR (400 MHz, $CDCl_3$): δ 7.82 (dd, $^3J_{HH}$ = 8.3 Hz, $^4J_{HH}$ = 1.3 Hz, 1H, PhH), 7.60 (d, $^3J_{HH}$ = 8.70 Hz, 1H, PhH), 7.55 (t, $^4J_{HH}$ = 1.8 Hz, 1H, PhH), 7.47 (dd, $^3J_{HH}$ = 8.1 Hz, $^3J_{HH}$ = 7.0 Hz, 1H, PhH), 7.38 (d, $^3J_{HH}$ = 8.70 Hz, 1H, PhH), 7.30 (d, $^4J_{HH}$ = 1.8 Hz, 2H, PhH), 7.27 (dd, $^3J_{HH}$ = 7.0 Hz, $^4J_{HH}$ = 1.3 Hz, 1H, PhH), 6.33 (s, 1H, O*H*), 1.38 (s, 18H, *t*Bu); ^{13}C{^{1}H} NMR (101 MHz, C_6D_6): δ 151.79 (s, 2C, Aryl-C), 150.61 (s, 1C, Aryl-C), 141.38 (s, 1C, Aryl-C), 138.11 (s, 1C, Aryl-C), 135.31 (s, 1C, Aryl-C), 132.41 (s, 1C, Aryl-C), 130.86 (s, 1C, Aryl-C), 129.44 (s, 1C, Aryl-C), 128.74 (s, 1C, Aryl-C), 125.53 (s, 1C, Aryl-C), 124.19 (s, 2C, Aryl-C), 122.77 (s, 1C, Aryl-C), 122.41 (s, 1C, Aryl-C), 121.91 (s, 1C, Aryl-C), 106.92 (s, 1C, Aryl-C), 35.07 (s, 1C, *C*H(CH_3)$_3$), 31.44 (s, 6C, CH(*C*H$_3$)$_3$).

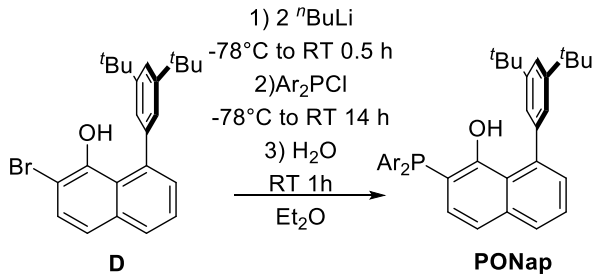

PONapH: In a glovebox, a stirring solution of **D** (600 mg, 1.46 mmol) in diethyl ether (10 mL) was cooled to -78 °C prior to the dropwise addition to 2 equivalents of *n*-butyl-lithium (1.1 mL, 2.5 M, 2.92 mmol). The solution was warmed to room temperature and the resulting suspension was stirred for 0.5 hours. The suspension was then cooled to -78 °C and a solution for di(2,6 dimethoxypehnyl)phosphine chloride (497 mg, 1.46 mmol) in THF (5 mL) was added dropwise. The resulting solution was allowed to warm to room temperature slowly over the course of 14 hours. In a glovebox containing degassed protic solvents, under an N_2 atmosphere,

water (10 mL) was added to the suspension and stirred for one hour. The pale-yellow suspension was extracted with Et_2O (2 x 25 mL) and the organic fractions were combined and washed with H_2O (3 x 5 mL). The organic fractions were combined, dried with $MgSO_4$, flirted, and evaporated to afford the crude product which was recrystallized from a saturated solution of Et_2O at -40°C for 16h (240 mg, 25.8 % yield) to afford pure **PONapH**.^{1}H NMR (400 MHz, C_6D_6): δ 7.81 (dd, $^3J_{HH}$ = 8.4 Hz, $^4J_{HP}$ = 5.4 Hz, 1H, PhH), 7.60 (dd, $^3J_{HH}$ = 8.4 Hz, $^4J_{HH}$ = 1.4 Hz, 1H, PhH), 7.48 (t, $^4J_{HH}$ = 1.8 Hz, 1H, PhH), 7.34 (d, $^4J_{HH}$ = 2.0 Hz, 2H, PhH), 7.23 (dd, $^3J_{HH}$ = 7.1 Hz, $^4J_{HH}$ = 1.4 Hz, 1H, PhH), 7.18 (d, $^3J_{HH}$ = 7.1 Hz, 1H, PhH), 7.16 (d, $^3J_{HH}$ = 7.5 Hz, 1H, PhH), 7.00 (t, $^3J_{HH}$ = 8.2 Hz, 2H, PhH), 6.20 (dd, $^3J_{HH}$ = 8.2 Hz, $^4J_{HP}$ = 2.9 Hz, 4H, PhH), 3.05 (s, 12H, OCH_3), 1.24 (s, 18H, ^{t}Bu); ^{31}P{^{1}H} NMR (121 MHz, C_6D_6): δ -65.68 (s, 1P). ^{13}C{^{1}H} NMR (101 MHz, C_6D_6): δ 162.83 (d, J_{CP} = 8.12 Hz, 2C, Aryl-C), 156.10 (d, J_{CP} = 20.3 Hz, 1C, Aryl-C), 149.66 (s, 2C, Aryl-C), 144.28 (s, 1C, Aryl-C), 140.10 (d, J_{CP} = 2.5 Hz, 1C, Aryl-C), 136.68 (s, 1C, Aryl-C), 132.30 (d, J_{CP} = 8.4 Hz, 1C, Aryl-C), 129.72 (s, 1C, Aryl-C), 129.01 (s, 1C, Aryl-C), 128.60 (s, 4C, Aryl-C), 125.18 (s, 1C, Aryl-C), 124.47 (s, 2C, Aryl-C), 122.28 (d, J_{CP} = 1.9 Hz, 1C, Aryl-C), 120.34 (s, 1C, Aryl-C), 120.21 (d, J_{CP} = 6.9 Hz, 1C, Aryl-C), 118.96 (d, J_{CP} = 3.7 Hz, 1C, Aryl-C), 113.93 (d, J_{CP} = 19.1 Hz, 1C, Aryl-C), 104.57 (d, $^4J_{CP}$ = 4.0 Hz, 4C, Aryl-C), 55.45 (s, 4C, OCH_3), 35.01 (s, 2C, *C*H(CH_3)$_3$), 31.73 (s, 6C, CH(*C*H$_3$)$_3$).

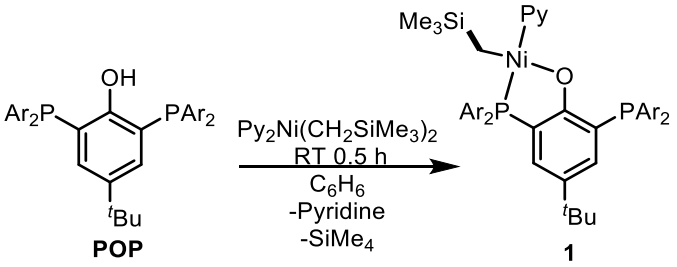

POP-Ni(py)(CH_2SiMe_3) (1): In the glove box, to a solution of $Py_2Ni(CH_2SiMe_3)_2$ (22 mg, 0.0593 mmol) in benzene (2 ml) in a vial was added a solution of **POPH** (42.83 mg, 0.0563

mmol) in benzene (4 ml). The mixture was stirred for 2 h under room temperature, forming a red-brown solution. Volatile materials were removed under vacuum and the residue was extracted with diethyl ether three times and dried in vacuo to provide the complex **1** (44 mg, 76%) as a yellowish solid. ^{1}H NMR (400 MHz, C_6D_6): δ 8.94-8.92 (m, 2H, PhH), 7.47−7.43 (m, 1H, PhH), 7.08−7.04 (t, $^3J_{HH}$ = 8.2 Hz, 2H, PhH), 7.04−7.00 (t, $^3J_{HH}$ = 8.2 Hz, 2H, PhH), 6.95−6.92 (m, 1H, PhH), 6.83−6.79 (m, 1H, PhH), 6.47−6.43 (m, 2H, PhH), 6.34−6.32 (dd, $^3J_{HH}$ = 8.2 Hz, $^4J_{HH}$ = 2.2 Hz, 4H, PhH), 6.29−6.26 (dd, $^3J_{HH}$ = 8.2 Hz, $^4J_{HH}$ = 3.5 Hz, 4H, PhH), 3.36 (s, 12H, OCH_3), 3.28 (s, 12H, OCH_3), 1.13 (s, 9H, $C(CH_3)_3$), 0.12 (s, 9H, $Si(CH_3)_3$), -0.71−-0.74 (d, $^3J_{HP}$ = 8.7 Hz, 2H, $NiCH_2Si$); ^{13}C{^{1}H} NMR (101 MHz, C_6D_6): 163.88 (d, $^2J_{CP}$ = 9.1 Hz, 4C, Ar-C), 161.77 (d, $^2J_{CP}$ = 1.5 Hz, 4C, Ar-C), 151.61 (m, 3C, Ar-C), 135.58 (s, 1C, Ar-C), 130.43 (m, 1C, Ar-C), 130.10 (s, 2C, Ar-C), 129.18 (s, 2C, Ar-C), 128.54 (s, 2C, Ar-C), 128.26 (m, 4C, Ar-C), 123.07 (d, $^3J_{CP}$ = 1.9 Hz, 2C, Ar-C), 118.65 (s, 1C, Ar-C), 112.77 (m, 1C, Ar-C), 105.04 (s, 4C, Ar-C), 104.74 (d, $^3J_{CP}$ = 4.1 Hz, 4C, Ar-C), 55.91 (s, 6C, OCH_3), 55.90 (s, 6C, OCH_3), 55.40 (s, 12C, OCH_3), 34.10 (s, 1C, $C(CH_3)_3$), 31.98 (s, 9C, $C(CH_3)_3$), 2.15 (s, 9C, $SiMe_3$), -18.25 (d, $^2J_{CP}$ = 29.0 Hz, 1C, $NiCH_2Si$); ^{31}P{^{1}H} NMR (121 MHz, C_6D_6): δ -5.31 (d, $^4J_{PP}$ = 8.9 Hz, 1P), -52.09 (d, $^4J_{PP}$ = 8.9 Hz, 1P). Anal. Calcd(%): C, 62.33; H, 6.46; N, 1.73. Found(%): C, 61.82; H, 6.33; N, 1.18.

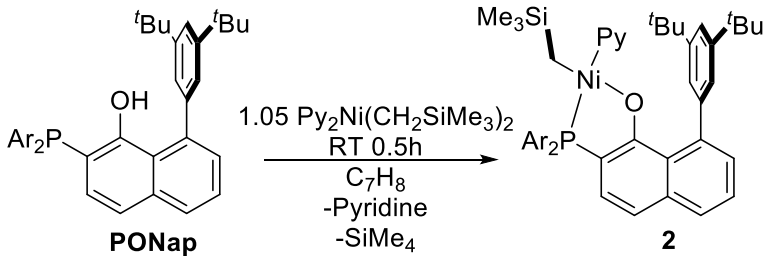

PONap-Ni (2): This complex was synthesized via a similar route for **1** and as isolated in 65% yield. ^{1}H NMR (400 MHz, C_6D_6): δ 8.45 (2nd order multiplet AA'BB', 2H, PhH), 7.89(dd, $^3J_{HH}$ =

8.3 Hz, $^4J_{HP}$ =10.1 Hz, 1H, PhH), 7.65 (dd, $^3J_{HH}$ = 8.0 Hz, $^4J_{HH}$ =1.4 Hz, 1H, PhH), 7.44 (d, $^4J_{HH}$ = 1.8 Hz, 2H, PhH), 7.31 (t, $^4J_{HH}$ = 1.8 Hz, 1H, PhH), 7.24 (t, $^3J_{HH}$ = 7.3 Hz, 1H, PhH), 7.16 (dd, $^3J_{HH}$ = 7.0 Hz, $^4J_{HH}$ = 1.4 Hz, 1H, PhH), 6.95-7.10 (overlapping multiplets, 4H, PhH), 6.87 (tt, $^3J_{HH}$ = 7.7 Hz, $^4J_{HH}$ = 1.7 Hz 1H, *p*-H C_5H_5N), 6.57 (t, $^3J_{HH}$ = 7.2 Hz, 2H, PhH), 6.20 (dd, $^3J_{HH}$ = 7.2 Hz, $^4J_{HP}$ = 3.6 Hz, 4H, PhH), 3.18 (s, 12H, OCH_3), 1.32 (s, 18H, *t*Bu), -0.24 (s, 9H, $SiMe_3$), -0.68 (d, $^3J_{HP}$= 9.0 Hz, 2H, Ni-CH_2); $^{13}C\{^1H\}$ NMR (101 MHz, C_6D_6): δ 173.82 (d, J_{CP}= 23.9 Hz, 1C, Aryl-C), 161.92 (d, J_{CP} = 1.4 Hz, 2C, Aryl-C), 151.21 (d, J_{CP} = 1.3 Hz, 2C, Aryl-C), 148.06 (s, 2C, Aryl-C), 146.88 (s, 1C, Aryl-C), 142.40 (d, J_{CP} = 2.3 Hz, 1C, Aryl-C), 139.54 (d, J_{CP} = 1.6 Hz, 1C, Aryl-C), 135.25 (s, 1C, Aryl-C), 130.36 (s, 1C, Aryl-C), 129.67 (s, 1C, Aryl-C), 129.28 (d, J_{CP} = 1.4 Hz, 1C, Aryl-C), 125.51 (s, 1C, Aryl-C), 125.06 (s, 2C, Aryl-C), 123.87 (d, J_{CP} = 1.6 Hz, 4C, Aryl-C), 118.84 (s, 1C, Aryl-C), 117.69 (d, $^2J_{CP}$ =56.8 Hz, 2C, Aryl-C), 112.82 (d, J_{CP} = 8.1 Hz, 1C, Aryl-C), 111.97 (d, $^2J_{CP}$ = 49.5 Hz, 2C, Aryl-C), 104.78 (d, $^4J_{CP}$ = 4.0 Hz, 4C, Aryl-C), 55.43(s, 4C, OCH_3), 35.00 (s, 2C, *C*H(CH_3)$_3$), 32.05 (s, 6C, CH(*C*H_3)$_3$), 2.23 (s, 3C, $SiMe_3$), -16.91 (d, $^2J_{CP}$ = 31.1 Hz, 1C, Ni-CH_2); $^{31}P\{^1H\}$ NMR (121 MHz, C_6D_6): δ -5.94 (s, 1P). Anal. Calcd(%): C, 68.37; H, 7.03; N, 1.63. Found(%): C, 68.27; N, 6.79; N, 1.29.

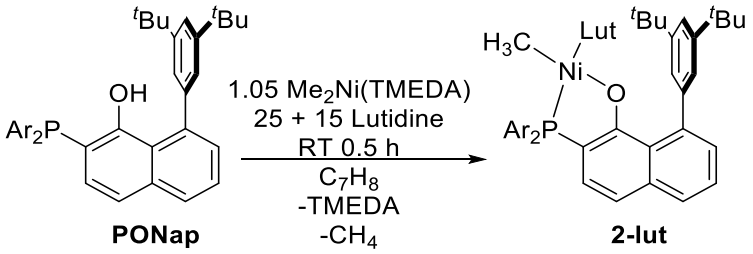

PONap-Ni(lut)(Me)(2-lut): In the glove box, to a thawing solution of $NiMe_2$(TMEDA) (38 mg, 0.19 mmol) in toluene(2 mL) was add a thawing solution of **PONapH** (120 mg, 0.19 mmol) and 25 equivalents of 2,6-lutidine (448 mg, 4.71 mmol) in toluene (2 mL). The strongly colored yellow solution was stirred while warming to room temperature for 10 minutes. While arming, 15 additional equivalents of 2,6-lutidine (268 mg, 2.82 mmol) were added and the solution was

stirred at room temperature for an additional 0.5 h. All volatiles were removed from solution which was triturated with hexanes (3 x 10 mL). The resulting residue was fractioned with *n*-pentane (12 mL) and toluene (8 mL), and the volatiles were subsequently removed from the toluene fraction yielding spectroscopically pure **2-lut** (98 mg, 63.6 % yield). ^{1}H NMR (400 MHz, C_6D_6): δ 7.83 (t, $^3J_{HH}$ = 9.2 Hz, 1H, PhH), 7.64 (dd, $^3J_{HH}$ = 7.5 Hz, 1H, PhH), 7.03-7.18 (overlapping multiplets, 5H, PhH), 7.01 (d, $^3J_{HH}$ = 8.1 Hz, 1H, PhH), 6.96 (t, $^4J_{HH}$ = 7.3 Hz, 1H, PhH), 6.39 (d, $^3J_{HH}$ = 7.6 Hz, 2H, PhH), 6.27 (dd, $^3J_{HH}$ = 8.0 Hz, $^4J_{HP}$ = 3.4 Hz, 4H, PhH), 3.22 (s, 6H, $(C_5H_3N)(CH_3)_2$), 3.21 (s, 12H, OCH_3), 1.25 (s, 18H, *t*Bu), -0.92 (d, $^3J_{HP}$ = 6.4 Hz, 3H. Ni-CH_3); ^{31}P{^{1}H} NMR (121 MHz, C_6D_6): δ -5.60. Anal. Calcd(%): C, 70.60; H, 6.91; N, 1.72. Found(%): C, 69.56; H. 6.79; N, 1.29.

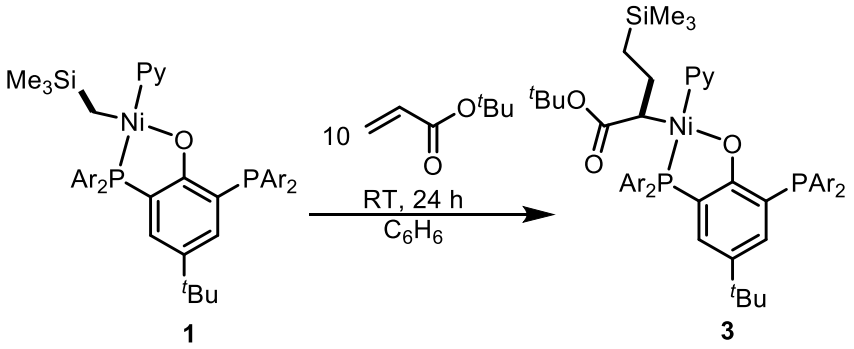

POP-Ni(py)(CCO)(3): In a glove box, to a yellow solution of **1** (49 mg, 0.050 mmol) in benzene (5 mL) was added 10 equivalents of tertbutyl acrylate (64 mg, 0.5 mmol). After 24 h, all volatiles were removed under vacuum and the residue was triturated with cold pentane (3 x 5 mL). The remaining residue was then dried under vacuum to afford crude **3** as an orange solid (16.5 mg, 28%). ^{31}P{^{1}H} NMR (121 MHz, C_6D_6): δ -6.62 ~ -7.26 (broad m), δ -52.85 ~ -53.45 (broad m).

Since only broad peaks were observed in ^{1}H NMR of **3** and addition of excess pyridine could sharpen peaks in ^{1}H NMR (Figure S2.2.17). Integrable NMR spectra of **3** were collected with 2

equiv. of additional pyridine. ^{1}H NMR (400 MHz, C_6D_6): δ 8.56-8.77 (overlapping multiplets, 4H, bound and free pyridine-H), δ 7.33 (d, $^3J_{HH}$ = 16 Hz, 2H, PhH), 7.00-7.12 (overlapping multiplets, 5H, PhH), 6.92 (broad s, 1H, free pyridine-H), 6.85 (broad s, 1H, PhH), 6.42-6.68 (overlapping multiplets, 4H, bound and free pyridine-H), 6.20-6.36 (d, overlapping multiplets, 8H, PhH), 3.59 (broad s, 6H, OCH_3), 3.26 (s, 6H, OCH_3), 3.26 (t, $^3J_{HH}$ = 12.8 Hz, 1H, nickel-CH), 3.20 (s, 6H, OCH_3), 3.12 (s, 6H, OCH_3), 1.99 (td, $^3J_{HH}$ = 12.8 Hz, $^3J_{HH}$ = 3.2 Hz, 1H, nickel-alkyl), 1.12 (s, 9H, $OC(CH_3)_3$), 1.09 (s, 9H, $C(CH_3)_3$), 1.02 (s, 1H, nickel alkyl), 0.69 (td, $^3J_{HH}$ = 12.8 Hz, $^3J_{HH}$ = 3.2 Hz, 1H, nickel-alkyl), 0.25 (s, 1H, nickel-alkyl), 0.06 (s, 9H, $Si(CH_3)_3$); $^{31}P\{^1H\}$ NMR (121 MHz, C_6D_6): δ -6.80 (d, $^4J_{PP}$ = 7.3 Hz, 1P), -53.17 (d, $^4J_{PP}$ = 7.3 Hz, 1P).

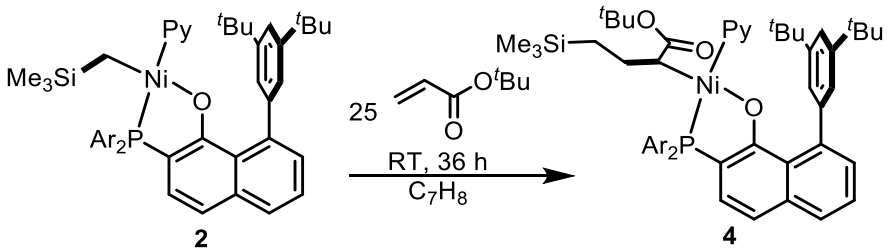

PONap-Ni(py)(CCO)(4): To a solution of **2** (135 mg, 0.157 mmol) in toluene (5 mL), in a glove box, was added 25 equivalents of tertbutyl acrylate (503.1 mg, 3.93 mmol). After 36 h, all volatiles were removed from the solution and the residue was triturated with hexanes (3 x 5 mL). The remaining residue was then fractioned with *n*-pentane (5 mL) and diethyl ether (10 mL). The diethyl ether fraction was evaporated to afford crude **4** (63 mg, 40.6 % yield). ^{1}H NMR (400 MHz, C_7D_8): δ 8.65 (broad s, $W_{1/2}$ = 36.8 Hz, 2H, *o*-pyridine), 7.65 (d, $^3J_{HH}$ = 8.1 Hz, 1H, PhH), 7.60 (broad m, 1H, PhH), 7.38 (s, 2H, PhH), 7.26 (t, $^3J_{HH}$ = 7.1 Hz, 1H, PhH), 6.99-7.19 (overlapping multiplets, 5H, PhH), 6.96 (d, $^3J_{HP}$ = 8.4 Hz, 2H, PhH), 6.70 (broad s, $W_{1/2}$ = 27.5 Hz, 2H, PhH), 6.33 (broad d, $^3J_{HH}$ = 7.8 Hz, 2H, PhH), 6.26 (d, $^3J_{HH}$=7.8 Hz, 2H, PhH), 3.47 (s, 6H, OCH_3), 3.36 (s, 1H, Ni-CH), 3.24 (s, 6H, OCH_3), 1.47 (s, 18H, ^{t}Bu), 1.32 (broad s, 9H, $W_{1/2}$

= 64 Hz, O^{t}Bu), 0.92 (t, $^3J_{HH}$ = 6.6 Hz, 2H, Ni-alkyl), 0.67 (broad multiplet, $W_{1/2}$= 31 Hz, 1H, Ni-alkyl), 0.31 (s, 1H, Ni-alkyl), -0.03 (s, 9H, $SiMe_3$); $^{31}P\{^1H\}$ NMR (121 MHz, C_6D_6): δ -6.15 (broad s, $W_{1/2}$= 37.1 Hz. 1P)

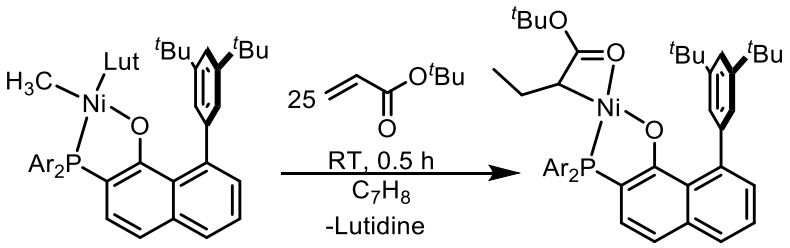

2-lut **5**

PONap-Ni (CCO): (5) Complex **5** was synthesized and purified in a similar way to **4** with the exception of using **2-lut** as the precursor. The reaction was completed in 0.5 h and was isolated in 70 % yield. ^1H NMR (400 MHz, C_6D_6): δ 7.68 (dd, $^3J_{HH}$ = 7.7 Hz, $^4J_{HP}$ = 1.8 Hz, 1H, PhH), 7.63 (dd, $^3J_{HH}$ = 7.4 Hz, $^3J_{HH}$ = 10.8 Hz, 1H, PhH), 7.56 (s, 2H, PhH), 7.47 (broad multiplet, 1H, PhH), 7.26-7.37 (overlapping multiplets, 2H, PhH), 6.99-7.07 (overlapping multiplets, 4H, PhH), 6.22 (dd, $^3J_{HH}$ = 8.4 Hz, $^4J_{HP}$ = 3.8 Hz, 2H, PhH), 6.16 (dd, $^3J_{HH}$ = 8.2 Hz, $^4J_{HP}$ = 3.8 Hz, 2H, PhH), 3.27 (s, 6H, OC*H*$_3$), 3.15 (broad s, $W_{1/2}$ = 15 Hz, 6H, OCH_3), 2.09 (broad m, 1H, Ni-C*H*), 1.54 (broad s, $W_{1/2}$ = 15 Hz, 18H, ^{t}Bu), 1.47 (s, 9H, O^{t}Bu), 1.19 (broad multiplet, 1H, Ni-CH-C*H*H), 0.81-0.86 (overlapping multiplets, 4H, Ni-CH-CH_2-C*H*$_3$ + Ni-CH-CH*H*-CH_3); $^{13}C\{^1H\}$ NMR (101 MHz, C_6D_6): δ 174.93 (d, J_{CP} = 22.5 Hz, 2C, Aryl-C), 161.97 (d, J_{CP} = 2.0 Hz, 2C, Aryl-C), 161.86 (broad s, 1C, Aryl-C), 147.72 (multiplet, 1C, Aryl-C), 145.70 (s, 1C, Aryl-C), 143.49 (multiplet, 1C, Aryl-C), 139.28 (s, 1C, Aryl-C), 131.21 (s, 1C, Aryl-C), 131.13 (s, 1C, Aryl-C), 128.88 (s, 2C, Aryl-C), 127.09 (s, 2C, Aryl-C), 126.42 (d, J_{CP} = 11.4 Hz, 1C, Aryl-C), 126.13 (s, 2C, Aryl-C), 119.15 (s, 1C, Aryl-C), 112.78 (d, J_{CP} = 8.7 Hz, 1C, Aryl-C), 108.25 (d, J_{CP} = 53.1 Hz, 1C, Aryl-C), 104.55 (d, J_{CP} = 4.4 Hz, 2C, Aryl-C), 104.30 (d, J_{CP} = 4.4 Hz, 2C, Aryl-C), 55.86 (s, 1C, O*C*$(CH_3)_3$), 55.47 (s, 2C, OCH_3), 55.43 (s, 2C, OCH_3),

35.05 (s, 2C, *C*H(CH_3)$_3$), 32.19 (s, 6C, CH(*C*H_3)$_3$), 28.86 (s, 3C, OC(*C*H_3)$_3$), 21.90 (d, $^2J_{CP}$= 25.5 Hz, 1C, Ni-*C*H), 20.06 (d, $^3J_{CP}$= 3.3 Hz, 1C, Ni-CH*C*H_2), 14.62 (s, 1C, Ni-CHCH_2*C*H_3); ^{31}P{^{1}H} NMR (121 MHz, C_6D_6, 298 K): δ -6.57 (broad s, 39.5 Hz, 1P); ^{31}P{^{1}H} NMR (121 MHz, C_7D_8, 193 K): δ -6.53 (broad s, 27.5 Hz, 1P), -8.08 (s, 1P). Anal. Calcd(%): C, 68.83; H, 7.10; N, 0. Found(%): C, 67.44; H, 6.89; N, 0.2.

3 Solution-State NMR Characterization and Discussion of 5

Encouraged by the structural confirmation of the chelate resulting from 2,1-insertion of acrylate in the solid-state, further NMR studies were performed to address the solution structure. The room temperature ^{1}H NMR spectrum of **5** shows the expected number of aromatic resonances as well as broad peaks corresponding to the two methoxy resonances in a 1:1 ratio. A broad resonance (δ 1.56) and a sharp resonance (δ 1.48) are assigned to the tert-butyl groups from the phosphine naphthoxide ligand and the ester group, respectively. Resonances for the Ni-bound alkyl moiety are observed at δ 2.1 as a broad multiplet for the methine, overlapping resonances at δ 0.76, and 1.19 for the diastereotopic methylene protons, and at δ 0.81 for the methyl protons, which were identified using multiplicity edited ^{1}H-^{13}C{^{1}H} HSQC. ^{13}C{^{1}H} NMR (Figure AD2.23) display five aliphatic resonances corresponding to the Ni-bound alkyl moiety. The resonances at δ 14.3, 19.7, and 21.3 are consistent with methyl, methylene, and methine groups, respectively. This assignment is further supported by higher magnitude J_{CP} value for the methine resonance (24.8 Hz) and low magnitude J_{CP} value for the methylene resonance (3.0 Hz). Furthermore, the multiplicity-edited ^{13}C{^{1}H}-^{1}H HSQC identifies the resonance at δ 19.7 as a methylene resonance with ^{1}H cross peaks at δ 0.76 and 1.19, the latter resonance overlapping with the tert-butyl resonances. A cross peak for the methyl peak was observed at δ 0.81, and for the methine, at δ 2.12. Although these data do not rule out a solution structure with

the carbonyl dissociating, they provide conclusive support for the Ni-alkyl group connectivity observed in the solid-state. Chain walking through β-H elimination and reinsertion at the other end of the olefin could give isomers in solution. The isomer where Ni walks to the end of the alkyl chain would not display a methyl group, while the remaining one with Ni migrating a single carbon would still have methyl, methylene, and methine motifs but in a different coupling pattern; both can be ruled out based on the NMR data. However, we cannot rule out a dynamic isomerization process with compound **5** as the major, and only detectible component.

Decoalesence of **5** is observed at low temperatures, NMR studies of **5** suggest the existence of two conformers in exchange, which in part elucidate the broadness observed of the resonances in the room-temperature ^{1}H and ^{31}P{1H} NMR spectra of **5**. Complex **5** was investigated further toward gleaning additional insights into potential isomerization processes. The ^{31}P{^{1}H} NMR spectrum of **5** shows a single broad resonance at δ -6.36 with a $W_{1/2}$= 58.1 Hz. Variable temperature ^{31}P{^{1}H} NMR spectra show the appearance of two sharp peaks upon cooling to 0 °C in a 10 to 1 ratio, at approximately δ -6.1 and -8.5, respectively. Upon further cooling to -60 °C, the ratio decreases to approximately 4.3:1. Cooling to -80 °C further decreases the ratio (3.1:1) and significant broadening is observed in the major isomer, but not the minor isomer (Figure AD2.26). Cooling to -90 °C shows further broadening and chemical shift change with both resonances overlapped. This observation could indicate the presence of two isomers stemming from reversible β-H elimination and reinsertion processes; alternatively, it could also indicate the presence of conformers which are not fluxional on the NMR time scale at low temperatures. The ^{1}H NMR shows sharpening of several resonances up-on cooling, as well as the decoalesence of the tert-butyl resonances on the naphthoxide ligand. Chemical shift changes are also observed for many of the resonances including the methoxy, the aromatic, and the Ni-alkyl groups. The apparent overlap of many of these resonances upon decoalesence render the

interpretation of the low temperature ^{1}H NMR spectra inconclusive. Because isomerization via chain walking would result in five- or six-membered chelates likely more stable than the alkyl species observed at room temperature, we favor the interpretation that the isomers observed at low temperatures are conformers.

4 Crystallographic Information

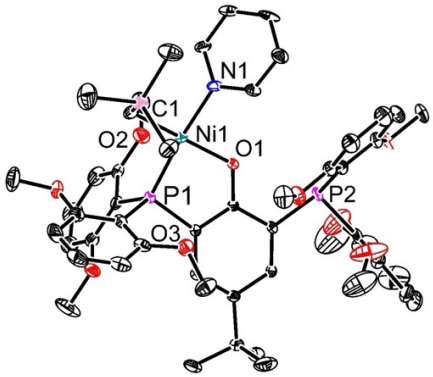

Figure S2.4.1. Solid-State Structure of **1**. Ellipsoids are show at the 50% probability level. Hydrogen atoms and solvent molecules excluded for clarity. Disordered $SiMe_3$ and OMe group excluded for clarity.

Special Refinement Details for 1: Complex **1** crystalizes in a P-1 space group with the full molecule in the asymmetric unit. The SiMe3 group is modelled with two-site disorder with occupancies of 0.78 and 0.22. One of the methoxy groups is also modelled with two-site disorder with occupancies of 0.78 and 0.22. The carbon on the lower occupancy disordered methoxy group is refined isotropically to prevent an NPD. A disordered benzene molecule is observed and is refined isotropically to prevent NPDs. There is likely disorder on the benzene molecule, despite efforts, it could not be modelled.

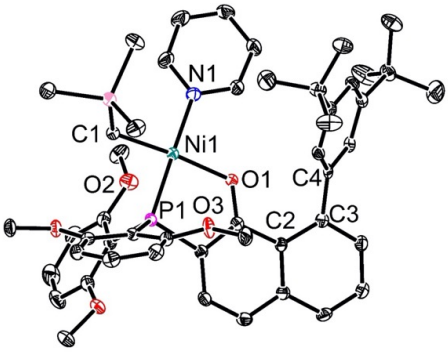

Figure S2.4.2. Solid-State Structure of **2**. Ellipsoids are show at the 50% probability level. Hydrogen atoms and solvent molecules excluded for clarity.

Special Refinement Details for 2: Complex **2** crystalizes as a twin in a P-1 space group with the full molecule and half of a benzene molecule in the asymmetric unit.

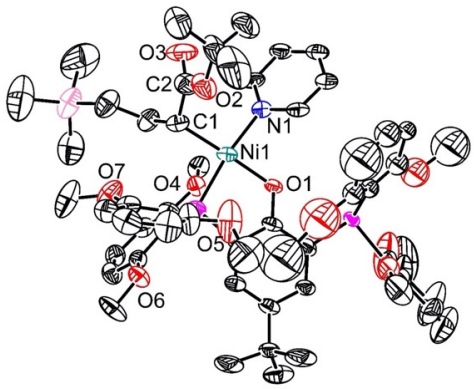

Figure S2.4.3. Solid-State Structure of **3**. Ellipsoids are show at the 50% probability level. Hydrogen atoms and solvent molecules excluded for clarity.

Special Refinement Details for 3: Complex **3** crystalizes in a P-1 space group with the full molecule in the asymmetric unit. The $SiMe_3$ group is modelled with two-site disorder with occupancies of 0.54 and 0.46. The unbound P center and the 2,6 dimethoxy aryl groups are modelled with two-site disorder with occupancies of 0.76 and 0.24. The data collected on this sample produces a moderate quality solid-state structure.

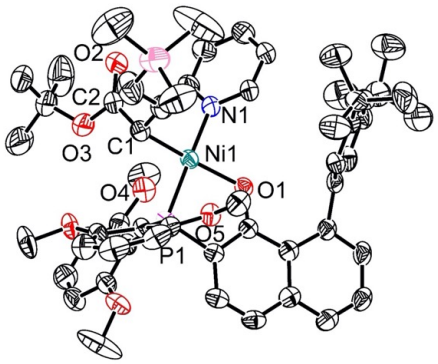

Figure S2.4.4. Solid-State Structure of **4**. Ellipsoids are show at the 50% probability level. Hydrogen atoms and solvent molecules excluded for clarity. Disorder also excluded for clarity.

Special Refinement Details for 4: Complex **4** crystallized in a $P_{21/c}$ space group with the full molecule in the asymmetric unit. Two-site disorder was modelled for the entire tert-butyl aryl group with relative occupanices of 0.78 and 0.22. Additional two site disorder was modelled for one of the dimethoxy aryl rings with relative occupancies of 0.78 and 0.22. Two of the carbons on the less-occupied dimethoxy ring were refined isotropically to prevent NPDs.

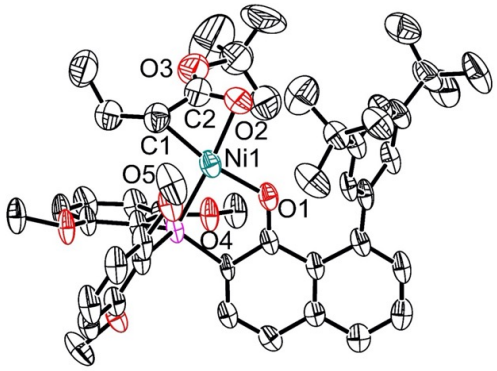

Figure S2.4.5. Solid-State Structure of **5**. Ellipsoids are show at the 50% probability level. Hydrogen atoms and solvent molecules excluded for clarity. Disorder of tert-butyl aryl also excluded for clarity.

Special Refinement Details for 5: Complex **5** crystallizes in a $P_{21/n}$ space group with an outer sphere ether molecule, all of which are present in the asymmetric unit. Two-site disorder is present in one of the tertbutyl groups on the aryl ring, with occupancies of 0.52 and 0.48. Additional solvent disorder could not be modelled successfully and was masked using SQUEEZE.

Table S2.4.1. Crystal and refinement data for complexes **1~5**

	1	**2**	**3**
Empirical formula	$C_{58}H_{63.9}NNi_{O8}P_2Si$	$C_{52}H_{63}NNiO_5PSi$	$C_{60.57}H_{78.28}NNiO_{11.34}P_2Si_{1.82}$
Formula weight	1067.7	899.78	1173.71
Temperature/K	100 K	100 K	100 K
Crystal system	Triclinic	Triclinic	Triclinic
Space group	P-1	P-1	P-1
a/Å	13.272(4)	11.2840(9)	13.366(8)
b/Å	13.914(7)	12.9467(10)	16.184(5)
c/Å	15.221(5)	16.3826(13)	16.570(5)
α/°	90.282(18)	91.142(5)	90.72(2)
β/°	101.120(14)	103.578(4)	97.09(2)
γ/°	90.58(2)	92.791(4)	101.70(2)
Volume/Å^3	2757.8(19)	2322.5	3480(3)
Z	2	2	2
ϱ_{calc}g/cm^3	1.286	1.287	1.120
μ/mm^{-1}	0.487	1.552	1.555
F(000)	1125.8	955.40	1246
Radiation	CuKα (λ = 1.54178)	CuKα (λ = 1.54178)	CuKα (λ = 1.54178)
Reflections collected	61600	9890	70100
Independent reflections	9916	9095	8812
Goodness-of-fit on F^2	1.141	1.059	1.077
Final R indexes	R_1 = 8.42 %	R_1 = 3.66 %	R_1 = 11.48 %
[I>=2σ (I)]	R_2 = 19.44 %	R_2 = 9.78 %	R_2 = 32.87 %

	4	**5**
Empirical formula	$C_{56}H_{71.78}NNiO_7PSi$	$C_{52}H_{68}NiO_8P$
Formula weight	988.67	910.72
Temperature/K	100 K	100 K
Crystal system	Monoclinic	Triclinic
Space group	$P_{21/C}$	$P_{21/n}$
a/Å	17.811(5)	15.546(4)
b/Å	20.024(6)	14.863(4)
c/Å	15.761(5)	23.621(9)
α/°	90	90
β/°	104.164(13)	103.26(2)
γ/°	90	90
Volume/Å^3	5450(3)	5312(3)
Z	4	4
ϱ_{calc}g/cm^3	1.205	1.139
μ/mm^{-1}	1.394	1.189
F(000)	2111.1	1948
Radiation	CuKα (λ = 1.54178)	CuKα (λ = 1.54178)
Reflections collected	101836	63894
Independent reflections	9392	4944
Goodness-of-fit on F^2	1.018	1.041
Final R indexes [I>=2σ (I)]	R_1 = 7.00 %	R_1 = 10.84 %
	R_2 = 20.59 %	R_2 = 30.15 %

5 Supplemental Data for Olefin Polymerization

5.1 General procedure for high throughput parallel polymerization reactor (PPR) runs for preparation of polyethylene and ethylene/tBA copolymers.

Polyolefin catalysis screening was performed in a high throughput parallel polymerization reactor (PPR) system. The PPR system was comprised of an array of 48 single cell (6 x 8 matrix) reactors in an inert atmosphere glovebox. Each cell was equipped with a glass insert with an internal working liquid volume of approximately 5 mL. Each cell had independent controls for pressure and was continuously stirred at 800 rpm. Catalyst, ligand, and metal precursor solutions, unless otherwise noted, were prepared in toluene. Ligands were metallated with 1:1 ligand:metal (L:M) ratio by premixing a solution of metal precursor with a solution of the ligand. All liquids (i.e., solvent, tBA, and catalyst solutions) were added via robotic syringes. Gaseous reagents (i.e.,

ethylene) were added via a gas injection port. Prior to each run, the reactors were heated to 50 °C, purged with ethylene, and vented.

All desired cells were injected with tBA followed with a portion of toluene (This step was skipped for ethylene homopolymerization). The reactors were heated to the run temperature and then pressured to the appropriate psig with ethylene. Catalyst or in situ metallated ligands were then added to the cells. Each catalyst addition was chased with a small amount of toluene so that after the final addition, a total reaction volume of 5 mL was reached. Upon addition of the catalyst, the PPR software began monitoring the pressure of each cell. The desired pressure (within approximately 2-6 psig) was maintained by the supplemental addition of ethylene gas by opening the valve at the set point minus 1 psi and closing it when the pressure reached 2 psi higher. All drops in pressure were cumulatively recorded as "Uptake" or "Conversion" of the ethylene for the duration of the run or until the uptake or conversion requested value was reached, whichever occurred first. Each reaction was then quenched by addition of 1% oxygen in nitrogen for 30 seconds at 40 psi higher than the reactor pressure. The shorter the "Quench Time", the more active the catalyst. In order to prevent the formation of too much polymer in any given cell, the reaction was quenched upon reaching a predetermined uptake level of 80psig. After all the reactors were quenched they were allowed to cool to about 60 °C. They were then vented and the tubes were removed. The polymer samples were then dried in a centrifugal evaporator at 60 °C for 12 hours, weighed to determine polymer yield and submitted for IR (tBA incorporation) and GPC (molecular weight) analysis.

5.2 General procedure for batch reactor runs for preparation of ethylene/tBA copolymers.

Polymerization reactions were conducted in a 2-L Parr batch reactor. The reactor was heated by an electrical heating mantle and cooled by an internal serpentine cooling coil containing cooling water. The water was pre-treated by passing through an Evoqua water purification

system. Both the reactor and the heating/cooling system were controlled and monitored by a Camile TG process computer. The bottom of the reactor was fitted with a dump valve, which empties the reactor contents into a lidded dump pot, which was prefilled with a catalyst-kill solution (typically 5 mL of an Irgafos / Irganox / toluene mixture). The lidded dump pot was vented to a 15-gal. blowdown tank, with both the pot and the tank N_2 purged. All chemicals used for polymerization or catalyst makeup are run through purification columns to remove any impurities that may affect polymerization. The toluene was passed through two columns, the first containing A2 alumina, the second containing Q5 reactant. The tert-butyl acrylate was filtered through activated alumina. The ethylene was passed through two columns, the first containing A204 alumina and 4 Å molecular sieves, the second containing Q5 reactant. The N2 used for transfers was passed through a single column containing A204 alumina, 4 Å molecular sieves and Q5 reactant.

The reactor was loaded first from the shot tank that contained toluene and tBA. The shot tank was filled to the load set points by use of a differential pressure transducer. After solvent/acrylate addition, the shot tank was rinsed twice with toluene. Then the reactor was heated up to the polymerization temperature set point. The ethylene was added to the reactor when the reaction temperature was reached to maintain the reaction pressure set point. Ethylene addition amounts were monitored by a micro-motion flowmeter.

The catalysts were handled in an inert atmosphere glovebox and were prepared as a solution in toluene. The catalyst was drawn into a syringe and pressure-transferred into the catalyst shot tank. This was followed by 3 rinses of toluene, 5 mL each. Catalyst was added when the reactor pressure set point was reached.

Immediately after catalyst addition the run timer was started. Usually within the first 2 min. of successful catalyst runs an exotherm was observed, as well as decreasing reactor pressure.

Ethylene was then added by the Camile to maintain reaction pressure set point in the reactor. These polymerizations were run for 75 min or until 40 g of ethylene uptake. Then the agitator was stopped, and the bottom dump valve was opened to empty reactor contents into the lidded dump pot. The lidded dump pot was closed and the contents were poured into trays placed in a lab hood where the solvent was evaporated off overnight. The trays containing the remaining polymer were then transferred to a vacuum oven, where they were heated up to 140 °C under vacuum to remove any remaining solvent. After the trays cooled to ambient temperature, the polymers were weighed for yield/efficiencies and submitted for polymer testing if so desired.

5.3 Orginal catalytic runs in high throughput parallel polymerization reactors (PPR)

Table S2.5.1 show a set of ethylene homopolymerization trials with **1**. In general, **1** showed extremely high activity (~400000kg/(mol·h)) at 90 ºC. These trials were stopped in ~10s to protect the reactor, and therefore resulting polyethylene features relatively low Mw and high PDI. This may not represent **1'**s typical performance.

Table S2.5.1. Ethylene/tBA copolymerization with in-situ mixed ligand **POPH** and $py_2Ni(CH_2SiMe_3)_2$ (**Ni**)

Entry[a]	time (s)	temp. (ºC)	Act. (kg/(mol·h))	$M_w/10^3$	PDI	Tm (ºC)
1	11	90	378947	9.3	5.3	123.9
2	10	90	417000	27.4	9.4	106.9
3	10	90	411429	16.8	6.5	107.0

[a]V(total)=5 mL, [Ni]=0.25 μmol, ethylene pressure=400 psi.

Table S2.5.2~ S5.4 show original analytic data of ethylene/tBA copolymerization with **1** and **2**.

Table S2.5.2. Ethylene/tBA copolymerization with *in-situ* mixed **POPH** + **Ni**.

Entry[a]	tBA (M)	T (ºC)	Act.[b]	t (min)	$M_w/10^3$	PDI	%Mol t-BA	Tm (ºC)
1	0.05	70	304	60	97.2	2.25	2.58	107.3
2	0.05	70	324	60	91.5	2.25	2.57	106.9
3	0.05	70	300	60	93.0	2.26	2.56	107.0
4	0.05	70	328	60	95.8	2.30	2.49	107.8
5	0.05	70	348	60	93.6	2.25	2.34	108.7
6	0.05	90	482	55	60.8	2.26	2.21	110.5
7	0.05	90	629	52	58.6	2.25	1.94	111.9
8	0.05	90	644	38	58.9	2.22	2.26	110.5
9	0.05	90	639	44	59.5	2.27	2.18	110.8
10	0.1	90	244	60	38.7	2.33	5.40	93.6
11	0.1	90	248	60	43.4	2.38	4.99	94.7
12	0.1	90	240	60	40.9	2.30	4.99	94.8
13	0.1	90	248	60	40.2	2.23	4.85	95.2
14	0.15	90	116	60	28.4	2.29	8.60	81.9
15	0.15	90	108	60	27.7	2.36	7.96	82.2
16	0.15	90	120	60	30.3	2.27	7.97	83.3
17	0.15	90	128	60	29.3	2.32	8.16	82.2
18	0.15	100	104	60	22.2	2.31	7.97	81.1
19	0.15	100	120	60	22.6	2.31	7.64	80.9
20	0.15	100	132	60	22.9	2.22	8.19	81.4
21	0.15	100	120	60	22.8	2.17	7.63	81.8
22	0.15	100	88	60	22.9	2.19	7.47	83.2
23	0.2	100	84	60	19.0	2.31	12.49	68.4
24	0.2	100	80	60	19.1	2.10	11.42	68.4

[a]V(total)=5 mL, [Ni]=0.25 μmol, ethylene pressure=400 psi. Polymerization runs were stopped when t=1 h or ethylene uptake reached a level of 80.13 psig (to prevent formation of two much polymer in the reactor), which ever occurred first (see section S5.1 for more details). [b]in kg/(mol·h).

Table S2.5.3. Ethylene/tBA copolymerization with isolated nickel complex **1.**

Entry[a]	T (ºC)	t (min)	Act. (kg/(mol·h))	$M_w/10^3$	PDI	%Mol t-BA	Tm (ºC)
1	90	37	618	54.7	2.07	2.17	110.8
2	90	37	595	54.3	2.17	2.20	109.4
3	90	37	659	53.1	2.20	2.24	109.9
4	90	54	517	55.9	2.08	2.10	111.4
5	90	45	604	55.8	2.12	2.06	111.3
6	90	44	575	50.6	2.31	2.26	109.6
7	90	33	848	56.5	2.12	2.01	110.3
8	90	32	871	58.7	2.13	1.97	110.2

[a]V(total)=5 mL, [**1**]=0.25 μmol, [tBA]=0.05 M, ethylene pressure=400 psi. Polymerization runs were stopped when ethylene uptake reached a level of 80.13 psig to prevent formation of two much polymer in the reactor.

Table S2.5.4. Ethylene/tBA copolymerization with isolated nickel complex **2**.

Entry[a]	Cat. (μmol)	tBA (M)	T (ºC)	t (min)	Act. (kg/(mol·h))	Mw	PDI	%Mol t-BA	Tm (ºC)
1	0.25	0.05	70	60	204	16.1	2.30	0.72	120.9
2	0.25	0.05	70	60	208	16.2	2.16	0.71	121.4
3	0.25	0.05	70	60	204	17.3	2.29	0.83	121.0
4	0.25	0.05	70	60	208	16.3	2.28	0.74	120.9
5	0.25	0.05	90	60	404	10.6	2.10	0.71	120.6
6	0.25	0.05	90	60	444	10.0	2.04	0.73	120.7
7	0.25	0.05	90	22	595	10.3	2.26	0.72	121.2
8	0.25	0.05	90	56	481	9.6	2.30	0.75	121.0
9	0.25	0.05	100	47	657	8.2	2.01	0.72	121.0
10	0.25	0.05	100	50	620	8.2	2.22	0.73	120.2
11	0.25	0.05	100	46	634	8.0	2.12	0.64	120.6
12	0.5	0.1	90	60	262	9.0	2.28	1.40	115.5
13	0.5	0.1	90	60	262	9.0	1.99	1.36	115.0
14	0.5	0.15	90	60	210	7.9	1.97	1.97	110.6
15	0.5	0.15	90	60	200	7.4	2.24	2.04	109.8
16	0.5	0.15	90	60	204	7.5	2.30	1.98	111.6

[a]V(total)=5 mL, [Ni]=0.25 μmol, ethylene pressure=400 psi. Polymerization runs were stopped when t=1 h or ethylene uptake reached 80.13 psi (<1 h), which ever occurred first.

5.5 Supplemental figures for ethylene/tBA copolymerizatin with different tBA concentration

Data for these figures are extracted from Table S2.5.2~S5.4 (Red: **1**, blue: **2**)

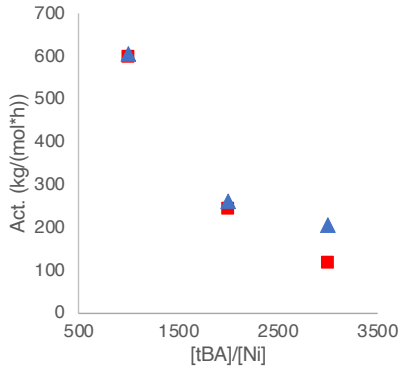

Figure S2.5.1. Catalytic activity of **1**/**2** with different equiv. of tBA

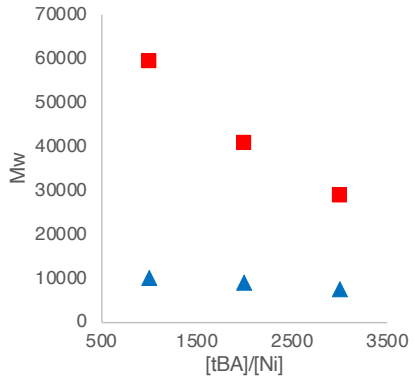

Figure S2.5.2. Molecular weights of ethylene/tBA copolymers with different equiv. of tBA

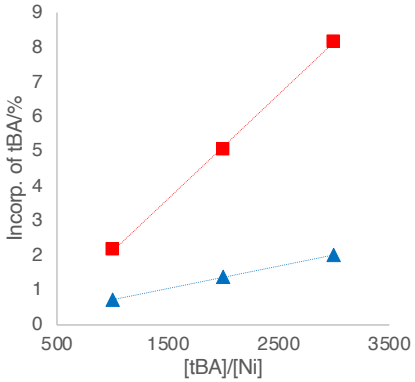

Figure S2.5.3. tBA incorporation of ethylene/tBA copolymers with different equiv. of tBA

6 NMR Characterization of ethylene/tBA copolymers

Methods: NMR spectra of ethylene/tBA copolymers were recorded on a Bruker 400 MHz using o-dichlorobenzene at 120 °C. ^{1}H NMR analysis of copolymers were done using a relaxation time (0.2 s), and an acquisition time (1.8 s) with the number of FID's collected per sample (512). ^{13}C{^{1}H} NMR analysis of copolymers were done using 90° pulse of 17.2 μs, a relaxation time (22.0 s), an acquisition time (5.3 s), and inverse-gated decoupling with the number of FID's collected per sample (1536).

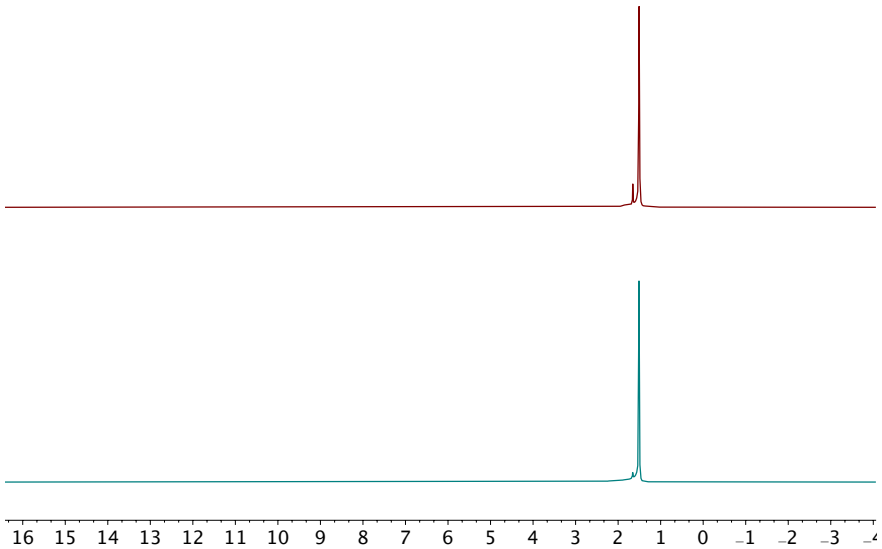

Figure S2.6.1. ^{1}H NMR spectra of ethylene/tBA copolymer P1 (top, collected from Table S2.5.3, entry 2) and P2 (bottom, collected from Table S2.5.4, entry 7)

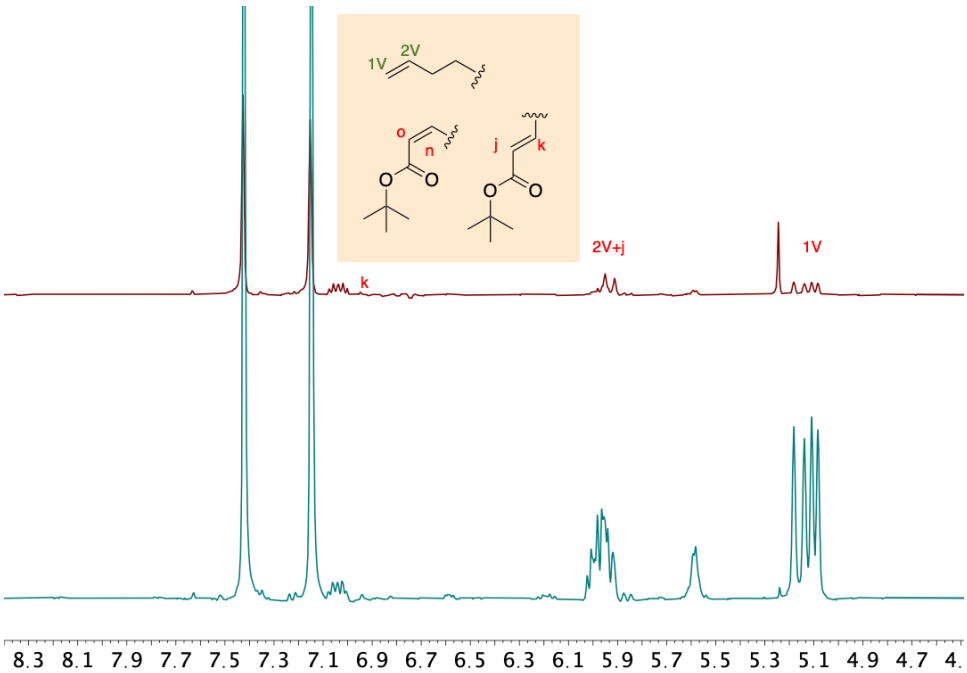

Figure S2.6.2. ^{1}H NMR spectra of ethylene/tBA copolymer P1 (top, collected from Table S2.5.3, entry 2) and P2 (bottom, collected from Table S2.5.4, entry 7): Part 2. Assignment is based on ^{1}H-^{1}H COSY NMR spectrum (Figure S2.6.3) and ref 37.

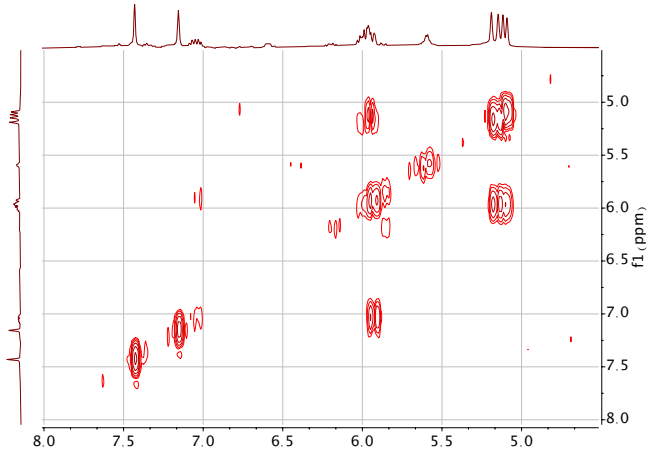

Figure S2.6.3. ^{1}H-^{1}H COSY NMR spectrum of ethylene/tBA copolymer P2 (collected from Table S2.5.4, entry 7)

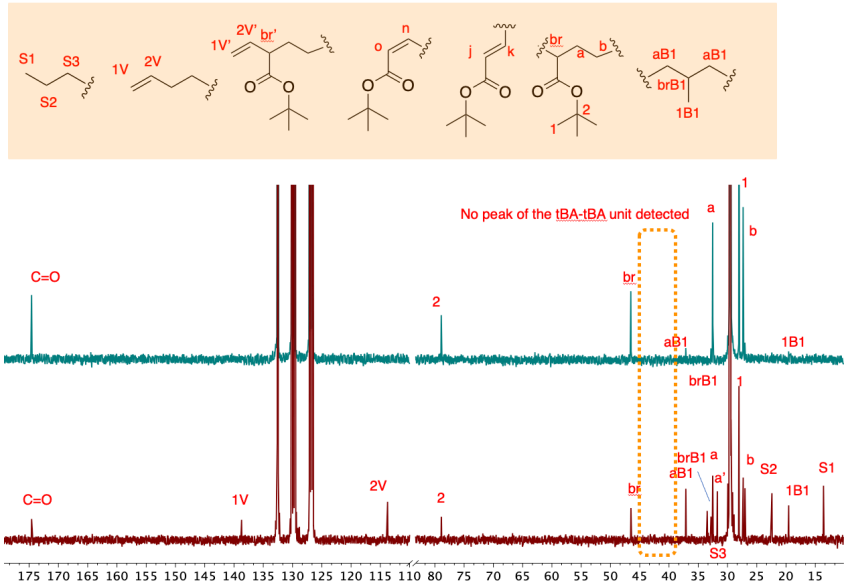

Figure S2.6.4. ^{13}C{^{1}H} NMR spectra of ethylene/tBA copolymer P1 (top, collected from Table S2.5.3, entry 2) and P2 (bottom, collected from Table S2.5.4, entry 7). Assignment is based on ref 37.

7. GPC curves of ethylene/tBA copolymers

Conventional GPC & Composition Results

LIMS #:	19-3295	Description:	*Library 370217 Vial 11*	Date:	5/7/19 13:03
Project:		Report by:			
For:	FileProc	Method:	Not Selected		

MWD Results: Conventional GPC		*Quadrant Analysis*			*Run Parameters:*	
Mn	43,280	25%	202260		Conc	1.8000
Mp	77,200	50%	94690	20	Inj. Vol.	480.0
Mv	88,500	75%	53950		Mass Inj.	0.8550
Mw	97,160	100%	20980		MassRec.	98.93%
Mz	178,790	Whole	67560		*System Parameters:*	
PDI	2.25	50% Ratio	3.96	-60	Flow Rate	1.0008
				271.64	Flow Marker	18.206
Comonomer Type	Octene				Ref Flow Marker	18.192
Avg SCB/1000TC	24.37				Rec. Flow Rate	
Avg Wt% Comonomer	19.7					
Avg Corrected Wt%	19.49					

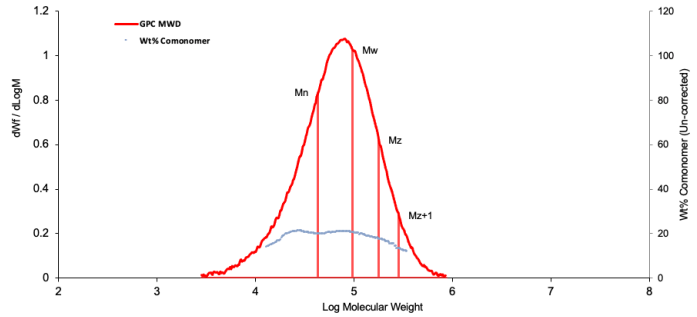

Figure S2.7.1. GPC curve of ethylene/tBA copolymer (Table S2.5.2, entry 1).

Conventional GPC & Composition Results

LIMS #:	19-6521	Description:	*Library 371847 Vial 43*	Date:	8/27/19 5:06
Project:		Report by:			
For:	FileProc	Method:	Not Selected		

MWD Results: Conventional GPC		*Quadrant Analysis*			*Run Parameters:*	
Mn	26,270	25%	112300		Conc	1.8000
Mp	48,930	50%	55950	0	Inj. Vol.	480.0
Mv	51,300	75%	32590		Mass Inj.	0.8550
Mw	55,810	100%	12700		MassRec.	76.95%
Mz	96,690	Whole	40040		*System Parameters:*	
PDI	2.12	50% Ratio	3.71	-60	Flow Rate	0.9989
				271.64	Flow Marker	18.182
Comonomer Type	Octene				Ref Flow Marker	18.201
Avg SCB/1000TC	4.06				Rec. Flow Rate	
Avg Wt% Comonomer	3.57					
Avg Corrected Wt%	3.25					

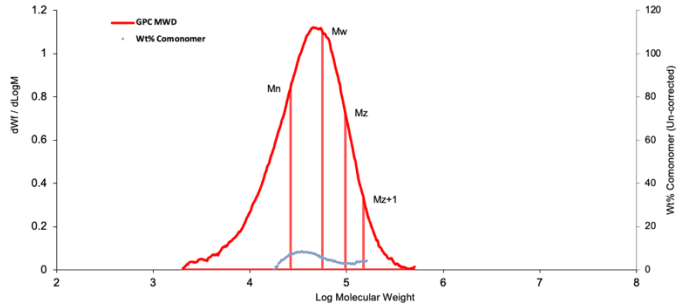

Figure S2.7.2. GPC curve of ethylene/tBA copolymer (Table S2.5.3, entry 5).

Conventional GPC & Composition Results

LIMS #:	19-6834	Description:	Library 372462 Vial 10	Date:	9/3/19 12:57
Project:		Report by:			
For:	FileProc	Method:	Not Selected		

MWD Results: Conventional GPC		Quadrant Analysis			Run Parameters:	
Mn	3,670	25%	16640		Conc	1.8000
Mp	7,530	50%	8190	10	Inj. Vol.	480.0
Mv	7,480	75%	4650		Mass Inj.	0.8550
Mw	8,170	100%	1780		MassRec.	114.47%
Mz	14,600	Whole	5760		System Parameters:	
PDI	2.22	50% Ratio	3.86	-60	Flow Rate	0.9980
				271.64	Flow Marker	18.182
Comonomer Type	Octene				Ref Flow Marker	18.219
Avg SCB/1000TC	9.47				Rec. Flow Rate	
Avg Wt% Comonomer	9.36					
Avg Corrected Wt%	7.58					

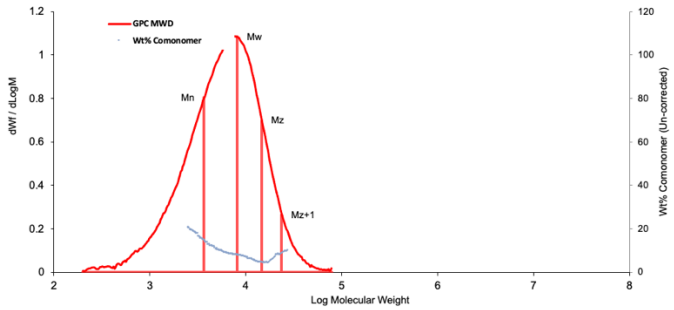

Figure S2.7.3. GPC curve of ethylene/tBA copolymer (Table S2.5.4, entry 10).

8 Kinetic Measurements

8.1 Procedures

Ethylene insertion(e1&e2). Unless specified, 0.0118 mmol of nickel complexes prepared using the above procedure was dissolved in C_6D_5Cl with pyridine in the glove box. The mixture was transferred to a J-Young tube and frozen in a liquid nitrogen bath. Then ethylene was added quantitatively via a gas bulb attached to the high vacuum line[72] prefilled with ethylene. The resulting mixture was warmed up to thawing temperature and shaken vigorously prior to pre-heated NMR probe for acquisition of spectra at specified temperature. Solvent residues were used as an internal standard. The decay of the concentration of the nickel (trimethylsilyl)methyl pyridine complex as well as the decay of the concentration of ethylene was recorded based on the ratio of the integration of bound phosphine to that of the internal standard accordingly.

tBA insertion (a1&a3). Unless specified, 0.0118 mmol of nickel complexes prepared using the above procedure was dissolved in protio-PhCl or 90% protio-PhCl/10% C_6D_5Cl with pyridine

in the glove box. The mixture was frozen in the coldwell pre-cooled by a liquid nitrogen bath, and *t*-butyl acrylate (tBA, or PhCl solution of tBA) was added via syringe (Total volume=0.75 ml). The resulting mixture was warmed up to thawing temperature and shaken vigorously prior to transferring to pre-heated NMR probe for acquisition of spectra at 50 ℃. NMR monitoring of tBA insertion were performed with a capillary insert with $CDCl_3$ solution of $MePPh_3^+Br^-$ inside as an external standard and the decay of the concentration of the nickel (trimethylsilyl)methyl pyridine complex was recorded based on the ratio of the integration of bound phosphine to that of the external standard accordingly.

tBA insertion into ethylene inserted species (a2). Unless specified, 0.0118 mmol of nickel complexes prepared using the above procedure was dissolved in C_6D_5Cl with pyridine in the glove box (total volume = Y mL, see below for clarification). The mixture was transferred to a J-Young tube, degassed via three freeze-pump-thaw cycles and kept frozen in a liquid nitrogen bath. Then ethylene was added via a gas bulb attached to the high vacuum line[6] prefilled with ethylene. The mixture was then warm up to room temperature and shaken vigorously. Decay of ethylene and decay of the nickel trimethylsilyl methyl complex were monitored via ^1H and ^{31}P NMR. Roughly at ~50% conversion of the nickel trimethylsilyl methyl complex, the mixture was frozen in a liquid nitrogen bath. Then residue ethylene was removed via four freeze-pump-thaw-backfill (with Ar or N_2) cycles. Complete removal of ethylene (>99.95%) was confirmed by ^1H NMR. Then the mixture was transferred to pre-heated NMR probe for acquisition of one sample spectrum at 50 ℃. Then the mixture was transferred into a glove box and frozen in the coldwell pre-cooled by a liquid nitrogen bath. Then *t*-butyl acrylate (tBA, or PhCl solution of tBA, X mL) was added via a syringe or micro-syringe (X+Y=0.75 mL) and the mixture was frozen again. The resulting mixture was warmed up to thawing temperature and shaken vigorously prior to transferring to pre-heated NMR probe. Spectra was collected immediately after reaching the

desired temperature. NMR monitoring of tBA insertion were performed with $P(O)Ph_3$ (0.2~0.4 equiv. to the nickel complex) as an internal standard and the decay of the concentration of the nickel (trimethylsilyl)methyl pyridine complex was recorded based on the ratio of the integration of bound phosphine to that of the internal standard in ^{31}P NMR accordingly.

Ethylene insertion into tBA inserted species (e3). Unless specified, 0.0059 mmol of the nickel complex **3** prepared using the above procedure was dissolved in C_7D_8 with pyridine in the glove box (total volume = 0.75 mL). The mixture was transferred to a J-Young tube, degassed via three freeze-pump-thaw cycles and kept frozen in a liquid nitrogen bath. Then ethylene was added via a gas bulb attached to the high vacuum line[6] prefilled with ethylene. The resulting mixture was warmed up to thawing temperature prior to pre-heated NMR probe for acquisition of spectra at the specified temperature. Solvent residues were used as an internal standard. The decay of the concentration of the nickel (trimethylsilyl)methyl pyridine complex as well as the decay of the concentration of ethylene was recorded based on the ratio of the integration of bound phosphine to that of the internal standard accordingly.

8.2 Kinetic Plots of tBA Insertion into Nickel (Trimethylsilyl)methyl Pyridine Complexes (a1)

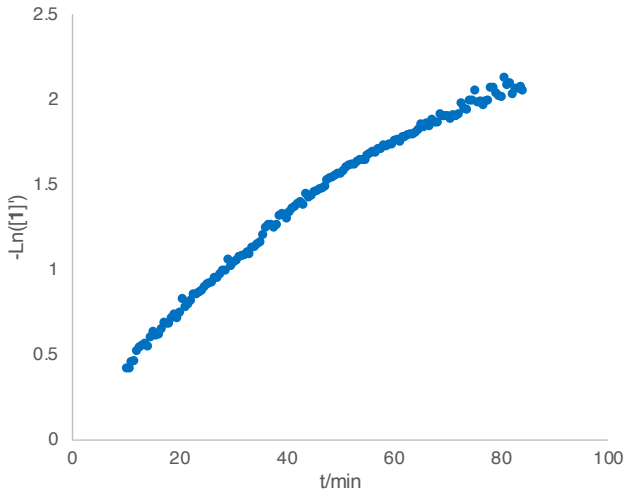

Figure S2.8.1. Log plot of relative concentration of **1** ([**1'**]=[**1**]/[**St**], St: internal standard) vs time as monitored by ^1H NMR spectroscopy.

(Note for Figure S2.8.1) Procedure: In the glove box, **1** (0.0059 mmol, 5.8 mg) was dissolved in C_6D_6 and the mixture was frozen in the coldwell pre-cooled by a liquid nitrogen bath, and *t*-butyl acrylate (100 equiv., 0.086 ml) was added via syringe (Total volume=0.75 ml). The resulting mixture was warmed up to thawing temperature prior to pre-heated NMR probe for acquisition of spectra at 30°C. No capillary was used the decay of the concentration of the nickel (trimethylsilyl)methyl pyridine complex was recorded based on the ratio of the integration of bound pyridine to that of the solvent residue.

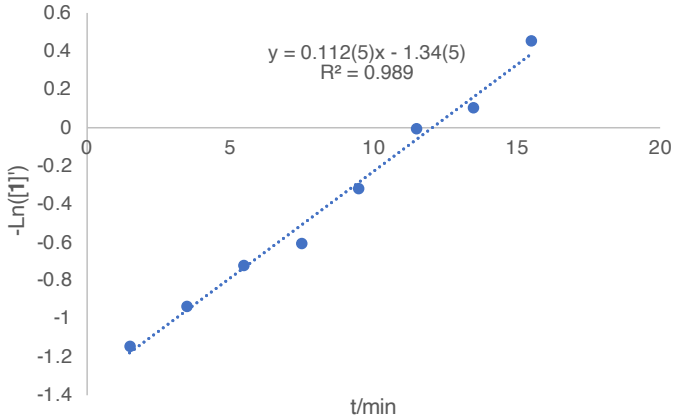

Figure S2.8.2. Log plot of relative concentration of **1** ([**1'**]=[**1**]/[**St**], St: external standard) vs time as monitored by ^{31}P NMR spectroscopy. Solvent: PhCl-H5. Temperature: 50 °C. Initial concentration: $[\mathbf{1}]_0$=0.0157 M; $[tBA]_0$=1.178 M (75 equiv.); $[py]_0$=0.0315 M (2 equiv.).

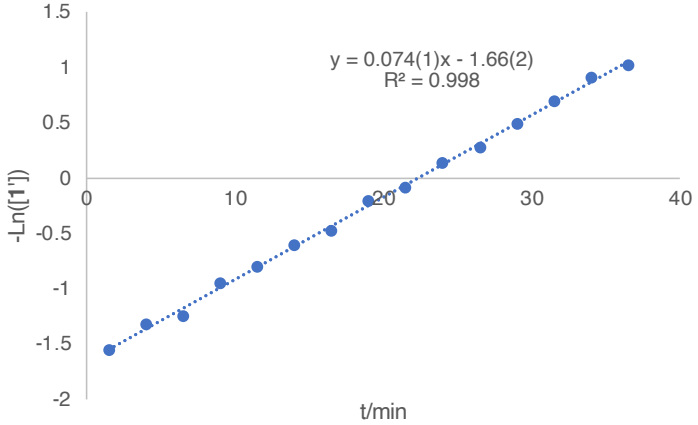

Figure S2.8.3. Log plot of relative concentration of **1** ([**1'**]=[**1**]/[**St**], St: external standard) vs time as monitored by ^{31}P NMR spectroscopy. Solvent: PhCl-H5. Temperature: 50 °C. Initial concentration: $[\mathbf{1}]_0$=0.0157 M; $[tBA]_0$=0.785 M (50 equiv.); $[py]_0$=0.0315 M (2 equiv.).

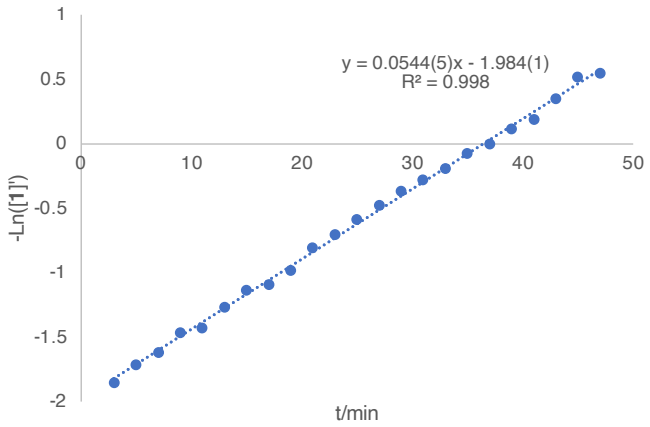

Figure S2.8.4. Log plot of relative concentration of **1** ([**1'**]=[**1**]/[**St**], St: external standard) vs time as monitored by ^{31}P NMR spectroscopy. Solvent: PhCl-H5. Temperature: 50 °C. Initial concentration: [**1**]$_0$=0.0157 M; [tBA]$_0$=0.550 M (35 equiv.); [py]$_0$=0.0315 M (2 equiv.).

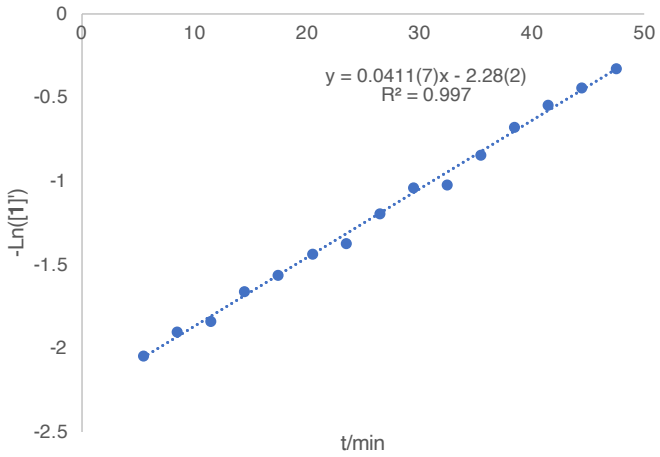

Figure S2.8.5. Log plot of relative concentration of **1** ([**1'**]=[**1**]/[**St**], St: external standard) vs time as monitored by ^{31}P NMR spectroscopy. Solvent: PhCl-H5. Temperature: 50 °C. Initial concentration: [**1**]$_0$=0.0157 M; [tBA]$_0$=0.393 M (25 equiv.); [py]$_0$=0.0315 M (2 equiv.).

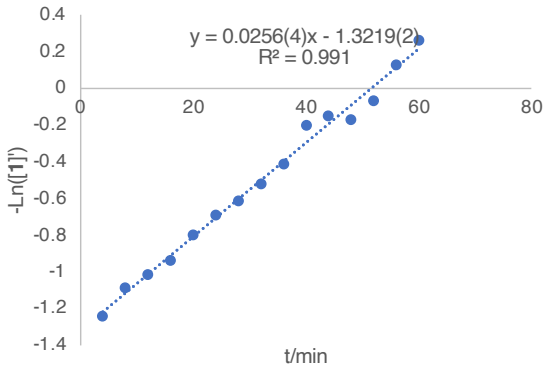

Figure S2.8.6. Log plot of relative concentration of 1 ([1']=[1]/[St], St: external standard) vs time as monitored by ^{31}P NMR spectroscopy. Solvent: PhCl-H5. Temperature: 50 °C. Initial concentration: $[1]_0$=0.0157 M; $[tBA]_0$=0.393 M (25 equiv.); $[py]_0$=0.0471 M (3 equiv.).

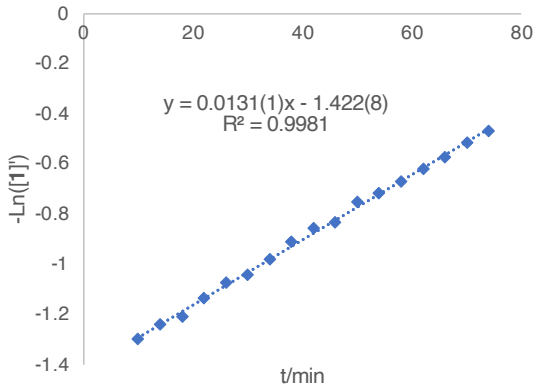

Figure S2.8.7. Log plot of relative concentration of **1** ([**1'**]=[**1**]/[**St**], St: external standard) vs time as monitored by ^{31}P NMR spectroscopy. Solvent: PhCl-H5. Temperature: 50 °C. Initial concentration: $[\mathbf{1}]_0$=0.0157 M; $[tBA]_0$=0.393 M (25 equiv.); $[py]_0$=0.0942 M (6 equiv.).

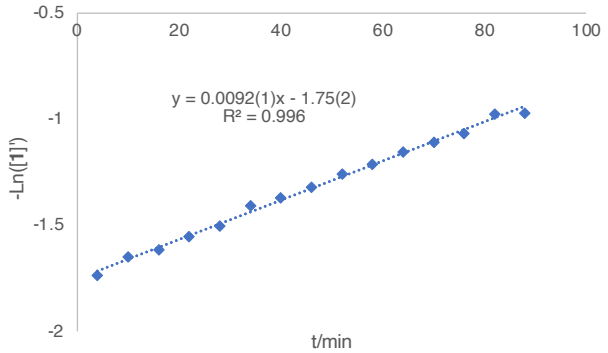

Figure S2.8.8. Log plot of relative concentration of **1** ([**1'**]=[**1**]/[**St**], St: external standard) vs time as monitored by ^{31}P NMR spectroscopy. Solvent: PhCl-H5. Temperature: 50 °C. Initial concentration: $[\mathbf{1}]_0$=0.0157 M; $[tBA]_0$=0.393 M (25 equiv.); $[py]_0$=0.142 M (9 equiv.).

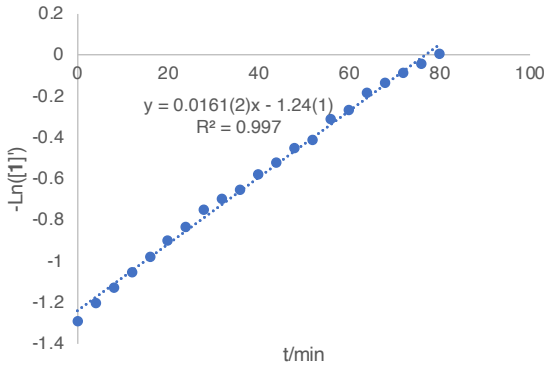

Figure S2.8.9. Log plot of relative concentration of **1** ([**1'**]=[**1**]/[**St**], St: external standard) vs time as monitored by ^{31}P NMR spectroscopy. Solvent: PhCl-H5. Temperature: 50 °C. Initial concentration: [**1**]$_0$=0.0157 M; [tBA]$_0$=0.157 M (10 equiv.); [py]$_0$=0.0315 M (2 equiv.).

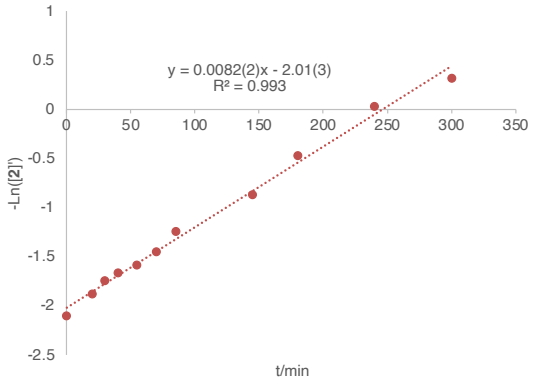

Figure S2.8.10. Log plot of relative concentration of **2** ([**2'**]=[**2**]/[**St**], St: external standard) vs time as monitored by ^{31}P NMR spectroscopy. Solvent: PhCl-H5. Temperature: 50 °C. Initial concentration: [**2**]$_0$=0.0157 M; [tBA]$_0$=1.57 M (100 equiv.); [py]$_0$=0.157 M (10 equiv.).

8.3 Kinetic Plots of Ethylene Insertion into Nickel Alkyl Pyridine Complexes (e1/e2)

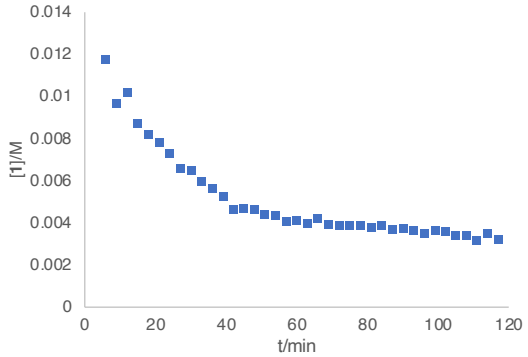

Figure S2.8.11. Plot of concentration of **1** vs time as monitored by ^{31}P NMR spectroscopy. Solvent: PhCl-D5. Temperature: 50 °C. Initial concentration: [**1**]$_0$=0.0157 M; [Ethylene]$_0$=0.236 M (15 equiv.); [py]$_0$=0.0315 M (2 equiv.).

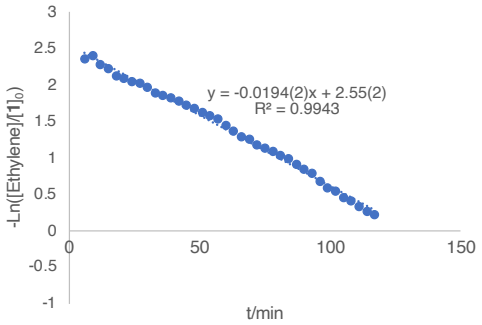

Figure S2.8.12. Log plot of relative concentration of ethylene ([Ethylene']=[Ethylene]/[**1**]$_0$) vs time as monitored by ^{1}H NMR spectroscopy. Solvent: PhCl-D5. Temperature: 50 °C. Initial concentration: [**1**]$_0$=0.0157 M; [Ethylene]$_0$=0.236 M (15 equiv.); [py]$_0$=0.0315 M (2 equiv.).

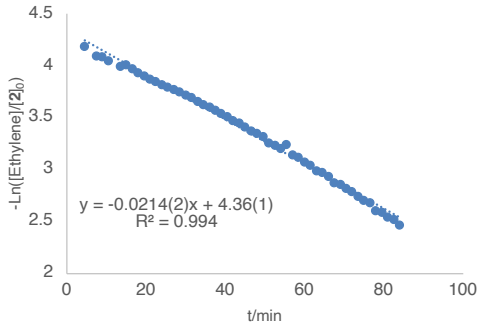

Figure S2.8.13. Log plot of relative concentration of ethylene ([Ethylene']=[Ethylene]/[**2**]$_0$) vs time as monitored by ^{1}H NMR spectroscopy. Solvent: PhCl-D5. Temperature: 50 °C. Initial concentration: [**1**]$_0$=0.0157 M; [Ethylene]$_0$=0.236 M (15 equiv.); [py]$_0$=0.0315 M (2 equiv.).

8.4 tBA Insertion into Ethylene Inserted Species (a2)

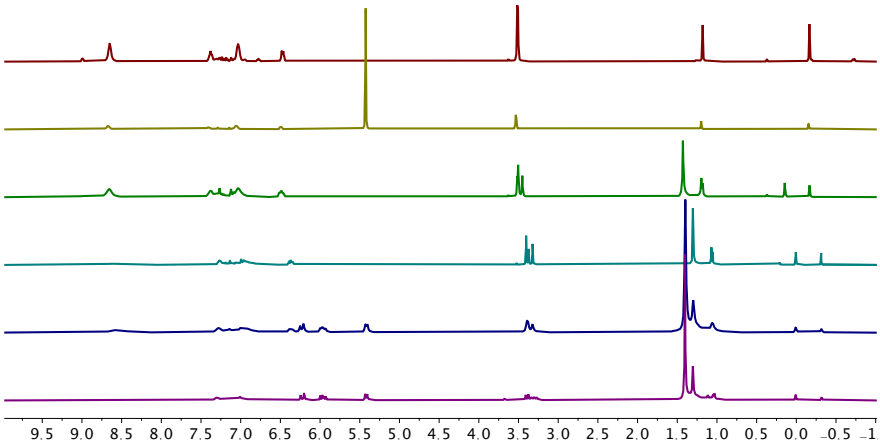

Figure S2.8.14. ^{1}H NMR spectra of (from top to bottom, C_6D_5Cl): a) **1** +10 equiv. of pyridine; b) after addition of 25 equiv. of ethylene; c) after removal of ethylene; d) spectrum recollected at 50 °C; e) after addition of 15 equiv. of tBA; f) after quantitative conversion of ethylene inserted species. Solvent: PhCl-D5. Initial concentration: [**1**]$_0$=0.0157 M; [py]$_0$=0.157 M (10 equiv.).

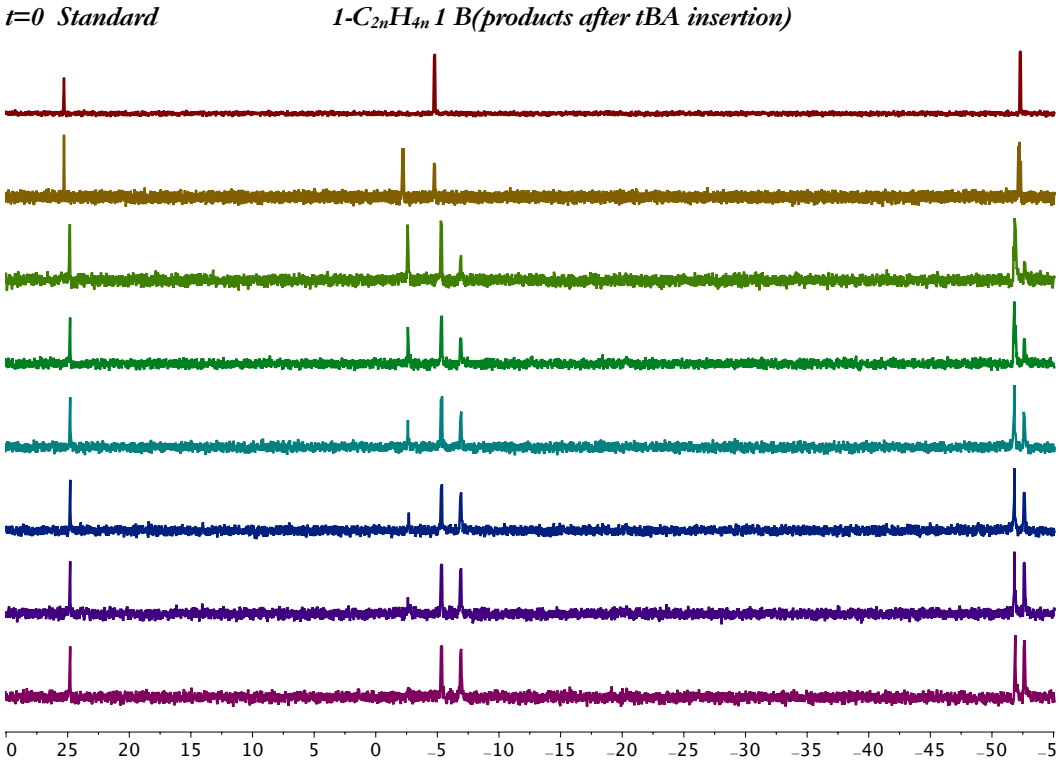

Figure S2.8.15. ^{31}P NMR monitoring of decay of ethylene inserted species (from top to bottom, C_6D_5Cl): a) **A** +10 equiv. of pyridine; b) before addition of tBA; c) after addition of 25 equiv. of ethylene; d) (last five) spectra collected every 20 s. Solvent: PhCl-D5. Temperature: 50 °C. Initial concentration: [**1**]$_0$=0.0157 M; [tBA]$_0$=0.236 M (15 equiv.); [py]$_0$=0.157 M (10 equiv.).

Kinetic Plot

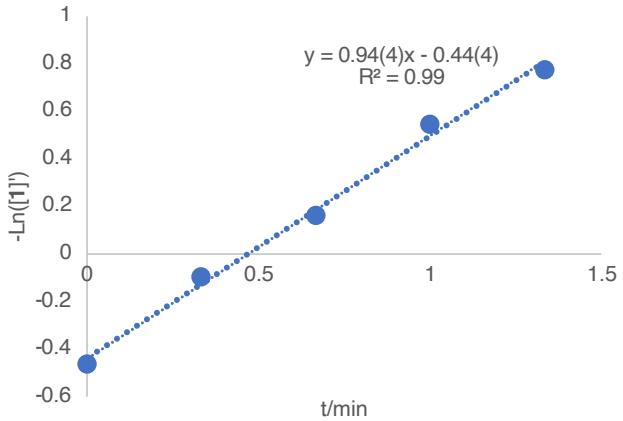

Figure S2.8.16. Log plot of relative concentration of **1** ([**1'**]=[**1**]/[**St**], St: internal standard) vs time as monitored by ^{31}P NMR spectroscopy. Solvent: PhCl-D5. Temperature: 50 °C. Initial concentration: [**1**]$_0$=0.0157 M; [tBA]$_0$=0.236 M (15 equiv.); [py]$_0$=0.157 M (10 equiv.).

8.5 Ethylene Insertion into tBA Inserted Species (e3)

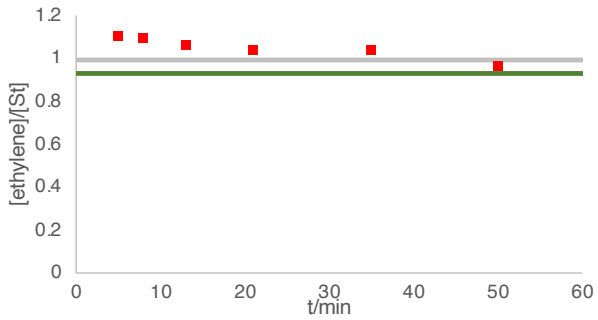

Figure S2.8.17. Plot of relative concentration of Ethylene ([Ethylene]/[St], St: external standard) vs time as monitored by ^{1}H NMR spectroscopy. Solvent: Tol-d8. Temperature: 50 °C. Initial concentration: [**1**]$_0$=0.0079 M; [Ethylene]$_0$=0.099 M (12.5 equiv.); [py]$_0$=0.079 M (10 equiv.). (red spots: measured value, grey line: 90% of initiatial concentration, green line: 85% of initiatial concentration)

As shown above, only 15% decrease of the concentration of ethylene in solution was observed. Therefore, ethylene concentration could be treated as a constant in first 50 minutes, which fits pseudo 1st order condition. A preliminary kinetic plot based on data collected in first 50 minutes was shown below (only the first half-life period involved).

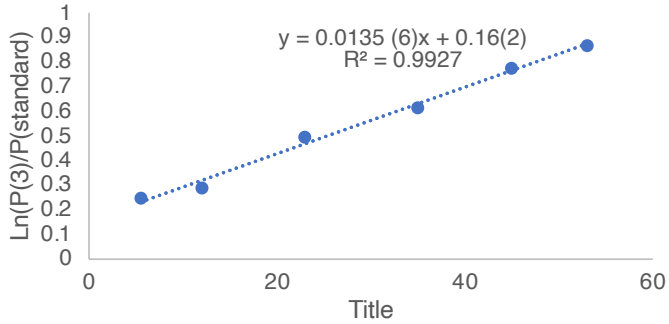

Figure S2.8.18. Log plot of relative concentration of **1** ([**1'**]=[**1**]/[**St**], St: internal standard) vs time as monitored by ^{1}H NMR spectroscopy. Solvent: Tol-d8. Temperature: 50 °C. Initial concentration: [**1**]$_0$=0.0079 M; [Ethylene]$_0$=0.099 M (12.5 equiv.), [py]$_0$=0.079 M (10 equiv.).

8.8 tBA Insertion into tBA Inserted Species

Discussion of Methods

Unless specified, data shown below come from experiments in part 2. As shown in Fig S4.1, phosphines in nickel (trimethylsilyl)methyl pyridine complex (**A**) and acylated nickel alkyl

complex (**B**, product of first tBA insertion) feature distinguished chemical shifts in ^{31}P NMR and they are also different from that of further inserted species. Based on changes of [**A**] and [**B**] over time, overall insertion rate of the second acrylate insertion can be obtained, which is shown below.

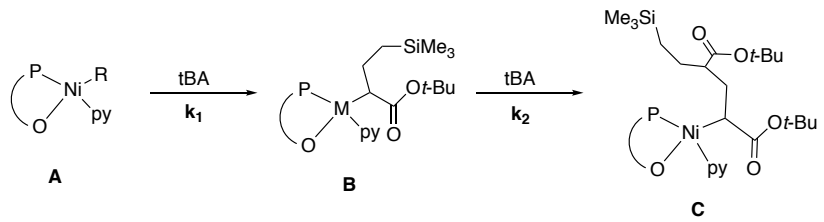

$$\frac{d[A]}{dt} = -k_1 \cdot [A] \quad \textbf{(i)}$$

$$[A] = [A]_0 \cdot e^{-k_1 t} \quad \textbf{(ii)}$$

$$\frac{d[B]}{dt} = k_1 \cdot [A] - k_2 \cdot [B] \quad \textbf{(iii)}$$

Based on (ii) and (iii),

$$k_2 \cdot [B] + \frac{d[B]}{dt} = k_1 \cdot [A]_0 \cdot e^{-k_1 t} \quad \textbf{(iv) ->}$$

$$k_2 \cdot e^{k_2 t} \cdot [B] + e^{k_2 t} \cdot \frac{d[B]}{dt} = k_1 \cdot [A]_0 \cdot e^{k_2 t} \cdot e^{-k_1 t} \quad \textbf{(v) ->}$$

$$\frac{d}{dt}(e^{k_2 t} \cdot [B]) = k_1 \cdot [A]_0 \cdot e^{(k_2 - k_1)t} \quad \textbf{(vi) ->}$$

$$e^{k_2 t} \cdot [B] = \frac{k_1}{k_2 - k_1} \cdot [A]_0 \cdot e^{(k_2 - k_1)t} + \mathrm{C} \quad \textbf{(vii) ->}$$

$$[B] = \frac{k_1}{k_2 - k_1} \cdot [A]_0 \cdot e^{-k_1 t} + \mathrm{C} \cdot e^{k_2 t} \quad \textbf{(viii)}$$

$$\mathrm{t=0,\ [B]=0,\ \therefore\ C} = -\frac{k_1}{k_2 - k_1} \cdot [A]_0 \quad \textbf{(ix)}$$

Based on (viii) and (ix),

$$[B] = \frac{k_1}{k_2 - k_1} \cdot [A]_0 \cdot (e^{-k_1 t} - e^{k_2 t}) \quad \textbf{(x)}$$

$$\text{(viii)/(iii) ->} \frac{[B]}{[A]} = \frac{k_1}{k_2 - k_1} \cdot (1 - e^{-(k_2 - k_1)t}) \quad \textbf{(xi)}$$

$$\text{If } p = k_2 - k_1, \frac{[B]}{[A]} = \frac{k_1}{p} \cdot (1 - e^{-pt}) \quad \textbf{(xii)}$$

[B]/[A] can be obtained from spectra, thereby p is solved via minimizing the difference of calculated curve (y axis: [B]/[A], x axis: time) and curve generated from exp in excel ("solver" add-on)

Sample Spectra

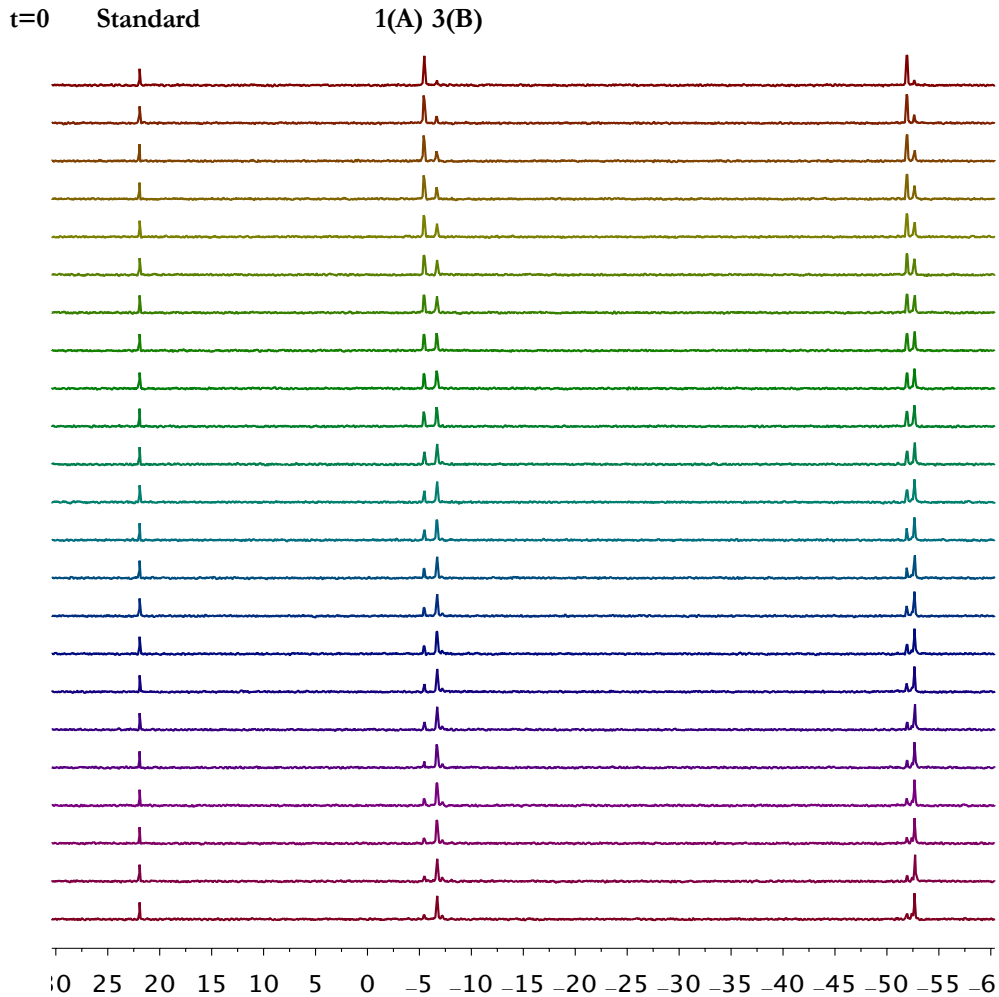

Figure S2.8.19, ^{31}P Plot of NMR monitoring of tBA insertion into **1.** Solvent: PhCl-H5. Temperature: 50 °C. Initial concentration: [**1**]$_0$=0.0157 M; [tBA]$_0$=0.550 M (35 equiv.); [py]$_0$=0.0315 M (2 equiv.).

Kinetic Plots

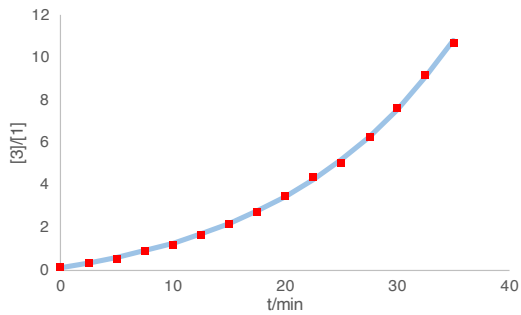

Figure S2.8.20. Plot of [**3**]/[**1**] v.s. time during tBA insertion. Solvent: PhCl-H5. Temperature: 50 °C. Initial concentration: $[\mathbf{1}]_0$=0.0157 M; $[tBA]_0$=0.785 M (50 equiv.); $[py]_0$=0.0315 M (2 equiv.). Red spots: experimental data; blue line: fitted curve.

- p=-0.0635, SSR (sum of squared residues) =0.0979, k_2=0.0107

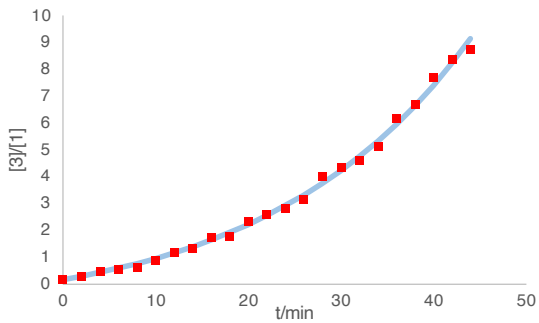

Figure S2.8.21. Plot of [**3**]/[**1**] v.s. time during tBA insertion Solvent: PhCl-H5. Temperature: 50 °C. Initial concentration: $[\mathbf{1}]_0$=0.0157 M; $[tBA]_0$=0.550 M (35 equiv.); $[py]_0$=0.0315 M (2 equiv.). Red spots: experimental data, blue line: fitted curve.

- p=-0.0461, SSR=0.588, k_2=0.0083

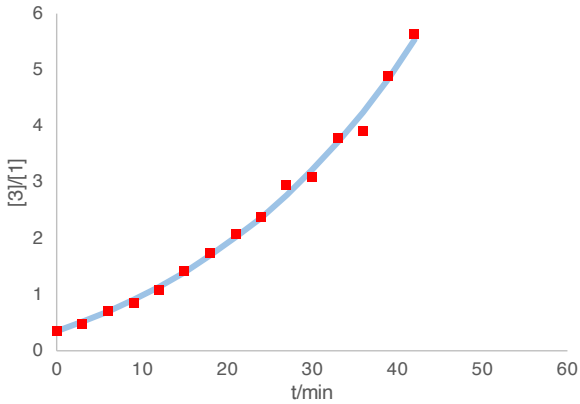

Figure S2.8.22. Plot of [**3**]/[**1**] v.s. time during tBA insertion Solvent: PhCl-H5. Temperature: 50 °C. Initial concentration: $[\mathbf{1}]_0$=0.0157 M; $[tBA]_0$=0.393 M (25 equiv.); $[py]_0$=0.0315 M (2 equiv.). Red spots: experimental data, blue line: fitted curve.

- p=-0.0356, SSR=0.206, k_2=0.0055

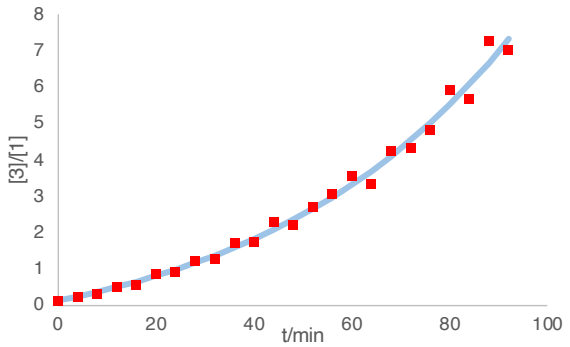

Figure S2.8.23. Plot of [**3**]/[**1**] v.s. time during tBA insertion. Solvent: PhCl-H5. Temperature: 50 °C. Initial concentration: [**1**]$_0$=0.0157 M; [tBA]$_0$=0.393 M (25 equiv.); [py]$_0$=0.0471 M (3 equiv.). Red spots: experimental data, blue line: fitted curve.

- p=-0.0195, SSR=1.133, k_2=0.0061

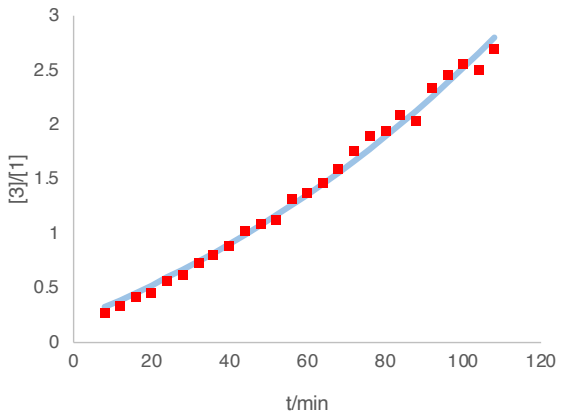

Figure S2.8.24. Plot of [**3**]/[**1**] v.s. time during tBA insertion. Solvent: PhCl-H5. Temperature: 50 °C. Initial concentration: [**1**]$_0$=0.0157 M; [tBA]$_0$=0.393 M (25 equiv.); [py]$_0$=0.0942 M (6 equiv.). Red spots: experimental data, blue line: fitted curve.

- p=-0.0083, SSR=0.118, k_2=0.0048

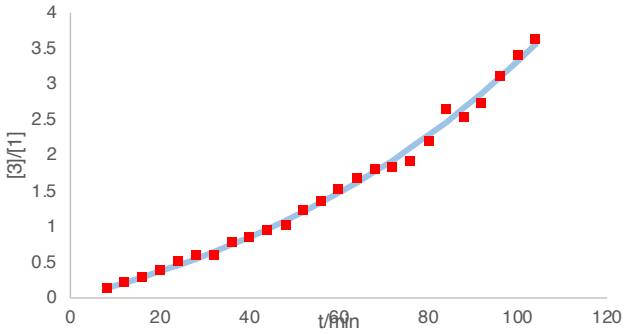

Figure S2.8.25. Plot of [**3**]/[**1**] v.s. time during tBA insertion Solvent: PhCl-H5. Temperature: 50 °C. Initial concentration: [**1**]$_0$=0.0157 M; [tBA]$_0$=0.157 M (10 equiv.); [py]$_0$=0.0315 M (2 equiv.). Red spots: experimental data, blue line: fitted curve.

- p=-0.0129, SSR=0.153, k_2=0.0032

Summary

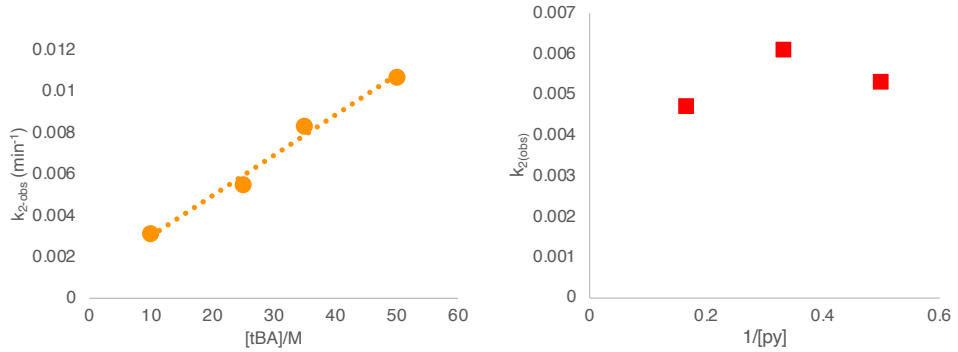

Figure S2.8.26. Plots (left: k_{obs} vs [tBA]; right: k_{obs} vs [py]) of coordination insertion of tBA into **3** (See Figure S2.8.20~S8.25 for details).

9 DFT calculation

Methods. Geometry optimizations in the gas phase were initially carried out using the GFN1-xTB method[73] as implemented in Entos Qcore Version 0.7.[74] The resulting structures were further optimized using hybrid meta-generalized gradient-approximation (hybrid meta-GGA) M06 functional[59] with Karlsruhe-family basis set of double-ζ valence def2-SVP[60-61] for all atoms as implemented in *Gaussian 16* rev. A.03.[75] Where possible, available X-ray crystal structures were used as an initial guess. The M06 functional was chosen as it performs better than many other functionals (e.g. ωB97X-D and TPSS) in predicting transition metal (TM) reaction barrier heights (TMBH21 dataset)[76-77] for reactions involving TMs.[75, 78] M06 has also been employed to study similar TM-catalyzed systems with excellent agreement with experimental results.[79-80] Minima and transition structures on the potential energy surface (PES) were confirmed as such by harmonic frequency analysis, showing respectively zero and one imaginary frequency, at the same level of theory. Where appropriate, intrinsic reaction coordinate (IRC) analyses[81-82] were performed to confirm that the found TSs connect to the right reactants and products.

Single point (SP) corrections were performed using M06 functional and def2-TZVP[60] basis set for all atoms. The implicit SMD continuum solvation model[62] was used to account for the solvent effect of chlorobenzene on the Gibbs energy profile. Gibbs energies were evaluated at the reaction temperature of 323.15 K, using a quasi-RRHO treatment of vibrational entropies.[83-84] Vibrational entropies of frequencies below 100 cm^{-1} were obtained according to a free rotor description, using a smooth damping function to interpolate between the two limiting descriptions. The free energies were further corrected using standard concentration of 1 mol/L, which was used in solvation calculations. SMD(chlorobenzene)-M06/def2-TZVP//M06/def2-SVP Gibbs energies are given and quoted in kcal mol^{-1} throughout. *Unless otherwise stated, these solvent-corrected values are used for discussion throughout the main text and in this supporting information.*

Non-covalent interactions (NCIs) were analyzed using NCIPLOT calculations.[85] The *.wfn* files for NCIPLOT were generated at M06/DGDZVP level of theory.[86-87] NCI indices calculated with NCIPLOT were visualized at a gradient isosurface value of $s = 0.5$ au. These are colored according to the sign of the second eigenvalue (λ_2) of the Laplacian of the density ($\nabla^2\rho$) over the range of -0.1 (blue = attractive) to +0.1 (red = repulsive). Molecular orbitals are visualized using an isosurface value of 0.05 throughout. All molecular structures and molecular orbitals were visualized using *PyMOL* software.[88] Geometries of all optimized structures (in *.xyz* format with their associated energy in Hartrees) are included in a separate folder named *structures_xyz* with an associated README file. All these data have been deposited with this Supporting Information. All Python scripts used for data analysis are taken from https://github.com/bobbypaton.

Conformational considerations. Where available, experimentally obtained X-ray crystal structures were used as initial guess for geometry optimization. Where different conformers exist in the

X-ray structures, all available conformers were used for geometry optimization and the final optimized, lowest energy structure is used. The ligand backbone from the lowest energy conformer is then kept fixed for all subsequent reaction paths. For olefin insertions, all possible coordination modes/orientations were considered in the geometry optimization and the lowest energy conformers are used for discussion.

9.1 Reaction pathways leading from POP-Ni-py (1)

9.1.1 The starting structure of POP-Ni-py (1)

The starting structure for the optimization of **POP-Ni-py** complex was taken from the experimentally obtained X-ray crystal structure. The henceforth optimized structure **1-c2** is shown in Figure S2.9.1. We found another optimized structure (**1**) that is lower in energy than **1-c2** and we take this as the zero energy reference for this reaction (Figure S2.9.1). Note that these two structures are essentially conformers and they differ in the spatial orientation of the trialkylsilylated polymer chain.

1	**1-c2**
ΔG = 0.0	ΔG = 9.8
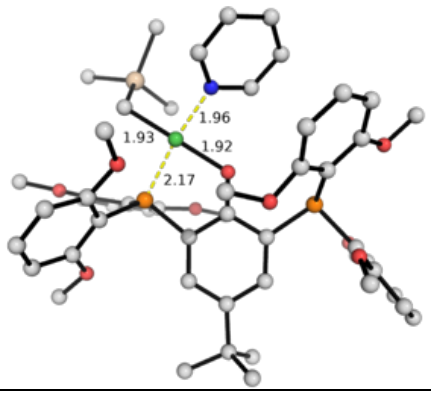	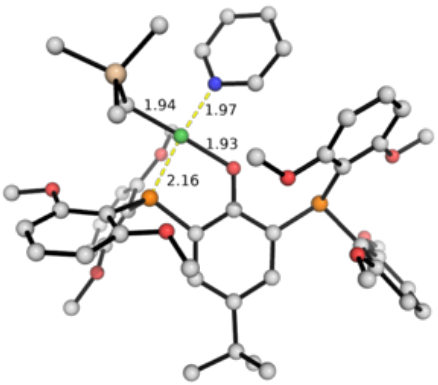

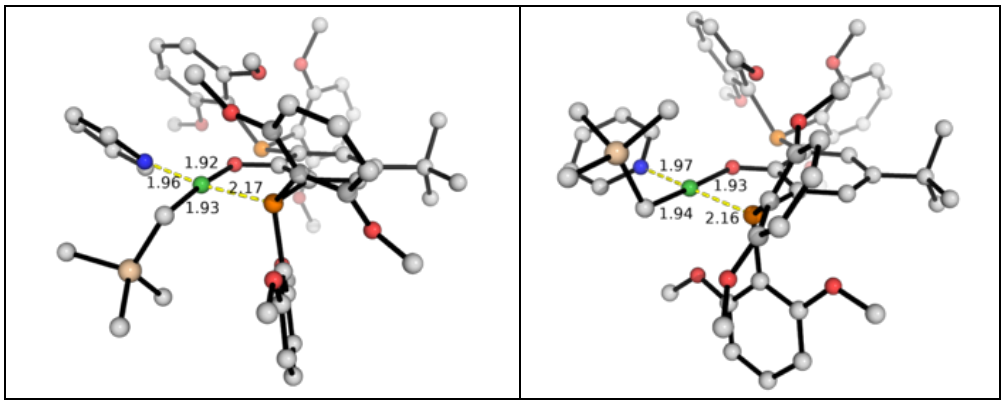

Figure S2.9.1. Optimized structures for the Ni(II) complex **POP-Ni-py**. The Gibbs energies are calculated at SMD (chlorobenzene)-M06/def2-TZVP//M06/def2-SVP level of theory and measured relative to the most sTable S2.pecies (**1**). Key bond distances are given in Å. Gibbs energy units are given in kcal mol^{-1}.

9.1.2 Ethylene-bound Ni(II) complex – displacement of pyridine by ethylene in POP-Ni-py

int1-et-c1	**int1-et-c2**
ΔG = 8.9	ΔG = 14.8
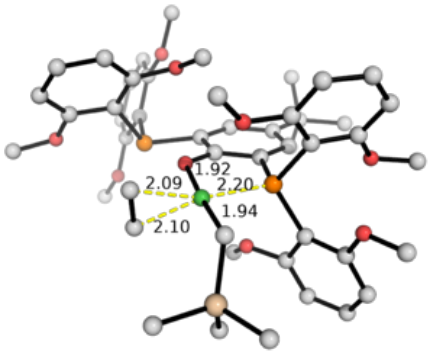	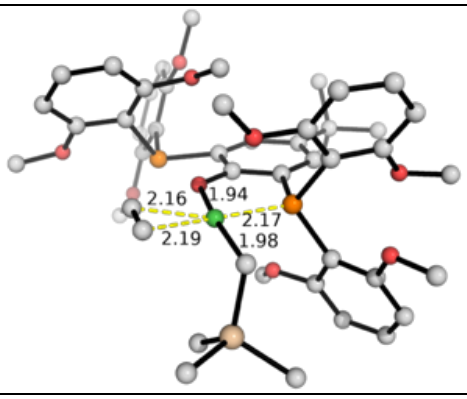

Figure S2.9.2. Optimized structures for the Ni(II) complex **POP-Ni-et**. The Gibbs energies are calculated relative to **POP-Ni-py** (**1**). Key bond distances are given in Å. Gibbs energy units are given in kcal mol^{-1}.

Herein we show the optimized structures of the Ni(II) complex where the pyridine ligand gets displaced by ethylene substrate. We denote these as **POP-Ni-et** complexes where the suffix "**et**" denotes ethylene. Two structures can be found (Figure S2.9.2). These differ in the orientations of the ethylene π-bond that is coordinated to the Ni-center. In **int1-et-c1**, the π-bond is perpendicular to the Ni square plane, whereas in **int1-et-c2**, the π-bond is parallel to and lying on the Ni square plane. Structure **int1-et-c1** is 5.9 kcal mol^{-1} more stable than **int1-et-c2**. For

the migratory insertion of ethylene substrate into the Ni–C bond, the ethylene has to be in **int1-et-c2** before insertion can occur (*vide infra*).

9.1.3 t-butylacrylate (tBA)-bound Ni(II) complex – displacement of pyridine by tBA in POP-Ni-py

We similarly show the optimized structures of the Ni(II) complex where the pyridine ligand gets displaced by t-butylacrylate (tBA) substrate. All possibilities were considered while minimizing / avoiding unphysical steric clashes. The optimized structures are given in Figure S2.9.3. We denote these as POP-Ni-ac complexes where the suffix "ac" denotes t-butylacrylate. tBA can coordinate either via the C=C π-bond or the O-atom of the carbonyl group. For the coordination via C=C π-bond to the Ni-center, both the C=C bond perpendicular (int1-ac-c1 and int1-ac-c2) and parallel (int1-ac-c3 and int1-ac-c4) to the Ni square plane can be found. As in the case of ethylene binding, the tBA binding with C=C π-bond perpendicular to the Ni square plane is lower in energy/more stable (by at least 4.4 kal mol^{-1}) than with C=C π-bond parallel to the Ni square plane. Comparing the latter two structures (int1-ac-c3 and int1-ac-c4) which the reaction must pass prior to migratory insertion, we found that int1-ac-c3, forming the observed tBA insertion product, is 5.1 kcal mol^{-1} more stable than int1-ac-c4, which forms the less favorable regioisomer (*vide infra*).

For tBA insertion, additionally, two structures with O-coordination were found (int1-ac-o1 and int1-ac-o2). These differ in the orientation of the *t*-butoxy group. Both these O-coordinated structures have lower energy than C=C π-bond coordinated species (by 2.2 kal mol^{-1} comparing the lowest energy coordination species, int1-ac-o1 and int1-ac-c1), suggesting that the initial coordination of tBA substrate would occur via O-coordination.

Coordination via C=C π-bond	
int1-ac-c1	**int1-ac-c2**
ΔG = 13.7	ΔG = 15.6

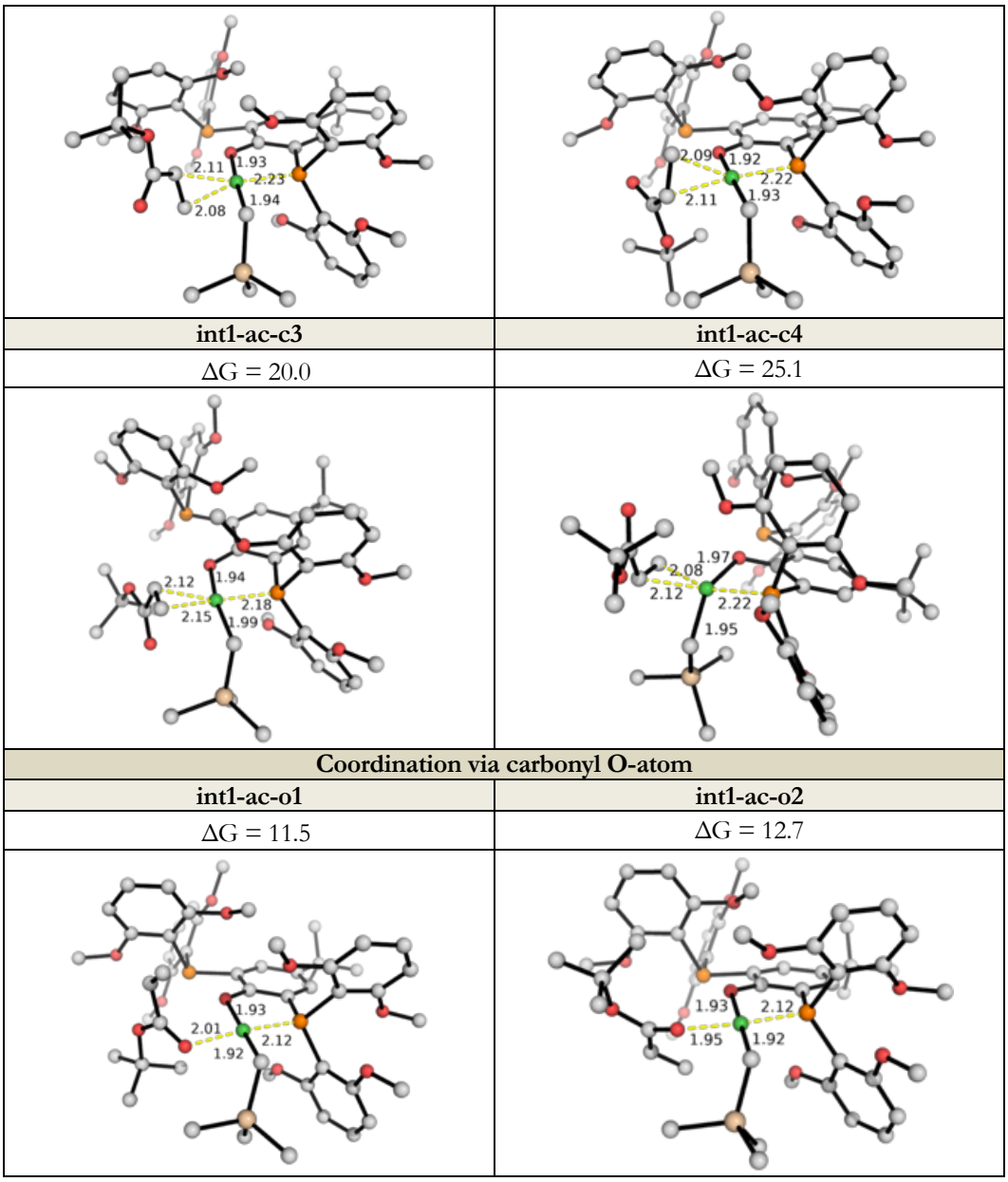

int1-ac-c3	int1-ac-c4
ΔG = 20.0	ΔG = 25.1
Coordination via carbonyl O-atom	
int1-ac-o1	**int1-ac-o2**
ΔG = 11.5	ΔG = 12.7

Figure S2.9.3. Optimized structures for the Ni(II) complex **POP-Ni-ac**. The Gibbs energies are calculated relative to **POP-Ni-py** (**1**). Key bond distances are given in Å. Gibbs energy units are given in kcal mol^{-1}.

*9.1.4 First insertion of substrate into POP-Ni-py (**1**)*

We investigated the comparative barriers of the insertion of ethylene vs tBA into catalyst **POP-Ni-py** (**1**). Figure S2.9.4 shows the reaction scheme and the Gibbs energy profile for the first insertion. The optimized TS structures and their key bond distances are given in Figure

S2.9.5. From this energy profile, we can see that the 2,1-insertion of acrylate tBA (**ts1-ac**, at 30.5 kcal mol^{-1}) has a lower activation barrier, by 2.6 kcal mol^{-1}, at the reaction temperature of 50 ^{o}C, than the insertion of ethylene (**ts1-et**, at 33.1 kcal mol^{-1}); the regioisomeric 1,2-insertion of tBA (**ts1-ac-r**) is the least favorable, with a barrier of 41.5 kcal mol^{-1}. Comparing the migratory insertion site selectivity of tBA (2,1-insertion vs 1,2-insertion), our calculation is in agreement with the observation that the migratory insertion of acrylate occurs at the β-carbon site of an α,β-unsaturated carbonyl, akin to conjugate addition.[10, 18, 24] Using simple transition state theory (TST), this translates to a rate of roughly **ts1-ac : ts1-et : ts1-ac-r** = 1 : 57 : 27 million. With this energy profile, it implicates that the insertion of acrylate can occur more easily than the insertion of ethylene, which is contradictory to the experimental observation that the first insertion of ethylene proceeds *ca.* 50 times faster than the tBA insertion. In addition, the overall barriers of 30.5 kcal mol^{-1} for tBA insertion and 33.1 kcal mol^{-1} for ethylene insertion seem pretty high. We anticipate that the Ni-catalyst **POP-Ni-py (1)** can undergo an isomerization before subsequent first insertion occurs, giving a lower activation barrier and correct substrate selectivity (see section 7.2).

The first insertion products have the β-H atom coordinated to the Ni-center, forming 4-membered nickelacycles (**int2-et**, **int2-ac** and **int2-ac-r**). These 4-m nickelacycles are lower in energy than the 5-m nickelacycles formed via γ-H atom coordination (**int2-et-5m**, **int2-ac-5m** and **int2-ac-r-5m**), as located by IRC analysis.

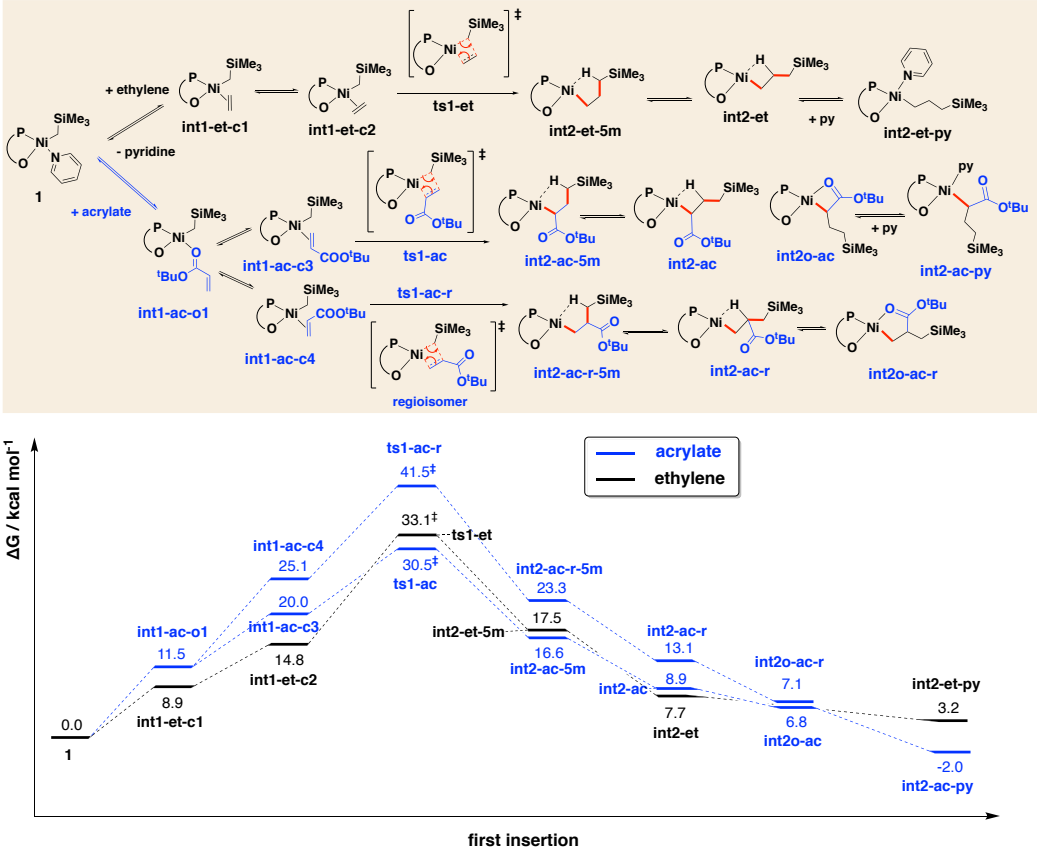

Figure S2.9.4. Gibbs energy profile for the first insertion of ethylene vs *t*-butylacrylate into catalyst **POP-Ni-py (1)**. The Gibbs energies are calculated at SMD(chlorobenzene)-M06/def2-TZVP//M06/def2-SVP level of theory. The energy of the species **POP-Ni-py** (**1**) is taken as a reference.

ts1-et	ts1-ac
ΔG‡ = 33.1	ΔG‡ = 30.5
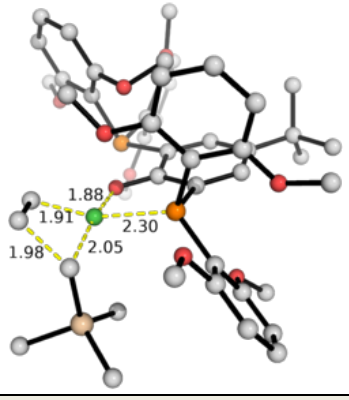	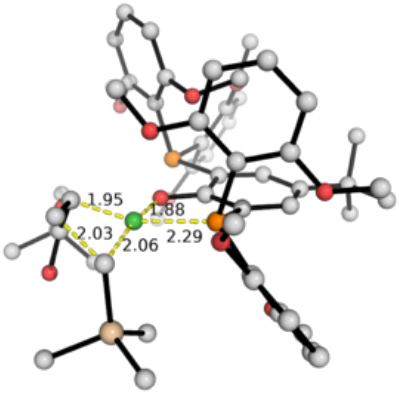
ts1-ac-r	
ΔG‡ = 41.5	

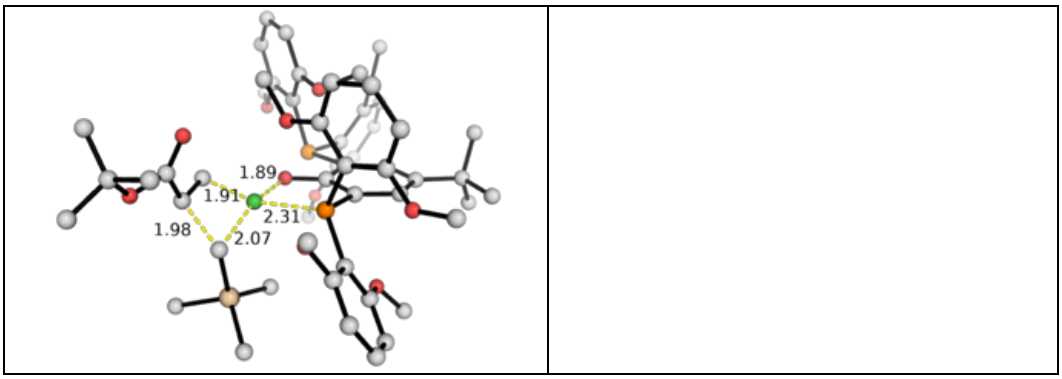

Figure S2.9.5. Optimized TS structures of first insertion of ethylene/tBA into Ni(II) complex **POP-Ni-ac 1**. Key bond distances are given in Å. Gibbs energy units are given in kcal mol^{-1}.

9.1.5 Second insertion of monomer into first insertion product of POP-Ni-py (1)

The insertion of second monomer after the first insertion of ethylene vs tBA into catalyst **POP-Ni-py 1** was studied. Figure S2.9.6 presents the Gibbs energy profile for the second insertion; optimized TS structures are given in Figure S2.9.7. In Figure S2.9.6 (a), we see that the second insertion of ethylene to first ethylene-inserted product has a rather low activation barrier of 9.4 kcal mol^{-1} (**ts3-et-et**, at 12.6 kcal mol^{-1}). The second insertion of tBA into first ethylene-inserted product has a slightly higher activation barrier, by 0.5 kcal mol^{-1} (**ts3-et-ac**, at 13.1 kcal mol^{-1}). This energetic difference is rather small and typically falls within the numerical accuracy of DFT. This implies that the rate of second insertion of ethylene would be rather similar to that of acrylate into first ethylene-inserted product. The insertion products having 4-membered nickelacycles via β-H agostic interaction with the Ni-center (**int4-et-et** and **int4-et-ac**) have lower energies than the 5-m nickelacycles formed via γ-H atom coordination (**int4-et-et-5m** and **int4-et-ac 5m**), as located by IRC analysis. We note that, however, these energetic differences do not affect the overall conclusion of the kinetic analyses as these species are not involved in turnover-frequency determining steps.

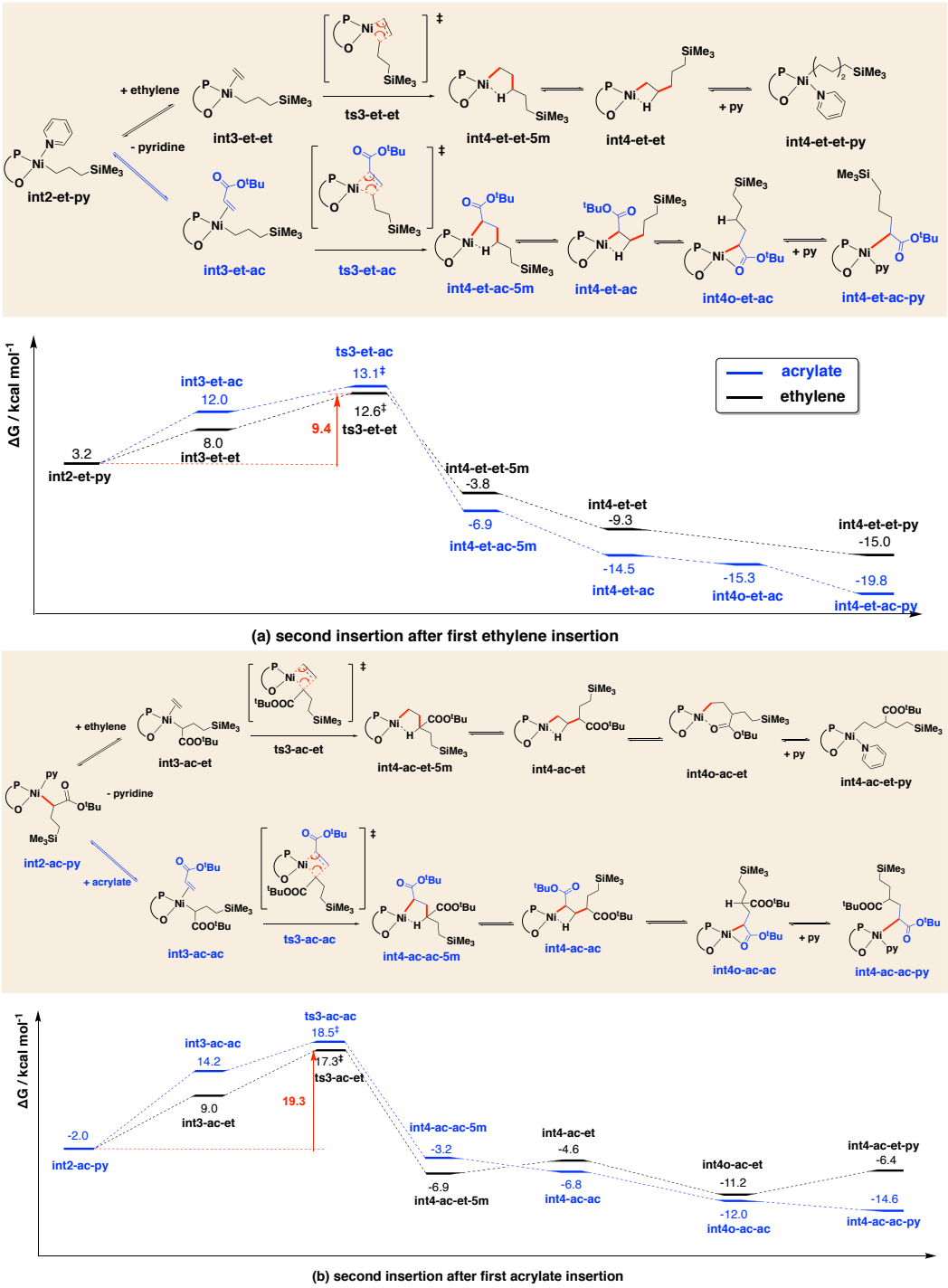

Figure S2.9.6. Gibbs energy profile for the second insertion of ethylene vs *t*-butylacrylate into first inserted product resulting from catalyst **POP-Ni-py (1)**. The energy of the species **POP-Ni-py** (**1**) is taken as a reference. **(a)** Second insertion after first ethylene insertion product and **(b)** second insertion after first acrylate insertion product.

ts3-et-et	**ts3-et-ac**
ΔG‡ = 12.6	ΔG‡ = 13.1
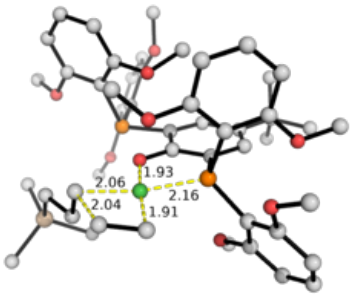	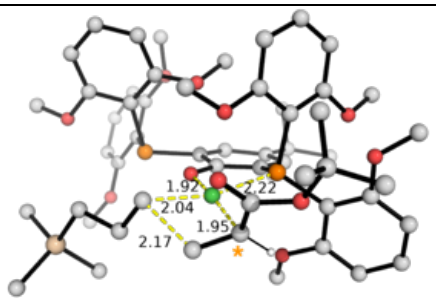
ts3-et-ac-c2	
ΔG‡ = 14.0	
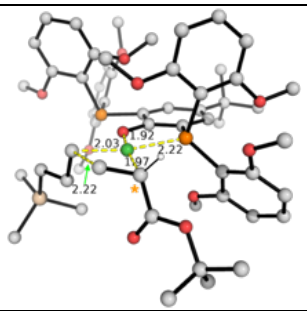	
ts3-ac-et	**ts3-ac-et-c2**
ΔG‡ = 17.3	ΔG‡ = 26.9
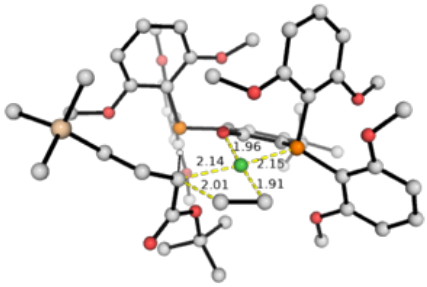	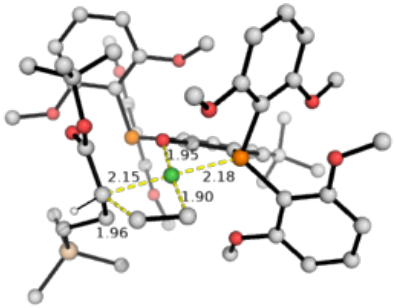
ts3-ac-ac	**ts3-ac-ac-c2**
ΔG‡ = 18.5	ΔG‡ = 18.5
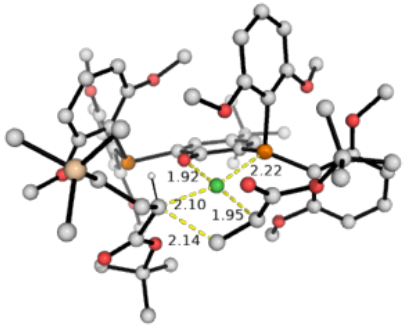	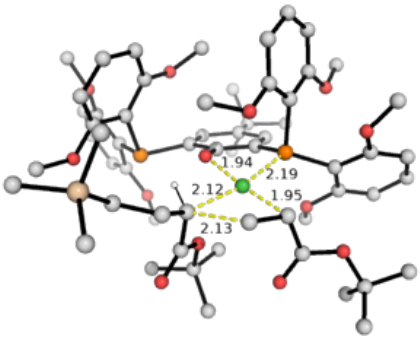

ts3-ac-ac-c3	
ΔG‡ = 27.7	
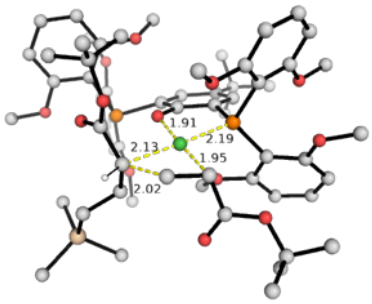	

Figure S2.9.7. Optimized TS structures of second insertion of ethylene/tBA into first inserted product arising from Ni(II) complex **POP-Ni-ac 1**. Key bond distances are given in Å. Gibbs energy units are given in kcal mol^{-1}.

For the second insertion of monomer into first acrylate-inserted product (Figure S2.9.6 (b)), the insertion of ethylene (**ts3-ac-et**, at 17.3 kcal mol^{-1}) has a barrier that is 1.2 kcal mol^{-1} lower than the second insertion of tBA (**ts3-ac-ac**, at 18.5 kcal mol^{-1}). The overall barrier for the second insertion into tBA-inserted product (28.9 kcal mol^{-1}) is much higher than the overall barrier for the second insertion into ethylene-inserted (9.4 kcal mol^{-1}), suggesting that the second insertion into acrylate-inserted product will be much more difficult than the second insertion into ethylene-inserted product.

9.2 Reaction pathways leading from the geometric isomer of the catalyst POP-Ni-py (1')

9.2.1 Geometric isomer POP-Ni-py (1') and its relavent substrate-bound complexes

Previous report by Morokuma and Nozaki on Pd phosphine-sulfonate-catalyzed polymerization[24] suggests that the olefin can insert to the growing polymer chain that is *trans* to the phosphorus atom. We herein consider the insertion to the geometric isomeric form of the **POP-Ni-py** catalyst, denoted as **1'**. The optimized structures of this pyridine-bound catalyst and the relevant substrate-bound complexes are shown in Figure S2.9.8. The relative energies are given with respect to the most stable form **POP-Ni-py 1**.

1'	
ΔG = 4.4	
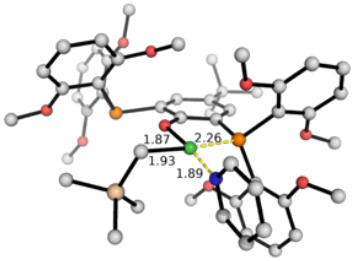	
Coordination of ethylene via C=C π-bond	
int1'-et-c1	**int1'-et-c2**
ΔG = 11.7	ΔG = 14.6
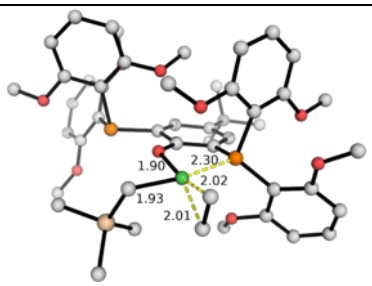	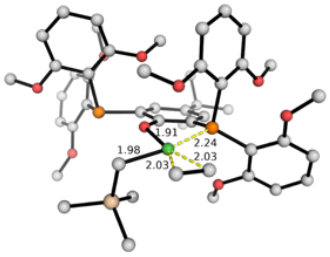
Coordination of tBA via C=C π-bond	
int1'-ac-c1	**int1'-ac-c2**
ΔG = 14.7	ΔG = 18.4
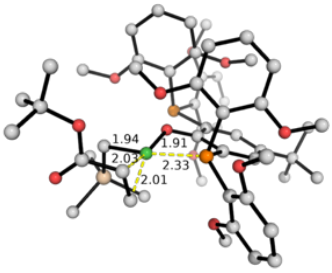	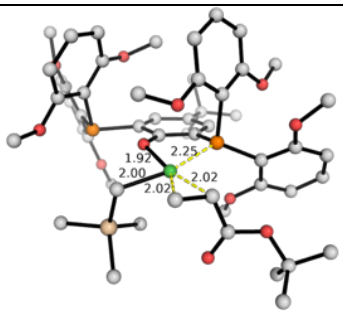
int1'-ac-c3	**int1'-ac-c4**
ΔG = 19.4	ΔG = 20.6
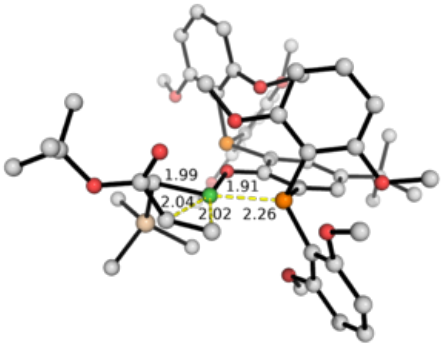	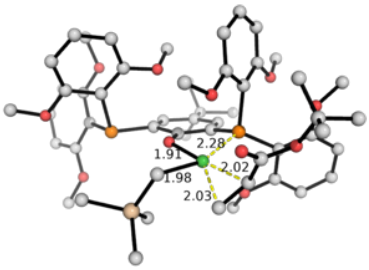

Coordination of tBA via carbonyl O-atom	
int1'-ac-o1	**int1'-ac-o2**
ΔG = 20.8	ΔG = 23.0
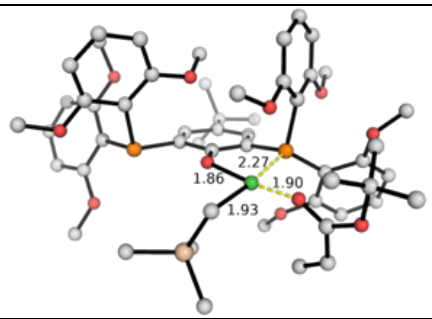	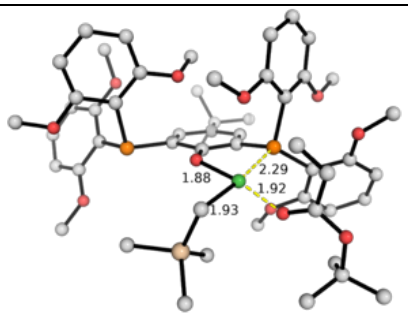

Figure S2.9.8. Optimized structures for the coordination complexes of the isomeric Ni-catalyst **1'**. The Gibbs energies are calculated relative to **POP-Ni-py** (**1**). Key bond distances are given in Å. Gibbs energy units are given in kcal mol^{-1}.

It is interesting to note here that, for the coordination complex with tBA monomer, the coordination via π_{CC} bond (**int1'-ac-c1**, at 14.7 kcal mol^{-1}) is much more stable, by 6.1 kcal mol^{-1}, than the coordination via oxygen atom (**int1'-ac-o1**, at 20.8 kcal mol^{-1}) (cf Figure S2.9.3). This differences possibly arise due to the electronic differences at Ni-metal relative to the ligand coordination from phenoxy-O and phosphine-P atoms. Herein the π donation is more favored than lone pair donation *cis* to P-atom, compared to the other way when tBA coordinates *trans* to P-atom (Figure S2.9.3).

9.2.3 First insertion of substrate into isomeric POP-Ni-py (1')

The insertion of ethylene vs tBA into isomeric POP-Ni-py **1'** was calculated. The Gibbs energy profile is shown in Figure S2.9.9 and the optimized TS structures are given in Figure S2.9.10. All values are given in kcal mol^{-1} and take the energy of the catalyst **1** as a reference. From this energy profile, we can see that the insertion of ethylene into the isomeric form of the Ni-catalyst has the lowest activation barrier (**ts1'-et**, at 20.5 kcal mol^{-1}). The insertion of tBA in either ways (**ts1'-ac**, at 23.7 kcal mol^{-1} and **ts1'-ac-r**, at 27.7 kcal mol^{-1}) are both less favorable. In particular, the insertion of ethylene is 3.2 kcal mol^{-1} more favorable than the 2,1-insertion of tBA, translating to a selectivity in favor of ethylene insertion by about 146 folds using simple TST.

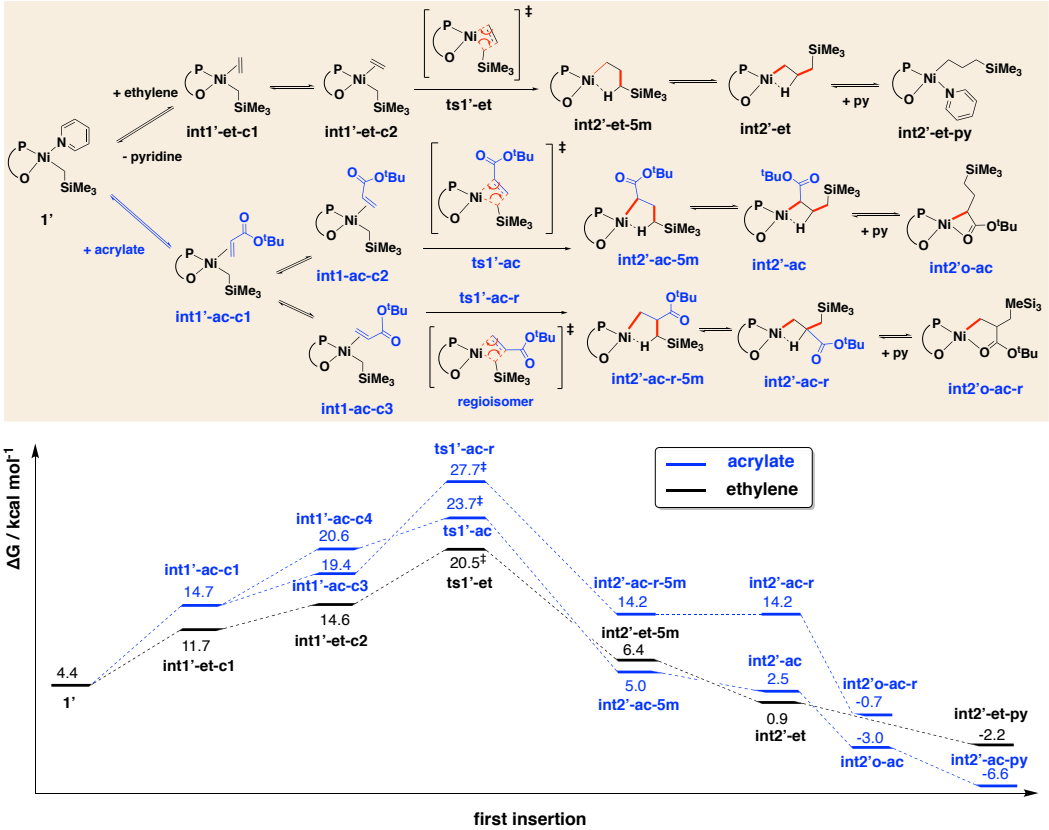

Figure S2.9.9. Gibbs energy profile for the first insertion of ethylene vs *t*-butylacrylate into isomeric form of the Ni-catalyst POP-Ni-py (1'). The Gibbs energies are calculated at SMD(chlorobenzene)-M06/def2-TZVP//M06/def2-SVP level of theory. The energy of the species POP-Ni-py (1) is taken as a reference.

More importantly, the overall barrier of 20.5 kcal mol^{-1} for ethylene insertion (taking the most stable catalyst **1** as the energy reference, assuming that the geometric isomers **1** and **1'** can interconvert rather easily) is much lower (by at least 10 kcal mol^{-1}) than the activation barriers observed for the insertion into catalyst **1** (Figure S2.9.4). In other words, if the isomerization of **1** to **1'** can occur easily (*vide infra*), then the insertion of ethylene will occur through the isomeric form of the catalyst via **ts1'-et**. This is in agreement with prior DFT studies of Pd-catalyzed ethylene polymerization[24] where the migratory insertion of the growing polymer chain can occur more readily when it is *trans* to P-atom (*trans* effect).

ts1'-et	ts1'-ac
ΔG‡ = 20.5	ΔG‡ = 23.7
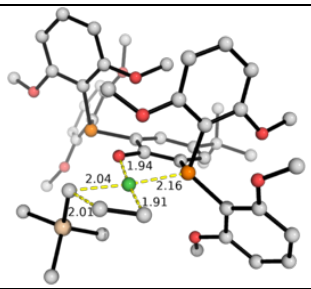	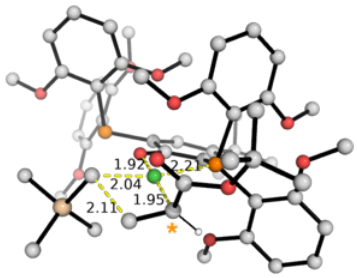
ts1'-ac-c2	**ts1'-ac-r**
ΔG‡ = 24.2	ΔG‡ = 27.7
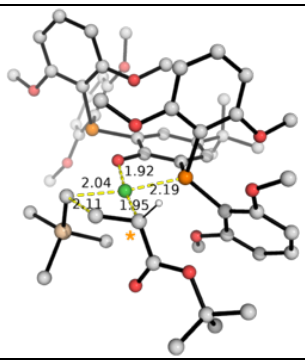	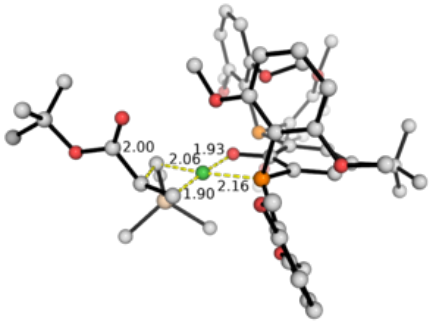

Figure S2.9.10. Optimized structures for the TS structures of first insertion of ethylene/tBA into Ni(II) complex **POP-Ni-ac 1**. Stereocenters in **ts1'-ac** and **ts1'-ac-c2** are marked with yellow asterisk (*). Key bond distances are given in Å. Gibbs energy units are given in kcal mol^{-1}.

Comparing the migratory insertion site selectivity of tBA, herein the migratory insertion of acrylate occurs more readily, by 4.0 kcal mol^{-1}, at the β-carbon site of the α,β-unsaturated carbonyl (**ts1'-ac**, at 23.7 kcal mol^{-1}) than at the α-carbon site (**ts1'-ac-r**, at 27.7 kcal mol^{-1}), as previously. For the migratory insertion at the β-carbon, two possibilities can occur (**ts1'-ac** and **ts1'-ac-c2**), giving a stereocenter at the α-carbon (Figure S2.9.10). We took the lowest TS for all subsequent second insertion.

9.2.3 Second insertion of monomer into first insertion product of isomeric POP-Ni-py (1')

The insertion of second monomer after the first insertion of ethylene vs tBA into the geometric isomeric catalyst **POP-Ni-py 1'** was studied. Figure S2.9.11 presents the Gibbs energy profile for the second insertion and Figure S2.9.12 gives the optimized TS structures. In Figure

S2.9.11 (a), we can see that the second insertion of ethylene to first ethylene-inserted product has a slightly higher barrier, by 1.7 kcal mol^{-1} (**ts3'-et-et**, at 22.5 kcal mol^{-1}) than the second insertion of acrylate tBA into first ethylene-inserted product (**ts3'-et-ac**, at 20.8 kcal mol^{-1}). This implies that the second insertion of tBA is predicted to occur more rapidly via this pathway, which is inconsistent with experimental observation that the second insertion of ethylene after first ethylene insertion occurs more rapidly than the second insertion of tBA. We note that, similar to first insertion, these second insertions where the growing chain originate from Ni-coordination site *cis* to the P-atom of the ligand have higher activation barriers than the corresponding second insertions where the growing polymer chain is *trans* to the P-atom (Figure S2.9.6 (a)). Again, we hypothesize that the initial catalyst **1** having growing polymer chain *cis* to the P-atom of the ligand can isomerize to its geometric isomer **1'** where the growing polymer chain is *trans* to the P-atom of the ligand before first insertion occurs (Figure S2.9.9). The ethylene insertion product **int2'-et-py** at -2.2 kcal mol^{-1} can undergo another isomerization to **int2-et-py**, at 3.2 kcal mol^{-1} before the second insertion of ethylene occurs. The isomerization serves to place the growing polymer chain *trans* to the P-atom of the ligand so that it can take advantage of the *trans* effect of the ligand, making the migratory insertion step easier to occur.

In the second insertion of monomer into the first acrylate-inserted product (Figure S2.9.11 (b)), we note that the insertion of tBA again has a lower barrier (**ts3'-ac-ac**, at 27.1 kcal mol^{-1}), by 1.2 kcal mol^{-1}, than the insertion of ethylene (**ts3'-ac-et**, at 28.3 kcal mol^{-1}), similar to that observed for the second insertion into first ethylene-inserted product in Figure S2.9.11 (a). This TS for the tBA insertion into tBA-inserted product (**ts3'-ac-ac**, activation barrier of 30.1 kcal mol^{-1}) has a very close activation barrier to TS **ts3-ac-ac** with an activation barrier of 29.7 kcal mol^{-1} (Figure S2.9.6 (b)).

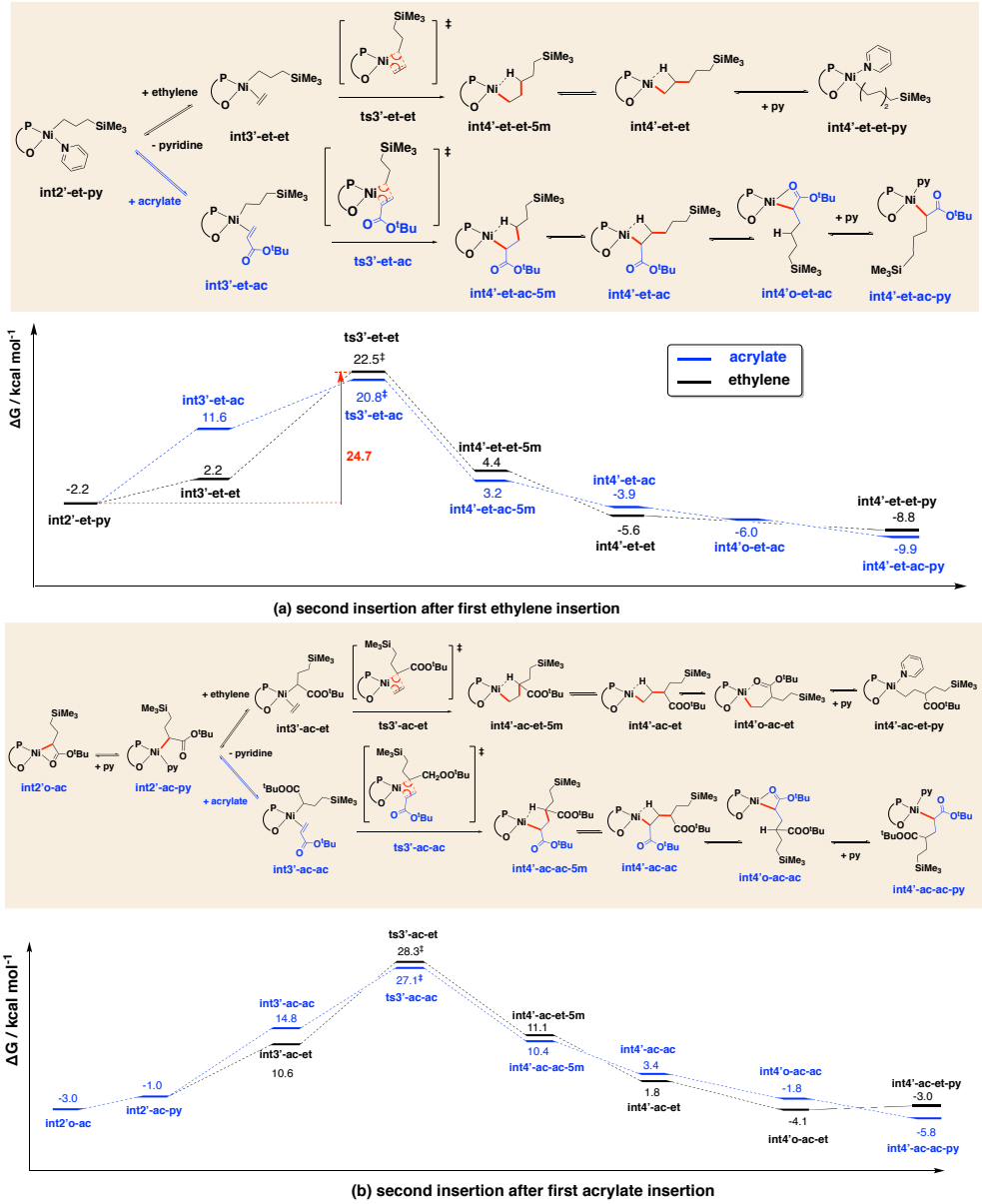

Figure S2.9.11. Gibbs energy profile for the second insertion of ethylene vs *t*-butylacrylate into first inserted product resulting from isomeric catalyst **POP-Ni-py 1'**. The Gibbs energies are calculated at SMD(chlorobenzene)-M06/def2-TZVP//M06/def2-SVP level of theory. The energy of the species **POP-Ni-py** (**1**) is taken as a reference. **(a)** Second insertion after first ethylene insertion product and **(b)** second insertion after first acrylate insertion product.

ts3'-et-et	ts3'-et-ac
ΔG = 22.5	ΔG = 20.8

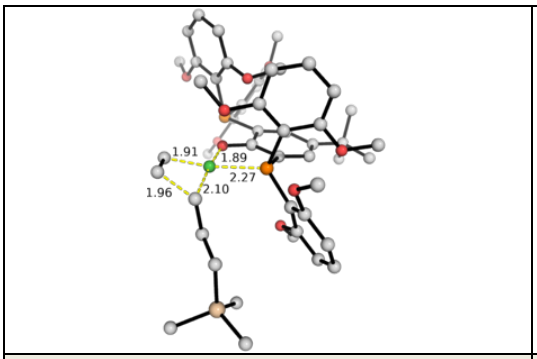	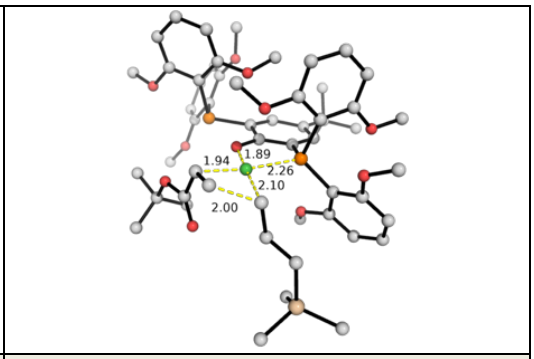
ts3'-ac-et	**ts3'-ac-ac**
ΔG = 28.3	ΔG = 27.1
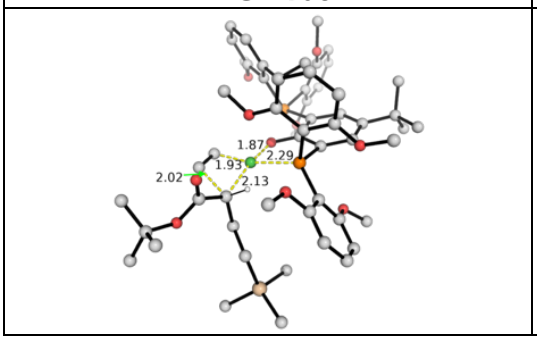	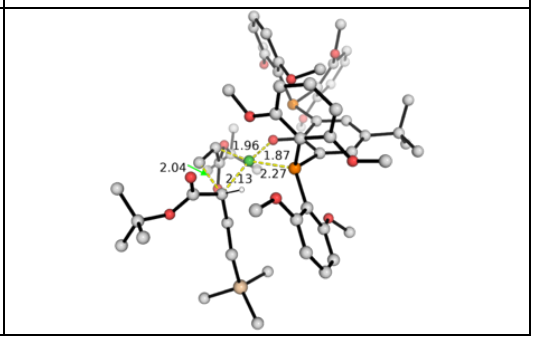

Figure S2.9.12. Optimized TS structures of second insertion of ethylene/tBA into first inserted product arising from isomeric Ni(II) complex **POP-Ni-ac 1'**. Key bond distances are given in Å. Gibbs energy units are given in kcal mol^{-1}.

9.3 Sterics and electronics effects in key transition states

9.3.1 Comparison of sterics and electronics of first and second isomerization

ts-5coord	ts-5coord-et	ts-5coord-ac
ΔΔG‡ = 27.1	ΔΔG‡ = 18.8	ΔΔG‡ = 22.3
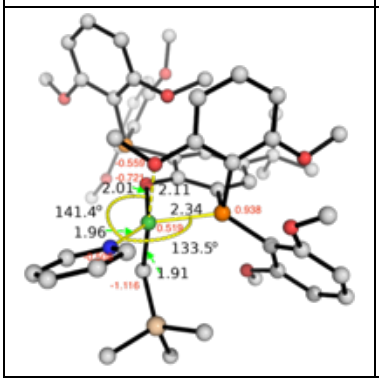	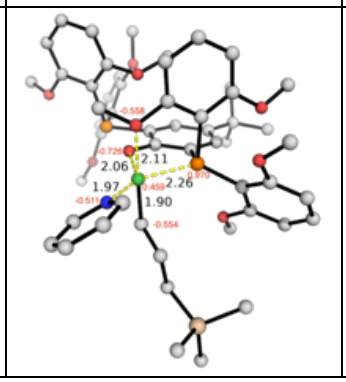	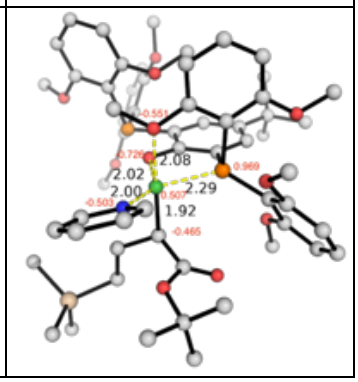

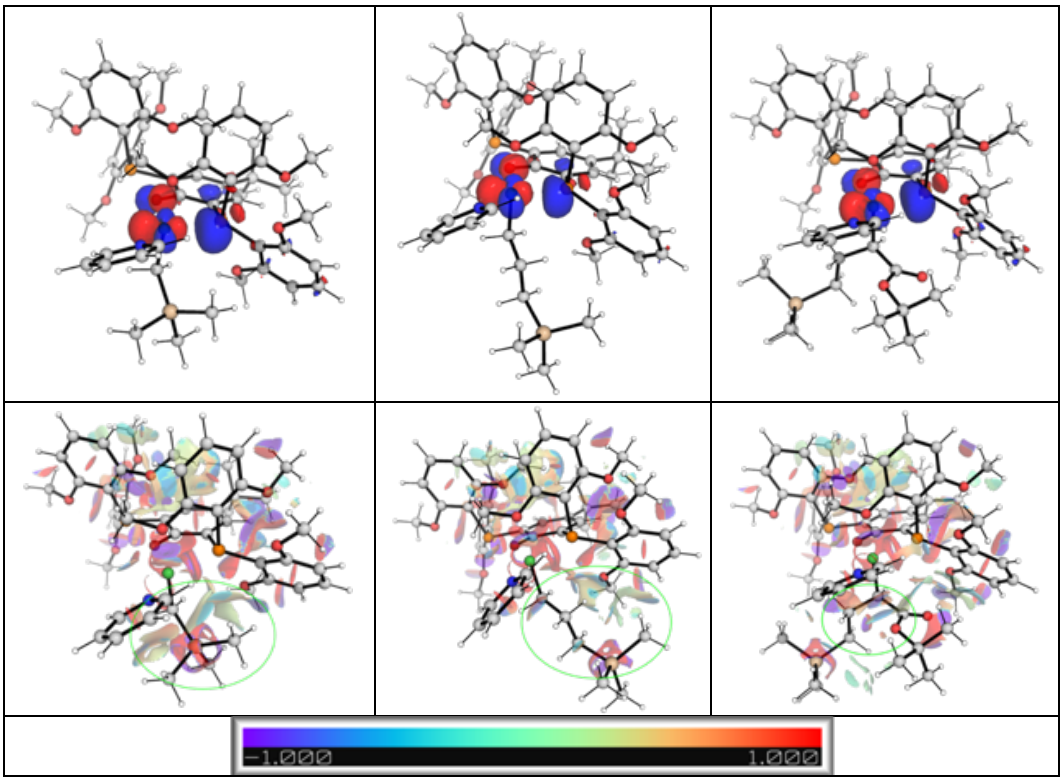

Figure S2.9.13. Optimized TS structures (first row), HOMO (middle row) and NCI plots (last row) for the isomerization of catalyst (**ts-5coord**), the isomerization of first ethylene-insertion product (**ts-5coord-et**) and the isomerization of first tBA-insertion product (**ts-5coord-ac**). Natural bond orbital (NBO) charges are given in red in the first row. Key bond distances are given in Å and angles are given in degrees. Isomerization barriers are given in kcal mol^{-1}.

9.3.2 Comparison of sterics and electronics of first insertion

ts1-et	ts1-ac
ΔG‡ = 33.1	ΔG‡ = 30.1
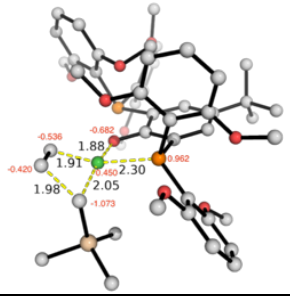	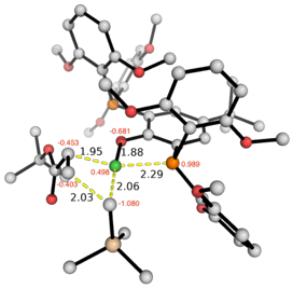

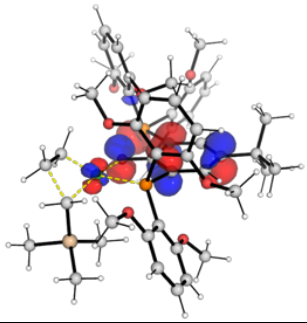	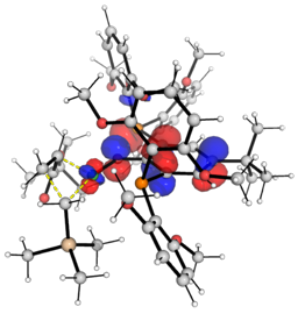
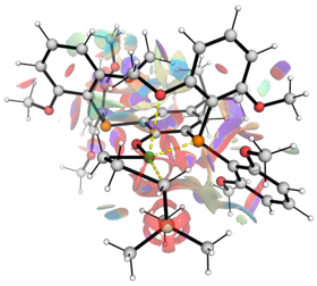	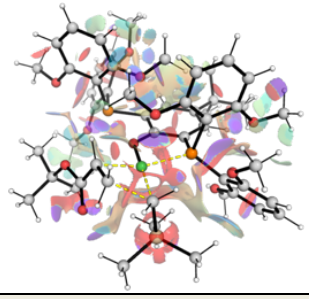
ts1'-et	**ts1'-ac**
$\Delta G^{\ddagger} = 20.5$	$\Delta G^{\ddagger} = 23.7$
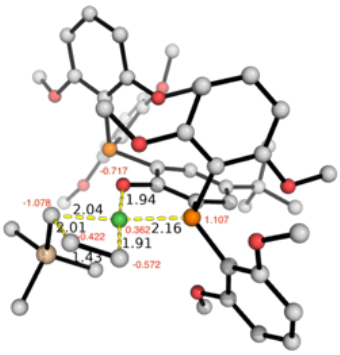	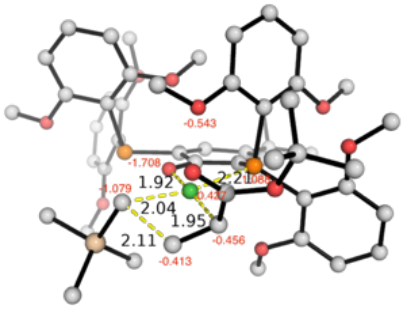
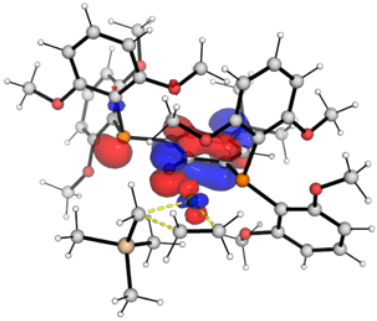	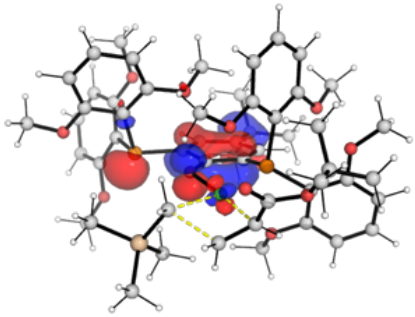

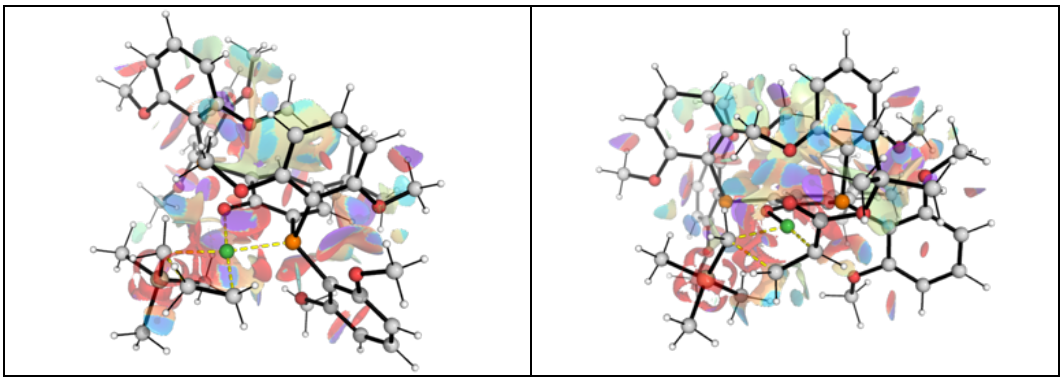

Figure S2.9.14. Optimized TS structures (first row), HOMO (middle row) and NCI plots (last row) for the first insertion into catalyst **1** and **1'**. Natural bond orbital (NBO) charges are given in red in the first row. TS free energies are relative to catalyst **1** and are given in kcal mol^{-1}. Key bond distances are given in Å.

	ts1-et	**ts1-ac**
$\Delta E^{(2)}$	-58.8	-66.2
donor	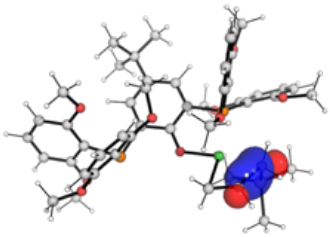	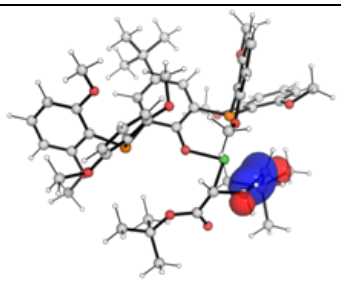
acceptor	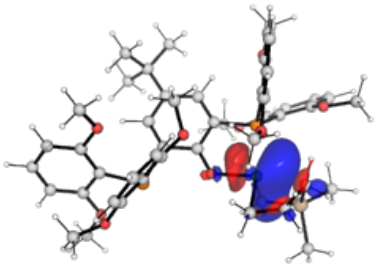	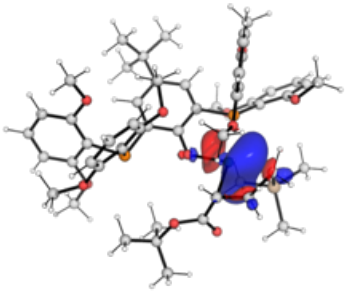
	ts1'-et	**ts1'-ac**
$\Delta E^{(2)}$	-76.8	-89.1
donor	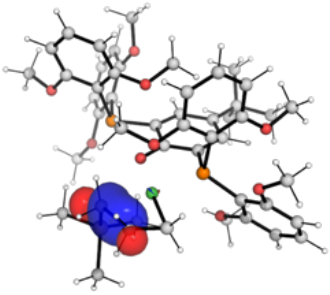	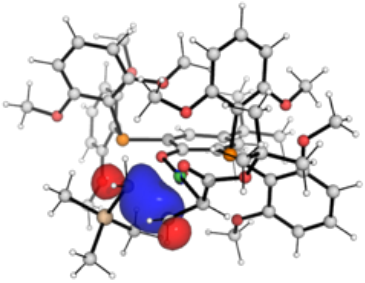

acceptor	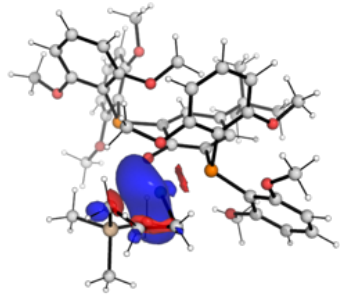	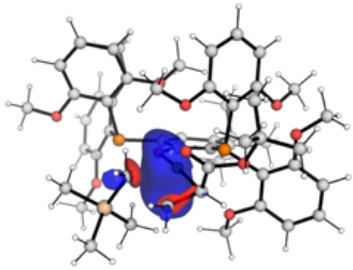

Figure S2.9.15. Natural bonding orbital (NBO) analysis using second-order perturbative stabilization energy ($\Delta E^{(2)}$), which gives the dominant bonding interactions between the nascently formed C–C σ-bond and the metal (Ni d* orbital). Energies are given in kcal mol^{-1}.

9.3.3 Comparison of sterics and electronics of O-chelates

int2'o-ac	int2o-ac
ΔG = -3.0	ΔG = 6.8
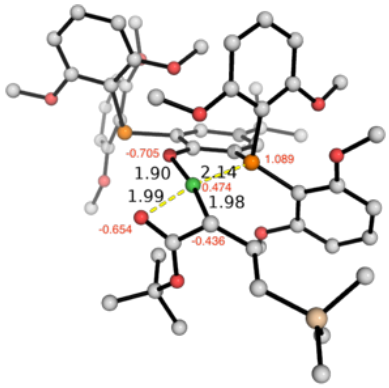	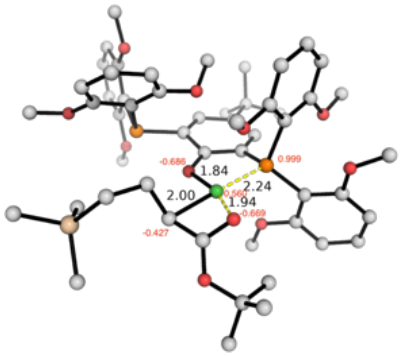
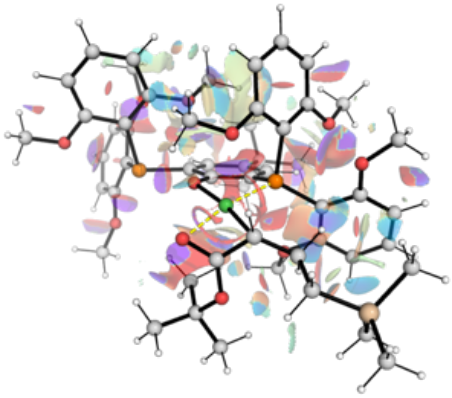	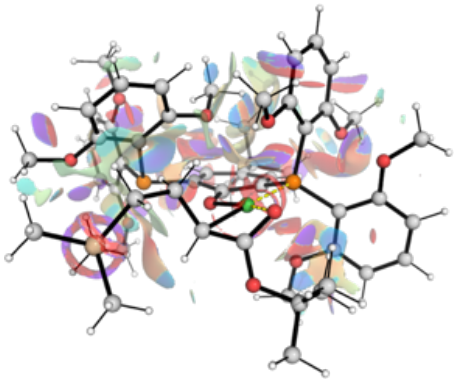

Figure S2.9.16. Optimized O-chelate structures from catalyst 1 and 1' after first insertion of tBA monomer (first row) and their associated NCI plots (last row). Natural bond orbital (NBO) charges are given in red in the first row. Free energies are relative to catalyst **1** and are given in kcal mol^{-1}. Key bond distances are given in Å.

	int2'o-ac	int2o-ac
$\Delta E^{(2)}$	-90.2	-90.7

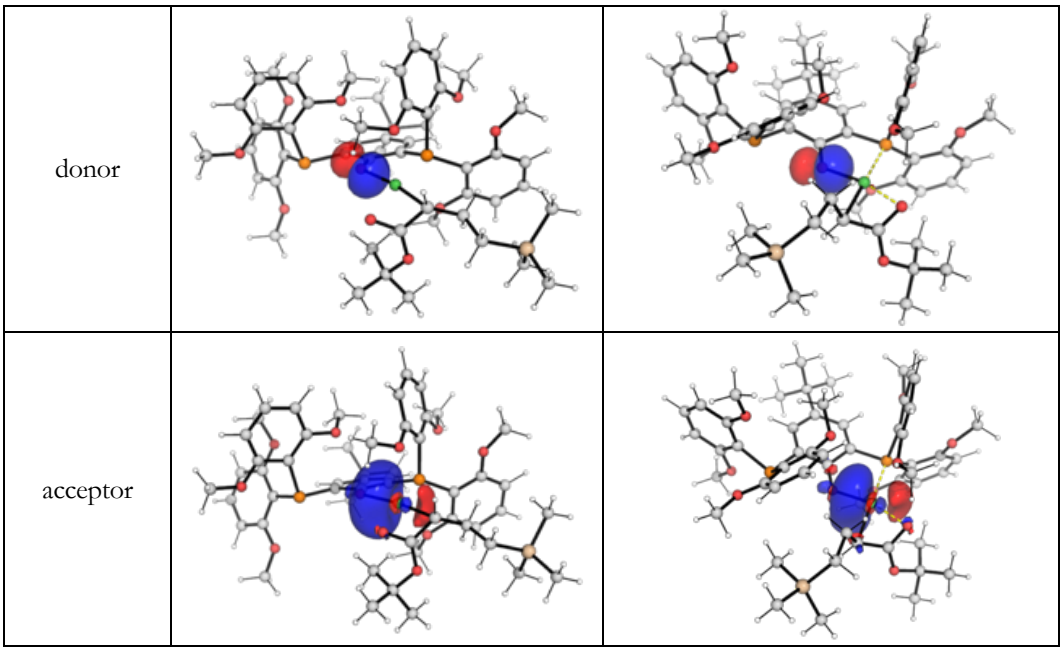

Figure S2.9.17. Natural bonding orbital (NBO) analysis using second-order perturbative stabilization energy ($\Delta E^{(2)}$), which gives the dominant bonding interactions between the ligand (O lone pair) and the metal (Ni d* orbital). Energies are given in kcal mol^{-1}.

9.4 Optimized geometries

Geometries of all optimized structures (in .xyz format with their associated energy in Hartrees) are included in a separate folder named *ESI_final_structures_xyz* with an associated README file. All these data have been deposited with this Supporting Information and uploaded to zenodo.org (DOI: 10.5281/zenodo.4593551).

10 Computational Investigation in isomerization

The isomerization of the square planar catalyst between **POP-Ni-py (1)** and its isomeric form **POP-Ni-py 1'** can occur via one of the three possible mechanisms: associative, dissociative or twisting through a tetrahedral TS and then back to square planar. This step is essential for the insertion of ethylene into the Ni–C bond via the lower TS **ts1'-et**, at 20.5 kcal mol^{-1}, rather than via **ts1-et**, at 33.1 kcal mol^{-1}. We herein consider these possibilities computationally:

Scheme S10.1. Possible mechanisms of isomerization between two geometric isomeric forms of the Ni-catalyst.

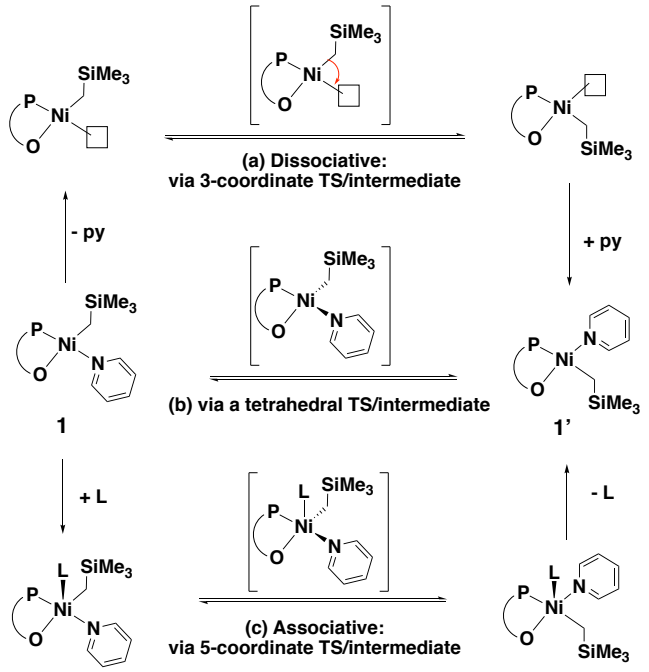

10.1 Dissociative mechanism

In a dissociative mechanism, the coordinating pyridine ligand leaves, giving a vacant site on Ni metal. Subsequently, the growing polymer chain can isomerize by moving from its original coordinating site to its adjacent, newly vacated coordination site. This is followed by recoordination of pyridine ligand at the site previously occupied by the growing polymer chain, giving the geometric isomeric form of the catalyst (Scheme S10.1a).

We first try to estimate the barrier to pyridine dissociation by doing a relaxed PES scan along the Ni–N(pyridine) bond. The gas phase energy scan is given in Figure S2.10.1. We can see that the loss of pyridine ligand is unfavorable and reversible. This is consistent with geometry optimization starting from initial guess structure of long (3.70 Å) Ni–N(pyridine) bond (by manually increasing this distance in catalyst **1** while maintaining the square plane of the Ni-center) which optimized back to catalyst **1**. To obtain the accurate Gibbs energy with solvent correction for the resulting structure after loss of pyridine coordination, we took the structure at point 5 in

Figure S2.10.1 and subjected it to geometry optimization. The final structure, **1a**, is 19.0 kcal mol^{-1} uphill (Figure S2.10.2). This gives the estimate of the dissociation barrier of pyridine as *ca.* 22 kcal mol^{-1} (this is nonetheless smaller than the isomerization barrier, *vide infra*). The loss of pyridine from this species, displaced by an agnostic interaction from the C–H group on trimethylsilyl, gives **1-3coord** which is 14.3 kcal mol^{-1} uphill (Figure S2.10.2). This species can further undergo isomerization to give the species **1-3coord** at 18.1 kcal mol^{-1} relative to catalyst **Ni-POP-py 1**.

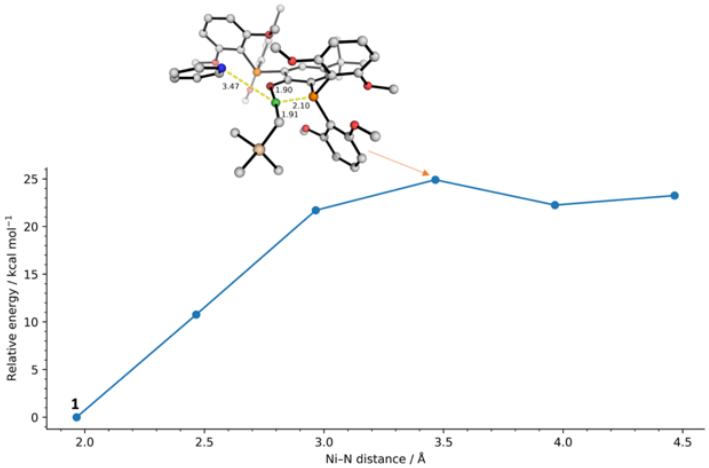

Figure S2.10.1. Relaxed PES scan along phenoxide O-Ni-C angle going from one 3-coordinate isomer to another. Relative energy values are computed at M06/def2-SVP in gas phase and used without further corrections. Key bond distances are given in Å.

Therefore, the loss of pyridine from catalyst **1** gives **1-3coord**, at 14.3 kcal mol^{-1}. We next set out to find the TS for the isomerization from **1-3coord** to **1'-3coord**.We initially tried direct TS search using the guess structure of placing the polymer chain in between the two Ni-coordination sites and QST2 method (in Gaussian 16 software, both *opt=modredundant* and *opt=qst2* methods) to no avail. We can, however, do a relaxed PES scan sweeping out the angle from one geometric isomer to the other to get an estimate of the barrier for such isomerization. This relaxed PES scan in gas phase is given in Figure S2.10.3, allowing us to estimate that the barrier for the isomerization from **1-3coord** to **1'-3coord** is about 24 kcal mol^{-1}. This estimate is valid since the

energy difference between **1-3coord** and **1'-3coord** in the gas phase ($\Delta\Delta E$ = 4.4 kcal mol^{-1}) is very similar to their Gibbs energy difference in solvent ($\Delta\Delta G$ = 3.8 kcal mol^{-1}). Given that species **1-3coord** is 14.3 kcal mol^{-1} uphill with respect to **Ni-POP-py 1**, we estimate that the barrier for isomerization of catalyst **Ni-POP-py 1** to its geometric isomer **Ni-POP-py 1'** via a 3-coordinate TS has an upper bound activation barrier of 38 kcal mol^{-1}, which is much higher than the barriers for the migratory insertion of monomer into Ni–C bond of catalyst **Ni-POP-py 1** (Figure S2.9.4).

1a	**1-3coord**
ΔG = 19.0	ΔG = 14.3
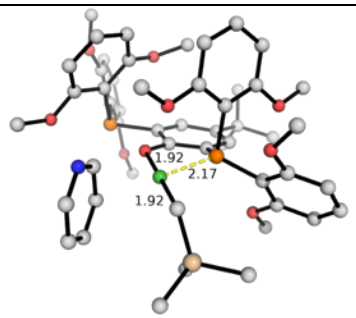	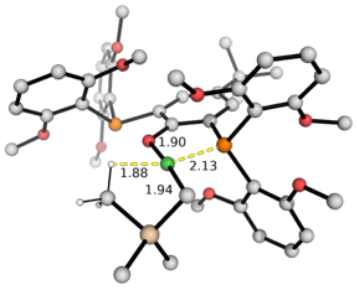
1'-3coord	**ts-3coord**
ΔG = 18.1	$\Delta G^{\ddagger}$ = 33.8
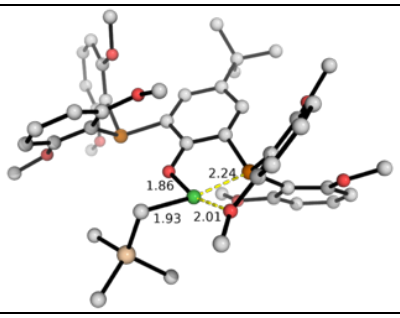	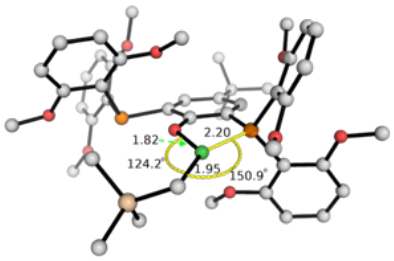

Figure S2.10.2. Optimized structures for the coordination complexes of the isomeric Ni-catalyst **1** and **1'** after losing pyridine coordination to give 3-coordinate species and the TS structure for the isomerization via 3-coordinate TS. The Gibbs energies are calculated relative to **POP-Ni-py** (**1**). Key bond distances are given in Å and angles are given in degrees. Gibbs energy units are given in kcal mol^{-1}.

Next, we took the structure with the highest energy from this PES scan (Figure S2.10.3) as an initial guess for the 3-coordinate isomerization TS search. We are able to locate the true TS **ts-**

3coord (Figure S2.10.4, verified by IRC) having a barrier of 33.8 kcal mol^{-1} relative to the catalyst **Ni-POP-py 1**.

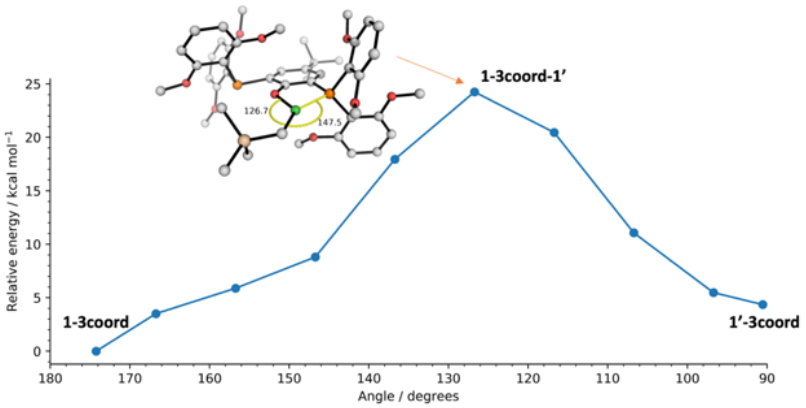

Figure S2.10.3. Relaxed PES scan along phenoxide O-Ni-C angle going from one 3-coordinate isomer to another. Relative energy values are computed at M06/def2-SVP in gas phase and used without further corrections. Key bond distances are given in Å.

In **1'-3coord** we see that the oxygen atom of an adjacent methoxy group on the ligand can coordinate to the Ni-metal. We wonder if this coordination can displace pyridine ligand in catalyst **1**, thus giving the isomeric **1'**. The optimized structures and their associated energetics are shown in Figure S2.10.4. The displacement of pyridine ligand by OMe group gives structure **1b**, which is endergonically uphill, at 27.1 kcal mol^{-1}. This requires an activation barrier of at least 27.1 kcal mol^{-1} and is unfavorable. This is perhaps unsurprising as a strong Ni–N(pyridine) interaction is lost and replaced by a weaker Ni–O(methoxy) interaction.

1b	**1c**
ΔG = 27.1	ΔG = 30.5
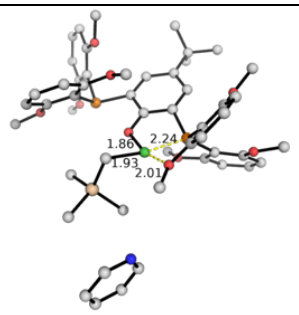	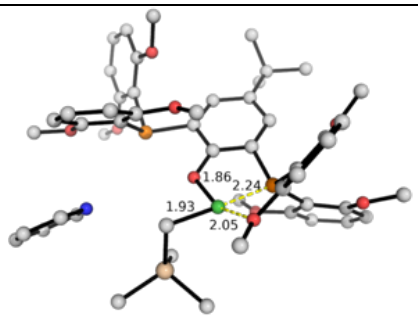

Figure S2.10.4. Optimized structures for the coordination complexes of the isomeric Ni-catalyst **1** and **1'** after losing pyridine coordination to give 3-coordinate species. The Gibbs energies are

calculated relative to **POP-Ni-py** (**1**). Key bond distances are given in Å. Gibbs energy units are given in kcal mol^{-1}.

This dissociative mechanism has an overall barrier of 33.8 kcal mol^{-1} which is higher than the isomerization barriers for the other two mechanistic possibilities (*vide infra*) and is thus unlikely for the isomerization of catalyst **1** to its geometric isomer **1'**.

10.2 Twisting mechanism via tetrahedral TS/intermediate

A similar dihedral angle scan mapping out one geometric isomer to the other passing through the tetrahedral TS/intermediate, to estimate how big the barrier is, was not successful due to the difficulties in defining the scanning coordinates. However, the direct TS search for the putative TS structure gives two TS conformers, **ts-tet** and **ts-tet-c2**, with the lowest activation barrier of 30.8 kcal mol^{-1} (**ts-tet**, Figure S2.10.5). This TS has been verified to be the true TS for the isomerization via tetrahedral TS using IRC analyses.

ts-tet	**ts-tet-c2**
ΔG‡ = 30.8	ΔG‡ = 31.4
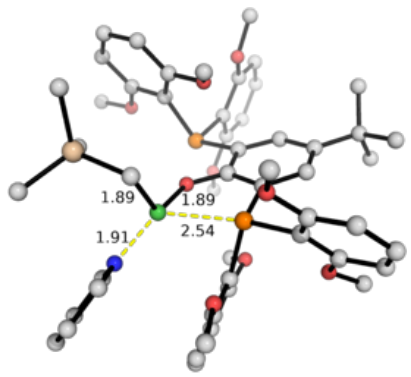	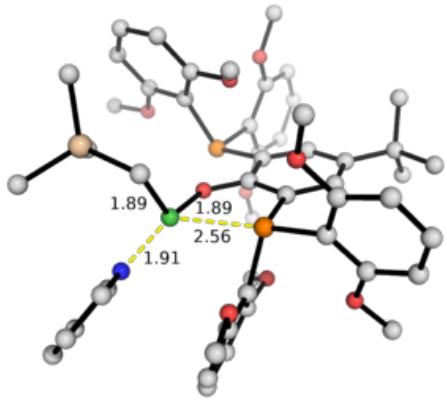

Figure S2.10.5. Optimized TS structures for the isomerization of catalyst **1** to **1'** via tetrahedral transition state. Two TS conformers were found. Key bond distances are given in Å. Gibbs energy units are given in kcal mol^{-1}.

10.3 Associative mechanism

In an associative mechanism, a fifth ligand coordinates to Ni-center, giving a 5-coordinate species. This can then undergo a Berry pseudorotation to isomerize the catalyst from one

geometric isomer to the other, before finally one ligand leaves to give back to the square planar species (Scheme S10.1c).

We first consider if an external ethylene molecule could serve as the fifth ligand by binding to the Ni-center. The direct optimization using ethylene binding to the Ni-center as an initial guess structure did not yield a stable 5-coordinate species. This species **1-et**, with ethylene unbound (Figure S2.10.6), is 6.6 kcal mol^{-1} uphill with respect to the most stable form of the catalyst **Ni-POP-py 1**. This is due to the unfavorable entropic effect associated with bringing in an additional ethylene molecule to the inner coordination shell of the Ni-metal. The absence of a stable 5-coordinate Ni-species with ethylene bound suggest that the coordination of ethylene to form 5-coodinate species is unlikely.

1-et	**1-5coord**
ΔG = 6.6	ΔG = 1.5
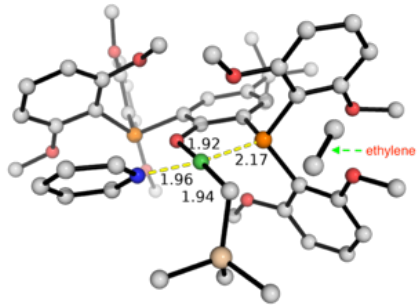	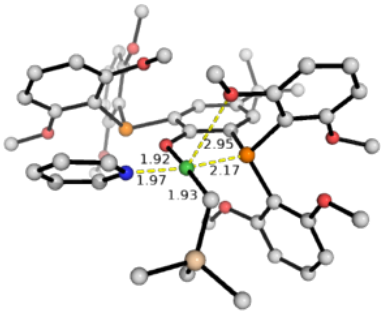
ts-5coord	**ts-5coord-c2**
ΔG‡ = 27.1	ΔG‡ = 28.3
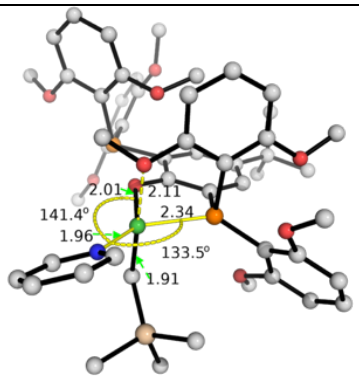	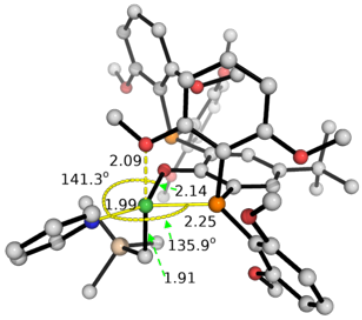

Figure S2.10.6. Optimized structures species involved in isomerization pathway via 5-coordinate Ni-complex. The Gibbs energies are calculated relative to **POP-Ni-py** (**1**). Key bond distances are given in Å and angles are given in degrees. Gibbs energy units are given in kcal mol^{-1}.

We found that the O-atom of the methoxy group on the ligand can serve as a fifth ligand in coordinating the Ni-center. This species, **1-5coord** (Figure S2.10.6), is 1.5 kcal mol^{-1} higher than catalyst **Ni-POP-py 1** (it is in fact a conformer of catalyst **1**). Two TS conformers for the pseudorotational barriers (**ts-5coord** and **ts-5coord-c2**, Figure S2.10.6) were found and verified by IRC to be the true TS structures for the isomerization of one catalyst form (catalyst **1**) to its geometric isomer (catalyst **1'**). The lowest energy conformer **ts-5coord** has a barrier of 27.1 kcal mol^{-1}, which is lower than the barriers via either 3-coordinate TS (**ts-3coord** at 33.8 kcal mol^{-1}, Figure S2.10.2) or tetrahedral TS (**ts-tet** at 30.8 kcal mol^{-1}, Figure S2.10.5). This is therefore the most likely mechanism: the isomerization of catalyst **Ni-POP-py 1** to its regioisomeric form **Ni-POP-py 1'** occurs via associative mechanism with a proximal OMe group serving as a binding ligand on the fifth coordination site before a pseudoroational TS gives the isomeric catalyst.

10.4 Other possibilities

The loss of P-coordination replaced by methoxy O-coordination was considered. However, the resulting species, **1d** and **1e**, both have very high energy such that their formation is highly endergonic and unfavorable (Figure S2.10.7). This is perhaps expected as the loss of stronger Ni–P coordination was replaced by weaker Ni–O(methoxy) interaction.

1d	**1e**
ΔG = 32.4	ΔG = 28.2

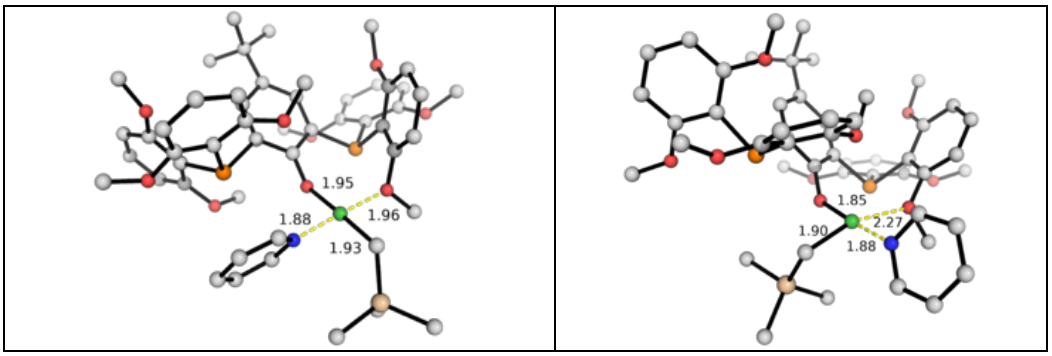

Figure S2.10.7. Optimized structures for the coordination complexes of Ni-catalyst **1** and **1'** where Ni–P interaction is displaced by Ni–O interaction. The Gibbs energies are calculated relative to **POP-Ni-py** (**1**). Key bond distances are given in Å. Gibbs energy units are given in kcal mol^{-1}.

11 Discussion of experimental and computational kinetic studies

11.1 Discussion of Enchainment Kinetics (Excluding Potential Isomerization)

The linear dependence indicates that pseudo-1st order rate constant (k_{obs-1}, rate=k_{obs-1}[Ni]) is proportional to the concentration of tBA and inversely proportional to the concentration of pyridine in the range of concentrations studied. To evaluate this behavior, we considered five mechanistic pathways: **A**: Dissociative mechanism and rate determining step pyridine dissociation; **B**. Dissociative mechanism and rate determining step migratory insertion; **C**. Associative mechanism and rate determining step tBA coordination; **D**. Associative mechanism and rate determining step pyridine dissociation; **E**. Associative mechanism and rate determining step migratory insertion. Corresponding rate equation and expressions of rate constants are shown below:

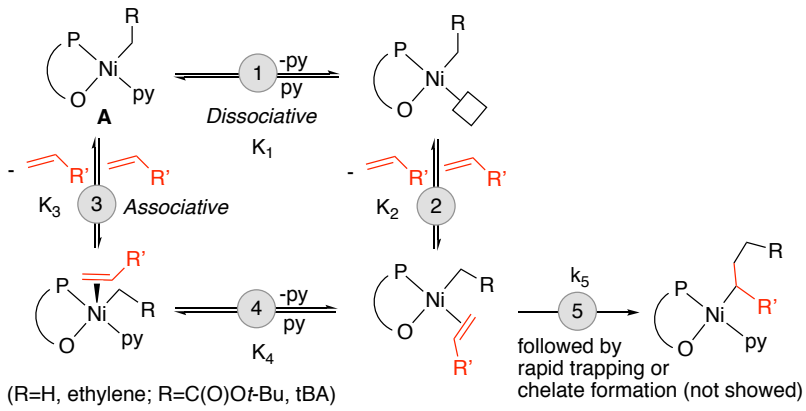

Path A: Dissociative mechanism & Rate determining step: pyridine dissociation (Note: tBA is used as the model monomer in this section and following sections. However, the conclusion also works for ethylene or other monomers)

$$\frac{d[A]}{dt} = -k_1 \cdot \frac{k_2[tBA]}{k_{-1}[py] + k_2[tBA]} \cdot [A]$$

$$k_{obs} = k_1 \cdot \frac{k_2[tBA]}{k_{-1}[py] + k_2[tBA]}$$

In this case,

1) If $k_{-1}[py] >> k_2[tBA]$, $k_{obs} \propto [tBA]/[py]$

2) Upper limit of kobs is k_1

3) In the double reciprocal plot (y axis: $1/k_{obs}$, x axis: [py]/[tBA]), slope=$1/(k_2K_1)$, Intercept=$1/k_1$

Path B: Dissociative mechanism & Rate determining step: migratory insertion

$$\frac{d[A]}{dt} = -K_1K_2 \cdot \frac{k_5[tBA]}{[py]} \cdot [A]$$

$$k_{obs} = -K_1K_2 \cdot \frac{k_5[tBA]}{[py]}$$

$$K_{tBA/py} = -K_1K_2$$

In this case,

1) $k_{obs} \propto$ [tBA]/[py]

2) In the double reciprocal plot (y axis: $1/k_{obs}$, x axis: [py]/[tBA]), slope= $1/(K_{tBA/py}k_3)$, Intercept=0

Path C: Associative mechanism & Rate determining step: tBuAc coordination

$$\frac{d[A]}{dt} = -k_3 \cdot \frac{k_4[tBA]}{k_{-3} + k_4} \cdot [A]$$

$$k_{obs} = k_3 \cdot \frac{k_4[tBA]}{k_{-3} + k_4}$$

In this case,

1) k_{obs} is not related to [py]

2) $k_{obs} \propto$ [tBA]

3) In the double reciprocal plot (y axis: $1/k_{obs}$, x axis: [py]/[tBA]), slope= $1/K_3k_4$, Intercept=0 (for different [tBA]); or slope= 0, Intercept=$1/(K_3k_4[tBA])+1/(k_3[tBA])$ (for different [py])

Path D: Associative mechanism & Rate determining step: py dissociation

$$\frac{d[A]}{dt} = -K_3k_4 \cdot \frac{k_5[tBA]}{k_{-4}[py] + k_5} \cdot [A]$$

$$k_{obs} = K_3k_4 \cdot \frac{k_5[tBA]}{k_{-4}[py] + k_5}$$

In this case,

1) If $k_{-4}[py] >> k_5[tBA]$, $k_{obs} \propto$ [tBA]/[py]

2) If $k_{-4}[py] << k_5[tBA]$, k_{obs} is proportional to [tBA] but not related to [py]

3) In the double reciprocal plot (y axis: $1/k_{obs}$, x axis: [py]/[tBA]), slope=$1/(K_3K_4k_5)$, Intercept= $1/(K_3k_4)$

Path E: Associative mechanism & Rate determining step: migratory insertion

$$\frac{d[A]}{dt} = -K_3K_4 \cdot \frac{k_5[tBA]}{[py]} \cdot [A]$$

$$k_{obs} = -K_3K_4 \cdot \frac{k_5[tBA]}{[py]}$$

$$K_{tBA/py} = -K_3K_4$$

In this case,

1) $k_{obs} \propto [tBA]/[py]$

2) In the double reciprocal plot (y axis: $1/k_{obs}$, x axis: [py]/[tBA]), slope= $1/(K_{tBA/py}k_3)$, Intercept=0

Notably, double reciprocal plot is not enough to differentiate path B and path E.

Mechanisms A, C, and D are expected to result in non-zero intercepts and therefore are inconsistent with the data. Mechanisms B and E both predict zero intercepts and are consistent with the data. Both of these reaction pathways implicate olefin insertion is slow comparing to ligand exchange (pyridine dissociation + olefin coordination). Note that an isomerization process that moves the alkyl group to the position trans to the phosphine, as previously proposed for asymmetric ligand systems cannot be addressed experimentally as it results in the same dependence on substrate concentration as the above cases (see below).

11.2 Discussion of Enchainment Kinetics (Including Isomerization)

Consider the first insertion of either ethylene or tBA. Herein we use tBA as an illustration; note that the case for ethylene will be the same.

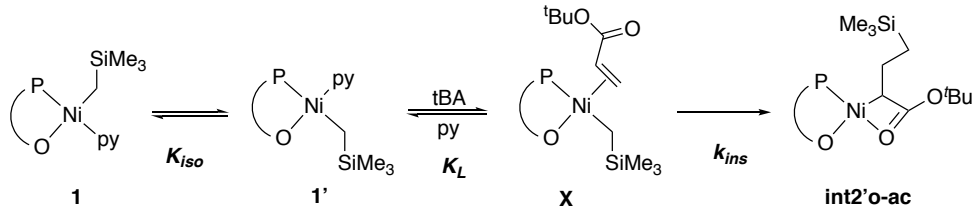

The overall rate of the formation of insertion product **int2'o-ac** is given by

$$rate = k_{ins} \cdot [\mathbf{X}] \qquad \text{(A)}$$

The isomerization step has the highest barrier for this transformation whereas the insertion step is rate-limiting after the isomerization. Applying the steady-state approximation to species **1'**, we have

$$0 = \frac{d[\mathbf{1}']}{dt} = k_{iso}\,[\mathbf{1}] - k_{-iso}\,[\mathbf{1}'] + k_{-L}\,[\mathbf{X}]\,[\mathrm{py}] - k_L\,[\mathbf{1}']\,[\mathrm{tBA}] \tag{B}$$

Consistent with experimental finding, the insertion step has a slower rate than olefin coordination such that a fast equilibrium exists between species **1'** and **X**. We then have

$$K_L = \frac{[\mathrm{py}][\mathbf{X}]}{[\mathrm{tBA}]\,[\mathbf{1}']} \implies [\mathbf{1}'] = \frac{[\mathrm{py}][\mathbf{X}]}{[\mathrm{tBA}]K_L} \tag{C}$$

where K_L is the equilibrium constant between species **1'** and **X**.

Substituting Equation (C) into (B), we have

$$\begin{aligned} 0 &= k_{iso}\,[\mathbf{1}] - k_{-iso}\frac{[\mathrm{py}][\mathbf{X}]}{[\mathrm{tBA}]K_L} + k_{-L}\,[\mathbf{X}]\,[\mathrm{py}] - k_L\frac{[\mathrm{py}][\mathbf{X}]}{[\mathrm{tBA}]K_L}\,[\mathrm{tBA}] \\ \implies [\mathbf{X}] &= \frac{k_{iso}[\mathbf{1}][\mathrm{tBA}]K_L}{k_{-iso}[\mathrm{py}]} = K_{iso}K_L\,[\mathbf{1}]\,\frac{[\mathrm{tBA}]}{[\mathrm{py}]} \end{aligned} \tag{D}$$

Putting Equation (D) in (A), we have the rate of insertion as

$$\begin{aligned} rate &= k_{ins}\cdot[\mathbf{X}] = k_{ins}K_{iso}K_L\,[\mathbf{1}]\,\frac{[\mathrm{tBA}]}{[\mathrm{py}]} \\ &= k_{ins(\mathrm{tBA})}K_{iso}K_{L(\mathrm{tBA})}\,[\mathbf{1}]\,\frac{[\mathrm{tBA}]}{[\mathrm{py}]} \end{aligned} \tag{E}$$

Similarly, the rate of insertion of ethylene is given by

$$rate = k_{ins(\mathrm{et})}K_{iso}K_{L(\mathrm{et})}\,[\mathbf{1}]\,\frac{[\mathrm{et}]}{[\mathrm{py}]} \tag{F}$$

Note that equation (E) is consistent with the findings of experiment measurement of tBA enchainment that pseudo-1st order rate constant ($k_{obs\text{-}1}$, rate=$k_{obs\text{-}1}$[Ni]) is proportional to the concentration of tBA and inversely proportional to the concentration of pyridine in the range of concentrations studied.

11.3 Comparison of Ethylene and tBA Enchainment

Based on (E) and (F), the relative rate of insertions is then given by

$$\begin{aligned}\frac{rate(\text{et})}{rate(\text{tBA})} &= \frac{k_{ins(\text{et})}K_{iso}K_{L(\text{et})}\,[\mathbf{1}]\,[\text{et}]}{k_{ins(\text{tBA})}K_{iso}K_{L(\text{tBA})}\,[\mathbf{1}]\,[\text{tBA}]} \\ &= \frac{k_{ins(\text{et})}K_{L(\text{et})}[\text{et}]}{k_{ins(\text{tBA})}K_{L(\text{tBA})}[\text{tBA}]} \\ &= \exp[-\Delta\Delta G^{\ddagger}/RT]\cdot\exp[-\Delta\Delta G/RT]\frac{[\text{et}]}{[\text{tBA}]}\end{aligned} \tag{G}$$

where $\Delta\Delta G^{\ddagger} = \Delta G^{\ddagger}_{ins(et)} - \Delta G^{\ddagger}_{ins(tBA)}$ is the difference between the activation barriers of the insertions and $\Delta\Delta G = \Delta G_{ins(et)} - \Delta G_{ins(tBA)}$ is the difference between the complexation/ coordination energies. Note that the barriers are measured for each *elementary step* in this analysis.

For the first insertion of ethylene (Figure S2.9.9), the barrier of insertion is 5.9 kcal mol^{-1} (from **int1'-et-c2** to **ts1'-et**), while the coordination energy is 10.2 kcal mol^{-1} (from **1'** to **int1'-et-c2**). For the first insertion of tBA, the barrier of insertion is 3.1 kcal mol^{-1} (from **int1'-ac-c4** to **ts1'-ac**), while the coordination energy is 16.2 kcal mol^{-1} (from **1'** to **int1'-ac-c4**). Therefore, this gives the difference between the activation barriers of insertion as 2.8 kcal mol^{-1} and the difference between the coordination energies as -6.0 kcal mol^{-1}. The overall difference in the first insertions of ethylene and tBA is thus (2.8 + (-6.0)) = -3.2 kcal mol^{-1}, i.e., the insertion of ethylene has a barrier that is 3.2 kcal mol^{-1} lower than the insertion of tBA. This is consistent with the energetic span model[25,26] where the concept of turnover frequency (TOF) determining intermediate (TDI) and TOF-determining transition state (TDTS) is used. For both insertions, the TDI is the catalyst **1'** whereas the insertion step is the TDTS. The barrier differences between the insertion of ethylene (16.1 kcal mol^{-1} from **1'** to **ts1'-et**) and the insertion of tBA (19.3 kcal mol^{-1} from **1'** to **ts1'-ac**) is 3.2 kcal mol^{-1}, consistent with the kinetic analysis above.

Using similar analysis for the second insertion (shown below second insertion of tBA into first ethylene-inserted product as an example), where the key rate-determining steps are the same as for the first insertion,

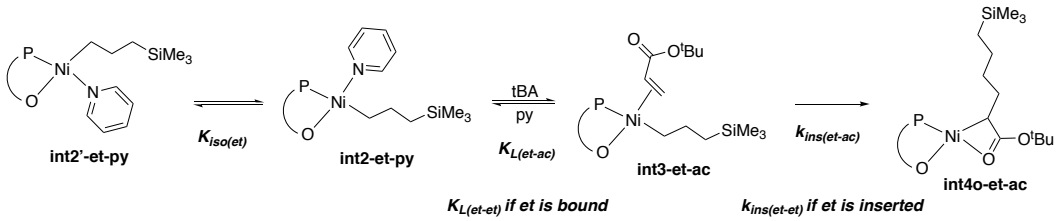

the relative rates for the second insertion of ethylene (et) vs tBA (ac) into first ethylene-inserted product is given by

$$\begin{aligned}\frac{rate(\text{et-et})}{rate(\text{et-ac})} &= \frac{k_{ins(\text{et-et})}K_{iso(et)}K_{L(\text{et-et})}\,[\textbf{int2'-et-py}]\,[\text{et}]}{k_{ins(\text{et-ac})}K_{iso(et)}K_{L(\text{et-ac})}\,[\textbf{int2'-et-py}]\,[\text{tBA}]} \\ &= \frac{k_{ins(\text{et-et})}K_{L(\text{et-et})}[\text{et}]}{k_{ins(\text{et-ac})}K_{L(\text{et-ac})}[\text{tBA}]} \\ &= \exp[-\Delta\Delta G^{\ddagger}/RT]\cdot\exp[-\Delta\Delta G/RT]\frac{[\text{et}]}{[\text{tBA}]}\end{aligned} \tag{H}$$

where again the differences between the Gibbs energy of activation $\Delta\Delta G^{\ddagger} = \Delta G^{\ddagger}_{ins(et-et)} - \Delta G^{\ddagger}_{ins(et-ac)}$ and of complexation/ coordination $\Delta\Delta G = \Delta G_{ins(et-et)} - \Delta G_{ins(et-ac)}$ are similarly defined.

11.4 Comparison of initiation vs propagation of ethylene (or tBA)

The rates of first insertion (initiation) and second insertion (propagation) can be similarly compared. For example, the relative rates of first insertion of ethylene into catalyst **1** and second insertion of ethylene into ethylene-inserted product **int2'-et-py** is given by

$$\begin{aligned}\frac{rate(\text{et})}{rate(\text{et-et})} &= \frac{k_{ins(\text{et})}K_{iso}K_{L(\text{et})}[\mathbf{1}][\text{et}]}{k_{ins(\text{et-et})}K_{iso(et)}K_{L(\text{et-et})}\,[\textbf{int2'-et-py}]\,[\text{et}]} \\ &= \frac{k_{ins(\text{et})}}{k_{ins(\text{et-et})}}\frac{K_{iso}}{K_{iso(et)}}\frac{K_{L(\text{et})}}{K_{L(\text{et-et})}}\frac{[\mathbf{1}]}{[\textbf{int2'-et-py}]} \\ &= \exp\left[-\Delta\Delta G^{\dagger}_{ins}/RT\right]\cdot\exp\left[-\Delta\Delta G_{iso}/RT\right]\cdot\exp\left[-\Delta\Delta G_{coord}/RT\right]\cdot\frac{[\mathbf{1}]}{[\textbf{int2'-et-py}]}\end{aligned} \tag{I}$$

From the energy profile in Figure S2.9.9, we see that the barrier for insertion of ethylene into catalyst **1'** (elementary step) is 5.9 kcal mol^{-1}; the insertion barrier of ethylene into **int2'-et-py** (Figure S2.9.11(a)) is 4.6 kcal mol^{-1}. This gives a barrier difference in the insertion of 1.3 kcal mol^{-1}. Similarly, the barrier difference in isomerization is 22.7 – 18.8 = 3.9 kcal mol^{-1}. The

difference in the coordination energies is 10.2 – 4.8 = 5.4 kcal mol^{-1}. This gives a total barrier difference of 10.6 kcal mol^{-1}. Using the energetic span model, the barrier for first insertion is 16.1 kcal mol^{-1} from the TDI (**1'**) to TDTS (**ts1'-et**); the barrier for second insertion into first ethylene-inserted product is 9.4 kcal mol^{-1} from the TDI (**int2-et-py**) to TDTS (**ts3-et-et**). This gives a barrier difference of 6.7 kcal mol^{-1} which is the sum of the differences in the coordination and insertion energies given by the elementary steps above (1.3 + 5.4) = 6.7 kcal mol^{-1}.

11.5 Comparison of propagation of ethylene (or tBA) into ethylene-initiated vs tBA-initiated species

The rates of second insertion (propagation) of each olefin into first ethylene- or tBA-inserted product can be similarly compared. The difference in the rates will arise from the first insertion of ethylene vs tBA, followed by the isomerization in each insertion product, as well as the second insertion into each first insertion product. We consider the insertion of ethylene into ethylene-inserted product vs into tBA-inserted product as an example; the insertion of tBA into ethylene-inserted product vs into tBA-inserted product is similar. The first insertion of ethylene (**ts1'-et**) is more favorable than the insertion of tBA (**ts1'-ac**) by 3.2 kcal mol^{-1}. Then, the isomerization of first ethylene-inserted product (**ts-5coord-et**, with a barrier of 18.8 kcal mol^{-1}) is in addition more favorable than the isomerization of first tBA-inserted product (**ts-5coord-ac**, with a barrier of 22.3 kcal mol^{-1}) by 3.5 kcal mol^{-1}. The subsequent ethylene insertion into first ethylene-inserted product (**ts3-et-et**, with a barrier of 9.4 kcal mol^{-1}) is in addition more favorable than the tBA insertion into first ethylene-inserted product (**ts3-et-ac**, with a barrier of 19.3 kcal mol^{-1}) by 9.9 kcal mol^{-1}. Taken together, this implies that the insertion of ethylene into ethylene-inserted product is *ca.* 10 orders of magnitude faster than into tBA-inserted product.

For the insertion of tBA into first ethylene-inserted vs tBA-inserted product, the insertion of tBA into first ethylene-inserted product (**ts3-et-ac**) has a barrier of 9.9 kcal mol^{-1}; the insertion of tBA into first tBA-inserted product has a barrier of 20.5 kcal mol^{-1}. This gives a difference in

the insertion step of 10.6 kcal mol^{-1}, which is very similar to the difference of insertion of ethylene into first ethylene-inserted and first tBA-inserted product (9.9 kcal mol^{-1} above). The differences in the first insertion of ethylene vs tBA and their subsequent isomerization are the same as above (3.2 kcal mol^{-1} and 3.5 kcal mol^{-1} respectively). Thus, we expect the insertion of tBA into tBA-inserted product to be *ca.* 10 orders of magnitude faster than into tBA-inserted product.

REFERENCES

(1) Chen, C., Designing catalysts for olefin polymerization and copolymerization: beyond electronic and steric tuning. *Nat. Rev. Chem.* **2018,** *2* (5), 6-14.

(2) Younkin, T. R.; Connor, E. F.; Henderson, J. I.; Friedrich, S. K.; Grubbs, R. H.; Bansleben, D. A., Neutral, single-component nickel (II) polyolefin catalysts that tolerate heteroatoms. *Science* **2000,** *287* (5452), 460-462.

(3) Nakamura, A.; Ito, S.; Nozaki, K., Coordination− insertion copolymerization of fundamental polar monomers. *Chem. Rev.* **2009,** *109* (11), 5215-5244.

(4) Carrow, B. P.; Nozaki, K., Transition-metal-catalyzed functional polyolefin synthesis: effecting control through chelating ancillary ligand design and mechanistic insights. *Macromolecules* **2014,** *47* (8), 2541-2555.

(5) Guan, Z.; Cotts, P.; McCord, E.; McLain, S., Chain walking: a new strategy to control polymer topology. *Science* **1999,** *283* (5410), 2059-2062.

(6) Arriola, D. J.; Carnahan, E. M.; Hustad, P. D.; Kuhlman, R. L.; Wenzel, T. T., Catalytic production of olefin block copolymers via chain shuttling polymerization. *Science* **2006,** *312* (5774), 714-719.

(7) Delferro, M.; Marks, T. J., Multinuclear olefin polymerization catalysts. *Chem. Rev.* **2011,** *111* (3), 2450-2485.

(8) Makio, H.; Terao, H.; Iwashita, A.; Fujita, T., FI Catalysts for olefin polymerization□ A comprehensive treatment. *Chem. Rev.* **2011,** *111* (3), 2363-2449.

(9) Johnson, L. K.; Mecking, S.; Brookhart, M., Copolymerization of ethylene and propylene with functionalized vinyl monomers by palladium (II) catalysts. *J. Am. Chem. Soc.* **1996,** *118* (1), 267-268.

(10) Guironnet, D.; Roesle, P.; Rünzi, T.; Göttker-Schnetmann, I.; Mecking, S., Insertion polymerization of acrylate. *J. Am. Chem. Soc.* **2009,** *131* (2), 422-423.

(11) Weng, W.; Shen, Z.; Jordan, R. F., Copolymerization of ethylene and vinyl fluoride by (phosphine-sulfonate) Pd (Me)(py) catalysts. *J. Am. Chem. Soc.* **2007,** *129* (50), 15450-15451.

(12) Johnson, L. K.; Killian, C. M.; Brookhart, M., New Pd (II)-and Ni (II)-based catalysts for polymerization of ethylene and. alpha.-olefins. *J. Am. Chem. Soc.* **1995,** *117* (23), 6414-6415.

(13) Williams, B. S.; Leatherman, M. D.; White, P. S.; Brookhart, M., Reactions of vinyl acetate and vinyl trifluoroacetate with cationic diimine Pd (II) and Ni (II) alkyl complexes: identification of problems connected with copolymerizations of these monomers with ethylene. *J. Am. Chem. Soc.* **2005,** *127* (14), 5132-5146.

(14) Dai, S.; Sui, X.; Chen, C., Highly Robust Palladium (II) α-Diimine Catalysts for Slow-Chain-Walking Polymerization of Ethylene and Copolymerization with Methyl Acrylate. *Angew. Chem. Int. Ed.* **2015,** *54* (34), 9948-9953.

(15) Chen, Z.; Liu, W.; Daugulis, O.; Brookhart, M., Mechanistic studies of Pd (II)-catalyzed copolymerization of ethylene and vinylalkoxysilanes: Evidence for a β-silyl elimination chain transfer mechanism. *J. Am. Chem. Soc.* **2016,** *138* (49), 16120-16129.

(16) Long, B. K.; Eagan, J. M.; Mulzer, M.; Coates, G. W., Semi-Crystalline Polar Polyethylene: Ester-Functionalized Linear Polyolefins Enabled by a Functional-Group-Tolerant, Cationic Nickel Catalyst. *Angew. Chem. Int. Ed.* **2016,** *55* (25), 7106-7110.

(17) Drent, E.; van Dijk, R.; van Ginkel, R.; van Oort, B.; Pugh, R. I., Palladium catalysed copolymerisation of ethene with alkylacrylates: polar comonomer built into the linear polymer chain. *Chemical Communications* **2002,** (7), 744-745.

(18) Ito, S.; Munakata, K.; Nakamura, A.; Nozaki, K., Copolymerization of vinyl acetate with ethylene by palladium/alkylphosphine− sulfonate catalysts. *Journal of the American Chemical Society* **2009,** *131* (41), 14606-14607.

(19) Nozaki, K.; Kusumoto, S.; Noda, S.; Kochi, T.; Chung, L. W.; Morokuma, K., Why did incorporation of acrylonitrile to a linear polyethylene become possible? Comparison of phosphine− sulfonate ligand with diphosphine and imine− phenolate ligands in the Pd-catalyzed ethylene/acrylonitrile copolymerization. *Journal of the American Chemical Society* **2010,** *132* (45), 16030-16042.

(20) Ito, S.; Kanazawa, M.; Munakata, K.; Kuroda, J.-i.; Okumura, Y.; Nozaki, K., Coordination− insertion copolymerization of allyl monomers with ethylene. *Journal of the American Chemical Society* **2011,** *133* (5), 1232-1235.

(21) Leicht, H.; Göttker-Schnetmann, I.; Mecking, S., Incorporation of vinyl chloride in insertion polymerization. *Angewandte Chemie International Edition* **2013,** *52* (14), 3963-3966.

(22) Jian, Z.; Baier, M. C.; Mecking, S., Suppression of chain transfer in catalytic acrylate polymerization via rapid and selective secondary insertion. *Journal of the American Chemical Society* **2015,** *137* (8), 2836-2839.

(23) Ota, Y.; Ito, S.; Kobayashi, M.; Kitade, S.; Sakata, K.; Tayano, T.; Nozaki, K., Crystalline Isotactic Polar Polypropylene from the Palladium-Catalyzed Copolymerization of Propylene and Polar Monomers. *Angew. Chem. Int. Ed.* **2016,** *55* (26), 7505-7509.

(24) Noda, S.; Nakamura, A.; Kochi, T.; Chung, L. W.; Morokuma, K.; Nozaki, K., Mechanistic studies on the formation of linear polyethylene chain catalyzed by palladium phosphine− sulfonate complexes: experiment and theoretical studies. *J. Am. Chem. Soc.* **2009,** *131* (39), 14088-14100.

(25) Ota, Y.; Ito, S.; Kuroda, J.-i.; Okumura, Y.; Nozaki, K., Quantification of the steric influence of alkylphosphine–sulfonate ligands on polymerization, leading to high-molecular-weight copolymers of ethylene and polar monomers. *J. Am. Chem. Soc.* **2014,** *136* (34), 11898-11901.

(26) Nakano, R.; Chung, L. W.; Watanabe, Y.; Okuno, Y.; Okumura, Y.; Ito, S.; Morokuma, K.; Nozaki, K., Elucidating the key role of phosphine− sulfonate ligands in palladium-catalyzed ethylene polymerization: Effect of ligand structure on the molecular weight and linearity of polyethylene. *ACS Catal.* **2016,** *6* (9), 6101-6113.

(27) Carrow, B. P.; Nozaki, K., Synthesis of functional polyolefins using cationic bisphosphine monoxide–palladium complexes. *J. Am. Chem. Soc.* **2012,** *134* (21), 8802-8805.

(28) Chen, M.; Yang, B.; Chen, C., Redox-Controlled Olefin (Co) Polymerization Catalyzed by Ferrocene-Bridged Phosphine-Sulfonate Palladium Complexes. *Angew. Chem. Int. Ed.* **2015,** *54* (51), 15520-15524.

(29) Tao, W. j.; Nakano, R.; Ito, S.; Nozaki, K., Copolymerization of ethylene and polar monomers by using Ni/IzQO catalysts. *Angew. Chem. Int. Ed.* **2016,** *55* (8), 2835-2839.

(30) Zhang, D.; Chen, C., Influence of Polyethylene Glycol Unit on Palladium-and Nickel-Catalyzed Ethylene Polymerization and Copolymerization. *Angew. Chem. Int. Ed.* **2017,** *56* (46), 14672-14676.

(31) Chen, M.; Chen, C., A Versatile Ligand Platform for Palladium-and Nickel-Catalyzed Ethylene Copolymerization with Polar Monomers. *Angew. Chem. Int. Ed.* **2018,** *57* (12), 3094-3098.

(32) Zhang, W.; Waddell, P. M.; Tiedemann, M. A.; Padilla, C. E.; Mei, J.; Chen, L.; Carrow, B. P., Electron-rich metal cations enable synthesis of high molecular weight, linear functional polyethylenes. *Journal of the American Chemical Society* **2018,** *140* (28), 8841-8850.

(33) Mitsushige, Y.; Yasuda, H.; Carrow, B. P.; Ito, S.; Kobayashi, M.; Tayano, T.; Watanabe, Y.; Okuno, Y.; Hayashi, S.; Kuroda, J., Methylene-bridged bisphosphine monoxide ligands for palladium-catalyzed copolymerization of ethylene and polar monomers. *ACS Macro Lett.* **2018,** *7* (3), 305-311.

(34) Tan, C.; Chen, C., Emerging palladium and nickel catalysts for copolymerization of olefins with polar monomers. *Angew. Chem.* **2019,** *131* (22), 7268-7276.

(35) Liu, F.-S.; Hu, H.-B.; Xu, Y.; Guo, L.-H.; Zai, S.-B.; Song, K.-M.; Gao, H.-Y.; Zhang, L.; Zhu, F.-M.; Wu, Q., Thermostable α-diimine nickel (II) catalyst for ethylene polymerization: effects of the substituted backbone structure on catalytic properties and branching structure of polyethylene. *Macromolecules* **2009,** *42* (20), 7789-7796.

(36) Ito, S.; Ota, Y.; Nozaki, K., Ethylene/allyl monomer cooligomerization by nickel/phosphine–sulfonate catalysts. *Dalton Trans* **2012,** *41* (45), 13807-13809.

(37) Xin, B. S.; Sato, N.; Tanna, A.; Oishi, Y.; Konishi, Y.; Shimizu, F., Nickel catalyzed copolymerization of ethylene and alkyl acrylates. *Journal of the American Chemical Society* **2017,** *139* (10), 3611-3614.

(38) Chen, M.; Chen, C., Rational design of high-performance phosphine sulfonate nickel catalysts for ethylene polymerization and copolymerization with polar monomers. *ACS Catal.* **2017,** *7* (2), 1308-1312.

(39) Rhinehart, J. L.; Mitchell, N. E.; Long, B. K., Enhancing α-diimine catalysts for high-temperature ethylene polymerization. *ACS Catal.* **2014,** *4* (8), 2501-2504.

(40) Zhang, Y.; Mu, H.; Pan, L.; Wang, X.; Li, Y., Robust bulky [P, O] neutral nickel catalysts for copolymerization

of ethylene with polar vinyl monomers. *ACS Catalysis* **2018,** *8* (7), 5963-5976.

(41) Lam, F.; Chan, K. S., Synthesis of acyclic dinucleating Schiff base-pyridine and schiff base-phosphine ligands. *Tetrahedron Lett.* **1995,** *36* (6), 919-922.

(42) Kim, J. S.; Sen, A.; Guzei, I. A.; Liable-Sands, L. M.; Rheingold, A. L., Synthesis and reactivity of bimetallic palladium (II) methyl complexes with new functional phosphine ligands. *J. Chem. Soc., Dalton Trans.* **2002,** (24), 4726-4731.

(43) Radlauer, M. R.; Day, M. W.; Agapie, T., Dinickel bisphenoxyiminato complexes for the polymerization of ethylene and α-olefins. *Organometallics* **2012,** *31* (6), 2231-2243.

(44) Gates, D. P.; Svejda, S. A.; Oñate, E.; Killian, C. M.; Johnson, L. K.; White, P. S.; Brookhart, M., Synthesis of branched polyethylene using (α-diimine) nickel (II) catalysts: influence of temperature, ethylene pressure, and ligand structure on polymer properties. *Macromolecules* **2000,** *33* (7), 2320-2334.

(45) Chen, Z.; Leatherman, M. D.; Daugulis, O.; Brookhart, M., Nickel-catalyzed copolymerization of ethylene and vinyltrialkoxysilanes: catalytic production of cross-linkable polyethylene and elucidation of the chain-growth mechanism. *J. Am. Chem. Soc.* **2017,** *139* (44), 16013-16022.

(46) Sahgal, A.; La, H.; Hayduk, W., Solubility of ethylene in several polar and non-polar solvents. *Can. J. Chem. Eng* **1978,** *56* (3), 354-357.

(47) Grau, E.; Broyer, J.-P.; Boisson, C.; Spitz, R.; Monteil, V., Supercritical behavior in free radical polymerization of ethylene in the medium pressure range. *Phys. Chem. Chem. Phys.* **2010,** *12* (37), 11665-11669.

(48) Mitsushige, Y.; Carrow, B. P.; Ito, S.; Nozaki, K., Ligand-controlled insertion regioselectivity accelerates copolymerisation of ethylene with methyl acrylate by cationic bisphosphine monoxide–palladium catalysts. *Chemical science* **2016,** *7* (1), 737-744.

(49) Guironnet, D.; Caporaso, L.; Neuwald, B.; Göttker-Schnetmann, I.; Cavallo, L.; Mecking, S., Mechanistic insights on acrylate insertion polymerization. *J. Am. Chem. Soc.* **2010,** *132* (12), 4418-4426.

(50) Berkefeld, A.; Drexler, M.; Möller, H. M.; Mecking, S., Mechanistic insights on the copolymerization of polar vinyl monomers with neutral Ni (II) catalysts. *J. Am. Chem. Soc.* **2009,** *131* (35), 12613-12622.

(51) Boffa, L. S.; Novak, B. M., Copolymerization of polar monomers with olefins using transition-metal complexes. *Chem. Rev.* **2000,** *100* (4), 1479-1494.

(52) Jin, D.; Schmeier, T. J.; Williard, P. G.; Hazari, N.; Bernskoetter, W. H., Lewis acid induced β-elimination from a nickelalactone: efforts toward acrylate production from CO2 and ethylene. *Organometallics* **2013,** *32* (7), 2152-2159.

(53) Jin, D.; Williard, P. G.; Hazari, N.; Bernskoetter, W. H., Effect of Sodium Cation on Metallacycle β-Hydride Elimination in CO2–Ethylene Coupling to Acrylates. *Chemistry–A European Journal* **2014,** *20* (11), 3205-3211.

(54) Plessow, P. N.; Weigel, L.; Lindner, R.; Schäfer, A.; Rominger, F.; Limbach, M.; Hofmann, P., Mechanistic details of the nickel-mediated formation of acrylates from CO2, ethylene and methyl iodide. *Organometallics* **2013,** *32* (11), 3327-3338.

(55) Langer, J.; Görls, H.; Fischer, R.; Walther, D., Organometallic Nickelamacrocycles of the Type [(R2R 'P) Ni (C2H4COO)] n: Synthesis and Self-Assembly to Form Different Molecular Architectures Tuned by the Phosphine. *Organometallics* **2005,** *24* (2), 272-279.

(56) Fischer, R.; Langer, J.; Malassa, A.; Walther, D.; Görls, H.; Vaughan, G., A key step in the formation of acrylic acid from CO 2 and ethylene: the transformation of a nickelalactone into a nickel-acrylate complex. *Chem. Commun.* **2006,** (23), 2510-2512.

(57) Guo, W.; Michel, C.; Schwiedernoch, R.; Wischert, R.; Xu, X.; Sautet, P., Formation of acrylates from ethylene and CO2 on Ni complexes: a mechanistic viewpoint from a hybrid DFT approach. *Organometallics* **2014,** *33* (22), 6369-6380.

(58) Jenkins, J. C.; Brookhart, M., A mechanistic investigation of the polymerization of ethylene catalyzed by neutral Ni (II) complexes derived from bulky anilinotropone ligands. *J. Am. Chem. Soc.* **2004,** *126* (18), 5827-5842.

(59) Zhao, Y.; Truhlar, D. G., The M06 suite of density functionals for main group thermochemistry, thermochemical kinetics, noncovalent interactions, excited states, and transition elements: two new functionals and

systematic testing of four M06-class functionals and 12 other functionals. *Theo. Chem. Acc.* **2008,** *120* (1-3), 215-241.

(60) Weigend, F.; Ahlrichs, R., Balanced basis sets of split valence, triple zeta valence and quadruple zeta valence quality for H to Rn: Design and assessment of accuracy. *Phys. Chem. Chem. Phys.* **2005,** *7* (18), 3297-3305.

(61) Weigend, F., Accurate Coulomb-fitting basis sets for H to Rn. *Phys. Chem. Chem. Phys.* **2006,** *8* (9), 1057-1065.

(62) Marenich, A. V.; Cramer, C. J.; Truhlar, D. G., Universal solvation model based on solute electron density and on a continuum model of the solvent defined by the bulk dielectric constant and atomic surface tensions. *The Journal of Physical Chemistry B* **2009,** *113* (18), 6378-6396.

(63) Sun, J.; Chen, M.; Luo, G.; Chen, C.; Luo, Y., Diphosphazane-monoxide and Phosphine-sulfonate Palladium Catalyzed Ethylene Copolymerization with Polar Monomers: A Computational Study. *Organometallics* **2019,** *38* (3), 638-646.

(64) Conley, M. P.; Jordan, R. F., cis/trans isomerization of phosphinesulfonate palladium (II) complexes. *Angew. Chem. Int. Ed.* **2011,** *50* (16), 3744-3746.

(65) Tran, Q. H.; Brookhart, M.; Daugulis, O., New Neutral Nickel and Palladium Sandwich Catalysts: Synthesis of Ultra-High Molecular Weight Polyethylene (UHMWPE) via Highly Controlled Polymerization and Mechanistic Studies of Chain Propagation. *J. Am. Chem. Soc.* **2020,** *142* (15), 7198-7206.

(66) Kozuch, S.; Shaik, S., How to conceptualize catalytic cycles? The energetic span model. *Acc. Chem. Res.* **2011,** *44* (2), 101-110.

(67) Pangborn, A. B.; Giardello, M. A.; Grubbs, R. H.; Rosen, R. K.; Timmers, F. J., Safe and convenient procedure for solvent purification. *Organometallics* **1996,** *15* (5), 1518-1520.

(68) Neuwald, B.; Caporaso, L.; Cavallo, L.; Mecking, S., Concepts for stereoselective acrylate insertion. *J. Am. Chem. Soc.* **2013,** *135* (3), 1026-1036.

(69) Low, C. H.; Rosenberg, J. N.; Lopez, M. A.; Agapie, T., Oxidative coupling with Zr (IV) supported by a noninnocent anthracene-based ligand: Application to the catalytic cotrimerization of alkynes and nitriles to pyrimidines. *J. Am. Chem. Soc.* **2018,** *140* (38), 11906-11910.

(70) Connor, E. F.; Younkin, T. R.; Henderson, J. I.; Waltman, A. W.; Grubbs, R. H., Synthesis of neutral nickel catalysts for ethylene polymerization–the influence of ligand size on catalyst stability. *Chem. Commun.* **2003,** (18), 2272-2273.

(71) Palmer, W. N.; Zarate, C.; Chirik, P. J., Benzyltriboronates: building blocks for diastereoselective carbon–carbon bond formation. *J. Am. Chem. Soc.* **2017,** *139* (7), 2589-2592.

(72) Burger, B. J.; Bercaw, J. E., Vacuum line techniques for handling air-sensitive organometallic compounds. ACS Publications: 1987.

(73) Grimme, S.; Bannwarth, C.; Shushkov, P., A robust and accurate tight-binding quantum chemical method for structures, vibrational frequencies, and noncovalent interactions of large molecular systems parametrized for all spd-block elements (Z= 1–86). *Journal of chemical theory and computation* **2017,** *13* (5), 1989-2009.

(74) Manby, F.; Miller, T.; Bygrave, P.; Ding, F.; Dresselhaus, T.; Batista-Romero, F.; Buccheri, A.; Bungey, C.; Lee, S.; Meli, R., entos: A quantum molecular simulation package. **2019**.

(75) Frisch, M. J.; Trucks, G. W.; Schlegel, H. B.; Scuseria, G. E.; Robb, M. A.; Cheeseman, J. R.; Scalmani, G.; Barone, V.; Petersson, G. A.; Nakatsuji, H.; Li, X.; Caricato, M.; Marenich, A. V.; Bloino, J.; Janesko, B. G.; Gomperts, R.; Mennucci, B.; Hratchian, H. P.; Ortiz, J. V.; Izmaylov, A. F.; Sonnenberg, J. L.; Williams; Ding, F.; Lipparini, F.; Egidi, F.; Goings, J.; Peng, B.; Petrone, A.; Henderson, T.; Ranasinghe, D.; Zakrzewski, V. G.; Gao, J.; Rega, N.; Zheng, G.; Liang, W.; Hada, M.; Ehara, M.; Toyota, K.; Fukuda, R.; Hasegawa, J.; Ishida, M.; Nakajima, T.; Honda, Y.; Kitao, O.; Nakai, H.; Vreven, T.; Throssell, K.; Montgomery Jr., J. A.; Peralta, J. E.; Ogliaro, F.; Bearpark, M. J.; Heyd, J. J.; Brothers, E. N.; Kudin, K. N.; Staroverov, V. N.; Keith, T. A.; Kobayashi, R.; Normand, J.; Raghavachari, K.; Rendell, A. P.; Burant, J. C.; Iyengar, S. S.; Tomasi, J.; Cossi, M.; Millam, J. M.; Klene, M.; Adamo, C.; Cammi, R.; Ochterski, J. W.; Martin, R. L.; Morokuma, K.; Farkas, O.; Foresman, J. B.; Fox, D. J. *Gaussian 16 Rev. C.01*, Wallingford, CT, 2016.

(76) Hu, L.; Chen, H., Assessment of DFT methods for computing activation energies of Mo/W-mediated reactions. *Journal of Chemical Theory and Computation* **2015,** *11* (10), 4601-4614.

(77) Sun, Y.; Chen, H., Performance of density functionals for activation energies of Re-catalyzed organic reactions. *Journal of Chemical Theory and Computation* **2014,** *10* (2), 579-588.

(78) Haoyu, S. Y.; He, X.; Li, S. L.; Truhlar, D. G., MN15: A Kohn–Sham global-hybrid exchange–correlation density functional with broad accuracy for multi-reference and single-reference systems and noncovalent interactions. *Chem. Sci.* **2016,** *7* (8), 5032-5051.

(79) Liu, Z.; Wang, Y.; Wang, Z.; Zeng, T.; Liu, P.; Engle, K. M., Catalytic intermolecular carboamination of unactivated alkenes via directed aminopalladation. *J. Am. Chem. Soc.* **2017,** *139* (32), 11261-11270.

(80) O'Duill, M. L.; Matsuura, R.; Wang, Y.; Turnbull, J. L.; Gurak Jr, J. A.; Gao, D.-W.; Lu, G.; Liu, P.; Engle, K. M., Tridentate directing groups stabilize 6-membered palladacycles in catalytic alkene hydrofunctionalization. *J. Am. Chem. Soc.* **2017,** *139* (44), 15576-15579.

(81) Fukui, K., The path of chemical reactions-the IRC approach. *Acc. Chem. Res.* **1981,** *14* (12), 363-368.

(82) Fukui, K., Formulation of the reaction coordinate. *The Journal of Physical Chemistry* **1970,** *74* (23), 4161-4163.

(83) Grimme, S., Supramolecular binding thermodynamics by dispersion-corrected density functional theory. *Chem. - Eur. J.* **2012,** *18* (32), 9955-9964.

(84) Funes-Ardoiz, I.; Paton, R., GoodVibes v2. 0.2. DOI: 2016.

(85) Contreras-García, J.; Johnson, E. R.; Keinan, S.; Chaudret, R.; Piquemal, J.-P.; Beratan, D. N.; Yang, W., NCIPLOT: a program for plotting noncovalent interaction regions. *Journal of chemical theory and computation* **2011,** *7* (3), 625-632.

(86) Sosa, C.; Andzelm, J.; Elkin, B. C.; Wimmer, E.; Dobbs, K. D.; Dixon, D. A., A local density functional study of the structure and vibrational frequencies of molecular transition-metal compounds. *The Journal of Physical Chemistry* **1992,** *96* (16), 6630-6636.

(87) Godbout, N.; Salahub, D. R.; Andzelm, J.; Wimmer, E., Optimization of Gaussian-type basis sets for local spin density functional calculations. Part I. Boron through neon, optimization technique and validation. *Canadian Journal of Chemistry* **1992,** *70* (2), 560-571.

(88) Schrödinger, L., The PyMOL molecular graphics system, version 1.7. 6.6. *Schrödinger LLC* **2015**.

CHAPTER 3

Olefin Coordination and Complex Isomerization Studies Relevant to Mechanism of Ni-Catalyzed Ethylene/Acrylate Copolymerization

This work was published in part as:

Organometallics **2022**, *41*, 2119.

Chapter 3

CONTRIBUTIONS AND ACKNOWLEDGEMENTS

Manar M. Shoshani, Shuoyan Xiong, and Theodor Agapie conceived the presented idea. M.M.S. and S.X. performed synthetic and mechanistic studies. James Lawniczak, Xinglong Zhang and Thomas F. Miller III performed DFT calculations and result analysis. M.M.S. and S.X. that is reproduced as this chapter. J.L., X.Z., T.F.M., and T.A. contributed to manuscript editing.

We are grateful to Dow (T.A.) and the Natural Sciences and Engineering Research Counsel of Canada (M.M.S.) for funding. X.Z. acknowledges the Agency for Science, Technology and Research (A*STAR), Singapore, for a National Science Scholarship. We thank Brad C. Bailey and Heather A. Spinney (Dow) for performing polymerization studies and polymer characterization, as well as insightful discussions. We thank Michael Takase and Lawrence Henling for assistance with X-ray crystallography and David VanderVelde for assistance with NMR spectroscopy. We thank Alex J. Nett, Briana S. Henderson, and Hannah Bailey (Dow) for assistance in collecting polymer characterization data (GPC, DSC, and FT-IR). Support has been provided for the Xray diffraction and NMR instrumentation via the Dow Next Generation Educator Fund. This work used the Bridges-2 system at the Pittsburgh Supercomputing Center (PSC). This material is based upon work supported by the National Science Foundation Graduate Research Fellowship under Grant No. DGE--1144469.

ABSTRACT

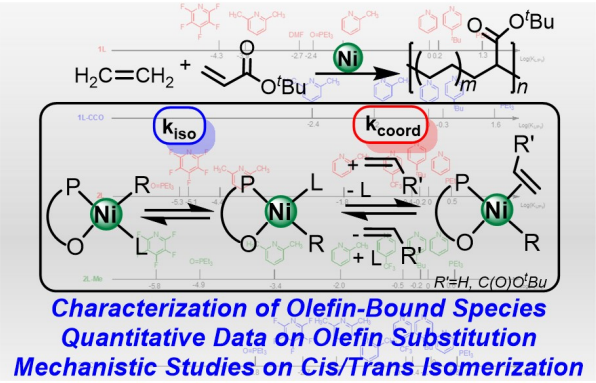

The insertion copolymerization of ethylene and acrylate remains a challenge in polymer synthesis due to decreased activities upon incorporation of polar monomer. Toward gaining mechanistic insight, two elusive four-membered chelated intermediates generated after acrylate insertion were prepared (**1-CCO** and **2-CCO**) and their ligand coordination and substitution behavior were studied. Specifically, an ethylene-coordinated species was characterized by NMR spectroscopy upon exposing **2-CCO** to ethylene at low temperatures, a rare observation for neutral late-transition metal polymerization catalysts. Thermodynamics of chelate-opening and monomer coordination from **2-CCO** were determined at -90 °C (ΔG of 0.4 kcal/mol for ethylene and 1.9 kcal/mol for 1-hexene). The Gibbs energy barrier of ligand exchange from pyridine to ethylene, a prerequisite for ethylene insertion in catalysis, was determined to be 3.3 kcal/mol. Ligand binding studies reveal that, compared to NiMe and $Ni(CH_2SiMe_3)$ complexes, acrylate inserted species **1L-CCO** and **2L-CCO** produce compressed thermodynamic binding-scales for both electronically and sterically

differentiating ligands, potentially related to their more electron deficient nickel centers as suggested by computational studies. Triethylphosphine complexes **1P**, **2P** and **2P-Me** were observed as both cis- and trans- isomers in solution. $^{31}P\{^{1}H\}$ EXSY NMR studies of **2P** reveal conversion between the cis and trans isomers that does not involve exchange with free PEt_3, supporting a mechanism of intramolecular isomerization. **2-CCO**, a neutral Ni(II) precatalyst that does not display an auxiliary ligand, serves as a highly active catalyst for copolymerization.

Chapter 3

GENERAL INTRODUCTION

The copolymerization of non-polar and polar monomers has garnered continued interest due to growing demand of diverse plastics in a plethora of industrial sectors.[1-6] Compared to the industrially employed radical process, coordination copolymerization has the potential to offer a precise control of copolymer microstructure and only requires mild conditions, and thus is considered as an economical and environmentally friendly alternative.[7-9] Several transition metal catalyst systems have been developed, with a focus on palladium and nickel complexes due to the low oxophilicity of these metal centers.[10-19] Among all reported systems, neutral nickel catalysts supported by bulky, asymmetric ligands stand out due to their high activity, low oxophillicity, and thermal stability, as well as the relatively low cost of the metal.[20-25]

Despite promise for catalysis, mechanistic details of this family of neutral Ni copolymerization catalysts are less explored.[26] Mechanistic studies have largely been restricted by the scarcity of isolable intermediates relevant to catalysis. For example, the success of isolating products of monomer insertion with diimine palladium and nickel complexes allows in-depth studies of olefin coordination, migratory insertion, and isomerization relevant to the copolymerization of ethylene and polar monomers including methyl acrylate,[12, 27] vinyl acetate,[28] and vinylalkoxysilanes.[29-31] Chain-walking with these symmetrical catalysts leads to the formation of highly branched copolymers,[7, 27, 32-33] deviating from the more widely used long chain polyolefins. In

contrast, neutral, asymmetric group 10 catalysts produce long chain copolymers with few branches,[14, 20] but gaining similar experimental insight of olefin coordination with these catalysts has been hampered by the presence of a strongly coordinating ligands L (e.g. pyridine or PR_3) that complete the square planar coordination sphere of the metal and must be substituted by olefin.[26, 34-35]Notably, the presence of olefin adducts have been observed with neutral, asymmetric N,O-chelated Pd catalysts and strong evidence of the presence of an ethylene adduct has been reported with a Ni-anilinotropone complex.[35-36]

We recently reported the nickel phosphine phenoxide complexes **1** and **2** (Figure 3.1a, b) that serve as thermally robust, highly active catalysts for the ethylene/acrylate copolymereization.[24] Potentially owing to the steric protection ortho to the phenoxide, acrylate inserted species from **1** and **2** were isolable, allowing the determination of kinetic details of chain propagation (Figure 3.1c). These indicate that the migratory insertion of olefins is relatively slow compared to ligand exchange. Overall, the ethylene enchainment after acrylate is the rate-determining step for copolymerization and the acrylate-inserted species is the resting state of catalysis. Investigations of olefin coordination has been impeded by the presence of pyridine in the coordination sphere and the thermodynamic preference for heterocycle binding. Notably, an auxiliary donor-free acrylate-inserted species, **2-CCO**, was prepared and isolated (Figure 3.1a). Herein, we report the observation of olefin-coordinated adducts using **2-CCO**, a rare demonstration for neutral Ni(II) precatalysts. We also report relative binding affinities for olefins and other donors relevant to copolymerization catalysis. In addition, facile

access to **2-CCO** allowed for the determination of thermodynamics of chelate opening by monomer coordination. Using **2**, we also report quantitative data relevant to mechanism of cis/trans isomerization. Notably, complex **2-CCO** is also an efficient catalyst in both ethylene homopolymerization and copolymerization with tert-butyl acrylate (tBA), represent the first example of ancillary ligand L free neutral nickel polymerization catalysts.

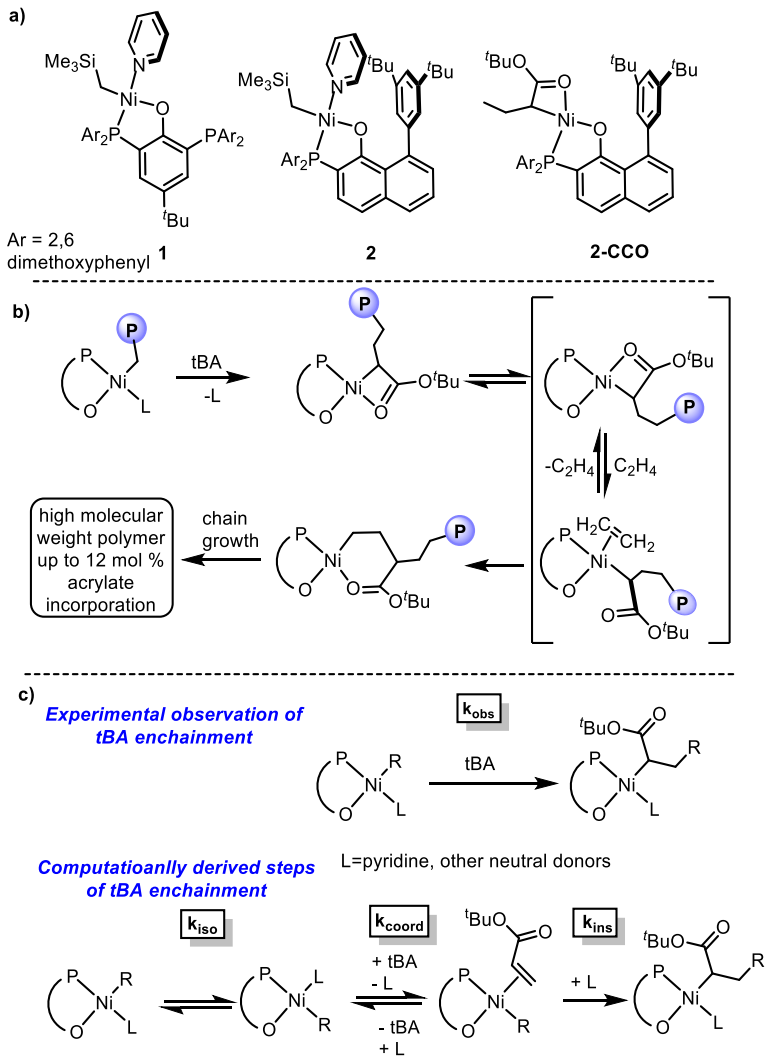

Figure 3.1. a) Nickel complex **1, 2, 2-CCO**. b) Mechanism of chain growth by Ni-phosphine phenoxide catalysts c) Experimental and computational steps for acrylate enchainment.

RESULTS AND DISCUSSION

Preparation and Characterization of Ni(CCO) Complexes

Compound **2lut-Me** was accessed by treating **PONap-H** with one equiv. of $NiMe_2$(TMEDA) in the presence of excess of lutidine (Figure 3.2a). Addition of excess tBA to an in situ generated solution of **2lut-Me** led to the isolation of **2-CCO** (Figure 3.2a), as previously reported.[24] Compound **2-CCO** represents the first spectroscopically and crystallographically characterized example of the auxiliary ligand free, four-membered chelate generated after acrylate insertion. Solution-state NMR characterization indicates the existence of two conformers that exchange on the NMR time scale. Specifically, two sets of sharp peaks were observed in the ^{1}H and ^{31}P{^{1}H} NMR spectra at temperatures ranging from 0 °C to -60 °C. The ratio of two conformers varies under different temperatures. Coalescence of the peaks corresponding to the two isomers was observed at 20 °C.

Akin to the synthesis and isolation of **2-CCO**, reaction of **POP-H** and one equiv. of $NiMe_2$(TMEDA) in the presence of excess of lutidine allowed for the generation of **1lut-Me** (Figure 3.2b). After removal of lutidine under vacuum, addition of excess tBA results in a color change from yellow to red over the course of 0.5 h. ^{31}P{^{1}H} NMR spectra revealed the consumption of **1lut-Me** and the appearance of a new species after removal of volatiles. The absence of lutidine resonances indicates the loss of this ligand and potential generation of acrylate inserted species that chelate to Ni. Indeed, the ^{1}H NMR spectra feature resonances similar to those observed for **2-**

CCO. The room temperature $^{31}P\{^{1}H\}$ NMR spectrum displays two sets of broad resonances corresponding to bound phosphine environments. Variable-temperature NMR spectroscopy was performed and the observed coalescence of the two species at 50 °C is consistent with a fluctional process between two conformers. Further interrogation via ^{1}H-^{1}H COSY experiments provides evidence of the tentative assignment of this species as **1-CCO**, the POP variant of **2-CCO**. Both are four-membered chelates generated after 2,1-insertion of tBA.

While crystallographic characterization of **1-CCO** has not been successful thus far, the solid-state structure of the PEt_3 adduct **1P-CCO** was obtained upon the addition of excess PEt_3 to **1-CCO** (Figure 3.2c). Single crystals of **1P-CCO** were grown via vapor diffusion of hexanes into the toluene solution of **1-CCO** with PEt_3 at -40 °C (Figure 3.2c). The solid-state structure reveals that the tBA indeed inserts in a 2,1-fashion into the Ni-CH_3 bond and is consistent with the assignment of **2-CCO** as the auxiliary donor-free compound generated after 2,1-insertion of tBA.

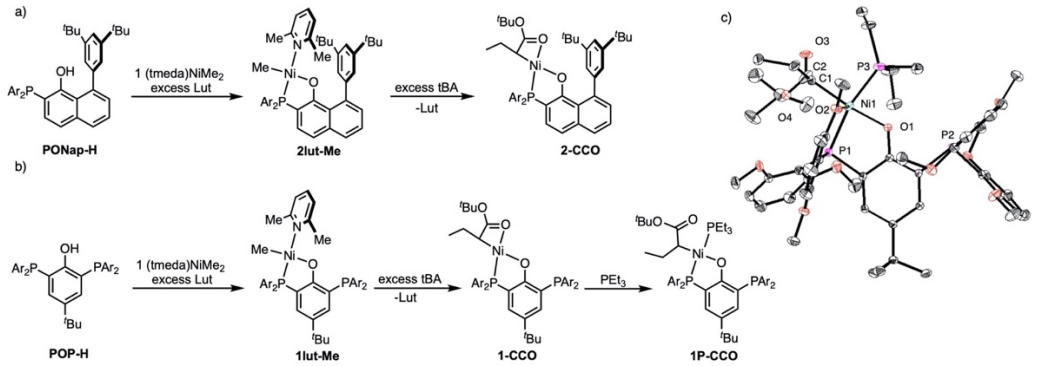

Figure 3.2. Preparation of nickel chelated-alkyl ether complexes (a and b) and ORTEP Depiction of **1P-CCO** (c, H-atoms excluded for clarity).

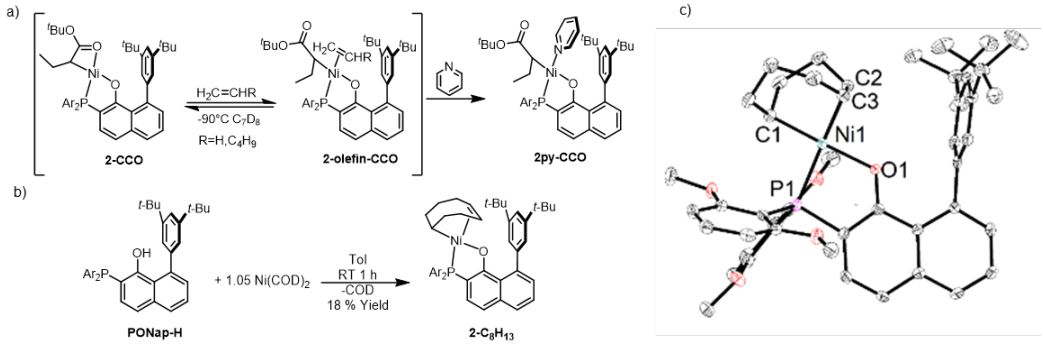

Figure 3.3. a) Equilibrium between 2-CCO and olefin-coordinated variants $2C_nH_{2n}$-CCO as well as reaction with pyridine to form 2py-CCO b) Formation of 2-C_8H_{13} c) ORTEP Depiction of **2-C_8H_{13}** (bottom). H-atoms are excluded for clarity.

As representative models for the proposed resting state in catalysis of ethylene/acrylate copolymerization, facile access to acrylate-inserted species, **1-CCO** and **2-CCO** provide a unique opportunity to investigate details relevant to the proposed rate-determining step. The mechanistic studies described below aim to gain insights related to the elementary steps of monomer enchainment, including chelate opening/olefin coordination and cis-trans isomerization. The auxiliary ligand-free nickel acrylate insertion complexes are integral to this study as they preclude additional ligands that obfuscate olefin coordination behavior and provide the possibility of quantitative determination of thermodynamics of chelate opening and binding affinities of olefins.

Investigation of Olefin Coordinated Complexes

Given the strain in the metallacycle of **1-CCO** and **2-CCO** and the lack of a strong fourth ligand, we targeted olefin coordination studies. Indeed, upon addition of 4 atmospheres of ethylene to a frozen solution of **2-CCO** in d_8-toluene, a new $^{31}P\{^1H\}$ NMR resonance at –19.3 ppm was observed at temperatures ranging from -90 to -70

°C, which was tentatively assigned to the ethylene adduct, **2et-CCO** (Scheme 1). Presence of a large excess of ethylene and the broadened resonances of two conformers of **2-CCO** at -90 °C precluded ^{1}H NMR assignment of the proposed **2et-CCO**.[37] The identity of **2et-CCO** was supported via ^{13}C{^{1}H} NMR, with the coordinated ethylene resonances appearing as broad multiplets at 104.5 and 102.5 ppm. These shifts are within the range of cationic Pd(II) ethylene adducts.[12, 38-39] The disappearance of resonances at temperatures above -70 °C and concomitant broadening of the remaining resonances along with reappearance of **2et-CCO** upon recooling to -90 °C, can be reasoned as a dynamic process with ethylene coordination and dissociation coupled with potential chelate dissociation and reassociation, respectively. The behaviour is consistent with the reversible formation of an ethylene adduct, and impeded isolation of **2et-CCO**.

In addition to the resonance corresponding to **2et-CCO** in ^{31}P{^{1}H} NMR, a new resonance also appears at approximately -7.8 ppm. This resonance may represent the formation of a separate isomer of an ethylene coordinated species, or a species which is the result of further reactivity of **2et-CCO**. To further confirm the assignment of the -19.4 ppm as the ethylene-coordinated species and expand the reactivity to other olefins of interest, **2-CCO** was exposed to 200 equivalents of 1-hexene at low temperatures. The resultant ^{31}P{^{1}H} NMR shows the partial formation of the analogous species, **2hex-CCO**, which displays a ^{31}P{^{1}H} resonance at approximately -20.6 ppm, yet a peak comparable to the unknown species observed at -7.8 ppm is not

observed. This scenario further supports that the unknown species may be an isomer of **2et-CCO** generated after further reactivity with ethylene.

To further support our assignment of **2et-CCO** and gain more insight into the unknown species, ^{13}C-labelled ethylene was employed. Addition of four atmospheres of ^{13}C-ethylene resulted in a slightly shifted resonance in ^{31}P{^{1}H} NMR at -19.6 ppm corresponding to **2et*-CCO**. The ^{13}C{^{1}H} NMR of the equilibrium mixture of **2-CCO** and **2et*-CCO** displayed a broad, high-intensity multiplet at approximately 99.0 and 95.5 ppm. The ~6 ppm chemical shift for **2et*-CCO** in comparison to **2et-CCO** may be the result of a low-lying paramagnetic state, potentially a tetrahedral Ni(II) species.[40-41] The ^{13}C olefin-based resonance disappears when the solution is warmed to temperatures above -70 °C, consistent with the behaviour observed in the ^{31}P{^{1}H} NMR spectra of **2et-CCO**. Lastly, further evidence of the assignment of the olefin adduct, **2et-CCO**, is provided by vacuum transferring pyridine to the frozen mixture of **2-CCO** and **2et-CCO** in toluene, which results in the complete conversion to the previously characterized, pyridine bound species **2py-CCO** (Figure 3.3a). These experiments, collectively, discount the potential assignment of the unknown species as an ethylene insertion compound.

Despite our best efforts, crystallographic characterization of **2et-CCO**, and **2et-CCO** was unattainable. Toward obtaining structural confirmation on an olefin adduct that could benchmark the chemical shifts observed in ^{31}P{^{1}H} and ^{13}C{^{1}H} NMR and attempt to locate the resonances of the bound olefin in ^{1}H NMR, we sought to employ a more stable chelated olefin. Previously reported Ni-phosphino phenoxide catalysts

were generated from biscyclooctadiene Ni(0) ($Ni(COD)_2$) as a precursor to generate the related cyclooct-4-enyl Ni complexes. Addition of $Ni(COD)_2$ to one equivalent of the PONap-H ligand at room temperature resulted in the formation of a cyclooct-4-enyl complex (**2-C_8H_{13}**) (Figure 3.3b).

Single-crystal XRD characterization revealed that **2-C_8H_{13}** (Figure 3.3c) features the olefin within the metallacycle coordinated to the Ni center trans to the phosphine donor. Importantly, the $^{31}P\{^1H\}$ NMR spectrum of **2-C_8H_{13}** displays a singlet at -18.00 ppm, a resonance consistent with the aforementioned olefin adducts of **2**. Similarly, $^{13}C\{^1H\}$ NMR of solution of **2-C_8H_{13}** displayed resonances corresponding to the bound olefin at 102.2 and 105.0 ppm with $^2J_{CP}$ coupling constants of 14.7 and 2.6 Hz. Both chemical shifts are in the vicinity of the olefin coordinated resonances observed in solution for **2et-CCO** and **2et*-CCO**. The ^1H NMR spectrum of **2-C_8H_{13}** features two multiplets corresponding to the coordinated olefin at 4.95 and 5.23 ppm. $^{13}C\{^1H\}x^1H$ HSQC confirms that these resonances are associated with the olefinic protons These proton resonances are consistent with the expected olefinic resonances bound to Ni(II).[37, 42] To serve as a direct comparison, cooling a d_8-toluene solution of **2-C_8H_{13}** to -90 °C was performed and corresponding NMR spectra were collected. $^{31}P\{^1H\}$ NMR at -90 °C displayed significant broadening compared to the room-temperature spectra which may indicate an exchange process potentially between enyl and allyl isomers, or different conformers. The ^1H NMR spectrum also observed broadening at -90 °C, including the olefinic resonances that bear $W_{1/2}$ of approximately 60 Hz. Significant broadening of olefinic resonances at -90 °C provides potential

reasoning to the challenges in assigning the coordinated ethylene resonance by ^{1}H NMR spectroscopy. Collectively, these experiments provide compelling evidence of the assignment of the ethylene coordinated species, **2et-CCO**, from the exposure of 4 atmospheres of ethylene to complex **2-CCO**.

Despite the lack of auxiliary donor, addition of 4 atmospheres of ethylene to complex **1-CCO** did not result in predominant formation of an ethylene coordination species similar to **2et-CCO** under a variety of temperature ranges. This suggests that **1et-CCO** may be a comparatively higher energy intermediate or **1-CCO** is a more stable species compared to **2-CCO**.

Methyl acrylate and tBA were also added to **1-CCO** and **2-CCO** targeting acrylate coordinated species. Even with a large excess of acrylate, no evidence of coordination was observed. This behavior indicates that coordination of acrylate is substantially disfavoured in comparison to chelate formation, an observation consistent with the copolymer microstructure lacking subsequent insertion of acrylates.

Thermodynamics of Chelate Opening

Intrigued by the observation of olefin coordinated species, we sought to gain quantitative measurements of the relative binding of olefins to neutral Ni(II) catalysts. As an isolable model for the resting state of catalysis, complex **2-CCO** was explored for reversible chelate opening through dissociation of the alkyl ester group and monomer coordination. Addition of ethylene led to an equilibrium mixture of **2-CCO** and **2et-CCO** at low temperatures. For comparison, the thermodynamics of chelate opening and 1-hexene coordination to access **2hex-CCO** was also studied.

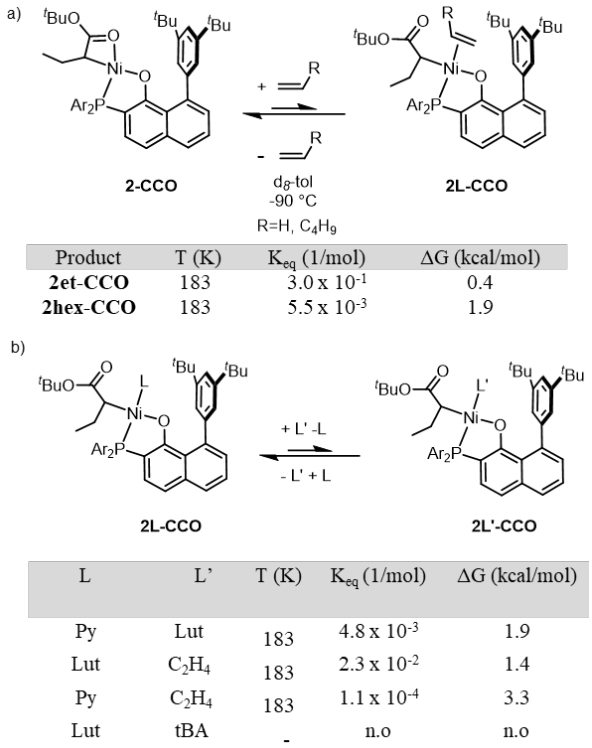

Product	T (K)	K_{eq} (1/mol)	ΔG (kcal/mol)
2et-CCO	183	3.0×10^{-1}	0.4
2hex-CCO	183	5.5×10^{-3}	1.9

L	L'	T (K)	K_{eq} (1/mol)	ΔG (kcal/mol)
Py	Lut	183	4.8×10^{-3}	1.9
Lut	C_2H_4	183	2.3×10^{-2}	1.4
Py	C_2H_4	183	1.1×10^{-4}	3.3
Lut	tBA	-	n.o	n.o

Figure 3.4. a) Thermodynamic values of ring opening and monomer coordination. b) Thermodynamic values of ligand exchange between ethylene and pyridines.

Thermodynamic scale for binding affinities of pyridine and olefinic donors to **1L-CCO** and **2L-CCO** (Blue denotes computational determination). Dotted red line denotes adjustment based on the crossover experiment. Binding scale adjustment was determined through modelling $^{31}P\{^1H\}$ and ^1H NMR resonances of **1py-CCO**, **1-CCO**, **2py-CCO**, and **2-CCO** from equimolar mixture of **1py-CCO** and **2-CCO** at room temperature. Analysis of thermodynamic data (Figure 3.4) at low temperature indicates that the equilibrium lies on the side of the chelate. The equilibrium mixture of **2-CCO** and **2et-CCO** at -90°C shows an equilibrium constant of 0.3 and ΔG of 0.4 kcal/mol, close to thermoneutral, consistent with the ability of these catalysts to perform efficient copolymerization. Coordination of 1-hexene requires a large excess

of olefin to observe an equilibrium mixture of **2-CCO** and **2hex-CCO.** The measured thermodynamic binding constant of 5.5 x 10^{-3} and ΔG of 1.9 kcal/mol is significantly less favorable to olefin coordination than for ethylene, a consequence of the bulkier α-olefin.

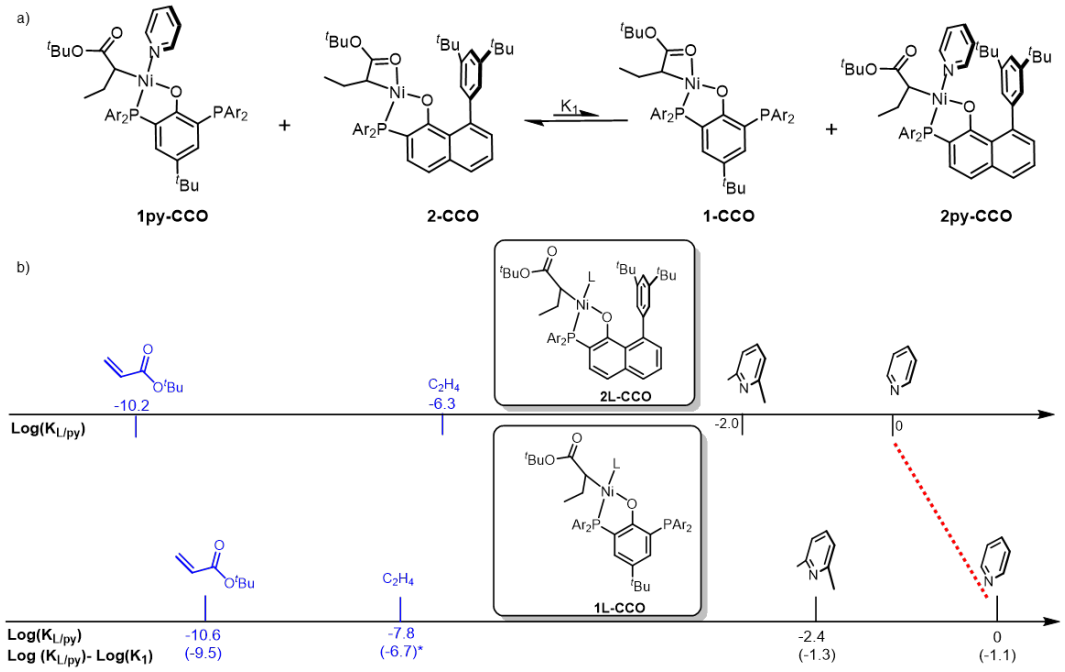

Figure 3.5. a) Pyridine binding competition experiment with **1py-CCO** and **2-CCO**.

Neutral Ni pre-catalysts employed in copolymerization catalysis typically feature a ligand L (e.g. pyridine) that must be substituted with olefin for propagation to occur.[43] Toward gaining quantitative data regarding the ligand substitution pre-equilibrium (Figure 3.1c), competitive binding of olefins vs different ancillary ligands, such as pyridine and lutidine, at neutral Ni(II) catalysts was explored.

Given the elusiveness of **2et-CCO** at temperatures above -70 °C, competitive binding experiments were conducted at -90 °C (Figure 3.4b). Pyridine and ethylene

proved to have binding affinities that were not conducive to direct comparison. Therefore, 2,6 lutidine was used as a weaker binding ligand for comparison. A solution of complex **3** and an excess of 2,6 lutidine in d_8-toluene in a J-Young tube was frozen and exposed to four atmospheres of ethylene. The solution was subsequently thawed and vigorously shaken, and NMR experiments were conducted at -90 °C. To ensure thermodynamic equilibrium was established the solution was warmed to -10 °C for one hour and re-cooled to -90 °C and the $^{31}P\{^1H\}$ NMR spectrum was recollected. This process was repeated until the relative intensities of **2et-CCO** and **2lut-CCO** were unchanged. The resulting integrals were used to calculate the equilibrium constant for ligand substitution, $K_{C2H4/lut}$, as 2.3 x 10^{-2} and ΔG of 1.4 kcal/mol. Separately, known amounts of pyridine and 2,6 lutidine were added to a sample of **2-CCO** in d_8-toluene and the solution was cooled to -90 °C. A similar procedure was employed to ensure the thermodynamic equilibrium was established and the resulting integrals were used to calculate the $K_{lut/py}$ of 2,6-lutidine binding from the pyridine-bound species (4.8 x 10^{-3}) and a ΔG of 1.9 kcal/mol. With these K_{eq} values determined, the binding affinity of ethylene from **2py-CCO** produces a Keq of 1.1 x 10^{-4} and a ΔG of 3.3 kcal/mol. Acrylate coordination via olefin or carbonyl group oxygen coordination was not observed (*vide supra*) precluding experimental determination of equilibrium constants involving the polar olefin. This aspect was investigated computationally (*vide infra*).

To address the impact of the ancillary phosphine-phenoxide ligand on the binding affinity of the labile ligands (L, Figure 3.1), a pyridine partition experiment between **1-**

CCO and **2-CCO** was performed. Equimolar amounts of **1py-CCO** and **2-CCO** (Figure 3.5a) were mixed and the concentration of **1py-CCO**, **2-CCO**, **1-CCO**, and **2py-CCO** were determined by ^{31}P NMR spectroscopy. The distribution shows approximately 80% of the pyridine stays bound on **1py-CCO** with approximately 20% of **2py-CCO** formation, corresponding to a K_1 of 8.0 x 10^{-2} and ΔG of 1.5 kcal/mol. This scenario indicates a higher binding affinity of pyridine to **1-CCO** than **2-CCO**, potentially owing to the more rigid bulk proximal to the neutral L donor in **2L** relative to **1L** impacting the planar pyridine ligand which extends further toward the aryl substituent in **2-CCO** than the chelate.

The above results allow direct comparison of the thermodynamic scales between **1L** and **2L** (Figure 3.5b) at room temperature. The experimentally determined donor binding at room temperature and computationally determined ones (indicated in blue), ethylene and tBA, show that for both ancillary ligands olefin binding is orders of magnitude disfavored relative to pyridines. The difference between ethylene and acrylate is, however, less pronounced with the POP-H compared to PONap-H ligand (**1** vs **2**) consistent with POP supporting a catalyst that incorporates more polar monomer.[24]

Experimental Ligand Binding Studies of 1 and 2 with Various Ligand Ls

Given that monomer enchainment after acrylate insertion is the propagation determining step in copolymerization, thermodynamic binding studies with a variety of electronically and sterically differentiating ligands was studied to gain insights relevant to monomer coordination. To further explore differences in L donor binding

affinity to Ni species relevant to olefin polymerization, in addition to **2-CCO** and **1-CCO, 1**, **2**, and **2lut-Me** were investigated as catalyst states prior to initiation and as models for the catalyst state after ethylene insertion. A series of pyridines with different electronic and steric properties were investigated. Ligands of more conical shape such as PEt_3 and $(O)PEt_3$, were also studied. These ligand binding competition studies afforded thermodynamic binding scales for the several nickel complexes; the logarithm of the K values relative to pyridine ($K_{L/py}$) are shown in Figure 3.6. Notably, a compression in relative binding energies was observed between **1L-CCO** (4.0 logK units) and **2L-CCO** (4.4) compared to **1L** (5.6), **2L** (5.8) and **2L-Me** (6.4). The difference in the spread of equilibrium constants appears for both sterically and electronically differentiated ligands, as observed with 2,6-lutidine and pentafluoropyridine. For example, the $\log(K_{Lut/Py})$ values for **1L-CCO** and **2L-CCO** are -2.4 and -2.0, compared to those of **1L**, **2L** and **2L-Me**, which are -3.9, -4.4 and -3.4, respectively. The $\log(K_{Py\text{-}F5/Py})$ value for **2L-CCO** is -2.7 whereas a significantly decreased relative binding affinity is observed for **2L** and **2L-Me** at -5.1 and -5.8, respectively. The origin of the compressed scale for ligand binding affinity to **1L-CCO**, **2L-CCO** is intriguing. Given the similarity in binding constants between **1L-CCO** and **2L-CCO** and their differences in the ancillary ligand architecture, the phenomenon observed is more likely due to the differences between the alkyl ligands on nickel (C-bonded ester enolate vs vs methyl/CH_2SiMe_3) instead of originated from the phosphine-phenoxide ligands.

Relatedly, ethylene and CO binding affinity studies to cationic Pd(II) catalysts for ethylene/CO copolymerization revealed that Pd-acetyl and Pd-acyl groups resulted in a relatively compressed binding affinity of C_2H_4 to CO compared to the Pd-CH_3 analogue.[39] This result is consistent with our observation of the C-bonded enolate in **1L-CCO** and **2L-CCO** featuring a compressed scale for binding affinities; whether this is the result of the electron-withdrawing nature of the enolate moiety in **1L-CCO**/**2L-CCO** or the larger steric profile of the ester, is unclear.

Targeting the effect of P,O-ligands, we then compare the binding affinity for ancillary ligands L with nickel complexes featuring the same alkyl but supported by different phosphine phenoxides. For ligands L featuring a large distal but distal steric profile such as P(O)Et_3 and 4-tertbutylpyridine (^{t}Bupy), a much smaller log($K_{L/Py}$) was observed with **2L**/**2L-Me** than with **1L**/**1L-Me**. Specifically, ^{t}Bupy is a weaker ligand than pyridine for **2L** and **2L-Me**, but a stronger one for **1L**. The above scenarios are potentially due to the steric repulsion between the rigid substituent 3,5-ditertbutylphenyl group on the P,O-ligand and the large substituents on L (ethyl for P(O)Et_3 or ^{t}Bu for ^{t}Bupy) that are far reaching. Note that during tBA coordination during catalysis, the ^{t}Bu substituent on tBA, which is two atoms away from the olefin moiety, may also be hindered by the phenoxide substituent and thus lead to higher barrier for tBA coordination, and subsequently, lower tBA incorporation. Indeed, ethylene/tBA copolymers produced by **2** feature much lower tBA incorporation than that produced by **1**.

To gain structural insight into ligand binding trends, single crystal X-ray diffraction studies were performed with **1L**, **1L-Me**, and **1L-CCO** featuring different ligands L (Figure 3.7). Among all seven complexes, **1P-CCO** features the shortest Ni-O distance, suggesting the strongest interaction between nickel and the axial methoxy group. For example, comparing **1P-CCO** and **1P**, differing only in the alkyl group coordinated to Ni, the Ni-O distance elongates from 2.701(2) Å to 2.967(3) Å, despite **1P-CCO** displaying a larger alkyl group. This is consistent with a more Lewis acidic nickel center in **1P-CCO** compared to **1L** and **1L-Me**, an aspect also supported by Mulliken population analysis. The increased polarisation of the Ni-C bond may be a contributor to the higher energy of ethylene insertion after acrylate insertion compared to consecutive ethylene insertions.[44] Furthermore, the more Lewis acidic metal center is expected to have a stronger interaction with the carbonyl group, stabilize the chelate, and slow down propagation, consistent with the experimental observation that ethylene enchainment from the chelate is the propagation determining step.

Analysis of the impact of the sterics of the pyridine ligand comparing **2lut-Me**, **1py-Me** and **1** shows almost identical Ni-N distances, but an increasing Ni-O distance (from 2.837(3) Å in **2lut-Me** to 3.086(3) Å in **1**) an indication of the ability of the substituents reaching out of the plane defined by the Ni coordination sphere to constrain axial coordination.

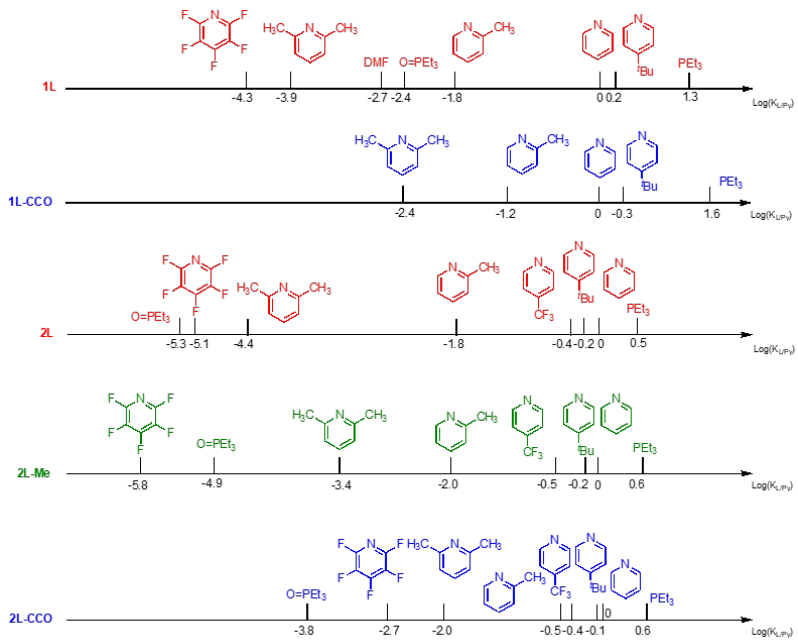

L	**1L** (1/mol)	**1L-CCO** (1/mol)	**2** (1/mol)	**2L-Me** (1/mol)	**2L-CCO** (1/mol)
PEt_3	1.3	1.6	0.5	0.6	0.6
4-^{t}Bu-Py	0.2	0.3	-0.2	-0.2	0.1
Py	0	0	0	0	0
2-Pic	-1.8	-1.2	-1.8	-2.0	-0.5
2,6-Lut	-3.9	-2.4	-4.4	-3.4	-2.0
Py-F_5	-4.3	N.D.	-5.1	-5.8	-2.7

Figure 3.6. Thermodynamic scales for binding affinities of neutral donors to **1L**, **1L-CCO**, **2L**, **2L-Me**, **2L-CCO** (top) and the table of selected values (bottom). Relative binding affinities determined by competition reactions with varying donors through either $^{31}P\{^1H\}$ NMR or ^1H NMR spectroscopy.

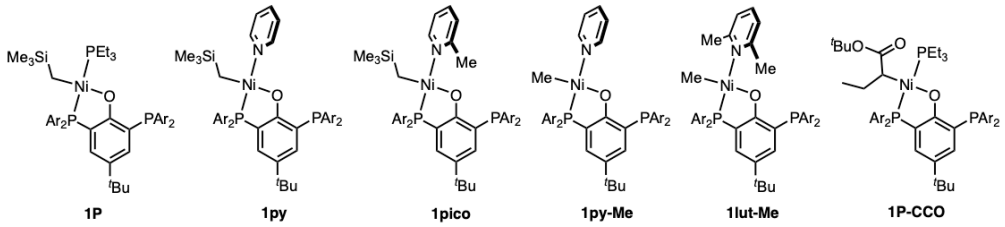

L	**1P**	**1py**	**1pico**	**1py-Me**	**1lut-Me**	**1P-CCO**
Ni-P	2.190(1)	2.134(1)	2.131(1)	2.132(1)	2.131(2)	2.211(1)
Ni-O	1.914(3)	1.926(2)	1.910(1)	1.915(2)	1.913(3)	1.922(1)
Ni-C	1.976(4)	1.950(4)	1.953(1)	1.927(3)	1.934(5)	1.983(3)
Ni-L	2.215(1)	1.938(3)	1.945(1)	1.934(2)	1.956(4)	2.230(1)
Ni-O'*	2.967(3)	2.837(3)	2.909(1)	2.927(2)	3.086(3)	2.701(2)

Figure 3.7. Selected bond lengths in Å of **1L-R** complexes (See SI for their solid-state structures).

Overall, the donor coordination studies of **1L**, **1L-CCO**, **2L**, **2L-Me**, and **2L-CCO** provide insights on the relative binding affinities of a series of neutral donors to catalytically relevant Ni species. The compression of relative binding constants in acrylate-inserted species is proposed to be a manifestation of the different electronic properties of the alkyl groups at Ni. Additionally, the rigidity of the phosphine phenoxide ligand was found to hinder binding of ligands with a large volume. Because these experiments allowed a single olefinic ligand comparison (for **2et-CCO**), we sought to employ DFT calculations to benchmark the experimental measurements and to extend the scales to olefins employed in copolymerization catalysis.

DFT calculation of ligand binding affinity of 2 with various polar olefins

The compression in relative binding energy scales for different catalyst systems, as shown in Figure 3.6, was explored computationally, to gauge the electronic effect of catalyst R-group substitutions. Ligand PONap-based catalyst systems **2L 2L-Me**, and **2L-CCO** were evaluated (Figure 3.8). The binding equilibria K_{bind} between the different ligands was quantified experimentally and used as a benchmark for the computational method. The binding energy ΔG_{bind} was related to the binding equilibrium constants K_{eq} obtained experimentally:

$$\Delta G_{bind} = RT\ln\Delta K_{bind} \quad (1)$$

The experimental binding equilibria for a set of representative ligands was converted to Gibbs free energies for the three catalyst systems **2L**, **2L-Me**, and **2L-CCO** (Figure 3.9) based on the experimental data (Figure 3.6). A consistent trend is seen where the electron-deficient R = ester substitution on **2L-CCO** results in lower experimental

binding energies. As the ester substituents has an electron withdrawing effect, these data suggest that stronger binding correlates with a more electron-deficient metal center. Some variation was observed in the rank ordering of the other two R-groups which may be due to the additional effect of sterics on the binding energies.

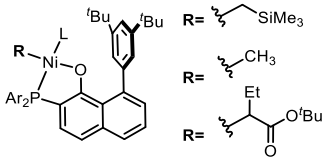

Figure 3.8. Ligand PONap-based catalyst systems explored computationally, with three R-group substitutions considered: **2L** (R = silane), **2L-Me** (R = Me), and **2L-CCO** (R = ester).

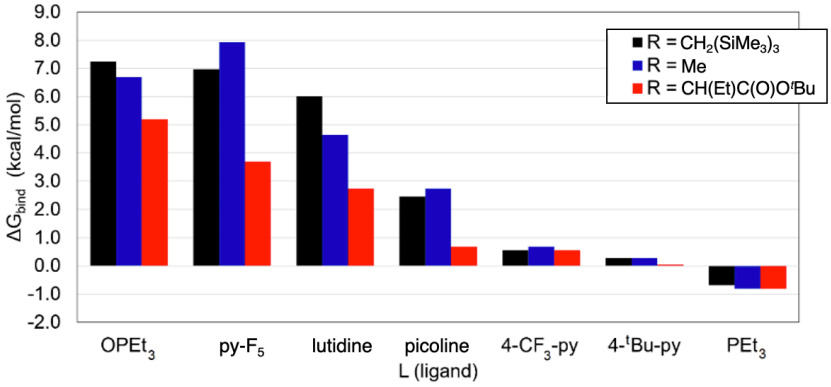

Figure 3.9. Experimental binding energies (relative to the pyridine-bound catalyst) for a representative set of monomers. A systematic decrease in binding energies for **2L-CCO** (R = ester) is observed.

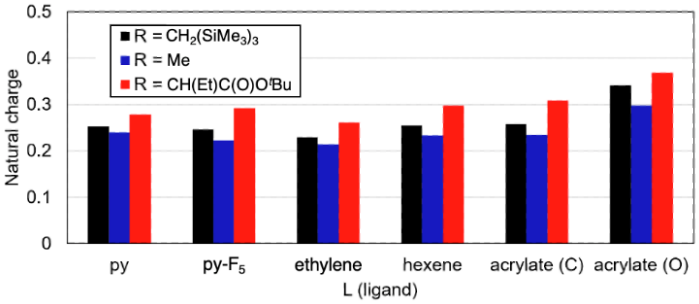

Figure 3.10. Natural charge of the Ni center as obtained from natural bond orbital (NBO) analysis. Acrylate (C) and (O) indicate binding of acrylate to Ni via the alkene or oxygen donor, respectively. A larger natural charge indicates a more electrophilic metal center. A consistently larger Ni natural charge for the **2L-CCO** (R = ester) compounds in comparison to the **2L-Me** (R = Me) and **2L** (R = silane) systems.

Relative binding energies for the three catalyst systems were calculated for an extended set of ligands that includes pyridines, non-polar monomers (e.g., ethylene, hexene), and polar monomers (Figure 3.10, see Supporting Information for full list of ligands considered). To visualize trends in the data, for a given ligand, the relative binding energy for **2L-CCO** was shown on the x-axis and the relative binding energy for either **2L** or **2L-Me** was plotted on the y-axis (Figure 3.11). There is a consistent trend in the binding energies of ligand based on the identity of the R-group substitution on the catalyst, as shown by the observation that all the points in Figure 3.11 lie above the y = x line. This indicates that there is an increase in the binding energies for **2L** and **2L-Me** catalyst systems, compared to the analogous **2L-CCO** system of the same ligand L (see Supporting Information for a regression analysis of the binding energies). Variation of the points away from the regression lines is considered to reflect the substrate-dependent effects of sterics on the relative binding energies.

A rationale for the R-group dependence of binding energies lies in the electronic effect. The NBO natural charge for Ni was calculated for the three R groups with the same ligands L. Larger computed natural charges at Ni were observed with the **2L-CCO** system, indicating the more electron deficient metal center (Figure 3.10). Our computational model was extended to the olefin coordination cases that were not accessible experimentally. The trend of lower binding energies for the **2L-CCO** was also observed for these olefins.

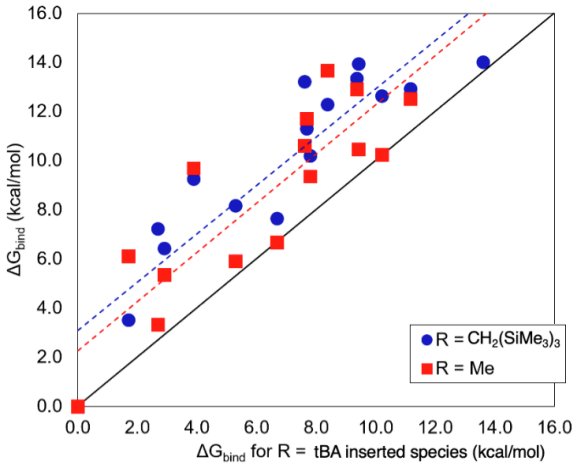

Figure 3.11. Calculated binding energies (relative to the pyridine-bound structure) shown for each ligand (each point is a unique monomer) and catalyst (distinguished by marker color and shape). For a given ligand, the relative binding energy of the **2L-CCO** catalyst (R = ester) is shown on the x-axis and compared the analogous monomer bound structure for the **2L** (R = silane) and **2L-Me** (R = methyl) catalyst systems (blue circle and red square, respectively). The dotted red and dotted blue lines represent the linear regression for R= Me and R=CH_2SiMe_3, respectively and the solid black line is a reference y=x line.

Cis-Trans Isomerization

The binding experiments described above provide insight regarding ligand coordination to analogues of catalysts after ethylene and tBA insertion; however, these studies are limited to examples where the ligand coordinates trans to the phosphine donor. Multiple computational studies of the mechanism of polymerization with asymmetric bidentate ligands invoked cis-trans isomerization prior to olefin migratory insertion.[14, 24, 45] Brookhart and Daugulis reported a rare example of isomerization of a neutral Pd methyl ethylene complex in solution. [36]An example of Ni-phosphine phenoxide complexes favoring the cis isomer displays crown ethers to support Lewis acids appended to the ligand framework.[39] The presence of the cis isomer in this system is reasoned to be due to π-interaction effects from the pendant Lewis acid. Beyond these reports, experimental information about the mechanism of

isomerization with catalytically relevant species is lacking. Given the computational evidence suggesting a cis-trans isomerization for the current catalysts,[24] further insight on the mechanism of cis-trans isomerization was sought.

The observation of both cis and trans isomers in some of the ligand binding studies prompted us to prepare and isolate **2P**, **2P-Me**, and **2P-CCO** for further investigation. A substantial amount of the P-P cis isomer (24% and 28%) was observed in both **2P** and **2P-Me** as supported by a set of two doublets with coupling constants of approximately 20 Hz in the ^{31}P NMR spectra, assigned to the two phosphine ligands. For comparison, the P-P trans isomers show a coupling constant of 330 Hz. Complex **2P-CCO** shows no detectable amount of the P-P cis isomer. Given that olefin enchainment after acrylate insertion is rate limiting, the absence of the P-P cis isomer indicates that a preequilibrium between the trans and cis isomers is substantially shifted toward trans, overall, energetically disfavoring isomerization and slowing propagation. With access to a mixture of P-P cis and P-P trans isomers for **2P** and **2P-Me**, experimental studies were focused on the mechanism of isomerization.

Potential mechanistic pathways of the isomerization process are outlined in Figure 3.12 with $Ni(PEt_3)(CH_2SiMe_3)$ as an example. Computational studies support an intramolecular mechanism involving coordination of a pendant ether group to generate a five-coordinate intermediate that undergoes a Berry pseudorotation, followed by ether dissociation (a);[46-47] An alternative associative mechanism involves intermolecular binding of a fifth ligand, PEt_3, followed by pseudorotation, and phosphine loss (b);[48-49] a dissociative mechanism involves loss of PEt_3 followed cis-

trans isomerization of the three-coordinate species, and reassociation of phosphine (c).[50-51]

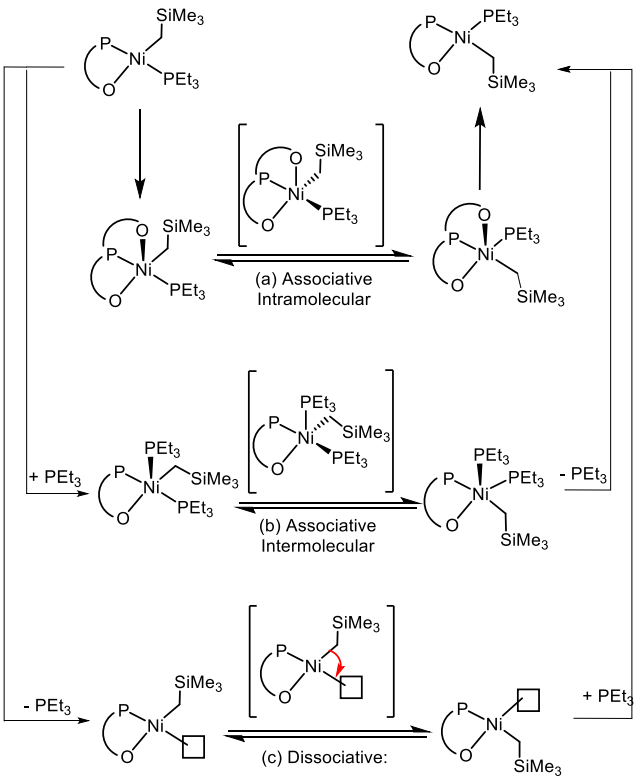

Figure 3.12. Potential mechanisms of cis-trans isomerization.

The observation of both P-P cis and P-P trans isomers with **2P** and **2P-Me**, allows studies of the ligand exchange dynamics using $^{31}P\{^{1}H\}$ 2D NOESY (EXSY)experiments, [52-53] EXSY studies with **2P** showed cross peaks corresponding to magnetization transfer between the P-P cis and P-P trans isomers at room temperature. When the EXSY experiment was performed in the presence of excess (10, 40 equivalents) of free PEt_3 and at higher temperatures, no cross peaks between free PEt_3 and the Ni species are observed. Using EXSYCalc, the magnetization transfer rates were determined through the exchange matrix with values ranging from

0.64 to 0.94 s^{-1} for the formation of the P-P cis isomer and 1.82 to 1.98 s^{-1} for the formation of the P-P trans isomer over the phosphine concentrations tested (Figure 3.13). The lack of substantial change of magnetization transfer rate with varying amounts of PEt_3 supports an intramolecular mechanism, such as (a), for isomer conversion.[47] An intermolecular mechanism (b or c) is inconsistent with the EXSY results. Notably, these results indicate that ligand substitution is slower than cis-trans isomerization under these conditions. **1P** also showed a small amount of P-P cis isomer (4%). Though magnetization transfer is not detectable under temperatures ranging from 25-65 °C through the EXSY experiments, significant broadening of the resonances in $^{31}P\{^1H\}$ NMR spectra are observed as the temperature increases. Although a dynamic process may be occurring at high temperatures, the interconversion of the isomers with **1P** is slower than for **2P**.

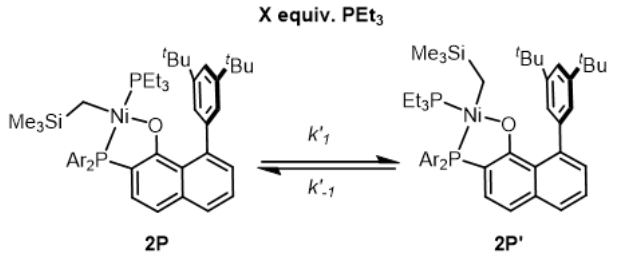

X	k'_1	k'_{-1}
0	0.6 s^{-1}	1.8 s^{-1}
10	0.9 s^{-1}	2.0 s^{-1}
40	0.9 s^{-1}	1.9 s^{-1}

Figure 3.13. Rates of magnetization transfer with varying equivalents of PEt_3.

Our studies, though not employing olefins, provide experimental support for the computational finding that the present phosphine phenoxide Ni catalysts undergo cis-trans isomerization via an intramolecular mechanism.

Using 3 as Auxiliary Donor Free Precatalysts for Polyolefin Synthesis

Our studies show that the competition for metal binding between the auxiliary ligands present in the precatalyst, pyridine or phosphine, and olefin monomers favors significantly the former. Therefore, we explored the impact of removing the auxiliary ligands (e.g. pyridine) on nickel catalyzed copolymerization of ethylene and polar monomers. Stable, coordinatively saturated metallocycle precatalysts prevent the use of the auxiliary ligand and has shown promising results in palladium catalyzed ethylene polymerization.[17] Examples of the nickel analogue are lacking; however, the effect of weaker ancillary ligands have been explored in Ni-phenoxyimine catalysts and weaker donor coordination leads to higher activity in ethylene polymerization and supresses β-H elimination.[43] Intermediates generated after monomer insertion are typically considered reactive and potentially not suitable as precatalysts. Given that **2-CCO** is the first structurally characterized, thermally robust four-membered chelate complex generated after tBA insertion, we explored its application as precatalyst in ethylene/tBA copolymerization.

Table 3.1. Ethylene/tBA copolymerization.

Entry[a]	catalyst	[tBA]/M	T (ºC)	Act.[b]	$M_w/10^3$	PDI	%Mol t-BA	Tm (ºC)
1	**2lut- Me**	0.025	70	333	16.7	2.2	0.4	128
2	**2lut- Me**	0.05	70	157	15.3	2.4	0.8	124
3	**2-CCO**	0.025	70	303	18.0	2.3	0.4	128
4	**2-CCO**	0.05	70	139	17.3	2.6	0.8	124
5[c]	**2**	0.05	70	206	16.5	2.3	0.8	121

[a] Unless specified, V(total)=5 mL, [Ni]=0.25 μmol, ethylene pressure=400 psi, toluene solvent, t=1 h, each entry represents multiply replicated runs (see Table S1~S3 for original data. [b] in (kg/(mol·h)). [c] Data has been reported in Ref 23.

Both the nickel complex featuring a weak auxiliary ligand (lutidine, **2lut-Me**) and auxiliary donor-free nickel complexes (**2-CCO**) are highly active in ethylene/tBA copolymerization (Table 1, Entry 1~4), and produce polymers with moderate molecular weight and tBA incorporation. Compared to **2** (Table 1, Entry 5), both are slightly less active overall, which is in contrast with previously reported effects of ligand L in ethylene polymerization. Notably, corresponding ethylene uptake curves revealed that **2lut-Me** and **2-CCO** consume ethylene much faster than **2** in the first 5 min of ethylene/tBA copolymerization. However, a significant decrease of ethylene consumption rate was observed at longer time, which may relate to their decreased stability (Figure 3.14). Overall, our observation indicates that the absence of strong auxiliary ligand L indeed accelerates the rate of monomer insertion, but it may also lead to a lower thermal stability. Given that high temperatures are preferred in industrial conditions, both aspects need to be taken into account in catalyst design.

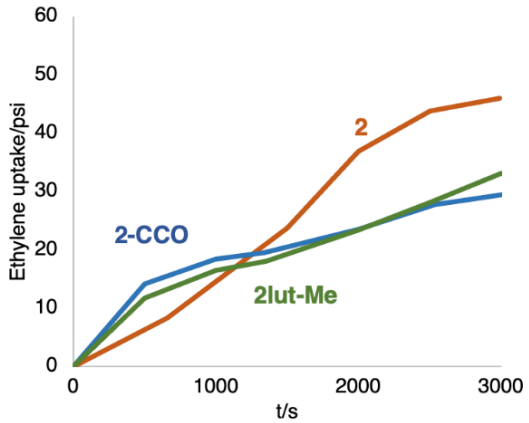

Figure 3.14. Ethylene uptake curves of **2** (Table S5.1, entry 13), **2lut-Me** (Table S5.1, entry 5) and **2-CCO** (Table S5.1, entry 10).

CONCLUSION

Auxiliary donor-free acrylate insertion compounds **1-CCO** and **2-CCO** were accessed through the insertion of tBA into Ni-Me bonds with the respective lutidine-bound precursors. Lack of a strong auxiliary donor in **2-CCO** allowed for the observation of olefin coordination complexes. Although equilibrium mixtures of **2-CCO** and olefin-bound species precluded isolation, the independently prepared COD-inserted complex **2-C_8H_{13}** was isolated and characterized structurally and by spectroscopy and supports the assignment of the olefin coordinated species. These data show that ethylene, but not acrylate, is capable of opening the chelate generated after acrylate insertion. Ligand binding studies have provided quantitative thermodynamic data regarding the impact of precatalyst structure on binding of donors such as olefins, pyridines, and phosphines.

A relatively compressed binding scale was observed with the acrylate inserted species (**1-CCO** and **2-CCO**) compared to the Ni-CH_2SiMe_3 and Ni-CH_3 complexes (**1, 2** and **2lut-Me**), which correlates with an increased Lewis acidity of Ni in the enolate complexes, as determined from computational studies. This behavior has an impact on catalytic performance by stabilizing the chelate and contributing to making the subsequent insertion rate limiting Addressing the impact of the supporting phosphine phenoxide, large donors were shown to have a higher binding affinity to complex **1-CCO** than **2-CCO**, likely due to the rigid steric-profile proximal to the phenoxide in **2-CCO**.

Complex **2P** provides a rare example of precatalyst that produces both cis and trans isomers in solution. $^{31}P\{^{1}H\}$ NMR EXSY experiments reveal an intramolecular mechanism of exchange between the cis and trans isomers and rule out involvement of free PEt_3. This mechanism is consistent with the mechanism of isomerization in ethylene/acrylate copolymerization found by computation.

Lastly, both **2-CCO** and **2lut-Me** serve as a competent single-component catalyst in ethylene/acrylate copolymerization. Analysis of their copolymerization behavior indicates that employing weak ancillary ligand L leads to both higher insertion rate and lower thermal stability, both of which should be taken into account in catalyst design.

Chapter 3

EXPERIMENTAL SECTION

General Considerations

All air- and water-sensitive compounds were manipulated under N_2 or Ar using standard Schlenk or glovebox techniques. The solvents for air- and moisture-sensitive reactions were dried over sodium benzophenone ketyl or calcium hydride or by the method of Grubbs.[54] Deuterated solvents were purchased from Cambridge Isotopes Lab, Inc.; C_6D_6, and C_7D_8 was dried over a purple suspension with Na/benzophenone ketyl and vacuum transferred. Ethylene (99.999%) was purchased from Matheson Tri-Gas and used without further purification. 2,6-lutidine was dried with sieves and distilled over $AlCl_3$ to remove 3-picoline and 4-picolline. 4-CF_3 pyridine, pentafluoropyridine, 2-picoline, and 4-tert-butyl pyridine were dried by stirring over CaH2 for greater than 12 hours and distilling. PEt_3 was purchased from Sigma Aldrich and purified by distillation prior to use. Triethylphosphine oxide was purchased from Combiblocks and used without further purification. 1-hexene was purchases from Sigma-Aldrich and distilled over Å sieves. t-butyl acrylate was dried over 3 Å sieves for greater than 72h, vacuum transferred, and passed over an activated alumina plug. Ligand **POPH**, **PONapH**, complexes **1**, **2**, **2lut-Me**, **2-CCO**,[24] $NiMe_2TMEDA$,[55] and $Nipy_2(CH_2Si(CH_3)_3$[56] were synthesized according to literature procedures. All ^1H, ^{13}C, and ^{31}P spectra of organic and organometallic compounds were recorded on Varian INOVA-400, or 500, or Bruker Cryoprobe 400 spectrometers. ^1H and ^{13}C chemical shifts are reported relative to residual solvent resonances.

Synthesis of Transition Metal Complexes

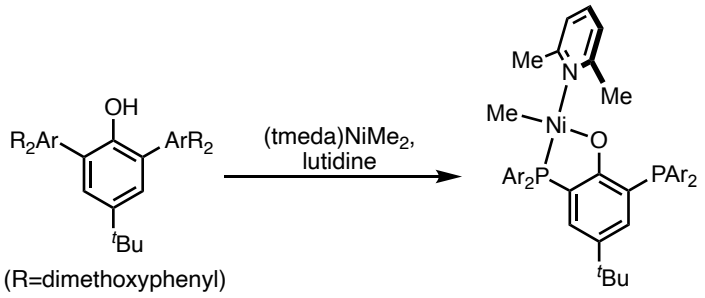

1lut-Me: In the glove box, to a thawing solution of $NiMe_2$(TMEDA) (38 mg, 0.19 mmol) in toluene (2 mL) was added a thawing solution of **POPH** (144 mg, 0.19 mmol) and 40 equivalents of 2,6-lutidine (717 mg, 7.54 mmol) in toluene (2 mL). The yellow solution was stirred while warming to room temperature for 30 minutes. After stirring for additional 30 min, all volatiles were removed from solution which was triturated with n-pentane (3 x 5 mL). The resulting residue was washed by n-pentane (5 mL) and diethyl ether (5 mL). The solids were collected via a filtration yielding spectroscopically pure **1lut-Me** (62 mg, 35 % Yield).

^{1}H NMR (400 MHz, C_6D_6): δ 7.58-7.52 (m, 1H, ArH), 7.14-7.05 (m, 5H, ArH), 6.75 (t, $^3J_{HH}$ = 7.6 Hz, 1H, lutidine-ArH), 6.40 (d, $^3J_{HH}$ = 7.6 Hz, 1H, lutidine-ArH), 6.36 (dd, $^3J_{HH}$ = 8.2 Hz, $^4J_{HP}$ = 3.4 Hz, 4H, ArH), 6.33 (dd, $^3J_{HH}$ = 8.2 Hz, $^4J_{HP}$ = 3.4 Hz, 4H, ArH), 3.37 (s, 6H, lutidine-CH_3), 3.30 (s, 12H, -OCH_3), 3.20 (s, 12H, -OCH_3), 1.22 (s, 9H, -$C(CH_3)_3$), -0.77 (d, J = 6.4 Hz, 3H, -$NiCH_3$). ^{13}C{^{1}H} NMR (101 MHz, C_6D_6): δ 163.56 (d, J_{CP} = 8.3 Hz, 4C, Aryl-C), 161.32 (s, 4C, Aryl-C), 159.24 (s, 2C, Aryl-C), 134.98 (s, 1C, Aryl-C), 132.43 (d, J_{CP} = 2.8 Hz, 1C, Aryl-C), 131.26 (s, 1C, Aryl-C), 129.42 (s, 2C, Aryl-C), 128.97 (s, 1C, Aryl-C), 128.23 (d, 2C, Aryl-C), 128.20 (s, 1C, Aryl-C), 125.15 (d, J_{CP} = 36.8 Hz, 1C, Aryl-C), 124.97 (s, 1C, Aryl-C), 120.46 (s, 2C, Aryl-C), 118.89 (d, J_{CP} = 31.3 Hz, 1C, Aryl-C), 113.02 (d, J_{CP} = 44.8 Hz, 1C, Aryl-C), 105.26 (s, 4C, Aryl-C), 104.25 (s, 4C, Aryl-C), 55.69 (s, 2C, Aryl-C), 55.67 (s, 2C, Aryl-C), 55.02 (s, 4C, Aryl-C), 33.78 (s, 1C, -$\underline{C}(CH_3)_3$), 32.05 (s, 3C, -$C(\underline{C}H_3)_3$), 25.71 (s, 2C, -CH_3), -23.85 (d, J=35.1 Hz, -$NiCH_3$). ^{31}P{^{1}H} NMR (121 MHz, C_6D_6, 298 K): δ - 5.08 (d, J_{PP}

= 11.0 Hz, 1P), - 52.71 (d, J_{PP} = 11.0 Hz, 1P). Anal. Calcd(%) for $C_{50}H_{59}NNiO_9P_2$: C: 63.98, H: 6.34, N: 1.49; found: C: 67.51, H: 6.02, N: 1.38.

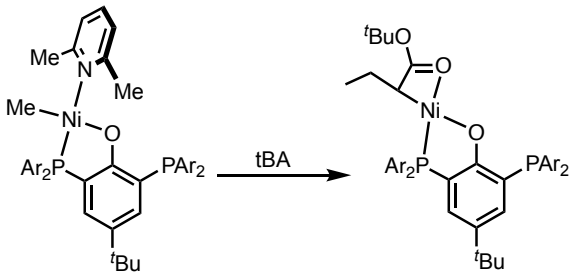

1-CCO: In the glove box, to a stirring solution of **1lut-Me** (73.1 mg, 0.078 mmol) in toluene (2 mL) was added 5 equiv. of tert-butyl acrylate (49.9 mg, 0.39 mmol). After 1 h, all volatiles were removed from the solution and the residue was triturated with cold hexanes (3*5 mL). The remaining residue was then washed with cold hexanes (5 mL) to afford **1-CCO** as reddish solids (28 mg, 38% yield). Complex **1-CCO** was only characterized by ^{1}H and ^{31}P{^{1}H} NMR due to its low thermal stability. ^{1}H NMR (400 MHz, C_6D_6): δ 7.35 (d, $^3J_{HP}$ = 12.7 Hz m, 1H, ArH), 7.07-6.81 (overlapping m, 5H, ArH), 6.38 (d, $^3J_{HH}$ = 8.2 Hz, 4H, ArH), 6.16 (d, $^3J_{HH}$ = 8.2 Hz, 4H, ArH), 3.33 (broad s, 12H, -OCH_3), 3.26 (broad s, 12H, -OCH_3), 1.56 (s, 9H, -$OC(CH_3)_3$), 1.34 (m, 1H, Ni-alkyl), 1.11 (overlapping m, 10H, -$C(CH_3)_3$ + Ni-alkyl), 0.86 (overlapping m, 4H, Ni-alkyl). ^{31}P{^{1}H} NMR (121 MHz, C_6D_6, 298 K): δ ~- 4.5 (broad), ~-8.0 (broad), - ~51 (broad, 1P).

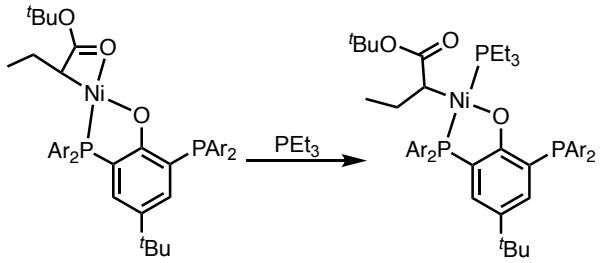

1P-CCO: In the glove box, to a solution of **1-CCO** (19.2 mg, 0.02 mmol) in toluene (2 mL) was added 5 equiv. of triethylphosphine (11.8 mg, 0.10 mmol). After stirred for 15 min, all

volatiles were removed under vacuum, affording quantitative formation of **1P-CCO** (21.2 mg, >95% yield). ^{1}H NMR (400 MHz, C_6D_6): δ 7.43-7.37 (m, 1H, ArH), 7.14-7.05 (m, 4H, ArH), 6.97-6.91 (m, 1H, ArH), 6.38 (ddd, J = 7.9, 5.2, 2.4 Hz, 4H, ArH), 6.34-6.29 (m, 4H, ArH), 3.46 (s, 6H, -OCH_3), 3.37 (s, 6H, -OCH_3), 3.21 (s, 6H, -OCH_3), 3.16 (s, 6H, -OCH_3), 2.15-2.05 (m, 2H, -PCH_2-), 2.00-1.89 (m, 2H, -PCH_2-), 1.81-1.70 (m, 1H, -PCH_2-), 1.67-1.57 (m, 1H, -PCH_2-), 1.41 (s, 9H, -OC(CH_3)$_3$), 1.35 (dt, J = 15.2, 7.6 Hz, 9 H, -PCH$_2$CH_3), 1.18-1.12 (Overlapping m+s (1.15), 11H, -C(CH_3)$_3$ + -NiCHRCH_2CH$_3$), 0.93-0.81 (Overlapping, 4H, -NiC*H*RCH$_2$CH_3). ^{13}C{^{1}H} NMR (101 MHz, C_6D_6): δ 163.81 (d, J = 8.3 Hz, 4C, Aryl-C), 162.48 (s, 4C, Aryl-C), 162.15 (s, 2C, Aryl-C), 133.44 (d, J = 6.5 Hz, 1C, Aryl-C), 131.42 (s, 1C, Aryl-C), 130.10 (d, J_{CP} = 7.7 Hz, 2C, Aryl-C), 128.96 (s, 2C, Aryl-C), 128.58 (d, 2C, Aryl-C), 125.66 (broad s, 2C, Aryl-C), 121.96 (d, J_{CP} = 96.8 Hz, 1C, Aryl-C), 118.87 (d, J_{CP} = 35.3 Hz, 1C, Aryl-C), 118.52 (d, J_{CP} = 39.8 Hz, 1C, Aryl-C), 105.48 (s, 2C, Aryl-C), 105.29 (s, 2C, Aryl-C), 104.01 (s, 1C, -O<u>C</u>(CH$_3$)$_3$),), 75.98(s, 2C, Acyl-C), 55.91 (s, 2C, Aryl-C), 55.80 (s, 2C, Aryl-C), 55.60 (s, 2C, Aryl-C), 55.30 (s, 2C, Aryl-C), 34.02 (s, 1C, -<u>C</u>(CH$_3$)$_3$), 32.31 (s, 3C, -C(<u>C</u>H$_3$)$_3$), 28.81 (s, 3C, -O<u>C</u>(<u>C</u>H$_3$)$_3$), 25.32 (s, 1C, -PCH$_2$-), 19.92 (s, 1C, Ni-CHR<u>C</u>H$_2$CH$_3$), 16.24 (s, 1C Ni-CHRCH$_2$<u>C</u>H$_3$), 14.56 (s, 1C, -PCH$_2$-),14.37 (s, 1C, -PCH$_2$-), 8.99 (broad s, 3C, -PCH$_2$<u>C</u>H$_3$), 5.93 (s, 1C, Ni-<u>C</u>HRCH$_2$CH$_3$),. ^{31}P{^{1}H} NMR (162 MHz, C_6D_6, 298 K): δ 11.65 (d, J_{PP} = 291.3 Hz, 1P), -12.01 (dd, J_{PP} = 291.3 Hz, 11.2, 1P), - 51.76 (d, J_{PP} = 11.2 Hz, 1P). Anal. Calcd(%) for $C_{56}H_{77}NiO_{11}P_3$: C: 62.40, H: 7.20; found: C: 63.28, H: 6.78.

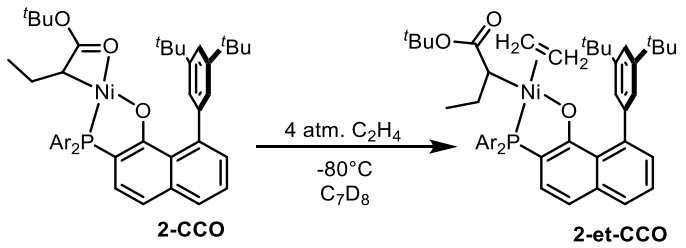

2et-CCO: A solution of complex **2-CCO** (5.6 mg, 0.0067 mmol) in C_7D_8 (0.6 mL) was prepared in the glovebox and transferred to a J-Young NMR tube. The J-Young NMR tube and a calibrated gas bulb (33.93 mL) were connected to a high-vacuum line. Dinitrogen in the J-Young tube was removed by three freeze-pump-thaw cycles of five minutes each. A separate vessel containing ethylene was connected to the high-vacuum line, cooled with liquid nitrogen, and placed under vacuum to remove residual dioxygen. The liquid nitrogen Dewar was them removed and ethylene was slowly transferred to the calibrated gas bulb. The calibrated gas bulb was sealed once the manometer read a pressure of 224 Torr. The ethylene in the calibrated gas bulb was then condensed in the J-Young NMR tube by cooling with liquid nitrogen over a period of 3 minutes. The J-Young NMR tube was then transferred to a dry-ice acetone bath and subsequently inserted to a pre-cooled NMR probe. Complex **2et-CCO** was characterized by $^{31}P\{^1H\}$ NMR. $^{31}P\{^1H\}$ NMR (121 MHz, C_6D_6, 183 K): δ -19.60 (broad s, 1P).

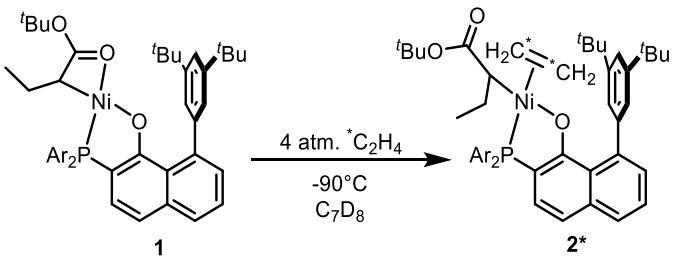

2et*-CCO: A similar protocol to generating **2et-CCO** was performed to characterize **2et*-CCO**, using $^{13}C_2H_4$ ethylene. Complex **2et*-CCO** was partially characterized by $^{13}C\{^1H\}$, and $^{31}P\{^1H\}$ NMR. $^{31}P\{^1H\}$ NMR (121 MHz, C_7D_8, 183 K): δ -19.60 (broad s, 1P). $^{13}C\{^1H\}$ NMR (101 MHz, C_7D_8, 183 K): δ 99.00 (broad d, 1C, $^1J_{CC}$= 48.2 Hz, $^{13}C_2H_4$) 95.46 (broad d, 1C, $^1J_{CC}$= 48.2 Hz, $^{13}C_2H_4$).

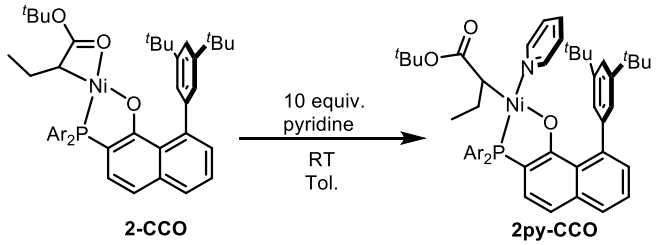

2py-CCO: To a solution of **2-CCO** (50 mg, 0.06 mmol) in 4 mL of diethyl ether in a 20 mL scintillation vial in the glovebox was added 10 equivalents of pyridine (80 mg, 0.06 mmol) in diethyl ether, affording quantitative generation of **2py-CCO**. ^{1}H NMR (400 MHz, C_6D_6, 298 K) ^{31}P{^{1}H} NMR (121 MHz, C_6D_6, 298 K): δ -19.60 (broad s, 1P).

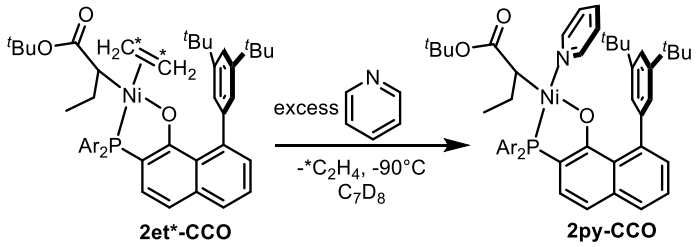

Conversion of Olefin Adduct 2et*-CCO to 2py-CCO: The previously characterized sample of **2et*-CCO** in a J-young tube was frozen in a liquid nitrogen Dewar and attached to the high vacuum line. A Schlenk tube of pyridine was also attached to the high vacuum line and an excess of pyridine was vacuum transferred to the sample of **2et*-CCO** over a period of 10 minutes. The J-young tube was then sealed, thawed in a dry ice-acetone bath and transferred to the precooled NMR spectrometer probe. The NMR experiments showed the displacement of ethylene as indicated by the disappearance of ^{31}P and ^{13}C resonances corresponding to **2et*-CCO** for both the bound phosphine ligand and the bound ethylene.

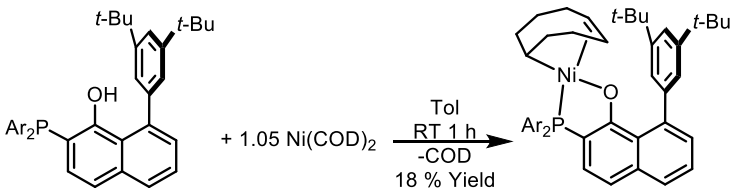

2-C_8H_{13}: In the glove box, to a solution of $Ni(COD)_2$ (35 mg, 0.125 mmol) in toluene (5 ml) in a vial was added a solution of **PONap-H** (80 mg, 0.125 mmol) in toluene (2 ml). The mixture was stirred for 2 h under room temperature, forming a dark yellow solution. Volatile materials were removed under vacuum and triturated with n-hexanes three times. The residue was washed with n-pentane and cold diethyl ether and subsequently was extracted with benzene and dried in vacuo to provide the complex **2-C_8H_{13}** (78 mg, 76%) as a yellowish solid. ^{1}H NMR (400 MHz, C_6D_6): δ 7.82(dd, $^3J_{HH}$ = 8.4 Hz, $^3J_{HH}$ = 9.2 Hz, 1H, PhH), 7.66(dd, $^3J_{HH}$ = 7.9 Hz, $^4J_{HH}$ = 1.8 Hz, 1H, PhH), 7.57(t, $^4J_{HH}$ = 1.9 Hz 1H, PhH), 7.30(apparent t, $^4J_{HH}$ = 1.6 Hz, 1H, ArH), 7.21-7.28(overlapping multiplets, 2H, ArH), 6.26(dd, $^3J_{HH}$ = 8.2 Hz, $^4J_{HP}$ = 3.3 Hz, 2H, PhH), 6.22(dd, $^3J_{HH}$ = 8.2 Hz, $^4J_{HP}$ = 3.3 Hz, 2H, PhH), 5.47(multiplet, 1H, olefinic-CH), 5.19(multiplet, 1H, olefinic H) 3.42(s, 6H, OCH_3), 3.04(s, 6H, OCH_3), 2.21(multiplet, 4H, aliphatic-H), 1.93(multiplet,2H, aliphatic-H), 1.47(s, 9H, O^{t}Bu), 1.48(s, 9H, tBu), 1.42(s, 9H, tBu), 0.78-1.60(overlapping multiplets, 4H, aliphatic H), 0.22(doublet of multiplets, $^3J_{HP}$= 14.2 Hz, 1H, Ni-CH). ^{13}C{^{1}H} NMR (101 MHz, C_6D_6): δ 172.61(d, J_{CP} = 27.5 Hz, 1C, Aryl-C), 161.97(d, J_{CP} = 2.0 Hz, 1C, Aryl-C), 161.86(d, J_{CP} = 2.0 Hz, 1C, Aryl-C), 147.93(s, 1C, Aryl-C), 147.72(s, 1C, Aryl-C), 147.31(s, 1C, Aryl-C), 143.05(d, J_{CP} = 2.8 Hz, 1C, Aryl-C), 138.45(d, J_{CP} = 2.8 Hz, 1C, Aryl-C), 129.88(d, J_{CP} = 11.5 Hz, 1C, Aryl-C), 129.51(d, J_{CP} = 2.5 Hz, 1C, Aryl-C), 128.22(s, 1C, Aryl-C), 126.97(s, 1C, Aryl-C), 127.09(s, 2C, Aryl-C), 126.63(s, 1C, Aryl-C), 125.13(s, 2C, Aryl-C), 122.75(s, 1C, Aryl-C), 122.57(s, 1C, Aryl-C), 118.92(s, 1C, Aryl-C), 114.33(d, J_{CP} = 60.1 Hz, 1C, Aryl-C), 113.53(d, J_{CP} = 42.4 Hz, 1C, Aryl-C), 111.76(d, J_{CP} = 7.2 Hz, 1C, Aryl-C), 109.30(d, J_{CP} = 42.4 Hz, 1C, Aryl-C), 104.91 (d, J_{CP} = 3.6 Hz, 1C, Aryl-C), 104.64(d, J_{CP} = 2.7 Hz, 1C, olefinic-C), 104.91(d, J_{CP} = 3.6 Hz, 1C, Aryl-C), 104.20(d, J_{CP} = 4.0 Hz, 1C, Aryl-C), 101.74(d, J_{CP} = 12.8 Hz, 1C, olefinic-C), 56.75(s, 2C, O*C*$(CH_3)_3$), 55.14(s, 2C, OCH_3), 39.91(d, 1C, $^2J_{CP}$= 5.2 Hz, aliphatic-C), 35.45 (s, 1C, aliphatic-

C), 34.96(d, $^{2}J_{CP}$= 12.0 Hz, 1C, Ni-CH), 32.16(s, 3C, CH(CH_3)$_3$), 32.00(s, 3C, CH(CH_3)$_3$), 31.74(s, 3C, CH(CH_3)$_3$), 30.29(s, 1C, aliphatic-C), 27.86(s, 1C, aliphatic-C), 20.06(d, $^{3}J_{CP}$= 3.3 Hz, 1C, Ni-CHCH_2), 25.99(multiplet, 1C, aliphatic C), 22.96(s, 1C, aliphatic C), 22.79(s, 1C, aliphatic C); $^{31}P\{^{1}H\}$ NMR (121 MHz, C_6D_6, 298 K): δ -19.61(s, 1P, Ni-*P*ONap). Anal. Calcd(%) for $C_{48}H_{57}NiO_5P$: C: 71.74, H: 7.15; found: C: 72.03, H: 7.33.

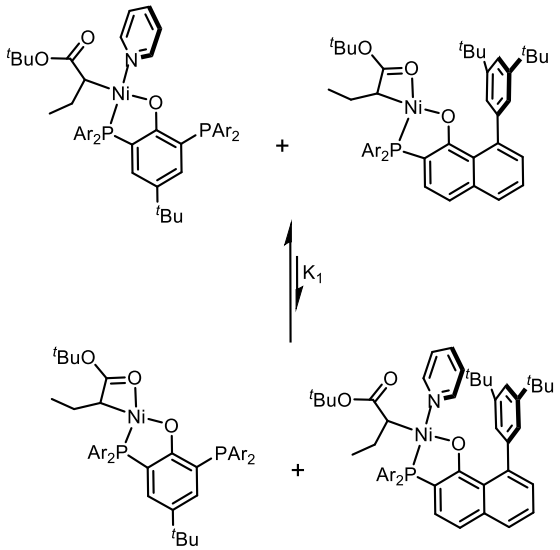

Pyridine Exchange Between 1L-CCO and 2L-CCO: A solution of **2-CCO** (8.4 mg, 0.01 mmol) in d6-benzene was transferred to a 20 mL scintillation vial in the glovebox with one equivalent of **1py-CCO** (10.4 mg, 0.01 mmol). The mixture was fully dissolved and transferred to an NMR tube after 0.5 hours. The four species, **1-CCO**, **1py-CCO**, **2-CCO**, and **2py-CCO** were identified by $^{31}P\{^{1}H\}$ NMR. The solution was monitored by NMR until relative intensities of the four species were unchanged, indicating equilibrium has been reached. Relative intensities of the four species were modelled indicating a K value of 8.0 x 10^{-2} and ΔG of 1.5 kcal/mol.

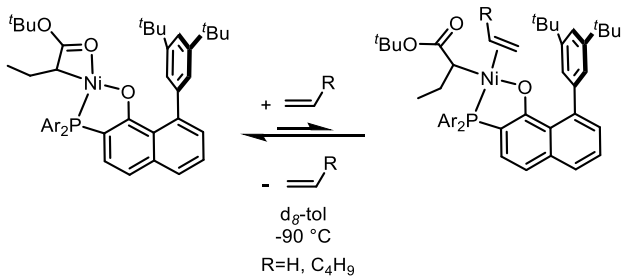

Quantitative determination of ring opening thermodynamics of 2-CCO by olefins: In the glovebox, to a solution of 2-CCO (6.3 mg, 0.0075 mmol) and internal standard hexamethyldisiloxane (6.8 mg, 0.0419 mmol) in d8-toluene (637 mg) was added an excess of olefin (ethylene or 1-hexene) at -78 °C. The solution was transferred to a precooled NMR probe and NMR spectra were recorded. The probe was them warned to -10 °C to allow the mixture to reach a thermodynamic equilibrium while hindering migratory insertion from proceeding. The mixture was recooled to -90 °C and NMR spectra were recollected. This process was repeated until the relative intensities of the starting material and the olefin coordination compounds were unchanged. The relative intensities by $^{31}P\{^{1}H\}$ NMR spectra were used to calculate the K values of 3.0 x 10^{-1} and 5.5 x 10^{-3} and the ΔG of 0.4 kcal/mol and 1.9 kcal/mol for ethylene and 1-hexene, respectively.

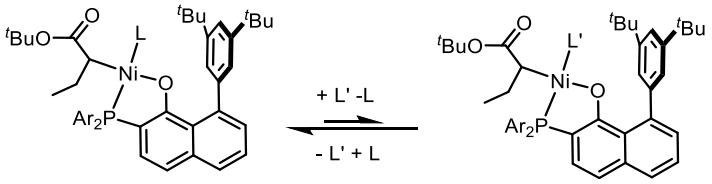

Thermodynamics of ligand exchange with pyridines and olefins at 183 K: A similar procedure to the above quantitative determination of thermodynamic binding constants was adapted to determine the relative thermodynamic binding constant between lutidine and ethylene. In order to determine the K value between pyridine and ethylene coordinated adduct to be 1.1 x 10^{-4} and a ΔG value of 1.4 kcal/mol, the K value for **2lut-CCO** and **2py-CCO**

was determined by mixing **2-CCO** (5.1 mg, 0.0061 mmol), lutidine (72 mg, 0.67 mmol) and pyridine (7.5 mg, 0.0948 mmol). The mixture was cooled to 183 K and the relative intensities observed in the $^{31}P\{^{1}H\}$ NMR spectrum was used to determine the K value of 4.8 x 10^{-3} and a ΔG value of 1.9 kcal/mol. These combined results allow the quantitative determination of the K value between pyridine and ethylene coordinated adducts of 1.1 x 10^{-4} and a ΔG value of 3.3 kcal/mol.

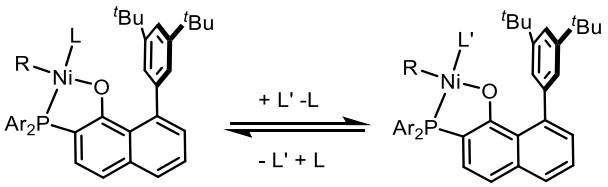

Quantitative determination of thermodynamics of ligand exchange for non-olefin donors: In the glovebox, to a solution of 2L-R (0.0122 mmol) and internal standard of hexamethyldisiloxane in C_6D_6 (406 mg) was added a known amount of a secondary ligand. The mixture was fully dissolved and transferred to an NMR tube. $^{31}P\{^{1}H\}$ and ^{1}H NMR spectra were collected in 20-minute intervals until the spectra were unchanged. The relative ratios were determined in one of two methods depending on the rate of exchange relative to the NMR timescale.

Method A. The rate of exchange is slow relative to the NMR timescale which lead to two separate species observed. The relative intensities of the two species are determined either by integration of Ni-CHR resonance in the ^{1}H NMR spectra or through the $^{31}P\{^{1}H\}$ NMR resonances.

Method B. The rate of exchange is fast relative to the NMR timescale which precludes the observation of two sets of resonances for the mixture of species. The relative intensities of the two species are determined by comparing the resonances of the purified species and

analyzing the separation of the methoxy resonance either of the ligand with different mixtures of both ligands.

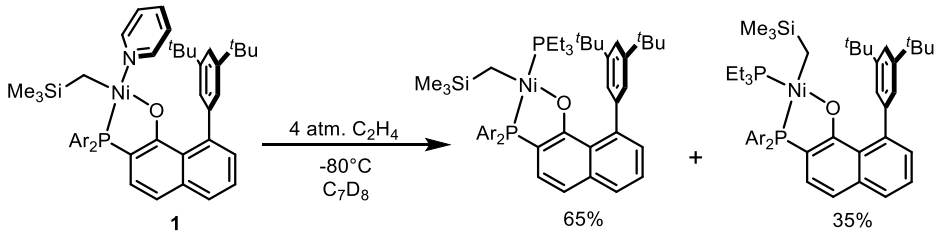

2P: In the glovebox, to a stirring solution of 2 (7.2 mg, 0.0085 mmol) in toluene (2 mL) was added 40 equivalents of PEt_3 (40 mg, 0.034 mmol). The solution was stirred for 0.5 h and all volatiles were removed in vacuo. The resultant solid was triturated with hexanes (3 x 3 mL) and extracted with 5 mL of toluene, filtered through a plug of celite and concentrated, affording quantitative formation of 2P. Both $^{31}P\{^1H\}$ and ^1H NMR suggest an approximate 2:1 mixture of the trans and cis isomer.

Trans isomer ^1H NMR (400 MHz, C_6D_6): δ 6.90-7.82 (overlapping multiplets with cis isomer, aromatic-H), 6.33 (dd, $^3J_{HH}$ = 8.2 Hz, $^4J_{HP}$ = 3.2 Hz, 4H, PhH), 3.31 (s, 12H, OC*H*$_3$), 1.38 (s, 18H, O*t*Bu), 1.20 (multiplet, 6H, Ni-C*H*$_2$-CH3), 0.99 (dt, $^3J_{HH}$ = 7.3 Hz, $^3J_{HP}$ = 14.2 Hz, 9H, Ni-CH$_2$-C*H*$_3$), 0.11 (s, 9H, SiMe$_3$), -0.80 (apparent t (dd), $^2J_{HP}$= 12.7 Hz, 2H, Ni-CH$_2$); $^{31}P\{^1H\}$ NMR (121 MHz, C_6D_6, 298 K): δ 12.09(d, $^2J_{PP}$= 325.2 Hz, 1P), -13.84(d, $^2J_{PP}$= 325.2 Hz, 1P);

Cis Isomer: ^1H NMR (400 MHz, C_6D_6): δ 6.90-7.82 (overlapping multiplets with cis isomer, aromatic-H), 6.23 (dd, $^3J_{HH}$ = 8.2 Hz, $^4J_{HP}$ = 3.2 Hz, 4H, PhH), 3.18 (s, 12H, OC*H*$_3$), 1.60 (s, 18H, O*t*Bu), 1.43 (overlapping multiplet, 6H, Ni-C*H*$_2$-CH3), 0.80 (dt, $^3J_{HH}$ = 7.5 Hz, $^3J_{HP}$ = 14.6 Hz, 9H, Ni-CH$_2$-C*H*$_3$), 0.22 (s, 9H, SiMe$_3$), -0.02 (broad multiplet, $W_{1/2}$= 18 Hz, 2H, Ni-CH$_2$); $^{31}P\{^1H\}$ NMR (121 MHz, C_6D_6, 298 K): δ 18.06 (d, $^2J_{PP}$= 19.6 Hz, 1P), -8.91(d, $^2J_{PP}$= 19.6 Hz, 1P).

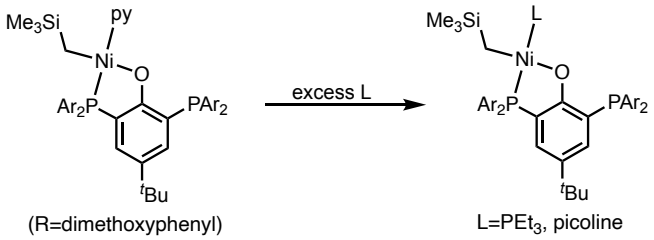

1P: In the glove box, to a solution of **1** (29.6 mg, 0.03 mmol) in toluene (1.5 mL) was added 1 equiv. of PEt_3 (3.5 mg, 0.03 mmol). The mixture was stirred for 10 min under room temperature, forming a red solution. After removal of volatiles, additional 1 equiv. of PEt_3 (3.5 mg, 0.03 mmol) and toluene (1.5 mL) was added to the residue. After stirring for 10 min, the volatiles were removed once again and the residue was triturated with pentane three times, forming the desired product as a red-orange solid (28.8 mg, 94%).^{1}H NMR (400 MHz, C_6D_6) of the major isomer: δ 7.45 (dd, $^3J_{HP}$ = 10.4 Hz, $^4J_{HH}$ = 2.4 Hz, 1H, PhH), 7.31 (broad s, 1H, PhH), 7.08−7.02 (m, 4H, PhH), 6.37 (dd, $^3J_{HH}$ = 8.0 Hz, $^4J_{HH}$ = 2.4 Hz, 4H, PhH), 6.27 (dd, $^3J_{HH}$ = 8.0 Hz, $^4J_{HH}$ = 3.2 Hz, 4H, PhH), 3.31 (s, 12H, OCH_3), 3.20 (s, 12H, OCH_3), 1.22-1.14 (m, 6H, $P(CH_2CH_3)_3$), 1.13 (s, 9H, $C(CH_3)_3$), 1.09-1.06 (t, $^3J_{HH}$ = 7.2 Hz, 9H, $P(CH_2CH_3)_3$), 0.15 (s, 9H, $Si(CH_3)_3$), -0.88−-0.94 (dd, $^3J_{HP}$ = 11.7 Hz, $^3J_{HP}$ = 11.5 Hz 2H, $NiCH_2Si$); $^{13}C\{^1H\}$ NMR (101 MHz, C_7D_8) of the major isomer: 164.31 (s, 2C, Ar-C), 164.19 (s, 2C, Ar-C), 162.31 (m, 2C, Ar-C), 133.44 (m, 1C, Ar-C), 131.60 (broad s, 1C, Ar-C), 130.37 (s, 4C, Ar-C), 126.49 (s, 2C, Ar-C), 105.82 (s, 8C, Ar-C), 104.51 (s, 4C, Ar-C), 104.47 (s, 4C, Ar-C), 56.18 (s, 4C, OCH_3), 55.62 (s, 4C, OCH_3), 34.44 (s, 1C, $C(CH_3)_3$), 32.71 (s, 3C, $C(CH_3)_3$), 14.64 (m, C, $P(CH_2CH_3)_3$), 9.04(m, C, $P(CH_2CH_3)_3$), 4.24 (s, 3C, $SiMe_3$), -26.37 (m, 1C, $NiCH_2Si$); $^{31}P\{^1H\}$ NMR (121 MHz, C_6D_6) of the major isomer: δ 12.19 (d, $^2J_{PP}$ = 197 Hz, 1P), -12.74 (d, $^2J_{PP}$ = 197 Hz, $^4J_{PP}$ = 7.1 Hz, 1P), -51.61 (d, $^4J_{PP}$ = 7.1 Hz, 1P); $^{31}P\{^1H\}$ NMR (121 MHz, C_6D_6) of the minor isomer: δ 21.02 (d, $^2J_{PP}$ = 12.3 Hz, 1P), -3.35 (d, $^2J_{PP}$ = 12.3 Hz, $^4J_{PP}$ = 8.5 Hz, 1P),

-50.37 (d, $^4J_{PP}$ = 8.5 Hz, 1P). Anal. Calcd(%) for $C_{52}H_{73}NiO_9P_3Si$: C: 61.12, H: 7.20; found: C: 63.35, H: 6.76.

1pico: In the glove box, to a solution of **1** (19.6 mg, 0.02 mmol) in toluene (2 mL) was added 25 equiv. of 2-picoline (46.5 mg, 0.5 mmol). After stirred for 15 min, all volatiles were removed under vacuum. Twice more, 25 equiv. of 2-picoline was added to the residue with 2 mL toluene and volatiles were removed after stirring for 15 min, affording quantitative formation of **1pico** (19.5 mg, >95% yield). ^{1}H NMR (400 MHz, C_6D_6): δ 8.97 (d, $^3J_{HH}$ = 5.6 Hz, 1H, PicoH), 7.46−7.39 (m, 1H, PhH), 7.31 (broad s, 1H, PhH), 7.08−7.05 (m, 4H, PhH), 6.96-6.93 (m, 1H, PhH), 6.77 (t, $^3J_{HH}$ = 7.3 Hz, 1H, PicoH), 6.53 (d, $^3J_{HH}$ = 7.3 Hz, 1H, PicoH), 6.42 (t, $^3J_{HH}$ = 6.5 Hz, 1H, PicoH), 6.32 (d, $^3J_{HH}$ = 8.4 Hz, 4H, PhH), 6.30 (d, $^3J_{HH}$ = 8.4 Hz, 4H, PhH), 3.60 (s, 3H, pico-CH_3), 3.45-3.15 (m, 24H, OCH_3), 1.12 (s, 9H, $C(CH_3)_3$), -0.29 (s, 9H, $Si(CH_3)_3$), -1.39 (broad, 2H, $NiCH_2Si$); $^{31}P\{^1H\}$ NMR (121 MHz, C_6D_6): δ -8.06 (d, $^2J_{PP}$ = 10.5 Hz, 1P), -54.75 (d, $^2J_{PP}$ = 10.5 Hz, 1P).

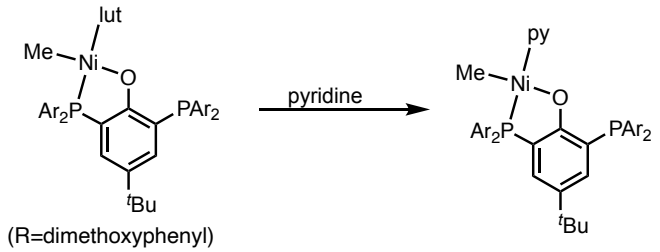

1py-Me: In the glove box, to a solution of **1lut-Me** (18.7 mg, 0.02 mmol) in toluene (2 mL) was added 15 equiv. of 2-picoline (23.7 mg, 0.3 mmol). After stirred for 15 min, all volatiles were removed under vacuum, affording quantitative formation of **1py-Me** (18.0 mg, >95% yield). ^{1}H NMR (400 MHz, C_6D_6): δ 8.59 (d, $^3J_{HH}$ = 5.4Hz, 2H, PyH), 7.51 (dt, , $^3J_{HP}$ = 10.4 Hz, $^4J_{HH}$ = 2.4 Hz, 1H, PhH), 7.10−7.00 (m, 4H, PhH), 6.97 (m, 1H, PhH), 6.78 (t, $^3J_{HH}$ = 5.4Hz, 1H), 6.41 (dd, $^3J_{HH}$ = 8.2 Hz, $^4J_{HH}$ = 2.3 Hz, 4H, PhH), 6.26 (dd, $^3J_{HH}$ = 8.3 Hz, $^4J_{HH}$ = 3.4 Hz, 4H, PhH), 3.34 (s, 6H, OCH_3), 3.25 (s, 12H, OCH_3), 1.15 (s, 9H, $C(CH_3)_3$), -0.49 (d,

$^{3}J_{HP}$ = 5.8 Hz, 3H, $NiCH_3$); $^{31}P\{^{1}H\}$ NMR (121 MHz, C_6D_6): δ -0.61 (d, $^{2}J_{PP}$ = 11.2 Hz, 1P), -50.01 (d, $^{2}J_{PP}$ = 11.2 Hz, 1P).

Quantitative-Determination-of-Ligand-Binding-Strengths

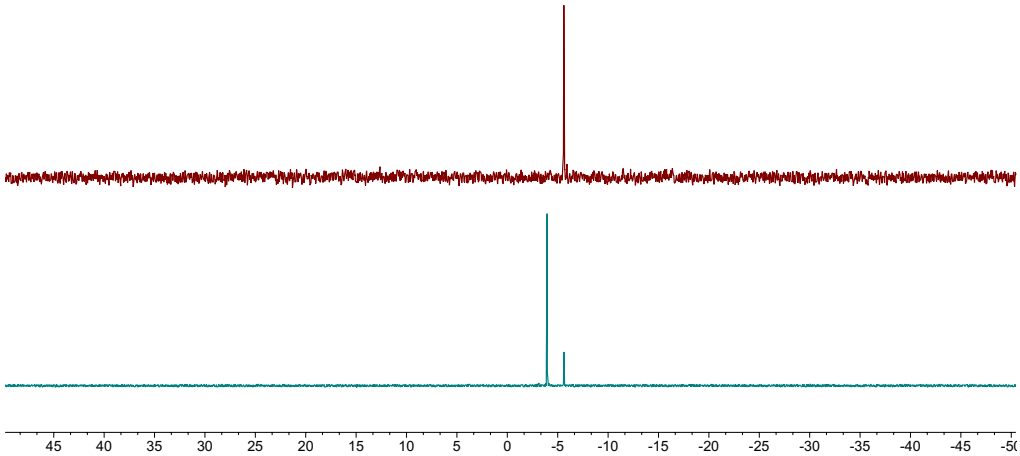

Figure S3.1. An example of the determination of K value via $^{31}P\{^{1}H\}$ NMR spectra (method 1): (Top) $^{31}P\{^{1}H\}$ NMR spectrum of **2lut-Me** and (bottom) $^{31}P\{^{1}H\}$ NMR spectrum of **2lut-Me** + 1 equiv. of lutidine.

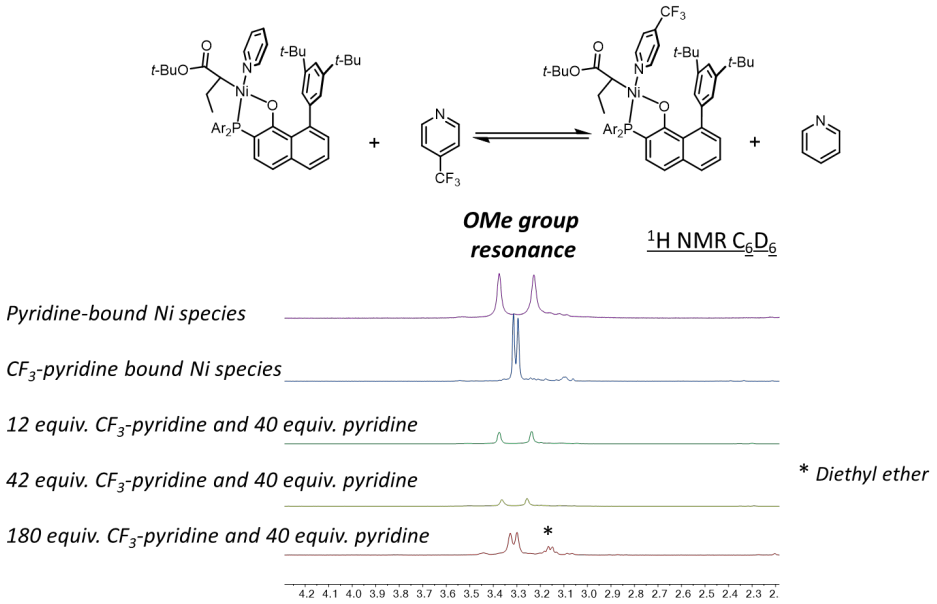

Figure S3.2. An example of the determination of K value via ^{1}H NMR spectra (method 2). Sample of $^{31}P\{^{1}H\}$ EXSY Experiment of 2P

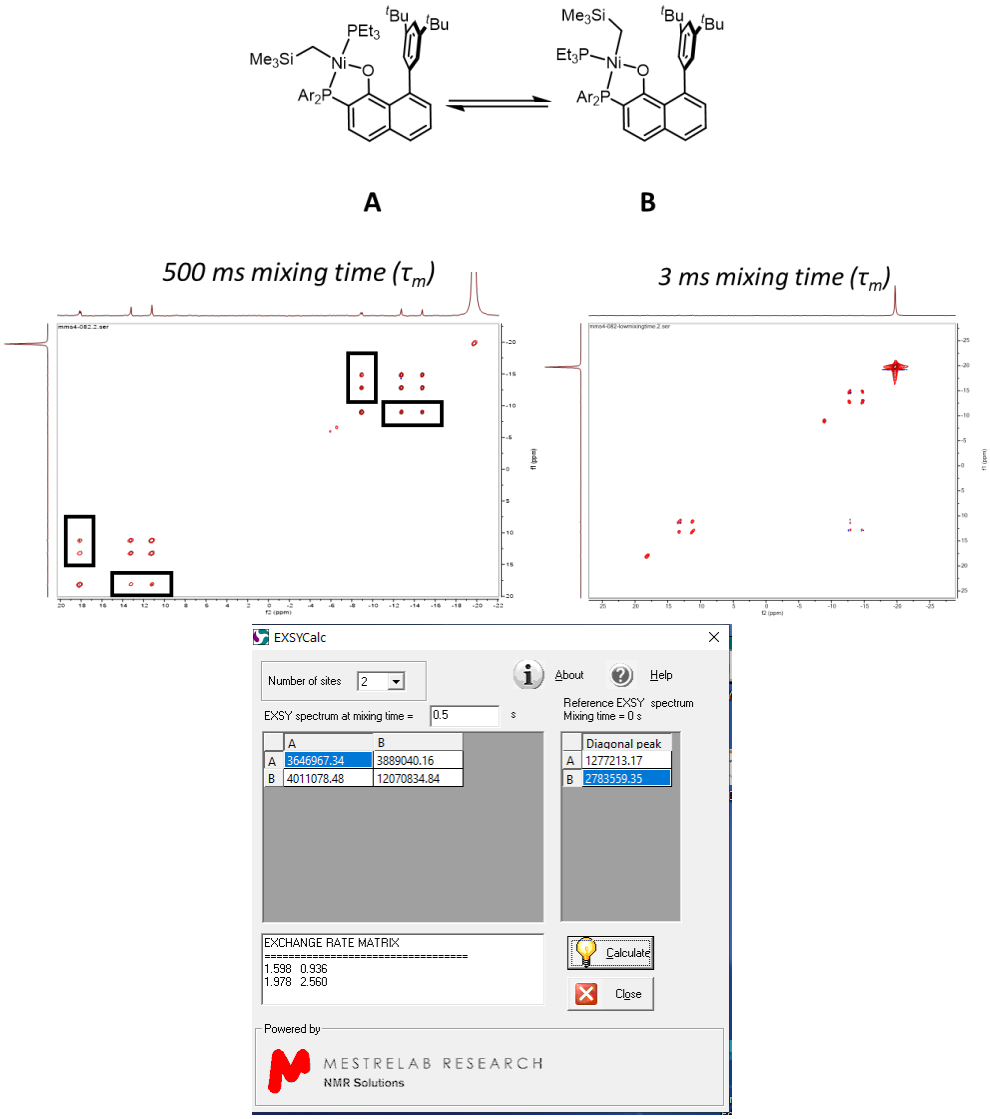

Supplemental information for olefin copolymerization

General procedure for high throughput parallel polymerization reactor (PPR) runs for preparation of polyethylene and ethylene/tBA copolymers.

Polyolefin catalysis screening was performed in a high throughput parallel polymerization reactor (PPR) system. The PPR system was comprised of an array of 48 single cell (6 x 8 matrix) reactors in an inert atmosphere glovebox. Each cell was equipped with a glass insert

with an internal working liquid volume of approximately 5 mL. Each cell had independent controls for pressure and was continuously stirred at 800 rpm. Catalysts were prepared in toluene. All liquids (i.e., solvent, tBA, and catalyst solutions) were added via robotic syringes. Gaseous reagents (i.e., ethylene) were added via a gas injection port. Prior to each run, the reactors were heated to 50 °C, purged with ethylene, and vented.

All desired cells were injected with tBA followed with a portion of toluene (This step was skipped for ethylene homopolymerization). The reactors were heated to the run temperature and then pressured to the appropriate psig with ethylene. Catalyst were then added to the cells. Each catalyst addition was chased with a small amount of toluene so that after the final addition, a total reaction volume of 5 mL was reached. Upon addition of the catalyst, the PPR software began monitoring the pressure of each cell. The desired pressure (within approximately 2-6 psig) was maintained by the supplemental addition of ethylene gas by opening the valve at the set point minus 1 psi and closing it when the pressure reached 2 psi higher. The pressure of each cell was monitored during and after the quench to ensure that no further ethylene consumption happens. The shorter the "Quench Time" (the duration between catalyst addition and oxygen quench), the more active the catalyst. All drops in pressure were cumulatively recorded as "Uptake" or "Conversion" of the ethylene for the duration of the run. After 1h, each reaction was then quenched by addition of 1% oxygen in nitrogen for 30 seconds at 40 psi higher than the reactor pressure. After all the reactors were quenched they were allowed to cool to about 60 °C. They were then vented and the tubes were removed. The polymer samples were then dried in a centrifugal evaporator at 60 °C for 12 hours, weighed to determine polymer yield and submitted for IR (tBA incorporation) and GPC (molecular weight) analysis. NMR analysis were performed separately for microstructural analysis.

General procedure for polymer characterization

a) Gel permeation chromatography (GPC)

High temperature GPC analysis was performed using a Dow Robot Assisted Delivery (RAD) system equipped with a Polymer Char infrared detector (IR5) and Agilent PLgel Mixed A columns. Decane (10 μL) was added to each sample for use as an internal flow marker. Samples were first diluted in 1,2,4-trichlorobenzene (TCB) stabilized with 300 ppm butylated hydroxyl toluene (BHT) at a concentration of 10 mg/mL and dissolved by stirring at 160°C for 120 minutes. Prior to injection the samples are further diluted with TCB stabilized with BHT to a concentration of 3 mg/mL. Samples (250 μL) are eluted through one PL-gel 20 μm (50 x 7.5 mm) guard column followed by two PL-gel 20 μm (300 x 7.5 mm) Mixed-A columns maintained at 160 °C with TCB stabilized with BHT at a flowrate of 1.0 mL/min. The total run time was 24 minutes. To calibrate for molecular weight (MW) Agilent EasiCal polystyrene standards (PS-1 and PS-2) were diluted with 1.5 mL TCB stabilized with BHT and dissolved by stirring at 160 °C for 15 minutes. These standards are analyzed to create a 3rd order MW calibration curve. Molecular weight units are converted from polystyrene (PS) to polyethylene (PE) using a daily Q-factor calculated to be around 0.4 using the average of 5 Dowlex 2045 reference samples.

b) Fourier-transform infrared spectroscopy (FTIR)

The 10 mg/mL samples prepared for GPC analysis are also utilized to quantify tert butyl acrylate (tBA) incorporation by Fourier Transform infrared spectroscopy (FTIR). A Dow robotic preparation station heated and stirred the samples at 160°C for 60 minutes then deposited 130 μL portions into stainless wells promoted on a silicon wafer. The TCB was evaporated off at 160°C under nitrogen purge. IR spectra were collected using a Nexus 6700 FT-IR equipped with a DTGS KBr detector from 4000-400 cm-1 utilizing 128 scans with a

resolution of 4. Ratio of tBA (C=O: 1762-1704 cm−1) to ethylene (CH2: 736-709 cm−1) peak areas were calculated and fit to a linear calibration curve to determine total tBA.

c) Differential scanning calorimetry (DSC)

Differential scanning calorimetry analyses was performed on solid polymer samples using a TA Instruments, Inc. Discovery Series or TA Instruments, Inc., DSC2500, programmed with: equilibrate at 175.00 °C; isothermal for 3 minutes, ramp 30.00 °C/min to 0.00 °C, ramp 10.00 °C/min to 175.00 °C. Data was analyzed using TA Trios software.

Original polymerization runs for ethylene/tBA copolymerization in high throughput parallel polymerization reactors (PPR)

Table S3.1. Ethylene copolymerization with **2lut-Me, 2-CCO and 2**.

Entry[a]	catalyst	[tBA]/M	Yield (mg)	Act.[b]	$M_w/10^3$	PDI	%Mol tBA	Tm (ºC)
1	**2lut-Me**	0.025	75	300	17.7	2.2	0.4	128
2	**2lut-Me**	0.025	89	356	16.6	2.2	0.4	129
3	**2lut-Me**	0.025	86	344	15.7	2.2	0.4	128
4	**2lut-Me**	0.05	40	160	14.8	2.3	0.8	124
5	**2lut-Me**	0.05	40	160	15.0	2.4	0.8	124
6	**2lut-Me**	0.05	38	152	16.3	2.5	0.8	124
7	**2-CCO**	0.025	73	296	18.2	2.2	0.5	127
8	**2-CCO**	0.025	75	300	18.1	2.4	0.4	128
9	**2-CCO**	0.025	79	316	17.8	2.4	0.4	128
10	**2-CCO**	0.05	33	132	17.2	2.4	0.8	125
11	**2-CCO**	0.05	36	144	17.6	2.5	0.8	124
12	**2-CCO**	0.05	35	140	17.0	2.7	0.8	124
13[c]	**2**	0.05	51	204	16.1	2.3	0.7	121

[a]Conditions unless specified: catalyst, 0.25 μmol; V(toluene)=5 ml; ethylene pressure=400 psi; T = 70 ºC; t = 1h.
[b] 1000 kg/(mol·h). [c]Data reported in Ref 24.

Crystallographic Information

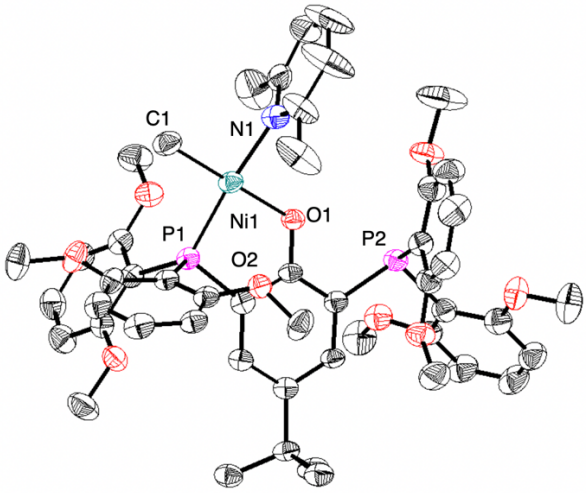

Figure S3.3: Solid-State Structure of **1lut-Me**. Ellipsoids are show at the 50% probability level. Hydrogen atoms excluded for clarity.

Special Refinement Details for 1lut-Me: Complex **1lut-Me** crystallizes in the triclinic P-1 space group with cocrystallized toluene in the asymmetric unit. The solvent molecules show relatively broad ellipsoids consistent with a high degree of thermal motion in the solid-state.

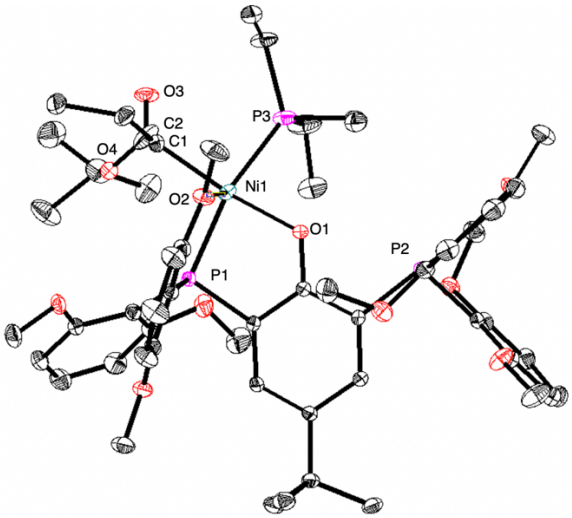

Figure S3.3: Solid-State Structure of **1P-CCO**. Ellipsoids are show at the 50% probability level. Hydrogen atoms excluded for clarity.

Special Refinement Details for 1P-CCO: Complex **1P-CCO** crystallizes in the monoclinic $P_{21/n}$ spacegroup. The inserted acrylate moiety suffers from two-site positional disorder and are freely refined to produce relative occupancies of 0.65 and 0.31. The small and plate-like nature of the crystal is responsible for the above average Rint value.

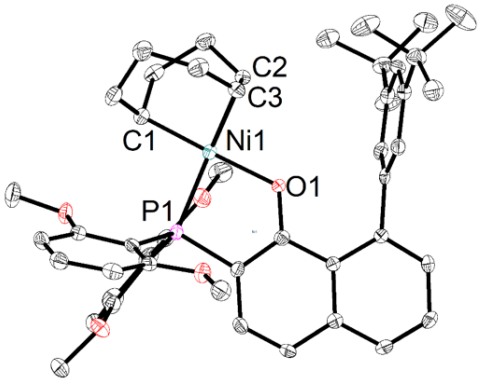

Figure S3.5: Solid-State Structure of **2-C_8H_{13}**. Ellipsoids are show at the 50% probability level. Hydrogen atoms excluded for clarity.

Special Refinement Details for 2-C_8H_{13}: Complex **2-C_8H_{13}** crystalizes in a P-1 space group with the full molecule in the asymmetric unit. The $SiMe_3$ group is modelled with two-site disorder with occupancies of 0.78 and 0.22. One of the methoxy groups is also modelled with two-site disorder with occupancies of 0.78 and 0.22. The carbon on the lower occupancy disordered methoxy group is refined isotropically to prevent a NPD. A disordered benzene molecule is observed and is refined isotropically to prevent NPDs. There is likely disorder on the benzene molecule, despite efforts, it could not be modelled.

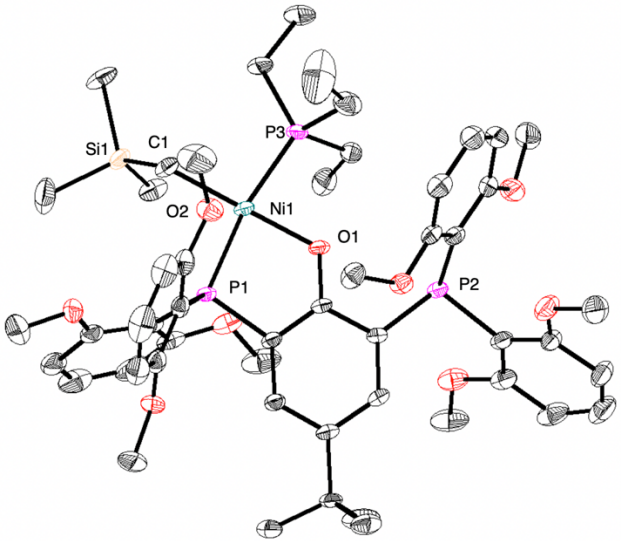

Figure S3.6: Solid-State Structure of **1P**. Ellipsoids are show at the 50% probability level. Hydrogen atoms excluded for clarity.

Special Refinement Details for 1P: Complex **1P** crystallizes in the orthorhombic Pca21 space group with cocrystallized diethyl ether in the asymmetric unit.

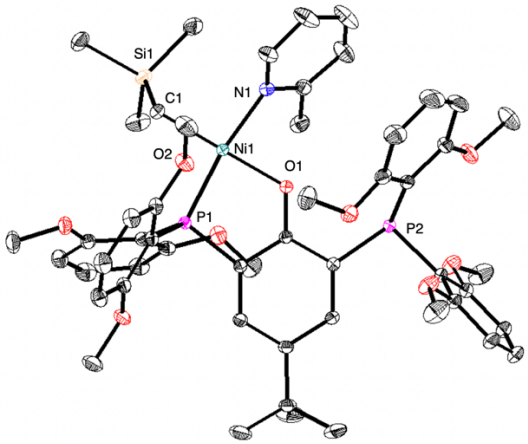

Figure S3.7: Solid-State Structure of **1pico**. Ellipsoids are show at the 50% probability level. Hydrogen atoms excluded for clarity.

Special Refinement Details for 1pico: Complex **1pico** crystallizes in the triclinic P-1 space group with a single molecule of benzene cocrystallized in the asymmetric unit along with a half of a benzene molecule.

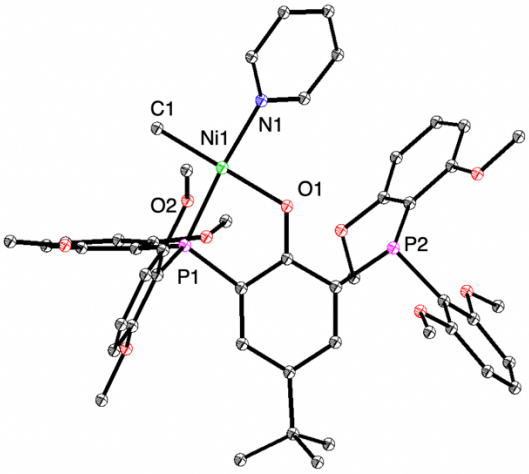

Figure S3.8: Solid-State Structure of **1py-Me**. Ellipsoids are show at the 50% probability level. Hydrogen atoms excluded for clarity.

Special Refinement Details for 1py-Me: Complex **1py-Me** crystallizes in the triclinic P-1 space group with cocrystallized benzene in the asymmetric unit. The solution suffers from a high Rint due to the small size of the single-crystalline sample along with the plate-like shape of the sample

Table S3.2: Crystal and refinement data (part 1)

	2-C_8H_{13}	**1P-CCO**
Empirical formula	$C_{48}H_{57}NiO_5P$	$C_{56.42}H7_{5.51}$ $NiO_{10.92}P_3$
Formula weight	803.61	1080.16
Temperature/K	100	100
Crystal system	Monoclinic	Monoclinic
Space group	$C_{2/c}$	P21/n
a/Å	41.799(11)	14.637(3)
b/Å	12.951(2)	16.793(4)
c/Å	15.734(5)	22.546(5)
α/°	90	90
β/°	105.463(16)	94.948(14)
γ/°	90	90
Volume/Å^3	8209(4)	5521(2)
Z	8	4
ρ_{calc}g/cm^3	0.066	0.496
μ/mm^{-1}	1.414	1.300
F(000)	3424	2298
Radiation	CuKα	MoKα
Reflections collected	7891	200549
Independent reflections	6893	9989
Goodness-of-fit on F^2	1.064	0.940
R_{int}	twinned	27.81%

Table S3.3: Crystal and refinement data (part 2)

	1lut-Me	**1py-Me**
CCDC		
Empirical formula	$C_{57}H_{67}NNiO_9P_2$	$C_{54}H_{61}NNiO_9P_2$
Formula weight	1030.76	988.68
Temperature/K	100	100
Crystal system	Triclinic	Triclinic
Space group	P-1	P-1
a/Å	12.408(2)	13.3937(14)
b/Å	14.666(6)	13.8200(15)
c/Å	15.040(4)	13.8909(14)
α/°	93.413(18)	79.649(6)
β/°	96.340(13)	76.070(10)
γ/°	96.33(2)	87.758(7)
Volume/Å^3	2965.5(14)	2454.9(5)
Z	2	2
ρ_{calc}g/cm^3	1.270	1.338
μ/mm^{-1}	1.528	1.656
F(000)	1092	1044
Radiation	CuKα	CuKα
Reflections collected	32411	116262
Independent reflections	6900	9583
Goodness-of-fit on F^2	1.071	1.076
R_{int}	8.60%	34.92%

Table S3.4: Crystal and refinement data (part 3)

	1P	**1pico**
CCDC		
Empirical formula	$C_{56}H_{83}NiO_{10}P_3Si$	$C_{67}H_{80}NNiO_9P_2Si$
Formula weight	1095.93	1192.06
Temperature/K	100	100
Crystal system	Orthorhombic	Triclinic
Space group	P-2ac	P-1
a/Å	26.600(9)	13.037(5)
b/Å	14.884(4)	13.920(3)
c/Å	14.618(3)	19.809(6)
α/°	90	96.29(3)
β/°	90	105.302(19)
γ/°	90	111.175(12)
Volume/Å^3	5788(3)	3148.3(18)
Z	4	2
ϱ_{calc}g/cm^3	1.258	1.257
μ/mm^{-1}	0.493	0.434
F(000)	2344	1266
Radiation	MoKα	MoKα
Reflections collected	117397	257499
Independent reflections	9541	9470
Goodness-of-fit on F^2	0.848	1.058
Final R indexes [I>=2σ (I)]	7.33%	5.74

Computational Details

DFT energy calculations and geometry optimizations in the gas phase are carried out with Gaussian software.[57] The hybrid meta-generalized gradient approximation (hybrid meta-GGA) functional M06[58] was used with the Karlsruhe-family double-ζ valence basis set def2-SVP.[59] M06 was chosen for its extensive benchmarking with organometallic systems[60] and from prior use in related systems.[24] When available, the initial guess for geometry optimization was the experimental X-ray crystal structure. Conformational sampling was performed using Entos Qcore software[61] by running an annealing MD trajectory for a given structure using the GFN-xTB1[62] potential energy surface, followed by optimization at the XTB level, and finally DFT optimization using the M06 functional. The critical points on the potential energy surface are confirmed with harmonic frequency analysis, where exactly zero imaginary frequencies are

seen for ground-state structures. Single point corrections are performed using the M06 functional and the triple-ζ def2-TZVP basis set. Implicit solvation effects by toluene solvent are considered by using the SMD continuum solvation model[61] as an additional single point correction with the ORCA software package.[63] Gibbs free energies are taken at 298.15 K. Natural charges at the nickel metal center were taken using natural bond orbital (NBO) analysis.[63]

In Figure 3.10, the following ligands bound to the Ni center were considered for each catalyst **2L** (R = silane), **2L-Me** (R = Me), and **2L-CCO** (R = ester): pyridine, 1,5-dimethylpyridine, 5-fluoropyridine, ethene, butene, hexene, methyl vinyl ether (binding at alkene), methyl vinyl ether (binding at O), vinyl acetate (binding at alkene), vinyl acetate (binding at O), *t*-butyl acrylate (binding at alkene), *t*-butyl acrylate (binding at O), acrylonitrile (binding at alkene), acrylonitrile (binding at N), methyl vinyl ketone (binding at alkene), and methyl vinyl ketone (binding at O).

Regression analysis was performed on the data in Figure 3.10. The lines of regression for the catalyst systems **2L** (R = silane) and **2L-Me** (R = Me) are $y = 0.98x + 3.07$ kcal/mol ($R^2 = 0.82$) and $y = 1.00x + 2.25$ kcal/mol ($R^2 = 0.79$), respectively.

REFERENCES

(1) Chen, C., Designing catalysts for olefin polymerization and copolymerization: beyond electronic and steric tuning. *Nat. Rev. Chem.* **2018,** *2* (5), 6-14.

(2) Nakamura, A.; Ito, S.; Nozaki, K., Coordination− insertion copolymerization of fundamental polar monomers. *Chem. Rev.* **2009,** *109* (11), 5215-5244.

(3) Carrow, B. P.; Nozaki, K., Transition-metal-catalyzed functional polyolefin synthesis: effecting control through chelating ancillary ligand design and mechanistic insights. *Macromolecules* **2014,** *47* (8), 2541-2555.

(4) Chen, E. Y.-X., Coordination polymerization of polar vinyl monomers by single-site metal catalysts. *Chem. Rev.* **2009,** *109* (11), 5157-5214.

(5) Luckham, S. L. J.; Nozaki, K., Toward the Copolymerization of Propylene with Polar Comonomers. *Acc. Chem. Res.* **2020**.

(6) Baur, M.; Lin, F.; Morgen, T. O.; Odenwald, L.; Mecking, S., Polyethylene materials with in-chain ketones from nonalternating catalytic copolymerization. *Science* **2021,** *374* (6567), 604-607.

(7) Guan, Z.; Cotts, P.; McCord, E.; McLain, S., Chain walking: a new strategy to control polymer topology. *Science* **1999,** *283* (5410), 2059-2062.

(8) Arriola, D. J.; Carnahan, E. M.; Hustad, P. D.; Kuhlman, R. L.; Wenzel, T. T., Catalytic production of olefin block copolymers via chain shuttling polymerization. *Science* **2006,** *312* (5774), 714-719.

(9) Makio, H.; Terao, H.; Iwashita, A.; Fujita, T., FI Catalysts for olefin polymerization□ A comprehensive treatment. *Chem. Rev.* **2011,** *111* (3), 2363-2449.

(10) Weng, W.; Shen, Z.; Jordan, R. F., Copolymerization of ethylene and vinyl fluoride by (phosphine-sulfonate) Pd (Me)(py) catalysts. *J. Am. Chem. Soc.* **2007,** *129* (50), 15450-15451.

(11) Guironnet, D.; Roesle, P.; Rünzi, T.; Göttker-Schnetmann, I.; Mecking, S., Insertion polymerization of acrylate. *J. Am. Chem. Soc.* **2009,** *131* (2), 422-423.

(12) Johnson, L. K.; Mecking, S.; Brookhart, M., Copolymerization of ethylene and propylene with functionalized vinyl monomers by palladium (II) catalysts. *J. Am. Chem. Soc.* **1996,** *118* (1), 267-268.

(13) Drent, E.; van Dijk, R.; van Ginkel, R.; van Oort, B.; Pugh, R. I., Palladium catalysed copolymerisation of ethene with alkylacrylates: polar comonomer built into the linear polymer chain. *Chem. Commun.* **2002,** (7), 744-745.

(14) Nakamura, A.; Anselment, T. M.; Claverie, J.; Goodall, B.; Jordan, R. F.; Mecking, S.; Rieger, B.; Sen, A.; Van Leeuwen, P. W.; Nozaki, K., Ortho-phosphinobenzenesulfonate: A superb ligand for palladium-catalyzed coordination–insertion copolymerization of polar vinyl monomers. *Acc. Chem. Res.* **2013,** *46* (7), 1438-1449.

(15) Tao, W. j.; Nakano, R.; Ito, S.; Nozaki, K., Copolymerization of ethylene and polar monomers by using Ni/IzQO catalysts. *Angew. Chem. Int. Ed.* **2016,** *55* (8), 2835-2839.

(16) Tao, W.; Akita, S.; Nakano, R.; Ito, S.; Hoshimoto, Y.; Ogoshi, S.; Nozaki, K., Copolymerisation of ethylene with polar monomers by using palladium catalysts bearing an N-heterocyclic carbene–phosphine oxide bidentate ligand. *Chem. Commun.* **2017,** *53* (17), 2630-2633.

(17) Carrow, B. P.; Nozaki, K., Synthesis of functional polyolefins using cationic bisphosphine monoxide–palladium complexes. *J. Am. Chem. Soc.* **2012,** *134* (21), 8802-8805.

(18) Dai, S.; Chen, C., Direct synthesis of functionalized high-molecular-weight polyethylene by copolymerization of ethylene with polar monomers. *Angew. Chem. Int. Ed.* **2016,** *55* (42), 13281-13285.

(19) Long, B. K.; Eagan, J. M.; Mulzer, M.; Coates, G. W., Semi-Crystalline Polar Polyethylene: Ester-Functionalized Linear Polyolefins Enabled by a Functional-Group-Tolerant, Cationic Nickel Catalyst. *Angew. Chem. Int. Ed.* **2016,** *55* (25), 7106-7110.

(20) Xin, B. S.; Sato, N.; Tanna, A.; Oishi, Y.; Konishi, Y.; Shimizu, F., Nickel catalyzed copolymerization of ethylene and alkyl acrylates. *J. Am. Chem. Soc.* **2017,** *139* (10), 3611-3614.

(21) Zhang, Y.; Mu, H.; Pan, L.; Wang, X.; Li, Y., Robust bulky [P, O] neutral nickel catalysts for copolymerization of ethylene with polar vinyl monomers. *ACS Catal.* **2018,** *8* (7), 5963-5976.

(22) Chen, M.; Chen, C., Rational design of high-performance phosphine sulfonate nickel catalysts for ethylene polymerization and copolymerization with polar monomers. *ACS Catal.* **2017,** *7* (2), 1308-1312.

(23) Tan, C.; Chen, C., Emerging palladium and nickel catalysts for copolymerization of olefins with polar monomers. *Angew. Chem.* **2019,** *131* (22), 7268-7276.

(24) Xiong, S.; Shoshani, M. M.; Zhang, X.; Spinney, H. A.; Nett, A. J.; Henderson, B. S.; Miller III, T. F.; Agapie, T., Efficient Copolymerization of Acrylate and Ethylene with Neutral P, O-Chelated Nickel Catalysts: Mechanistic Investigations of Monomer Insertion and Chelate Formation. *J. Am. Chem. Soc.* **2021,** *143* (17), 6516-6527.

(25) Wang, X.-l.; Zhang, Y.-p.; Wang, F.; Pan, L.; Wang, B.; Li, Y.-s., Robust and Reactive Neutral Nickel Catalysts for Ethylene Polymerization and Copolymerization with a Challenging 1,1-Disubstituted Difunctional Polar Monomer. *ACS Catal.* **2021**, 2902-2911.

(26) Berkefeld, A.; Drexler, M.; Möller, H. M.; Mecking, S., Mechanistic insights on the copolymerization of polar vinyl monomers with neutral Ni (II) catalysts. *J. Am. Chem. Soc.* **2009,** *131* (35), 12613-12622.

(27) Allen, K. E.; Campos, J. s.; Daugulis, O.; Brookhart, M., Living polymerization of ethylene and copolymerization of ethylene/methyl acrylate using "sandwich" diimine palladium catalysts. *ACS Catal.* **2015,** *5* (1), 456-464.

(28) Williams, B. S.; Leatherman, M. D.; White, P. S.; Brookhart, M., Reactions of vinyl acetate and vinyl trifluoroacetate with cationic diimine Pd (II) and Ni (II) alkyl complexes: identification of problems connected with copolymerizations of these monomers with ethylene. *J. Am. Chem. Soc.* **2005,** *127* (14), 5132-5146.

(29) Chen, C.; Luo, S.; Jordan, R. F., Cationic polymerization and insertion chemistry in the reactions of vinyl ethers with (α-diimine) PdMe+ species. *J. Am. Chem. Soc.* **2010,** *132* (14), 5273-5284.

(30) Chen, Z.; Liu, W.; Daugulis, O.; Brookhart, M., Mechanistic studies of Pd (II)-catalyzed copolymerization of ethylene and vinylalkoxysilanes: Evidence for a β-silyl elimination chain transfer mechanism. *J. Am. Chem. Soc.* **2016,** *138* (49), 16120-16129.

(31) Chen, Z.; Leatherman, M. D.; Daugulis, O.; Brookhart, M., Nickel-catalyzed copolymerization of ethylene and vinyltrialkoxysilanes: catalytic production of cross-linkable polyethylene and elucidation of the chain-growth mechanism. *J. Am. Chem. Soc.* **2017,** *139* (44), 16013-16022.

(32) Guo, L.; Dai, S.; Sui, X.; Chen, C., Palladium and nickel catalyzed chain walking olefin polymerization and copolymerization. *ACS Catal.* **2016,** *6* (1), 428-441.

(33) Dai, S.; Sui, X.; Chen, C., Highly Robust Palladium (II) α-Diimine Catalysts for Slow-Chain-Walking Polymerization of Ethylene and Copolymerization with Methyl Acrylate. *Angew. Chem. Int. Ed.* **2015,** *54* (34), 9948-9953.

(34) Berkefeld, A.; Mecking, S., Deactivation pathways of neutral Ni (II) polymerization catalysts. *J. Am. Chem. Soc.* **2009,** *131* (4), 1565-1574.

(35) Jenkins, J. C.; Brookhart, M., A mechanistic investigation of the polymerization of ethylene catalyzed by neutral Ni (II) complexes derived from bulky anilinotropone ligands. *J. Am. Chem. Soc.* **2004,** *126* (18), 5827-5842.

(36) Tran, Q. H.; Brookhart, M.; Daugulis, O., New Neutral Nickel and Palladium Sandwich Catalysts: Synthesis of Ultra-High Molecular Weight Polyethylene (UHMWPE) via Highly Controlled Polymerization and Mechanistic Studies of Chain Propagation. *J. Am. Chem. Soc.* **2020,** *142* (15), 7198-7206.

(37) Svejda, S. A.; Johnson, L. K.; Brookhart, M., Low-temperature spectroscopic observation of chain growth and migratory insertion barriers in (α-diimine) Ni (II) olefin polymerization catalysts. *J. Am. Chem. Soc.* **1999,** *121* (45), 10634-10635.

(38) Mecking, S.; Johnson, L. K.; Wang, L.; Brookhart, M., Mechanistic studies of the palladium-catalyzed copolymerization of ethylene and α-olefins with methyl acrylate. *J. Am. Chem. Soc.* **1998,** *120* (5), 888-899.

(39) Rix, F. C.; Brookhart, M.; White, P. S., Mechanistic studies of the palladium (II)-catalyzed copolymerization of ethylene with carbon monoxide. *J. Am. Chem. Soc.* **1996,** *118* (20), 4746-4764.

(40) Chandran, D.; Lee, K. M.; Chang, H. C.; Song, G. Y.; Lee, J.-E.; Suh, H.; Kim, I., Ni (II) complexes with ligands derived from phenylpyridine, active for selective dimerization and trimerization of ethylene. *J. Organomet. Chem.* **2012,** *718*, 8-13.

(41) Chapleski, R. C.; Kern, J. L.; Anderson, W. C.; Long, B. K.; Roy, S., A mechanistic study of microstructure modulation in olefin polymerizations using a redox-active Ni (II) α-diimine catalyst. *Catal. Sci. Technol.* **2020,** *10* (7), 2029-2039.

(42) Leatherman, M. D.; Svejda, S. A.; Johnson, L. K.; Brookhart, M., Mechanistic studies of nickel (II) alkyl agostic cations and alkyl ethylene complexes: investigations of chain propagation and isomerization in (α-diimine) Ni (II)-catalyzed ethylene polymerization. *J. Am. Chem. Soc.* **2003,** *125* (10), 3068-3081.

(43) Kenyon, P.; Falivene, L.; Caporaso, L.; Mecking, S., Ancillary Ligands Impact Branching Microstructure in Late-Transition-Metal Polymerization Catalysis. *ACS Catal.* **2019,** *9* (12), 11552-11556.

(44) Thompson, M. E.; Baxter, S. M.; Bulls, A. R.; Burger, B. J.; Nolan, M. C.; Santarsiero, B. D.; Schaefer, W. P.; Bercaw, J. E., . sigma.-Bond metathesis for carbon-hydrogen bonds of hydrocarbons and Sc-R (R= H, alkyl, aryl) bonds of permethylscandocene derivatives. Evidence for noninvolvement of the. pi. system in electrophilic activation of aromatic and vinylic CH bonds. *J. Am. Chem. Soc.* **1987,** *109* (1), 203-219.

(45) Noda, S.; Nakamura, A.; Kochi, T.; Chung, L. W.; Morokuma, K.; Nozaki, K., Mechanistic studies on the formation of linear polyethylene chain catalyzed by palladium phosphine− sulfonate complexes: experiment and theoretical studies. *J. Am. Chem. Soc.* **2009,** *131* (39), 14088-14100.

(46) Zhou, X.; Lau, K.-C.; Petro, B. J.; Jordan, R. F., cis/trans Isomerization of o-Phosphino-Arenesulfonate Palladium Methyl Complexes. *Organometallics* **2014,** *33* (24), 7209-7214.

(47) Casares, J. A.; Espinet, P., Dynamic Behavior of [Pd (C6F5) 2 (SPPy n Ph3-n)] Complexes: Evidence for a Turnstile Mechanism in Intramolecular Exchange. *Inorg. Chem.* **1997,** *36* (24), 5428-5431.

(48) Macchioni, A.; Bellachioma, G.; Cardaci, G.; Travaglia, M.; Zuccaccia, C.; Milani, B.; Corso, G.; Zangrando, E.; Mestroni, G.; Carfagna, C., Counterion effect on CO/styrene copolymerization catalyzed by cationic palladium (II) organometallic Complexes: an interionic structural and dynamic investigation based on NMR spectroscopy. *Organometallics* **1999,** *18* (16), 3061-3069.

(49) Redfield, D. A.; Nelson, J. H.; Henry, R. A.; Moore, D. W.; Jonassen, H. B., Isomerism energetics and mechanisms for palladium (II) phosphine complexes containing 5-methyl-and 5-trifluoromethyltetrazoles. *J. Am. Chem. Soc.* **1974,** *96* (20), 6298-6309.

(50) Casado, A. L.; Casares, J. A.; Espinet, P., Mechanism of the Uncatalyzed Dissociative Cis− Trans Isomerization of Bis (pentafluorophenyl) bis (tetrahydrothiophene): A Refinement. *Inorg. Chem.* **1998,** *37* (16), 4154-4156.

(51) Romeo, R.; D'Amico, G.; Sicilia, E.; Russo, N.; Rizzato, S., β-hydrogen kinetic effect. *J. Am. Chem. Soc.* **2007,** *129* (17), 5744-5755.

(52) Bircher, H.; Bender, B. R.; von Philipsborn, W., Interconversion of diastereomeric complexes involved in Rh (I)-catalyzed asymmetric hydrogenation: A (31P, 31P) EXSY NMR study. *Magnetic resonance in chemistry* **1993,** *31* (3), 293-298.

(53) Londaitsbehere, A.; Herrera, M.; Salgado, A.; Mosquera, M. E.; Cuenca, T.; Cano, J., Nondissociative Mechanism for the Inversion of the Configuration in Cyclopentadienyl Di (aryloxo) titanium Complexes: An Entropy Discussion. *Organometallics* **2017,** *36* (20), 3904-3911.

(54) Pangborn, A. B.; Giardello, M. A.; Grubbs, R. H.; Rosen, R. K.; Timmers, F. J., Safe and convenient procedure for solvent purification. *Organometallics* **1996,** *15* (5), 1518-1520.

(55) Connor, E. F.; Younkin, T. R.; Henderson, J. I.; Waltman, A. W.; Grubbs, R. H., Synthesis of neutral nickel catalysts for ethylene polymerization–the influence of ligand size on catalyst stability. *Chem. Commun.* **2003,** (18), 2272-2273.

(56) Palmer, W. N.; Zarate, C.; Chirik, P. J., Benzyltriboronates: building blocks for diastereoselective carbon–carbon bond formation. *J. Am. Chem. Soc.* **2017,** *139* (7), 2589-2592.

(57) Frisch, M. J.; Trucks, G. W.; Schlegel, H. B.; Scuseria, G. E.; Robb, M. A.; Cheeseman, J. R.; Scalmani, G.; Barone, V.; Petersson, G. A.; Nakatsuji, H.; Li, X.; Caricato, M.; Marenich, A. V.; Bloino, J.; Janesko, B. G.; Gomperts, R.; Mennucci, B.; Hratchian, H. P.; Ortiz, J. V.; Izmaylov, A. F.; Sonnenberg, J. L.; Williams; Ding, F.; Lipparini, F.; Egidi, F.; Goings, J.; Peng, B.; Petrone, A.; Henderson, T.; Ranasinghe, D.; Zakrzewski, V. G.; Gao, J.; Rega, N.; Zheng, G.; Liang, W.; Hada, M.; Ehara, M.; Toyota, K.; Fukuda, R.; Hasegawa, J.; Ishida, M.; Nakajima, T.; Honda, Y.; Kitao, O.; Nakai, H.; Vreven, T.; Throssell, K.; Montgomery Jr., J. A.; Peralta, J. E.; Ogliaro, F.; Bearpark, M. J.; Heyd, J. J.; Brothers, E. N.; Kudin, K. N.; Staroverov, V. N.; Keith, T. A.; Kobayashi, R.; Normand, J.; Raghavachari, K.; Rendell, A. P.; Burant,

J. C.; Iyengar, S. S.; Tomasi, J.; Cossi, M.; Millam, J. M.; Klene, M.; Adamo, C.; Cammi, R.; Ochterski, J. W.; Martin, R. L.; Morokuma, K.; Farkas, O.; Foresman, J. B.; Fox, D. J. *Gaussian 16 Rev. C.01*, Wallingford, CT, 2016.

(58) Zhao, Y.; Truhlar, D. G., The M06 suite of density functionals for main group thermochemistry, thermochemical kinetics, noncovalent interactions, excited states, and transition elements: two new functionals and systematic testing of four M06-class functionals and 12 other functionals. *Theoretical Chemistry Accounts* **2008,** *120* (1-3), 215-241.

(59) Weigend, F.; Ahlrichs, R., Balanced basis sets of split valence, triple zeta valence and quadruple zeta valence quality for H to Rn: Design and assessment of accuracy. *Phys. Chem. Chem. Phys.* **2005,** *7* (18), 3297-3305.

(60) Haoyu, S. Y.; He, X.; Li, S. L.; Truhlar, D. G., MN15: A Kohn–Sham global-hybrid exchange–correlation density functional with broad accuracy for multi-reference and single-reference systems and noncovalent interactions. *Chem. Sci.* **2016,** *7* (8), 5032-5051.

(61) Manby, F.; Miller, T.; Bygrave, P.; Ding, F.; Dresselhaus, T.; Batista-Romero, F.; Buccheri, A.; Bungey, C.; Lee, S.; Meli, R., entos: A quantum molecular simulation package. **2019**.

(62) Grimme, S.; Bannwarth, C.; Shushkov, P., A robust and accurate tight-binding quantum chemical method for structures, vibrational frequencies, and noncovalent interactions of large molecular systems parametrized for all spd-block elements (Z= 1–86). *Journal of chemical theory and computation* **2017,** *13* (5), 1989-2009.

(63) Reed, A. E.; Weinstock, R. B.; Weinhold, F., Natural population analysis. *The Journal of Chemical Physics* **1985,** *83* (2), 735-746.

CHAPTER 4

Highly Active and Thermally Robust Nickel Enolate Catalysts for the Synthesis of Ethylene/Acrylate Copolymers

This work was published in part as:

Angew. Chem. Int. Ed. **2022**, *61*, e202206637.

Chapter 4

CONTRIBUTIONS AND ACKNOWLEDGEMENTS

Shuoyan Xiong and Theodor Agapie conceived the presented idea. S.X. performed synthesis experiments and polymer characterization and analyzed the catalysis data. Alexandria Hong performed synthesis experiments. Brad C. Bailey, Heather A. Spinney, Todd D. Senecal and Hannah Bailey performed polymerization studies and polymer characterization. S.X. drafted the manuscript that is reproduced as this chapter. A.H., B.C.B., H.A.S., T.D.S., H.B., and T.A. contributed to manuscript editing.

We are grateful to Dow for funding (T.A.) and to the Caltech SURF program for a Ronan Armaan Mack fellowship (A.H.). We thank Jerzy Klosin, Alex J. Nett for insightful discussions. We thank Heidi Clements for GPC and tBA incorporation analysis. We thank Michael K. Takase for assistance with X-ray crystallography and David VanderVelde for assistance with NMR spectroscopy. Support has been provided for the X-ray diffraction and NMR instrumentation via the Dow Next Generation Educator Fund. S.X. acknowledge Manar Shoshani for assistance in refinement of solid-state structures and Yu Chen for assistance in generating topographical steric maps.

ABSTRACT

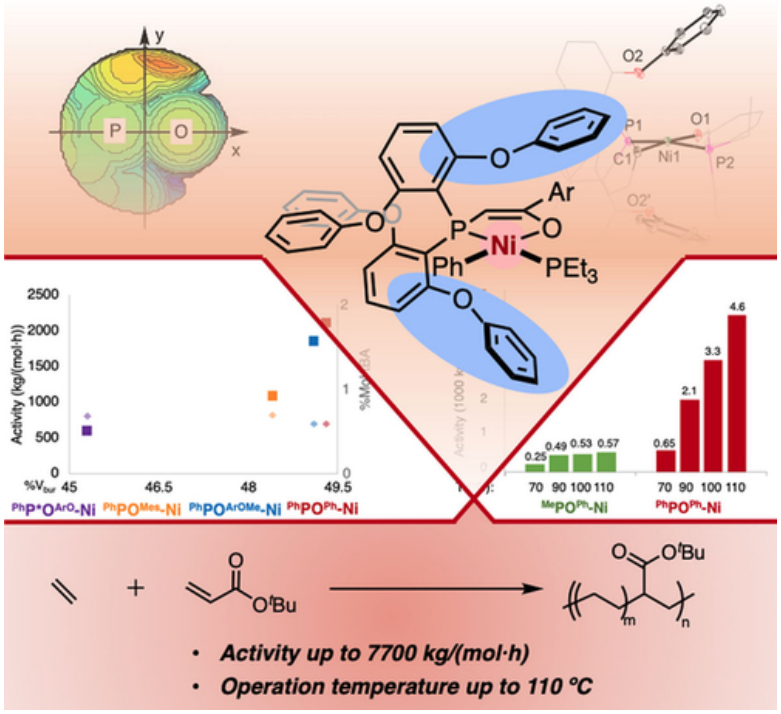

The insertion copolymerization of polar olefins and ethylene remains a significant challenge in part due to catalysts' low activity and poor thermal stability. Herein we demonstrate a strategy toward addressing these obstacles through ligand design. Neutral nickel phosphine enolate catalysts with large phosphine substituents reaching the axial positions of Ni achieve activity of up to $7.7*10^3$ kg/(mol*h) (efficiency > $35*10^3$ g copolymer/g Ni) at 110 °C, notable for ethylene/acrylate copolymerization. NMR analysis of resulting copolymers reveals highly linear microstructures with main-chain ester functionality. Structure-performance studies indicate a strong correlation between axial steric hindrance and catalyst performance.

Chapter 4

GENERAL INTRODUCTION

Polyolefins account for over half of global plastic production.[1-2] Incorporation of polar functionalities via coordination copolymerization can provide value-added polyolefins with precisely controlled physical and mechanical properties and potential degradability.[3-7] Catalysts based on Pd and Ni are attractive candidates due to their lower oxophilicity and decreased inhibition by heteroatoms compared to early transition metals. Common bidentate ligands for Pd and Ni catalysts are based on imine, phosphine, phosphine oxide, phenoxide, and sulfonate donors (Figure 4.1a). [8-24] While being able to produce copolymers with a variety of functionalities and polymer topologies, their low activity hinders industrial applications.[25] Ni catalysts are of special interest given potential economic and environmental advantages.[9, 20, 26] However, major issues remain in Ni-catalyzed copolymerization with polar monomers, such as low activity and poor performance at elevated temperatures applied in industry (e.g. >100 ºC).[20, 27-30] In general, these catalysts are screened at temperatures ≤70 ºC and thermally robust examples typically require elaborate ligand frameworks.[31-35] Additionally, most nickel catalysts cannot copolymerize ethylene with monomers having polar groups directly attached to the vinyl [35-37] except a few recent examples.[6, 11, 16, 29, 38-40]

To address these obstacles, a variety of catalyst design strategies, including steric and electronic tuning and introduction of weak coordination sites or secondary Lewis acidic metal centers, have been applied to modify ligand systems known for polar

functional polymer synthesis.[41-47] Separately, new ligand platforms have been introduced for applications in copolymerization with polar monomers.[10, 48-51]

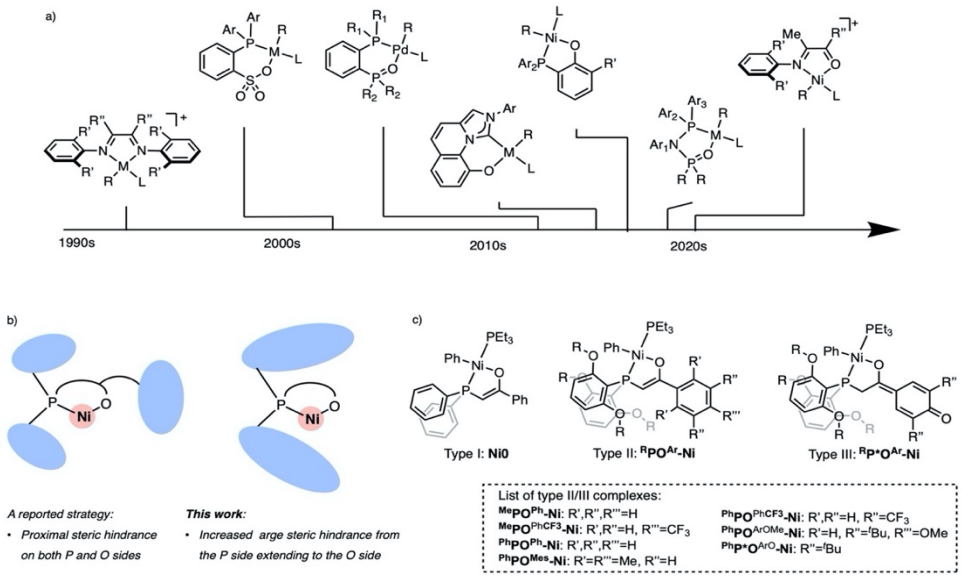

Figure 4.1. a) Representative Pd and Ni catalysts supported by bidentate ligands for copolymerization of ethylene and polar monomers; b) Rationale of catalyst design in this work; c) Lists of catalysts studied in this work.

Nickel phosphine enolate catalysts are notable for their high activity and thermal stability in producing α-olefins (Shell-Higher-Olefin-Process).[20, 52] In general, these catalysts are not able to produce high Mw polymers or to incorporate polar comonomers. Prior studies toward improving their activity and broaden the scope of applications resulted in modified ligand structures, some of which show promise for polyethylene production.[53-58] A variant with a pendant sulfonate moiety supports Ni-Na multimetallic catalysts that produce polyethylene.[59-60] These Ni-Na catalysts can also copolymerize ethylene and polar monomers in which the vinyl and the functional group are separated by ≥2 methylene units. Despite these progresses, the nickel enolate systems only show moderate activity for polyethylene production and have not been

reported to incorporate vinyl polar monomers.

In terms of catalyst design based on asymmetric ligands, a potential strategy is to introduce steric hindrance from the direction of both donors (Figure 4.1b).[38, 61-62] With the enolate group locating the substituent away from the metal center, we targeted increased steric bulk from only the phosphine side (Figure 4.1b). Through combined quantitative steric analysis and polymerization studies, we confirmed that the introduction of steric bulk covering the axial positions of Ni can convert this type of olefin oligomerization catalyst into highly active, thermally stable polymerization catalysts (Figure 4.1c). Specifically, the observed activity in ethylene/tBA copolymerization reaches $7.7*10^3$ kg/(mol*h) (efficiency > 35000 g copolymer/g Ni) at 110 °C. The effects of substituents on the phosphine and enolate side on tBA incorporation, activity, branching and chain termination are reported.

RESULTS AND DISCUSSION

Design and Synthesis of Complexes

To convert the SHOP-type ethylene oligomerization catalyst to high-performance polymerization catalysts, efficient suppression of β-H elimination is essential.[63-66] Based on our previous studies of the impact of proximal steric hindrance on the copolymerization of ethylene and polar monomers,[38, 67] we decided to introduce four ether groups ortho to the phosphine to ensure efficient axial shielding and inhibition of β-H elimination (Figure 4.1b-c). Previous synthetic methods involve a β-keto

phosphorus(V) ylide intermediate, which did not provide a reliable route for installing bulky phosphine moieties (Figure 4.2a).[59] Further, this method requires one of the aryl substituents on the phosphorus(V) transferring to nickel,[58] which would introduce an undesired variation in structure-performance studies if substituents on the phosphine vary. Bulky substituents on phosphine are required for the targeted axial shielding. We thus employed an alternate metalation route involving salt metathesis between a nickel halide precursor and the lithium enolate of the corresponding β-keto phosphine (Figure 4.2b).[68-71] Characterization of **^{Me}PO^{Ph}-Ni** by single crystal X-ray diffraction (scXRD) reveals a square planar geometry with the two phosphines trans to each other, and short metal-ether oxygen distances (Ni1-O2 ~3 Å, Figure 3a-b). Notably, the methoxy group point toward the axial positions of nickel but do not reach them.

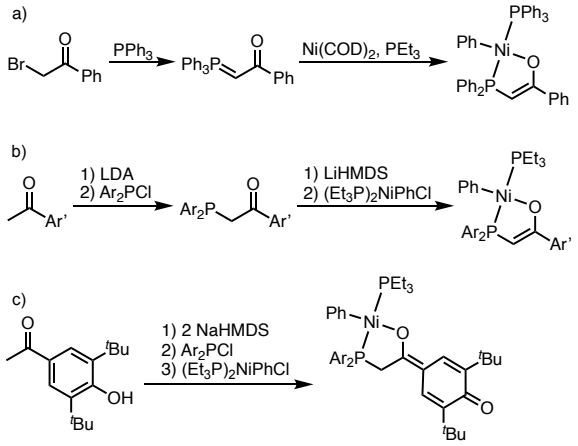

Figure 4.2. Preparation of type I (a), Type II (b) and type III (c) nickel phosphine enolate complexes.

Based on this structure, we anticipated that larger substituents ortho to the phosphine may extend the steric shielding to the axial positions. Bisphenoxyphenyl was selected as phosphine substituent, and the corresponding phosphorus chloride

was synthesized in a one-pot, three-step procedure. Next, proligand ^{Ph}**PC(H)CO**^{Ph} and complex ^{Ph}**PO**^{Ph}**-Ni** were synthesized similarly to their methoxy analogues (Figure 4.2b). The solid-state structure of ^{Ph}**PO**^{Ph}**-Ni** shows that the phenoxy substituents provide steric shielding extending toward the enolate side (Figure 4.3a). The axial positions of the nickel center are covered from both the top and bottom directions, leading to a sandwich-like geometry. Three additional nickel phosphine enolate complexes (^{Ph}**PO**^{PhCF3}**-Ni**, ^{Ph}**PO**^{Mes}**-Ni**, ^{Ph}**PO**^{ArOMe}**-Ni**) with large bisphenoxyphenyl phosphine substituents were prepared from substituted acetophenones with the goal of tuning the ligand electronics as well as sterics on the enolate side. To study the effect of ligand backbone, a different type of phosphine enolate complex, ^{Ph}**P*O**^{ArO}**-Ni**, was prepared via a modified procedure (Figure 4.2c). Instead of the vinyl linkage, it features a methylene unit between the P and O donors.

The majority of the prepared metal complexes were characterized by scXRD. This family of nickel phosphine enolate complexes allows quantitative structural comparison across a range of steric profiles (Figure 4.3b-c). Analysis by Cavallo's SambVca 2.1 program[72-75] provided topographical steric maps and percent buried volume data (%V_{bur}) related to ligands' space filling properties (Figure 4.3c). Inspection of the topographical maps clearly shows that **Ni0** is open along the axial coordination sites. In agreement, %V_{bur} for **Ni0** is the lowest of all Ni complexes characterized structurally. Consistent with the constrained axial space (Figure 4.3a), %V_{bur} for ^{Ph}**PO**^{Ph}**-Ni** is near 49.3, significantly larger than %V_{bur} for **Ni0** (38.7) and ^{Me}**PO**^{Ph}**-Ni** (46.3). Though the mesityl group is bulkier than the phenyl, ^{Ph}**PO**^{Mes}**-Ni** features a

slightly smaller %Vbur than ^{Ph}**PO**^{Ph}**-Ni** (48.4% vs 49.1%) and features less occupied axial space especially at the bottom, potentially resulting from the repulsion between the mesityl and the ether groups. While ^{Ph}**P*O**^{ArO}**-Ni** features the shortest Ni1-O2 distance (2.905(2) Å) among all complexes, the phenoxy groups only partially fill axial space on one side of the Ni center likely due to the higher flexibility of the backbone.

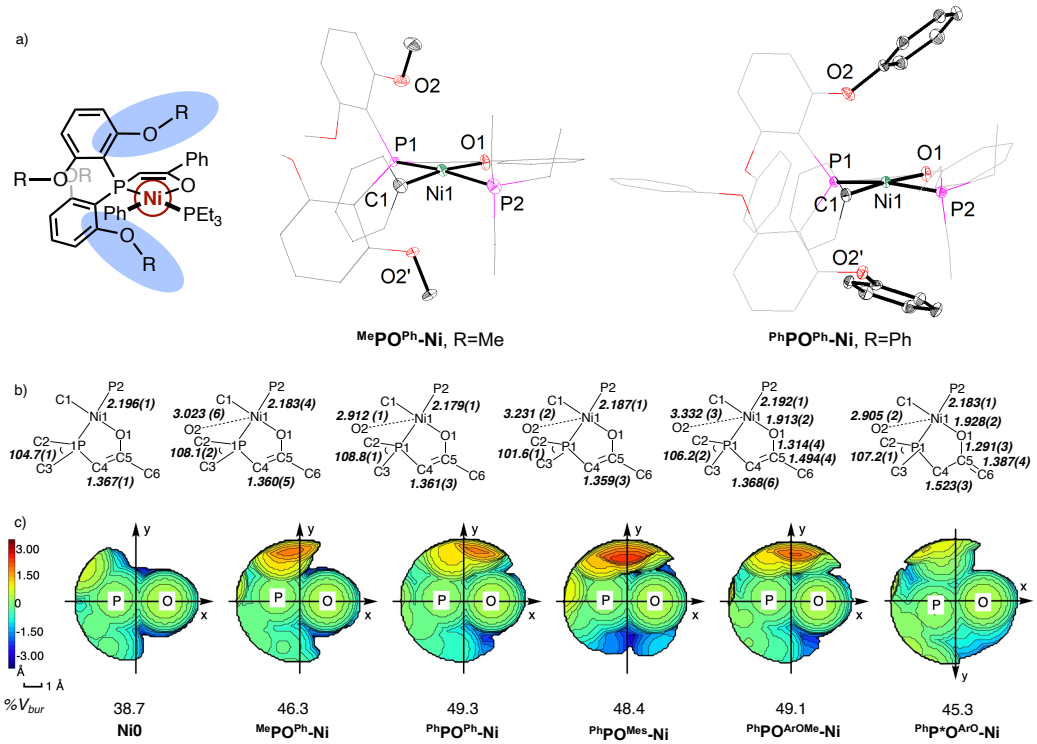

Figure 4.3. a) Depiction of the sandwiched-like geometry of the Ni center and solid-state structures of ^{Me}**PO**^{Ph}**-Ni** and ^{Ph}**PO**^{Ph}**-Ni**. Only ellipsoids of atoms that coordinate to nickel or locate axial to nickel are shown (50% probability). Hydrogen atoms are excluded for clarity and other atoms are shown in wire-frame. b) Selected bond angles (°), distances (Å) and c) topographical steric maps with %V_{bur} of **Ni0**, ^{Me}**PO**^{Ph}**-Ni**, ^{Ph}**PO**^{Ph}**-Ni**, ^{Ph}**PO**^{Mes}**-Ni**, ^{Ph}**PO**^{ArOMe}**-Ni**, ^{Ph}**P*O**^{ArO}**-Ni**. For topographical maps and %V_{bur}, the Ni atom defines the origin of xyz coordinate system. Only the P,O-ligand included in calculation and steric visualization. These maps are in the same orientation as shown in part a). Blue indicates occupied space in the -z direction (toward back as drawn in a), where the phosphine-enolate ligands are located, and red indicates +z direction. For ^{Ph}**P*O**^{ArO}**-Ni**, the y-axis is flipped so the larger axial shielding locates on the top. See SI section S4 for more details.

Ethylene Homopolymerization

While sandwich-like α-diimine or salicylaldiminato Pd or Ni catalysts have been studied extensively,[62, 76-81] analogous P,O type catalysts have not been reported. To evaluate this ligand design strategy, we first screened the catalysts via ethylene polymerization at 90 ºC in high throughput parallel reactors (Table 4.1). Polymerization was stopped after consumption of a set amount of ethylene to prevent buildup of polymer that may alter the solution properties and result in mass transport limitations. In a single run, 140~300 mg of polyethylene was produced. The catalysts are all highly active (~40000~113000 kg/(mol·h)) with 4 equiv. of $Ni(COD)_2$ as the phosphine scavenger (entry 1~5).[59, 82-83] Compared to **Ni0**, bulkier catalysts produce polymers with significantly higher Mw. Specifically, polyethylene produced by **^{Ph}PO^{Ph}-Ni**, which has a sandwich-like geometry, features Mw nearly 10 times higher than that by **Ni0**, indicating significant inhibition of β-H elimination and demonstrating the importance of axial steric hindrance.[32, 79] Previously, Ni-Na multimetallic catalysts supported by phosphine-enolate-sulfonate ligands generate high Mw polyethylene with high dispersity (PDI 11~25), though the ligands design elements promoting this performance are unclear.[60] Ethylene homopolymerization trials without $Ni(COD)_2$ were also conducted with **^{Me}PO^{Ph}-Ni** and **^{Ph}PO^{Ph}-Ni** (Table 4.1, entry 6~7). Although decrease of activity was observed compared to entries 2~3, it is notable that both catalysts remained highly active even in the absence of phosphine scavenger.

Table 4.1. Ethylene homopolymerization.

Entry	Cat.	$Ni(COD)_2$/Cat.	Act. [c]	M_w[d]	PDI	T_m/°C
1	**Ni0**	4	70	1.3	2.3	122
2	**$^{Me}PO^{Ph}$-Ni**	4	114	4.1	3.1	120
3	**$^{Ph}PO^{Ph}$-Ni**	4	82	11.9	3.3	124
4	**$^{Ph}PO^{Mes}$-Ni**	4	49	5.5	2.7	120
5	**$^{Ph}PO^{PhCF3}$-Ni**	4	60	9.4	2.8	124
6	**$^{Me}PO^{Ph}$-Ni**	0	48	4.5	2.3	121
7	**$^{Ph}PO^{Ph}$-Ni**	0	19	13.7	2.5	126

[a] V = 5 mL, [Catalyst] = 0.05 mM, [$Ni(COD)_2$] = 0.2 mM, ethylene pressure = 400 psi, T= 90 °C, toluene solvent; each entry represents multiple replicated runs (see SI section S5 for detailed procedure and table S4.3 for original data). [b] Mol/L. [c] Activity in 1000 kg/(mol·h). [d] kg/mol.

Ethylene/Acrylate Copolymerization Results

Encouraged by above promising results with nickel catalysts featuring bulky substituents on phosphine, we explored polar polyolefin synthesis. Ethylene/acrylate copolymers were chosen as the target due to their wide applications and the reported ester tolerance of Ni enolate catalysts.[60, 84] Overall, these catalysts are highly active (200~2100 kg/(mol*h)) at 70 and 90 ºC with $Ni(COD)_2$ as the phosphine scavenger, producing copolymers with moderate tBA incorporation (0.5~2.8%) (Table 4.2, entry 1~15). Comparing entry 1~6 with entries 7, 11, 12~15, significant higher activity was observed with these catalysts at 90 ºC than at 70 ºC, indicating good thermal stability. Compared to **$^{Me}PO^{Ph}$-Ni**, **$^{Ph}PO^{Ar}$-Ni** catalysts show significantly higher activity and produce copolymers with higher Mw and lower tBA concentration (entry 1, 7, 8 vs entry 2~5, 10~14). This effect may be related to the stronger steric shielding provided by the phenoxy groups than by the methoxy groups.

These complexes can also function as single-component catalysts (Entry 16~18, table 4.2). Comparing entry 7 vs 16, 10 vs 17 and 16 vs 18, **^{Me}PO^{Ph}-Ni** shows much lower activity (by 60%) in the absence of $Ni(COD)_2$ while **^{Ph}PO^{Ph}-Ni** and **^{Ph}P*O^{ArO}-Ni** only show ~25% difference. This scenario is likely a result of more facile dissociation and weaker coordination of PEt_3 at the more sterically hindered Ni centers in **^{Ph}PO^{Ph}-Ni** and **^{Ph}P*O^{ArO}-Ni**.

Notably, the phenoxy-substituted systems produce polyethylene and ethylene/tBA copolymers with similar Mw values, within 30% (entries 3~5, table 4.1 vs entries 10, 12, 13, table 4.2, respectively). In contrast, significantly lower Mw values are observed with previously reported catalysts. For example, the presence of acrylates (methyl acrylate, butyl acrylate and tBA) leads to ~90% decrease in Mw for polymer produced by Pd-IzQO, Ni imine ketone, and Ni phosphine phenoxide catalysts.[10, 12, 29, 85] This observation implies that chain transfer specific to acrylate insertion compared to overall chain transfer events in this enolate system is lower than in previous systems. Therefore, acrylate is not the limiting factor for Mw under copolymerization conditions.

Different from reported P,O-Ni catalysts,[11, 29, 38] incorporation ratio of tBA is nearly solely controlled by substituents on the phosphine in this enolate system and substituents on the oxygen side have minimal effects likely because the relatively remote location of these groups (Table 4.2, entries 2~4 or entries 10, 12~15).

Table 4.2. Ethylene/tBA copolymerization.

Entry	Cat.	$Ni(COD)_2$ /Cat.	[tBA] /M	T (°C)	A.[b]	M_w[c]	PDI	%Mol tBA	T_m/ °C
1	^{Me}**PO**^{Ph}**-Ni**	4	0.05	70	0.25	4.6	2.0	1.4	114
2	^{Ph}**PO**^{Ph}**-Ni**	4	0.05	70	0.68	14.5	2.3	0.6	123
3	^{Ph}**PO**^{Mes}**-Ni**	4	0.05	70	0.40	7.6	2.1	0.6	115
4	^{Ph}**PO**^{PhCF3}**-Ni**	4	0.05	70	0.62	19.3	3.2	0.4	124
5	^{Ph}**PO**^{ArOMe}**-Ni**	4	0.05	70	0.59	18.6	2.4	0.6	123
6[d]	^{Ph}**P*O**^{ArO}**-Ni**	4	0.05	70	0.20	19.6	2.6	0.7	123
7	^{Me}**PO**^{Ph}**-Ni**	4	0.05	90	0.49	3.5	1.9	1.6	113
8[d]	^{Me}**PO**^{Ph}**-Ni**	4	0.1	90	0.19	2.6	2.1	2.8	77
9	^{Me}**PO**^{PhCF3}**-Ni**	4	0.05	90	0.77	6.2	3.2	1.4	114
10	^{Ph}**PO**^{Ph}**-Ni**	4	0.05	90	2.1	10.9	2.5	0.6	122
11	^{Ph}**PO**^{Ph}**-Ni**	4	0.1	90	1.16	8.9	2.6	1.2	118
12	^{Ph}**PO**^{Mes}**-Ni**	4	0.05	90	1.09	7.0	2.1	0.7	116
13	^{Ph}**PO**^{PhCF3}**-Ni**	4	0.05	90	1.34	10.1	2.2	0.5	122
14	^{Ph}**PO**^{ArOMe}**-Ni**	4	0.05	90	1.85	15.2	2.3	0.6	123
15	^{Ph}**P*O**^{ArO}**-Ni**	4	0.05	90	0.59	15.1	2.4	0.7	123
16	^{Me}**PO**^{Ph}**-Ni**	0	0.05	90	0.21	2.9	2.1	2.0	113
17	^{Ph}**PO**^{Ph}**-Ni**	0	0.05	90	1.59	10.6	2.5	0.6	122
18	^{Ph}**P*O**^{ArO}**-Ni**	0	0.05	90	0.45	11.3	2.5	0.6	122

[a] Unless specified, V = 5 mL, [Catalyst] = 0.25 μmol, ethylene pressure = 400 psi, toluene solvent; each entry represents multiple replicated runs. (see SI for detailed procedure and table S4.4 for original data). [b] Activity in 1000 kg/(mol·h). [c] kg/mol. [d] polymerization was stopped at 1h.

Steric Influence of Enolate Ligands on Copolymerization Activity

The series of catalysts reported here allows for studies of the relationship between structural parameters and catalyst performance. In these comparisons, it is important to exclude the variation in tBA incorporation levels. Previous mechanistic studies of

another P,O-chelated neutral nickel catalyst have identified ethylene insertion after acrylate is the rate-limiting step for overall copolymerization,[38] therefore higher levels of tBA incorporation lead to lower catalyst activity. In this regard, **^{Ph}PO^{Ph}-Ni**, **^{Ph}PO^{Mes}-Ni**, **^{Ph}PO^{ArOMe}-Ni**, and **^{Ph}P*O^{ArO}-Ni** were selected for comparison because they produce copolymers with similar tBA limiting the effect of that aspect on activity.

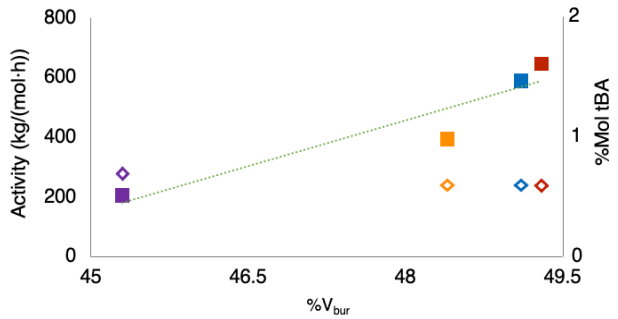

Figure 4.4. Correlation between activity in ethylene/tBA copolymerization and %V$_{bur}$ (in square) at 70 °C (Purple: **^{Ph}P*O^{ArO}-Ni**, orange: **^{Ph}PO^{Mes}-Ni**, blue: **^{Ph}PO^{ArOMe}-Ni**, red: **^{Ph}PO^{Ph}-Ni**. Corresponding %Mol tBA shown in diamonds). Activity data extracted from table 4.2.

Most notably, correlation of %Vbur and the catalytic activity of **^{Ph}PO^{Ph}-Ni**, **^{Ph}PO^{Mes}-Ni**, **^{Ph}PO^{ArOMe}-Ni**, and **^{Ph}P*O^{ArO}-Ni** leads to a strong positive relationship (Figure 4.4). For example, **^{Ph}P*O^{ArO}-Ni**, having a methylene unit in the ligand backbone, shows a more open steric environment comparing to its type II analogue, **^{Ph}PO^{ArOMe}-Ni**. Actually, its %V$_{bur}$ value (45.3) is close to the one of **^{Me}PO^{Ph}-Ni** (46.3). Indeed, the activity of **^{Ph}P*O^{ArO}-Ni** (200 kg/(mol·h) at 70 °C) is much less than that of **^{Ph}PO^{ArOMe}-Ni** (590 kg/(mol·h) at 70 °C) but close to that of **^{Me}PO^{Ph}-Ni** (250 kg/(mol·h at 70 °C). Notably, this relationship is not observed in ethylene homopolymerization (Figure S4.7). Overall, the above results demonstrate the important role of axial ether groups and the accuracy of %V$_{bur}$ as an index for examining axial steric hindrance and potential

predictor of catalyst performance in polar polyolefin synthesis. Previous examples of correlations between steric profile and polymerization catalyst performance includes impact on polyethylene Mw in Pd catalyzed polymerization.[63]

Microstructural Analysis of Copolymers

In addition to activity and copolymer Mw, axial shielding may also affect copolymer microstructure since the same elementary steps, such as β-H elimination and olefin (re)insertion, are implicated. Microstructure analysis was performed using ^{1}H and ^{13}C{^{1}H} NMR spectroscopy.[11, 38] Copolymers produced by **^{Me}PO^{Ph}-Ni**, **^{Me}PO^{PhCF3}-Ni**, **^{Ph}PO^{Ph}-Ni**, **^{Ph}PO^{PhCF3}-Ni**, and **^{Ph}PO^{Mes}-Ni** under otherwise identical conditions were examined (Table 4.3).

Table 4.3. Microstructural analysis of ethylene/tBA copolymers[a].

	A	**B**	**C**	**D**	**E**
%I-tBA[b]	61%	48%	59%	52%	71%
N(Methyl)/1000C	2.7	1.6	1.7	1.1	4.0
N(2-Propenyl) /1000C	2.1	1.9	0.6	1.0	1.8
N(Methyl) /N(2-Propenyl)	1.3	0.84	2.8	1.1	2.2

[a] **A~F**: Ethylene/tBA copolymers produced in entry 7, 9, 10, 13, 12 of table 4.2, respectively. (Catalyst: **^{Me}PO^{Ph}-Ni** (**A**), **^{Me}PO^{PhCF3}-Ni** (**B**), **^{Ph}PO^{Ph}-Ni** (**C**), **^{Ph}PO^{PhCF3}-Ni** (**D**), **^{Ph}PO^{Mes}-Ni** (**E**). [b] Percentage of internal tBA units vs all tBA units. see SI for details.

In all samples, significant amount of internal tBA units is present, confirming that these nickel phosphine enolate catalysts are able to incorporate acrylate into copolymer main-chain. The percentage of internal tBA units (%I-tBA) depends on catalyst identity. For the same phosphine substituents, %I-tBA varies by 10 to 20% from **^{Ph}PO^{Mes}-Ni** (71%) to **^{Ph}PO^{PhCF3}-Ni** (52%) or from **^{Me}PO^{Ph}-Ni** (61%) to **^{Me}PO^{PhCF3}-Ni** (48%), due to changes on the enolate substituent. Since %I-tBA reflects the selectivity between

ethylene insertion and β-H elimination from the $NiCHR_2$ species generated after a tBA insertion, the above results imply that the substituents on the enolate side can impact these elementary reaction steps. Unlike copolymer Mw or activity, **^{Me}PO^{Ph}-Ni** and **^{Ph}PO^{Ph}-Ni** produce copolymers feature similar %I-tBA values suggesting that the phosphine and enolate substituents can have decoupled effects.

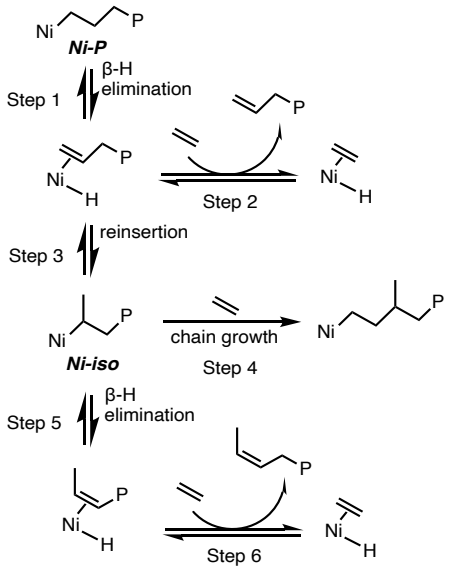

Figure 4.5. Pathways of the formation of the methyl branch, terminal vinyl, and 2-propenyl.

Copolymers **A**~**E** are all highly linear, similar to copolymers produced by other types of asymmetric Pd and Ni complexes.[11, 18, 20, 84] Notably, all copolymers feature a significant amount of 2-propenyl end group. Proposed mechanisms for the formation of methyl branch and vinyl and propenyl chain ends (Figure 4.5) show that ***Ni-iso*** is at the branching point between the formation of a methyl branch (step 4) and a 2-propenyl end group (steps 5 and 6).[86] The ratio of N(Methyl)/N(2-Propenyl) represents the selectivity between chain propagation and β-H elimination after ***Ni-iso***. Substituents on both P and O sides affect this selectivity (Table 4.3): 1) CF3 substitution leads to higher

preference for β-H elimination (e.g. **D** vs **C**); 2) bulkier phosphine substituents promote chain propagation (e.g. comparing phenoxy to methoxy: **C** vs **A**). The above microstructure analysis highlights that the substituents on the enolate side can alter the selectivity between ethylene enchainment and β-H elimination processes after formation of $NiCHR_2$ species, though this is a relatively subtle effect compared to the large impact of the phosphine substitution on activity and Mw.

High-Temperature Ethylene/Acrylate Copolymerization by ^{Ph}PO^{Ph}-Ni

Significant increase in activity was observed with all catalysts in copolymerization at 90 vs 70 ºC, suggesting high thermal stability. With **^{Me}PO^{Ph}-Ni** and **^{Ph}PO^{Ph}-Ni** as model catalysts, further investigations were performed of their temperature dependent performance. While increasing the temperature from 70 ºC to 90 ºC leads to doubled activity for **^{Me}PO^{Ph}-Ni** and tripled for **^{Ph}PO^{Ph}-Ni** (Figure 4.6a), <10% increase was observed with **^{Me}PO^{Ph}-Ni** but ~2.2-fold for **^{Ph}PO^{Ph}-Ni** from 90 ºC to 110 ºC. To determine the origin of this difference, the ethylene uptake over time was monitored as an *in-situ* measure of the rates of chain propagation. Both catalysts are highly active within the time range of catalysis at 90 ºC (Figure 4.6b), however, a significant slowdown of ethylene consumption over time was observed with **^{Me}PO^{Ph}-Ni** at 110 ºC, indicating severe catalyst deactivation. In contrast, **^{Ph}PO^{Ph}-Ni** remains highly active at 110 ºC. We suspect this remarkable thermal stability of **^{Ph}PO^{Ph}-Ni** results from the large axial shielding provided by axial phenoxy groups.

Encouraged by its high thermal stability, further ethylene/tBA copolymerizations with **^{Ph}PO^{Ph}-Ni** were conducted under at 110 °C (Table 4.4). Similar activities were observed in copolymerization with and without $Ni(COD)_2$ (entry 3 vs entry 4), indicating that the PEt_3 dissociation from **^{Ph}PO^{Ph}-Ni** at 110 °C is facile under copolymerization conditions. The highest activity reaches $7.7*10^3$ kg/(mol·h) (Entry 3), a notable level in ethylene/acrylate copolymerization (see SI and Figure S4.20 for comparisons), which is comparable to activities of many nickel catalysts in ethylene homopolymerization.[45]

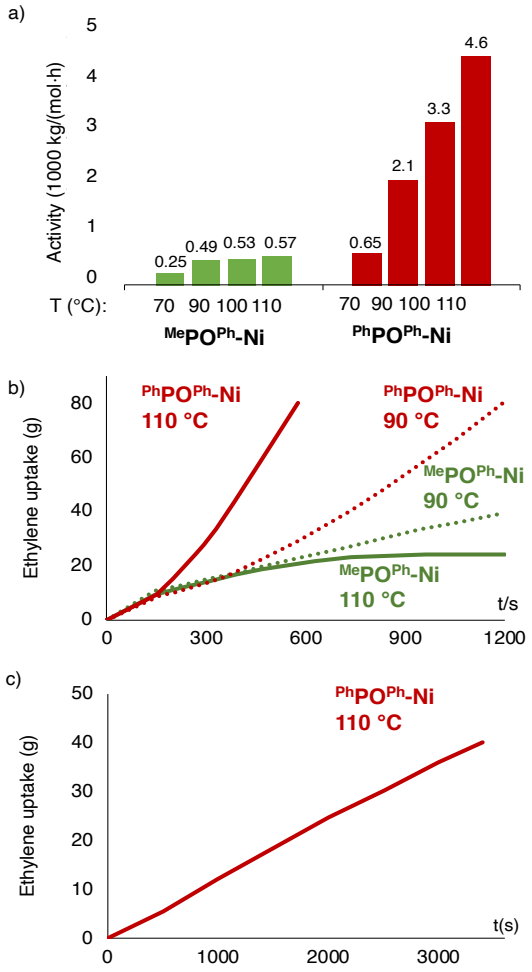

Figure 4.6. a) Temperature dependence of catalytic activity for **^{Me}PO^{Ph}-Ni** and **^{Ph}PO^{Ph}-Ni** (original runs: 70 °C & 90 °C: table 4.2, entries 1, 2, 7, 10; 100 °C & 110 °C: table S4.6 and table

4, entry 1). b) Ethylene uptake curves of ethylene/tBA copolymerization by **^{Me}PO^{Ph}-Ni** and **^{Ph}PO^{Ph}-Ni** at 90 °C and 110 °C. See Table S4.6 for other analytic data for these polymerization runs. c) Ethylene uptake curves of ethylene/tBA copolymerization by **^{Ph}PO^{Ph}-Ni** in a batch reactor at 110 °C (Table 4.4, entry 7). See SI for detailed procedures.

Table 4.4. High-temperature ethylene/tBA copolymerization.[a]

Entry	Cat.	$Ni(COD)_2$ /Cat.	[tBA] /M	T (°C)	A.[b]	M_w[c]	PDI	%Mol tBA	T_m/ °C
1	**^{Ph}PO^{Ph}-Ni**	0.05	4	0.05	4.6	7.8	2.5	0.6	121
2	**^{Ph}PO^{Ph}-Ni**	0.05	4	0.10	3.2	6.5	2.4	1.1	118
3	**^{Ph}PO^{Ph}-Ni**	0.025	4	0.025	7.6	9.3	2.4	0.4	124
4	**^{Ph}PO^{Ph}-Ni**	0.025	0	0.025	7.7	9.5	2.5	0.4	123
5	**^{Ph}PO^{Ph}-Ni**	0.025	0	0.10	2.9	7.8	2.6	1.4	120
6[d]	**^{Ph}PO^{Ph}-Ni**	0.043	0	0.054	5.0	10.3	2.8	0.3	125
7[d]	**^{Ph}PO^{Ph}-Ni**	0.043	0	0.11	2.3	11.1	2.6	0.5	125

[a] V = 5 mL, ethylene pressure = 400 psi, T= 110 °C, toluene solvent; polymerization was stopped after consuming a set amount of ethylene; each entry represents multiple replicated runs (see SI section S5 for detailed procedure and table S6.6 for original data). [b] Activity in 1000 kg/(mol·h). [c] kg/mol.[d] Copolymerization in a batch reactor. Condition: V = 550 mL, 23.7 μmol **^{Ph}PO^{Ph}-Ni** ([Ni]=0.043 mM), ethylene pressure = 430 psi, T= 110 °C, t = 26 min (entry 6), or 56 min (entry 7). See SI section S5 for detailed procedure.

To further investigate the thermal stability and productivity limits of the **^{Ph}PO^{Ph}-Ni**, we next conducted ethylene/tBA copolymerization in a batch reactor under more practical conditions (Table 4.4, entry 6~7). Comparing entry 1 vs entry 6, or entry 2 vs entry 7, similar activities were observed in copolymerization under different scales but otherwise similar conditions. Ethylene uptake curve revealed that catalyst **^{Ph}PO^{Ph}-Ni** remains highly active for at least 56 min in batch reactors (Figure 4.6c). Consequently, the catalyst efficiency reaches >35000 g copolymer/g Ni. Previously, a bulky Ni-diimine catalyst was reported to be moderately stable in ethylene homopolymerization at 100 ºC for 20 min.[31] Herein, we demonstrate a significant improvement of thermal stability of

Ni catalysts in the more challenging ethylene/acrylate copolymerization at a higher temperature.

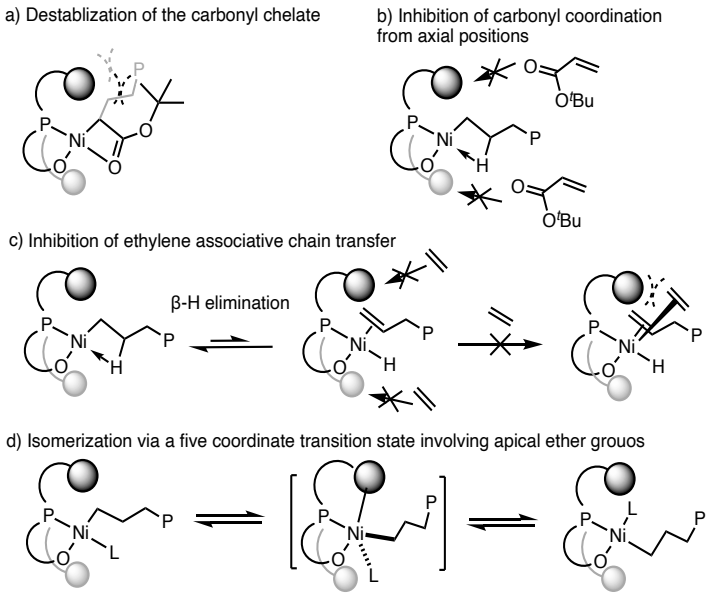

Figure 4.7. Depiction of roles of the apical steric hindrance in copolymerization.

Roles of Axial Shielding in Catalysis

Overall, the above results highlight the importance of large axial shielding for catalyst activity, thermal stability, and polymer Mw in this system. Specifically, an efficient strategy is to introduce four phenoxy groups ortho to P in the phosphine-enolate system that constitutes the sandwich-like geometry, as demonstrated by ^{Ph}**PO**^{Ph}**-Ni** and ^{Ph}**PO**^{ArOMe}**-Ni**. Considering the elementary steps involved in copolymerization, the desired chain propagation may be impeded by β-H elimination and formation of a carbonyl chelate complex.[87] The former leads to molecular weight suppression, while the latter increases the barrier of subsequent insertion and thus decreases the activity.[88] From this chelate complex, further catalyst deactivation may occur via a variety of

pathways, generating Ni(0), Ni(I) complexes or ligand disproportionation byproducts.[28, 89-92] Based on topographical steric maps of these semi-sandwich complexes, the phenoxy groups act as axial shielding on both the P and the O side in one direction, which may: 1) destabilize the carbonyl chelate intermediate, 2) prevent the axial coordination of the carbonyl group in tBA to nickel,[41, 93] 3) inhibit associative ethylene coordination that leads to chain transfer, [94-96] and 4) act as the fifth ligand in cis-trans isomerization via Berry-pseudorotation, a step required for lowest-energy propagation pathway (Figure 4.7).[38, 64]

CONCLUSION

In summary, we reported a series of Ni complexes derived from phosphine enolate SHOP catalysts. Through rational design of axial steric hindrance, the donor set corresponding to prototypical ethylene oligomerization catalysts was able to support highly active polymerization catalysts that are suitable for the synthesis of ester-functionalized polyethylene. The best catalyst, **^{Ph}PO^{Ph}-Ni**, shows activity of up to ~$7.7*10^3$ kg/(mol·h) (efficiency over 35000 g copolymer/g Ni) at 110 ºC, a record level for activity and thermal stability in ethylene/acrylate copolymerization. The phenoxy group ortho to phosphine leads to a sandwich-like geometry and provides axial shielding that is crucial for these catalysts' activity and high temperature performance. The versatile supporting ligands also allow control of copolymer microstructure via electronic and/or steric tuning of ligand substituents. The relatively

simple synthetic route to this ligand system is expected to allow further modulation of catalyst performance for the copolymerization of ethylene and polar monomers.

Chapter 4

EXPERIMENTAL SECTION

General Considerations

All air- and water-sensitive compounds were manipulated under N_2 or Ar using standard Schlenk or glovebox techniques. The solvents for air- and moisture-sensitive reactions were dried over sodium benzophenone/ketyl, calcium hydride, or by the method of Grubbs.[28] Deuterated solvents were purchased from Cambridge Isotopes Lab, Inc.; C_6D_6, was dried over a purple suspension with Na/benzophenone ketyl and vacuum transferred. t-Butyl acrylate was dried over 4 Å sieves for greater than 72h. 2,4,6-Trimethylacetophenone was dried over 4 Å sieves for greater than 72h, vacuum transferred, and passed over an activated alumina plug. Acetophenone, dimethoxybenzene, and triethylphosphine were dried over calcium hydride and vacuum-transferred or distilled prior to use. 4-Trifluoromethylacetophenone. 3', 5'-di-tert-butyl-4'-hydroxyacetophenone and 1,3-diphenoxybenzene were purified by sublimation. 2.5 M ^{n}BuLi in hexanes, lithium diisopropylamide (LDA), lithium bis(trimethylsilyl)amide (LiHMDS) were purchased from Sigma-Aldrich and used without further purification. Bis(dimethoxyphenyl)phosphine chloride,[97] $(Et_3P)_2NiPhCl$,[13] and complex **Ni0**[98] were synthesized according to literature procedures. All ^{1}H, ^{13}C, and ^{31}P spectra of organic and organometallic compounds were recorded on Varian Mercury 300, Varian INOVA-400, or Bruker Cryoprobe 400 spectrometers. ^{1}H and ^{13}C chemical shifts are reported relative to residual solvent resonances.

Synthesis of Ligands and Transition Metal Complexes

Bis(diphenoxyphenyl) phosphine chloride: At -78 °C, ^{n}BuLi (11 mL, 2.5 M in hexane, 26.5 mmol, 1.1 equiv) was added dropwise to a solution of 1,3-diphenoxybenzene (6.55 g, 25 mmol, 1.0 equiv) in tetrahydrofuran (100 mL) under nitrogen. The reaction mixture was warmed up to 0 °C, stirred

for 5 h, and cooled to -78 °C. To this mixture was added Cl_2PNMe_2 (1.75 g, 12 mmol, 0.48 equiv.) dropwise. The reaction mixture was then warmed up to room temperature and stirred for 2 h. Ethereal HCl (2 M, 12.5 mL, 25 mmol, 2.0 equiv) was added at -78 °C and the mixtures were then warmed up and stirred for 20 min. Volatiles are fully removed and the residue was redissolved in toluene. The solids were filtered off over Celite and volatiles were removed once again. The resulting solids were washed by hexane (40 mL) and ether (20 mL), yielding the bis(diphenoxyphenyl) phosphine chloride as white or pale pink solids (4.44 g, 7.5 mmol, 63%).

Since this chlorophosphine is not stable over time in solution only ^{1}H NMR and ^{31}P{^{1}H} NMR data is given.

^{1}H NMR (400 MHz, C_6D_6) δ 6.97 (dd, J = 8.7, 7.2 Hz, 8H), 6.87 (d, J = 8.7 Hz, 8H), 6.81 (d, J = 7.2 Hz, 4H), 6.70 (t, J = 8.2 Hz, 2H), 6.39 (dd, J = 8.2, 2.7 Hz, 4H). ^{31}P{^{1}H} NMR (121 MHz, C_6D_6): δ 55.60 (s).

3', 5'-Di-tert-butyl-4'-methoxyacetophenone were synthesized according to literature.[99]

^{1}H NMR (400 MHz, $CDCl_3$) δ 7.89 (s, 2H, ArH), 3.72 (s, 3H, -OCH_3), 2.58 (s, 3H, -C(O)CH_3), 1.46 (s, 18H, -C(CH_3)$_3$). ^{13}C{^{1}H} NMR (101 MHz, $CDCl_3$): δ 198.10 (s), 164.26 (s), 144.27 (s), 132.04 (s), 127.28 (s), 64.57 (s), 36.05 (s), 32.05 (s), 26.64 (s).*General synthesis route for ligands* ***^{R}PO^{Ar}H*** *and metal complexes* ***^{R}PO^{Ar}-Ni***

Ligands ***^{R}PO^{Ar}H:*** In the glove box, to a precooled (-78 °C) solution of the (substituted) acetophenone (0.5 mmol) in diethyl ether (5 mL) was added a precooled (-78 °C) solution (2 mL) of LDA (M equiv., see below for actual numbers) in diethyl ether. The mixture was stirred for 30 min at (-78 °C), then slowly warmed up to room temperature and stirred for another 45 min at room temperature. All volatiles were removed from solution which was triturated with pentane (2 x 5 mL). The resulting residue was dissolved in THF (4 mL) and cooled to -78 °C.

To this solution was added a THF solution (3 mL) of corresponding diaryl phosphine chloride (N equiv., see below for actual numbers). The mixture was then slowly warmed up to room temperature and stirred for additional 8 h. Next, volatiles were removed under vacuum, and the residue was dissolved in benzene and filtered through Celite. The volatile materials were removed once more under vacuum. The residue was triturated with pentane (2 x 5 mL) and or washed with hexanes (5 mL) and ether (5 mL) to yield ligands (**^{R}PO^{Ar}H**) as white or pale yellow solids.

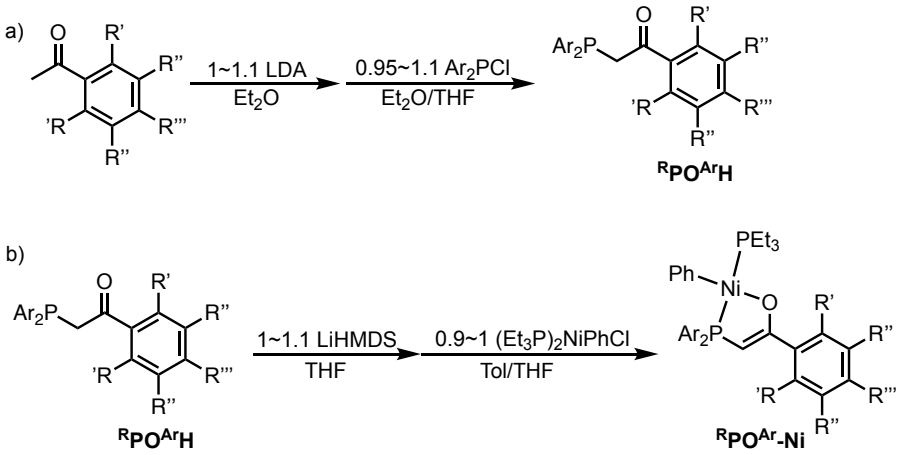

Metal complexes ***^{R}PO^{Ar}-Ni:*** In the glove box, to a precooled (-78 °C) solution of the ligand **^{R}PO^{Ar}H** (0.2 mmol) in tetrahydrofuran (THF) (2 mL) was added a precooled (-78 °C) solution (2 mL) of LiHMDS (33.4 mg, 0.2 mmol) in THF. The mixture was then slowly warmed up to room temperature and stirred for 8 h at room temperature. All volatiles were removed from solution which was triturated with pentane (2 x 5 mL). The resulting residue was dissolved in toluene (4 mL) and cooled to -78 °C. To this solution was added a toluene solution (2 mL) of $(PEt_3)_2NiPhCl$ (81.4 mg, 0.2 mmol). The mixture was then slowly warmed up to room temperature and stirred for additional 24 h. Next, the mixture was filtered through Celite and volatiles were removed under vacuum. The residue was washed with pentane (5~10 mL),

hexanes (1 mL), and diethyl ether (2 mL), yielding metal complexes (**^{R}PO^{Ar}-Ni**) as yellow or orange solids.

^{Me}PO^{Ph}H: R'=R"=R'"=H. M= 1.05, N= 0.95. Yield: 65 %. ^{1}H NMR (400 MHz, C_6D_6) δ 8.09 (ddt, *J* = 6.7, 3.1, 1.4 Hz, 2H, ArH), 7.16 – 6.99 (m, 5H, ArH), 6.26 (ddd, *J* = 8.3, 2.5, 1.4 Hz, 4H, ArH), 4.37 (dd, *J* = 2.3, 1.3 Hz, 2H, -CH_2-), 3.21 (s, 12H, -CH_3). ^{13}C{^{1}H} NMR (101 MHz, C_6D_6): δ 197.65 (d, *J* = 9.9 Hz), 162.83 (d, *J* = 8.7 Hz), 138.62 (s), 131.90 (s), 129.63 (s), 129.07 (d, J = 3.4 Hz), 116.60 (s), 116.29 (s), 104.68 (s), 67.83 (s), 65.92 (s), 55.50 (s), 38.46 (d, *J* = 19.7 Hz). ^{31}P{^{1}H} NMR (121 MHz, C_6D_6): δ -47.15 (s).

^{Me}PO^{PhCF3}H: R'=R"=H, R'"=CF_3. M= 1.05, N= 0.95. Yield: 17%. ^{1}H NMR (400 MHz, C_6D_6) δ 7.91 – 7.84 (m, 2H, ArH), 7.25 (d, *J* = 8.1 Hz, 2H, ArH), 7.02 (tt, *J* = 8.3, 0.7 Hz, 2H, ArH), 6.23 (dd, *J* = 8.3, 2.6 Hz, 4H, ArH), 4.29 (d, *J* = 2.6 Hz, 1H, -CH2-), 3.18 (s, 12H, -CH3). ^{13}C{^{1}H} NMR (101 MHz, C_6D_6): δ 196.96 (d, J = 10.1 Hz), 162.68 (d, J = 8.7 Hz), 141.03 (s), 133.09 (q, J = 32.2 Hz), 129.89 (s), 129.33 (d, J = 4.0 Hz), 126.02 (broad s), 125.18 (q, J = 3.8 Hz), 115.67 (d, J = 30.4 Hz), 104.57 (s), 55.42 (s), 38.80 (d, J = 21.3 Hz). ^{19}F{^{1}H} NMR (121 MHz, C_6D_6): δ -62.69 (s). ^{31}P{^{1}H} NMR (121 MHz, C_6D_6): δ -46.46 (s).

^{Ph}PO^{Ph}H: R'=R"=R'"=H. M=1.05, N=1.05. Yield: 74%. ^{1}H NMR (400 MHz, C_6D_6) δ 7.94 – 7.89 (m, 2H, ArH), 7.03 – 6.90 (m, 11H, ArH), 6.89 – 6.84 (m, 8H, ArH), 6.83 – 6.77 (m, 4H, ArH), 6.71 (ddd, *J* = 8.6, 7.9, 0.8 Hz, 2H, ArH), 6.40 (dd, *J* = 8.2, 2.4 Hz, 4H, ArH), 4.63 (d, *J* = 3.2 Hz, 2H, -CH_2-). ^{13}C{^{1}H} NMR (101 MHz, C_6D_6): δ 196.98 (d, *J* = 8.9 Hz), 161.22 (d, *J* = 9.4 Hz), 157.36 (s), 137.90 (s), 132.21 (s), 130.07 (s), 129.79 (s), 129.08 (d, *J* = 3.6 Hz), 123.45 (s), 120l.86 (d, *J* = 31.4 Hz), 119.89 (s), 112.92 (s), 37.89 (d, *J* = 18.9 Hz). ^{31}P{^{1}H} NMR (121 MHz, C_6D_6): δ -45.95 (s).

^{Me}PO^{Mes}H: R'=R'"=Me, R"=H. M=1, N=1. Yield: 66%. ^{1}H NMR (400 MHz, C_6D_6) δ 7.02 – 6.97 (m, 8H, ArH), 6.92 – 6.79 (m, 12H, ArH), 6.71 (ddd, *J* = 8.6, 7.9, 0.8 Hz, 2H, ArH), 6.52

(s, 2H, ArH), 6.39 (dd, *J* = 8.2, 2.4 Hz, 4H, ArH), 4.64 (d, *J* = 4.3 Hz, 2H, -CH_2-), 2.07 (s, 6H, mesityl-CH_3), 2.00 (s, 3H, mesityl-CH_3). $^{13}C\{^1H\}$ NMR (101 MHz, C_6D_6): δ 207.27 (d, *J* = 12.7 Hz), 161.55 (d, *J* = 9.1 Hz), 157.37 (s), 141.01 (s), 137.87(s), 133.90 (s), 130.10 (s), 129.84 (s), 128.89(s), 123.56 (s), 121.03 (d, *J* = 31.3 Hz), 120.12 (s), 112.71 (s), 42.79 (d, *J* = 20.5 Hz), 20.98 (s), 19.88 (s), 19.85 (s). $^{31}P\{^1H\}$ NMR (121 MHz, C_6D_6): δ -49.64 (s).

^{Ph}**PO**^{PhCF3}**H**: R'=R"=H, R'"=CF_3. M=1, N=1. Yield: 79%. ^1H NMR (400 MHz, C_6D_6) δ 7.71 (dt, *J* = 7.9, 0.8 Hz, 2H, ArH), 7.12-7.04 (m, 2H, ArH), 6.92-6.98 (m, 8H, ArH), 6.87-6.75 (m, 12H, ArH), 6.69 (ddd, *J* = 8.6, 7.9, 0.8 Hz, 2H, ArH), 6.38 (dd, *J* = 8.2, 2.4 Hz, 4H, ArH), 4.53 (d, *J* = 3.3 Hz, 2H, -CH_2-). $^{13}C\{^1H\}$ NMR (101 MHz, C_6D_6): δ 196.14 (d, *J* = 8.9 Hz), 161.16 (d, *J* = 9.4 Hz), 157.17 (s), 140.19 (d, *J* = 1.3 Hz), 133.34 (q, *J* = 32.3 Hz), 130.32 (s), 129.86 (s), 129.34 (d, *J* = 4.0 Hz), 128.73 (s), 125.22 (d, *J* = 3.8 Hz), 123.63 (s), 119.76 (s), 112.91 (s), 38.09 (d, *J* = 19.5 Hz), 26.17 (s). $^{19}F\{^1H\}$ NMR (121 MHz, C_6D_6): δ -62.84 (s). $^{31}P\{^1H\}$ NMR (121 MHz, C_6D_6): δ -45.75(s).

^{Ph}**PO**^{ArOMe}**H**: R'=H, R"=^{t}Bu, R'"=OMe. M=1, N=1. Yield: 79%. ^1H NMR (400 MHz, C_6D_6) δ 8.16 (s, 1H), 6.97 (dd, *J* = 8.7 7.3 Hz, 8H, ArH), 6.92-6.86 (m, 8H, ArH), 6.82-6.75 (m, 4H, ArH), 6.70 (ddd, *J* = 8.7, 7.9, 0.8 Hz, 2H, ArH), 6.39 (dd, *J* = 8.2, 2.4 Hz, 4H, ArH), 4.70 (d, *J* = 3.4 Hz, 2H, -CH_2-), 3.30 (s, 3H, -OCH_3), 1.30 (s, 18H, -$C(CH_3)_3$). $^{13}C\{^1H\}$ NMR (101 MHz, C_6D_6): δ 196.62 (d, *J* = 7.6 Hz), 163.70 (s), 161.22 (d, *J* = 9.4 Hz), 157.38 (s), 143.44 (s), 132.92 (s), 130.05 (s), 129.80 (s), 123.45 (s), 120.80 (d, *J* = 31.6 Hz), 119.93 (s), 112.80 (s), 67.85 (s), 37.66 (d, *J* = 18.9 Hz), 35.93 (s), 32.10 (s), 32.04(s). $^{31}P\{^1H\}$ NMR (121 MHz, C_6D_6): δ -45.20(s).

^{Me}**PO**^{Ph}**-Ni**: Yield: 65%. ^1H NMR (400 MHz, C_6D_6) δ 8.06 – 7.99 (m, 2H, ArH), 7.36 – 7.29 (m, 2H, ArH), 7.20 (t, J = 7.6 Hz, 3H, ArH), 7.14 – 7.01 (m, 4H, ArH), 6.78 (t, J = 7.3 Hz, 2H, ArH), 6.66 (t, J = 7.2 Hz, 1H, ArH), 6.28 (dd, J = 8.2, 3.4 Hz, 4H, ArH), 5.67 (t, J = 1.5 Hz, 1H, -CH-), 3.28 (s, 12H, -CH3), 1.46 – 1.33 (m, 6H, -CH2), 1.13 (dt, J = 15.1, 7.6 Hz, 9H, -CH3).

$^{13}C\{^1H\}$ NMR (101 MHz, C_6D_6): δ 176.89 (d, J = 25.1 Hz), 161.78 (s), 153.09 (t, J = 33.2 Hz), 141.27 (d, J = 14.4 Hz), 137.49 (q, J = 3.3 Hz), 129.53 (s), 127.35 (d, J = 2.2 Hz), 124.90 (d, J = 2.8 Hz), 119.99 (s), 114.43 (s), 113.97 (s), 105.03 (t, J = 3.4 Hz), 83.94 (s), 83.37 (s), 56.01 (d, J = 2.3 Hz), 13.81 (d, J = 21.1 Hz), 8.21 (d, J = 2.2 Hz). $^{31}P\{^1H\}$ NMR (162 MHz, C_6D_6) δ 14.22 (d, J = 301.9 Hz), -8.61 (d, J = 301.8 Hz). Anal. Calcd(%) for $C_{36}H_{44}NiO_5P_2$: C: 63.83, H: 6.55, found: C: 64.46, H: 6.10.

^{Me}PO^{PhCF3}-Ni: Yield: 68%. ^1H NMR (400 MHz, C_6D_6) 7.85 (d, J = 8.1 Hz, 2H), 7.36 (d, J = 8.2 Hz, 2H), 7.28 (dq, J = 8.0, 1.3 Hz, 2H), 7.06 (t, J = 8.2 Hz, 2H), 6.78 (t, J = 7.4 Hz, 2H), 6.71 – 6.62 (m, 1H), 6.27 (dd, J = 8.2, 3.4 Hz, 4H), 5.66 (t, J = 1.8 Hz, 1H), 3.27 (s, 12H), 1.44 – 1.30 (m, 6H), 1.13 (dt, J = 15.1, 7.6 Hz, 9H). $^{13}C\{^1H\}$ NMR (101 MHz, C_6D_6): δ 174.86 (dd, J = 26.9, 8.0 Hz), 161.65 (s), 152.28 (dd, J = 33.7, 30.7 Hz), 144.51 (d, J = 15.4 Hz), 137.36 (t, J = 3.7 Hz), 129.77 (s), 129.18 (d, J = 31.8 Hz), 127.38 (s), 125.00 (t, J = 2.6 Hz), 124.78 (q, J = 3.9 Hz), 120.16 (t, J = 2.4 Hz), 113.62 (d, J = 2.2 Hz), 113.15 (d, J = 2.1 Hz), 104.86 (d, J = 4.2 Hz), 86.45 (s), 85.90 (s), 55.90 (s), 13.80 (d, J = 21.4 Hz), 8.19 (s). $^{31}P\{^1H\}$ NMR (121 MHz, C_6D_6): δ 14.43 (d, *J* = 301.8 Hz, 1P), -8.73 (d, *J* = 302.0 Hz, 1P). $^{19}F\{^1H\}$ NMR (121 MHz, C_6D_6): δ -61.93 (s). Anal. Calcd(%) for $C_{37}H_{43}F_3NiO_5P_2$: C: 59.62, H: 5.82, found: C: 59.12, H: 5.75.

^{Ph}PO^{Ph}-Ni: Yield: 76%. ^1H NMR (400 MHz, C_6D_6) δ 7.63 (d, *J* = 7.2 Hz, 2H, ArH), 7.44 (d, *J* = 6.2, 1.6 Hz, 2H, ArH), 7.14-6.07 (m, 3H, ArH), 7.01 (ddd, *J* = 9.3, 5.5, 2.1 Hz, 8H, ArH), 6.95-6.87 (m, 11H, ArH), 6.84 (ddt, *J* = 8.4, 7.0, 1.1 Hz, 4H, ArH), 6.71 (t, *J* = 8.4 Hz, 2H, ArH), 6.43 (dd, *J* = 8.4, 3.0 Hz, 4H, ArH), 5.30-5.27 (m, 1H, -CHP-), 1.23 (ddd, *J* = 9.2, 7.5, 1.7 Hz, 6H), 0.97 (dt, *J* = 15.3, 7.5 Hz, 9H). $^{13}C\{^1H\}$ NMR (101 MHz, C_6D_6): δ 179.66-178.32 (m), 159.48 (s), 158.00 (s), 152.37-150.71 (m), 140.72 (d, *J* = 14.9 Hz), 138.16 (s), 129.74 (s), 129.71 (s), 128.59 (s), 127.93 (s), 127.47 (d, *J* = 32.0 Hz), 125.42 (d, *J* = 3.1 Hz), 123.20 (s), 120.66 (s), 119.98 (s), 113.27 (s), 82.27 (d, *J* = 55.4 Hz), 13.55 (d, *J* = 22.3 Hz), 7.99 (s). $^{31}P\{^1H\}$ NMR (121

MHz, C_6D_6): δ 14.56 (d, *J* = 305.0 Hz, 1P), -6.92 (d, *J* = 305.0 Hz, 1P). Anal. Calcd(%) for $C_{56}H_{52}NiO_5P_2$: C: 72.66, H: 5.66, found: C: 73.16, H: 5.37.

$^{Ph}PO^{Mes}$-Ni: Modification of synthesis: After addition of $(PEt_3)_2NiPhCl$, the mixture was then heated to 70 ℃ under nitrogen with stirring for 12 h. Yield: 45%. ^1H NMR (400 MHz, C_6D_6) δ 7.56 (d, *J* = 7.1 Hz, 2H, ArH), 7.10 – 6.77 (m, 23H, ArH), 6.71-6.64 (m, 4H, ArH), 6.37-6.31 (m, 4H, ArH), 5.12 (d, *J* = 1.7 Hz, 1H, -CH-), 2.35 (s, 6H, mesityl-CH_3), 2.05 (s, 3H, mesityl-CH_3), 1.22-1.11 (m, 6H, -CH_2P-), 0.95 (dt, *J* = 15.1, 7.5 Hz, 9H, -CH_3). $^{13}C\{^1H\}$ NMR (101 MHz, C_6D_6): δ 181.73 (dd, *J* = 27.0, 8.1 Hz), 160.25 (s), 157.16 (s), 152.89 (dd, *J* = 35.2, 28.1 Hz), 140.65 (d, *J* = 15.1 Hz), 135.36 (s), 134.92 (s), 129.77 (s), 129.42 (s), 128.59 (s), 125.26, 123.83 (s), 121.16 (s), 120.52 (s), 111.14 (s), 85.80 (d, *J* = 59.2 Hz), 13.27 (d, *J* = 22.3 Hz), 8.07 (s). $^{31}P\{^1H\}$ NMR (121 MHz, C_6D_6): δ 14.42 (d, *J* = 304.8 Hz, 1P), -6.92 (d, *J* = 304.8 Hz, 1P). Anal. Calcd(%) for $C_{59}H_{58}NiO_5P_2$: C: 73.23, H: 6.04, found: C: 72.92, H: 6.22.

$^{Ph}PO^{CF3}$-Ni: Modification of synthesis: 1) After addition of $(PEt_3)_2NiPhCl$, the mixture was then heated to 70 ℃ under nitrogen with stirring for 12 h; 2) after removed volatiles (2nd time), the residue was washed with pentane (5 mL) and hexanes (5 mL). Yield: 52%. ^1H NMR (400 MHz, C_6D_6) δ 7.60 (d, *J* = 7.2 Hz, 2H, ArH), 7.30 (s, 4H, ArH), 6.99 (dd, *J* = 8.6, 7.2 Hz, 8H, ArH), 6.94-6.81 (m, 15H, ArH), 6.71 (t, *J* = 8.2 Hz, 2H, ArH), 6.42 (dd, *J* = 8.2, 3.2 Hz, 4H, ArH), 5.27 (s, 1H, -CH-), 1.22 (ddd, *J* = 9.2, 7.6, 1.8 Hz, 6H, -CH_2P-), 0.97 (dt, *J* = 15.1 Hz, 7.6 Hz, 9H, -CH_3). $^{13}C\{^1H\}$ NMR (101 MHz, C_6D_6): δ 177.08-176.73 (m), 159.44(s), 157.90 (s), 151.04-150.40 (m), 143.99 (d, *J* = 15.2 Hz), 138.04 (s), 129.97 (s), 129.78 (s), 129.36-129.71 (m), 128.39 (s), 127.34 (s), 125.51 (s), 124.61 (s), 123.33 (s), 120.83(s), 119.83 (s), 113.32 (s), 84.74 (d, *J* = 54.5 Hz), 13.52 (d, *J* = 22.2 Hz), 7.97 (s). $^{19}F\{^1H\}$ NMR (121 MHz, C_6D_6): δ -62.00 (s). $^{31}P\{^1H\}$ NMR (121 MHz, C_6D_6): δ 14.40 (d, *J* = 304.7 Hz, 1P), -8.78 (d, *J* = 304.7 Hz, 1P). Anal. Calcd(%) for $C_{57}H_{51}F_3NiO_5P_2$: C: 68.90, H: 5.17, found: C: 68.66, H: 4.87.

$^{Ph}PO^{ArOMe}$-Ni: Modification of synthesis: 1) After addition of $(PEt_3)_2NiPhCl$, the mixture was then heated to 70 °C under nitrogen with stirring for 12 h; 2) after removed volatiles (2nd time), the residue was washed with pentane (5 mL) and hexanes (5 mL). Yield: 72%. ^{1}H NMR (400 MHz, C_6D_6): δ 7.61 (d, *J* = 7.3 Hz, 2H, ArH), 7.47 (s, 2H, ArH), 7.03-6.77 (m, 23H, ArH), 6.66 (t, *J* = 8.3 Hz, 2H, ArH), 6.37 (d, *J* = 8.3 Hz, 4H, ArH), 5.13 (broad s, 1H, -CH-), 3.36 (s, 3H, -OCH_3), 1.42 (s, 18H, -$C(CH_3)_3$), 1.28-1.16 (m, 6H, -CH_2P-), 0.94 (dt, *J* = 15.1 Hz, 7.5 Hz, 9H, -CH_3). ^{13}C{^{1}H} NMR (101 MHz, C_6D_6): δ 178.97 (broad s), 159.43 (s), 159.11 (s), 157.68 (s), 151.49 (s), 141.68 (s), 137.77 (s), 134.42 (d, *J* = 14.3 Hz), 129.31 (s), 129.22 (s), 125.47 (s), 124.98 (s), 122.82 (s), 120.24 (s), 119.61 (s), 113.00 (s), 80.52 (d, *J* = 55.2 Hz), 63.54 (s), 35.54 (s), 35.54 (s), 32.11 (s), 13.12 (d, *J* = 22.1 Hz), 7.63 (s). ^{31}P{^{1}H} NMR (121 MHz, C_6D_6): δ 14.24 (d, *J* = 305.5 Hz, 1P), -7.21 (d, *J* = 305.5 Hz, 1P). Anal. Calcd(%) for $C_{65}H_{70}NiO_6P_2$: C: 73.11, H: 6.61, found: C: 72.32, H: 6.65.

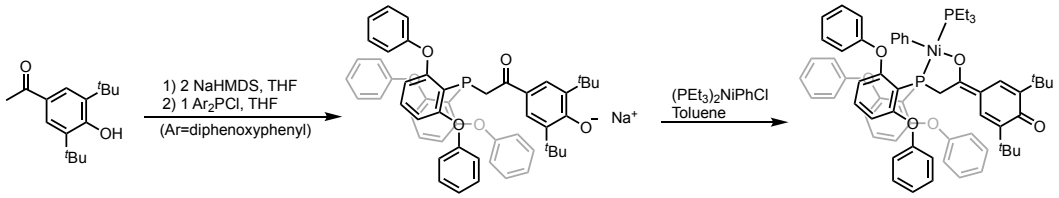

Metal complex ***$^{Ph}P^*O^{ArO}$-Ni:*** In the glove box, to a precooled (-78 °C) solution of 3', 5'-di-tert-butyl-4'-hydroxyacetophenone (124 mg, 0.5 mmol) in diethyl ether (5 mL) was added a precooled (-78 °C) solution (2 mL) of LDA (1.03 mol, 2.05 equiv.,) in diethyl ether. The mixture was stirred for 30 min at (-78 °C), then slowly warmed up to room temperature and stirred for another 24 h at room temperature, yielding a pale orange suspension. All volatiles were removed from solution which was triturated with pentane (2 x 5 mL). The resulting residue was dissolved in THF (4 mL) and cooled to -78 °C. To this solution was added a THF solution (3 mL) of corresponding bis(diphenoxyphenyl) phosphine chloride (280.5 mg, 0.49 mmol, 0.95 equiv.). The mixture was

then slowly warmed up to room temperature and stirred for additional 8 h. Next, volatiles were removed under vacuum and the residue **A** was washed with diethyl ether (2 x 5 mL) and used directly in the next step.

In the glove box, to a precooled (-78 ℃) solution of **A** in toluene (5 mL) at -78 ℃ was added a toluene solution (2 mL) of $(PEt_3)_2NiPhCl$ (200 mg, 0.49 mmol). The mixture was then slowly warmed up to room temperature and heated to 70 ℃ under nitrogen with stirring for 12 h. Next, the mixture was filtered through Celite and volatiles were removed under vacuum. The residue was washed with pentane (5~10 mL), hexanes (5 mL) and diethyl ether (2 mL), yielding metal complexes ^{Ph}**P*O**^{ArO}**-Ni** as bright yellow solids (Yields: 216 mg, 40%).

^{1}H NMR (400 MHz, C_6D_6): δ 7.94 (d, *J* = 2.5 Hz, 1H, ArH), 7.53 (d, *J* = 7.4 Hz, 2H, ArH), 7.30 (d, *J* = 2.6 Hz, 1H, ArH), 7.04 (dd, *J* = 8.7, 7.2 Hz, 8H, ArH), 6.92-6.77 (m, 15H, ArH), 6.56 (t, *J* = 8.3 Hz, 2H, ArH), 6.17 (d, *J* = 8.3 Hz, 4H, ArH), 4.74 (d, *J* = 10.6 Hz, 2H, $-CH_2-$), 1.85 (s, 9H, $-C(CH_3)_3$), 1.68 (s, 9H, $-C(CH_3)_3$), 1.04 (dd, 6H, *J* = 8.6, 6.8 Hz, $-CH_2P-$), 0.73 (dt, *J* = 15.3 Hz, 7.6 Hz, 9H, $-CH_3$). ^{13}C{^{1}H} NMR (101 MHz, C_6D_6): δ 183.61 (s), 160.41 (s), 156.53 (s), 142.33 (s), 140.56 (s), 137.33 (s), 132.05 (s), 130.17(s), 130.02 (s), 128.59 (s), 126.34 (s), 126.10 (s), 124.58 (s), 121.38 (s), 120.36 (s), 111.92 (s), 39.94 (d, *J* = 31.7 Hz), 35.86 (s), 30.44 (s), 30.26 (s), 13.29 (d, *J* = 23.6 Hz), 7.61 (s). ^{31}P{^{1}H} NMR (121 MHz, C_6D_6): δ 13.66 (d, *J* = 312.9 Hz, 1P), 0.10 (d, *J* = 312.9 Hz, 1P). Anal. Calcd(%) for $C_{64}H_{68}NiO_6P_2$: C: 72.94, H: 6.50, found: C: 73.85, H: 6.11.

Crystallographic Information

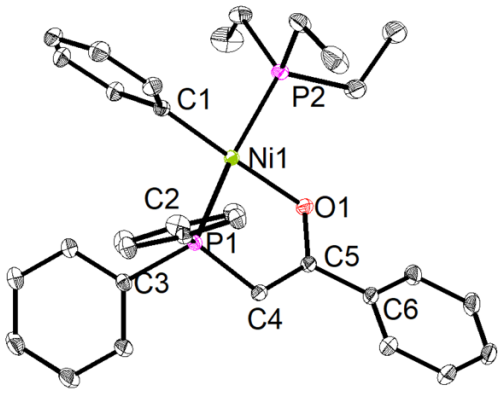

Figure S4.1. Solid-State Structure of **Ni0**. Ellipsoids are show at the 50% probability level. Hydrogen atoms and solvent molecules excluded for clarity.

Special Refinement Details for Ni0: Complex **Ni0** crystalizes in a P2(1)c space group with the full molecule in the asymmetric unit.

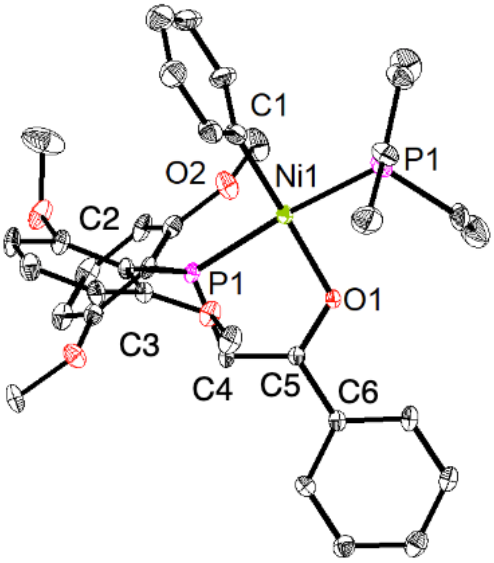

Figure S4.2. Solid-State Structure of **^{Me}PO^{Ph}-Ni**. Ellipsoids are show at the 50% probability level. Hydrogen atoms and solvent molecules excluded for clarity.

Special Refinement Details for ^{Me}PO^{Ph}-Ni: Complex **^{Me}PO^{Ph}-Ni** crystalizes in a P-1 space group with the full molecule in the asymmetric unit.

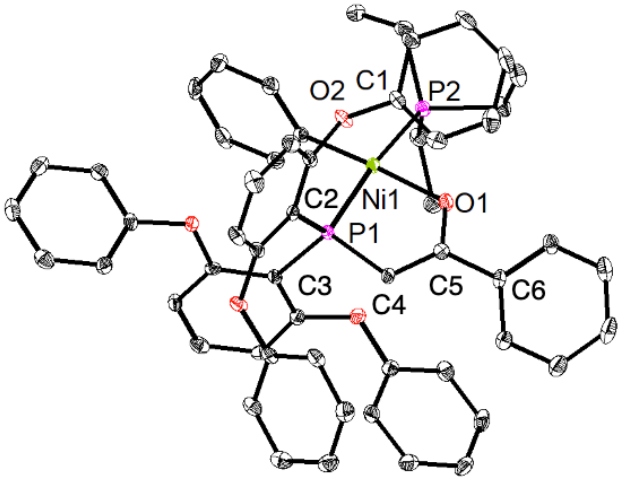

Figure S4.3. Solid-State Structure of **^{Ph}PO^{Ph}-Ni**. Ellipsoids are show at the 50% probability level. Hydrogen atoms and solvent molecules excluded for clarity.

Special Refinement Details for ^{Ph}PO^{Ph}-Ni: Complex **^{Ph}PO^{Ph}-Ni** crystalizes in a P-1 space group with the full molecule in the asymmetric unit.

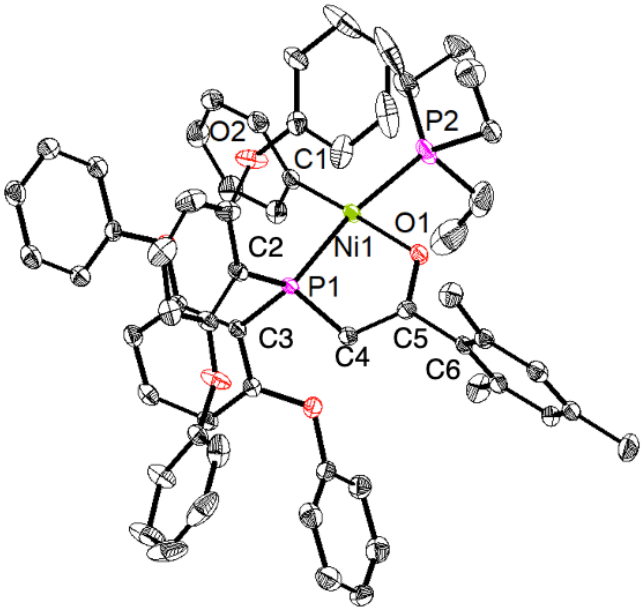

Figure S4.4. Solid-State Structure of **^{Ph}PO^{Mes}-Ni**. Ellipsoids are show at the 50% probability level. Hydrogen atoms and solvent molecules excluded for clarity.

Special Refinement Details for ^{Ph}PO^{Mes}-Ni: Complex **^{Ph}PO^{Mes}-Ni** crystalizes in a P-2(1)/c space group with the full molecule in the asymmetric unit. One of the Et group in PEt_3 is modelled with two-site disorder with occupancies of 0.62 and 0.38 (only one part is shown in figure 3.2).

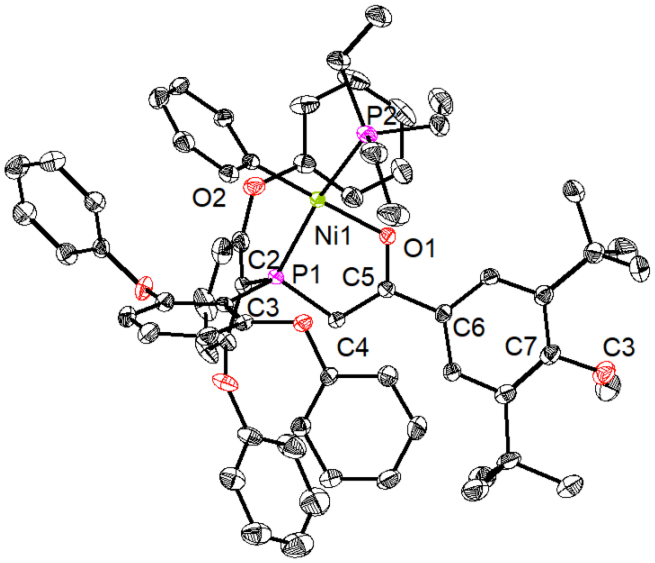

Figure S4.5. Solid-State Structure of ^{Ph}**PO**^{ArOMe}**-Ni**. Ellipsoids are show at the 50% probability level. Hydrogen atoms and solvent molecules excluded for clarity.

Special Refinement Details for ^{Ph}PO^{ArOMe}-Ni: Complex ^{Ph}**PO**^{ArOMe}**-Ni** crystalizes in a P-2(1)c space group with the full molecule in the asymmetric unit.

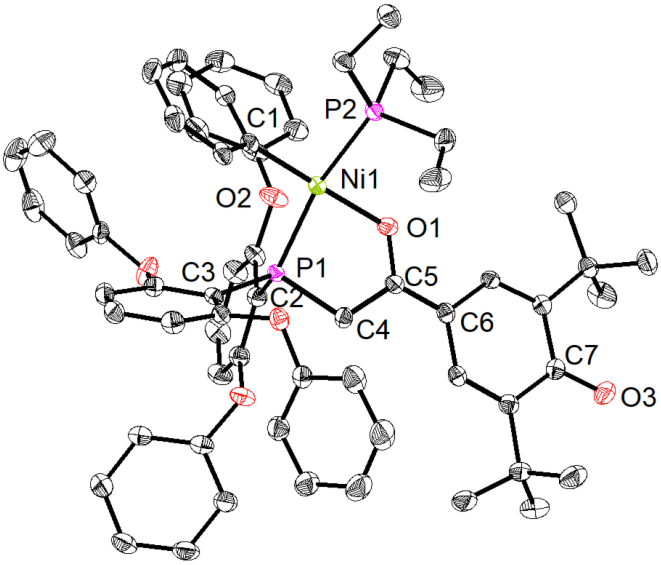

Figure S4.6. Solid-State Structure of ^{Ph}**P*O**^{ArO}**-Ni**. Ellipsoids are show at the 50% probability level. Hydrogen atoms and solvent molecules excluded for clarity.

Special Refinement Details for ^{Ph}P*O^{ArO}-Ni: Complex ^{Ph}**P*O**^{ArO}**-Ni** crystalizes in a P-2(1)c space group with the full molecule in the asymmetric unit.

Crystallographic Information

Table S4.1. Crystal and refinement data for complexes **Ni0**, **^{R}P*O^{Ar}-Ni**s, and **^{Ph}P*O^{ArO}-Ni**.

	NiH	**^{Me}PO^{Ph}-Ni**	**^{Ph}PO^{Ph}-Ni**
Empirical formula	$C_{32}H_{33}NiO_5P_2$	$C_{36}H_{44}NiO_5P_2$	$C_{56}H_{52}NiO_5P_2$
Formula weight	557.3	677.36	925.65
Temperature/K	100 K	100 K	100 K
Crystal system	Monoclinic	Triclinic	Triclinic
Space group	P-2(1)c	P-1	P-1
a/Å	17.542(16)	9.241(19)	12.693(6)
b/Å	8.406(3)	9.97(2)	13.396(3)
c/Å	20.05(2)	18.65(4)	14.751(6)
α/°	90	91.17(7)	92.266(8)
β/°	108.57(2)	97.76(6)	94.621(1)
γ/°	90	101.09(5)	100.070(6)
Volume/Å^3	2803(4)	1669(6)	2457.8(15)
Z	4	2	2
ϱ_{calc}g/cm^3	1.320	1.348	1.312
μ/mm^{-1}	0.829	0.718	0.510
F(000)	1176	716	1020
Radiation	MoKα (λ = 0.71073)	MoKα (λ = 0.71073)	MoKα (λ = 0.71073)
Reflections collected	51639	38726	79639
Independent reflections	11532	7506	7641
Goodness-of-fit on F^2	1.167	1.276	0.978
Final R indexes [I>=2σ (I)]	R_1 = 4.02 % R_2 = 15.37%	R_1 = 7.79 % R_2 = 21.49 %	R_1 = 5.19 % R_2 = 9.29 %

	^{Ph}P*O^{Mes}-Ni	**^{Ph}P*O^{ArOMe}-Ni**	**^{Ph}P*O^{ArO}-Ni**
Empirical formula	$C_{59}H_{58}NiO_5P_2$	$C_{65}H_{70}NiO_6P_2$	$C_{64}H_{68}NiO_6P_2$
Formula weight	967.80	1067.9	1053.83
Temperature/K	100 K	100 K	100 K
Crystal system	Monoclinic	Monoclinic	Monoclinic
Space group	P-2(1)c	P-2(1)c	P-2(1)c
a/Å	11.340(3)	12.5879(12)	15.5540(16)
b/Å	14.723(4)	18.312(3)	21.475(3)
c/Å	29.769(9)	13.3885(16)	17.684(2)
α/°	90	90	90
β/°	100.28(3)	116.991(7)	106.525(7)
γ/°	90	90	90
Volume/Å^3	4890(4)	2750.0(6)	5663.0(12)
Z	4	4	4
ϱ_{calc}g/cm^3	1.315	1.290	1.236
μ/mm^{-1}	0.513	1.472	1.423
F(000)	2040	1132	1246
Radiation	MoKα (λ = 0.71073)	CuKα (λ = 1.54178)	CuKα (λ = 1.54178)
Reflections collected	85040	38726	73832
Independent reflections	13734	10050	8817
Goodness-of-fit on F^2	1.167	0.858	0.978
Final R indexes [I>=2σ(I)]	R_1 = 7.70 % R_2 = 22.42%	R_1 = 3.63 % R_2 = 10.85 %	R_1 = 5.17 % R_2 = 14.84 %

Topographical analyses. Topographical maps of **Ni0**, **^{R}P*O^{Ar}-Ni**s, and **^{Ph}P*O^{ArO}-Ni** and corresponding percent buried volume data (%V_{bur}) were generated by Cavallo's SambVca 2.1 (Salerno molecular buried volume calculation) program.[72-75]

More details for %V_{bur} calculation and steric maps:

1) The nickel atom (Ni1) defines the center of the xyz coordinate system,

2) Ni(PEt$_3$)Ph fragment was excluded;

3) Bondi radii was scaled by 1.17; [74]

4) Mesh spacing for numerical integration was 0.10;

5) Sphere radius was set to 3.5 Å;

6) H atoms were excluded.

For all compounds except **^{Ph}P*O^{ArO}-Ni**, xz-plane was defined as shown in the figure below and the z -axis was defined by the right-hand rule. For **^{Ph}P*O^{ArO}-Ni**, the y-axis is flipped (left-handed coordinate system) so the larger axial shielding locates on the top. Note that for a specific complex, the %Vbur remained the same with Ni1 in the origin even the xyz coordination system rotated or flipped.

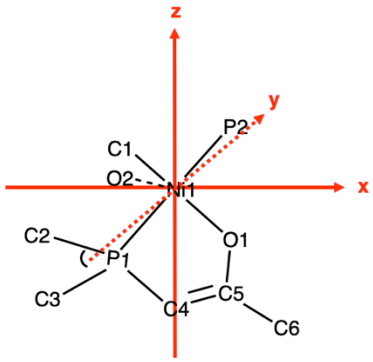

Supplemental Information for Ethylene Homopolymerization and Ethylene/tBA Copolymerization

General procedure for high throughput parallel polymerization reactor (PPR) runs. Polyolefin catalysis screening was performed in a high throughput parallel polymerization reactor (PPR) system. The PPR system was comprised of an array of 48 single cell (6 x 8 matrix) reactors in an inert atmosphere glovebox. Each cell was equipped with a glass insert with an internal working liquid volume of approximately 5 mL. Each cell had independent controls for pressure and was continuously stirred at 800 rpm. Catalyst solutions (with $Ni(COD)_2$ if necessary) were prepared in toluene. All liquids (i.e., solvent, tBA, and catalyst solutions) were added via robotic syringes. Gaseous reagents (i.e., ethylene) were added via a gas injection port. Prior to each run, the reactors were heated to 50 °C, purged with ethylene, and vented.

All desired cells were injected with tBA followed with a portion of toluene (This step was skipped for ethylene homopolymerization). The reactors were heated to the run temperature and then pressured to the appropriate psig with ethylene. Catalyst solutions (with $Ni(COD)_2$ if necessary) were then added to the cells. Each catalyst addition was chased with a small amount of toluene so that after the final addition, a total reaction volume of 5 mL was reached. Upon addition of the catalyst, the PPR software began monitoring the pressure of each cell. The desired pressure (within approximately 2-6 psig) was maintained by the supplemental addition of ethylene gas by opening the valve at the set point minus 1 psi and closing it when the pressure reached 2 psi higher. All drops in pressure were cumulatively recorded as "Uptake" or "Conversion" of the ethylene for the duration of the run or until the uptake or conversion requested value was reached, whichever occurred first. Each reaction was then quenched by addition of 1% oxygen in nitrogen for 30 seconds at 40 psi higher than the reactor pressure. The pressure of each cell was monitored during and after the quench to

ensure that no further ethylene consumption happens. The shorter the "Quench Time" (the duration between catalyst addition and oxygen quench), the more active the catalyst. In order to prevent the formation of too much polymer in any given cell, the reaction was quenched upon reaching a predetermined uptake level of 80 psig. After all the reactors were quenched, they were allowed to cool to about 60 °C. They were then vented, and the tubes were removed. The polymer samples were then dried in a centrifugal evaporator at 60 °C for 12 hours, weighed to determine polymer yield and used in subsequent IR (tBA incorporation), GPC, DSC and NMR (copolymer microstructures) analysis.

Measurement of ethylene uptake curves. Upon addition of the catalyst, the PPR software began monitoring the pressure of each cell. The desired pressure (within approximately 2-6 psig) was maintained by the supplemental addition of ethylene gas by opening the valve at the set point minus 1 psi and closing it when the pressure reached 2 psi higher. For example, the pressure was maintained between approximately 399-402 psi if the original pressure was set to 400 psi. All drops in pressure were cumulatively recorded as "Uptake" or "Conversion" of the ethylene for the duration of the run. The unit of this "Uptake" is in psi and the uptake curves over time were used to analyze the real-time activity of catalysts and rates of chain propagation.

General procedure for batch reactor runs for preparation of ethylene/tBA copolymers. Polymerization reactions were conducted in a 2-L Parr batch reactor. The reactor was heated by an electrical heating mantle and cooled by an internal serpentine cooling coil containing cooling water. The water was pre-treated by passing through an Evoqua water purification system. Both the reactor and the heating/cooling system were controlled and monitored by a Camile TG process computer. The bottom of the reactor was fitted with a dump valve, which empties the reactor contents into a lidded dump pot, which was prefilled with a catalyst-kill solution (typically 5 mL of an Irgafos / Irganox / toluene mixture). The lidded dump pot was vented

to a 15-gal. blowdown tank, with both the pot and the tank N_2 purged. All chemicals used for polymerization or catalyst makeup are run through purification columns to remove any impurities that may affect polymerization. The toluene was passed through two columns, the first containing A2 alumina, the second containing Q5 reactant. The tert-butyl acrylate was filtered through activated alumina. The ethylene was passed through two columns, the first containing A204 alumina and 4 Å molecular sieves, the second containing Q5 reactant. The N2 used for transfers was passed through a single column containing A204 alumina, 4 Å molecular sieves and Q5 reactant.

The reactor was loaded first from the shot tank that contained toluene and tBA. The shot tank was filled to the load set points by use of a differential pressure transducer. After solvent/acrylate addition, the shot tank was rinsed twice with toluene. Then the reactor was heated up to the polymerization temperature set point. The ethylene was added to the reactor when the reaction temperature was reached to maintain the reaction pressure set point. Ethylene addition amounts were monitored by a micro-motion flowmeter.

The catalysts were handled in an inert atmosphere glovebox and were prepared as a solution in toluene. The catalyst was drawn into a syringe and pressure-transferred into the catalyst shot tank. This was followed by 3 rinses of toluene, 5 mL each. Catalyst was added when the reactor pressure set point was reached.

Immediately after catalyst addition the run timer was started. Usually within the first 2 min. of successful catalyst runs an exotherm was observed, as well as decreasing reactor pressure. Ethylene was then added by the Camile to maintain reaction pressure set point in the reactor. These polymerizations were run for 75 min or until 40 g of ethylene uptake. Then the agitator was stopped, and the bottom dump valve was opened to empty reactor contents into the lidded dump pot. The lidded dump pot was closed and the contents were poured into trays placed in

a lab hood where the solvent was evaporated off overnight. The trays containing the remaining polymer were then transferred to a vacuum oven, where they were heated up to 140 °C under vacuum to remove any remaining solvent. After the trays cooled to ambient temperature, the polymers were weighed for yield/efficiencies and submitted for polymer testing if so desired.

Procedure for gel permeation chromatography (GPC). High temperature GPC analysis was performed using a Dow Robot Assisted Delivery (RAD) system equipped with a Polymer Char infrared detector (IR5) and Agilent PLgel Mixed A columns. Decane (10 μL) was added to each sample for use as an internal flow marker. Samples were first diluted in 1,2,4-trichlorobenzene (TCB) stabilized with 300 ppm butylated hydroxyl toluene (BHT) at a concentration of 10 mg/mL and dissolved by stirring at 160°C for 120 minutes. Prior to injection the samples are further diluted with TCB stabilized with BHT to a concentration of 3 mg/mL. Samples (250 μL) are eluted through one PL-gel 20 μm (50 x 7.5 mm) guard column followed by two PL-gel 20 μm (300 x 7.5 mm) Mixed-A columns maintained at 160 °C with TCB stabilized with BHT at a flowrate of 1.0 mL/min. The total run time was 24 minutes. To calibrate for molecular weight (MW) Agilent EasiCal polystyrene standards (PS-1 and PS-2) were diluted with 1.5 mL TCB stabilized with BHT and dissolved by stirring at 160 °C for 15 minutes. These standards are analyzed to create a 3rd order MW calibration curve. Molecular weight units are converted from polystyrene (PS) to polyethylene (PE) using a daily Q-factor calculated to be around 0.4 using the average of 5 Dowlex 2045 reference samples.

Procedure for Fourier-transform infrared spectroscopy (FTIR). The 10 mg/mL samples prepared for GPC analysis are also utilized to quantify tert-butyl acrylate (tBA) incorporation by Fourier Transform infrared spectroscopy (FTIR). A Dow robotic preparation station heated and stirred the samples at 160°C for 60 minutes then deposited 130 μL portions into stainless wells promoted on a silicon wafer. The TCB was evaporated off at 160°C under nitrogen purge.

IR spectra were collected using a Nexus 6700 FT-IR equipped with a DTGS KBr detector from 4000-400 cm-1 utilizing 128 scans with a resolution of 4. Ratio of tBA (C=O: 1762-1704 cm−1) to ethylene (CH2: 736-709 cm−1) peak areas were calculated and fit to a linear calibration curve to determine total tBA.

Differential scanning calorimetry (DSC). Differential scanning calorimetry analyses was performed on solid polymer samples using a TA Instruments, Inc. Discovery Series or TA Instruments, Inc., DSC2500, programmed with the following method: Equilibrate at 175.00 °C; Isothermal for 3 minutes; Ramp 30.00 °C/min to 0.00 °C; Ramp 10.00 °C/min to 175.00 °C; Data was analyzed using TA Trios software.

NMR characterization. NMR spectra of ethylene/tBA copolymers were recorded on a Bruker 400 MHz using o-dichlorobenzene at 120 °C. ^{1}H NMR analysis of copolymers were done using a relaxation time (0.2 s), and an acquisition time (1.8 s) with the number of FID's collected per sample (512). ^{13}C{^{1}H} NMR analysis of copolymers were done using 90° pulse of 17.2 μs, a relaxation time (22.0 s), an acquisition time (5.3 s), and inverse-gated decoupling with the number of FID's collected per sample (1536). Analysis of the spectra was based on literature.[11, 38]

Supplemental Data for Ethylene Polymerization and Ethylene/tBA Copolymeri-zation

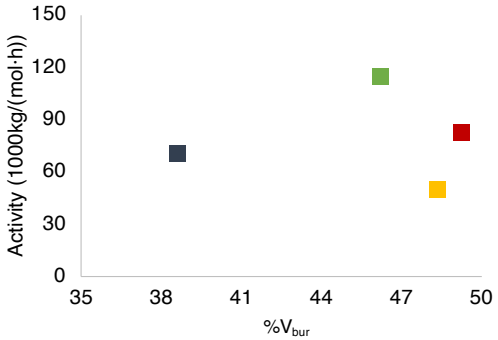

Figure S4.7. Correlation between ethylene homopolymerization activity and %V_{bur} (in square) at 90 °C (Dark blue: **Ni0**, green: **^{Me}PO^{Ph}-Ni**, orange: **^{Ph}PO^{Mes}-Ni**, red: **^{Ph}PO^{Ph}-Ni**). Activity data extracted from table 4.1.

Table S4.2 show the results of a set of ethylene/tBA copolymerization trials, which are summarized in Figure 4.6a (Figure 4.6a also includes entry 1, 2, 7, 10 from Table 4.2, and entry 1 from Table 4.4).

Table S4.2. Ethylene/tBA copolymerization with **^{Me}PO^{Ph}-Ni**, **^{Ph}PO^{Ph}-Ni**, **^{Ph}PO^{PhCF3}-Ni** under different temperatures (some data are also included in Table 1).

Entry[a]	catalyst	T (ºC)	Act. (kg/(mol·h))	$M_w/10^3$	PDI	%Mol tBA	Tm (ºC)
1	**^{Me}PO^{Ph}-Ni**	100	534	2.5	1.9	1.5	115
2	**^{Me}PO^{Ph}-Ni**	110	574	2.4	1.9	1.4	114
3	**^{Ph}PO^{Ph}-Ni**	100	3274	9.1	2.5	0.6	121

[a]Conditions unless specified: catalyst, 0.25 μmol; $Ni(COD)_2$, 1 μmol; [tBA] = 0.05 M, V(toluene)=5 ml; ethylene pressure=400 psi; polymerization runs were stopped when ethylene uptake reached 80 psi.

Original polymerization runs for ethylene/tBA copolymerization

Table S4.3. Original runs of table 4.1.

Entry[a]	catalyst	$Ni(COD)_2$ /Cat.	T (ºC)	time (s)	yield (mg)	Act.[b]	$M_w/10^3$	PDI	Tm (ºC)
1	**Ni0**	4	90	41	182	64	1.25	2.1	122
2	**Ni0**	4	90	41	208	73	1.47	2.7	123
3	**Ni0**	4	90	38	195	74	1.28	2.3	122
4	**^{Me}PO^{Ph}-Ni**	4	90	38	294	111	3.6	2.8	121
5	**^{Me}PO^{Ph}-Ni**	4	90	35	281	116	4.5	3.3	118
6	**^{Ph}PO^{Ph}-Ni**	4	90	49	271	80	11.4	3.2	123
7	**^{Ph}PO^{Ph}-Ni**	4	90	46	245	77	13.4	3.7	125
8	**^{Ph}PO^{Ph}-Ni**	4	90	41	255	90	10.9	3.1	125
9	**^{Ph}PO^{Mes}-Ni**	4	90	72	264	53	7.8	2.6	121
10	**^{Ph}PO^{Mes}-Ni**	4	90	65	199	44	3.2	2.7	118
11	**^{Ph}PO^{PhCF3}-Ni**	4	90	65	285	63	9.2	3	124
12	**^{Ph}PO^{PhCF3}-Ni**	4	90	63	252	58	9.8	2.7	124
13	**^{Ph}PO^{PhCF3}-Ni**	4	90	54	225	60	9.3	2.6	125
14	**^{Me}PO^{Ph}-Ni**	0	90	73	229	45	5.1	2.1	121
15	**^{Me}PO^{Ph}-Ni**	0	90	65	226	50	3.9	2.4	120
16	**^{Ph}PO^{Ph}-Ni**	0	90	118	146	18	14.3	2.5	126
17	**^{Ph}PO^{Ph}-Ni**	0	90	113	152	19	13	2.5	126

[a]Conditions unless specified: catalyst, 0.25 μmol; V(toluene)=5 ml; ethylene pressure=400 psi; polymerization runs were stopped when ethylene uptake reached 80 psi. [b]Activity in 10^6 g/(mol*h).

Table S4.4. Original runs of table 4.2.

Entry[a]	catalyst	Ni(COD)$_2$/ Cat.	[tBA]/ M	T (ºC)	time (s)	yield (mg)	Act.[b]	$M_w/10^3$	PDI	%Mol tBA	Tm (ºC)
1	^{Me}**PO**^{Ph}**-Ni**	4	0.05	70	3513	57	234	4.6	1.9	1.3	111
2	^{Me}**PO**^{Ph}**-Ni**	4	0.05	70	3101	55	255	4.6	2	1.4	114
3	^{Ph}**PO**^{Ph}**-Ni**	4	0.05	70	2152	120	803	16.5	2.2	0.5	122
4	^{Ph}**PO**^{Ph}**-Ni**	4	0.05	70	1970	95	694	16.2	2.2	0.7	123
5	^{Ph}**PO**^{Ph}**-Ni**	4	0.05	70	1922	59	442	12.6	2.2	0.5	123
6	^{Ph}**PO**^{Ph}**-Ni**	4	0.05	70	1878	103	789	12.6	2.3	0.5	-
7	^{Ph}**PO**^{Mes}**-Ni**	4	0.05	70	3600	102	408	7.9	2.1	0.6	115
8	^{Ph}**PO**^{Mes}**-Ni**	4	0.05	70	3433	91	382	7.3	2.1	0.6	114
9	^{Ph}**PO**^{PhCF3}**-Ni**	4	0.05	70	1972	58	424	17.5	3	0.3	123
10	^{Ph}**PO**^{PhCF3}**-Ni**	4	0.05	70	2201	125	818	21.1	3.3	0.4	124
11	^{Ph}**PO**^{ArOMe}**-Ni**	4	0.05	70	2204	89	486	17.2	2.3	0.6	123
12	^{Ph}**PO**^{ArOMe}**-Ni**	4	0.05	70	2334	113	697	19.9	2.5	0.5	123
13	^{Ph}**P*O**^{ArO}**-Ni**	4	0.05	70	3601	42	168	18.8	2.5	0.6	123
14	^{Ph}**P*O**^{ArO}**-Ni**	4	0.05	70	3515	58	238	20.3	2.6	0.7	123
15	^{Me}**PO**^{Ph}**-Ni**	4	0.05	90	2141	75	504	3.9	2	1.4	112
16	^{Me}**PO**^{Ph}**-Ni**	4	0.05	90	2338	70	431	3	1.9	1.6	114
17	^{Me}**PO**^{Ph}**-Ni**	4	0.05	90	1789	67	539	3.7	1.9	1.4	113
18	^{Me}**PO**^{Ph}**-Ni**	4	0.1	90	3600	46	184	2.7	2.1	2.5	76
19	^{Me}**PO**^{Ph}**-Ni**	4	0.1	90	3296	44	192	2.4	2	3	78
20	^{Me}**PO**^{PhCF3}**-Ni**	4	0.05	90	1470	84	823	6.2	3.2	1.4	114
21	^{Me}**PO**^{PhCF3}**-Ni**	4	0.05	90	1586	86	781	6.3	3.3	1.4	114
22	^{Me}**PO**^{PhCF3}**-Ni**	4	0.05	90	1588	79	716	6.2	3.1	1.4	114
23	^{Ph}**PO**^{Ph}**-Ni**	4	0.05	90	680	103	2181	10.5	2.5	0.6	122
24	^{Ph}**PO**^{Ph}**-Ni**	4	0.05	90	763	117	2208	11.9	2.3	0.6	122
25	^{Ph}**PO**^{Ph}**-Ni**	4	0.05	90	743	100	1938	10.3	2.7	0.6	122
26	^{Ph}**PO**^{Ph}**-Ni**	4	0.1	90	1199	99	1189	9.3	2.6	1.2	118
27	^{Ph}**PO**^{Ph}**-Ni**	4	0.1	90	1127	89	1137	8.4	2.5	1.1	118
28	^{Ph}**PO**^{Mes}**-Ni**	4	0.05	90	1521	121	1146	7	2.1	0.7	116
29	^{Ph}**PO**^{Mes}**-Ni**	4	0.05	90	1502	107	1026	6.9	2	0.7	116
30	^{Ph}**PO**^{PhCF3}**-Ni**	4	0.05	90	777	72	1334	10	2.2	0.5	122
31	^{Ph}**PO**^{PhCF3}**-Ni**	4	0.05	90	899	84	1345	10.2	2.2	0.5	122
32	^{Ph}**PO**^{ArOMe}**-Ni**	4	0.05	90	1206	140	1672	15.2	2.3	0.6	122
33	^{Ph}**PO**^{ArOMe}**-Ni**	4	0.05	90	935	132	2033	-	-	0.6	123
34	^{Ph}**P*O**^{ArO}**-Ni**	4	0.05	90	2275	87	551	14.7	2.5	0.7	122
35	^{Ph}**P*O**^{ArO}**-Ni**	4	0.05	90	1870	82	631	15.4	2.3	0.7	123
36	^{Me}**PO**^{Ph}**-Ni**	0	0.05	90	3600	51	204	2.9	2	1.9	112
37	^{Me}**PO**^{Ph}**-Ni**	0	0.05	90	3600	53	212	2.9	2.1	2	114
38	^{Ph}**PO**^{Ph}**-Ni**	0	0.05	90	966	104	1550	11.5	2.5	0.6	122
39	^{Ph}**PO**^{Ph}**-Ni**	0	0.05	90	826	93	1621	9.7	2.5	0.6	122
40	^{Ph}**P*O**^{ArO}**-Ni**	0	0.05	90	2617	93	512	12.4	2.4	0.6	122
41	^{Ph}**P*O**^{ArO}**-Ni**	0	0.05	90	3412	94	397	10.2	2.5	0.6	122

[a]Conditions unless specified: catalyst, 0.25 µmol; V(toluene)=5 ml; ethylene pressure=400 psi; polymerization runs were stopped when ethylene uptake reached 80 psi. [b]Activity in 10^3 g/(mol*h).

Table S4.5. Original runs of table S4.2.

Entry[a]	catalyst	$Ni(COD)_2$/ Cat.	[tBA]/ M	T (ºC)	time (s)	yield (mg)	Act.[b]	M_w/ 10^3	PDI	%Mol tBA	Tm (ºC)
1	^{Me}**PO**^{Ph}**-Ni**	4	0.05	100	3601	71	284	2.7	1.9	1.4	111
2	^{Me}**PO**^{Ph}**-Ni**	4	0.05	100	1882	87	666	2.6	1.9	1.5	115
3	^{Me}**PO**^{Ph}**-Ni**	4	0.05	100	2886	81	404	2.4	1.8	1.4	114
4	^{Ph}**PO**^{Ph}**-Ni**	4	0.05	100	556	125	3237	9.1	2.5	0.6	121
5	^{Ph}**PO**^{Ph}**-Ni**	4	0.05	100	567	130	3302	9.4	2.6	0.6	122
6	^{Ph}**PO**^{Ph}**-Ni**	4	0.05	100	540	127	3387	8.6	2.4	0.6	121
7	^{Ph}**PO**^{Ph}**-Ni**	4	0.05	100	545	120	3171	9.4	2.6	0.6	121
8	^{Me}**PO**^{Ph}**-Ni**	4	0.05	110	946	48	731	2.5	2.0	1.4	-
9	^{Me}**PO**^{Ph}**-Ni**	4	0.05	110	2066	60	418	2.2	1.8	1.4	114

[a]Conditions unless specified: catalyst, 0.25 μmol; V(toluene)=5 ml; ethylene pressure=400 psi; polymerization runs were stopped when ethylene uptake reached 80 psi. [b]Activity in 10^3 g/(mol*h).

Table S4.6. Original runs of figure 4.6 (ethylene uptake curves).

Entry[a]	catalyst	$Ni(COD)_2$/ Cat.	[tBA]/M	T (ºC)	time (s)	yield (mg)	Act.[b]	M_w/ 10^3	PDI	%Mol tBA	Tm (ºC)
1[c]	^{Me}**PO**^{Ph}**-Ni**	4	0.1	90	3296	44	192	2.4	2	3	78
2[d]	^{Ph}**PO**^{Ph}**-Ni**	4	0.1	90	1199	99	1189	9.3	2.6	1.2	118
3[e]	^{Ph}**PO**^{Ph}**-Ni**	4	0.1	110	576	126	3150	6.7	2.4	1.0	119
4	^{Me}**PO**^{Ph}**-Ni**	4	0.1	110	3600	25	99	9.1	2.5	0.6	121
5[f]	^{Ph}**PO**^{Ph}**-Ni**	0	0.1	110	1200	119	2855	7.8	2.5	1.3	120

[a]Conditions unless specified: catalyst, 0.25 μmol; V(toluene)=5 ml; ethylene pressure=400 psi; polymerization runs were stopped when ethylene uptake reached 80 psi. [b]Activity in 10^3 g/(mol*h). [c]Also included in table S6.3 as entry 18. [d]Also included in table S6.3 as entry 25. [e]Also included in table S6.6 as entry 4. [f]Also included in table S6.6 as entry 14, [Ni]=0.125 μmol .

Table S4.7. Original runs of table 4.4 (PPR).

Entry[a]	catalyst	[Cat.]/ μmol	$Ni(COD)_2$/ Cat.	[tBA]/ M	Time (s)	Yield (mg)	Act.[b]	M_w/ 10^3	PDI	%Mol tBA	Tm (ºC)
1	^{Ph}**PO**^{Ph}**-Ni**	0.25	4	0.05	362	106	4217	7.5	2.3	0.5	121
2	^{Ph}**PO**^{Ph}**-Ni**	0.25	4	0.05	341	108	4561	7.2	2.4	0.6	121
3	^{Ph}**PO**^{Ph}**-Ni**	0.25	4	0.05	403	138	4931	8.6	2.7	0.6	122
4	^{Ph}**PO**^{Ph}**-Ni**	0.25	4	0.1	576	126	3150	6.7	2.4	1.0	119
5	^{Ph}**PO**^{Ph}**-Ni**	0.25	4	0.1	534	121	3263	6.4	2.4	1.1	118
6	^{Ph}**PO**^{Ph}**-Ni**	0.25	4	0.1	584	130	3205	6.3	2.5	1.2	118
7	^{Ph}**PO**^{PhCF3}**-Ni**	0.125	4	0.025	396	105	7636	7.0	2.3	0.3	123
8	^{Ph}**PO**^{PhCF3}**-Ni**	0.125	4	0.025	437	112	7381	11.9	2.4	0.2	123
9	^{Ph}**PO**^{Ph}**-Ni**	0.125	0	0.025	562	116	7229	9.6	2.5	0.4	123
10	^{Ph}**PO**^{Ph}**-Ni**	0.125	0	0.025	510	131	7399	9.9	2.6	0.4	123
11	^{Ph}**PO**^{Ph}**-Ni**	0.125	0	0.025	473	132	8032	9.2	2.5	0.3	123
12	^{Ph}**PO**^{Ph}**-Ni**	0.125	0	0.025	464	133	8259	9.3	2.5	0.5	123
13	^{Ph}**PO**^{Ph}**-Ni**	0.125	0	0.1	1112	117	3029	7.8	2.6	1.4	119
14	^{Ph}**PO**^{Ph}**-Ni**	0.125	0	0.1	1200	119	2855	7.8	2.5	1.3	120

[a]Conditions unless specified: V(toluene)=5 ml; ethylene pressure=400 psi; T= 110 ºC; polymerization runs were stopped when ethylene uptake reached 80 psi. [b]Activity in 10^3 g/(mol*h).

Table S4.8. Original runs of table 4.4 (Batch).

Entry[a]	catalyst	$Ni(COD)_2$/Cat.	tBA/mmol	Time (min)	Yield (g)	Act.[b]	Efficiency[c]	M_w/ 10^3	PDI	%Mol tBA	Tm (ºC)
1	^{Ph}**PO**^{Ph}**-Ni**	0	29.5	26.2	50.1	4954	36900	10.3	2.8	0.3	125
2	^{Ph}**PO**^{Ph}**-Ni**	0	58.5	56.6	50.1	2293	36900	11.1	2.6	0.5	125

[a]Conditions: V(toluene)=550 ml; 23.7 μmol Ni catalyst, ethylene pressure=430 psi; T= 110 ºC; polymerization runs were stopped when ethylene consumption reached 40 g. [b]Activity in 10^3 g/(mol*h). [c]Efficiency in g copolymer/g Ni.

Microstructural analysis of ethylene/tBA copolymers

The following sections summarize methods and results of microstructural analysis. Analysis of the spectra was based on literature.[11, 38]

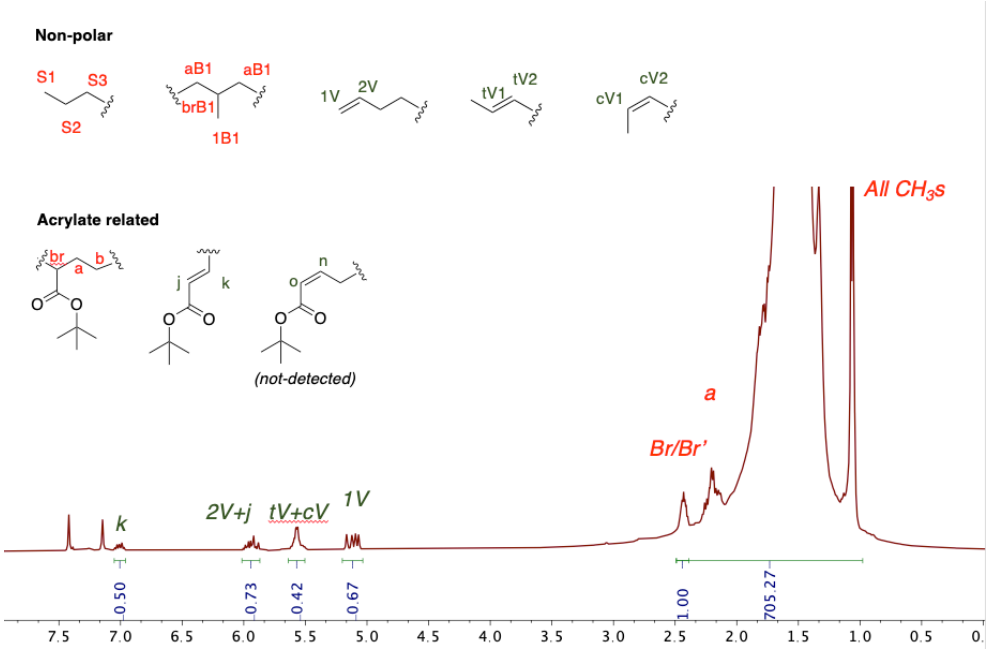

Figure S4.8. A sample ^{1}H NMR spectrum of ethylene/tBA copolymers (C. entry 10, table 2) with peaks assigned to specific microstructural features.

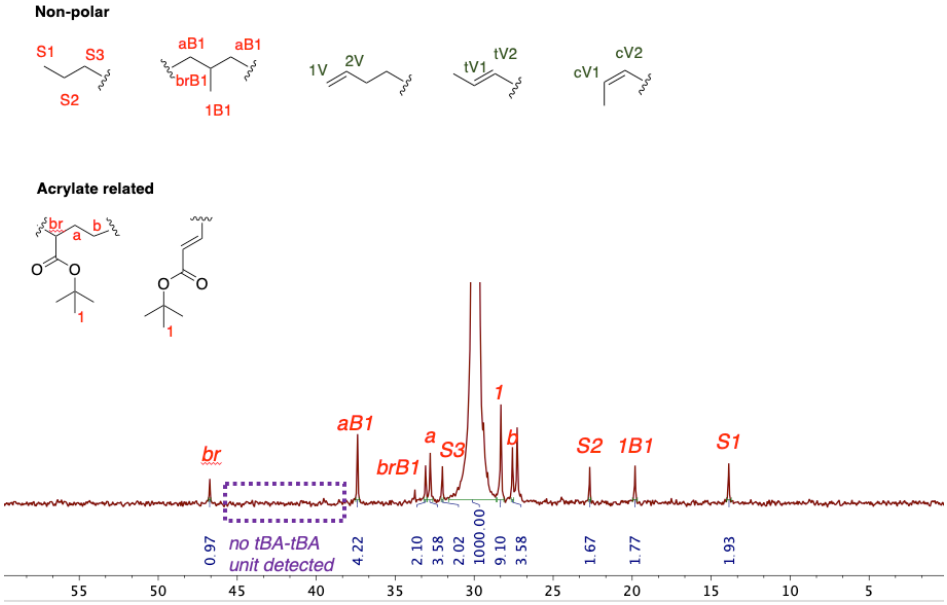

Figure S4.9. A sample $^{13}C\{^{1}H\}$ NMR spectrum of ethylene/tBA copolymers (C, entry 10, table 2) with peaks assigned to specific microstructural features.

Calculation of Mn based on ^{1}H NMR spectra

Mn can be calculated from ^{1}H NMR spectra. Below is an example based on sample **C**.

Note that the integration of br/br' set to 1, therefore all values of integration in ^{1}H NMR spectra are all relevant numbers of protons per occurrence of a tBA units (labeled as rX)

rX = relevant number of carbon atoms

rX-H = relevant number of proton atoms = 705.27+ 0. 67 + 0.42 + 0.73 + 0.5 = 707.59

Each ethylene unit has 2 carbon and 4 protons

For tBA units, each tBA unit has 6 carbon and 12 protons exclude the ester group (-C(O)O-). Note that the relevant number of tBA units is 1 (reference).

Therefore **rX = 0.5 * rX-H + 1**

rC = relevant number of polymer chain

rC = 0.5 * 0.67 + 0.5 * 0.42 + 0.5 = 1.045

M_n = (rX * 12 + rX-H * 1 + 2 * Mol Wt (O))/rC = ((0.5 * rX-H + 1) * 12 + rX-H + 2 * 16)/rC = (7 * 707.59 + 6 + 32)/1.045 = 4.776 ~ 4.8k.

For comparison, the molecular weight obtained by GPC is $M_n = M_w$ / PDI = 10.9k / 2.5 =4.36 k

Methods of microstructural analysis

- **%Mol tBA (NMR):** Calculation of % Mol tBA (NMR) is based on the ^{1}H NMR spectrum and section S7.1.2.

rR = relevant number of repeating units = 0.5 * (rX-4) = 0.25 * rX-H - 1.5

Relevant number of tBA units = 1

% Mol tBA = 1 / rR = 1 / (0.25 * rX-H - 1.5)

For sample **C**, % Mol tBA = 1 / (0.25 * 707.59 - 1.5) = 0.6 %, which is consistent with the result obtained from quantitative FTIR.

- **%I-tBA:** the percentage of internal tBA units over all tBA units. Use sample **C** as an example:

Calculation of **%I-tBA** is based on the $^{13}C\{^{1}H\}$ NMR spectrum. Note that all tBA units have t-butyl group (peak 1) but only internal tBA units have saturated α- and β-carbon (peak a, b).

% I -tBA = (0.5 * Integration of peak b)/(0.333 * Integration of peak 1) = 59%

- **%T-tBA:** the percentage of terminal tBA units over all tBA units.

%T-tBA = 1 - %I-tBA

For sample **C**, **%T-tBA** = 41%

- **%Vinyl:** the ratio of the number of terminal vinyl units over the number of tBA units in percentage, which is calculated based on the ^{1}H NMR spectra and section S7.1.2. Use sample **C** as an example:

rV = relevant number of vinyls = 0.5 * integration of peak 1V

rT-tBA = relevant number of terminal tBA = integration of peak k (if cis-end tBA is not present)

%Vinyl/%T-tBA=rV/rT-tBA

For sample **C**, % Vinyl = 21%

- **%2-Propenyl:** the ratio of the number of 2-propenyl units over the number of tBA units in percentage.

Similar to % Vinyl,

% 2-Propenyl/%T-tBA = (0.5 * integration of peak (TV+CV))/integration of peak k (if cis-end tBA is not present)

For sample **C**, % Vinyl = 17%

- **%HomoPE:** the minimum amount of polyethylene present in the product in percentage. This concept is adopted from literature,[85] with 2-propenyl taken into account.

%HomoPE = (%Vinyl + % Propenyl - % I-tBA)/((%Vinyl + % Propenyl + % T-tBA)

- **N(Methyl):** Calculation of **N(Methyl)** is based on the $^{13}C\{^{1}H\}$ NMR spectrum (unit: 1/1000C).

For sample **C**, **N(Methyl)** = 1000 * 1.77 / (1000 + 3.55 + 3.58 + 2.10 + 3.58 + 1.93 + 1.67 + 2.02) = 1.7

- **N(2-Propenyl):** Calculation of **N(2-Propenyl)** is based on the ^{1}H NMR spectrum (unit: 1/1000C).

N(2-Propenyl) = 1000 * relevant number of propenyl/rX = 1000 * (0.5 * integration of peak (TV+CV)/(0.5 * rX-H + 1)

For sample **C**, **N(2-Propenyl)** = 0.6

7.1.4 Results of microstructural analysis

Copolymer samples **A~E** are Ethylene/tBA copolymers produced in entry 7, 9, 10, 13, 12 of table 2, respectively.

Table S4.10 Lists of catalysts and copolymer samples they produced.

	A	**B**	**C**	**D**	**E**
Catalyst	**^{Me}PO^{Ph}-Ni**	**^{Me}PO^{PhCF3}-Ni**	**^{Ph}PO^{Ph}-Ni**	**^{Ph}PO^{PhCF3}-Ni**	**^{Ph}PO^{Mes}-Ni**
Entries in table 2	7	9	10	13	12

Table S4.11. Comparison of Mw values obtained from GPC and NMR analysis.

	A	**B**	**C**	**D**	**E**
Mn(GPC)/10^3	1.84	1.93	4.36	4.59	3.33
Mn(NMR)/10^3	1.61	2.29	4.76	5.07	3.70

In general, the Mw values obtained from these two methods matches, with errors of 9%~18%.

Table S4.12. Analysis of distributions of tBA units.

	A	B	C	D	E
% I-tBA	61%	48%	59%	52%	71%
% T-tBA	39%	52%	41%	48%	29%
% Vinyl	26%	24%	21%	34%	44%
%2-Propenyl	22%	44%	17%	47%	57%
%HomoPE	0%	2%	0%	0%	0%
Mn(NMR)/10^3	1.61	2.29	4.76	5.07	3.70

Table S4.13. Analysis of non-polar moieties.

	A	B	C	D	E
N(Methyl)[a]	2.7	1.6	1.7	1.1	4.0
N(2-Propenyl)[a]	2.1	1.9	0.6	1.0	1.8

[b]1/1000C.

^{1}H and ^{13}C{^{1}H} spectra of ethylene/tBA copolymers

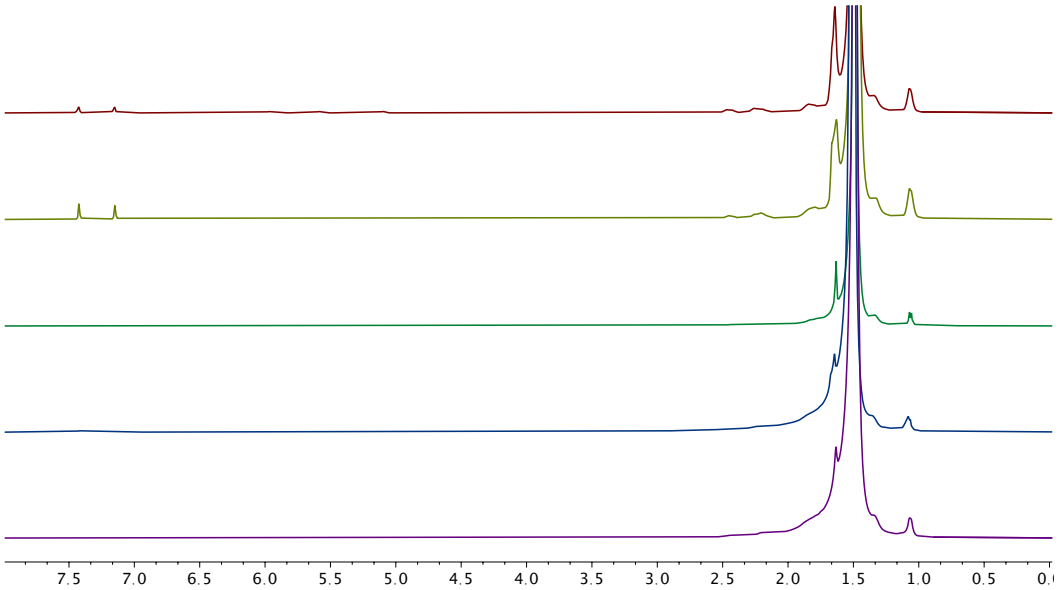

Figure S4.14. ^{1}H NMR spectra of ethylene/tBA copolymer **A~E** (top to bottom).

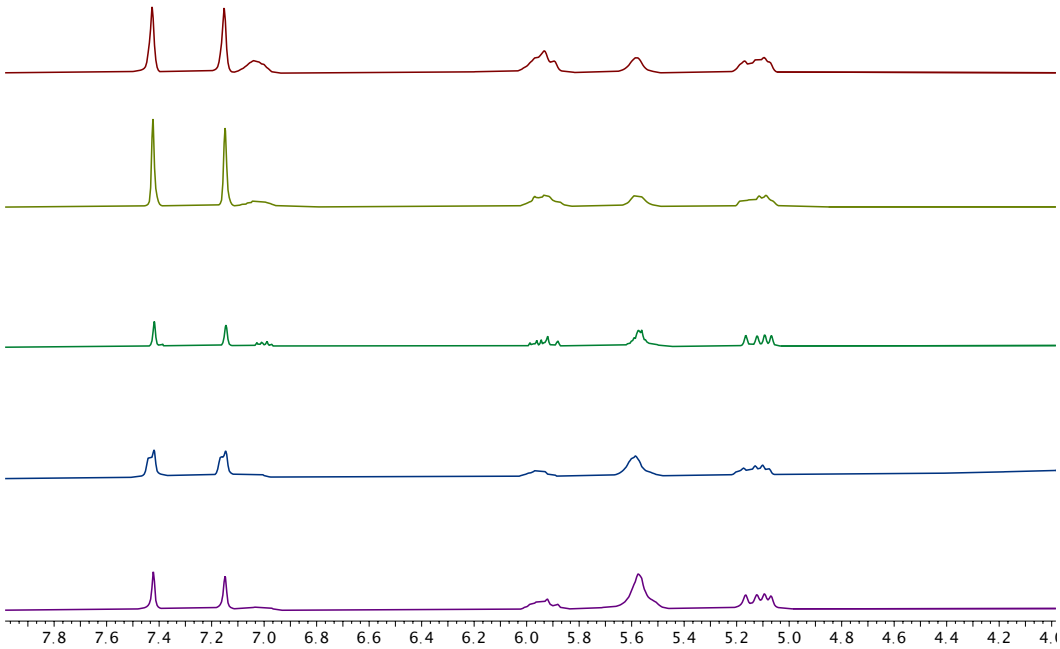

Figure S4.15. ^{1}H NMR spectra of ethylene/tBA copolymer **A~E** (top to bottom, olefinic region).

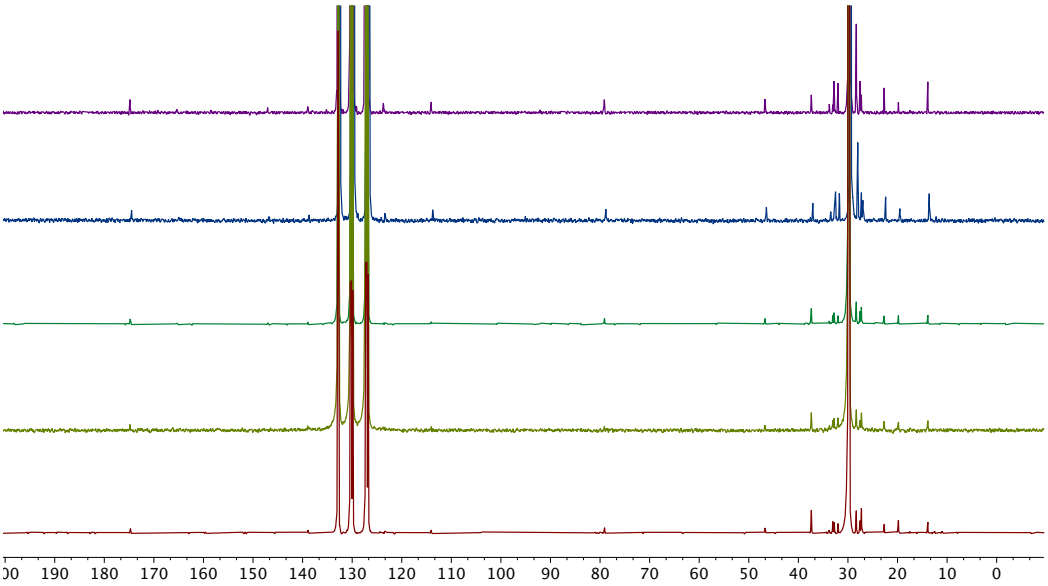

Figure S4.16. ^{13}C{^{1}H} NMR spectra of ethylene/tBA copolymer **A~E** (top to bottom).

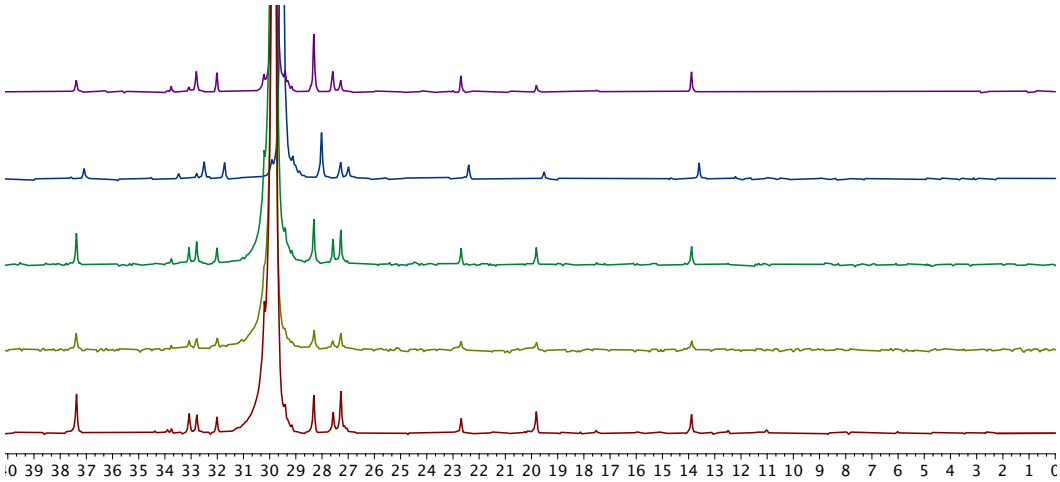

Figure S4.17. Scaled $^{13}C\{^{1}H\}$ NMR spectra of ethylene/tBA copolymer **A~E** (top to bottom, alkyl region).

Samples of GPC curves of homopolyethylene and ethylene/tBA copolymers

MWD Results: Conventional GPC	
Mn	3,550
Mp	8,740
Mv	9,940
Mw	11,430
Mz	31,920
PDI	3.22

Quadrant Analysis		
25%	24430	
50%	10050	0
75%	5180	
100%	1650	
Whole	6720	
50% Ratio	5.05	-60
		271.64

Run Parameters:	
Conc	1.8000
Inj. Vol.	480.0
Mass Inj.	0.8550
MassRec.	95.54%
System Parameters:	
Flow Rate	0.9993
Flow Marker	18.616
Ref Flow Marker	18.629
Rec. Flow Rate	

Comonomer Type	Octene
Avg SCB/1000TC	3.19
Avg Wt% Comonomer	4.09
Avg Corrected Wt%	2.55

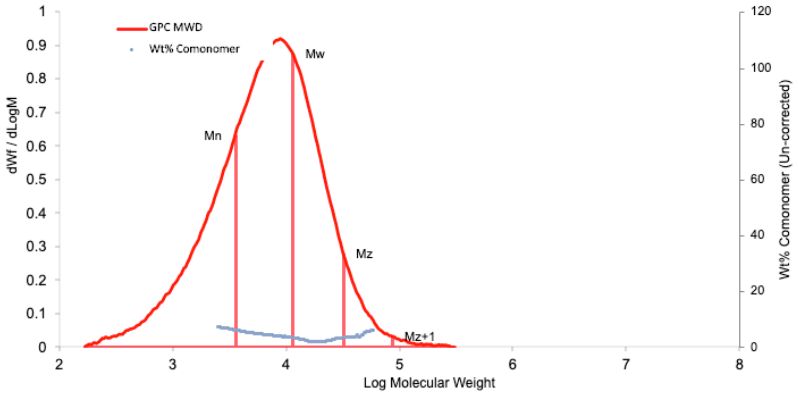

Figure S4.18. GPC curve of homopolyethylene (table S6.2, entry 6).

MWD Results: Conventional GPC		*Quadrant Analysis*			*Run Parameters:*	
Mn	5,190	25%	24480		Conc	1.8000
Mp	10,320	50%	11820	10	Inj. Vol.	480.0
Mv	10,830	75%	6660		Mass Inj.	0.8550
Mw	11,880	100%	2490		MassRec.	99.71%
Mz	21,550	Whole	8230		*System Parameters:*	
PDI	2.29	50% Ratio	3.97	-60	Flow Rate	0.9945
				271.64	Flow Marker	18.616
Comonomer Type	Octene				Ref Flow Marker	18.719
Avg SCB/1000TC	7.3				Rec. Flow Rate	
Avg Wt% Comonomer	7.26					
Avg Corrected Wt%	5.84					

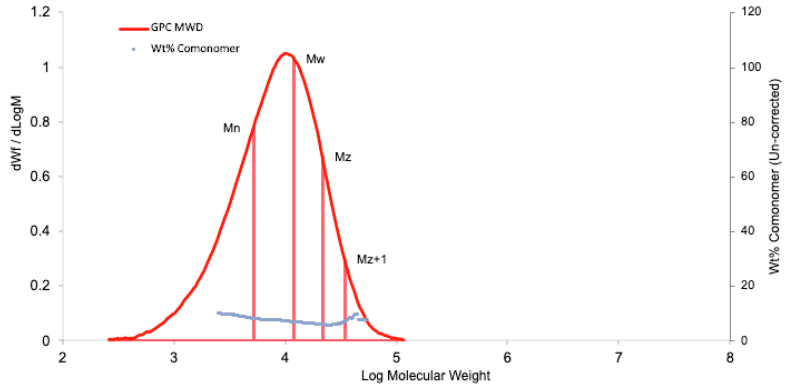

Figure S4.19. GPC curve of ethylene/tBA copolymers (table S6.3, entry 24).

Catalyst comparison

The catalysts reported here are notable for high activity and thermal stability for polar polyolefin synthesis. A variety of catalysts have been developed for ethylene/acrylate copolymerization.[11-13, 15-17, 22-24, 29, 32, 38, 41-42, 47, 49, 51, 61, 63, 81, 83, 85, 100-149] Previous examples of nickel catalyzed ethylene acrylate copolymerization are relatively rare, with the majority supported by phenoxide/napthoxide-based ligands. [10-11, 16, 29, 38, 83, 85, 102] To compare the performance of our best catalyst, **^{Ph}PO^{Ph}-Ni** to prior examples, two metrics were ploted: catalyst activity and optimized reaction temperature (Figure S8.1). Previously reported ethylene/acrylate copolymerization experiments were included if they feature: 1) activity > 0.5 kg/(mol*h) and 2) copolymer Mw>2500. In addition, experiments are excluded if they were performed with large amounts of activator/masking reagents on a scale comparable to the amount of acrylate (additives:acrylates > 1:10). Overall, experiments under 468 different reaction conditions, or 229

different catalysts, from 75 scientific papers are included in catalyst comparison.[11-13, 15-17, 22-24, 29, 32, 38, 41-42, 47, 49, 51, 61, 63, 81, 83, 85, 100-149] Reaction conditions, such the ethylene pressure, catalyst and monomer concentration, may differ, therefore these comparisons should be considered qualitative.

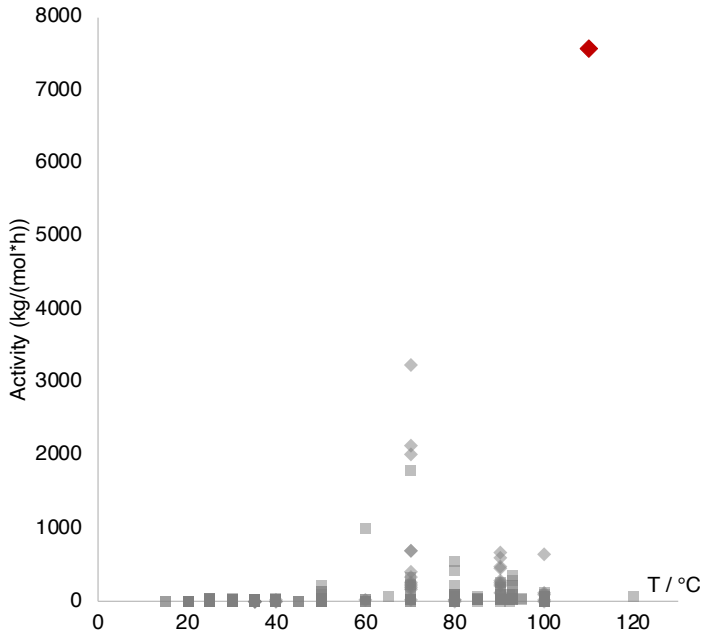

Figure S4.20. Comparison of ^{Ph}**PO**^{Ph}**-Ni** (red diamond) with reported Pd and Ni catalysts for ethylene/acrylate copolymerization (half-transparent diamonds: acrylate = tBA; half-transparent square: other acrylates were used; darker color indicates overlapping data points; reported catalysts are included if they: 1) shows activity higher than 0.5 kg/(mol*h) in ethylene acrylate copolymerization and 2) produce copolymers with Mw>2500).

Overall, most examples show limited activities of less than 100 kg/(mol·h) (423 out of 468 experiments, or 200 out of 229 catalysts) , though being able to produce copolymers with varying molecular weights, branching distribution and polar monomer incorporation. An important aspect to consider is that increased acrylate incorporation will result in lower activity, which affects some of the systems compared. Many palladium catalysts are able to produce polar polyethylene at relatively high temperatures. Notably, several recent developed nickel and palladium catalysts show remarkably improved activity at elevated temperatures (70~90 ºC). As

shown in figure 8, the highest activity was observed at 70 ºC. Only one of these reports describes a palladium example with operation temperature >100 ºC though the activity is relatively low (63 kg/(mol·h)).[128] As shown in figure S4.20, $^{Ph}PO^{Ph}$-Ni displays significant improved activity at elevated temperatures compared to previous reports.

REFERENCES

(1) Chen, C., Designing catalysts for olefin polymerization and copolymerization: beyond electronic and steric tuning. *Nat. Rev. Chem.* **2018,** *2* (5), 6-14.

(2) Hustad, P. D., Frontiers in olefin polymerization: Reinventing the world's most common synthetic polymers. *Science* **2009,** *325* (5941), 704-707.

(3) Boffa, L. S.; Novak, B. M., Copolymerization of polar monomers with olefins using transition-metal complexes. *Chem. Rev.* **2000,** *100* (4), 1479-1494.

(4) Franssen, N. M.; Reek, J. N.; de Bruin, B., Synthesis of functional 'polyolefins': state of the art and remaining challenges. *Chem. Soc. Rev.* **2013,** *42* (13), 5809-5832.

(5) Zou, C.; Chen, C., Polar-functionalized, crosslinkable, self-healing, and photoresponsive polyolefins. *Angew. Chem. Int. Ed* **2020,** *59* (1), 395-402.

(6) Baur, M.; Lin, F.; Morgen, T. O.; Odenwald, L.; Mecking, S., Polyethylene materials with in-chain ketones from nonalternating catalytic copolymerization. *Science* **2021,** *374* (6567), 604-607.

(7) Nakamura, A.; Ito, S.; Nozaki, K., Coordination− insertion copolymerization of fundamental polar monomers. *Chem. Rev.* **2009,** *109* (11), 5215-5244.

(8) Johnson, L. K.; Killian, C. M.; Brookhart, M., New Pd (II)-and Ni (II)-based catalysts for polymerization of ethylene and. alpha.-olefins. *J. Am. Chem. Soc.* **1995,** *117* (23), 6414-6415.

(9) Younkin, T. R.; Connor, E. F.; Henderson, J. I.; Friedrich, S. K.; Grubbs, R. H.; Bansleben, D. A., Neutral, single-component nickel (II) polyolefin catalysts that tolerate heteroatoms. *Science* **2000,** *287* (5452), 460-462.

(10) Liang, T.; Goudari, S. B.; Chen, C., A simple and versatile nickel platform for the generation of branched high molecular weight polyolefins. *Nat. Commun.* **2020,** *11* (1), 1-8.

(11) Xin, B. S.; Sato, N.; Tanna, A.; Oishi, Y.; Konishi, Y.; Shimizu, F., Nickel catalyzed copolymerization of ethylene and alkyl acrylates. *J. Am. Chem. Soc.* **2017,** *139* (10), 3611-3614.

(12) Nakano, R.; Nozaki, K., Copolymerization of propylene and polar monomers using Pd/IzQO catalysts. *J. Am. Chem. Soc.* **2015,** *137* (34), 10934-10937.

(13) Tao, W. j.; Nakano, R.; Ito, S.; Nozaki, K., Copolymerization of ethylene and polar monomers by using Ni/IzQO catalysts. *Angew. Chem. Int. Ed.* **2016,** *55* (8), 2835-2839.

(14) Carrow, B. P.; Nozaki, K., Synthesis of functional polyolefins using cationic bisphosphine monoxide–palladium complexes. *J. Am. Chem. Soc.* **2012,** *134* (21), 8802-8805.

(15) Zhang, W.; Waddell, P. M.; Tiedemann, M. A.; Padilla, C. E.; Mei, J.; Chen, L.; Carrow, B. P., Electron-rich metal cations enable synthesis of high molecular weight, linear functional polyethylenes. *J. Am. Chem. Soc.* **2018,** *140* (28), 8841-8850.

(16) Chen, M.; Chen, C., A Versatile Ligand Platform for Palladium-and Nickel-Catalyzed Ethylene Copolymerization with Polar Monomers. *Angew. Chem. Int. Ed.* **2018,** *57* (12), 3094-3098.

(17) Drent, E.; van Dijk, R.; van Ginkel, R.; van Oort, B.; Pugh, R. I., Palladium catalysed copolymerisation of ethene with alkylacrylates: polar comonomer built into the linear polymer chain. *Chem. Commun.* **2002,** (7), 744-745.

(18) Nakamura, A.; Anselment, T. M.; Claverie, J.; Goodall, B.; Jordan, R. F.; Mecking, S.; Rieger, B.; Sen, A.; Van Leeuwen, P. W.; Nozaki, K., Ortho-phosphinobenzenesulfonate: A superb ligand for palladium-catalyzed coordination–insertion copolymerization of polar vinyl monomers. *Acc. Chem. Res.* **2013,** *46* (7), 1438-1449.

(19) Chen, Z.; Brookhart, M., Exploring ethylene/polar vinyl monomer copolymerizations using Ni and Pd α-diimine catalysts. *Acc. Chem. Res.* **2018,** *51* (8), 1831-1839.

(20) Mu, H.; Pan, L.; Song, D.; Li, Y., Neutral nickel catalysts for olefin homo-and copolymerization: relationships between catalyst structures and catalytic properties. *Chem. Rev.* **2015,** *115* (22), 12091-12137.

(21) Carrow, B. P.; Nozaki, K., Transition-metal-catalyzed functional polyolefin synthesis: effecting control through chelating ancillary ligand design and mechanistic insights. *Macromolecules* **2014,** *47* (8), 2541-2555.

(22) Alberoni, C.; D'Alterio, M. C.; Balducci, G.; Immirzi, B.; Polentarutti, M.; Pellecchia, C.; Milani, B., Tunable "In-Chain" and "At the End of the Branches" Methyl Acrylate Incorporation in the Polyolefin Skeleton through Pd (II) Catalysis. *ACS Catal.* **2022,** *12* (6), 3430-3443.

(23) Ge, Y.; Li, S.; Wang, H.; Dai, S., Synthesis of Branched Polyethylene and Ethylene-MA Copolymers Using Unsymmetrical Iminopyridyl Nickel and Palladium Complexes. *Organometallics* **2021,** *40* (17), 3033-3041.

(24) Cui, L.; Jian, Z., A N-bridged strategy enables hemilabile phosphine–carbonyl palladium and nickel catalysts to mediate ethylene polymerization and copolymerization with polar vinyl monomers. *Polym. Chem* **2020,** *11* (38), 6187-6193.

(25) Tan, C.; Zou, C.; Chen, C., Material Properties of Functional Polyethylenes from Transition-Metal-Catalyzed Ethylene–Polar Monomer Copolymerization. *Macromolecules* **2022**.

(26) Mu, H.; Zhou, G.; Hu, X.; Jian, Z., Recent advances in nickel mediated copolymerization of olefin with polar monomers. *Coor. Chem. Rev.* **2021,** *435*, 213802.

(27) Xie, T.; McAuley, K. B.; Hsu, J. C.; Bacon, D. W., Gas phase ethylene polymerization: Production processes, polymer properties, and reactor modeling. *Ind. & Eng. Chem. Res.* **1994,** *33* (3), 449-479.

(28) Waltman, A. W.; Younkin, T. R.; Grubbs, R. H., Insights into the deactivation of neutral nickel ethylene polymerization catalysts in the presence of functionalized olefins. *Organometallics* **2004,** *23* (22), 5121-5123.

(29) Zhang, Y.; Mu, H.; Pan, L.; Wang, X.; Li, Y., Robust bulky [P, O] neutral nickel catalysts for copolymerization of ethylene with polar vinyl monomers. *ACS Catal.* **2018,** *8* (7), 5963-5976.

(30) Baier, M. C.; Zuideveld, M. A.; Mecking, S., Post-metallocenes in the industrial production of polyolefins. *Angew. Chem. Int. Ed.* **2014,** *53* (37), 9722-9744.

(31) Rhinehart, J. L.; Brown, L. A.; Long, B. K., A robust Ni (II) α-diimine catalyst for high temperature ethylene polymerization. *J. Am. Chem. Soc.* **2013,** *135* (44), 16316-16319.

(32) Dai, S.; Sui, X.; Chen, C., Highly Robust Palladium (II) α-Diimine Catalysts for Slow-Chain-Walking Polymerization of Ethylene and Copolymerization with Methyl Acrylate. *Angew. Chem. Int. Ed.* **2015,** *54* (34), 9948-9953.

(33) Long, B. K.; Eagan, J. M.; Mulzer, M.; Coates, G. W., Semi-Crystalline Polar Polyethylene: Ester-Functionalized Linear Polyolefins Enabled by a Functional-Group-Tolerant, Cationic Nickel Catalyst. *Angew. Chem. Int. Ed* **2016,** *55* (25), 7106-7110.

(34) Fu, X.; Zhang, L.; Tanaka, R.; Shiono, T.; Cai, Z., Highly robust nickel catalysts containing anilinonaphthoquinone ligand for copolymerization of ethylene and polar monomers. *Macromolecules* **2017,** *50* (23), 9216-9221.

(35) Zhang, H.; Zou, C.; Zhao, H.; Cai, Z.; Chen, C., Hydrogen-Bonding-Induced Heterogenization of Nickel and Palladium Catalysts for Copolymerization of Ethylene with Polar Monomers. *Angew. Chem.* **2021**.

(36) Takeuchi, D.; Chiba, Y.; Takano, S.; Osakada, K., Double-Decker-Type Dinuclear Nickel Catalyst for Olefin Polymerization: Efficient Incorporation of Functional Co-monomers. *Angew. Chem. Int. Ed* **2013,** *52* (48), 12536-12540.

(37) Tan, C.; Chen, C., Emerging palladium and nickel catalysts for copolymerization of olefins with polar monomers. *Angew. Chem.* **2019,** *131* (22), 7268-7276.

(38) Xiong, S.; Shoshani, M. M.; Zhang, X.; Spinney, H. A.; Nett, A. J.; Henderson, B. S.; Miller III, T. F.; Agapie, T., Efficient Copolymerization of Acrylate and Ethylene with Neutral P, O-Chelated Nickel Catalysts: Mechanistic Investigations of Monomer Insertion and Chelate Formation. *J. Amer. Chem. Soc.* **2021,** *143* (17), 6516-6527.

(39) Wang, X.-l.; Zhang, Y.-p.; Wang, F.; Pan, L.; Wang, B.; Li, Y.-s., Robust and Reactive Neutral Nickel Catalysts for Ethylene Polymerization and Copolymerization with a Challenging 1,1-Disubstituted Difunctional Polar Monomer. *ACS Catal.* **2021,** *11* (5), 2902-2911.

(40) Zhang, Y.; Jian, Z., 2-Phosphine-pyridine-N-oxide palladium and nickel catalysts for ethylene polymerization

and copolymerization with polar monomers. *Polymer* **2020**, 122410.

(41) Li, M.; Wang, X.; Luo, Y.; Chen, C., A Second-Coordination-Sphere Strategy to Modulate Nickel-and Palladium-Catalyzed Olefin Polymerization and Copolymerization. *Angew. Chem. Int. Ed.* **2017,** *56* (38), 11604-11609.

(42) Zhang, D.; Chen, C., Influence of Polyethylene Glycol Unit on Palladium-and Nickel-Catalyzed Ethylene Polymerization and Copolymerization. *Angew. Chem. Int. Ed.* **2017,** *56* (46), 14672-14676.

(43) Chen, M.; Chen, C., Rational design of high-performance phosphine sulfonate nickel catalysts for ethylene polymerization and copolymerization with polar monomers. *ACS Catal.* **2017,** *7* (2), 1308-1312.

(44) Wang, X.-l.; Zhang, Y.-p.; Wang, F.; Pan, L.; Wang, B.; Li, Y.-s., Robust and Reactive Neutral Nickel Catalysts for Ethylene Polymerization and Copolymerization with a Challenging 1, 1-Disubstituted Difunctional Polar Monomer. *ACS Catal.* **2021,** *11* (5), 2902-2911.

(45) Xiao, D.; Cai, Z.; Do, L. H., Accelerating ethylene polymerization using secondary metal ions in tetrahydrofuran. *Dalton Trans* **2019,** *48* (48), 17887-17897.

(46) Zhang, Y.; Wang, C.; Mecking, S.; Jian, Z., Ultrahighly Branched Main-Chain-Functionalized Polyethylenes via Inverted Insertion Selectivity. *Angew. Chem. Int. Ed.* **2020**.

(47) Yang, B.; Xiong, S.; Chen, C., Manipulation of polymer branching density in phosphine-sulfonate palladium and nickel catalyzed ethylene polymerization. *Polym. Chem* **2017,** *8* (40), 6272-6276.

(48) Jung, J.; Yasuda, H.; Nozaki, K., Copolymerization of Nonpolar Olefins and Allyl Acetate Using Nickel Catalysts Bearing a Methylene-Bridged Bisphosphine Monoxide Ligand. *Macromolecules* **2020,** *53* (7), 2547-2556.

(49) Li, K.; Ye, J.; Wang, Z.; Mu, H.; Jian, Z., Indole-bridged bisphosphine-monoxide palladium catalysts for ethylene polymerization and copolymerization with polar monomers. *Polym. Chem* **2020**.

(50) Gao, J.; Yang, B.; Chen, C., Sterics versus electronics: Imine/phosphine-oxide-based nickel catalysts for ethylene polymerization and copolymerization. *J. Catal.* **2019,** *369*, 233-238.

(51) Zhu, N.; Liang, T.; Huang, Y.; Pang, W.; Chen, M.; Tan, C., Influences of ligand backbone substituents on phosphinecarbonylpalladium and-nickel catalysts for ethylene polymerization and copolymerization with polar monomers. *Inorg. Chem.* **2021,** *60* (17), 13080-13090.

(52) Keim, W., Oligomerization of Ethylene to α-Olefins: Discovery and Development of the Shell Higher Olefin Process (SHOP). *Angew. Chem. Int. Ed* **2013,** *52* (48), 12492-12496.

(53) Starzewski, K. A. O.; Witte, J., Highly Active Ylide-Nickel Catalysts for the Polymerization of Ethylene. *Angewandte Chemie International Edition in English* **1985,** *24* (7), 599-601.

(54) Pietsch, J.; Braunstein, P.; Chauvin, Y., Nickel phenyl complexes with chelating κ 2-P, O ligands as catalysts for the oligomerization of ethylene into linear α-olefins. *New Journal of Chemistry* **1998,** *22* (5), 467-472.

(55) Gibson, V. C.; Tomov, A.; White, A. J.; Williams, D. J., The effect of bulky substituents on the olefin polymerisation behaviour of nickel catalysts bearing [P, O] chelate ligands. *Chem. Commun.* **2001,** (8), 719-720.

(56) Heinicke, J.; Köhler, M.; Peulecke, N.; Keim, W., The impact of P substituents on the oligomerization of ethylene with nickel 2-diphenyl and 2-dicyclohexylphosphinophenolate phosphine catalysts. *J. Catal.* **2004,** *225* (1), 16-23.

(57) Kuhn, P.; Sémeril, D.; Matt, D.; Chetcuti, M. J.; Lutz, P., Structure–reactivity relationships in SHOP-type complexes: tunable catalysts for the oligomerisation and polymerisation of ethylene. *Dalton Trans* **2007,** (5), 515-528.

(58) Wan, D.-W.; Gao, Y.-S.; Li, J.-F.; Shen, Q.; Sun, X.-L.; Tang, Y., Synthesis, structure, and ethylene polymerization behavior of nickel complexes based on benzoylmethylenetri (2-alkoxylphenyl) phosphorane. *Dalton Trans* **2012,** *41* (15), 4552-4557.

(59) Klabunde, U.; Mulhaupt, R.; Herskovitz, T.; Janowicz, A.; Calabrese, J.; Ittel, S., Ethylene homopolymerization with P, O-chelated nickel catalysts. *J. Polym. Sci., Part A: Polym. Chem* **1987,** *25* (7), 1989-2003.

(60) Klabunde, U.; Itten, S. D., Nickel catalysis for ethylene homo-and co-polymerization. *Journal of Molecular Catalysis* **1987,** *41* (1-2), 123-134.

(61) Dai, S.; Chen, C., Direct synthesis of functionalized high-molecular-weight polyethylene by copolymerization of ethylene with polar monomers. *Angew. Chem. Int. Ed.* **2016,** *55* (42), 13281-13285.

(62) Tran, Q. H.; Brookhart, M.; Daugulis, O., New neutral nickel and palladium sandwich catalysts: synthesis of ultra-high molecular weight polyethylene (UHMWPE) via highly controlled polymerization and mechanistic studies of chain propagation. *J. Amer. Chem. Soc.* **2020,** *142* (15), 7198-7206.

(63) Ota, Y.; Ito, S.; Kuroda, J.-i.; Okumura, Y.; Nozaki, K., Quantification of the steric influence of alkylphosphine–sulfonate ligands on polymerization, leading to high-molecular-weight copolymers of ethylene and polar monomers. *J. Am. Chem. Soc.* **2014,** *136* (34), 11898-11901.

(64) Noda, S.; Nakamura, A.; Kochi, T.; Chung, L. W.; Morokuma, K.; Nozaki, K., Mechanistic studies on the formation of linear polyethylene chain catalyzed by palladium phosphine− sulfonate complexes: experiment and theoretical studies. *J. Am. Chem. Soc.* **2009,** *131* (39), 14088-14100.

(65) Wang, C.; Kang, X.; Dai, S.; Cui, F.; Li, Y.; Mu, H.; Mecking, S.; Jian, Z., Efficient Suppression of Chain Transfer and Branching via Cs-Type Shielding in a Neutral Nickel(II) Catalyst. *Angew. Chem. Int. Ed.* **2021,** *60* (8), 4018-4022.

(66) Li, K.; Mu, H.; Kang, X.; Jian, Z., Suppression of Chain Transfer and Promotion of Chain Propagation in Neutral Anilinotropone Nickel Polymerization Catalysis. *Macromolecules* **2022**.

(67) Radlauer, M. R.; Day, M. W.; Agapie, T., Bimetallic effects on ethylene polymerization in the presence of amines: Inhibition of the deactivation by lewis bases. *J. Amer. Chem. Soc.* **2012,** *134* (3), 1478-1481.

(68) Fryzuk, M. D.; Gao, X.; Rettig, S. J., Coordination chemistry of a mixed donor bidentate ligand with nickel. A tetrameric enolate of sodium that binds a phosphine donor. *Canadian journal of chemistry* **1995,** *73* (7), 1175-1180.

(69) Bouaoud, S. E.; Braunstein, P.; Grandjean, D.; Matt, D.; Nobel, D., Complexes of functional phosphines. 10. Palladium complexes with the ligands (diphenylphosphino) acetophenone,(Ph2PCHCOPh)-and Ph2PCHC (Ph) OPPh2. Crystal and molecular structure of cis-[PdCl2 {Ph2PCH: C (Ph) OPPh2}]. *Inorg. Chem.* **1986,** *25* (21), 3765-3770.

(70) Braunstein, P.; Chauvin, Y.; Nähring, J.; DeCian, A.; Fischer, J.; Tiripicchio, A.; Ugozzoli, F., Rhodium (I) and iridium (I) complexes with β-Keto phosphine or phosphino enolate ligands. Catalytic transfer dehydrogenation of cyclooctane. *Organometallics* **1996,** *15* (26), 5551-5567.

(71) Agostinho, M.; Rosa, V.; Avilés, T.; Welter, R.; Braunstein, P., Synthesis and characterization of Co and Ni complexes stabilized by keto-and acetamide-derived P, O-type phosphine ligands. *Dalton Trans* **2009,** (5), 814-822.

(72) Falivene, L.; Credendino, R.; Poater, A.; Petta, A.; Serra, L.; Oliva, R.; Scarano, V.; Cavallo, L., SambVca 2. A web tool for analyzing catalytic pockets with topographic steric maps. *Organometallics* **2016,** *35* (13), 2286-2293.

(73) Falivene, L.; Cao, Z.; Petta, A.; Serra, L.; Poater, A.; Oliva, R.; Scarano, V.; Cavallo, L., Towards the online computer-aided design of catalytic pockets. *Nat. Chem.* **2019,** *11* (10), 872-879.

(74) Poater, A.; Cosenza, B.; Correa, A.; Giudice, S.; Ragone, F.; Scarano, V.; Cavallo, L., SambVca: A web application for the calculation of the buried volume of N-heterocyclic carbene ligands. Wiley Online Library: 2009.

(75) Ragone, F.; Poater, A.; Cavallo, L., Flexibility of N-heterocyclic carbene ligands in ruthenium complexes relevant to olefin metathesis and their impact in the first coordination sphere of the metal. *J. Am. Chem. Soc.* **2010,** *132* (12), 4249-4258.

(76) Camacho, D. H.; Salo, E. V.; Ziller, J. W.; Guan, Z., Cyclophane-based highly active late-transition-metal catalysts for ethylene polymerization. *Angew. Chem. Int. Ed* **2004,** *43* (14), 1821-1825.

(77) Chen, Z.; Mesgar, M.; White, P. S.; Daugulis, O.; Brookhart, M., Synthesis of branched ultrahigh-molecular-weight polyethylene using highly active neutral, single-component Ni (II) catalysts. *ACS Catal.* **2015,** *5* (2), 631-636.

(78) Tran, Q. H.; Wang, X.; Brookhart, M.; Daugulis, O., Cationic α-Diimine Nickel and Palladium Complexes Incorporating Phenanthrene Substituents: Highly Active Ethylene Polymerization Catalysts and Mechanistic Studies of syn/anti Isomerization. *Organometallics* **2020**.

(79) Wang, C.; Kang, X.; Dai, S.; Cui, F.; Li, Y.; Mu, H.; Mecking, S.; Jian, Z., Efficient Suppression of Chain Transfer and Branching via Cs-Type Shielding in a Neutral Nickel (II) Catalyst. *Angew. Chem. Int. Ed* **2021,** *60* (8), 4018-4022.

(80) Schiebel, E.; Voccia, M.; Falivene, L.; Göttker-Schnetmann, I.; Caporaso, L.; Mecking, S., Neutral Unsymmetrical Coordinated Cyclophane Polymerization Catalysts. *Angew. Chem. Int. Ed* **2021**.

(81) Liu, Y. S.; Harth, E., Distorted Sandwich α-Diimine PdII Catalyst: Linear Polyethylene and Synthesis of Ethylene/Acrylate Elastomers. *Angew. Chem. Int. Ed* **2021**.

(82) Radlauer, M. R.; Day, M. W.; Agapie, T., Dinickel bisphenoxyiminato complexes for the polymerization of ethylene and α-olefins. *Organometallics* **2012,** *31* (6), 2231-2243.

(83) Tahmouresilerd, B.; Xiao, D.; Do, L. H., Rigidifying Cation-Tunable Nickel Catalysts Increases Activity and Polar Monomer Incorporation in Ethylene and Methyl Acrylate Copolymerization. *Inorg. Chem.* **2021**.

(84) Ittel, S. D.; Johnson, L. K.; Brookhart, M., Late-metal catalysts for ethylene homo-and copolymerization. *Chem. Rev.* **2000,** *100* (4), 1169-1204.

(85) Wang, X.-l.; Zhang, Y.-p.; Wang, F.; Pan, L.; Wang, B.; Li, Y.-s., Robust and Reactive Neutral Nickel Catalysts for Ethylene Polymerization and Copolymerization with a Challenging 1,1-Disubstituted Difunctional Polar Monomer. *ACS Catal.* **2021**, 2902-2911.

(86) Zhang, Y.; Kang, X.; Jian, Z., Selective branch formation in ethylene polymerization to access precise ethylene-propylene copolymers. *Nat. Commun.* **2022,** *13* (1), 1-9.

(87) Berkefeld, A.; Drexler, M.; Möller, H. M.; Mecking, S., Mechanistic insights on the copolymerization of polar vinyl monomers with neutral Ni (II) catalysts. *J. Amer. Chem. Soc.* **2009,** *131* (35), 12613-12622.

(88) Guironnet, D.; Roesle, P.; Rünzi, T.; Göttker-Schnetmann, I.; Mecking, S., Insertion polymerization of acrylate. *J. Amer. Chem. Soc.* **2009,** *131* (2), 422-423.

(89) Foley, S. R.; Stockland, R. A.; Shen, H.; Jordan, R. F., Reaction of vinyl chloride with late transition metal olefin polymerization catalysts. *J. Amer. Chem. Soc.* **2003,** *125* (14), 4350-4361.

(90) Mariott, W. R.; Rodriguez-Delgado, A.; Chen, E. Y.-X., Chain termination and transfer reactions in the acrylate polymerization by a monometallic chiral zirconocenium catalyst system. *Macromolecules* **2006,** *39* (4), 1318-1327.

(91) Chen, C.; Jordan, R. F., Palladium-catalyzed dimerization of vinyl ethers to acetals. *J. Amer. Chem. Soc.* **2010,** *132* (30), 10254-10255.

(92) Ölscher, F.; Göttker-Schnetmann, I.; Monteil, V.; Mecking, S., Role of Radical Species in Salicylaldiminato Ni (II) Mediated Polymer Chain Growth: A Case Study for the Migratory Insertion Polymerization of Ethylene in the Presence of Methyl Methacrylate. *J. Am. Chem. Soc.* **2015,** *137* (46), 14819-14828.

(93) Mecking, S., Olefin polymerization by late transition metal complexes—a root of Ziegler catalysts gains new ground. *Angew. Chem. Int. Ed* **2001,** *40* (3), 534-540.

(94) Nakano, R.; Chung, L. W.; Watanabe, Y.; Okuno, Y.; Okumura, Y.; Ito, S.; Morokuma, K.; Nozaki, K., Elucidating the key role of phosphine− sulfonate ligands in palladium-catalyzed ethylene polymerization: Effect of ligand structure on the molecular weight and linearity of polyethylene. *ACS Catal.* **2016,** *6* (9), 6101-6113.

(95) Mecking, S.; Johnson, L. K.; Wang, L.; Brookhart, M., Mechanistic studies of the palladium-catalyzed copolymerization of ethylene and α-olefins with methyl acrylate. *J. Amer. Chem. Soc.* **1998,** *120* (5), 888-899.

(96) Deng, L.; Woo, T. K.; Cavallo, L.; Margl, P. M.; Ziegler, T., The role of bulky substituents in Brookhart-type Ni (II) diimine catalyzed olefin polymerization: a combined density functional theory and molecular mechanics study. *J. Amer. Chem. Soc.* **1997,** *119* (26), 6177-6186.

(97) Neuwald, B.; Caporaso, L.; Cavallo, L.; Mecking, S., Concepts for stereoselective acrylate insertion. *J. Am. Chem. Soc.* **2013,** *135* (3), 1026-1036.

(98) Klabunde, U.; Tulip, T.; Roe, D.; Ittel, S., Reaction of nickel polymerization catalysts with carbon monoxide. *J. Organomet. Chem.* **1987,** *334* (1-2), 141-156.

(99) Falsini, M.; Catarzi, D.; Varano, F.; Ceni, C.; Dal Ben, D.; Marucci, G.; Buccioni, M.; Volpini, R.; Di Cesare Mannelli, L.; Lucarini, E., Antioxidant-conjugated 1, 2, 4-triazolo [4, 3-a] pyrazin-3-one derivatives: Highly potent and selective human A2A adenosine receptor antagonists possessing protective efficacy in neuropathic pain. *Journal of medicinal chemistry* **2019,** *62* (18), 8511-8531.

(100) Johnson, L. K.; Mecking, S.; Brookhart, M., Copolymerization of ethylene and propylene with functionalized

vinyl monomers by palladium (II) catalysts. *J. Am. Chem. Soc.* **1996,** *118* (1), 267-268.

(101) Takano, S.; Takeuchi, D.; Osakada, K.; Akamatsu, N.; Shishido, A., Dipalladium catalyst for olefin polymerization: Introduction of acrylate units into the main chain of branched polyethylene. *Angew. Chem. Int. Ed.* **2014,** *53* (35), 9246-9250.

(102) Zhang, Y.; Mu, H.; Wang, X.; Pan, L.; Li, Y., Elaborate tuning in ligand makes a big difference in catalytic performance: bulky nickel catalysts for (co) polymerization of ethylene with promising vinyl polar monomers. *ChemCatChem* **2019,** *11* (9), 2329-2340.

(103) Saki, Z.; D'Auria, I.; Dall'Anese, A.; Milani, B.; Pellecchia, C., Copolymerization of Ethylene and Methyl Acrylate by Pyridylimino Ni (II) Catalysts Affording Hyperbranched Poly (ethylene-co-methyl acrylate) s with Tunable Structures of the Ester Groups. *Macromolecules* **2020,** *53* (21), 9294-9305.

(104) Ye, J.; Mu, H.; Wang, Z.; Jian, Z., Heteroaryl backbone strategy in bisphosphine monoxide palladium-catalyzed ethylene polymerization and copolymerization with polar monomers. *Organometallics* **2019,** *38* (15), 2990-2997.

(105) Zou, C.; Liao, D.; Pang, W.; Chen, M.; Tan, C., Versatile PNPO ligands for palladium and nickel catalyzed ethylene polymerization and copolymerization with polar monomers. *J. Catal.* **2021,** *393*, 281-289.

(106) Jenkins, J. C.; Brookhart, M., A mechanistic investigation of the polymerization of ethylene catalyzed by neutral Ni (II) complexes derived from bulky anilinotropone ligands. *J. Am. Chem. Soc.* **2004,** *126* (18), 5827-5842.

(107) Popeney, C. S.; Camacho, D. H.; Guan, Z., Efficient incorporation of polar comonomers in copolymerizations with ethylene using a cyclophane-based Pd (II) α-diimine catalyst. *J. Am. Chem. Soc.* **2007,** *129* (33), 10062-10063.

(108) Neuwald, B.; Olscher, F.; Göttker-Schnetmann, I.; Mecking, S., Limits of activity: weakly coordinating ligands in arylphosphinesulfonato palladium (II) polymerization catalysts. *Organometallics* **2012,** *31* (8), 3128-3137.

(109) Piche, L.; Daigle, J. C.; Rehse, G.; Claverie, J. P., Structure–Activity Relationship of Palladium Phosphanesulfonates: Toward Highly Active Palladium-Based Polymerization Catalysts. *Chem. - Eur. J.* **2012,** *18* (11), 3277-3285.

(110) Wucher, P.; Goldbach, V.; Mecking, S., Electronic influences in phosphinesulfonato palladium (II) polymerization catalysts. *Organometallics* **2013,** *32* (16), 4516-4522.

(111) Jian, Z.; Wucher, P.; Mecking, S., Heterocycle-substituted phosphinesulfonato palladium (II) complexes for insertion copolymerization of methyl acrylate. *Organometallics* **2014,** *33* (11), 2879-2888.

(112) Pan, H.; Zhu, L.; Li, J.; Zang, D.; Fu, Z.; Fan, Z., A thermal stable α-diimine palladium catalyst for copolymerization of ethylene with functionalized olefins. *Journal of Molecular Catalysis A: Chemical* **2014,** *390*, 76-82.

(113) Zhu, L.; Fu, Z.-S.; Pan, H.-J.; Feng, W.; Chen, C.; Fan, Z.-Q., Synthesis and application of binuclear α-diimine nickel/palladium catalysts with a conjugated backbone. *Dalton Trans* **2014,** *43* (7), 2900-2906.

(114) Allen, K. E.; Campos, J. s.; Daugulis, O.; Brookhart, M., Living polymerization of ethylene and copolymerization of ethylene/methyl acrylate using "sandwich" diimine palladium catalysts. *ACS Catal.* **2015,** *5* (1), 456-464.

(115) Chen, M.; Yang, B.; Chen, C., Redox-Controlled Olefin (Co) Polymerization Catalyzed by Ferrocene-Bridged Phosphine-Sulfonate Palladium Complexes. *Angew. Chem. Int. Ed.* **2015,** *54* (51), 15520-15524.

(116) Hu, H.; Chen, D.; Gao, H.; Zhong, L.; Wu, Q., Amine–imine palladium catalysts for living polymerization of ethylene and copolymerization of ethylene with methyl acrylate: incorporation of acrylate units into the main chain and branch end. *Polym. Chem* **2016,** *7* (3), 529-537.

(117) Mitsushige, Y.; Carrow, B. P.; Ito, S.; Nozaki, K., Ligand-controlled insertion regioselectivity accelerates copolymerisation of ethylene with methyl acrylate by cationic bisphosphine monoxide–palladium catalysts. *Chem. Sci.* **2016,** *7* (1), 737-744.

(118) Wang, R.; Zhao, M.; Chen, C., Influence of ligand second coordination sphere effects on the olefin (co) polymerization properties of α-diimine Pd (II) catalysts. *Polym. Chem* **2016,** *7* (23), 3933-3938.

(119) Wu, Z.; Chen, M.; Chen, C., Ethylene polymerization and copolymerization by palladium and nickel catalysts containing naphthalene-bridged phosphine–sulfonate ligands. *Organometallics* **2016,** *35* (10), 1472-1479.

(120) Zou, W.; Chen, C., Influence of backbone substituents on the ethylene (co) polymerization properties of α-diimine Pd (II) and Ni (II) catalysts. *Organometallics* **2016,** *35* (11), 1794-1801.

(121) Liang, T.; Chen, C., Side-arm control in phosphine-sulfonate palladium-and nickel-catalyzed ethylene polymerization and copolymerization. *Organometallics* **2017,** *36* (12), 2338-2344.

(122) Sui, X.; Hong, C.; Pang, W.; Chen, C., Unsymmetrical α-diimine palladium catalysts and their properties in olefin (co) polymerization. *Mater. Chem. Front.* **2017,** *1* (5), 967-972.

(123) Tao, W.; Akita, S.; Nakano, R.; Ito, S.; Hoshimoto, Y.; Ogoshi, S.; Nozaki, K., Copolymerisation of ethylene with polar monomers by using palladium catalysts bearing an N-heterocyclic carbene–phosphine oxide bidentate ligand. *Chem. Commun.* **2017,** *53* (17), 2630-2633.

(124) Wu, Z.; Hong, C.; Du, H.; Pang, W.; Chen, C., Influence of ligand backbone structure and connectivity on the properties of phosphine-sulfonate Pd (II)/Ni (II) catalysts. *Polymers* **2017,** *9* (5), 168.

(125) Zhai, F.; Solomon, J. B.; Jordan, R. F., Copolymerization of ethylene with acrylate monomers by amide-functionalized α-diimine Pd catalysts. *Organometallics* **2017,** *36* (9), 1873-1879.

(126) Zhao, M.; Chen, C., Accessing multiple catalytically active states in redox-controlled olefin polymerization. *ACS Catal.* **2017,** *7* (11), 7490-7494.

(127) Zhong, S.; Tan, Y.; Zhong, L.; Gao, J.; Liao, H.; Jiang, L.; Gao, H.; Wu, Q., Precision synthesis of ethylene and polar monomer copolymers by palladium-catalyzed living coordination copolymerization. *Macromolecules* **2017,** *50* (15), 5661-5669.

(128) Cai, Z.; Do, L. H., Thermally Robust Heterobimetallic Palladium–Alkali Catalysts for Ethylene and Alkyl Acrylate Copolymerization. *Organometallics* **2018,** *37* (21), 3874-3882.

(129) Ding, L.; Cheng, H.; Li, Y.; Tanaka, R.; Shiono, T.; Cai, Z., Efficient ethylene copolymerization with polar monomers using palladium anilinonaphthoquinone catalysts. *Polym. Chem* **2018,** *9* (45), 5476-5482.

(130) Guo, L.; Liu, Y.; Sun, W.; Du, Q.; Yang, Y.; Kong, W.; Liu, Z.; Chen, D., Synthesis, characterization, and olefin (co) polymerization behavior of unsymmetrical α-diimine palladium complexes containing bulky substituents at 4-position of aniline moieties. *J. Organomet. Chem.* **2018,** *877*, 12-20.

(131) Du, C.; Zhong, L.; Gao, J.; Zhong, S.; Liao, H.; Gao, H.; Wu, Q., Living (co) polymerization of ethylene and bio-based furfuryl acrylate using dibenzobarrelene derived α-diimine palladium catalysts. *Polym. Chem* **2019,** *10* (16), 2029-2038.

(132) Liao, Y.; Zhang, Y.; Cui, L.; Mu, H.; Jian, Z., Pentiptycenyl substituents in insertion polymerization with α-diimine nickel and palladium species. *Organometallics* **2019,** *38* (9), 2075-2083.

(133) Li, S.; Dai, S., 8-Arylnaphthyl substituent retarding chain transfer in insertion polymerization with unsymmetrical α-diimine systems. *Polym. Chem* **2020,** *11* (45), 7199-7206.

(134) Park, D.-A.; Byun, S.; Ryu, J. Y.; Lee, J.; Lee, J.; Hong, S., Abnormal N-Heterocyclic Carbene–Palladium Complexes for the Copolymerization of Ethylene and Polar Monomers. *ACS Catal.* **2020,** *10* (10), 5443-5453.

(135) Tan, C.; Qasim, M.; Pang, W.; Chen, C., Ligand–metal secondary interactions in phosphine–sulfonate palladium and nickel catalyzed ethylene (co) polymerization. *Polym. Chem* **2020,** *11* (2), 411-416.

(136) Xu, M.; Yu, F.; Li, P.; Xu, G.; Zhang, S.; Wang, F., Enhancing chain initiation efficiency in the cationic allyl-nickel catalyzed (co) polymerization of ethylene and methyl acrylate. *Inorg. Chem.* **2020,** *59* (7), 4475-4482.

(137) Zhang, Y.; Wang, C.; Mecking, S.; Jian, Z., Ultrahigh branching of main-chain-functionalized polyethylenes by inverted insertion selectivity. *Angew. Chem.* **2020,** *132* (34), 14402-14408.

(138) Zhong, L.; Zheng, H.; Du, C.; Du, W.; Liao, G.; Cheung, C. S.; Gao, H., Thermally robust α-diimine nickel and palladium catalysts with constrained space for ethylene (co) polymerizations. *J. Catal.* **2020,** *384*, 208-217.

(139) Zhou, G.; Mu, H.; Jian, Z., A comprehensive picture on catalyst structure construction in palladium catalyzed ethylene (co) polymerizations. *J. Catal.* **2020,** *383*, 215-220.

(140) Akita, S.; Nozaki, K., Copolymerization of ethylene and methyl acrylate by palladium catalysts bearing IzQO ligands containing methoxyethyl ether moieties and salt effects for polymerization. *Polymer Journal* **2021,** *53* (9), 1057-1060.

(141) Chen, S.-Y.; Pan, R.-C.; Liu, Y.; Lu, X.-B., Bulky o-Phenylene-Bridged Bimetallic α-Diimine Ni (II) and Pd

(II) Catalysts in Ethylene (Co) polymerization. *Organometallics* **2021,** *40* (22), 3703-3711.

(142) Dai, S.; Li, G.; Lu, W.; Liao, Y.; Fan, W., Suppression of chain transfer via a restricted rotation effect of dibenzosuberyl substituents in polymerization catalysis. *Polym. Chem* **2021,** *12* (22), 3240-3249.

(143) Ge, Y.; Li, S.; Fan, W.; Dai, S., Flexible "Sandwich"(8-Alkylnaphthyl α-Diimine) Catalysts in Insertion Polymerization. *Inorg. Chem.* **2021,** *60* (8), 5673-5681.

(144) Guo, L.; Hu, X.; Lu, W.; Xu, G.; Liu, Q.; Dai, S., Investigations of ligand backbone effects on bulky diarylmethyl-based nickel (II) and palladium (II) catalyzed ethylene polymerization and copolymerization. *J. Organomet. Chem.* **2021,** *952*, 122046.

(145) Hai, Z.; Lu, Z.; Li, S.; Cao, Z.-Y.; Dai, S., The synergistic effect of rigid and flexible substituents on insertion polymerization with α-diimine nickel and palladium catalysts. *Polym. Chem* **2021,** *12* (32), 4643-4653.

(146) Li, S.; Dai, S., Highly efficient incorporation of polar comonomers in copolymerizations with ethylene using iminopyridyl palladium system. *J. Catal.* **2021,** *393*, 51-59.

(147) Lu, W.; Xu, G.; Chang, G.; Wang, H.; Dai, S., Synthesis of highly branched polyethylene and ethylene-MA copolymers using hybrid bulky α-diimine Pd (II) catalysts. *J. Organomet. Chem.* **2021,** *956*, 122118.

(148) Wang, G.; Peng, D.; Sun, Y.; Chen, C., Interplay of supramolecular chemistry and photochemistry with palladium-catalyzed ethylene polymerization. *CCS Chemistry* **2021,** *3* (7), 2025-2034.

(149) Xia, J.; Han, Y.-F.; Kou, S.; Zhang, Y.; Jian, Z., Exploring steric effect of electron-donating group in palladium and nickel mediated ethylene polymerization and copolymerization with polar monomers. *European Polymer Journal* **2021,** *160*, 110781.

CHAPTER 5

Impacts of Labile Ligands on Catalyst Initiation and Chain Propagation in Ni-Catalyzed Ethylene/Acrylate Copolymerization

This work was published in part as:

ACS Catalysis, **2023**, 13, 5000-5006.

CONTRIBUTIONS AND ACKNOWLEDGEMENTS

Shuoyan Xiong and Theodor Agapie conceived the presented idea. S.X. performed synthesis experiments, polymer characterization, and analyzed the catalysis data. Priyabrata Ghana performed synthesis experiments. Brad. C. Bailey, Heather A. Spinney, and Briana S Henderson performed polymerization studies and polymer characterization. Matthew R. Espinosa performed single-crystal X-ray diffraction (scXRD) studies. S.X. drafted the manuscript that is reproduced as this chapter. P.G., B.C.B., H.A.S., B.S.H., and T.A. contributed to manuscript editing.

We are grateful to Dow (T.A.) for funding. We thank Alex J. Nett and Todd D. Senecal for insightful discussions. We thank Manar M. Shoshani and Linh N.V. Le for assistance with X-ray crystallography, and David VanderVelde for assistance with NMR spectroscopy. We thank Heidi Clements, Hannah Bailey, and Katie Muron for assistance in collecting polymer characterization data (GPC, DSC, FT-IR). Support has been provided for the X-ray diffraction and NMR instrumentation via the Dow Next Generation Educator Fund.

ABSTRACT

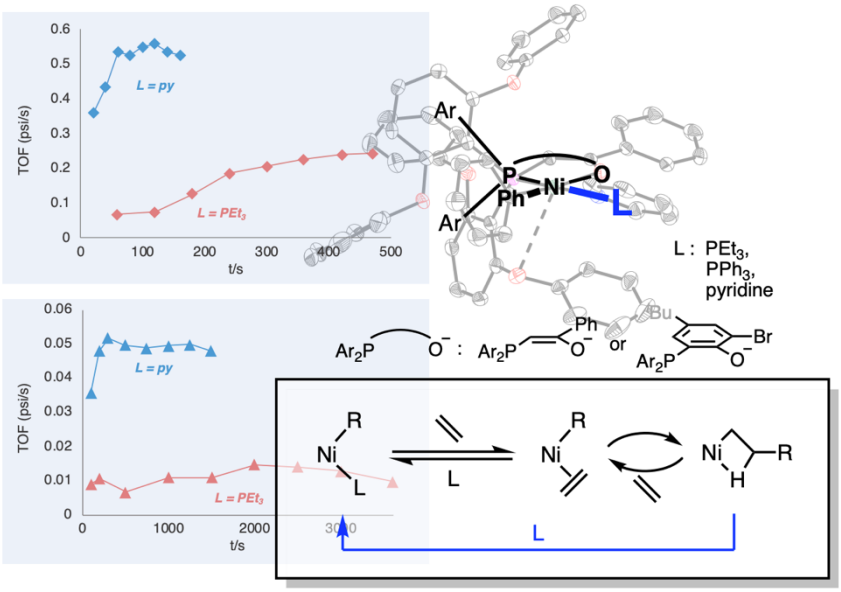

Polar polyolefin synthesis by coordination polymerization is of high interest, but catalysts' low activity limits industrial implementation. Herein, we report that the nature of labile ligand, L, significantly impacts the performance of neutral nickel catalysts supported by bidentate phosphine-phenoxide and phosphine-enolate ligands in ethylene/acrylate copolymerization. By tuning L, the copolymerization activity of one newly developed catalyst, **2-py**, reaches ~24000 kg/(mol*h). *In situ* studies indicate that a weaker L leads to faster chain propagation and more efficient catalyst initiation. Overall, this work demonstrates the impact of a strategy to improve catalyst activity in polar polyolefin synthesis complementary to design optimization for the bidentate ligand.

Chapter 5

GENERAL INTRODUCTION

Polyolefins account for over half of global plastic production.[1-2] Incorporation of polar groups can provide value-added materials with desirable physical and mechanical properties and potential degradability.[3-10] Metal catalyzed coordination copolymerization is of interest due to better expected control over monomer incorporation and polymer microstructure relative to industrialized radical process.[6, 11-14] However, polar groups can significantly inhibit this catalysis through coordination to the metal site, and thus prevent practical implementation.[1, 6]

Late transition metal catalysts supported by bidentate ligands have shown promise in the coordination copolymerization involving polar olefins.[6, 15-34] Despite significant progress, major limitations include the low catalytic activity, low thermal stability of catalysts, and low molecular weight (Mw) of resulting copolymers.[1, 15, 35] Catalyst design strategies beyond steric and electronic tuning of the bidentate ligands are of increasing interest.[1, 35]

Late transition metal precatalysts typically display a bidentate ligand and a labile ligand (L) in addition to a metal-hydrocarbyl motif (Figure 5.1a). Ligand L requires substitution by olefin to initiate catalysis. Therefore, additives that compete for these ligands such as $Ni(COD)_2$ or borane Lewis acids or phase transfer strategies have been employed to promote initiation.[36-43] The effects of L on Ni-catalyzed ethylene polymerization have been studied, highlighting impacts on activity, branching and associated isomerization.[36, 44-48] However, the effect of L on Ni-catalyzed

copolymerization of ethylene with polar olefins has not been studied systematically.[27, 33, 49-52] For neutral Pd catalysts, only limited effects on ethylene/acrylate copolymerization were reported with ligand L. For example, ligand L-free version of a Pd phosphine sulfonate catalyst showed <35% increase in activity compared to analogues with labile ligands (e.g. $OPBu_3$, DMSO) for L.[45] The small effect of the additional donor is potentially related to the presence of a large excess of coordinating polar groups in copolymerization with polar monomers. Herein, we report studies of two types of neutral Ni catalysts toward addressing the impact of ligand L on the copolymerization of ethylene and acrylate.

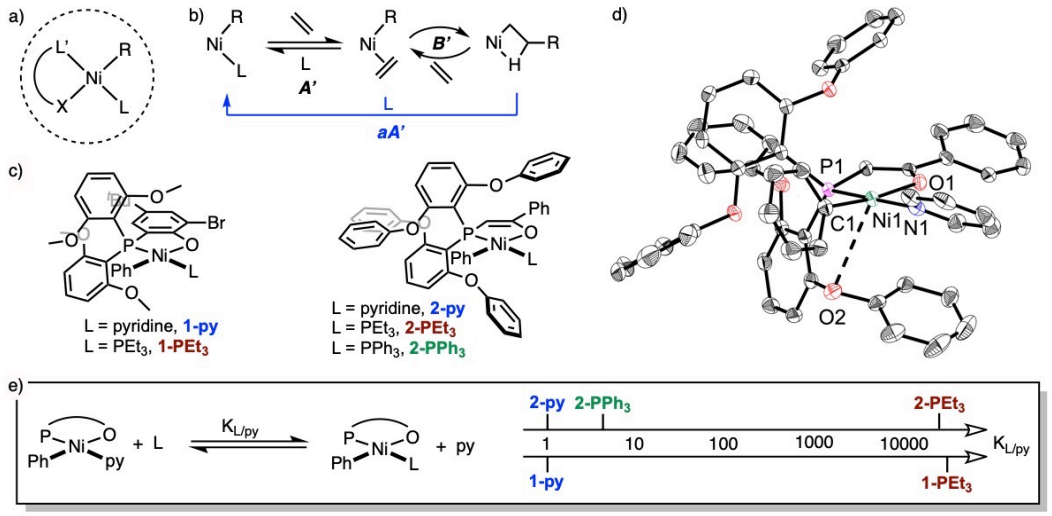

Figure 5.1. a) Depiction of neutral Ni catalysts; b) Potential reaction pathways involving ligand L in catalysis; c) Ni catalysts studied in this work; d) Solid-state structure of **^{Ph}PO^{Ph}-Ni(py)**. Only one molecule in the asymmetric unit is shown for clarity. Hydrogen atoms and solvent molecules are excluded. Ellipsoids are shown at the 50% probability level; e) Reversible ligand binding and relative binding strength of ligand Ls with two types of complexes.

RESULTS AND DISCUSSION

Neutral Ni catalysts are attractive given their relatively high efficiency and low cost of nickel.[17] P,O-chelated Ni complexes represent a high-performance class of catalysts with potential for further improvement for the synthesis of polar polyolefins.[8, 17, 32-34, 53-56] We have previously studied the thermodynamics of olefin and polar group coordination to the nickel center and found both are orders of magnitude weaker than binding of typical labile ligands (e.g. PEt_3).[34 56] We therefore anticipated that ligand L could compete for binding to metal with vinyl and ester groups present under ethylene/acrylate copolymerization conditions even under relatively low concentrations of L as is the case for single component catalysts (Figure 5.1b). Once coordinated, substitution of ligand L by olefins is required for subsequent monomer insertion during initiation or propagation.

We focused our study of the influence of ligand L on two types of catalysts, the Ni phosphine phenoxide and Ni phosphine enolate systems. Although both feature promising activity and thermal stability in ethylene/acrylate copolymerization further improvements are desirable.[55] Five complexes were selected, **1-PEt$_3$**, **1-py**, **2-PEt$_3$**, **2-PPh$_3$**, and **2-py** (Figure 5.1c)**.** Within the same bidentate ligand class (phosphine-phenoxide vs phosphine-phenolate), they differ only in the labile ligand L.

The synthesis of **1-PEt$_3$** was analogous to **2-PEt$_3$** (see SI), which was previously reported.[55] Preparation of the pyridine adduct for both, **1-py** and **2-py**, was attempted by substitution of PEt_3 upon addition of a large excess of pyridine to **1-PEt$_3$** or **2-**

PEt_3. However, the ligand exchange was slow and the equilibrium between these two types of adducts is far on the side of the **PEt_3** adduct. Based on ligand exchange experiments (SI Section S3), the equilibrium constant, $K_{PEt3/py}$, is approximately ~25000 for **1-PEt_3/1-py** and 20000 for **2-PEt_3/2-py** (Figure 5.1e), indicating the significant difference in the binding energies of PEt_3 and Py.

The large $K_{PEt3/py}$ favoring phosphine binding prevents efficient synthesis of the pyridine adduct from corresponding PEt_3 adduct. Instead, deprotonation of the P,O proligand with $LiN(SiMe_3)_2$ followed by salt metathesis with NiPhCl(tmeda), where tmeda = N,N,N',N'-tetramethylethylenediamine, afforded **1-py** and **2-py** (SI Section S2). The $^{31}P\{^1H\}$ NMR spectrum of the product features a sharp singlet at ~-0.6 ppm for **1-py**, and ~-2.6 ppm for **2-py** (Figure AB5.1-5.2, AB5.5), matching the new resonance observed in the ligand exchange studies. The PPh_3 adduct, **2-PPh_3**, can be prepared by ligand substitution from **2-py** quantitatively (See SI section S2). A small equilibrium constant was observed between the pyridine adduct and the PPh_3 adduct (~4, $K_{PPh3/py}$, Figure 5.1e). The identity of **1-PEt_3**, **1-py**, **2-py** were further confirmed by single crystal X-ray diffraction (scXRD), which reveals a square-planar geometry and and an ether oxygen oriented over the axial position of Ni (Figure 5.1d and Figure S5.4.1-3).

The influence of ligand L on ethylene/acrylate copolymerization was studied. All five catalysts show high activity and thermal stability in the copolymerization of ethylene and tert-butyl acrylate as single-component catalysts (tBA, Table 5.1). Under otherwise identical conditions (Entry 1 vs 2, and 4 vs 5), the pyridine adducts (**1-py**

and **2-py**) show activity ~5 times higher than that of the corresponding PEt_3 adducts (**1-PEt$_3$** and **2-PEt$_3$**, respectively), indicating that a weaker ligand L does facilitate catalysis. On the other hand, **2-PPh$_3$**, and **2-py** feature similar activity (Entry 6 vs 7), consistent with the similar binding affinities of pyridine and PPh_3. Resulting copolymers feature similar molecular weights (Mw) and tBA incorporation. This is notable given that strategies of increasing activity are typically coupled with significant changes in polymer Mw or polar monomer incorporation.[41, 57-60]

To further evaluate the effect of ligand L, ethylene/tBA copolymerization was conducted with **2-PPh$_3$** and varying equivalents of PEt_3 (Table 5.1, entry 7~10). Addition of 1 equiv. of PEt_3 leads to ~70% decrease in activity (entry 7 vs 8), demonstrating the significant inhibitory effect of a strong ligand L on catalysis, even at low concentration. Increase in PEt_3 concentrations leads to further decrease in activity (entry 8~10). Specifically, *in-situ* mixture of **2-PPh$_3$** and 10 equivalent of PEt_3 feature activity ~1/10 that of activity of the **2-PPh$_3$** + 1 PEt_3 mixture. Notably, addition of a large excess of PEt_3 (e.g.) also leads to significant decrease in copolymer Mw, implying that ligand L impacts chain transfer. Overall, the above scenarios further confirm the substantial influence of ligand L on ethylene/acrylate copolymerization.

Table 5.1. Ethylene/acrylate copolymerization results.[a]

Entry	catalyst	[tBA]/M	T/°C	Act.[c]	Mw/10^3	PDI	%Mol tBA	Tm/°C
1	**1-PEt$_3$**	0.05	90	0.21	63.1	2.3	1.7	114
2	**1-PEt$_3$**	0.10	90	0.12	41.3	2.6	3.5	104
3	**1-py**	0.05	90	1.1	78.4	2.3	1.6	115
4	**1-py**	0.10	90	0.44	55.0	2.2	3.2	105
5	**2-PEt$_3$**	0.05	90	1.38	10.3	2.3	0.5	122
6	**2-py**	0.05	90	6.2	10.3	2.5	0.6	122
7	**2-PPh$_3$**	0.05	90	5.6	12.2	2.1	0.5	122
8	**2-PPh$_3$** + 1 PEt$_3$	0.05	90	1.87	11.1	2.1	0.5	122
9	**2-PPh$_3$** + 2 PEt$_3$	0.05	90	1.20	10.2	2.4	0.5	122
10	**2-PPh$_3$** + 10 PEt$_3$	0.05	90	0.18	3.7	2.4	0.5	121
11	**2-PEt$_3$**	0.05	110	3.7	8.4	2.5	0.6	122
12	**2-py**	0.05	110	13.3	6.8	2.4	0.6	123
13	**2-py**	0.10	110	4.7	6.8	2.5	1.2	114
14	**2-py**	0.15	110	2.9	6.6	2.3	1.6	112
15[b]	**2-PEt$_3$**	0.025	90	3.0	11.3	2.3	0.3	125
16[b]	**2-py**	0.025	90	13.6	12.5	2.6	0.3	124
17[b]	**2-PEt$_3$**	0.025	110	7.4	8.6	2.5	0.3	124
18[b]	**2-py**	0.025	110	24	8.1	2.5	0.3	124
19[c]	**2-py**	0.054	110	10.6	10.6	2.3	0.5	124
20[c]	**2-py**	0.11	110	4.9	9.5	2.2	0.8	123

[a]Unless specified, V = 5 mL, [Ni] = 0.05 mM, ethylene pressure = 400 psi, toluene solvent. Polymerizations were stopped after consuming a set amount of ethylene (reaction time: 2.5~60 min; see Table S5.6.1 for specific polymerization times. Each entry represents multiple replicated runs. 85~145 mg of copolymer was produced in each run. See SI section S5 for detailed procedures and Table S5.6.1 for original catalytic runs. [b][Ni]=0.025 mM. [c] Copolymerization in a batch reactor. Condition: V = 550 mL, 23.7 μmol **^{Ph}PO^{Ph}-Ni** ([Ni]=0.043 mM), ethylene pressure = 430 psi, T= 110

°C, t = 8 min (entry 19), or 15 min (entry 20), polymerizations were stopped after ethylene uptake reached 40g. See SI section S5 for detailed procedure. [d]Activity in 1000 kg/(mol·h).

To understand how ligand L affects copolymerization activity, *in-situ* measurements of ethylene uptake over time during catalysis were performed with **1-PEt$_3$**, **1-py**, **2-PEt$_3$** and **2-py** (Figure 5.2a). Though both ethylene and tBA are involved in copolymerization, ~99% of repeating units in resulting copolymers are ethylene-based. Therefore, ethylene uptake over time, plotted as turnover frequency (TOF) was used to evaluate catalyst performance in this copolymerization. Notably, a higher maximum TOF was observed with the pyridine adduct (~ 0.05 psi/s for **1-py** and > 0.5 psi/s for **2-py**) compared to the analogous PEt$_3$ adduct (~ 0.015 psi/s for **1-PEt$_3$** and ~ 0.25 psi/s for **2-PEt$_3$**). The maximum and steady state value of TOF corresponds to the rate of chain propagation. Therefore, the above difference indicates that chain propagation is faster with the pyridine adduct and, hence, implies that ligand L significantly impacts the propagation. In addition, an induction period to reach maximum TOF was observed for both **2-PEt$_3$** and **2-py**, but it is much shorter for **2-py** (c.a. 60 s) compared **2-PEt$_3$** (> 300 s) under otherwise identical conditions. For these neutral catalysts, replacement of ligand L by ethylene is necessary for catalyst initiation. The shorter induction period of **2-py** indicates that substitution of pyridine by olefins is more facile than of PEt$_3$. This is consistent with the ligand's relative binding strengths. Copolymerization by **2-PPh$_3$** in the presence of different concentrations of PEt$_3$ (Figure S5.6.1), shows impact on both catalyst initiation and chain propagation further confirming the abovementioned effects of L on copolymerization catalysis.

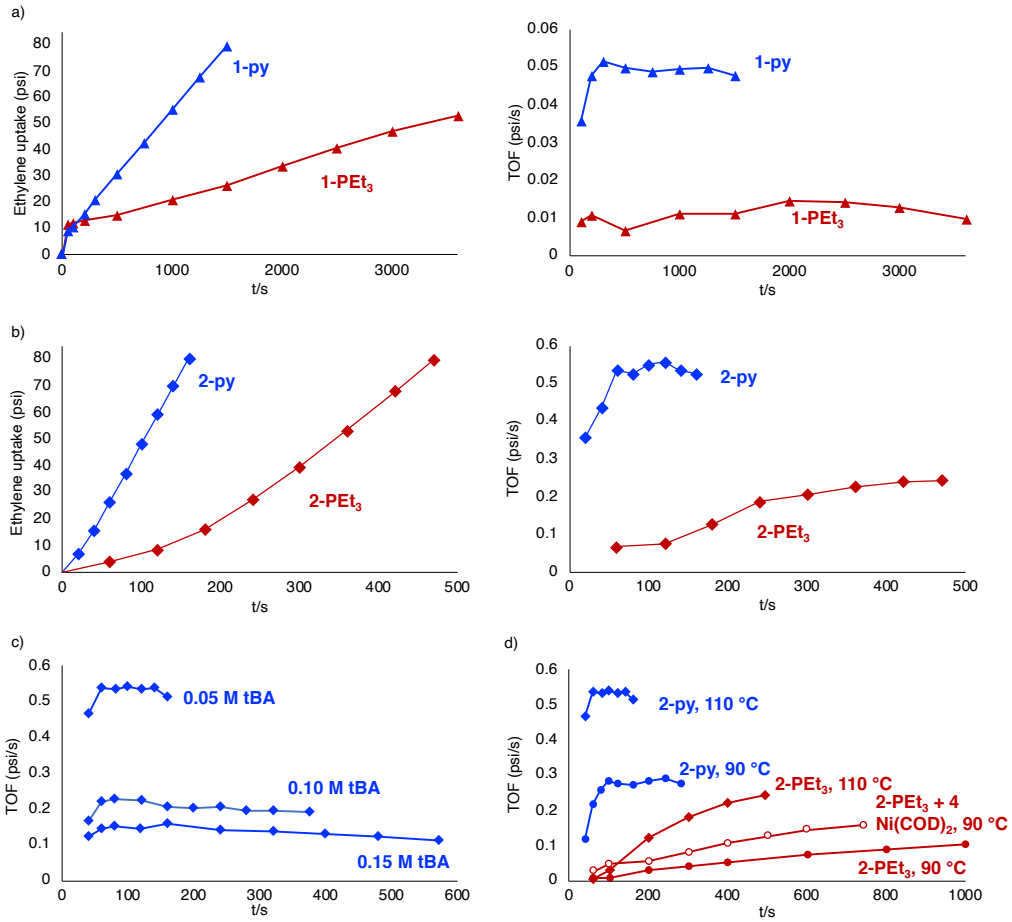

Figure 5.2. a) Ethylene uptake curves (left) and corresponding TOF (right) vs time for **1-PEt$_3$** (red) and **1-py** (blue). Conditions for a): V (total) = 5mL, [Ni Cat.] = 0.05 mM, [tBA] = 0.05 M, ethylene pressure = 400 psi, T = 90 °C, toluene solvent. b) Ethylene uptake curves (left) and corresponding TOF (right) vs time for **2-PEt$_3$** (red) and **2-py** (blue). Conditions for b): V (total) = 5mL, [Ni Cat.] = 0.025 mM, [tBA] = 0.025 M, ethylene pressure = 400 psi, T = 110 °C, toluene solvent. c) Rate of ethylene uptake (TOF) vs time with different tBA concentrations (Catalyst: **2-py**). d) Rate of ethylene uptake (TOF) vs time for **2-PEt$_3$** and **2-py** with/without Ni(COD)$_2$ at different temperatures. Conditions for c) and d) unless specified: V (total) = 5mL, [Ni Cat.] = 0.05 mM, [tBA] = 0.05 M, ethylene pressure = 400 psi, T = 110 °C, toluene solvent. See Table S5.6.2-3 for original catalytic runs.

Overall, the above results demonstrate that ligand L impacts catalyst initiation and propagation, which is notable given that the concentration of L is c.a. ~1000 times lower than acrylate and ethylene concentration is even higher than acrylate.[61-62] The ester group of acrylate can also substitute L, though it is a significantly weaker ligand compared to pyridine and phosphines.[56] We thus performed ethylene uptake studies

with **2-py** under different acrylate concentrations (Figure 5.2b, Table S5.6.2), which revealed that the catalyst initiation has a similar induction period under all conditions. However, a significant difference was observed in maximum TOF. These observations indicate that initiation is independent of acrylate concentration, likely being driven by ethylene insertion, consistent with kinetics studies on related systems,[34] although ethylene and acrylate induced initiation could also be undistinguishable. The lower maximum TOF at higher tBA concentrations is consistent with more frequent acrylate insertions, generating the resting state of the catalyst with a chelating pendant ester that undergoes slow ethylene insertion.[34, 56] Structural analysis of the copolymer indeed show higher tBA incorporation, that keep the catalyst in the less reactive form.

In addition to L, reaction temperatures and activators can also impact catalyst initiation and chain propagation. Their effects were evaluated via ethylene uptake analysis (Figure 5.2c). Increase in temperature leads to higher maximum TOFs (rate of ethylene uptake) and shorter induction period for both catalysts. For example, for **2-py** maximum TOF increases from 0.3 psi/s (90 °C) to 0.5 psi/s (110 °C), and it is achieved in ~100 s and <60 s, respectively. This is consistent with higher rates of chain propagation and initiation at higher temperature. Again, the maximum TOF is different between the two catalysts even at different temperatures, indicating that the presence of different L in the reaction mixture still impacts propagation. $Ni(COD)_2$ is commonly employed as a phosphine scavenger to promote catalyst initiation. Indeed, catalyst activation of **2-PEt$_3$** with $Ni(COD)_2$ results in marginally faster initiation and a higher maximum TOF. However, the improvement relative to no activator is small

and both catalyst initiation and chain propagation are slower than **2-py.** Therefore, adding scavengers of the labile ligand L is not sufficient to achieve the intrinsic activity of system **2** as promoted by the bidentate phosphine enolate ligand.

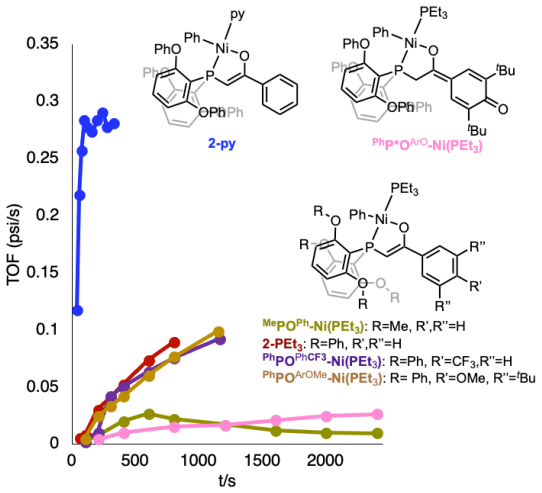

Figure 5.3. Influence of structures of enolate ligands on rates of catalyst "initiation" and propagation. Conditions unless specified: V (total) = 5mL, [Ni] = 0.05 mM, [tBA] = 0.05 M, ethylene pressure = 400 psi, T = 90 °C, toluene solvent. See Table S5.6.4 for original catalytic runs.

Typical catalyst improvement strategies are primarily focused on the design of ancillary bidentate ligands. For comparison, the effect of the nature of ligand L vs bidentate ligand structures on catalyst initiation and propagation were evaluated. A set of reported Ni enolate catalysts featuring different substituents and chelating frameworks based on the phosphine enolate motif were screened (Figure 5.3). Changes in the nature of the PO chelate (**^{Ph}P*O^{ArO}-Ni(PEt$_3$)** vs **^{Ph}PO^{ArO}-Ni(PEt$_3$)**) and substituents ortho to the phosphine (**2-PEt$_3$** vs **^{Me}PO^{Ph}-Ni(PEt$_3$)**) lead to a 2~4-fold differences in maximum TOF. These relative changes are comparable to the

effects observed upon varying L. Importantly, the highest activity is derived from changing L.

Overall, the above results further demonstrate the significance of ligand L on both catalyst initiation and chain propagation even upon changes in the nature of ancillary ligand or addition of activator ($Ni(COD)_2$). Therefore, in new catalyst development, careful comparison should be made to evaluate the effect of ligand L, as its impact may mask the intrinsic performance derived from the design of the ancillary bidentate ligand. Moreover, given that altering ligand L is more facile than the bidentate ligand, this is an alternate strategy in catalyst optimization.

Table 5.2. Analysis of copolymer microstructures.[a]

	P	**P***
Catalyst	**2-PEt$_3$**	**2-py**
Methyl/1000C	1.7	2.0
2-Propenyl/1000C	0.6	0.9

[a] Sample P and P* are copolymers produced by **2-PEt3** and **2-py** under otherwise identical conditions. (**P**: reported in ref 55 as sample C; **P***: table S5.6.1, entry 15). See SI Section S5.7.1-2 for more details.

Ligand L has been reported to impact branching in ethylene homopolymerization by Ni-imino-phenoxide catalysts at low temperatures (≤30 °C).[47] Our results here provide a related example in a more complicated reaction system, ethylene/tBA copolymerization, and at more industrially relevant temperatures (90~110 °C). Compared to copolymers generated by **2-PEt$_3$**, copolymers from **2-py** show slightly higher levels of methyl branch and 2-propenyl end (~120%, ~150%, respectively). Nonetheless, these copolymers remain highly linear (methyl branch ≤2/1000C). These features indicate that polymerization activity can be increased by appropriate selection of L, without dramatically altering polymer microstructure.

CONCLUSION

In summary, labile ligand L significantly impacts catalyst activity in ethylene/acrylate copolymeriza-tion, while its impact on copolymer microstructure is moderate. Specifically, replacing PEt3 by pyridine leads to a 4~5-fold increase in copolymerization activ-ity. Importantly, L affects not only the initiation, but also propagation, even in the presence of an activa-tor. These results may have practical applications given that low activity is a major limiting factor for coordination copolymerization involving polar mon-omers, and optimization of ligand L is more facile than changes in the ancillary ligand.

Chapter 5

EXPERIMENTAL SECTION

1. General Considerations

All air- and water-sensitive compounds were manipulated under N_2 or Ar using standard Schlenk or glovebox techniques. The solvents for air- and moisture-sensitive reactions were dried over sodium benzophenone/ketyl, calcium hydride, or by the method of Grubbs.[1] Deuterated solvents were purchased from Cambridge Isotopes Lab, Inc.; C_6D_6, was dried over a purple suspension with Na/benzophenone ketyl and vacuum transferred. tert-Butyl acrylate was dried over 4 Å sieves for greater than 72h. 2,4,6-Trimethylacetophenone was dried over 4 Å sieves for greater than 72h, vacuum transferred, and passed over an activated alumina plug. Acetophenone, dimethoxybenzene, and triethylphosphine were dried over calcium hydride and vacuum-transferred or distilled prior to use. Lithium bis(trimethylsilyl)amide (LiHMDS) were purchased from Sigma-Aldrich and used without further purification. Bis(dimethoxyphenyl)phosphine chloride, bis(diphenoxyphenyl)phosphine chloride, Metal precursor (tmeda)NiPhCl, phosphine enolate ligand ^{Ph}**PO**^{Ph}**H**, complex **2-PEt$_3$**, ^{Me}**PO**^{Ph}**-Ni(PEt$_3$)Ph**, ^{Ph}**PO**^{Mes}**-Ni(PEt$_3$)Ph**, ^{Ph}**PO**^{ArOMe}**-Ni(PEt$_3$)Ph**, ^{Ph}**PO**^{PhCF3}**-Ni(PEt$_3$)Ph**, and ^{Ph}**P*O**^{ArO}**-Ni(PEt$_3$)Ph** were synthesized according to literature procedures.[2-4] All ^{1}H, ^{13}C, and ^{31}P spectra of organic and organometallic compounds were recorded on Varian INOVA-400, or Bruker Cryoprobe 400 spectrometers. ^{1}H and ^{13}C chemical shifts are reported relative to residual solvent resonances.

2. Preparation of Metal Complexes

Synthesis of 2-bromo-4-tert-butyl-6-bis(2',6'-dimethoxyphenyl)phosphinophenol (^{MeO}POBrH)

A Schlenk flask fitted with a screw-in Teflon stopper was charged with a solution of 1,3-dibromo-5-(tert-butyl)-2-(methoxymethoxy)benzene (3.52 g, 10.0 mmol) in THF (40 mL) and cooled to -78 °C under nitrogen. A hexane solution of n-butyllithium (4 mL, 2.5 M, 10.0 mmol) was added dropwise via syringe. After stirring for an additional 30 min at -78 °C, a solution of bis(2,6-dimethoxyphenyl)phosphine chloride (3.41 g, 10.0 mmol) in THF (20 mL) was added dropwise via cannula. After complete addition, the reaction was allowed to warm up to room temperature and stirred for an additional 3 h, yielding a yellow solution. The solution was then concentrated to ~20 mL. Degassed MeOH (10 mL) was added, followed by the addition of concentrated aqueous HCl (5 mL). The resulting mixture was degassed immediately via three freeze-pump-thaw cycle with a liquid nitrogen bath. After stirring for 4 h under room temperature, volatiles were removed under vacuum. In a N_2-filled glovebox (no exclusion of water), the resulting pale-yellow residue was taken up in CH_2Cl_2 (40 mL), washed with saturated aqueous solutions of K_2CO_3 (3 x 10 mL) and NH_4Cl (3 x 10 mL), dried over $MgSO_4$, and filtered through Celite. The volatiles were removed under reduced pressure. In a glovebox (exclusion of water and oxygen), the resulting pale-yellow solid was dissolved in ether and filtered through Celite. The volatile materials were removed once more under vacuum and the resulting mixture was washed by hexanes (10 mL) and the solid was collected via vacuum filtration. Further recrystallization from cold, concentrated Et_2O solution yields 2-bromo-4-tert-butyl-6-bis(2',6'-dimethoxyphenyl)phosphinophenol (**^{MeO}POBrH**, 4.05 g, 70% yield) as a white powder. ^{1}H NMR (400 MHz, C_6D_6): δ 7.97 (dd, *J* = 13.0, 2.5 Hz, 1H, ArH), 7.80 (d, *J* = 2.4 Hz, 1H, OH), 7.62 (d, *J* = 2.4 Hz, 1H, ArH), 7.0 (dt, *J* = 8.3, 1.1 Hz, 2H, ArH), 6.20 (dd, *J* = 8.3, 2.9 Hz, 4H,

ArH), 3.14 (s, 12H, OCH_3), 1.15 (s, 9H, $C(CH_3)_3$). $^{13}C\{^1H\}$ NMR (101 MHz, C_6D_6): δ 161.89 (d, *J* = 8.4 Hz, 4C, Aryl-C), 153.94 (d, *J* = 4.8 Hz, 1C, Aryl-C), 142.51 (d, *J* = 12.8 Hz, 1C, Aryl-C), 132.64 (d, *J* = 42.0 Hz, 1C, Aryl-C), 130.71 (s, 1C, Aryl-C), 129.79 (s, 2C, Aryl-C), 125.48 (d, *J* = 17.2 Hz, 1C, Aryl-C), 112.91 (d, *J* = 22.7 Hz, 2C, Aryl-C), 109.38 (s, 1C, Aryl-C), 104.25 (s, 4C, Aryl-C), 55.26 (s, 4C, OCH_3), 34.08 (s, 1C, $\underline{C}(CH_3)_3$), 31.51 (s, 3C, $C(\underline{C}H_3)_3$). $^{31}P\{^1H\}$ NMR (162 MHz, C_6D_6) δ -55.2 (s).

Synthesis of ^{MeO}POBr-Ni(PEt$_3$)Ph (1-PEt$_3$)

In a Schlenk tube, a solid mixture of **^{MeO}POBrH** (75 mg, 0.14 mmol) and $LiCH_2SiMe_3$ (13 mg, 0.14 mmol) was treated with cold (+5 °C) benzene (8 mL). The resulting mixture was slowly warmed to room temperature and stirred for an additional 1 hour. To this reaction mixture, a benzene solution (2 mL) of $[NiCl(Ph)(PEt_3)_2]$ (53 mg, 0.14 mmol, 1 equiv.) was added at room temperature. The resulting yellow suspension was heated to 80 °C for 18 hours under nitrogen atmosphere. After completion of the reaction, as confirmed by an aliquot ^{31}P NMR, the reaction mixture was filtered into a 20 mL glass vial, and the yellow filtrate was evaporated to dryness under reduced pressure. The resulting residue was washed with hexane (3 × 5 mL) at room temperature and dried under reduced pressure for 3 hours to obtain **1-PEt$_3$** as an analytically pure yellow solid. Yield: 90 mg (0.11 mmol, 82%).

^1H NMR (400 MHz, C_6D_6): δ 7.73 (dd, *J* = 9.9, 1.7 Hz, 1H, ArH), 7.61 (d, *J* = 1.7 Hz, 1H, ArH), 7.19 (d, *J* = 7.3 Hz, 2H, ArH), 7.02 (t, *J* = 8.3 Hz, 2H, ArH), 7.62 (t, *J* = 7.2 Hz, 2H, ArH), 6.62 (t, *J* = 7.2 Hz, 1H, ArH), 6.18 (dd, $^3J_{H,H}$ = 8.4 Hz, $^4J_{H,P}$ = 3.4 Hz, 4H, ArH), 3.18 (s, 12H, -OC*H*$_3$), 1.49 (m, 6H, PC*H*$_2$), 1.18 (m, 9H, PCH$_2$C*H*$_3$), 1.14 (s, 9H, $C(CH_3)_3$). $^{13}C\{^1H\}$ NMR (101 MHz, C_6D_6): δ 168.75 (dd, *J* = 30.4, 7.4 Hz, 2C, Aryl-C), 161.56 (s, 4C, Aryl-C), 151.59 (dd, *J* = 32.4, 7.4 Hz, 2C, Aryl-C), 137.27 (t, *J* = 3.7 Hz, 2C, Aryl-C), 136.11 (d, *J* = 6.5 Hz, 1C, Aryl-C), 131.34 (d, *J* = 1.5 Hz, 1C, Aryl-C), 130.32 (s, 2C, Aryl-C), 127.09 (d, *J* = 2.2 Hz, 1C, Aryl-C),

125.63 (d, J = 49.4 Hz, 1C, Aryl-C), 125.02 (t, J = 2.5 Hz, 2C, Aryl-C), 120.09 (t, J = 2.2 Hz, 1C, Aryl-C), 113.46 (d, J = 14.8 Hz, 1C, Aryl-C), 110.54 (dd, J = 45.2, 1.8 Hz, 2C, Aryl-C), 104.20 (d, J = 4.2 Hz, 4C, Aryl-C), 55.48 (s, 4C, OCH_3), 33.80 (s, 1C, $\underline{C}(CH_3)_3$), 31.92 (s, 3C, $C(\underline{C}H_3)_3$), 13.94 (d, J = 22.0 Hz, 3C, $P\underline{C}H_2CH_3$), 8.28 (s, 3C, $PCH_2\underline{C}H_3$). $^{31}P\{^1H\}$ NMR (162 MHz, C_6D_6) δ 15.0 (d, J = 298.8 Hz, 1P), -3.6 (d, J = 298.8 Hz, 1P). Anal. Calcd(%) for $C_{38}H_{49}BrNiO_5P_2$: C: 58.04, H: 6.28; found: C: 58.87, H: 6.34.

Synthesis of ^{MeO}POBr-Ni(py)Ph (1-py)

In the glove box, to a precooled (-78 °C) solution of the ligand **^{MeO}POBrH** (107 mg, 0.2 mmol) in tetrahydrofuran (THF) (2 mL) was added a precooled (-78 °C) solution (2 mL) of LiHMDS (33.4 mg, 0.2 mmol) in THF. The mixture was then slowly warmed up to room temperature and stirred for 8 h at room temperature. All volatiles were removed from solution which was triturated with pentane (2 x 5 mL). The resulting residue was dissolved in toluene (4 mL) and cooled to -78 °C. To this solution was added a toluene solution (2 mL) of (tmeda)NiPhCl (57.2 mg, 0.2 mmol) and pyridine (79 mg, 1.0 mmol). The mixture was then slowly warmed up to room temperature and stirred for additional 24 h. Next, the mixture was filtered through Celite and volatiles were removed under vacuum. The resulting solids were further washed with pentane (5~10 mL*3), hexanes (1 mL), and diethyl ether (1 mL), yielding metal complexes (**1-py**) as analytically pure yellow solids (97 mg, yield: 65%).

^1H NMR (400 MHz, C_6D_6): δ 8.95 – 8.89 (m, 2H, ArH), 7.71 (d, J = 2.3 Hz, 1H, ArH), 7.66 (dd, J = 11.3, 2.4 Hz, 1H, ArH), 7.60 (d, J = 7.2 Hz, 2H, ArH), 7.02 (t, J = 8.3 Hz, 2H, ArH), 6.82 (t, J = 7.2 Hz, 2H, ArH), 6.78 – 6.73 (m, 1H, ArH), 6.71-6.67 (m, 1H, ArH), 6.42 (t, J = 6.4 Hz, 2H, ArH), 6.17 (dd, J = 8.3, 3.8 Hz, 4H, ArH), 3.17 (s, 12H, $-OCH_3$), 1.14 (s, 9H, -^{t}Bu). $^{13}C\{^1H\}$ NMR (101 MHz, C_6D_6): δ 167.38 (d, J = 23.5 Hz, 2C, ArC), 161.51 (s, 4C, ArC), 155.34 (d, J = 48.0 Hz, 1C, ArC), 151.81 (s, 2C, ArC), 138.35 (s, 2C, ArC), 136.47 (s, 1C, ArC), 136.12

(d, J = 6.9 Hz, 1C, ArC), 131.58 (s, 1C, ArC), 130.79 (s, 2C, ArC), 126.88 (s, 1C, ArC), 126.46 (s, 1C, ArC), 125.42 (s, 2C, ArC), 123.51 (s, 2C, ArC), 121.30 (s, 1C, ArC), 112.96 (d, J = 16.2 Hz, 1C, ArC), 110.05 (d, J = 54.5 Hz, 1C, ArC), 104.18(s, 4C, ArC), 55.36 (s, 4C, -OMe), 33.86 (s, 1C, -$\underline{C}(CH_3)_3$), 31.98 (s, 3C, -C($\underline{C}H_3)_3$). $^{31}P\{^1H\}$ NMR (162 MHz, C_6D_6) δ -0.63 (s). Anal. Calcd(%) for $C_{37}H_{38}BrNNiO_5P$: C: 59.47, H: 5.26, N: 1.87; found: C: 60.37, H: 5.40, N: 2.13.

Synthesis of $^{Ph}PO^{Ph}$-Ni(py)Ph (2-py)

In the glove box, to a precooled (-78 °C) solution of the ligand **$^{Ph}PO^{Ph}H$** (134.4 mg, 0.2 mmol) in tetrahydrofuran (THF) (2 mL) was added a precooled (-78 °C) solution (2 mL) of LiHMDS (33.4 mg, 0.2 mmol) in THF. The mixture was then slowly warmed up to room temperature and stirred for 8 h at room temperature. All volatiles were removed from solution which was triturated with pentane (2 x 5 mL). The resulting residue was dissolved in toluene (4 mL) and cooled to -78 °C. To this solution was added a toluene solution (2 mL) of (tmeda)NiPhCl (57.2 mg, 0.2 mmol) and pyridine (79 mg, 1.0 mmol). The mixture was then slowly warmed up to room temperature and stirred for additional 24 h. Next, the mixture was filtered through Celite and volatiles were removed under vacuum. After washed with pentane (5~10 mL*3), hexanes (1 mL), and cold diethyl ether (2 mL), the resulting solids was further purified by precipitation from cold, concentrated solution in diethyl ether, yielding metal complexes (**2-py**) as yellow-brownish solids (44 mg, yield: 25%).

^1H NMR (400 MHz, C_6D_6) δ 8.08 – 7.98 (m, 4H, 4ArH), 7.49 (dd, J = 7.6, 2.0 Hz, 2H, 2ArH), 7.12 – 7.06 (m, 3H, ArH), 7.03 – 6.94 (m, 11H, ArH), 6.95 – 6.88 (m, 8H, ArH), 6.85 – 6.80 (m, 4H, ArH), 6.75 (t, J = 8.2 Hz, 2H, ArH), 6.69 – 6.64 (m, 1H, ArH), 6.60-6.55 (m, 1H, ArH), 6.47 (dd, J = 8.2, 3.3 Hz, 4H, ArH), 6.21-6.16 (m, 2H, ArH), 5.23 (broad s, 1H, -C$\underline{H}$C(O)-). $^{13}C\{^1H\}$ NMR (101 MHz, C_6D_6): δ 177.67 (d, J = 20.7 Hz), 159.16 (s), 158.10 (s), 155.82 (d, J = 44.3 Hz), 151.22(s). 140.14 (d, J = 15.6 Hz), 138.76 (s), 136.00 (s), 130.12 (s), 129.76(s), 127.80 (s), 127.61

(s), 127.42 (s), 125.75 (s), 123.09 (s), 122.96 (s), 121.73 (s), 120.49 (s), 119.82 (s), 113.73 (s), 82.45 (d, J = 58.7 Hz). $^{31}P\{^{1}H\}$ NMR (162 MHz, C_6D_6) δ -2.63 (s). Anal. Calcd(%) for $C_{55}H_{42}NNiO_5P$: C: 74.51, H: 4.78, N: 1.58; Found (%): C, 74.15; H, 5.07; N, 1.17.

Synthesis of $^{Ph}PO^{Ph}$-Ni(PPh$_3$)Ph (2-PPh$_3$)

In the glove box, to a solution of **2-py** (35.44 mg, 0.04 mmol) in toluene (6 mL) was added 1 equiv. of PPh_3 (10.48 mg, 0.04 mmol). After stirring for 15 min, all volatiles were removed under vacuum. To the residue was added toluene (6 mL) and the volatiles were removed under vacuum again. The above step was repeated for several times until quantitative converion of **2-py** to **2-PPh$_3$** (41.8 mg, >97% yield).

^{1}H NMR (400 MHz, C_6D_6) δ 7.50 (ddd, J = 9.8, 7.7, 1.8 Hz, 8H, ArH), 7.08 – 6.88 (m, 30H, ArH), 6.87 – 6.81 (m, 4H, Raha), 6.73 – 6.66 (m, 3H, ArH), 6.60 (t, J = 7.7 Hz, 2H, ArH), 6.42 (dd, J = 8.2, 3.2 Hz, 4H, ArH), 5.18 (d, J = 1.7 Hz, 1H, ArH). ^{31}P NMR (162 MHz, C_6D_6) δ -5.98 (d, *J* = 303 Hz), 23.44 (d, *J* = 303 Hz).

3. Ligand Exchange Studies

Representative procedure. In the glovebox, to a solution of **2-PEt$_3$** (0.0059 mmol, 5.5 mg) and in C_6D_6 (438 mg) was added a known amount of pyridine. The mixture was fully dissolved and transferred to an NMR tube. The rate of exchange is slow relative to the NMR timescale which lead to two separate species observed. $^{31}P\{^{1}H\}$ and ^{1}H NMR spectra were collected in 1-h intervals until the spectra remained unchanged. The relative intensities of the two species are determined through the $^{31}P\{^{1}H\}$ NMR resonances.

Results.

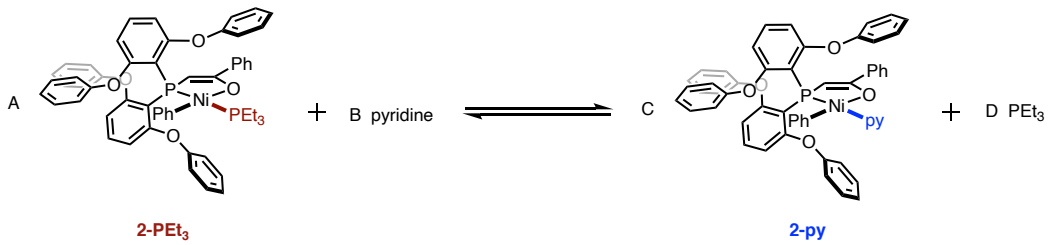

Entry	A_0	B_0	$A_{Equilbrium}$	$B_{Equilbrium}$	$C_{Equilbrium}$	$D_{Equilbrium}$	$K_{py/PEt3}$	$\mathbf{K_{PEt3/py}}$
1	1	150	0.92	~150	0.08	0.08	0.0000464	**21600**
2	1	1000	0.80	~1000	0.20	0.20	0.000050	**20000**
3	1	1500	0.76	~1500	0.24	0.24	0.0000505	**19800**

Therefore $K_{P/py}$~ 20000, log $K_{PEt3/py}$~ 4.3.

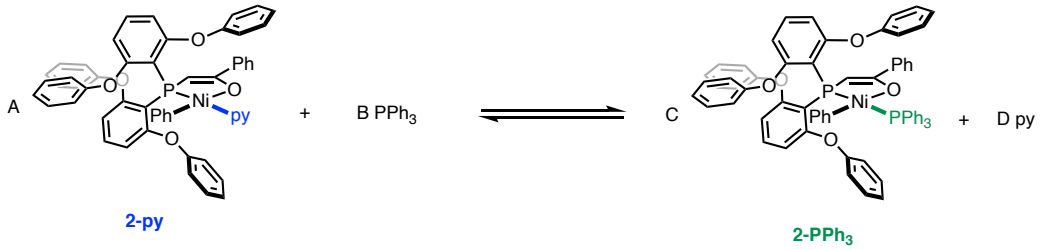

Entry	A_0	B_0	C_0	D_0	$A_{Equilbrium}$	$B_{Equilbrium}$	$C_{Equilbrium}$	$D_{Equilbrium}$	$\mathbf{K_{PPh3/py}}$
1	1	1	0	0	0.35	0.35	0.65	0.65	**3.4**
2	1	2	0	0	0.15	1.15	0.85	0.85	**4.2**
3	1	4	1	1	0.14	3.14	0.86	1.86	**3.6**

Therefore $K_{P/py}$~ 4, log $K_{PPh3/py}$~ 0.6.

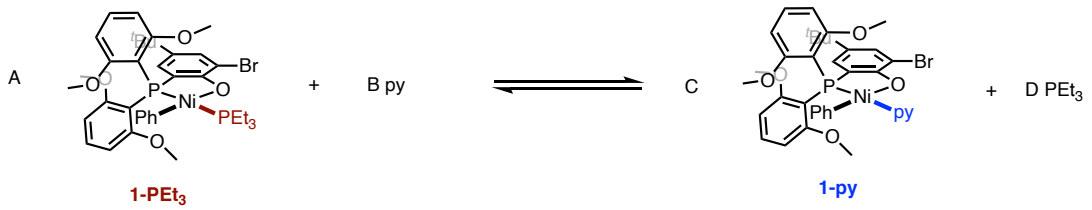

Entry	A_0	B_0	$A_{Equilbrium}$	$B_{Equilbrium}$	$C_{Equilbrium}$	$D_{Equilbrium}$	$K_{py/PEt3}$	$\mathbf{K_{PEt3/py}}$
1	1	200	0.92	~200	0.08	0.08	0.0000348	**28800**
2	1	500	0.87	~500	0.13	0.13	0.0000388	**25800**
3	1	3000	0.71	~3000	0.29	0.29	0.0000395	**25326**

Therefore $K_{P/py}$~ 25000, log $K_{PEt3/py}$~ 4.4.

4. Crystallographic Information

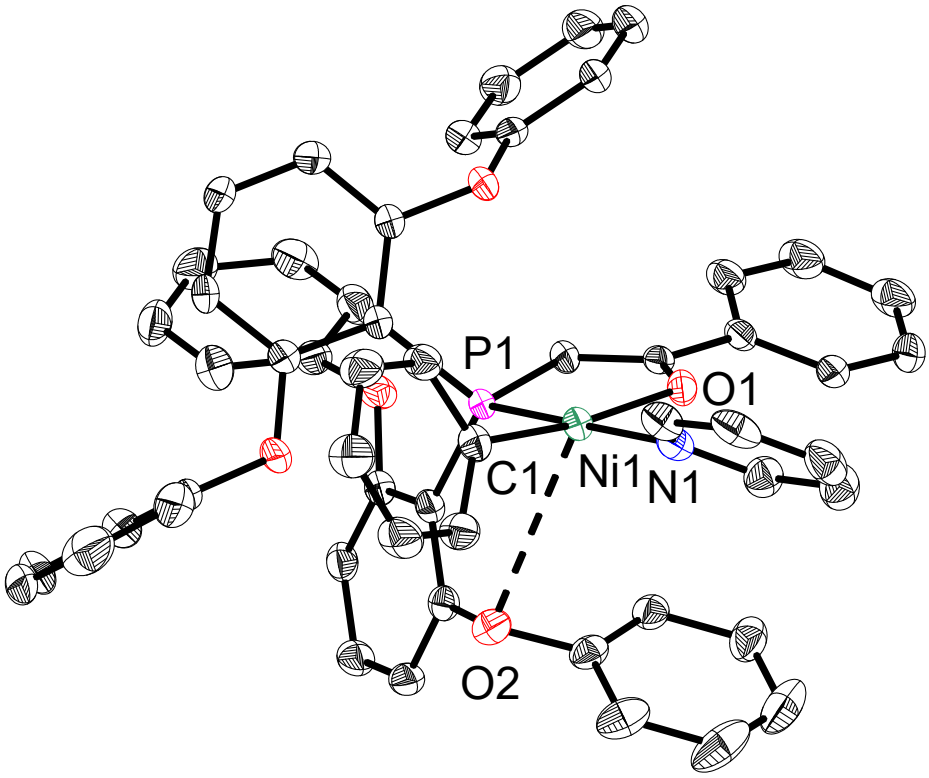

Figure S5.4.1. Solid-State Structure of **2-py**. Ellipsoids are shown at the 50% probability level. Hydrogen atoms and solvent molecules excluded for clarity.

Special Refinement Details for 2-py: Complex **2-py** crystalizes as needles/needle-like thin blocks in a P-1 space group with two molecules in the asymmetric unit (only one is shown in figure S22 for clarity), as well as one outer-sphere diethyl ether molecule.

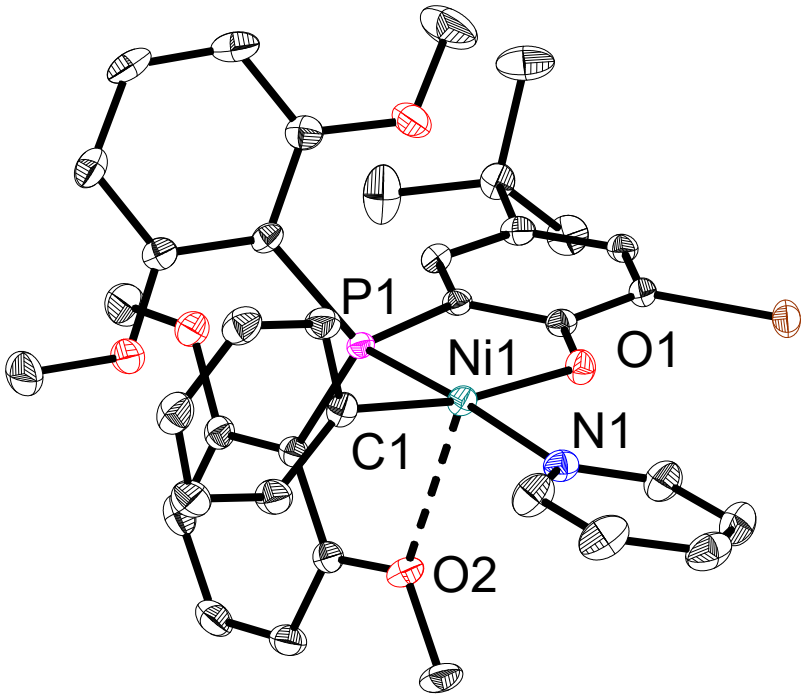

Figure S5.4.2. Solid-State Structure of **1-py**. Ellipsoids are shown at the 50% probability level. Hydrogen atoms and solvent molecules excluded for clarity.

Special Refinement Details for 1-py: Complex **1-py** crystalizes in a P-1 space group with one molecule in the asymmetric unit.

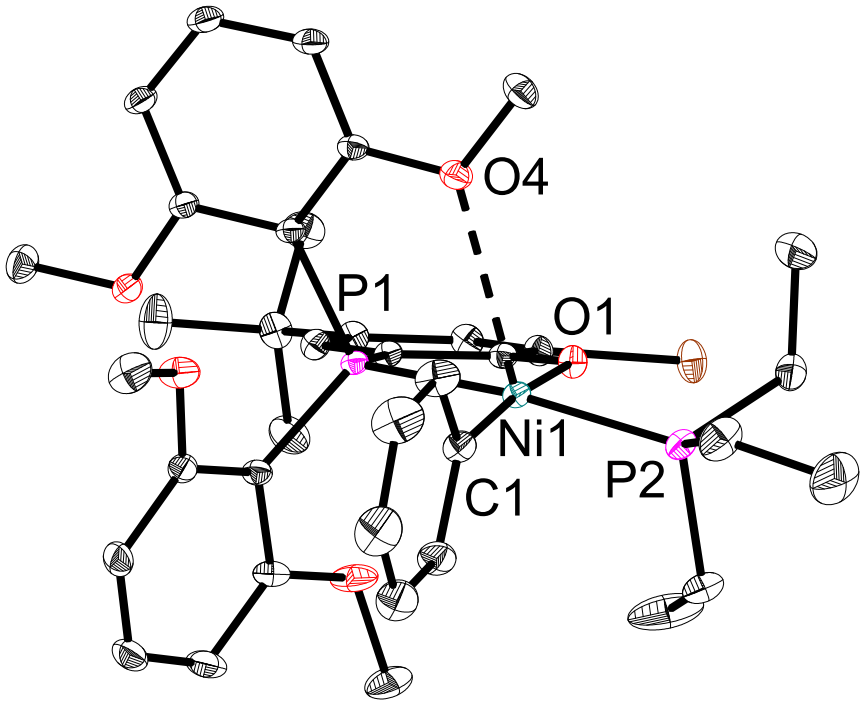

Figure S5.4.3. Solid-State Structure of **1-PEt$_3$**. Ellipsoids are shown at the 50% probability level. Hydrogen atoms and solvent molecules excluded for clarity.

Special Refinement Details for 1-PEt$_3$: Complex **1-PEt$_3$** crystalizes in a P-1 space group with one molecule in the asymmetric unit.

Crystallographic Information

Table S5.4.1. Crystal and refinement data.

	1-PEt$_3$	**1-py**	**2-py**
CCDC	2240825	2240827	2240826
Empirical formula	$C_{38}H_{49}BrNiO_5P_2$	$C_{37}H_{39}BrNNiO_5P$	$C_{57}H_{47}NNiO_{5.5}P$
Formula weight	786.3	747.3	923.6
Temperature/K	100	100.0	100
Crystal system	Triclinic	Monoclinic	Triclinic
Space group	P-1	$P2_1/n$	P-1
a/Å	10.3124(4)	11.6704(12)	12.607(1)
b/Å	13.674(3)	20.7729(18)	17.131(1)
c/Å	14.277(3)	14.1219(11)	23.826(1)
α/°	98.571(11)	90	90.931(2)
β/°	100.819(12)	95.872(8)	91.839(2)
γ/°	103.599(13)	90	99.079(2)
Volume/Å^3	1882.2(7)	3405.6(5)	5077.2(4)
Z	2	4	4
ϱ_{calc}g/cm^3	1.388	1.458	1.208
μ/mm^{-1}	1.702	2.993	1.232
F(000)	821	1535	1932
Radiation	MoKα (λ = 0.71073)	CuKα (λ = 1/54178)	CuKα (λ = 1/54178)
Reflections collected	89011	11904	118128
Independent reflections	20596	6520	19869
Goodness-of-fit on F^2	1.018	1.033	1.049
Final R indexes [I>=2σ (I)]	R_1 = 2.90 %, R_2 = 7.17 %	R_1 = 3.06 %, R_2 = 7.94 %	R_1 = 6.24 %, R_2 = 19.19 %

5. Procedures for Polymerization and Polymer characterization

5.1 General procedure for high throughput parallel polymerization reactor (PPR) runs for preparation of polyethylene and ethylene/tBA copolymers.

Polyolefin catalysis screening was performed in a high throughput parallel polymerization reactor (PPR) system. The PPR system was comprised of an array of 48 single cell (6 x 8 matrix) reactors in an inert atmosphere glovebox. Each cell was equipped with a glass insert with an internal working liquid volume of approximately 5 mL. Each cell had independent controls for pressure and was continuously stirred at 800 rpm. Catalyst solutions (with $Ni(COD)_2$ if necessary) were prepared in toluene. All liquids (i.e., solvent, tBA, and catalyst solutions) were added via robotic syringes. Gaseous reagents (i.e., ethylene) were added via a gas injection port. Prior to each run, the reactors were heated to 50 °C, purged with ethylene, and vented.

All desired cells were injected with tBA followed with a portion of toluene (This step was skipped for ethylene homopolymerization). The reactors were heated to the run temperature and then pressured to the appropriate psig with ethylene. Catalyst solutions (with $Ni(COD)_2$ if necessary) were then added to the cells. Each catalyst addition was chased with a small amount of toluene so that after the final addition, a total reaction volume of 5 mL was reached. Upon addition of the catalyst, the PPR software began monitoring the pressure of each cell. The desired pressure (within approximately 2-6 psig) was maintained by the supplemental addition of ethylene gas by opening the valve at the set point minus 1 psi and closing it when the pressure reached 2 psi higher. All drops in pressure were cumulatively recorded as "Uptake" or "Conversion" of the ethylene for the duration of the run or until the uptake or conversion requested value was reached, whichever occurred first. Each reaction was then quenched by addition of 1% oxygen in nitrogen for 30 seconds at 40 psi higher than the reactor pressure. The pressure of each cell was monitored during and after the quench to ensure that no further

ethylene consumption happens. The shorter the "Quench Time" (the duration between catalyst addition and oxygen quench), the more active the catalyst. In order to prevent the formation of too much polymer in any given cell, the reaction was quenched upon reaching a predetermined uptake level of 80 psig. After all the reactors were quenched, they were allowed to cool to about 60 °C. They were then vented, and the tubes were removed. The polymer samples were then dried in a centrifugal evaporator at 60 °C for 12 hours, weighed to determine polymer yield and used in subsequent IR (tBA incorporation), GPC (molecular weight), DSC (melting temperature) and NMR (copolymer microstructures) analysis.

5.1.1 Measurement of ethylene uptake curves

Upon addition of the catalyst, the PPR software began monitoring the pressure of each cell. The desired pressure (within approximately 2-6 psig) was maintained by the supplemental addition of ethylene gas by opening the valve at the set point minus 1 psi and closing it when the pressure reached 2 psi higher. For example, the pressure was maintained between approximately 399-402 psi if the original pressure was set to 400 psi. All drops in pressure were cumulatively recorded as "Uptake" or "Conversion" of the ethylene for the duration of the run. The unit of this "Uptake" is in psi and the uptake curves over time were used to analyze the real-time activity of catalysts and rates of chain propagation.

5.2 General procedure for batch reactor runs for preparation of ethylene/tBA copolymers.

Polymerization reactions were conducted in a 2-L Parr batch reactor. The reactor was heated by an electrical heating mantle and cooled by an internal serpentine cooling coil containing cooling water. The water was pre-treated by passing through an Evoqua water purification system. Both the reactor and the heating/cooling system were controlled and monitored by a Camile TG process computer. The bottom of the reactor was fitted with a dump valve, which

empties the reactor contents into a lidded dump pot, which was prefilled with a catalyst-kill solution (typically 5 mL of an Irgafos / Irganox / toluene mixture). The lidded dump pot was vented to a 15-gal. blowdown tank, with both the pot and the tank N_2 purged. All chemicals used for polymerization or catalyst makeup are run through purification columns to remove any impurities that may affect polymerization. The toluene was passed through two columns, the first containing A2 alumina, the second containing Q5 reactant. The tert-butyl acrylate was filtered through activated alumina. The ethylene was passed through two columns, the first containing A204 alumina and 4 Å molecular sieves, the second containing Q5 reactant. The N2 used for transfers was passed through a single column containing A204 alumina, 4 Å molecular sieves and Q5 reactant.

The reactor was loaded first from the shot tank that contained toluene and tBA. The shot tank was filled to the load set points by use of a differential pressure transducer. After solvent/acrylate addition, the shot tank was rinsed twice with toluene. Then the reactor was heated up to the polymerization temperature set point. The ethylene was added to the reactor when the reaction temperature was reached to maintain the reaction pressure set point. Ethylene addition amounts were monitored by a micro-motion flowmeter.

The catalysts were handled in an inert atmosphere glovebox and were prepared as a solution in toluene. The catalyst was drawn into a syringe and pressure-transferred into the catalyst shot tank. This was followed by 3 rinses of toluene, 5 mL each. Catalyst was added when the reactor pressure set point was reached.

Immediately after catalyst addition the run timer was started. Usually within the first 2 min. of successful catalyst runs an exotherm was observed, as well as decreasing reactor pressure. Ethylene was then added by the Camile to maintain reaction pressure set point in the reactor. These polymerizations were run until 40 g of ethylene uptake. Then the agitator was stopped,

and the bottom dump valve was opened to empty reactor contents into the lidded dump pot. The lidded dump pot was closed and the contents were poured into trays placed in a lab hood where the solvent was evaporated off overnight. The trays containing the remaining polymer were then transferred to a vacuum oven, where they were heated up to 140 °C under vacuum to remove any remaining solvent. After the trays cooled to ambient temperature, the polymers were weighed for yield/efficiencies and submitted for polymer testing if so desired.

5.3 General procedure for polymer characterization

5.3.1 Gel permeation chromatography (GPC)

High temperature GPC analysis was performed using a Dow Robot Assisted Delivery (RAD) system equipped with a Polymer Char infrared detector (IR5) and Agilent PLgel Mixed A columns. Decane (10 μL) was added to each sample for use as an internal flow marker. Samples were first diluted in 1,2,4-trichlorobenzene (TCB) stabilized with 300 ppm butylated hydroxyl toluene (BHT) at a concentration of 10 mg/mL and dissolved by stirring at 160°C for 120 minutes. Prior to injection the samples are further diluted with TCB stabilized with BHT to a concentration of 3 mg/mL. Samples (250 μL) are eluted through one PL-gel 20 μm (50 x 7.5 mm) guard column followed by two PL-gel 20 μm (300 x 7.5 mm) Mixed-A columns maintained at 160 °C with TCB stabilized with BHT at a flowrate of 1.0 mL/min. The total run time was 24 minutes. To calibrate for molecular weight (MW) Agilent EasiCal polystyrene standards (PS-1 and PS-2) were diluted with 1.5 mL TCB stabilized with BHT and dissolved by stirring at 160 °C for 15 minutes. These standards are analyzed to create a 3rd order MW calibration curve. Molecular weight units are converted from polystyrene (PS) to polyethylene (PE) using a daily Q-factor calculated to be around 0.4 using the average of 5 Dowlex 2045 reference samples.

5.3.2 Fourier-transform infrared spectroscopy (FTIR)

The 10 mg/mL samples prepared for GPC analysis are also utilized to quantify tert-butyl acrylate (tBA) incorporation by Fourier Transform infrared spectroscopy (FTIR). A Dow robotic preparation station heated and stirred the samples at 160°C for 60 minutes then deposited 130 μL portions into stainless wells promoted on a silicon wafer. The TCB was evaporated off at 160°C under nitrogen purge. IR spectra were collected using a Nexus 6700 FT-IR equipped with a DTGS KBr detector from 4000-400 cm-1 utilizing 128 scans with a resolution of 4. Ratio of tBA (C=O: 1762-1704 cm−1) to ethylene (CH2: 736-709 cm−1) peak areas were calculated and fit to a linear calibration curve to determine total tBA.

5.3.3 Differential scanning calorimetry (DSC)

Differential scanning calorimetry analyses was performed on solid polymer samples using a TA Instruments, Inc. Discovery Series or TA Instruments, Inc., DSC2500, programmed with the following method:

Equilibrate at 175.00 °C

Isothermal for 3 minutes

Ramp 30.00 °C/min to 0.00 °C

Ramp 10.00 °C/min to 175.00 °C

Data was analyzed using TA Trios software.

5.3.4 NMR characterization

NMR spectra of ethylene/tBA copolymers were recorded on a Bruker 400 MHz using o-dichlorobenzene at 120 °C. ^{1}H NMR analysis of copolymers were done using a relaxation time (0.2 s), and an acquisition time (1.8 s) with the number of FID's collected per sample (512). ^{13}C{^{1}H} NMR analysis of copolymers were done using 90° pulse of 17.2 μs, a relaxation time

(22.0 s), an acquisition time (5.3 s), and inverse-gated decoupling with the number of FID's collected per sample (1024). Analysis of the spectra was based on literature.[32, 34]

6. Original catalytic runs of ethylene/tBA copolymerization

6.1 Supplemental ethylene uptake curves

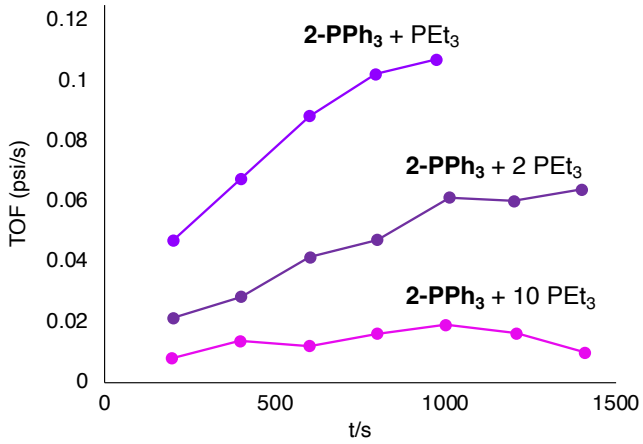

Figure S5.6.1. Rate of ethylene uptake (TOF) vs time with different PEt_3 concentrations (Catalyst: **2-PPh$_3$**). Condition: V = 5 mL, [Ni] = 0.05 mM, ethylene pressure = 400 psi, [tBA] = 0.05 M, toluene solvent. See Table S5.6.5 for original catalytic runs.

6.2 Original catalytic runs of ethylene/tBA copolymerization included in Table 5.1

Table S5.6.1. Original data for Table 5.1.

Entry	Catalyst	[Ni]/mM	[tBA]/M	T/ºC	t/s	Isolated Yield/mg	Activity[b]	Mw/10^3	PDI	%Mol tBA	Tm /ºC
1	**1-PEt$_3$**	0.05	0.05	90	3601	47	190	60.27	2.22	1.79	113
2	**1-PEt$_3$**	0.05	0.05	90	3600	54	220	65.20	2.38	1.67	114
3	**1-PEt$_3$**	0.05	0.05	90	3601	57	230	63.92	2.21	1.66	114
4	**1-PEt$_3$**	0.05	0.1	90	3600	31	120	39.75	2.25	3.47	104
5	**1-PEt$_3$**	0.05	0.1	90	3600	31	120	42.83	2.95	3.48	103
6	**1-py**	0.05	0.05	90	1761	125	1020	79.63	2.24	1.66	115
7	**1-py**	0.05	0.05	90	1457	114	1130	76.73	2.58	1.61	115
8	**1-py**	0.05	0.05	90	1504	122	1170	78.96	2.13	1.47	N.D.
9	**1-py**	0.05	0.1	90	3601	104	420	54.16	2.17	3.25	105
10	**1-py**	0.05	0.1	90	3600	118	470	55.79	2.17	3.23	105
11	**2-PEt$_3$**	0.05	0.05	90	1304	117	1300	10.34	2.27	0.50	122
12	**2-PEt$_3$**	0.05	0.05	90	1125	113	1400	10.14	2.41	0.55	122

13	**2-PEt$_3$**	0.05	0.05	90	1213	115	1400	10.62	2.41	0.54	122
14	**2-PEt$_3$**	0.05	0.05	90	1274	124	1400	10.06	2.20	0.53	122
15	**2-py**	0.05	0.05	90	296	114	5500	10.32	2.32	0.57	122
16	**2-py**	0.05	0.05	90	280	123	6300	11.04	2.84	0.56	121
17	**2-py**	0.05	0.05	90	252	118	6800	9.16	2.76	0.56	121
18	**2-py**	0.05	0.05	90	323	141	6300	10.66	2.25	0.52	122
19	**2-PPh$_3$**	0.05	0.05	90	342	128	5400	11.95	2.13	0.51	121
20	**2-PPh$_3$**	0.05	0.05	90	320	126	5700	13.12	1.92	N.D.	124
21	**2-PPh$_3$**	0.05	0.05	90	304	124	5900	11.38	2.18	0.50	121
22	**2-PPh$_3$** + 1 PEt$_3$	0.05	0.05	90	973	126	1860	11.24	2.20	0.50	120
23	**2-PPh$_3$** + 1 PEt$_4$	0.05	0.05	90	1096	140	1840	10.06	2.24	0.53	122
24	**2-PPh$_3$** + 1 PEt$_5$	0.05	0.05	90	865	115	1910	11.96	1.94	0.45	122
25	**2-PPh$_3$** + 2 PEt$_3$	0.05	0.05	90	1545	119	1110	10.27	2.34	0.51	122
26	**2-PPh$_3$** + 2 PEt$_4$	0.05	0.05	90	1268	108	1230	9.86	2.38	0.51	122
27	**2-PPh$_3$** + 2 PEt$_5$	0.05	0.05	90	1309	114	1250	10.57	2.61	0.50	122
28	**2-PPh$_3$** + 10 PEt$_6$	0.05	0.05	90	3601	40	160	3.16	2.22	0.47	121
29	**2-PPh$_3$** + 10 PEt$_7$	0.05	0.05	90	3601	46	190	3.57	2.21	0.46	121
30	**2-PPh$_3$** + 10 PEt$_8$	0.05	0.05	90	3600	47	190	4.50	2.82	0.48	121
31	**2-PEt$_3$**	0.05	0.05	110	493	126	3700	8.55	2.48	0.66	120
32	**2-PEt$_3$**	0.05	0.05	110	454	113	3600	7.84	2.45	0.58	122
33	**2-PEt$_3$**	0.05	0.05	110	417	111	3800	8.10	2.34	0.49	121
34	**2-py**	0.05	0.05	110	169	142	12100	6.63	2.43	0.70	123
35	**2-py**	0.05	0.05	110	159	143	12900	6.70	2.55	0.66	122
36	**2-py**	0.05	0.05	110	145	150	14900	7.17	2.18	0.52	122
37	**2-py**	0.05	0.1	110	399	135	4900	7.40	2.60	1.11	113
38	**2-py**	0.05	0.1	110	368	121	4700	6.74	2.34	1.14	115
39	**2-py**	0.05	0.1	110	376	120	4600	6.17	2.48	1.20	113
40	**2-py**	0.05	0.15	110	587	117	2900	6.68	2.43	1.51	113
41	**2-py**	0.05	0.15	110	571	118	3000	6.48	2.24	1.60	111
42	**2-PEt$_3$**	0.025	0.025	90	587	117	3400	11.43	2.37	0.33	125
43	**2-PEt$_3$**	0.025	0.025	90	571	118	2600	11.13	2.29	0.32	125
44	**2-py**	0.025	0.025	90	323	130	11600	14.09	3.37	0.31	125
45	**2-py**	0.025	0.025	90	302	120	11400	12.03	2.43	0.30	123
46	**2-py**	0.025	0.025	90	323	131	11700	12.38	2.15	0.29	123
47	**2-py**	0.025	0.025	90	209	143	19700	11.66	2.54	0.24	126
48	**2-PEt$_3$**	0.025	0.025	110	492	120	7000	14.09	3.37	0.31	125
49	**2-PEt$_3$**	0.025	0.025	110	470	122	7500	12.03	2.43	0.30	123
50	**2-PEt$_3$**	0.025	0.025	110	455	116	7300	12.38	2.15	0.29	123
51	**2-PEt$_3$**	0.025	0.025	110	452	119	7600	11.66	2.54	0.24	126
52	**2-py**	0.025	0.025	110	186	138	21000	8.56	2.42	0.32	124
53	**2-py**	0.025	0.025	110	180	144	23000	7.72	2.53	0.32	124

54	**2-py**	0.025	0.025	110	162	135	24000	7.96	2.56	0.33	124
55	**2-py**	0.025	0.025	110	139	136	28000	8.27	2.36	0.29	123

[a]Unless specified, V = 5 mL, [Ni] = 0.05 mM, ethylene pressure = 400 psi, toluene solvent; polymerization was stopped after consuming a set amount of ethylene. [b]Activity in kg/(mol·h).

6.3 Original ethylene/tBA copolymerization runs of ethylene uptake curves included in Figure 5.2

Table S5.6.2. Original runs of ethylene uptake curves in Figure 5.2a

Entry	Catalyst	[Ni]/mM	[tBA]/M	T/°C	t/s	Isolated Yield/mg	Activity[b]	Mw/10^3	PDI	%Mol tBA	Tm/°C
1	**2-PEt$_3$**	0.025	0.025	110	470	122	7500	12.03	2.43	0.3	123
2	**2-py**	0.025	0.025	110	162	135	24000	7.96	2.56	0.33	124

[a]Unless specified, V = 5 mL, ethylene pressure = 400 psi, toluene solvent; polymerization was stopped after consuming a set amount of ethylene. Entries 1~2 were also included in table S5.6.1 as entry 49, and 54, respectively. [b]Activity in kg/(mol·h).

Table S5.6.3. Original runs of ethylene uptake curves in Figure 5.2b-c

Entry[a]	Catalyst	[Ni(COD)$_2$]/ mM	[tBA]/M	T/°C	t/s	Isolated Yield/mg	Activity[b]	Mw/10^3	PDI	%Mol tBA	Tm/°C
1	**1-PEt$_3$**	0.05	0.05	90	3601	57	230	63.92	2.21	1.66	114
2	**1-py**	0.05	0.05	90	1504	122	1170	78.96	2.13	1.47	N.D.
3[c]	**2-py**	0	0.05	110	159	143	12900	6.7	2.55	0.66	122
4	**2-py**	0	0.10	110	376	120	4600	6.17	2.48	1.2	110
5	**2-py**	0	0.15	110	571	118	3000	6.48	2.24	1.6	111
6	**2-py**	0	0.05	90	323	141	6300	10.66	2.25	0.52	122
7	**2-PEt$_3$**	0	0.05	90	1053	101	1380	10.6	2.40	0.5	122
8	**2-PEt$_3$**	0.20	0.05	90	743	100	2000	12.3	2.70	0.6	122

[a]Unless specified, V = 5 mL, [Ni] = 0.05 mM, ethylene pressure = 400 psi, toluene solvent; polymerization was stopped after consuming a set amount of ethylene. Entries 1~4 were also included in table S5.6.1 as entry 35, 39, 41, and 16, respectively. [b]Activity in kg/(mol·h). [c]Reported in ref 3 (Table S6.3, entry 37). [d]Reported in ref 3 (Table S6.3, entry 24).

Table S5.6.4. Original runs for ethylene uptake curves in Figure 3

Entry[a]	Catalyst	[Ni(COD)$_2$]/ mM	[tBA]/M	T/°C	t/s	Isolated Yield/mg	Activity[b]	Mw/10^3	PDI	%Mol tBA	Tm/°C
1[c]	**^{Me}PO^{Ph}-Ni(P)**	0	0.05	90	3600	51	210	2.9	2.1	2.0	114
2	**2-PEt$_3$**	0	0.05	90	1053	101	1380	10.6	2.4	0.5	122
3	**^{Ph}PO^{PhCF3}-Ni(P)**	0	0.05	90	1156	106	1320	6.3	2.2	0.5	122
4	**^{Ph}PO^{ArOMe}-Ni(P)**	0	0.05	90	1148	116	1460	11.5	2.5	0.6	121
5[d]	**^{Ph}P*O^{ArO}-Ni(P)**	0	0.05	90	3412	94	400	10.2	2.5	0.6	122

[a]Unless specified, V = 5 mL, [Ni] = 0.05 mM, ethylene pressure = 400 psi, toluene solvent; polymerization was stopped after consuming a set amount of ethylene. [b]Activity in kg/(mol·h). [c]Reported in ref 3 (Table S6.3, entry 37). [d]Reported in ref 3 (Table S6.3, entry 24).

Table S5.6.5. Original ethylene/tBA copolymerization runs of ethylene uptake curves included in Figure S5.6.1.

Entry	Catalyst	T/°C	t/s	Isolated Yield/mg	Activity[b]	Mw/10^3	PDI	%Mol tBA	Tm/°C
1	**2-PPh$_3$** + 1 PEt$_3$	90	973	126	1860	11.24	2.20	0.50	120
2	**2-PPh$_3$** + 2 PEt$_3$	90	1545	119	1110	10.27	2.34	0.51	122
3	**2-PPh$_3$** + 10 PEt$_6$	90	3601	40	160	3.16	2.22	0.47	121

[a]Unless specified, V = 5 mL, [Ni] = 0.05 mM, ethylene pressure = 400 psi, [tBA] = 0.05 M, toluene solvent; polymerization was stopped after consuming a set amount of ethylene. Entries 1~3 were also included in table S5.6.1 as entry 22, 25, 28, and 16, respectively. [b]Activity in kg/(mol·h).

7. Characterization of ethylene/tBA copolymers

7.1 Samples of ^{1}H and ^{13}C{^{1}H} spectra of ethylene/tBA copolymers

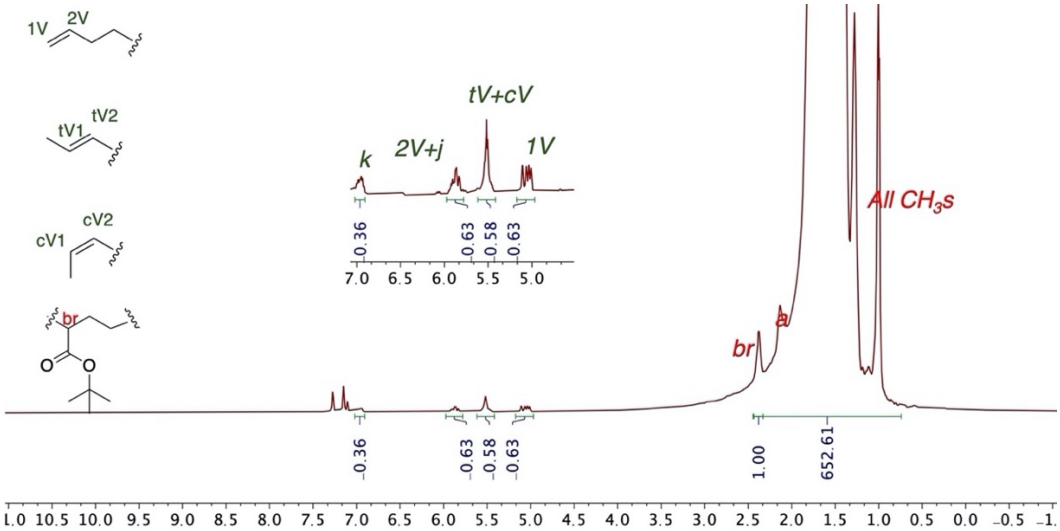

Figure S5.7.1. ^{1}H NMR spectrum of ethylene/tBA copolymer **P*** (Table 5.6.1, entry 15).

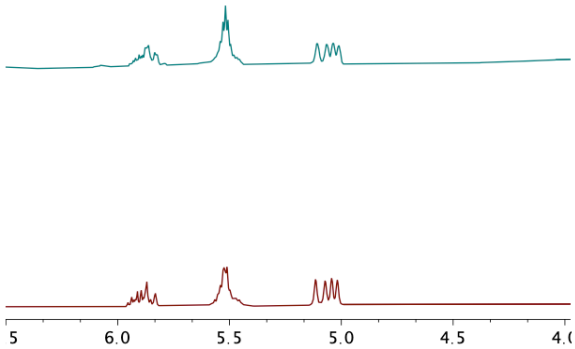

Figure S5.7.2. Comparison of ^{1}H NMR spectra of ethylene/tBA copolymer **P*** (top) and **P** (bottom) (Note: Copolymer samples **P** is the copolymers produced by **^{Ph}PO^{Ph}-Ni(P)** and has been reported in ref 2b as sample C. Sample P and P* were produced in ethylene/tBA copolymerization by **^{Ph}PO^{Ph}-Ni(P)** or **^{Ph}PO^{Ph}-Ni(py)** under otherwise identical conditions.)

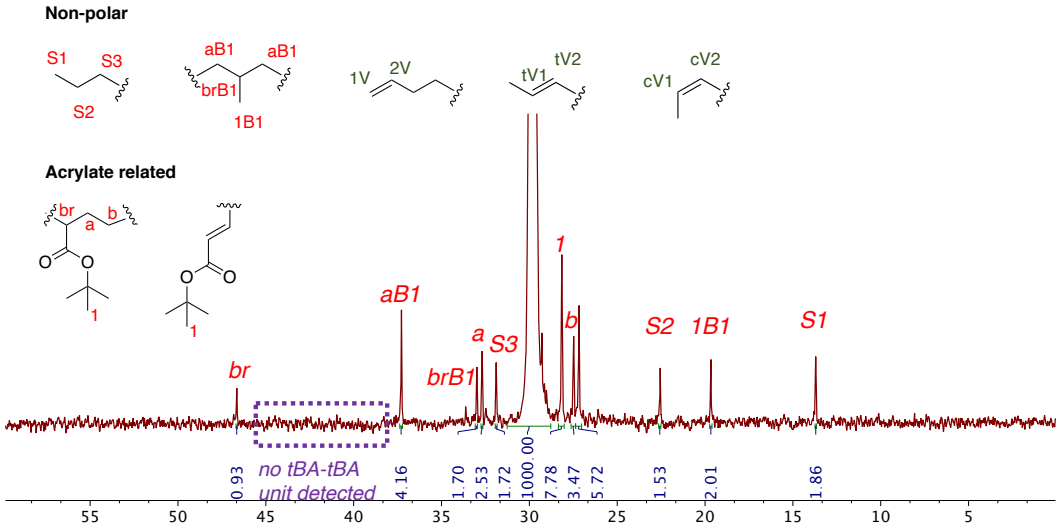

Figure S5.7.3. ^{13}C{^{1}H} NMR spectrum of ethylene/tBA copolymer **P*** with peaks assigned to specific microstructural features.

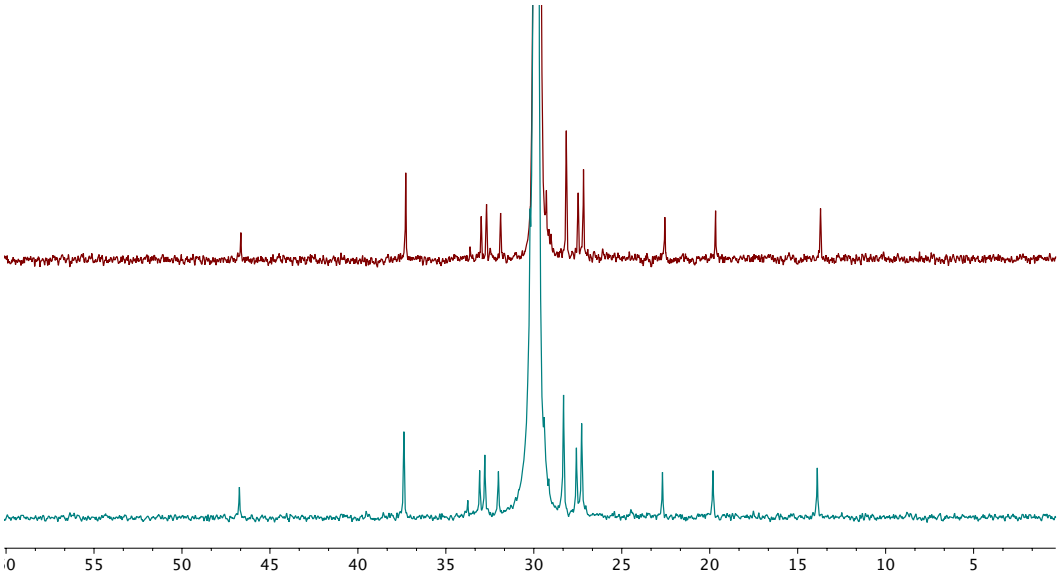

Figure S5.7.4. Comparison of $^{13}C\{^{1}H\}$ NMR spectra of ethylene/tBA copolymer **P*** (top) and **P** (bottom)

7.2 Microstructural analysis

Calculation of Mn based on ^{1}H NMR spectra

Below shown the calculation of Mn from a ^{1}H NMR spectrum (Figure S5.7.1). Note that the integration of the resonance of *br* set to 1, therefore all values of integration in ^{1}H NMR spectra are all relevant numbers of protons per occurrence of a tBA units (labeled as rX)

rX = relevant number of carbon atoms

rX-H = relevant number of proton atoms = 652.63 + 0. 63 + 0.58 + 0.63 + 0.36 = 654.83

Each ethylene unit has 2 carbon and 4 protons

For tBA units, each tBA unit has 6 carbon and 12 protons exclude the ester group (-C(O)O-). Note that the relevant number of tBA units is 1 (reference).

Therefore **rX = 0.5 * rX-H + 1**

rC = relevant number of polymer chain

rC = 0.5 * 0.63 + 0.5 * 0.58 + 0.36 = 0.965

M_n = (rX * 12 + rX-H * 1 + 2 * Mol Wt (O))/rC = ((0.5 * rX-H + 1) * 12 + rX-H + 2 * 16)/rC = (7 * 654.83 + 6 + 32)/0.965 = 4.789k ~ 4.8k

For comparison, the molecular weight obtained by GPC is M_n =4.45 k

Methods of microstructural analysis

- **%Mol tBA (NMR)**

Calculation of % Mol tBA (NMR) is based on the ^{1}H NMR spectrum and section S7.1.2.

rR = relevant number of repeating units = 0.5 * (rX-4) = 0.25 * rX-H - 1.5

Relevant number of tBA units = 1

% Mol tBA = 1 / rR = 1 / (0.25 * rX-H - 1.5)

For sample **P***, % Mol tBA = 1 / (0.25 * 654.83 - 1.5) = 0.6 %, which is consistent with the result obtained from quantitative FTIR.

- **%I-tBA**

%I-tBA is the percentage of internal tBA units over all tBA units. Calculation of **%I-tBA** is based on the ^{13}C{^{1}H} NMR spectrum. Note that all tBA units have t-butyl group (peak 1) but only internal tBA units have saturated α- and β-carbon (peak a, b). For sample **P***:

% I -tBA = (0.5 * Integration of peak b)/(0.333 * Integration of peak 1) = 67%

- **%T-tBA**

%T-tBA is the percentage of terminal tBA units over all tBA units.

%T-tBA = 1 - %I-tBA

For sample **P***, **%T-tBA** = 33%

- **%Vinyl**

% Vinyl is the ratio of the number of terminal vinyl units over the number of tBA units in percentage.

% Vinyl is calculated based on the ^{1}H NMR spectra and section S7.1.2. For sample **P***:

rV = relevant number of vinyls = 0.5 * integration of peak 1V

rT-tBA = relevant number of terminal tBA = integration of peak k (if cis-end tBA is not present)

%Vinyl/%T-tBA=rV/rT-tBA

For sample **P***, % Vinyl = 29%

- **N(Methyl)**

Calculation of **N(Methyl)** is based on the ^{13}C{^{1}H} NMR spectrum (unit: 1/1000C).

N(Methyl) = 1000 * Integration of 1B1/Intergration of all main-chain carbons

For sample **P***, **N(Methyl)** = 2.0

- **N(2-Propenyl)**

Calculation of **N(2-Propenyl)** is based on the ^{1}H NMR spectrum (unit: 1/1000C).

N(2-Propenyl) = 1000 * relevant number of propenyl/rX = 1000 * (0.5 * integration of peak (TV+CV)/(0.5 * rX-H + 1)

For sample **P***, **N(2-Propenyl)** = 0.9

Comparison of copolymer microstructures

Copolymer samples **P** is the copolymers produced by **^{Ph}PO^{Ph}-Ni(P)** (reported in ref 2b as sample C). Sample P and P* were produced in ethylene/tBA copolymerization by **^{Ph}PO^{Ph}-Ni(P)** or **^{Ph}PO^{Ph}-Ni(py)** under otherwise identical conditions.

Table S5.7.1 Comparison of ethylene/tBA copolymers **P** and **P***.

	P	**P***
Catalyst	**$^{Ph}PO^{Ph}$-Ni(P)**	**$^{Ph}PO^{Ph}$-Ni(py)**
Mn(GPC)/10^3	4.36	4.45
% I-tBA	59%	67%
% T-tBA	41%	33%
% Vinyl	21%	29%
Methyl/1000C	1.7	2.0
2-Propenyl/1000C	0.6	0.9
Mn(NMR)/10^3	4.76	4.78

7.3 A samples of GPC curves of ethylene/tBA copolymers

Conventional GPC & Composition Results

LIMS #:	22-0604	Description:	Library 385457 Vial 19
Project:		Report by:	
For:	FileProc	Method:	Not Selected

MWD Results: Conventional GPC		Quadrant Analysis			Run Parameters:	
Mn	4,450	25%	21270		Conc	2.0000
Mp	8,990	50%	10300	10	Inj. Vol.	250.0
Mv	9,410	75%	5800		Mass Inj.	0.5000
Mw	10,320	100%	2150		MassRec.	88.50%
Mz	18,640	Whole	7160		System Parameters:	
PDI	2.32	50% Ratio	3.97	-60	Flow Rate	1.0010
				271.64	Flow Marker	18.501
Comonomer Type	Octene				Ref Flow Marker	18.482
Avg SCB/1000TC	9.61				Rec. Flow Rate	
Avg Wt% Comonomer	9.24					
Avg Corrected Wt%	7.69					

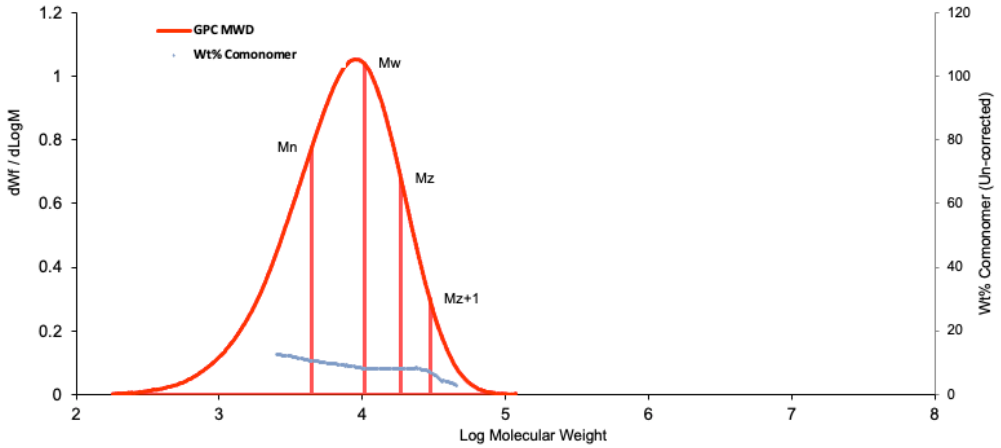

Figure S5.7.5. GPC curve of ethylene/tBA copolymers (table S5.6.1, entry 15).

7.4 A sample of DSC curves of ethylene/tBA copolymers

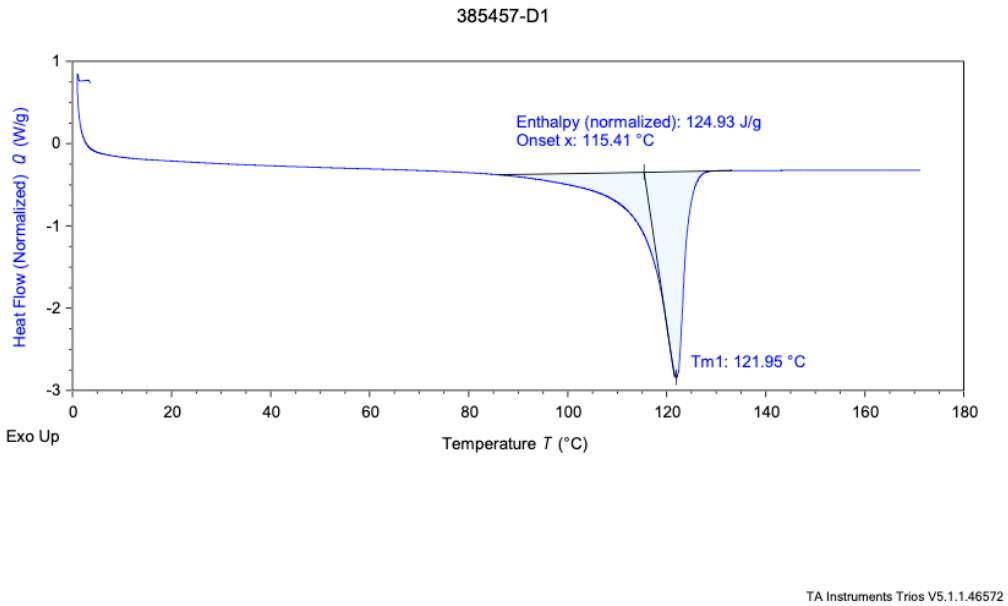

Figure S5.7.6. GPC curve of ethylene/tBA copolymers (table S5.6.1, entry 15).

8. Catalyst comparison

The catalysts reported here are notable for high activity and thermal stability for polar polyolefin synthesis. A variety of catalysts have been developed for ethylene/acrylate copolymerization.[19-20, 22, 24, 29, 32-34, 45, 48, 51, 57, 59, 66-124] Previous examples of nickel catalyzed ethylene acrylate copolymerization are relatively rare, with the majority supported by phenoxide/napthoxide-based ligands. [32-34, 67-68, 70, 121, 125] To compare the performance of our best catalyst, **2-py** to prior examples, two metrics were plotted: catalyst activity and tBA incorporation (Figure S5.8.1).

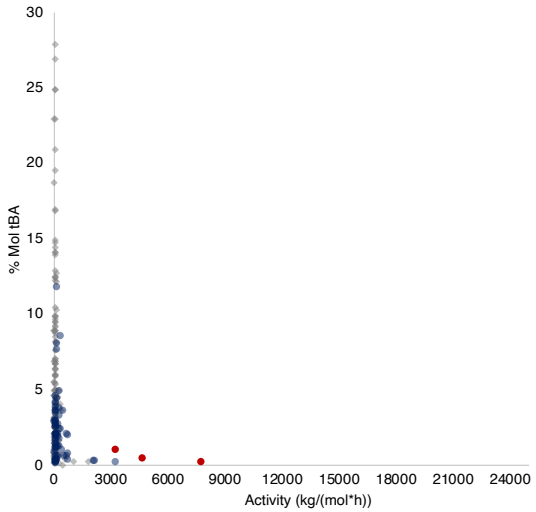

Figure S5.8.1. Reported Pd and Ni catalysts for ethylene/acrylate copolymerization (Squares: palladium examples; rounds: nickel examples, red rounds: **2-PEt$_3$**, darker color indicates overlapping data points; reported catalysts are included if they: 1) shows activity higher than 0.5 kg/(mol*h) in ethylene acrylate copolymerization and 2) produce copolymers with Mw>2500).

Previously reported ethylene/acrylate copolymerization experiments were included if they feature: 1) activity > 0.5 kg/(mol*h) and 2) copolymer Mw>2500. In addition, experiments are excluded if they were performed with large amounts of activator/masking reagents on a scale comparable to the amount of acrylate (additives:acrylates > 1:10). Overall, experiments under 468 different reaction conditions, or 229 different catalysts, from 75 scientific papers are included in catalyst comparison.[19-20, 22, 24, 29, 32-34, 45, 48, 51, 57, 59, 66-124] Reaction conditions, such the ethylene pressure, catalyst and monomer concentration, may differ, therefore these comparisons should be considered qualitative.

Overall, most examples show limited activities of less than 100 kg/(mol·h) (423 out of 468 experiments, or 200 out of 229 catalysts), though being able to produce copolymers with varying molecular weights, branching distribution and polar monomer incorporation. An important aspect to consider is that increased acrylate incorporation will result in lower activity, which affects some of the systems compared. Specifically, both catalyst activity and tBA incorporation are limited for Ni-catalyzed ethylene/acrylate copolymerization, except a recent example

showing ability to incorporate up to 12 mol% tBA.[34] **2-PEt$_3$**, a catalyst we recently reported, displays significant improved activity (yellow data points) compared to previous reports.

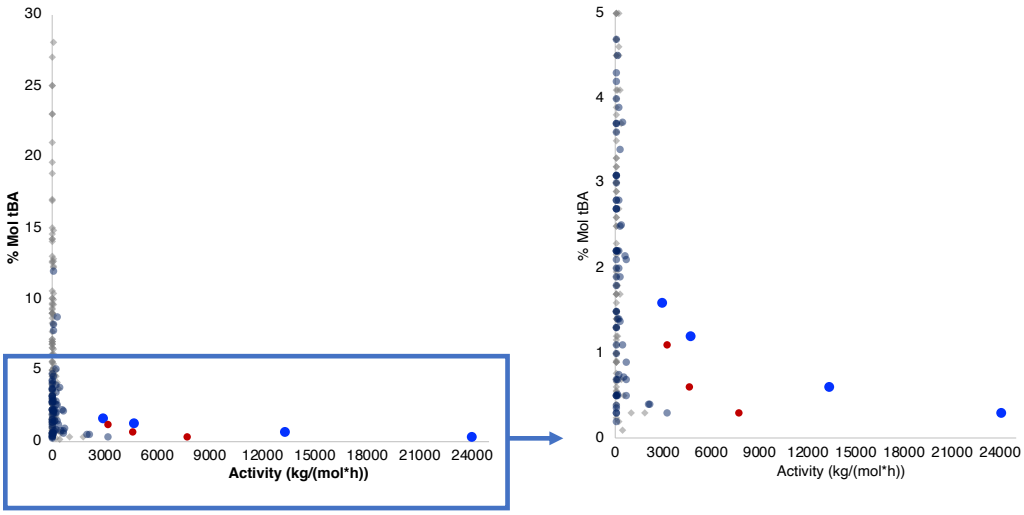

Figure S5.8.2. Comparison of **2-py** with reported Pd and Ni catalysts for ethylene/acrylate copolymerization (Squares: palladium examples; rounds: nickel examples, red rounds: **2-PEt$_3$**, blue rounds: **2-py** darker color indicates overlapping data points; reported catalysts are included if they: 1) shows activity higher than 0.5 kg/(mol*h) in ethylene acrylate copolymerization and 2) produce copolymers with Mw>2500)

The best catalyst included in this work, **2-py**, displays further improvements in activity (Figure S5.8.2).

REFERENCES

(1) Chen, C., Designing catalysts for olefin polymerization and copolymerization: beyond electronic and steric tuning. *Nat. Rev. Chem.* **2018,** *2* (5), 6-14.

(2) Hustad, P. D., Frontiers in olefin polymerization: Reinventing the world's most common synthetic polymers. *Science* **2009,** *325* (5941), 704-707.

(3) Boffa, L. S.; Novak, B. M., Copolymerization of polar monomers with olefins using transition-metal complexes. *Chem. Rev.* **2000,** *100* (4), 1479-1494.

(4) Nakamura, A.; Ito, S.; Nozaki, K., Coordination− insertion copolymerization of fundamental polar monomers. *Chem. Rev.* **2009,** *109* (11), 5215-5244.

(5) Franssen, N. M.; Reek, J. N.; de Bruin, B., Synthesis of functional 'polyolefins': state of the art and remaining challenges. *Chem. Soc. Rev.* **2013,** *42* (13), 5809-5832.

(6) Carrow, B. P.; Nozaki, K., Transition-metal-catalyzed functional polyolefin synthesis: effecting control through chelating ancillary ligand design and mechanistic insights. *Macromolecules* **2014,** *47* (8), 2541-2555.

(7) Zou, C.; Chen, C., Polar-functionalized, crosslinkable, self-healing, and photoresponsive polyolefins. *Angew. Chem. Int. Ed.* **2020,** *59* (1), 395-402.

(8) Baur, M.; Lin, F.; Morgen, T. O.; Odenwald, L.; Mecking, S., Polyethylene materials with in-chain ketones from nonalternating catalytic copolymerization. *Science* **2021,** *374* (6567), 604-607.

(9) Tan, C.; Zou, C.; Chen, C., Material Properties of Functional Polyethylenes from Transition-Metal-Catalyzed Ethylene–Polar Monomer Copolymerization. *Macromolecules* **2022**.

(10) Tan, C.; Zou, C.; Chen, C., An Ionic Cluster Strategy for Performance Improvements and Product Morphology Control in Metal-Catalyzed Olefin–Polar Monomer Copolymerization. *J. Am. Chem. Soc.* **2022**.

(11) Guan, Z.; Cotts, P.; McCord, E.; McLain, S., Chain walking: a new strategy to control polymer topology. *Science* **1999,** *283* (5410), 2059-2062.

(12) Arriola, D. J.; Carnahan, E. M.; Hustad, P. D.; Kuhlman, R. L.; Wenzel, T. T., Catalytic production of olefin block copolymers via chain shuttling polymerization. *Science* **2006,** *312* (5774), 714-719.

(13) Delferro, M.; Marks, T. J., Multinuclear olefin polymerization catalysts. *Chem. Rev.* **2011,** *111* (3), 2450-2485.

(14) Makio, H.; Terao, H.; Iwashita, A.; Fujita, T., FI Catalysts for olefin polymerization A comprehensive treatment. *Chem. Rev.* **2011,** *111* (3), 2363-2449.

(15) Tan, C.; Chen, C., Emerging palladium and nickel catalysts for copolymerization of olefins with polar monomers. *Angew. Chem.* **2019,** *131* (22), 7268-7276.

(16) Nakamura, A.; Anselment, T. M.; Claverie, J.; Goodall, B.; Jordan, R. F.; Mecking, S.; Rieger, B.; Sen, A.; Van Leeuwen, P. W.; Nozaki, K., Ortho-phosphinobenzenesulfonate: A superb ligand for palladium-catalyzed coordination–insertion copolymerization of polar vinyl monomers. *Acc. Chem. Res.* **2013,** *46* (7), 1438-1449.

(17) Mu, H.; Pan, L.; Song, D.; Li, Y., Neutral nickel catalysts for olefin homo-and copolymerization: relationships between catalyst structures and catalytic properties. *Chem. Rev.* **2015,** *115* (22), 12091-12137.

(18) Chen, Z.; Brookhart, M., Exploring ethylene/polar vinyl monomer copolymerizations using Ni and Pd α-diimine catalysts. *Acc. Chem. Res.* **2018,** *51* (8), 1831-1839.

(19) Johnson, L. K.; Mecking, S.; Brookhart, M., Copolymerization of ethylene and propylene with functionalized vinyl monomers by palladium (II) catalysts. *J. Am. Chem. Soc.* **1996,** *118* (1), 267-268.

(20) Dai, S.; Sui, X.; Chen, C., Highly Robust Palladium (II) α-Diimine Catalysts for Slow-Chain-Walking

Polymerization of Ethylene and Copolymerization with Methyl Acrylate. *Angew. Chem. Int. Ed.* **2015,** *54* (34), 9948-9953.

(21) Zhang, Y.; Wang, C.; Mecking, S.; Jian, Z., Ultrahighly Branched Main-Chain-Functionalized Polyethylenes via Inverted Insertion Selectivity. *Angew. Chem. Int. Ed.* **2020**.

(22) Drent, E.; van Dijk, R.; van Ginkel, R.; van Oort, B.; Pugh, R. I., Palladium catalysed copolymerisation of ethene with alkylacrylates: polar comonomer built into the linear polymer chain. *Chem. Commun.* **2002,** (7), 744-745.

(23) Chen, M.; Chen, C., Rational design of high-performance phosphine sulfonate nickel catalysts for ethylene polymerization and copolymerization with polar monomers. *ACS Catal.* **2017,** *7* (2), 1308-1312.

(24) Zhang, D.; Chen, C., Influence of Polyethylene Glycol Unit on Palladium-and Nickel-Catalyzed Ethylene Polymerization and Copolymerization. *Angew. Chem. Int. Ed.* **2017,** *56* (46), 14672-14676.

(25) Teator, A. J.; Bielawski, C. W., Remote control grubbs catalysts that modulate ring-opening metathesis polymerizations. *J. Polym. Sci., Part A: Polym. Chem* **2017,** *55* (18), 2949-2960.

(26) Radlauer, M. R.; Day, M. W.; Agapie, T., Bimetallic effects on ethylene polymerization in the presence of amines: Inhibition of the deactivation by lewis bases. *J. Am. Chem. Soc.* **2012,** *134* (3), 1478-1481.

(27) Radlauer, M. R.; Buckley, A. K.; Henling, L. M.; Agapie, T., Bimetallic Coordination Insertion Polymerization of Unprotected Polar Monomers: Copolymerization of Amino Olefins and Ethylene by Dinickel Bisphenoxyiminato Catalysts. *J. Am. Chem. Soc.* **2013,** *135* (10), 3784-3787.

(28) Takeuchi, D.; Chiba, Y.; Takano, S.; Osakada, K., Double-Decker-Type Dinuclear Nickel Catalyst for Olefin Polymerization: Efficient Incorporation of Functional Co-monomers. *Angew. Chem. Int. Ed.* **2013,** *52* (48), 12536-12540.

(29) Takano, S.; Takeuchi, D.; Osakada, K.; Akamatsu, N.; Shishido, A., Dipalladium catalyst for olefin polymerization: Introduction of acrylate units into the main chain of branched polyethylene. *Angew. Chem. Int. Ed.* **2014,** *53* (35), 9246-9250.

(30) Klabunde, U.; Itten, S. D., Nickel catalysis for ethylene homo-and co-polymerization. *Journal of Molecular Catalysis* **1987,** *41* (1-2), 123-134.

(31) Keim, W.; Behr, A.; Gruber, B.; Hoffmann, B.; Kowaldt, F. H.; Kuerschner, U.; Limbaecker, B.; Sistig, F. P., Reactions of chelate ylides with nickel(0) complexes. *Organometallics* **1986,** *5* (11), 2356-2359.

(32) Xin, B. S.; Sato, N.; Tanna, A.; Oishi, Y.; Konishi, Y.; Shimizu, F., Nickel catalyzed copolymerization of ethylene and alkyl acrylates. *J. Am. Chem. Soc.* **2017,** *139* (10), 3611-3614.

(33) Zhang, Y.; Mu, H.; Pan, L.; Wang, X.; Li, Y., Robust bulky [P, O] neutral nickel catalysts for copolymerization of ethylene with polar vinyl monomers. *ACS Catal.* **2018,** *8* (7), 5963-5976.

(34) Xiong, S.; Shoshani, M. M.; Zhang, X.; Spinney, H. A.; Nett, A. J.; Henderson, B. S.; Miller III, T. F.; Agapie, T., Efficient Copolymerization of Acrylate and Ethylene with Neutral P, O-Chelated Nickel Catalysts: Mechanistic Investigations of Monomer Insertion and Chelate Formation. *J. Am. Chem. Soc.* **2021,** *143* (17), 6516-6527.

(35) Cai, Z.; Xiao, D.; Do, L. H., Cooperative Heterobimetallic Catalysts in Coordination Insertion Polymerization. *Comments Inorg. Chem.* **2019,** *39* (1), 27-50.

(36) Jones, G. R.; Basbug Alhan, H. E.; Karas, L. J.; Wu, J. I.; Harth, E., Switching the Reactivity of Palladium Diimines with "Ancillary" Ligand to Select between Olefin Polymerization, Branching Regulation, or Olefin Isomerization. *Angew. Chem.* **2021,** *133* (3), 1659-1664.

(37) Dalibart, M.; Derouault, J.; Granger, P.; Chapelle, S., Spectroscopic investigations of complexes between acetonitrile and aluminum trichloride. 1. Aluminum chloride-acetonitrile solutions. *Inorg. Chem.* **1982,** *21* (3), 1040-1046.

(38) Chen, E. Y.-X.; Marks, T. J., Cocatalysts for metal-catalyzed olefin polymerization: activators, activation processes, and structure− activity relationships. *Chem. Rev.* **2000,** *100* (4), 1391-1434.

(39) Metz, M. V.; Schwartz, D. J.; Stern, C. L.; Marks, T. J.; Nickias, P. N., New perfluoroarylborane activators for single-site olefin polymerization. Acidity and cocatalytic properties of a "superacidic" perfluorodiboraanthracene. *Organometallics* **2002,** *21* (20), 4159-4168.

(40) Noda, S.; Kochi, T.; Nozaki, K., Synthesis of allylnickel complexes with phosphine sulfonate ligands and their application for olefin polymerization without activators. *Organometallics* **2009,** *28* (2), 656-658.

(41) Cai, Z.; Shen, Z.; Zhou, X.; Jordan, R. F., Enhancement of chain growth and chain transfer rates in ethylene polymerization by (phosphine-sulfonate) PdMe catalysts by binding of B (C6F5) 3 to the sulfonate group. *ACS Catal.* **2012,** *2* (6), 1187-1195.

(42) Basbug Alhan, H. E.; Jones, G. R.; Harth, E., Branching regulation in olefin polymerization via lewis acid triggered isomerization of monomers. *Angew. Chem.* **2020,** *132* (12), 4773-4779.

(43) Zaccaria, F.; Zuccaccia, C.; Cipullo, R.; Budzelaar, P. H.; Vittoria, A.; Macchioni, A.; Busico, V.; Ehm, C., Methylaluminoxane's molecular cousin: A well-defined and "complete" al-activator for molecular olefin polymerization catalysts. *ACS Catal.* **2021,** *11* (8), 4464-4475.

(44) Zhang, D.; Guironnet, D.; Göttker-Schnetmann, I.; Mecking, S., Water-soluble complexes [(κ2-P, O-phosphinesulfonato) PdMe (L)] and their catalytic properties. *Organometallics* **2009,** *28* (14), 4072-4078.

(45) Neuwald, B.; Ölscher, F.; Göttker-Schnetmann, I.; Mecking, S., Limits of activity: weakly coordinating ligands in arylphosphinesulfonato palladium (II) polymerization catalysts. *Organometallics* **2012,** *31* (8), 3128-3137.

(46) Skupov, K. M.; Marella, P. R.; Simard, M.; Yap, G. P.; Allen, N.; Conner, D.; Goodall, B. L.; Claverie, J. P., Palladium aryl sulfonate phosphine catalysts for the copolymerization of acrylates with ethene. *Macromolecular rapid communications* **2007,** *28* (20), 2033-2038.

(47) Kenyon, P.; Falivene, L.; Caporaso, L.; Mecking, S., Ancillary Ligands Impact Branching Microstructure in Late-Transition-Metal Polymerization Catalysis. *ACS Catal.* **2019,** *9* (12), 11552-11556.

(48) Liu, Y. S.; Harth, E., Distorted Sandwich α-Diimine PdII Catalyst: Linear Polyethylene and Synthesis of Ethylene/Acrylate Elastomers. *Angew. Chem. Int. Ed.* **2021**.

(49) Zhang, Y.; Zhang, Y.; Chi, Y.; Jian, Z., Influence of initiating groups on phosphino-phenolate nickel catalyzed ethylene (co) polymerization. *Dalton Trans* **2020,** *49* (8), 2636-2644.

(50) Jung, J.; Yasuda, H.; Nozaki, K., Copolymerization of Nonpolar Olefins and Allyl Acetate Using Nickel Catalysts Bearing a Methylene-Bridged Bisphosphine Monoxide Ligand. *Macromolecules* **2020,** *53* (7), 2547-2556.

(51) Tao, W. j.; Nakano, R.; Ito, S.; Nozaki, K., Copolymerization of ethylene and polar monomers by using Ni/IzQO catalysts. *Angew. Chem. Int. Ed.* **2016,** *55* (8), 2835-2839.

(52) Ito, S.; Ota, Y.; Nozaki, K., Ethylene/allyl monomer cooligomerization by nickel/phosphine–sulfonate catalysts. *Dalton Trans* **2012,** *41* (45), 13807-13809.

(53) Zou, C.; Si, G.; Chen, C., A general strategy for heterogenizing olefin polymerization catalysts and the synthesis of polyolefins and composites. *Nat. Commun.* **2022,** *13* (1), 1-12.

(54) Lin, F.; Morgen, T. O.; Mecking, S., Living Aqueous Microemulsion Polymerization of Ethylene with Robust Ni (II) Phosphinophenolato Catalysts. *J. Am. Chem. Soc.* **2021,** *143* (49), 20605-20608.

(55) Xiong, S.; Hong, A.; Bailey, B. C.; Spinney, H. A.; Senecal, T. D.; Bailey, H.; Agapie, T., Highly Active and Thermally Robust Nickel Enolate Catalysts for the Synthesis of Ethylene-Acrylate Copolymers. *Angew. Chem. Int. Ed.* **2022**.

(56) Shoshani, M. M.; Xiong, S.; Lawniczak, J. J.; Zhang, X.; Miller, T. F.; Agapie, T., Phosphine-Phenoxide Nickel Catalysts for Ethylene/Acrylate Copolymerization: Olefin Coordination and Complex Isomerization Studies Relevant to the Mechanism of Catalysis. *Organometallics* **2022**.

(57) Akita, S.; Nozaki, K., Copolymerization of ethylene and methyl acrylate by palladium catalysts bearing IzQO ligands containing methoxyethyl ether moieties and salt effects for polymerization. *Polymer Journal* **2021,**

53 (9), 1057-1060.

(58) Xiao, D.; Cai, Z.; Do, L. H., Accelerating ethylene polymerization using secondary metal ions in tetrahydrofuran. *Dalton Trans* **2019,** *48* (48), 17887-17897.

(59) Cai, Z.; Do, L. H., Thermally Robust Heterobimetallic Palladium–Alkali Catalysts for Ethylene and Alkyl Acrylate Copolymerization. *Organometallics* **2018,** *37* (21), 3874-3882.

(60) Xiao, D.; Do, L. H., In Situ Generated Heterometallic Nickel–Zinc Catalysts for Ethylene Polymerization. *Organometallics* **2018,** *37* (18), 3079-3085.

(61) Sahgal, A.; La, H.; Hayduk, W., Solubility of ethylene in several polar and non-polar solvents. *Can. J. Chem. Eng* **1978,** *56* (3), 354-357.

(62) Grau, E.; Broyer, J.-P.; Boisson, C.; Spitz, R.; Monteil, V., Supercritical behavior in free radical polymerization of ethylene in the medium pressure range. *Phys. Chem. Chem. Phys.* **2010,** *12* (37), 11665-11669.

(63) Waltman, A. W.; Younkin, T. R.; Grubbs, R. H., Insights into the deactivation of neutral nickel ethylene polymerization catalysts in the presence of functionalized olefins. *Organometallics* **2004,** *23* (22), 5121-5123.

(64) Marshall, W. J.; Grushin, V. V., Activation of chlorobenzene with Ni(0) N,N-chelates A remarkably profound effect of a minuscule change in ligand structure. *Canadian Journal of Chemistry* **2005,** *83* (6-7), 640-645.

(65) Guironnet, D.; Roesle, P.; Rünzi, T.; Göttker-Schnetmann, I.; Mecking, S., Insertion polymerization of acrylate. *J. Am. Chem. Soc.* **2009,** *131* (2), 422-423.

(66) Nakano, R.; Nozaki, K., Copolymerization of propylene and polar monomers using Pd/IzQO catalysts. *J. Am. Chem. Soc.* **2015,** *137* (34), 10934-10937.

(67) Zhang, Y.; Mu, H.; Wang, X.; Pan, L.; Li, Y., Elaborate tuning in ligand makes a big difference in catalytic performance: bulky nickel catalysts for (co) polymerization of ethylene with promising vinyl polar monomers. *ChemCatChem* **2019,** *11* (9), 2329-2340.

(68) Chen, M.; Chen, C., A Versatile Ligand Platform for Palladium-and Nickel-Catalyzed Ethylene Copolymerization with Polar Monomers. *Angew. Chem. Int. Ed.* **2018,** *57* (12), 3094-3098.

(69) Saki, Z.; D'Auria, I.; Dall'Anese, A.; Milani, B.; Pellecchia, C., Copolymerization of Ethylene and Methyl Acrylate by Pyridylimino Ni (II) Catalysts Affording Hyperbranched Poly (ethylene-co-methyl acrylate) s with Tunable Structures of the Ester Groups. *Macromolecules* **2020,** *53* (21), 9294-9305.

(70) Tahmouresilerd, B.; Xiao, D.; Do, L. H., Rigidifying Cation-Tunable Nickel Catalysts Increases Activity and Polar Monomer Incorporation in Ethylene and Methyl Acrylate Copolymerization. *Inorg. Chem.* **2021**.

(71) Li, M.; Wang, X.; Luo, Y.; Chen, C., A Second-Coordination-Sphere Strategy to Modulate Nickel-and Palladium-Catalyzed Olefin Polymerization and Copolymerization. *Angew. Chem. Int. Ed.* **2017,** *56* (38), 11604-11609.

(72) Ye, J.; Mu, H.; Wang, Z.; Jian, Z., Heteroaryl backbone strategy in bisphosphine monoxide palladium-catalyzed ethylene polymerization and copolymerization with polar monomers. *Organometallics* **2019,** *38* (15), 2990-2997.

(73) Cui, L.; Jian, Z., A N-bridged strategy enables hemilabile phosphine–carbonyl palladium and nickel catalysts to mediate ethylene polymerization and copolymerization with polar vinyl monomers. *Polym. Chem* **2020,** *11* (38), 6187-6193.

(74) Zou, C.; Liao, D.; Pang, W.; Chen, M.; Tan, C., Versatile PNPO ligands for palladium and nickel catalyzed ethylene polymerization and copolymerization with polar monomers. *J. Catal.* **2021,** *393*, 281-289.

(75) Jenkins, J. C.; Brookhart, M., A mechanistic investigation of the polymerization of ethylene catalyzed by neutral Ni (II) complexes derived from bulky anilinotropone ligands. *J. Am. Chem. Soc.* **2004,** *126* (18), 5827-5842.

(76) Popeney, C. S.; Camacho, D. H.; Guan, Z., Efficient incorporation of polar comonomers in

copolymerizations with ethylene using a cyclophane-based Pd (II) α-diimine catalyst. *J. Am. Chem. Soc.* **2007,** *129* (33), 10062-10063.

(77) Piche, L.; Daigle, J. C.; Rehse, G.; Claverie, J. P., Structure–Activity Relationship of Palladium Phosphanesulfonates: Toward Highly Active Palladium-Based Polymerization Catalysts. *Chem. - Eur. J.* **2012,** *18* (11), 3277-3285.

(78) Wucher, P.; Goldbach, V.; Mecking, S., Electronic influences in phosphinesulfonato palladium (II) polymerization catalysts. *Organometallics* **2013,** *32* (16), 4516-4522.

(79) Jian, Z.; Wucher, P.; Mecking, S., Heterocycle-substituted phosphinesulfonato palladium (II) complexes for insertion copolymerization of methyl acrylate. *Organometallics* **2014,** *33* (11), 2879-2888.

(80) Ota, Y.; Ito, S.; Kuroda, J.-i.; Okumura, Y.; Nozaki, K., Quantification of the steric influence of alkylphosphine–sulfonate ligands on polymerization, leading to high-molecular-weight copolymers of ethylene and polar monomers. *J. Am. Chem. Soc.* **2014,** *136* (34), 11898-11901.

(81) Pan, H.; Zhu, L.; Li, J.; Zang, D.; Fu, Z.; Fan, Z., A thermal stable α-diimine palladium catalyst for copolymerization of ethylene with functionalized olefins. *Journal of Molecular Catalysis A: Chemical* **2014,** *390*, 76-82.

(82) Zhu, L.; Fu, Z.-S.; Pan, H.-J.; Feng, W.; Chen, C.; Fan, Z.-Q., Synthesis and application of binuclear α-diimine nickel/palladium catalysts with a conjugated backbone. *Dalton Trans* **2014,** *43* (7), 2900-2906.

(83) Allen, K. E.; Campos, J. s.; Daugulis, O.; Brookhart, M., Living polymerization of ethylene and copolymerization of ethylene/methyl acrylate using "sandwich" diimine palladium catalysts. *ACS Catal.* **2015,** *5* (1), 456-464.

(84) Chen, M.; Yang, B.; Chen, C., Redox-Controlled Olefin (Co) Polymerization Catalyzed by Ferrocene-Bridged Phosphine-Sulfonate Palladium Complexes. *Angew. Chem. Int. Ed.* **2015,** *54* (51), 15520-15524.

(85) Dai, S.; Chen, C., Direct synthesis of functionalized high-molecular-weight polyethylene by copolymerization of ethylene with polar monomers. *Angew. Chem. Int. Ed.* **2016,** *55* (42), 13281-13285.

(86) Hu, H.; Chen, D.; Gao, H.; Zhong, L.; Wu, Q., Amine–imine palladium catalysts for living polymerization of ethylene and copolymerization of ethylene with methyl acrylate: incorporation of acrylate units into the main chain and branch end. *Polym. Chem* **2016,** *7* (3), 529-537.

(87) Mitsushige, Y.; Carrow, B. P.; Ito, S.; Nozaki, K., Ligand-controlled insertion regioselectivity accelerates copolymerisation of ethylene with methyl acrylate by cationic bisphosphine monoxide–palladium catalysts. *Chem. Sci.* **2016,** *7* (1), 737-744.

(88) Wang, R.; Zhao, M.; Chen, C., Influence of ligand second coordination sphere effects on the olefin (co) polymerization properties of α-diimine Pd (II) catalysts. *Polym. Chem* **2016,** *7* (23), 3933-3938.

(89) Wu, Z.; Chen, M.; Chen, C., Ethylene polymerization and copolymerization by palladium and nickel catalysts containing naphthalene-bridged phosphine–sulfonate ligands. *Organometallics* **2016,** *35* (10), 1472-1479.

(90) Zou, W.; Chen, C., Influence of backbone substituents on the ethylene (co) polymerization properties of α-diimine Pd (II) and Ni (II) catalysts. *Organometallics* **2016,** *35* (11), 1794-1801.

(91) Liang, T.; Chen, C., Side-arm control in phosphine-sulfonate palladium-and nickel-catalyzed ethylene polymerization and copolymerization. *Organometallics* **2017,** *36* (12), 2338-2344.

(92) Sui, X.; Hong, C.; Pang, W.; Chen, C., Unsymmetrical α-diimine palladium catalysts and their properties in olefin (co) polymerization. *Mater. Chem. Front.* **2017,** *1* (5), 967-972.

(93) Tao, W.; Akita, S.; Nakano, R.; Ito, S.; Hoshimoto, Y.; Ogoshi, S.; Nozaki, K., Copolymerisation of ethylene with polar monomers by using palladium catalysts bearing an N-heterocyclic carbene–phosphine oxide bidentate ligand. *Chem. Commun.* **2017,** *53* (17), 2630-2633.

(94) Wu, Z.; Hong, C.; Du, H.; Pang, W.; Chen, C., Influence of ligand backbone structure and connectivity on the properties of phosphine-sulfonate Pd (II)/Ni (II) catalysts. *Polymers* **2017,** *9* (5), 168.

(95) Yang, B.; Xiong, S.; Chen, C., Manipulation of polymer branching density in phosphine-sulfonate palladium and nickel catalyzed ethylene polymerization. *Polym. Chem* **2017,** *8* (40), 6272-6276.

(96) Zhai, F.; Solomon, J. B.; Jordan, R. F., Copolymerization of ethylene with acrylate monomers by amide-functionalized α-diimine Pd catalysts. *Organometallics* **2017,** *36* (9), 1873-1879.

(97) Zhao, M.; Chen, C., Accessing multiple catalytically active states in redox-controlled olefin polymerization. *ACS Catal.* **2017,** *7* (11), 7490-7494.

(98) Zhong, S.; Tan, Y.; Zhong, L.; Gao, J.; Liao, H.; Jiang, L.; Gao, H.; Wu, Q., Precision synthesis of ethylene and polar monomer copolymers by palladium-catalyzed living coordination copolymerization. *Macromolecules* **2017,** *50* (15), 5661-5669.

(99) Ding, L.; Cheng, H.; Li, Y.; Tanaka, R.; Shiono, T.; Cai, Z., Efficient ethylene copolymerization with polar monomers using palladium anilinonaphthoquinone catalysts. *Polym. Chem* **2018,** *9* (45), 5476-5482.

(100) Guo, L.; Liu, Y.; Sun, W.; Du, Q.; Yang, Y.; Kong, W.; Liu, Z.; Chen, D., Synthesis, characterization, and olefin (co) polymerization behavior of unsymmetrical α-diimine palladium complexes containing bulky substituents at 4-position of aniline moieties. *J. Organomet. Chem.* **2018,** *877*, 12-20.

(101) Zhang, W.; Waddell, P. M.; Tiedemann, M. A.; Padilla, C. E.; Mei, J.; Chen, L.; Carrow, B. P., Electron-rich metal cations enable synthesis of high molecular weight, linear functional polyethylenes. *J. Am. Chem. Soc.* **2018,** *140* (28), 8841-8850.

(102) Du, C.; Zhong, L.; Gao, J.; Zhong, S.; Liao, H.; Gao, H.; Wu, Q., Living (co) polymerization of ethylene and bio-based furfuryl acrylate using dibenzobarrelene derived α-diimine palladium catalysts. *Polym. Chem* **2019,** *10* (16), 2029-2038.

(103) Liao, Y.; Zhang, Y.; Cui, L.; Mu, H.; Jian, Z., Pentiptycenyl substituents in insertion polymerization with α-diimine nickel and palladium species. *Organometallics* **2019,** *38* (9), 2075-2083.

(104) Li, K.; Ye, J.; Wang, Z.; Mu, H.; Jian, Z., Indole-bridged bisphosphine-monoxide palladium catalysts for ethylene polymerization and copolymerization with polar monomers. *Polym. Chem* **2020**.

(105) Li, S.; Dai, S., 8-Arylnaphthyl substituent retarding chain transfer in insertion polymerization with unsymmetrical α-diimine systems. *Polym. Chem* **2020,** *11* (45), 7199-7206.

(106) Park, D.-A.; Byun, S.; Ryu, J. Y.; Lee, J.; Lee, J.; Hong, S., Abnormal N-Heterocyclic Carbene–Palladium Complexes for the Copolymerization of Ethylene and Polar Monomers. *ACS Catal.* **2020,** *10* (10), 5443-5453.

(107) Tan, C.; Qasim, M.; Pang, W.; Chen, C., Ligand–metal secondary interactions in phosphine–sulfonate palladium and nickel catalyzed ethylene (co) polymerization. *Polym. Chem* **2020,** *11* (2), 411-416.

(108) Xu, M.; Yu, F.; Li, P.; Xu, G.; Zhang, S.; Wang, F., Enhancing chain initiation efficiency in the cationic allyl-nickel catalyzed (co) polymerization of ethylene and methyl acrylate. *Inorg. Chem.* **2020,** *59* (7), 4475-4482.

(109) Zhang, Y.; Wang, C.; Mecking, S.; Jian, Z., Ultrahigh branching of main-chain-functionalized polyethylenes by inverted insertion selectivity. *Angew. Chem.* **2020,** *132* (34), 14402-14408.

(110) Zhong, L.; Zheng, H.; Du, C.; Du, W.; Liao, G.; Cheung, C. S.; Gao, H., Thermally robust α-diimine nickel and palladium catalysts with constrained space for ethylene (co) polymerizations. *J. Catal.* **2020,** *384*, 208-217.

(111) Zhou, G.; Mu, H.; Jian, Z., A comprehensive picture on catalyst structure construction in palladium catalyzed ethylene (co) polymerizations. *J. Catal.* **2020,** *383*, 215-220.

(112) Chen, S.-Y.; Pan, R.-C.; Liu, Y.; Lu, X.-B., Bulky o-Phenylene-Bridged Bimetallic α-Diimine Ni (II) and Pd (II) Catalysts in Ethylene (Co) polymerization. *Organometallics* **2021,** *40* (22), 3703-3711.

(113) Dai, S.; Li, G.; Lu, W.; Liao, Y.; Fan, W., Suppression of chain transfer via a restricted rotation effect of dibenzosuberyl substituents in polymerization catalysis. *Polym. Chem* **2021,** *12* (22), 3240-3249.

(114) Ge, Y.; Li, S.; Fan, W.; Dai, S., Flexible "Sandwich"(8-Alkylnaphthyl α-Diimine) Catalysts in Insertion

Polymerization. *Inorg. Chem.* **2021,** *60* (8), 5673-5681.

(115) Ge, Y.; Li, S.; Wang, H.; Dai, S., Synthesis of Branched Polyethylene and Ethylene-MA Copolymers Using Unsymmetrical Iminopyridyl Nickel and Palladium Complexes. *Organometallics* **2021,** *40* (17), 3033-3041.

(116) Guo, L.; Hu, X.; Lu, W.; Xu, G.; Liu, Q.; Dai, S., Investigations of ligand backbone effects on bulky diarylmethyl-based nickel (II) and palladium (II) catalyzed ethylene polymerization and copolymerization. *J. Organomet. Chem.* **2021,** *952*, 122046.

(117) Hai, Z.; Lu, Z.; Li, S.; Cao, Z.-Y.; Dai, S., The synergistic effect of rigid and flexible substituents on insertion polymerization with α-diimine nickel and palladium catalysts. *Polym. Chem* **2021,** *12* (32), 4643-4653.

(118) Li, S.; Dai, S., Highly efficient incorporation of polar comonomers in copolymerizations with ethylene using iminopyridyl palladium system. *J. Catal.* **2021,** *393*, 51-59.

(119) Lu, W.; Xu, G.; Chang, G.; Wang, H.; Dai, S., Synthesis of highly branched polyethylene and ethylene-MA copolymers using hybrid bulky α-diimine Pd (II) catalysts. *J. Organomet. Chem.* **2021,** *956*, 122118.

(120) Wang, G.; Peng, D.; Sun, Y.; Chen, C., Interplay of supramolecular chemistry and photochemistry with palladium-catalyzed ethylene polymerization. *CCS Chemistry* **2021,** *3* (7), 2025-2034.

(121) Wang, X.-l.; Zhang, Y.-p.; Wang, F.; Pan, L.; Wang, B.; Li, Y.-s., Robust and Reactive Neutral Nickel Catalysts for Ethylene Polymerization and Copolymerization with a Challenging 1,1-Disubstituted Difunctional Polar Monomer. *ACS Catal.* **2021**, 2902-2911.

(122) Xia, J.; Han, Y.-F.; Kou, S.; Zhang, Y.; Jian, Z., Exploring steric effect of electron-donating group in palladium and nickel mediated ethylene polymerization and copolymerization with polar monomers. *European Polymer Journal* **2021,** *160*, 110781.

(123) Zhu, N.; Liang, T.; Huang, Y.; Pang, W.; Chen, M.; Tan, C., Influences of ligand backbone substituents on phosphinecarbonylpalladium and-nickel catalysts for ethylene polymerization and copolymerization with polar monomers. *Inorg. Chem.* **2021,** *60* (17), 13080-13090.

(124) Alberoni, C.; D'Alterio, M. C.; Balducci, G.; Immirzi, B.; Polentarutti, M.; Pellecchia, C.; Milani, B., Tunable "In-Chain" and "At the End of the Branches" Methyl Acrylate Incorporation in the Polyolefin Skeleton through Pd (II) Catalysis. *ACS Catal.* **2022,** *12* (6), 3430-3443.

(125) Liang, T.; Goudari, S. B.; Chen, C., A simple and versatile nickel platform for the generation of branched high molecular weight polyolefins. *Nat. Commun.* **2020,** *11* (1), 1-8.

CHAPTER 6

Acrylate-Induced β-H Elimination in Insertion Polymerization

Chapter 6

CONTRIBUTIONS AND ACKNOWLEDGEMENTS

Shuoyan Xiong and Theodor Agapie conceived the presented idea. S.X. performed synthetic and mechanistic studies and polymer characterization and analyzed the catalysis data. Alexandria Hong performed mechanistic studies. Brad C. Bailey, Heather A. Spinney, Briana S. Henderson, and Steve Marshall performed polymerization studies and polymer characterization. S.X. wrote the chapter.

We are grateful to Dow for funding (T.A.). We thank Alex J. Nett and Todd D. Senecal for insightful discussions. We thank Heidi Clements for GPC and tBA incorporation analysis. We thank Michael K. Takase and Manar M. Shoshani for assistance with X-ray crystallography and David VanderVelde for assistance with NMR spectroscopy. Support has been provided for the X-ray diffraction and NMR instrumentation via the Dow Next Generation Educator Fund.

ABSTRACT

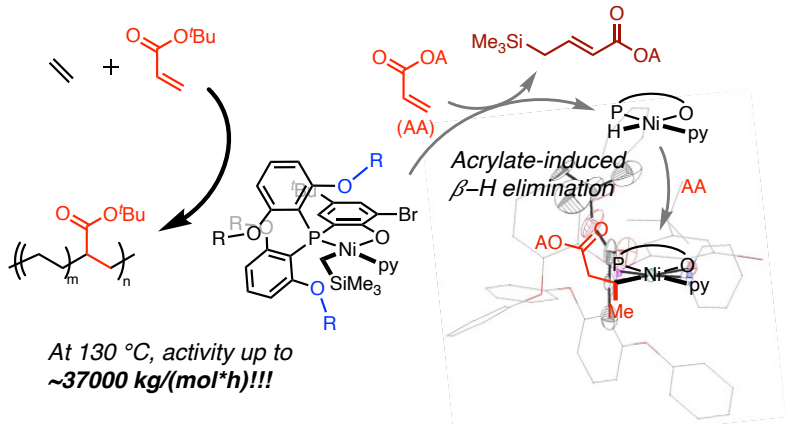

Polar monomer-induced β-H elimination is a key elementary step in polar polyolefin synthesis by coordination polymerization, but remains underexplored. Herein, we show that a bulky neutral Ni catalyst, **^{PhO}PO^{Br}-Ni**, is not only a high-performance catalyst in ethylene/acrylate copolymerization (activity up to ~37000 kg/(mol*h) at 130 °C in a batch reactor), but also a suitable platform for investigation of acrylate-induced β-H elimination. **^{PhO}PO^{Br}-NiCCO**, a novel Ni alkyl complex generated after acrylate induced β-H elimination and subsequent acrylate insertion, was identified and crystallographically characterized. A combination of catalysis and mechanistic studies reveals the role of β-H elimination in copolymerization catalysis as a chain-termination pathway, and its potential in controlling polymer microstructure in polar polyolefin synthesis.

Chapter 6

GENERAL INTRODUCTION

Polyolefins account for over half of global plastic production.[1-8] Coordination copolymerization of non-polar and polar monomers is of high interest as it can provide value-added functional polyolefins with diverse but controlled material properties and potential degradability.[3, 7, 9-12] Despite significant progresses in catalyst developments over past three decades, [2, 4, 13-36] industrial implementations of this process are limited by catalysts' low activity (typically <1000 kg/(mol*h), thermal stability (typically <100 °C) and low molecular weight (MW) of resulting copolymers.[10, 17, 19, 37-40]

Elucidation of copolymerization mechanism has significantly benefited catalyst developments.[2, 4, 6, 11, 17, 29-30, 41-44] Polar monomer-induced β-H elimination is a key elementary step in copolymerization of ethylene and polar monomers as it competes with monomer insertion after polar monomer insertion, the limiting step of this polymerization (Figure 6.1).[37, 45] Considerable efforts have been focused on β-H elimination after ethylene and α-olefin insertion.[46-58] Specifically, Brookhart and Diao characterized several β-agostic species that are key intermediates in polymerization of α-olefins.[46-47, 53, 56, 59] For polar monomer-induced β-H elimination, Mecking and Sen reported spectroscopic evidence of Pd hydride species, internal olefins and double-inserted Pd species, however, no solid-state structure has been reported.[60-63] Further, these studies are based on systems that exhibit no or low reactivity in copolymerization of ethylene and polar monomers.

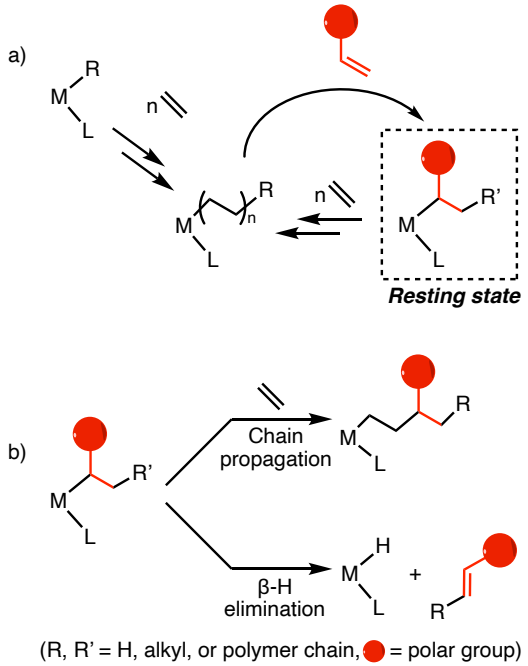

Figure 6.1. a) Depiction of olefin insertion in copolymerization catalysis and the resting state. b) Two possible reactions after polar monomer insertion.

Nickel catalysts have been a recent focus in polar polyolefin synthesis due to nickel's relatively low cost and promising performance.[17-19] Though being of high interest, β-H elimination has been little detailed, potentially due to the lack of a suitable catalyst system that undergoes facile β-H elimination while still being productive in copolymerization. Herein we report on the β-H elimination behavior of high-performance Ni phosphine phenoxide catalysts (activity up to ~37000 kg/(mol*h) at 130 °C in a batch reactor). An intermediate, **^{PhO}PO^{Br}-NiCCO**, generated from the putative Ni-hydride, was crystallographically characterized. These results provide insights into how catalyst design impacts Mw and chain-end functionality in polar polyolefin synthesis.

RESULTS AND DISCUSSION

Catalyst Design, Preparation and Characterization

The intermediates generated after β-H elimination are expected to be highly reactive toward further insertion or decomposition. Previous mechanistic studies have identified several catalyst deactivation pathways starting from inter- and intramolecular interactions axial to the nickel center.[60, 63-67] To stabilize reactive intermediates, a catalyst featuring large axial shielding was designed (Figure 6.2a). Increasing proximal steric hindrance has also shown promise in improving catalytic activity and thermal stability in Ni catalysts supported by anionic PO ligands.[22, 37, 40, 68-72] Two neutral Ni complexes, **^{MeO}PO^{Br}-Ni** and **^{PhO}PO^{Br}-Ni**, were synthesized as single-component catalysts for ethylene/acrylate copolymerization and precursors for investigation of β-H elimination (Figure 6.2a). Structural characterization by single-crystal X-ray diffraction (scXRD), in combination with topographical steric analysis by Cavallo's SambVca 2.1,[73-74] confirms that axial positions of the Ni center in both complexes are covered from both the top and bottom directions (Figure 6.2b and Figure S6.1). Notably, the phenoxy group in **^{PhO}PO^{Br}-Ni** also provides steric shielding extending to the O side, while the methoxy group in **^{MeO}PO^{Br}-Ni** provides steric shielding only on the P side.

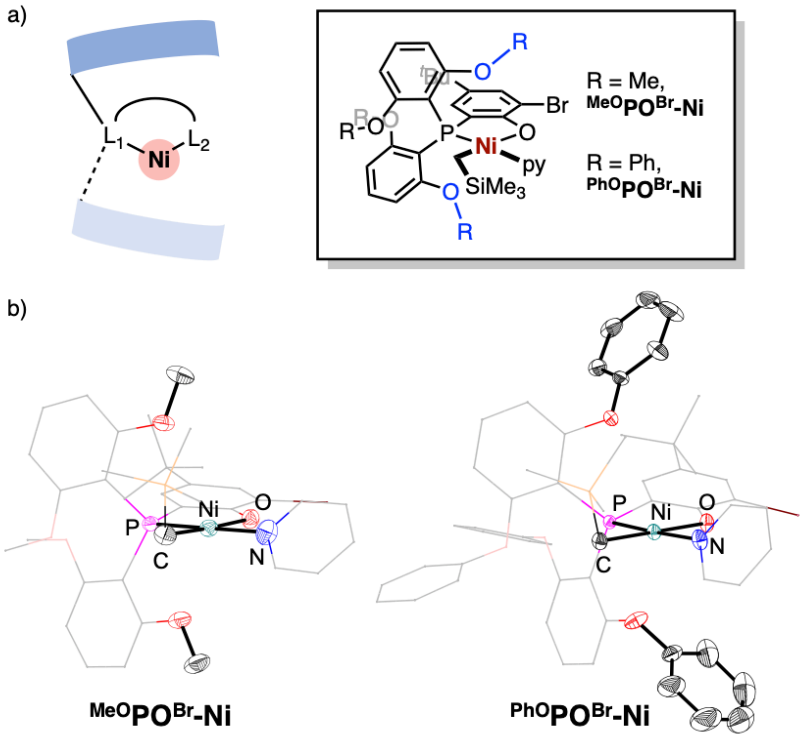

Figure 6.2 a) Depiction of the catalyst design strategy and two new catalysts in this work. b) Solid-state structures of ^{MeO}**PO**^{Br}**-Ni** and ^{PhO}**PO**^{Br}**-Ni**.

Catalytic Synthesis of Ethylene/Acrylate Copolymers at High Temperatures

Both ^{MeO}**PO**^{Br}**-Ni** and ^{PhO}**PO**^{Br}**-Ni** are highly active in ethylene/acrylate copolymerization (Table 1, entry 1~5). The bulkier catalyst, ^{PhO}**PO**^{Br}**-Ni**, shows significantly higher activity than ^{MeO}**PO**^{Br}**-Ni** but produces copolymers with lower tBA incorporation (entry 1 vs 3, or 2 vs 5), consistent with structure-performance relationships of Ni catalysts reported previously.[22, 34, 40] Notably, ^{PhO}**PO**^{Br}**-Ni** is significantly more active at 110 °C than at 90 °C (entry 3 vs 5) and an activity of ~33000 kg/(mol*h) was achieved at 110 °C in a batch reactor (entry 6), in contrast with the optimized temperatures for reported Ni phosphine phenoxide catalysts typically ranging between 50 and 90 °C.[22, 40, 45, 70] A few Ni catalysts reported recently

are active under similar conditions, however, they produce copolymers with lower M_w (<10000) compared to copolymers by ^{PhO}**PO**^{Br}**-Ni** (25000~30000).[34] At 130 °C, ^{PhO}**PO**^{Br}**-Ni** shows an activity of ~37000 kg/(mol*h) in a batch reactor (entry 8). To the best of our knowledge, this is the first example of ethylene/acrylate coordination copolymerization at temperatures above 110 °C. These results show promise for potential practical applications as low activity, low thermal stability, and low copolymer MW are three major limitations.[17, 75]

Table 6.1. Ethylene/tBA copolymerization results.

Entry[a]	catalyst	T (ºC)	tBA (M)	Act.[b]	Mw[c]	PDI	%Mol tBA	Tm (ºC)
1	^{MeO}**PO**^{Br}**-Ni**	90	0.10	720	47.0	2.2	3.4	106
2	^{MeO}**PO**^{Br}**-Ni**	110	0.10	440	17.8	2.4	2.9	107
3	^{PhO}**PO**^{Br}**-Ni**	90	0.10	9700	32.9	2.4	0.7	123
4	^{PhO}**PO**^{Br}**-Ni**	90	0.15	5700	30.0	2.3	1.0	120
5	^{PhO}**PO**^{Br}**-Ni**	110	0.10	17800	26.0	2.4	0.7	123
6[d]	^{PhO}**PO**^{Br}**-Ni**	110	0.054	33000	28.4	2.2	0.3	127
7[d]	^{PhO}**PO**^{Br}**-Ni**	110	0.108	14000	24.9	2.2	0.6	125
8[d]	^{PhO}**PO**^{Br}**-Ni**	130	0.054	37000	15.6	2.6	0.3	127

[a] V = 5 mL, [Catalyst] = 0.05 mM, ethylene pressure = 400 psi, toluene solvent; each entry represents multiple replicated runs (see Experimental section 3 for detailed procedure and Table S6.6.4 for original data). [b] Activity in kg/(mol·h). [c] kg/mol. [d] Copolymerization in a batch reactor. Condition: V = 550 mL, [Ni]=0.043 mM, ethylene pressure = 430 psi, t = 3.5 min (entry 6), 6.5 min (entry 7), or 3 min (entry 8), ethylene consumption = 40 g. See Experimental section 3 for detailed procedure.

Identification of β-H Elimination and Subsequent Acrylate Reinsertion

With these two highly active and robust catalysts, tBA insertion and subsequent reactions were investigated. Treatment of ^{PhO}**PO**^{Br}**-Ni** with excess tBA results in a color change from yellow to red. Monitoring of ^{1}H and ^{31}P{^{1}H} NMR spectra

confirmed the consumption of ^{PhO}**PO**^{Br}**-Ni**. One broad resonance appears in ^{31}P{^{1}H} NMR spectra over time (Figure S6.6, 9), and four new resonances were observed in ^{1}H NMR spectra in a ~1:9:9:9 ratio (Figure S6.7~8, 10): one new doublet in the olefinic region (δ ~5.8 ppm), one in the upfield region corresponding to a Me_3Si-containing species (δ ~0 ppm), and two ^{t}BuO- resonances (δ 1.2-1.5 ppm). These results suggest reactivity with two acrylates and generation of a new olefinic species. Combination of ^{1}H-^{1}H COSY NMR and GC-MS analysis revealed the identity of the internal olefin as ^{tBu}**IO**^{Si} (Figure 6.3a, Figure S6.11-14). Further ^{1}H, ^{31}P{^{1}H} and ^{1}H-^{1}H COSY NMR analysis suggests the identity of the other species as ^{PhO}**PO**^{Br}**-NiCCO**^{tBu}, which is generated via tBA insertion into a Ni hydride complex (^{PhO}**PO**^{Br}**-NiH**, Figure 6.3a, Figure S6.15-17).

Structural Characterization of ^{PhO}PO^{Br}-Ni(py)CCO

Despite numerous attempts, isolation of ^{PhO}**PO**^{Br}**-NiCCO**^{tBu} as a solid was not successful. It decomposes quickly at room temperature, both under vacuum and in solution. Nonetheless, single crystals were obtained from tBA insertion experiments in the presence of of tBA and pyridine and scXRD analysis confirmed the identity of ^{PhO}**PO**^{Br}**-NiCCO**^{tBu} (Figure 6.3b). To the best of our knowledge, this is the first structural characterization of an intermediate generated after polar-monomer induced β-H elimination relevant to polar polyolefin synthesis. The Ni(1)-C(1) distance in ^{PhO}**PO**^{Br}**-NiCCO**^{tBu} (2.030(5) Å) is longer than that in ^{PhO}**PO**^{Br}**-Ni** (1.949(2) Å) or in reported Ni complexes resulting from tBA insertion into a metal alkyl moiety (1.972(8)~2.003(8) Å).[37, 45] This comparison suggests a weakened Ni-alkyl bond in

^{PhO}**PO**^{Br}**-NiCCO**^{tBu}, potentially due to steric repulsion induced by the bulky phenoxy and tBu groups. These steric interactions may also promote the facile β-H elimination in crowded intermediate ^{PhO}**PO**^{Br}**-Ni**^{Si}**CCO**^{tBu}.

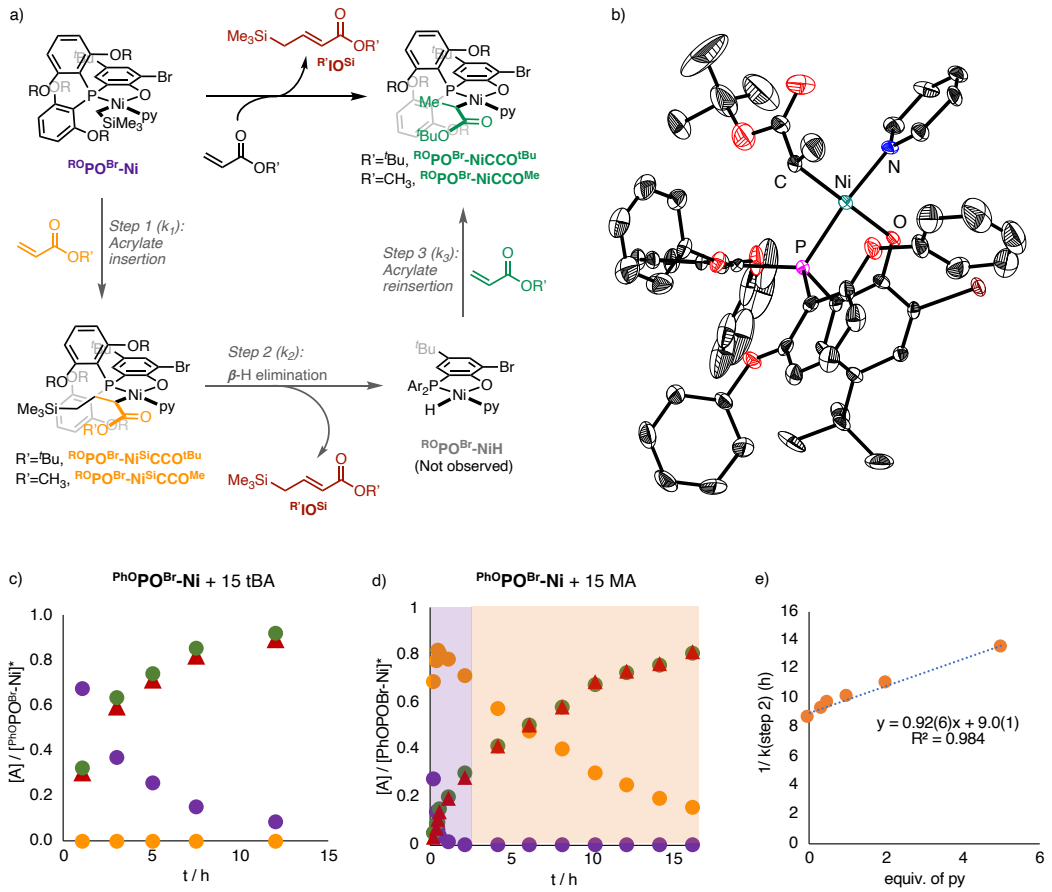

Figure 6.3. a) Generation of the internal olefin (**IO**^{Si}) and the acrylate-inserted species, as well as the corresponding three-step pathway. b) Solid-state structure of ^{PhO}**PO**^{Br}**-NiCCO**^{tBu}. c-d) Kinetic profiles of reaction of tBA and MA with ^{PhO}**PO**^{Br}**-Ni** ([Ni] = [^{PhO}**PO**^{Br}**-Ni**]$_{t=0}$ = 0.0118 M, [py] = 0, [Acrylate] = 0.177 M, solvent: C_6D_6, V(total) = 0.5 mL, T = 25 ºC.) e) Plot of the reverse of *pseudo*-1st order rate constant of β-H elimination (1/k(step 2), or $1/k_2$) vs [py]/[Ni$_{t=0}$] for ^{PhO}**PO**^{Br}**-Ni**. ([Ni] = 0.0118 M, [py] = 0039-0.059 M, [MA] = 0.59 M, solvent: C_6D_6, V(total) = 0.5 mL, T = 25 ºC). See Experimental section 6~7 for details.

Kinetics of β-H Elimination

Identification of the internal olefin and ^{PhO}**PO**^{Br}**-NiCCO**^{tBu}, in combination with *in-situ* ^{1}H and ^{31}P{^{1}H} NMR monitoring, established a kinetic profile of the reactions

with tBA (Figure 6.3c). The concentration of ^{PhO}**PO**^{Br}**-NiCCO**^{tBu} is roughly equal to that of **IO**^{Si} during the course of the reaction and the two putative intermediates, ^{PhO}**POBr-NiC**^{Si}**COO**^{tBu} and ^{PhO}**PO**^{Br}**-NiH**, were not observed, indicating that step 1 is rate determining in this reaction and step 2 is slower than step 3. Notably, analogous kinetic analysis of reactions with methyl acrylate (MA) revealed faster initial acrylate insertion (step 1) and lower tendency for β-H elimination after acrylate compared to tBA reactions (Figure 6.3c-d). As a result, ^{PhO}**PO**^{Br}**-Ni**^{Si}**CCO**^{Me} was observed as an intermediate. Further, acrylate insertion (step 1) and β-H elimination (step 2) are differentiable in the kinetic profile (Figure 6.3d), allowing direct, quantitative kinetic studies of β-H elimination to elucidate the mechanism. With varying acrylate and pyridine concentrations (15 or 50 equiv. of MA, 0~5 equiv. of pyridine), a near-linear correlation was observed between the inverse of *pseudo*-1st order rate constant for β-H elimination ($1/k_2$) and the pyridine concentration ([py], Figure 6.3e). These observations are consistent with pyridine being involved in the rate-limiting step of β-H elimination (step 2, Figure 6.3a, Experimental section 8). k_2 does not depend on [MA] (Table S6.6, Figure S6.46), indicating that MA is not involved in this portion of the mechanism. Comparing MA and tBA reaction with ^{PhO}**PO**^{Br}**-Ni** (Figure 6.3c vs 3d), initial insertion (step 1) is faster with MA, the smaller monomer, as evidenced by the faster decrease of ^{PhO}**PO**^{Br}**-Ni**. In contrast, β-H elimination (step 2) is faster from the insertion product derived from the larger monomer, as evidenced by the kinetics of internal olefin (**IO**^{Si}) generation. For example, the amount of ^{tBu}**IO**^{Si} is nearly twice as the amount of ^{Me}**IO**^{Si} at ~3 h under otherwise identical conditions.

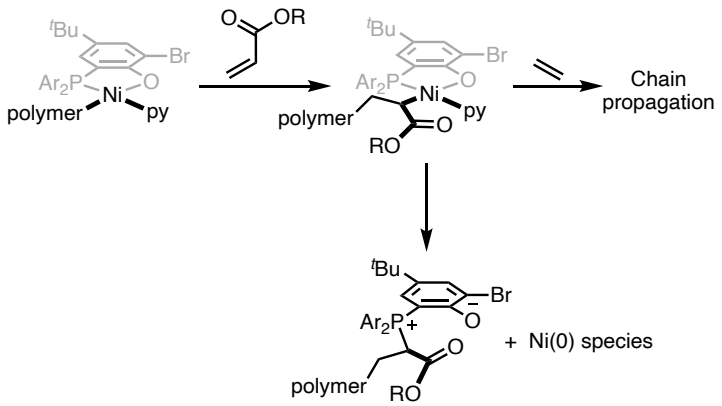

Figure 6.4. A potential catalyst deactivation pathway that generates phosphonium species.

Effects of Catalyst and Acrylate Structures on β-H Elimination

Next, effects of catalyst structure on acrylate-induced β-H elimination and subsequent reactions were investigated by comparing the reaction of tBA with **^{PhO}PO^{Br}-Ni** and with **^{MeO}PO^{Br}-Ni**. Initial tBA insertion for the latter is faster by almost an order of magnitude (0.042(1) min^{-1} vs 0.0061(1) min^{-1}, Figure S6.32 vs S33), while subsequent β-H elimination is slower, as indicated by slower **^{tBu}IO^{Si}** generation (Figure 6.3c vs Figure S6.31). These observations are consistent with the behavior observed when the size of the monomer was changed – larger steric profiles induce lower rate of insertion but faster β-H elimination. Competing with β-H elimination, side reactions likely generating phosphonium species were also observed with the smaller ligand (Figure S6.30-31), as indicated by the peak observed at ~8 ppm in the ^{31}P{^{1}H} NMR spectra of **^{MeO}PO^{Br}-Ni** upon treatment with tBA. These species are potentially related to catalyst deactivation pathways during catalysis (Figure 6.4).[66, 76] These species were not observed in reactions of acrylate with **^{PhO}PO^{Br}-Ni**. These results suggest that the larger axial shielding in **^{PhO}PO^{Br}-Ni** compared to **^{MeO}PO^{Br}-Ni** is crucial for

stabilizing intermediates generated in acrylate-induced reactions and disfavoring undesired side reactions, as suggested by the higher activity (Table 1). However, this comes with a disadvantage of a slower reaction with acrylate and, therefore, decreased incorporation into the polymer.

Notably, analysis of the polymers shows that although **^{PhO}PO^{Br}-Ni** produces copolymers with lower acrylate incorporation, it actually features significantly higher turnover frequencies of acrylate (TOF_{tBA}) compared to **^{MeO}PO^{Br}-Ni** under otherwise identical conditions (Table S6.2, by ~3 fold at 90 °C or ~10 fold at 110 °C). Given that the resting state of this catalysis is the intermediate generated after acrylate insertion and that back to back tBA insertion is very slow,[37] the higher TOF_{tBA} implies that subsequent ethylene insertion and / or β-H elimination (Figure 6.1b) is faster with **^{PhO}PO^{Br}-Ni** compared to **^{MeO}PO^{Br}-Ni**. Additional analysis of polymer microstructures may provide insights into the competition between β-H elimination and ethylene insertion after tBA insertion (Table S6.5).

Investigation of β-H Elimination via Analysis of Copolymer Microstructures

β-H elimination subsequent to acrylate insertion results in ester chain-ends, while competing ethylene insertion results in in-chain acrylate units (Figure 6.1b). In copolymers produced by **POP-Ni**, **^{MeO}PO^{Br}-Ni**, and **^{PhO}PO^{Br}-Ni**, 23~66% of unsaturated chain-ends are ester chain-ends despite acrylate content being below 3% in these samples, confirming that acrylate-induced β-H elimination is an important pathway for chain-termination. On the other hand, the majority of tBA units locate in-chain (73~97%), indicating that ethylene insertion rather than β-H elimination

remains the major event occurring after tBA insertion. In this regard, the aforementioned higher TOF_{tBA} of **$^{PhO}PO^{Br}$-Ni** compared to **$^{MeO}PO^{Br}$-Ni** suggests that ethylene insertion after tBA insertion is faster with **$^{PhO}PO^{Br}$-Ni** than with **$^{MeO}PO^{Br}$-Ni**. Changes in tBA concentration with **$^{PhO}PO^{Br}$-Ni** show minimal effects on the terminal tBA / total tBA ratio even though the total tBA is affected. This is consistent with kinetic results showing that tBA is not involved in the rate-determining step of β-H elimination, therefore, upon each insertion propagation vs termination is independent of tBA concentration (Figure 6.5). Notably, doubling in terminal tBA / all tBA units and tripling in terminal tBA / chain were achieved by tunning reaction temperature, ethylene pressure and acrylate concentration. These results demonstrate potential strategies to control acrylate-induced β-H elimination and polymer microstructure. Changing the catalyst structure further expands on the range of tBA incorporation profiles.

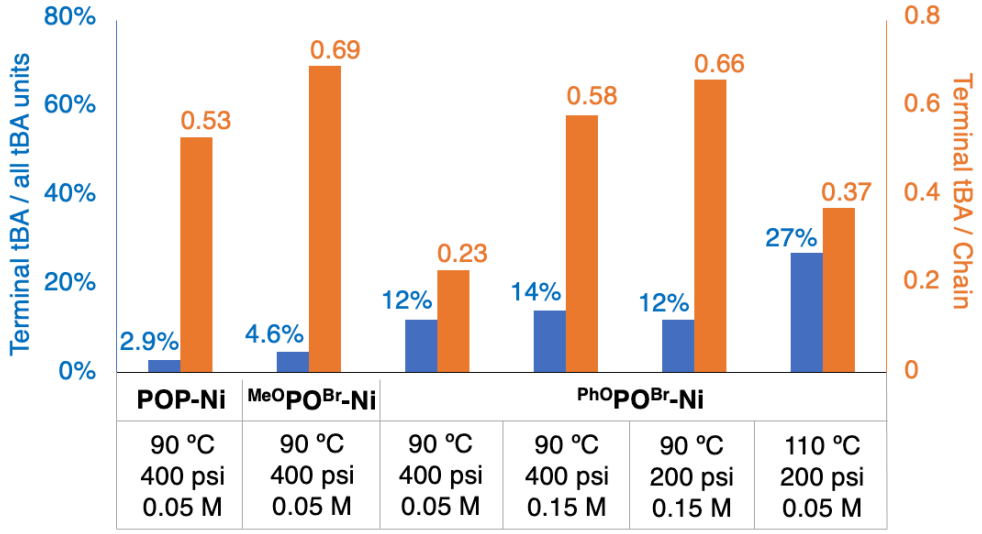

Figure 6.5. Structural analysis of ethylene/acrylate copolymers (See Table S6.5 for details).

Chapter 6

CONCLUSION

In summary, ^{PhO}**PO**^{Br}**-Ni** is a catalyst featuring excellent activity and thermostability in ethylene/acrylate copolymerization. Additionally, this ligand class allowed for investigations of polar monomer (acrylate)-induced β-H elimination, an underexplored elementary step in polar polyolefin synthesis. Increased ligand sterics promote this transformation, while also being essential for preventing reactive intermediates from decomposition and thus affording efficient catalysis. A combination of mechanistic and catalysis studies demonstrate the role of acrylate-induced β-H elimination as a chain-termination mechanism in copolymerization and its potential in controlling polymer microstructures, providing insights for future studies targeting catalyst developments and polymer synthesis.

C h a p t e r 6

EXPERIMENTAL SECTION

1. Procedures for Synthesis of Ligands and Metal Complexes

1.1. General Considerations

All air- and water-sensitive compounds were manipulated under N_2 or Ar using standard Schlenk or glovebox techniques. The solvents for air- and moisture-sensitive reactions were dried over sodium benzophenone/ketyl, calcium hydride, or by the method of Grubbs.[39] Deuterated solvents were purchased from Cambridge Isotopes Lab, Inc.; C_6D_6, was dried over a purple suspension with Na/benzophenone ketyl and vacuum transferred. t-Butyl acrylate was dried over 4 Å sieves for greater than 72h. 2.5 M ^{n}BuLi in hexanes were purchased from Sigma-Aldrich and used without further purification. 1,3-Dibromo-5-(tert-butyl)-2-(methoxymethoxy)benzene,[77] bis(dimethoxyphenyl)phosphine chloride,[62] bis(diphenoxyphenyl)phosphine chloride,[34] $py_2Ni(CH_2SiMe_3)_2$[78] and 2-bromo-4-tertbutyl-5-bis(dimethoxyphenyl)phosphino)phenol[44] were synthesized according to literature procedures. All ^{1}H, ^{13}C, and ^{31}P spectra of organic and organometallic compounds were recorded on Varian INOVA-400, or Bruker Cryoprobe 400 spectrometers. ^{1}H and ^{13}C chemical shifts are reported relative to residual solvent resonances.

1.2. Synthesis of Ligands and Metal Complexes

Ligand ^{PhO}***POBrH****:* A Schlenk flask fitted with a screw-in Teflon stopper was charged with a solution of 1,3-dibromo-5-(tert-butyl)-2-(methoxymethoxy)benzene (3.52 g, 10.0 mmol) in THF (40 mL) and cooled to -78 °C under nitrogen. A hexane solution of *n*-butyllithium (4 mL, 2.5 M, 10.0 mmol) was added dropwise via syringe. After stirring for an additional 30 min at -78 °C, a solution of bis(2,6-diphenoxyphenyl)phosphine chloride (5.89g, 10.0 mmol) in THF (20 mL) was added dropwise via cannula. After complete addition, the reaction was allowed to warm up

to room temperature and stirred for an additional 3 h, yielding a yellow solution. The solution was then concentrated to ~20 mL and degassed MeOH (10 mL) and concentrated aqueous HCl (10 mL, degassed by three freeze-pump-thaw cycles with a liquid nitrogen bath prior to usage) were added. After stirring for 12 h under room temperature, volatiles were removed under vacuum. In a N_2-filled glovebox (no exclusion of water), the resulting yellow residue was taken up in CH_2Cl_2 (20 mL), washed with saturated aqueous solutions of K_2CO_3 (3 x 10 mL) and NH_4Cl (3 x 10 mL), dried over $MgSO_4$, and filtered through Celite. The volatiles were removed under reduced pressure. In a glovebox (exclusion of water and oxygen), the resulting pale-yellow solid was was washed by cold pentane (3 x 20 mL), then dissolved in Et_2O and filtered through Celite. The volatile materials were removed once more under vacuum, yielding ^{PhO}**POBrH** (3.82g, 95% purity) as gel-like solids. This material was then used in metalation as the proligand without further purification. ^{1}H NMR (400 MHz, C_6D_6, *note: only resonances assigned to protons of the desired product were listed*): δ 7.69 (dd, *J* = 9.7, 2.3 Hz, 1H, ArH), 7.33 (d, *J* = 2.3 Hz, 1H, ArH), 6.98 – 6.92 (m, 8H, ArH), 6.85 – 6.75 (m, 12H, ArH), 6.72 – 6.64 (m, 3H, ArH + ArOH), 6.44 (dd, *J* = 8.2, 2.8 Hz, 4H, ArH), 0.99 (s, 9H, -Si(CH_3)$_3$); ^{31}P{^{1}H} NMR (162 MHz, C_6D_6): δ -51.70 (s).

Complex ^{PhO}***POBr-Ni:*** In the glove box, to a solution of $Py_2Ni(CH_2SiMe_3)_2$ (44 mg, 0.119 mmol) in benzene (4 ml) in a vial was added a solution of ^{PhO}**POBrH** (92.9 mg, 0.119 mmol) in benzene (8 ml). The mixture was stirred for 2 h under room temperature, forming a red-brown solution. Volatile materials were removed under vacuum. The residue was extracted with pentane (3 x 5 mL), then washed by cold pentane (3 x 15 mL), pentane (3 x 5 mL) and hexanes (3 x 2 mL), The solid was collected via vacuum filtration, and redissolved in Et_2O, filtered through Celite. The volatile materials were removed once more under vacuum, yielding spectroscopically pure ^{PhO}**POBr-Ni** (50 mg, 45%) as yellow-orange solids. ^{1}H NMR (400 MHz, C_6D_6): δ 8.76 (dd, *J* = 4.9, 1.6 Hz, 2H, ArH), 7.71 – 7.65 (m, 1H, ArH), 7.51 (d, *J* = 2.3 Hz, 1H, ArH), 7.12 – 7.07

(m, 8H, ArH), 7.06 – 6.99 (m, 8H, ArH), 6.88 – 6.79 (m, 5H, ArH), 6.77 – 6.70 (m, 2H, ArH), 6.56 – 6.48 (m, 5H, ArH), 0.90 (s, 9H, -^{t}Bu), -0.00 (s, 9H, -$SiMe_3$), -0.61 (d, J = 9.8 Hz, 2H, $NiCH_2Si$). $^{13}C\{^1H\}$ NMR (101 MHz, C_6D_6): δ 168.74 (d, J = 25.2 Hz, 1C, ArC), 160.01 (s, 4C, ArC), 155.86 (s, 4C, ArC), 151.68 (s, 2C, ArC), 136.44 (s, 1C, ArC), 135.97 (d, J = 7.6 Hz, 1C, ArC), 132.80 (s, 1C, ArC), 130.45 (s, 2C, ArC), 129.92 (s, 8C, ArC), 128.59 (s, 1C, ArC), 126.45 (d, J = 2.8 Hz, 1C, ArC), 124.06 (s, 4C, ArC), 123.27 (s, 2C, ArC), 123.20 (d, J = 52.4 Hz, 1C, ArC), 120.56 (s, 8C, ArC), 114.06 (d, J = 44.4 Hz, 2C, ArC), 110.72 (d, J = 4.0 Hz, 4C, ArC), 33.73 (s, 1C, -$\underline{C}(CH_3)_3$), 31.65 (s, 3C, -$C(\underline{C}H_3)_3$), 2.64 (s, 3C, $SiMe_3$), -16.11 (d, J = 27.2 Hz, 1C, $NiCH_2Si$); $^{31}P\{^1H\}$ NMR (121 MHz, C_6D_6): δ -2.49 (s, 1P). Anal. Calcd(%) for $C_{55}H_{53}BrNNiO_5PSi$: C, 65.69; H, 5.31; N, 1.39. Found(%): C, 66.12; H, 5.40; N, 1.11.

Complex ***^{MeO}POBr-Ni*:** In the glove box, to a solution of $Py_2Ni(CH_2SiMe_3)_2$ (44 mg, 0.119 mmol) in benzene (4 ml) in a vial was added a solution of **^{MeO}POBrH** (63.3mg, 0.119 mmol) in benzene (8 ml). The mixture was stirred for 2 h under room temperature, forming a red-brown solution. Volatile materials were removed under vacuum. The residue was extracted with pentane (3 x 5 mL), then washed by pentane (3 x 10 mL), hexanes (3 x 5 mL) and Et_2O (2 x 2 mL). The solid was collected via vacuum filtration, and redissolved in benzene, filtered through Celite. The volatile materials were removed once more under vacuum, yielding **^{MeO}POBr-Ni** (50 mg, 45%) as brown solids. ^1H NMR (400 MHz, C_6D_6): δ 9.19 (d, J = 6.5 Hz, 2H, ArH), 7.68 (d, J = 2.3 Hz, 1H, ArH), 7.62 (dd, J = 11.1, 2.4 Hz, 1H, ArH), 7.10 (t, J = 8.3 Hz, 2H, ArH), 6.93 – 6.81 (m, 1H, ArH), 6.60 (t, J = 7.3 Hz, 2H, ArH), 6.28 (dd, J = 8.3, 3.7 Hz, 4H, ArH), 3.27 (s, 12H, -OCH_3), 1.13 (s, 9H, -^{t}Bu), -0.13 (s, 9H, -$SiMe_3$), -0.59 (d, J = 9.2 Hz, 2H, $NiCH_2Si$). $^{13}C\{^1H\}$ NMR (101 MHz, C_6D_6): δ 168.17 (d, J = 24.5 Hz, 2C, ArC), 161.73 (s, 4C, ArC), 151.60 (s, 2C, ArC), 136.61 (s, 1C, ArC), 135.60 (d, J = 7.4 Hz, 1C, ArC), 131.52 (s, 1C, ArC), 130.81 (s, 2C, ArC), 128.60 (s, 1C, ArC), 126.33 (d, J = 2.8 Hz, 1C, ArC), 123.75 (s, 2C, ArC), 112.74 (d, J =

15.2 Hz, 1C, ArC), 110.85 (d, *J* = 48.5 Hz, 1C, ArC), 104.69 (d, *J* = 4.6 Hz, 4C, ArC), 55.51 (s, 4C, -OMe), 33.81 (s, 1C, -$\underline{C}(CH_3)_3$), 32.02 (s, 3C, -C($\underline{C}H_3)_3$), 2.30 (s, 3C, $SiMe_3$), -17.74 (d, *J* = 30.0 Hz, 1C, $NiCH_2Si$); $^{31}P\{^1H\}$ NMR (121 MHz, C_6D_6): δ -5.08 (s, 1P). Anal. Calcd(%) for $C_{35}H_{45}BrNNiO_5PSi$: C, 55.50; H, 5.99; N, 1.85. Found(%): C, 55.02; H, 5.77; N, 1.72.

2. Topographical Analyses

Results

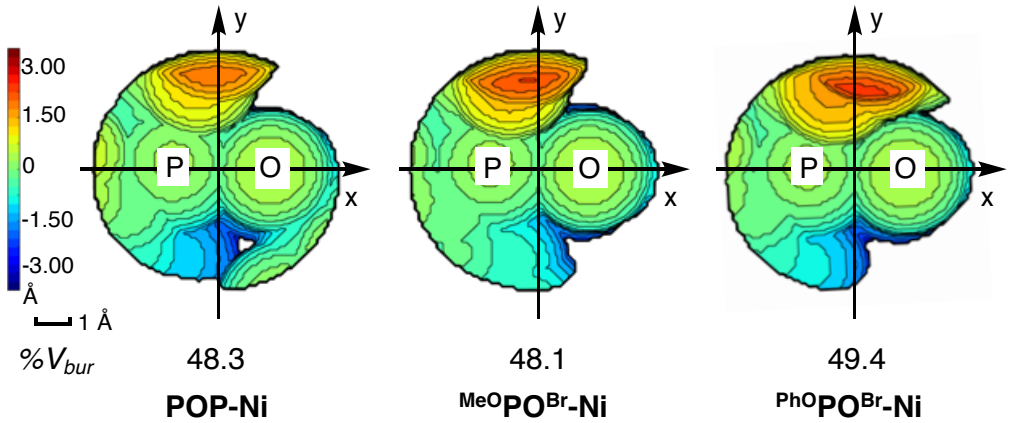

Figure S6.1. Topographical steric maps with %V_{bur} of **POP-Ni**, **^{MeO}PO^{Br}-Ni**, and **^{PhO}PO^{Br}-Ni**. The Ni atom defines the origin of xyz coordinate system. Only the P,O-ligand included in calculation and steric visualization. Blue indicates occupied space in the -z direction (toward back as drawn in a), where the phosphine-phenoxide ligands are located, and red indicates +z direction. See section S3 for more details.

Details for topographical analyses. Topographical maps of **POP-Ni**, **^{MeO}PO^{Br}-Ni**, and **^{MeO}PO^{Br}-Ni** and corresponding percent buried volume data (%V_{bur}) were generated by Cavallo's SambVca 2.1 (Salerno molecular buried volume calculation) program.[73-74, 79-80]

More details for %V_{bur} calculation and steric maps:

1) The nickel atom (Ni1) defines the center of the xyz coordinate system,

2) <u>Ni(PEt$_3$)Ph fragment was excluded</u>;

3) Bondi radii was scaled by 1.17; [74]

4) Mesh spacing for numerical integration was 0.10;

5) Sphere radius was set to 3.5 Å;

6) H atoms were excluded.

7) xz-Plane was defined as shown in the figure below and the y -axis was defined by the right-hand rule (for **POP-Ni**) or the reverse (for the other two). This is to ensure the larger axial shielding locates on the top for easier comparison. Note that for a specific complex, the %Vbur remained the same with Ni1 in the origin even the xyz coordination system rotated or flipped.

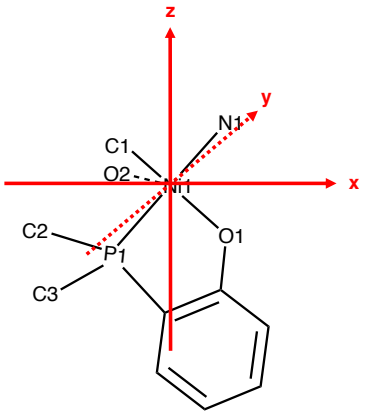

3. Procedures for Polymerization and Polymer Characterization

3.1. General procedure for high throughput parallel polymerization reactor (PPR) runs.

Polyolefin catalysis screening was performed in a high throughput parallel polymerization reactor (PPR) system. The PPR system was comprised of an array of 48 single cell (6 x 8 matrix) reactors in an inert atmosphere glovebox. Each cell was equipped with a glass insert with an internal working liquid volume of approximately 5 mL. Each cell had independent controls for pressure and was continuously stirred at 800 rpm. Catalyst solutions were prepared in toluene. All liquids (i.e., solvent, tBA, and catalyst solutions) were added via robotic syringes. Gaseous reagents (i.e., ethylene) were added via a gas injection port. Prior to each run, the reactors were heated to 50 °C, purged with ethylene, and vented.

All desired cells were injected with tBA followed with a portion of toluene (This step was skipped for ethylene homopolymerization). The reactors were heated to the run temperature and then pressured to the appropriate psig with ethylene. Catalyst solutions were then added to the cells. Each catalyst addition was chased with a small amount of toluene so that after the final addition, a total reaction volume of 5 mL was reached. Upon addition of the catalyst, the PPR software began monitoring the pressure of each cell. The desired pressure (within approximately 2-6 psig) was maintained by the supplemental addition of ethylene gas by opening the valve at the set point minus 1 psi and closing it when the pressure reached 2 psi higher. All drops in pressure were cumulatively recorded as "Uptake" or "Conversion" of the ethylene for the duration of the run or until the uptake or conversion requested value was reached, whichever occurred first. Each reaction was then quenched by addition of 1% oxygen in nitrogen for 30 seconds at 40 psi higher than the reactor pressure. The pressure of each cell was monitored during and after the quench to ensure that no further ethylene consumption

happens. The shorter the "Quench Time" (the duration between catalyst addition and oxygen quench), the more active the catalyst. In order to prevent the formation of too much polymer in any given cell, the reaction was quenched upon reaching a predetermined uptake level of 80 psig. After all the reactors were quenched, they were allowed to cool to about 60 °C. They were then vented, and the tubes were removed. The polymer samples were then dried in a centrifugal evaporator at 60 °C for 12 hours, weighed to determine polymer yield and used in subsequent IR (tBA incorporation), GPC, DSC and NMR (copolymer microstructures) analysis.

3.2. General procedure for batch reactor runs for preparation of ethylene/tBA copolymers.

Polymerization reactions were conducted in a 2-L Parr batch reactor. The reactor was heated by an electrical heating mantle and cooled by an internal serpentine cooling coil containing cooling water. The water was pre-treated by passing through an Evoqua water purification system. Both the reactor and the heating/cooling system were controlled and monitored by a Camile TG process computer. The bottom of the reactor was fitted with a dump valve, which empties the reactor contents into a lidded dump pot, which was prefilled with a catalyst-kill solution (typically 5 mL of an Irgafos / Irganox / toluene mixture). The lidded dump pot was vented to a 15-gal. blowdown tank, with both the pot and the tank N_2 purged. All chemicals used for polymerization or catalyst makeup are run through purification columns to remove any impurities that may affect polymerization. The toluene was passed through two columns, the first containing A2 alumina, the second containing Q5 reactant. The tert-butyl acrylate was filtered through activated alumina. The ethylene was passed through two columns, the first containing A204 alumina and 4 Å molecular sieves, the second containing Q5 reactant. The N2 used for transfers was passed through a single column containing A204 alumina, 4 Å molecular sieves and Q5 reactant.

The reactor was loaded first from the shot tank that contained toluene and tBA. The shot tank was filled to the load set points by use of a differential pressure transducer. After solvent/acrylate addition, the shot tank was rinsed twice with toluene. Then the reactor was heated up to the polymerization temperature set point. The ethylene was added to the reactor when the reaction temperature was reached to maintain the reaction pressure set point. Ethylene addition amounts were monitored by a micro-motion flowmeter.

The catalysts were handled in an inert atmosphere glovebox and were prepared as a solution in toluene. The catalyst was drawn into a syringe and pressure-transferred into the catalyst shot tank. This was followed by 3 rinses of toluene, 5 mL each. Catalyst was added when the reactor pressure set point was reached.

Immediately after catalyst addition the run timer was started. Ethylene was then added by the Camile to maintain reaction pressure set point in the reactor. These polymerizations were run for 60 min or until 40 g of ethylene uptake. Then the agitator was stopped, and the bottom dump valve was opened to empty reactor contents into the lidded dump pot. The lidded dump pot was closed, and the contents were poured into trays placed in a lab hood where the solvent was evaporated off overnight. The trays containing the remaining polymer were then transferred to a vacuum oven, where they were heated up to 140 °C under vacuum to remove any remaining solvent. After the trays cooled to ambient temperature, the polymers were weighed for yield/efficiencies and submitted for polymer testing if so desired.

3.3. Procedure for gel permeation chromatography (GPC).

High temperature GPC analysis was performed using a Dow Robot Assisted Delivery (RAD) system equipped with a Polymer Char infrared detector (IR5) and Agilent PLgel Mixed A columns. Decane (10 μL) was added to each sample for use as an internal flow marker. Samples were first diluted in 1,2,4-trichlorobenzene (TCB) stabilized with 300 ppm butylated

hydroxyl toluene (BHT) at a concentration of 10 mg/mL and dissolved by stirring at 160°C for 120 minutes. Prior to injection the samples are further diluted with TCB stabilized with BHT to a concentration of 3 mg/mL. Samples (250 μL) are eluted through one PL-gel 20 μm (50 x 7.5 mm) guard column followed by two PL-gel 20 μm (300 x 7.5 mm) Mixed-A columns maintained at 160 °C with TCB stabilized with BHT at a flowrate of 1.0 mL/min. The total run time was 24 minutes. To calibrate for molecular weight (MW) Agilent EasiCal polystyrene standards (PS-1 and PS-2) were diluted with 1.5 mL TCB stabilized with BHT and dissolved by stirring at 160 °C for 15 minutes. These standards are analyzed to create a 3rd order MW calibration curve. Molecular weight units are converted from polystyrene (PS) to polyethylene (PE) using a daily Q-factor calculated to be around 0.4 using the average of 5 Dowlex 2045 reference samples.

3.4. Procedure for fourier-transform infrared spectroscopy (FTIR).

The 10 mg/mL samples prepared for GPC analysis are also utilized to quantify tert-butyl acrylate (tBA) incorporation by Fourier Transform infrared spectroscopy (FTIR). A Dow robotic preparation station heated and stirred the samples at 160°C for 60 minutes then deposited 130 μL portions into stainless wells promoted on a silicon wafer. The TCB was evaporated off at 160°C under nitrogen purge. IR spectra were collected using a Nexus 6700 FT-IR equipped with a DTGS KBr detector from 4000-400 cm-1 utilizing 128 scans with a resolution of 4. Ratio of tBA (C=O: 1762-1704 cm−1) to ethylene (CH2: 736-709 cm−1) peak areas were calculated and fit to a linear calibration curve to determine total tBA.

3.5. Differential scanning calorimetry (DSC).

Differential scanning calorimetry analyses was performed on solid polymer samples using a TA Instruments, Inc. Discovery Series or TA Instruments, Inc., DSC2500, programmed with

the following method: Equilibrate at 175.00 °C; Isothermal for 3 minutes; Ramp 30.00 °C/min to 0.00 °C; Ramp 10.00 °C/min to 175.00 °C; Data was analyzed using TA Trios software.

3.6. NMR characterization.

NMR spectra of ethylene/tBA copolymers were recorded on a Bruker 400 MHz using o-dichlorobenzene at 120 °C. ^{1}H NMR analysis of copolymers were done using a relaxation time (0.2 s), and an acquisition time (1.8 s) with the number of FID's collected per sample (512). ^{13}C{^{1}H} NMR analysis of copolymers were done using 90° pulse of 17.2 μs, a relaxation time (22.0 s), an acquisition time (5.3 s), and inverse-gated decoupling with the number of FID's collected per sample (1536). Analysis of the spectra was based on literature.[22, 37]

4. Supplemental Data for Ethylene/tBA Copolymerization

4.1. Analysis of turnover frequency of acrylate (TOF_{tBA})

Table S6.2. Supplemental data for ethylene/acrylate copolymerization.

Entry[a]	catalyst	T/°C	[tBA]/M	Act.[b]	$M_w/10^3$	PDI	%Mol tBA	Tm/°C	TOF_{tBA}[c]
1	^{MeO}**PO^{Br}-Ni**	90	0.05	1550	73.3	2.4	1.5	115	***803***
2	^{MeO}**PO^{Br}-Ni**	90	0.10	720	47.0	2.2	3.4	106	***750***
3	^{MeO}**PO^{Br}-Ni**	90	0.15	410	35.4	2.3	4.8	98.6	***610***
4	^{PhO}**PO^{Br}-Ni**	90	0.025	29000	47.0	2.3	0.2	128	***2400***
5	^{PhO}**PO^{Br}-Ni**	90	0.05	21000	38.5	2.3	0.3	126	***2500***
6	^{PhO}**PO^{Br}-Ni**	90	0.10	9700	32.9	2.4	0.7	123	***2500***
7	^{PhO}**PO^{Br}-Ni**	90	0.15	5700	30.0	2.3	1.0	120	***1900***
8	^{MeO}**PO^{Br}-Ni**	110	0.10	440	17.8	2.4	2.9	107	***420***
9	^{PhO}**PO^{Br}-Ni**	110	0.10	18000	26.0	2.4	0.7	123	***4400***
10	^{PhO}**PO^{Br}-Ni**	110	0.15	10000	17.0	2.5	1.2	119	***4100***

[a]Unless specified, V = 5 mL, [Ni] = 0.05 mM, ethylene pressure = 400 psi, toluene solvent. Polymerization was stopped after consuming a set amount of ethylene and each entry represents multiple replicated runs. Entries 2, 8, 6, 7, 9 were also included in table 1 as entry 1~5. See Experimental section 3 for detailed procedures and Table S6.4 for original catalytic runs. [b]Activity in 1000 kg/(mol·h). [c]Turnover frequency of TBA = Mol of tBA inserted / (Mol of catalyst x time (in hours)).

As shown in the Table S6.2, ^{PhO}**PO^{Br}-Ni** produces copolymers with lower acrylate incorporation compared to ^{MeO}**PO^{Br}-Ni**. However, the former actually features a significantly higher turnover frequency of acrylate (TOF_{tBA}) compared to the latter under otherwise identical conditions (e.g. entry 2 vs 6, or 3 vs 7, or 8 vs 9). It's also notable that the temperature shows significant impact on TOF_{tBA} while the impact of tBA concentration is moderate.

4.2. Supplemental ethylene./acrylate copolymerization results.

Table S6.3. Catalysis results for Figure 6.5 and Table S6.5.

Entry[a]	catalyst	T/°C	E/psi	A	A/M	Act.[b]	Mw[c]	PDI	%Mol A	Tm (°C)
1[d]	**POP-Ni**	90	400	tBA	0.05	660	55.1	2.2	2.1	111
2	**^{MeO}PO^{Br}-Ni**	90	400	tBA	0.05	1550	73.3	2.4	1.5	115
3	**^{PhO}PO^{Br}-Ni**	90	400	tBA	0.05	21000	38.5	2.3	0.3	126
4[e]	**^{PhO}PO^{Br}-Ni**	90	400	tBA	0.15	5700	30.0	2.3	1.0	120
5	**^{PhO}PO^{Br}-Ni**	90	200	tBA	0.15	910	21.9	2.1	1.5	118
6	**^{PhO}PO^{Br}-Ni**	110	200	tBA	0.05	8300	15.9	2.4	0.7	123

[a] V = 5 mL, [Catalyst] = 0.05 mM, ethylene pressure = 400 psi, toluene solvent; each entry represents multiple replicated runs (see section S3 for detailed procedure and Table S6.4 for original data). [b] Activity in kg/(mol·h). [c] kg/mol. [d] Reported in ref 1. [e] Also included in table 1 as entry 4.

4.3 Original polymerization runs for ethylene/tBA copolymerization

Table S6.4 Original runs of Table 1, S2~3.

Entry	catalyst	T/°C	E (psi)	A	A/M	time/s	Yield/mg	Act.[c]	Mw[d]	PDI	%Mol A	Tm (°C)
1	^{MeO}**POBr-Ni**	70	400	tBA	0.05	1050	55	754	112.2	2.8	2.4	114
2	^{MeO}**POBr-Ni**	70	400	tBA	0.05	1390	72	746	127.5	2.5	2.3	114
3	^{MeO}**POBr-Ni**	90	400	tBA	0.05	1003	111	1594	72	2.4	1.5	115
4	^{MeO}**POBr-Ni**	90	400	tBA	0.05	1133	118	1499	74.6	2.5	1.5	116
5	^{MeO}**POBr-Ni**	90	400	tBA	0.1	2057	105	735	46.7	2.2	3.3	106
6	^{MeO}**POBr-Ni**	90	400	tBA	0.1	2223	105	680	47.3	2.2	3.4	106
7	^{MeO}**POBr-Ni**	90	400	tBA	0.15	3601	104	416	35.5	2.2	4.9	98
8	^{MeO}**POBr-Ni**	90	400	tBA	0.15	3601	103	412	35.2	2.3	4.7	99
9	^{PhO}**POBr-Ni**	90	400	tBA	0.05	116	193	23922	37.9	2.3	0.3	126
10	^{PhO}**POBr-Ni**	90	400	tBA	0.05	129	164	18317	39.1	2.3	0.3	126
11	^{PhO}**POBr-Ni**	90	400	tBA	0.1	232	155	9610	33	2.4	0.7	122
12	^{PhO}**POBr-Ni**	90	400	tBA	0.1	238	162	9816	32.7	2.3	0.8	123
13	^{PhO}**POBr-Ni**	90	400	tBA	0.15	355	141	5717	30.1	2.3	1.0	121
14	^{PhO}**POBr-Ni**	90	400	tBA	0.15	345	137	5714	29.9	2.3	0.9	120
15	^{MeO}**POBr-Ni**	110	400	tBA	0.1	3600	119	476	27.7	2.4	3.0	107
16	^{MeO}**POBr-Ni**	110	400	tBA	0.1	3600	109	436	25	2.3	3.2	107
17	^{MeO}**POBr-Ni**	110	400	tBA	0.1	3601	103	412	25.2	2.4	2.6	107
18	^{PhO}**POBr-Ni**	110	400	tBA	0.1	135	163	17353	18.8	2.5	0.7	123
19	^{PhO}**POBr-Ni**	110	400	tBA	0.1	130	159	17550	18.1	2.4	0.7	122
20	^{PhO}**POBr-Ni**	110	400	tBA	0.1	126	162	18550	16.5	2.5	0.7	123
21	^{PhO}**POBr-Ni**	110	400	tBA	0.15	217	154	10241	6.6	2.5	1.2	120
22	^{PhO}**POBr-Ni**	110	400	tBA	0.15	216	156	10241	7.2	2.5	1.1	120
23	^{PhO}**POBr-Ni**	110	200	tBA	0.05	226	132	8414	15.7	2.8	2.4	114
24	^{PhO}**POBr-Ni**	110	200	tBA	0.05	231	133	8282	16.2	2.5	2.3	114
25	^{PhO}**POBr-Ni**	90	200	tBA	0.15	1471	94	920	21.5	2.1	1.6	116
26	^{PhO}**POBr-Ni**	90	200	tBA	0.15	1547	98	912	21.7	2.1	1.5	117
27	^{PhO}**POBr-Ni**	90	200	tBA	0.15	1841	115	899	22.4	2.2	1.5	121
28	^{MeO}**POBr-Ni**	90	400	tBA	0.05	1003	111	1594	72	2.4	1.5	115
29	^{MeO}**POBr-Ni**	90	400	tBA	0.05	1133	118	1499	74.6	2.5	1.5	116
30	^{MeO}**POBr-Ni**	90	400	tBA	0.15	3601	104	416	35.5	2.2	4.9	98
31	^{MeO}**POBr-Ni**	90	400	tBA	0.15	3601	103	412	35.2	2.3	4.7	99
32	^{PhO}**POBr-Ni**	90	400	tBA	0.025	84	166	28339	48.4	2.3	0.2	128
33	^{PhO}**POBr-Ni**	90	400	tBA	0.025	88	176	28925	45.6	2.2	0.2	128
34	^{PhO}**POBr-Ni**	90	400	tBA	0.05	116	193	23922	37.9	2.3	0.3	126
35	^{PhO}**POBr-Ni**	90	400	tBA	0.05	129	164	18317	39.1	2.3	0.3	126
36	^{PhO}**POBr-Ni**	110	400	tBA	0.15	217	154	10241	6.6	2.5	1.2	120
37	^{PhO}**POBr-Ni**	110	400	tBA	0.15	216	156	10241	7.2	2.5	1.1	120

[a] V = 5 mL, [Catalyst] = 0.05 mM, ethylene pressure = 400 psi, toluene solvent; see Experimental section 3 for detailed procedure. [b] Activity in kg/(mol·h). [c] kg/mol.

5. Characterization of Ethylene/tBA Copolymers

Microstructural analysis of ethylene/tBA copolymers

The following sections summarize methods and results of microstructural analysis. Analysis of the spectra was based on literature.[22, 34, 37]

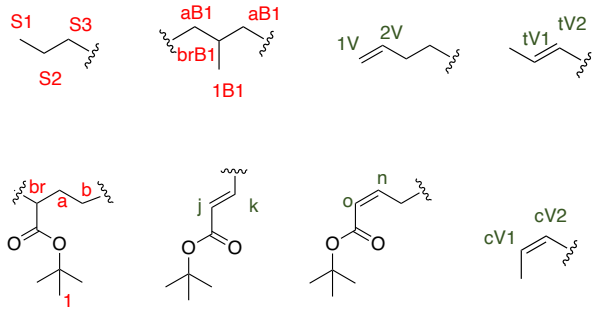

Figure S6.2. Microstructural features identified in ^{1}H and ^{31}C{^{1}H} NMR analysis.

Copolymer samples **A~F** are ethylene/tBA copolymers produced in entry 1~6 of Table S6.4, respectively.

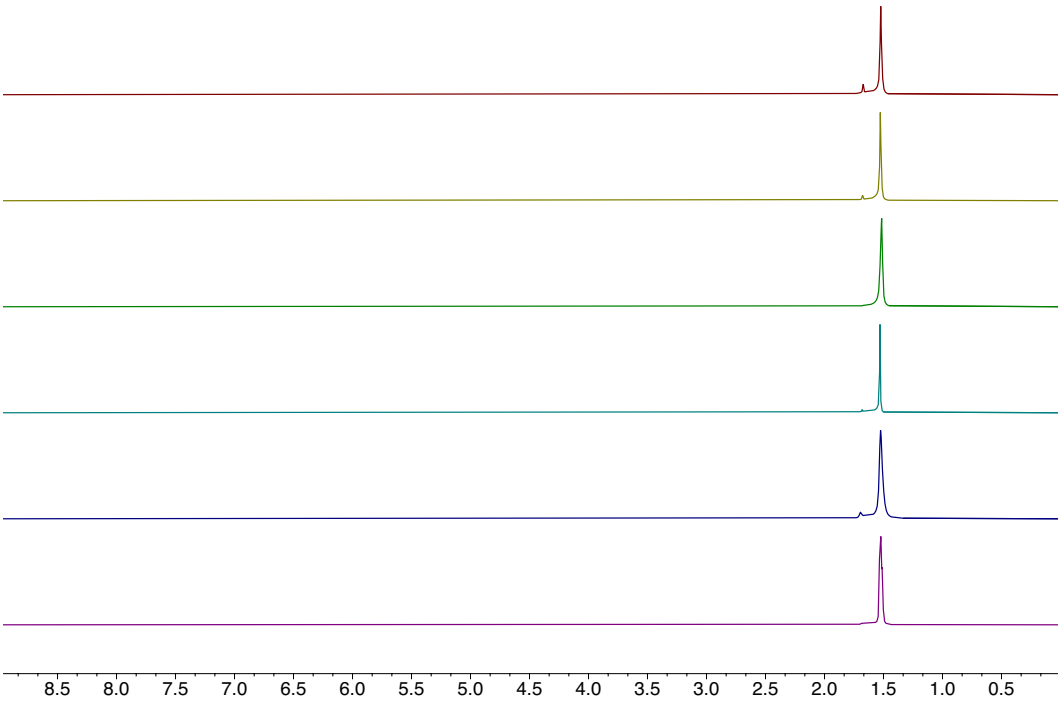

Figure S6.3. ^{1}H NMR spectra of ethylene/tBA copolymer **A~F** (top to bottom).

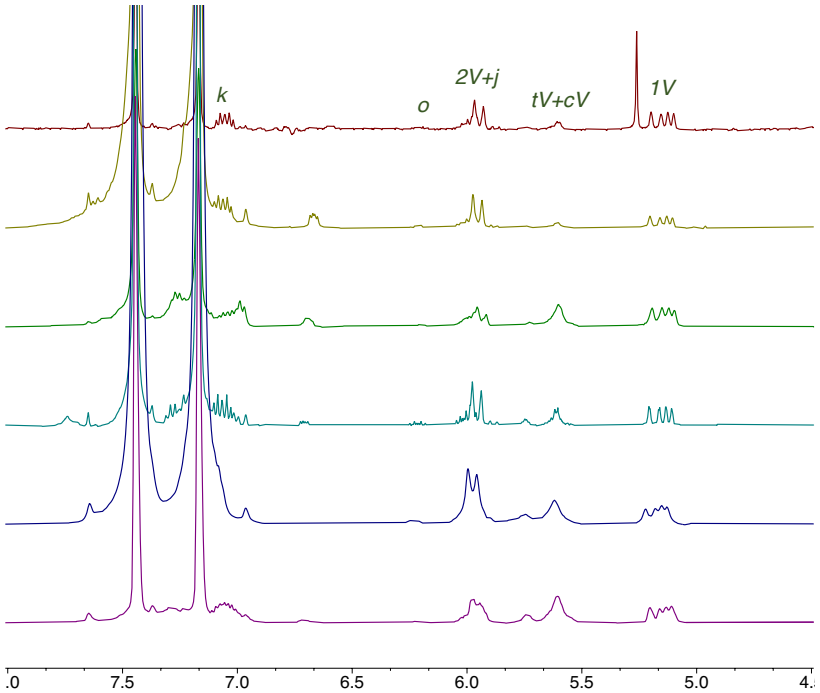

Figure S6.4. ^{1}H NMR spectra of ethylene/tBA copolymer **A~F** (top to bottom, olefinic region).

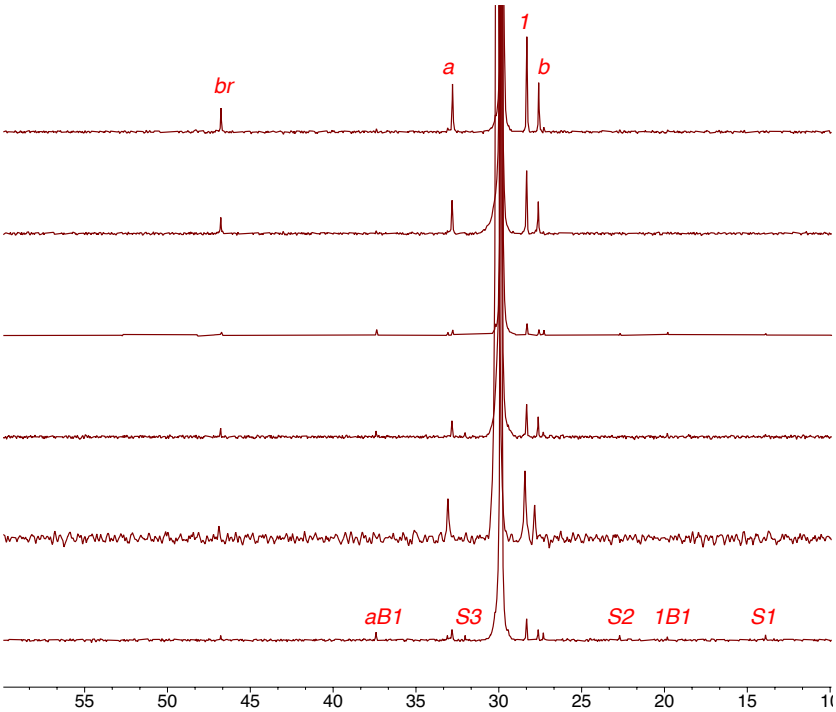

Figure S6.5. Scaled ^{13}C{^{1}H} NMR spectra of ethylene/tBA copolymer **A~F** (top to bottom, alkyl region).

Table S6.5. Microstructural analysis of ethylene/acrylate copolymers.[a]

	A	**B**	**C**	**D**	**E**	**F**
Catalyst	**POP-Ni**	**^{MeO}PO^{Br}-Ni**	**^{PhO}PO^{Br}-Ni**	**^{PhO}PO^{Br}-Ni**	**^{PhO}PO^{Br}-Ni**	**^{PhO}PO^{Br}-Ni**
T (ºC)	90	90	90	90	90	110
E/psi	400	400	400	400	200	200
[tBA]/M	0.05	0.05	0.05	0.15	0.15	0.05
%Mol tBA	2.1%	1.5%	0.3%	1.0%	1.5%	0.7%
tBA/chain	18	15	1.9	4.2	5.5	1.5
Terminal tBA/ chain	0.53	0.69	0.23	0.58	0.66	0.37
%Terminal tBA/ tBA	2.9%	4.6%	12.1%	14.0%	12.1%	27.2%
Vinyl/chain	0.39	0.24	0.44	0.25	0.18	0.29
2-Propenyl/ chain	0.08	0.06	0.33	0.16	0.16	0.31
Vinyl+propenyl/E units[b]	0.06%	0.03%	0.13%	0.09%	0.10%	0.26%

[a] Copolymer samples **A~F** are ethylene/tBA copolymers produced in entry 1~6 of Table S6.3, respectively. See Experimental section 4 for more details. [b] 'Vinyl+propenyl': the sum of numbers of the vinyl and 2-propenyl units per chain. 'E units': the number of ethylene units in one chain.

6. Investigations of Acrylate-Induced Reactions

Procedures. Unless specified, 0.0059 mmol of the Ni catalyst prepared using the above procedure was dissolved in C_6D_6 and transferred to a J-Young tube. The solution was frozen in the Coldwell pre-cooled by a liquid nitrogen bath, and *t*-butyl acrylate (tBA) was added via syringe (Total volume = 0.50 ml). The resulting mixture was warmed up to thawing temperature and shaken vigorously prior to transferring to pre-heated NMR probe for acquisition of spectra at 25 ºC. NMR monitoring of tBA insertion were performed by monitoring the ^{1}H and ^{31}P{^{1}H} NMR.

tBA insertion into ^{PhO}***PO***^{Br}***-Ni***

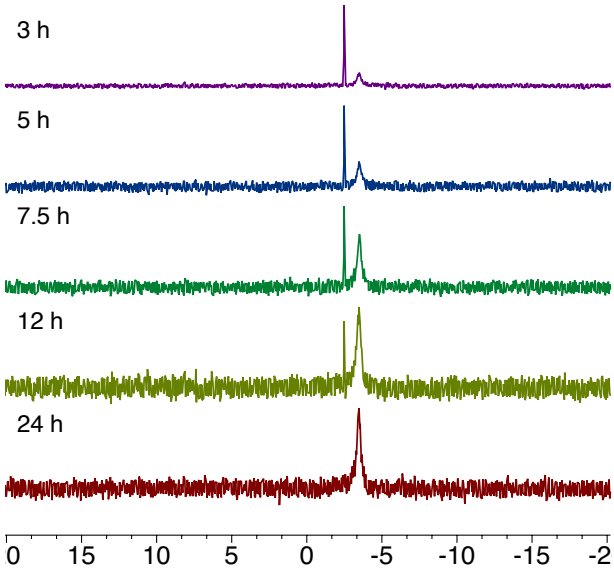

Figure S6.6. ^{31}P{^{1}H} NMR monitoring of reaction of tBA with ^{PhO}**PO**^{Br}**-Ni** (Condition: [^{PhO}**PO**^{Br}**-Ni**] = 0.0118 M, [tBA] = 0.177 M, solvent: C_6D_6, V = 0.5 mL).

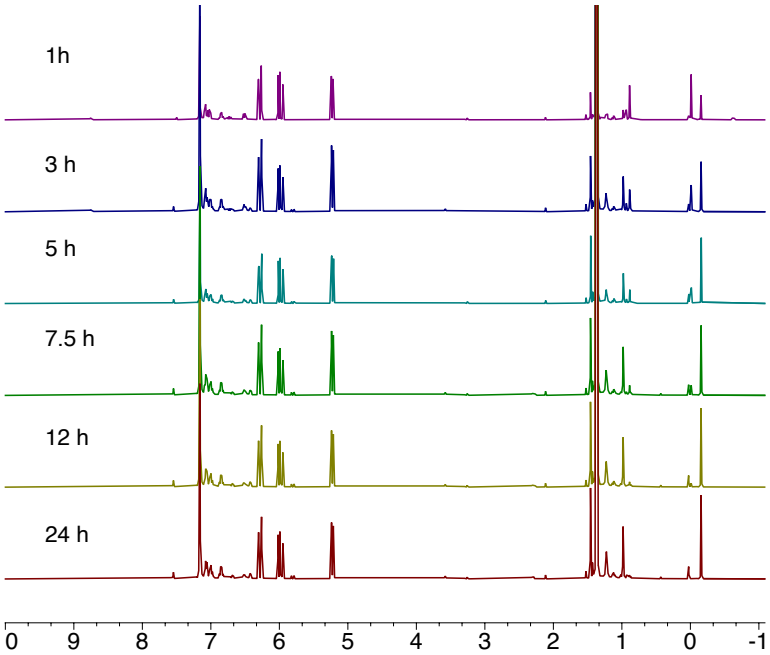

Figure S6.7. ^{1}H NMR monitoring of reaction of tBA with **^{PhO}PO^{Br}-Ni** (Condition: [**^{PhO}PO^{Br}-Ni**] = 0.0118 M, [tBA] = 0.177 M, solvent: C_6D_6, V = 0.5 mL).

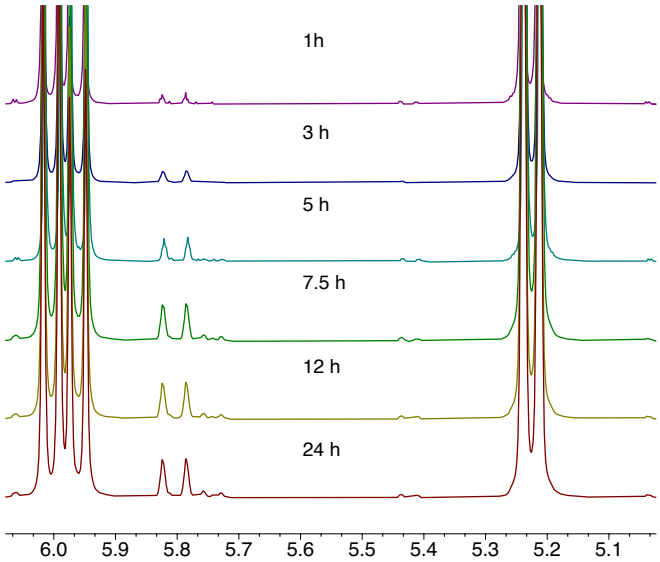

Figure S6.8. ^{1}H NMR monitoring of reaction of tBA with **^{PhO}PO^{Br}-Ni** (Olefinic region, condition: [**^{PhO}PO^{Br}-Ni**] = 0.0118 M, [tBA] = 0.177 M, solvent: C_6D_6, V = 0.5 mL).

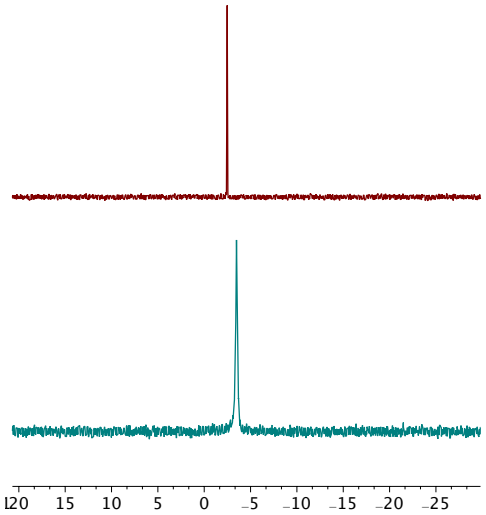

Figure S6.9. $^{31}P\{^{1}H\}$ NMR spectra of ^{PhO}**PO**^{Br}**-Ni** (top) and tBA inserted products (bottom, after removal of volatiles)

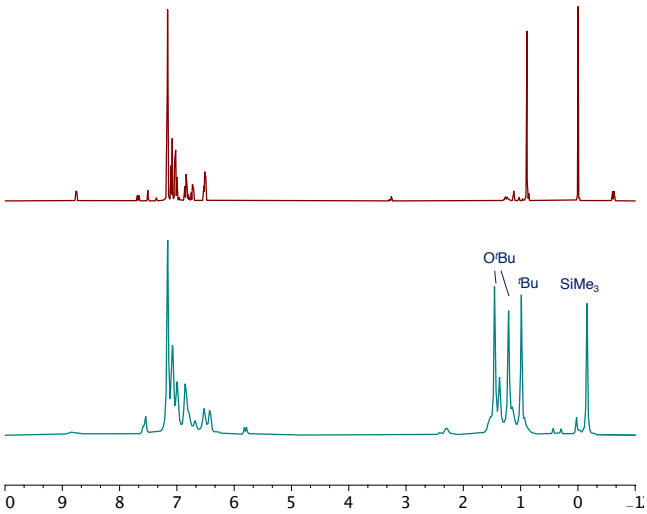

Figure S6.10. $^{31}P\{^{1}H\}$ NMR spectra of ^{PhO}**PO**^{Br}**-Ni** (top) and tBA inserted products (bottom, after removal of volatiles)

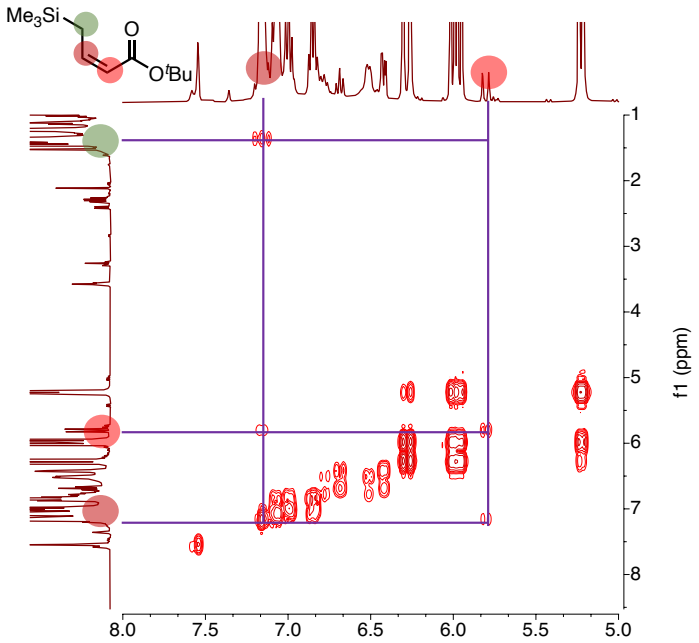

Figure S6.11. Identifying the internal olefin: ^{1}H-^{1}H COSY NMR spectrum of products generated from tBA reaction with ^{PhO}**POBr-Ni**.

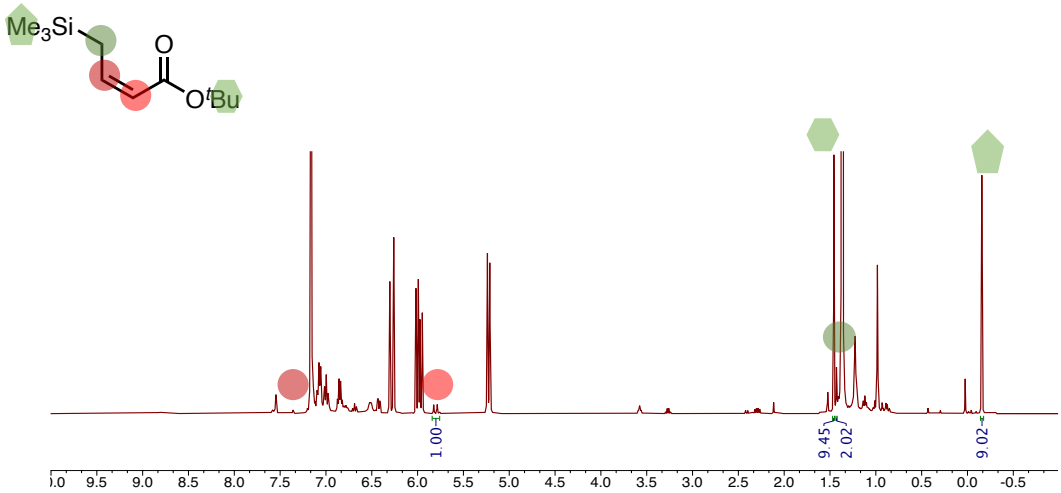

Figure S6.12. Identifying the internal olefin: ^{1}H NMR characterization of the internal olefin from the mixture generated from tBA reaction with ^{PhO}**PO^{Br}-Ni**.

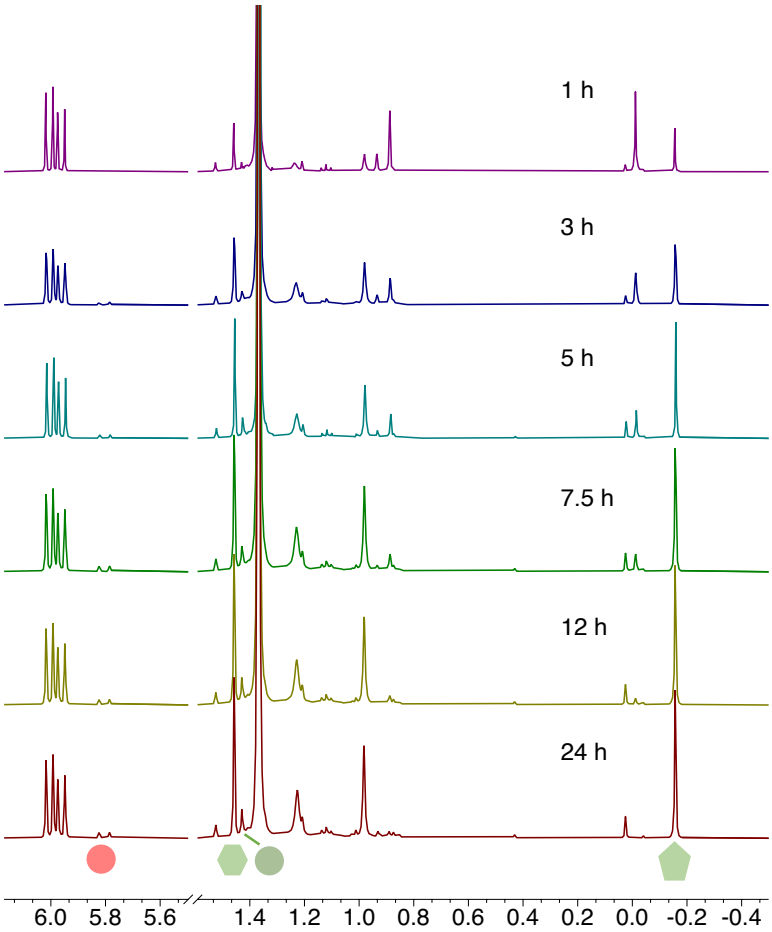

Figure S6.13. ^{1}H NMR monitoring of generation of the internal olefin overtime (Condition: [^{PhO}**PO**^{Br}**-Ni**] = 0.0118 M, [tBA] = 0.177 M, solvent: C_6D_6, V = 0.5 mL).

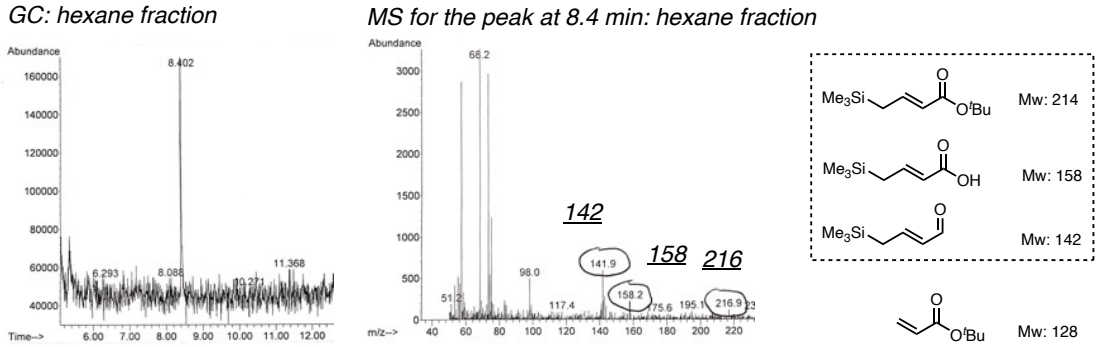

Figure S6.14. Identifying the internal olefin: GC-mass analysis of the mixture generated from tBA reaction with ^{PhO}**PO**^{Br}**-Ni**.

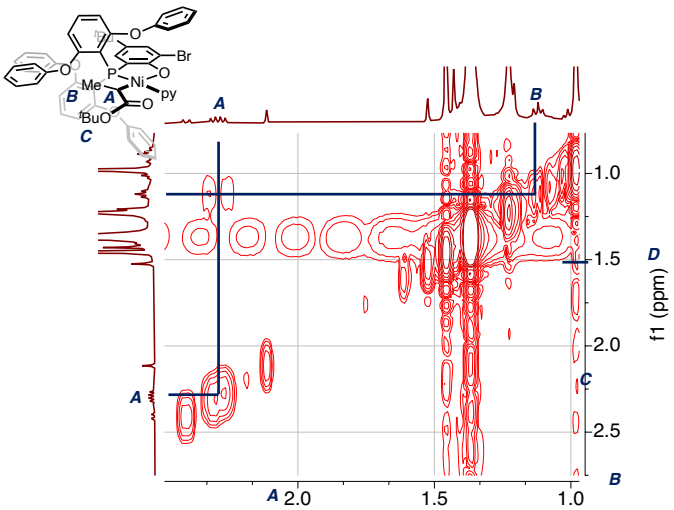

Figure S6.15. Identifying the tBA reinsertion product (**^{PhO}PO^{Br}-Ni(py)CCO**): ^{1}H-^{1}H COSY NMR spectrum of products generated from tBA reaction with **^{PhO}PO^{Br}-Ni**.

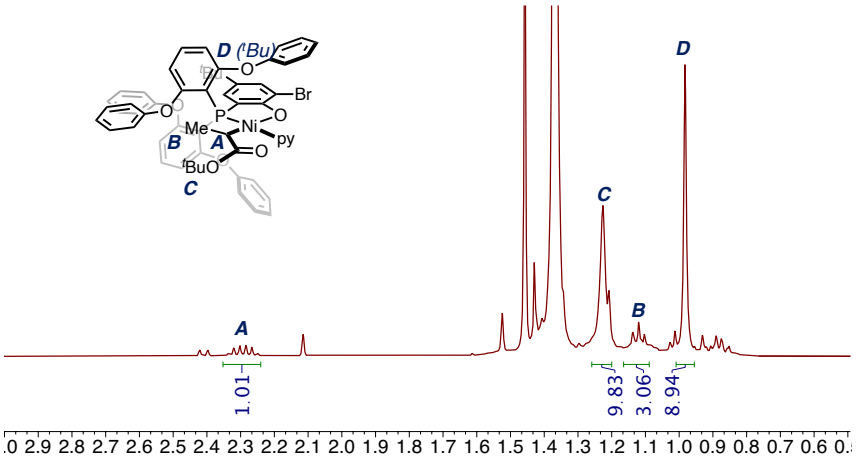

Figure S6.16. Identifying the tBA reinsertion product (**^{PhO}PO^{Br}-Ni(py)CCO**): ^{1}H NMR spectrum of products generated from tBA reaction with **^{PhO}PO^{Br}-Ni**.

MA insertion into ***^{PhO}PO^{Br}-Ni***

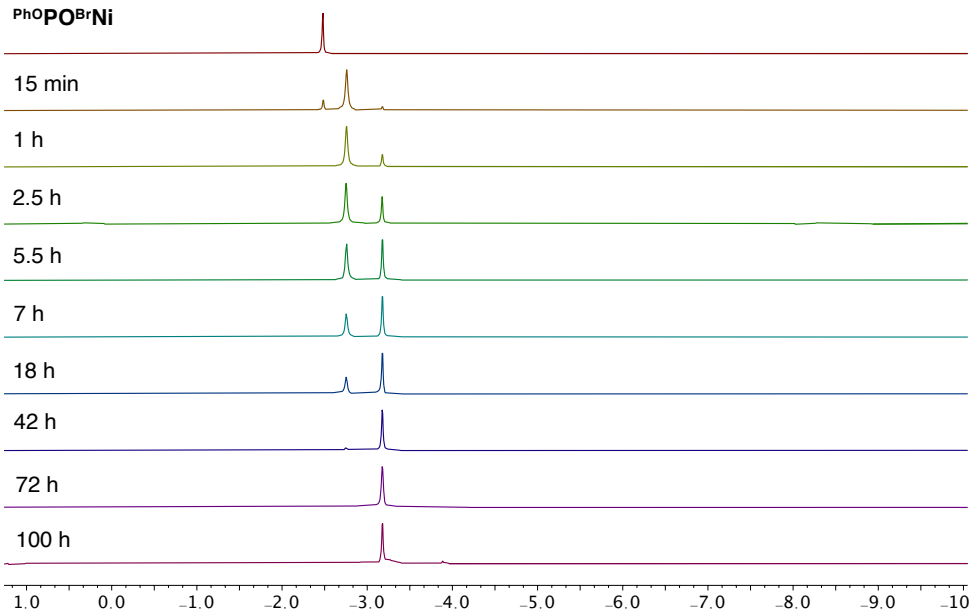

Figure S6.17. $^{31}P\{^{1}H\}$ NMR monitoring of reaction of MA with **^{PhO}PO^{Br}-Ni** (Condition: [**^{PhO}PO^{Br}-Ni**] = 0.0118 M, [MA] = 0.177 M, solvent: C_6D_6, V = 0.5 mL).

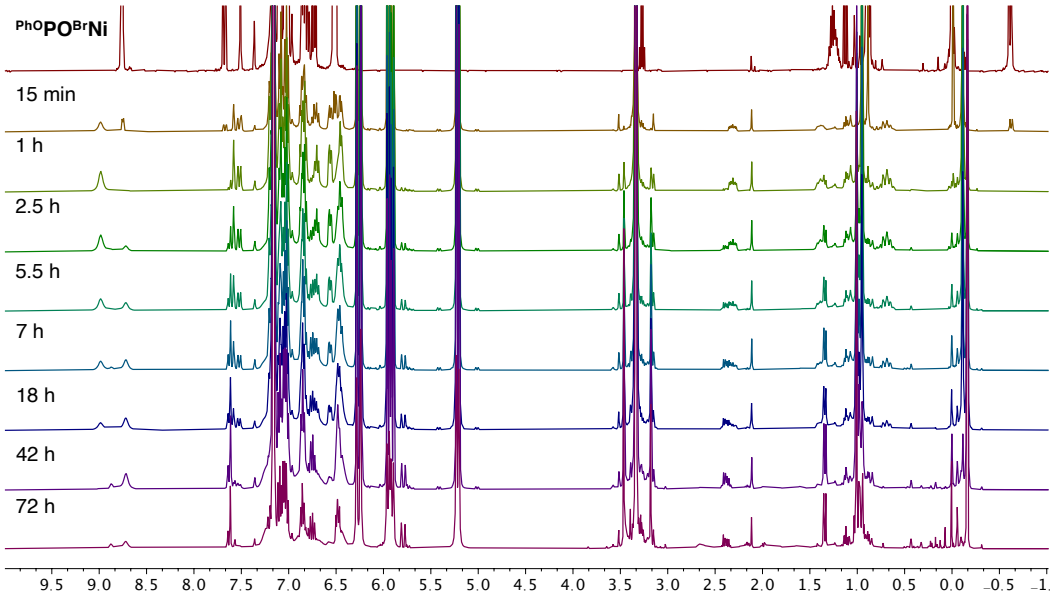

Figure S6.18. ^{1}H NMR monitoring of reaction of MA with **^{PhO}PO^{Br}-Ni** (Condition: [**^{PhO}PO^{Br}-Ni**] = 0.0118 M, [MA] = 0.177 M, solvent: C_6D_6, V = 0.5 mL).

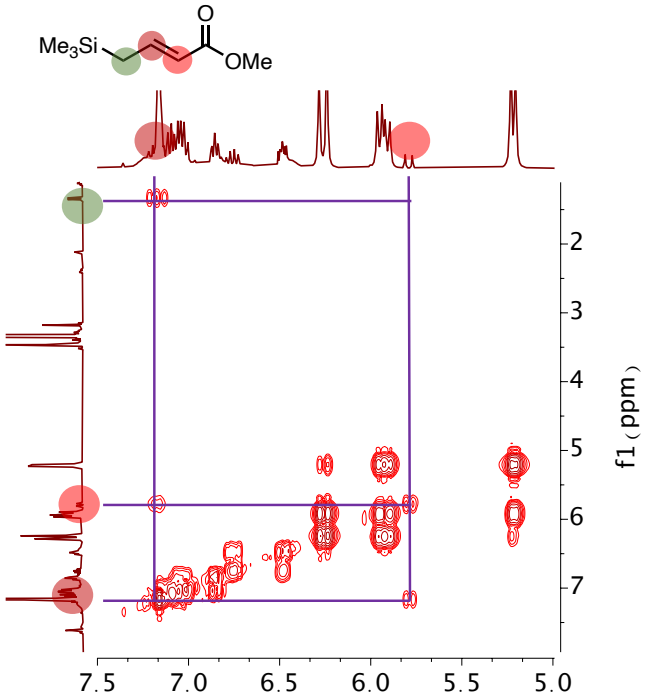

Figure S6.19. Identifying the internal olefin: ^{1}H-^{1}H COSY NMR spectrum of products generated from MA reaction with ^{PhO}**PO**^{Br}**-Ni**.

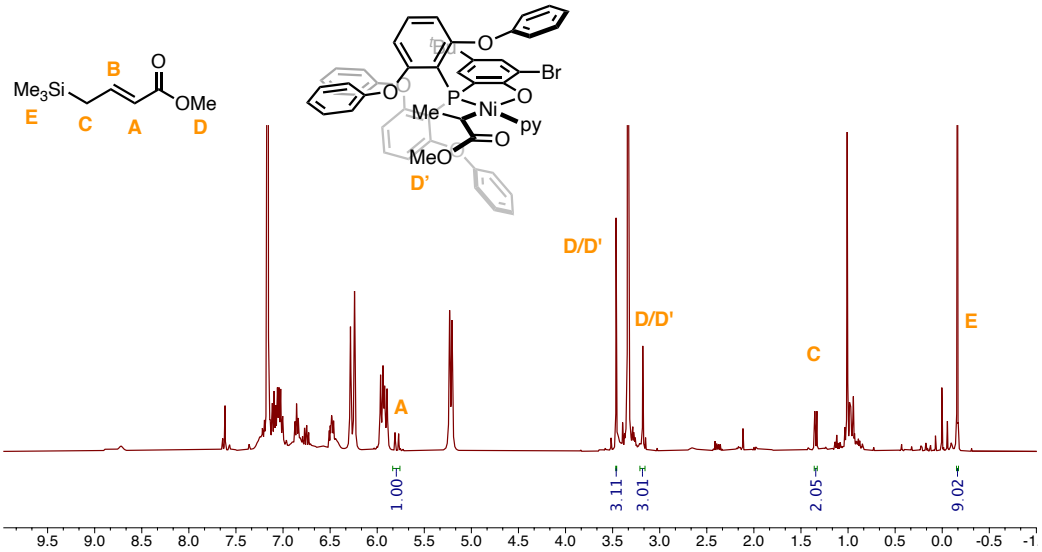

Figure S6.20. Identifying the internal olefin and ^{PhO}**PO**^{Br}**-NiCCO**^{M}: ^{1}H NMR characterization of the internal olefin from the mixture generated from MA reaction with ^{PhO}**PO**^{Br}**-Ni**.

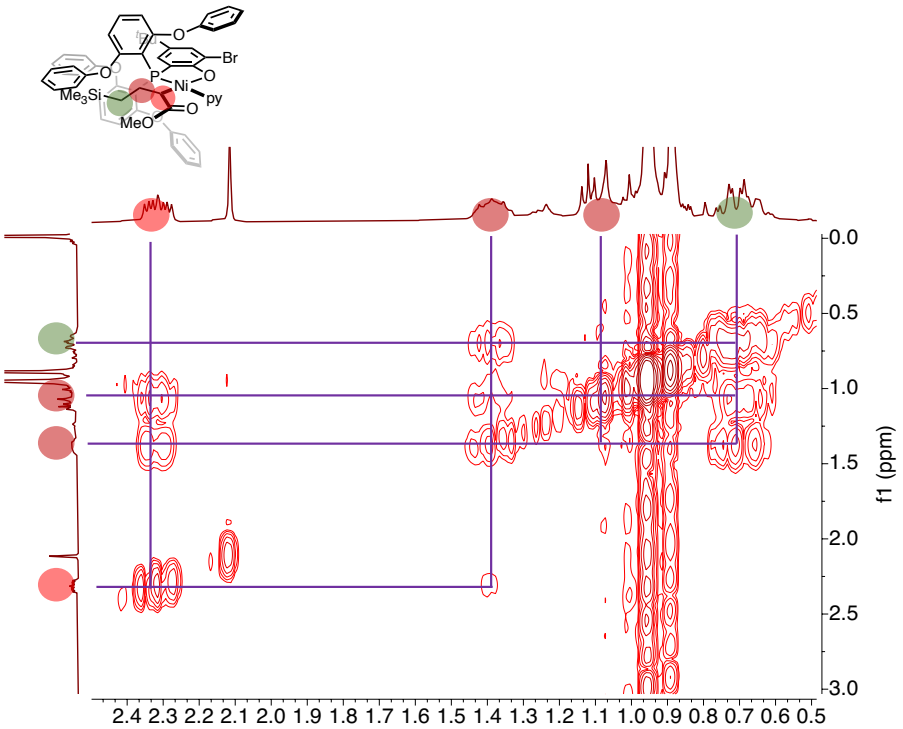

Figure S6.21. Identifying the first MA product (**^{PhO}PO^{Br}-Ni^{Si}CCO^{M}**): ^{1}H-^{1}H COSY NMR spectrum of tBA reaction with **^{PhO}PO^{Br}-Ni** (15 min).

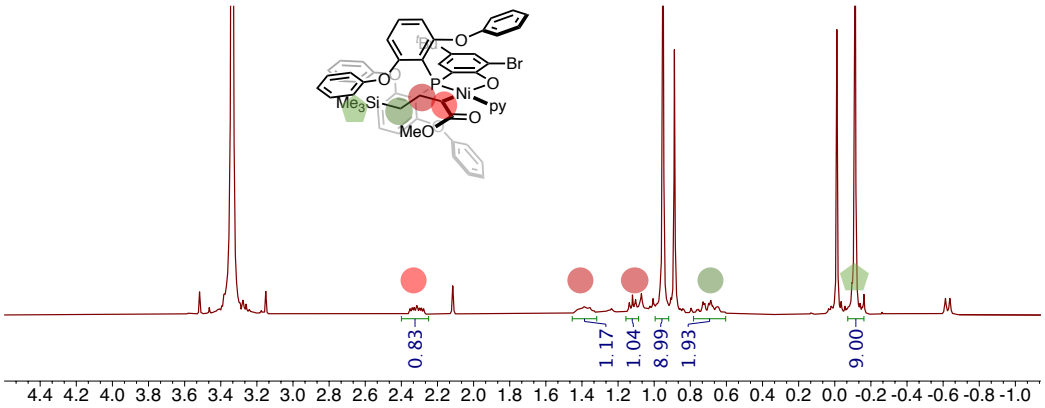

Figure S6.22. Identifying the first MA product (**^{PhO}PO^{Br}-Ni^{Si}CCO^{M}**): ^{1}H NMR spectrum of products generated from tBA reaction with **^{PhO}PO^{Br}-Ni**.

tBA insertion into ***^{MeO}PO^{Br}-Ni***

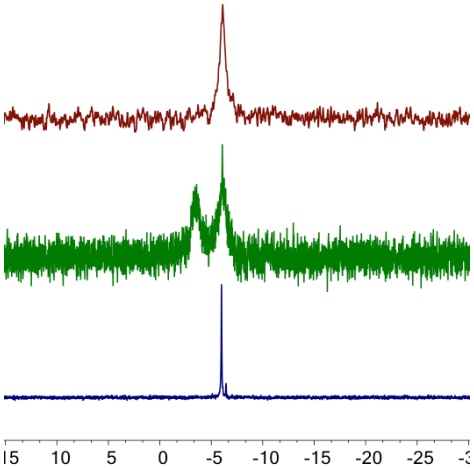

Figure S6.23. ^{31}P{^{1}H} NMR spectra of **^{MeO}PO^{Br}-Ni** + 50 tBA (t = 75 min), residue after removal of volatiles (medium) and the product after addition of 2 equiv. of pyridine (bottom).

Addition of excess tBA to **^{MeO}PO^{Br}-Ni** leads to generation of new species featuring one broad resonance in ^{31}P{^{1}H} NMR spectrum (Figure S6.23), which are converted to two broad resonances after removal of volatiles. After addition of 2 equiv. of pyridine, these new broad resonances collapse to one sharp resonance.

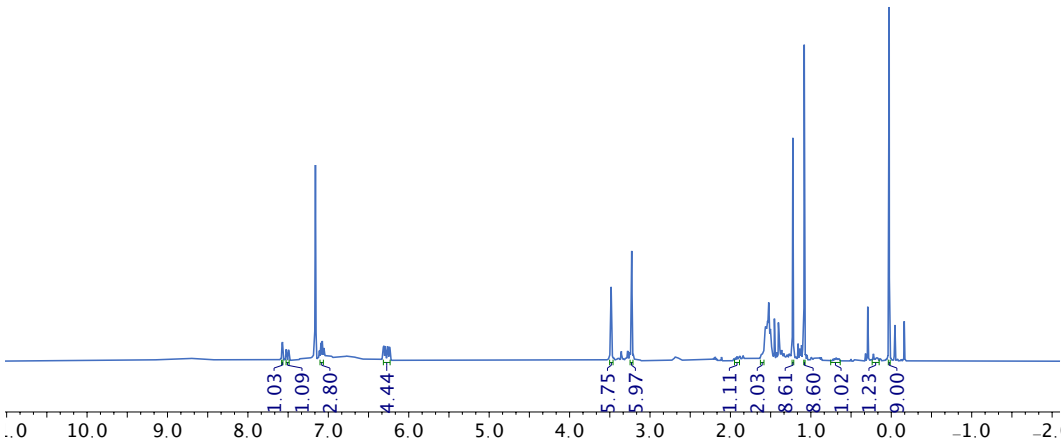

Figure S6.24. ^{1}H NMR spectrum of the tBA insertion product (**^{MeO}PO^{Br}-Ni^{Si}CCO**) with 2 equiv. of pyridine.

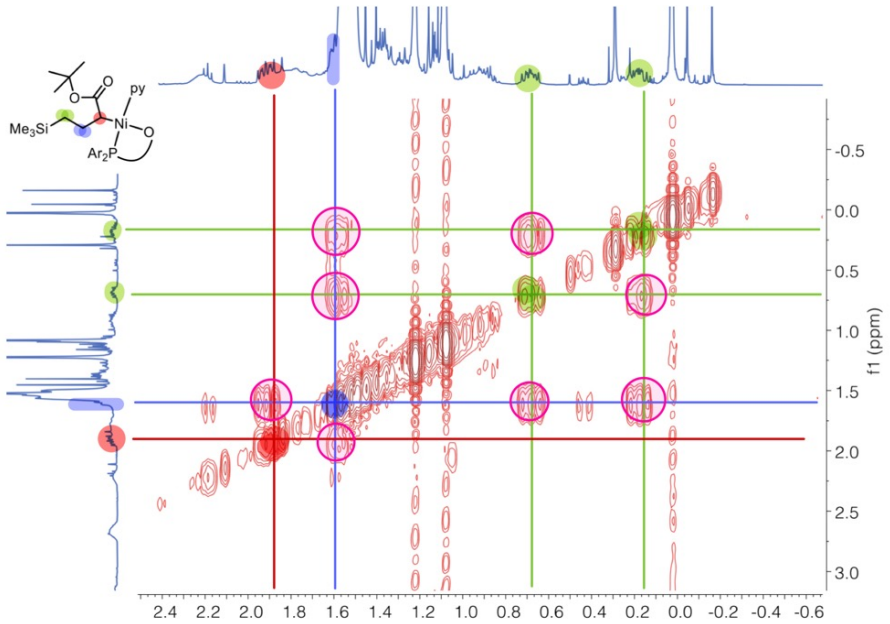

Figure S6.25. ^{1}H-^{1}H COSY NMR spectrum of tBA insertion product (**^{MeO}PO^{Br}-Ni^{Si}CCO**) with 2 equiv. of pyridine.

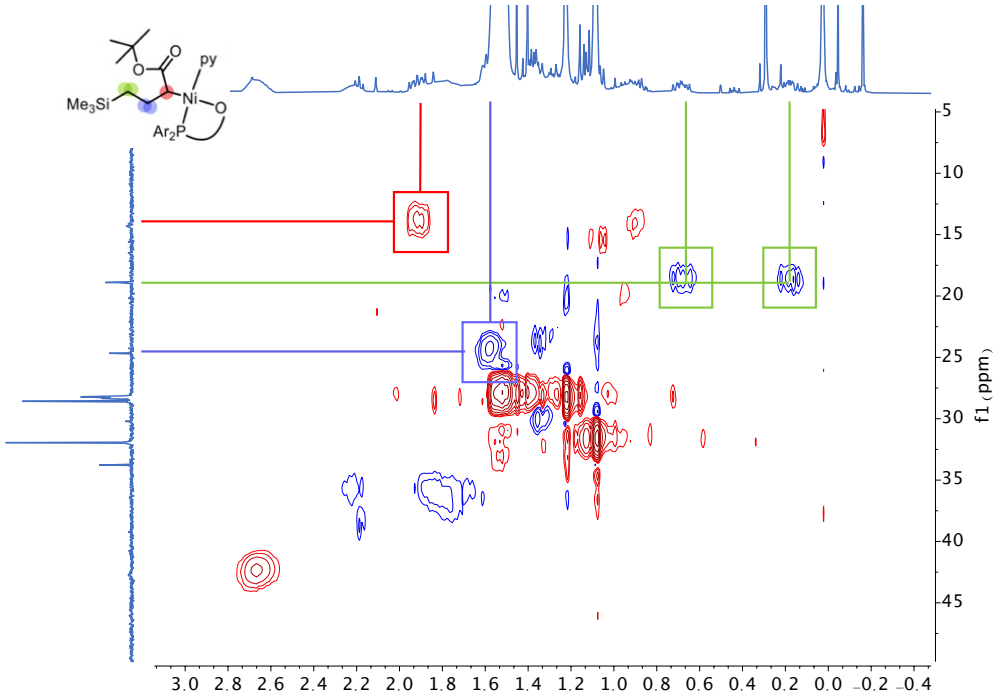

Figure S6.26. ^{1}H-^{13}C HSQC NMR spectrum of tBA insertion product (**^{MeO}PO^{Br}-Ni^{Si}CCO**) with 2 equiv. of pyridine.

Based on ^{1}H, ^{1}H-^{1}H COSY, ^{1}H-^{13}C HSQC NMR analysis (Figure S6.24-26), the major product was identified as **^{MeO}PO^{Br}-Ni(py)C^{Si}CO**, the species generated after first tBA insertion.

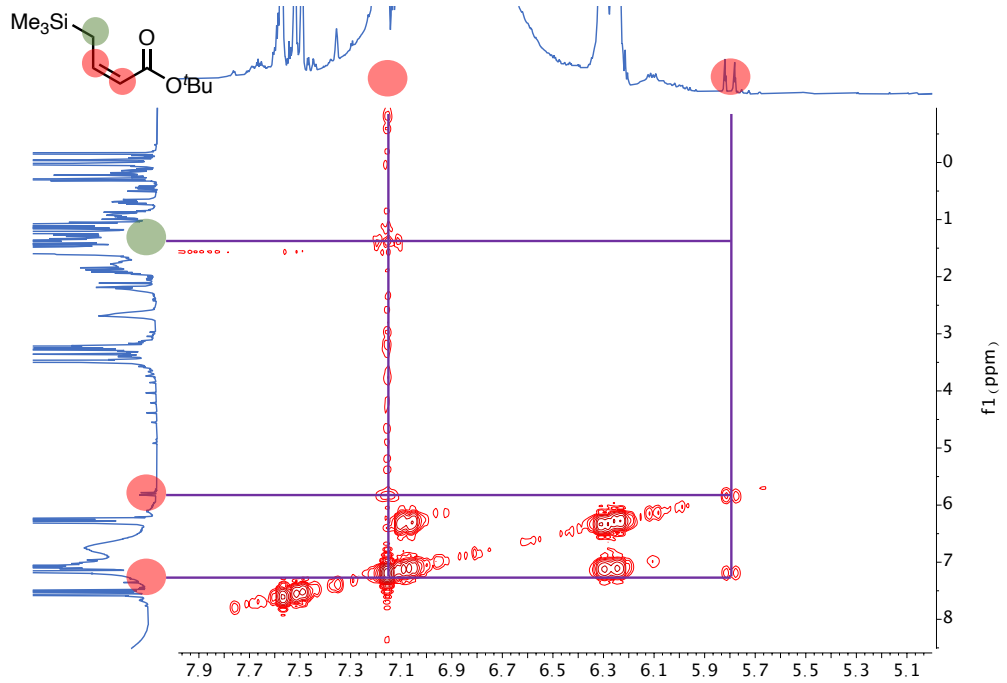

Figure S6.27. Possible observation of the internal olefin: ^{1}H-^{1}H COSY NMR spectrum of tBA insertion product (**^{MeO}PO^{Br}-Ni^{Si}CCO**) with 2 equiv. of pyridine.

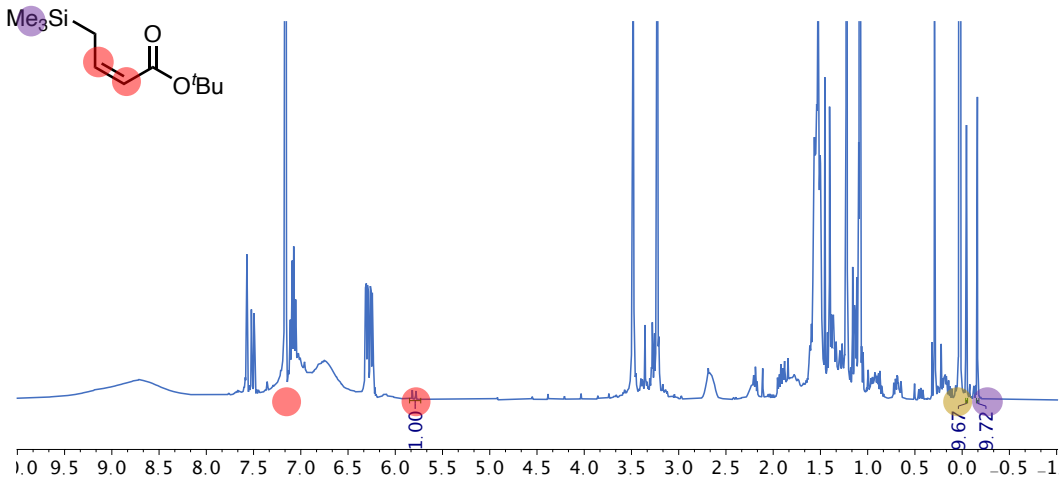

Figure S6.28. Possible observation of the internal olefin: ^{1}H NMR spectrum of the tBA insertion product (**^{MeO}PO^{Br}-Ni^{Si}CCO**) with 2 equiv. of pyridine.

Though **^{MeO}PO^{Br}-Ni(py)C^{Si}CO** is the major product (c.a. >90% NMR yields), other minor species were also observed during this reaction, including the internal olefin generated from β-H elimination.

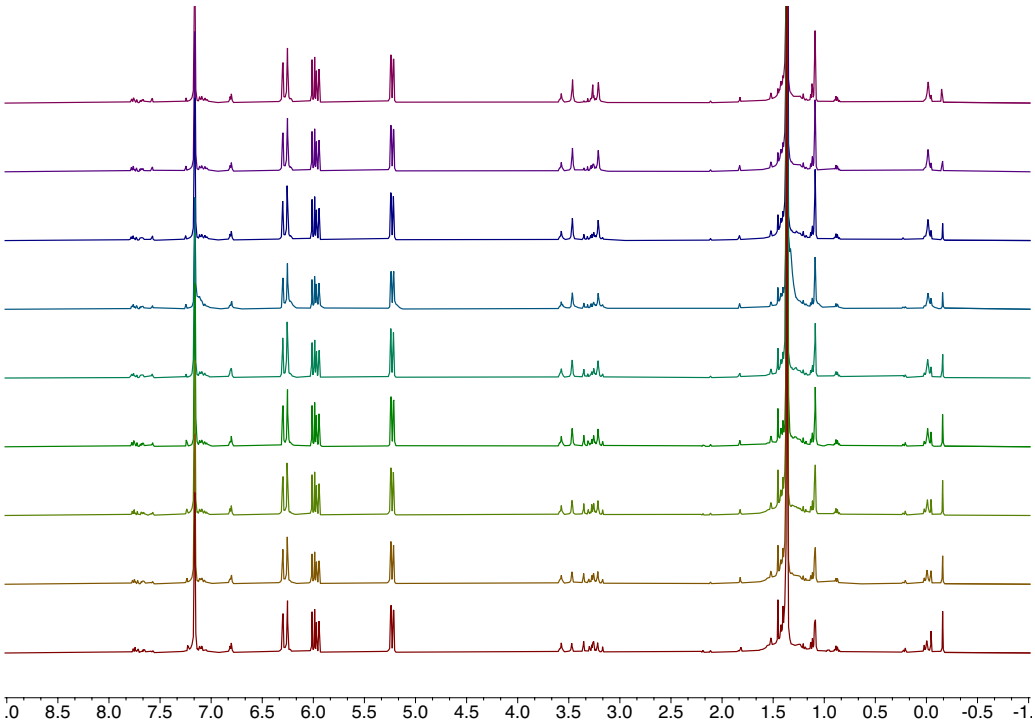

Figure S6.29. ^{1}H NMR monitoring of reaction of tBA with **^{MeO}PO^{Br}-Ni** (Condition: [**^{MeO}PO^{Br}-Ni**] = 0.0118 M, [tBA] = 0.177 M, solvent: C_6D_6, V(total) = 0.5 mL, T = 25 ºC).

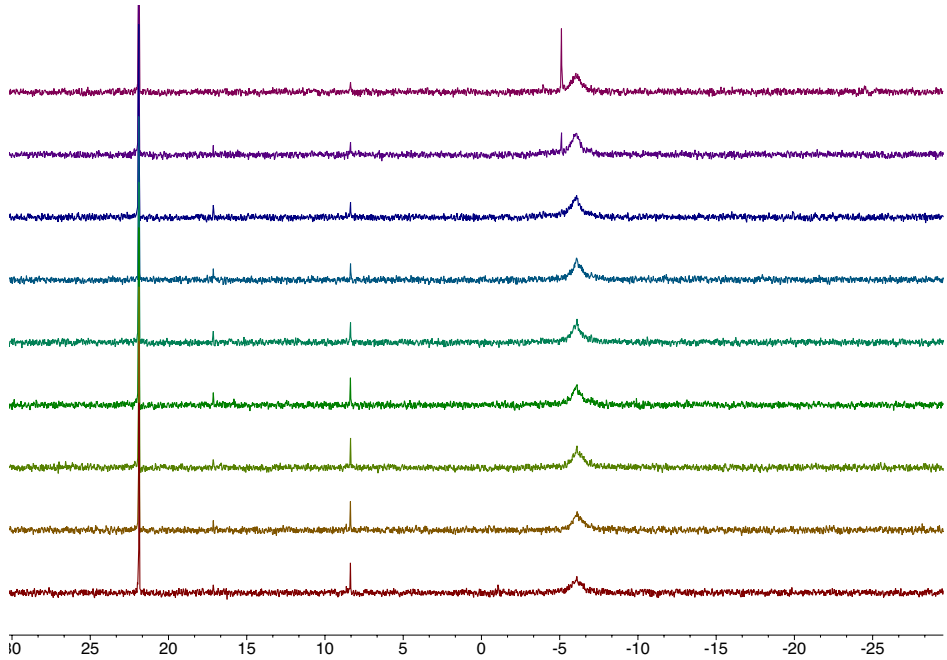

Figure S6.30. $^{31}P\{^{1}H\}$ NMR monitoring of reaction of tBA with **$^{MeO}PO^{Br}$-Ni** (Condition: [**$^{MeO}PO^{Br}$-Ni**] = 0.0118 M, [tBA] = 0.177 M, solvent: C_6D_6, V(total) = 0.5 mL, T = 25 °C. An external standard, $Ph_3PMe^+Br^-$, was added in a sealed capillary)

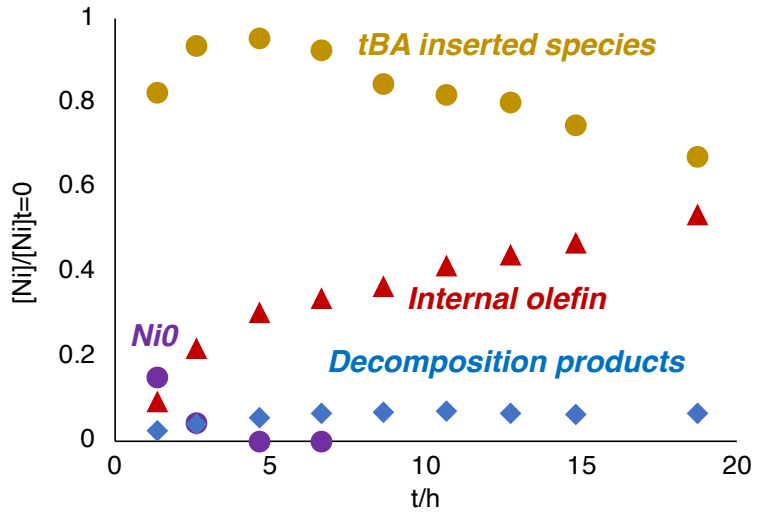

Figure S6.31. A kinetic profile of tBA insertion and subsequent reactions with **$^{MeO}PO^{Br}$-Ni**. (Purple: **$^{MeO}PO^{Br}$-Ni** (**Ni0**), brown: tBA inserted products, red: the internal olefin, blue: new species assigned to Ar_3PR^+ species based on literature.[66, 76] Note: differentiation of the first insertion product, **$^{MeO}PO^{Br}$-Ni(py)C^{Si}CO** and subsequent insertion product, **$^{MeO}PO^{Br}$-Ni(py)CCO**, is challenging and thus only the sum of them are shown as brown circles).

NMR monitoring was conducted for an elongated period (Figure S6.29-30). Differentiation of two tBA reinsertion products, **^{MeO}PO^{Br}-Ni(py)CCO** and **^{MeO}PO^{Br}-Ni(py)C^{Si}CO** is challenging in both ^{1}H and ^{31}P{^{1}H} NMR. Generation of significant amount of internal olefin was observed, though in a rate slower than that with **^{PhO}PO^{Br}-Ni** under otherwise identical conditions.

In addition to the internal olefin and tBA inserted Ni complexes, new species featuring broad resonances ~8 ppm in ^{31}P{^{1}H} NMR spectra were also observed over time. These resonances are close to ^{31}P{^{1}H} resonances of several reported phosphonium species (Ar_3PR^+).[76] One possible pathway to generate phosphonium species after tBA insertion is reductive elimination from the tBA inserted products (Figure 6.4). Similar pathways have been reported with Pd methyl complexes.[66] We proposed that similar process may also happen during ethylene/acrylate copolymerization by **^{MeO}PO^{Br}-Ni** and possibly other P,O-Ni catalysts as a pathway of catalyst deactivation. Notably, neither of above phenomena was observed in reaction of tBA with **^{PhO}PO^{Br}-Ni** in aforementioned NMR studies, though it cannot be ruled out that decomposition of **^{PhO}PO^{Br}-Ni** occurs via a similar pathway in catalysis.

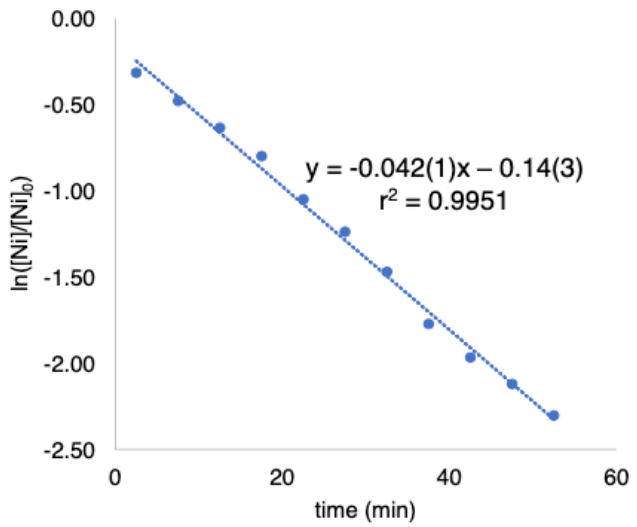

Figure S6.32. Log plot of relative concentration of ^{MeO}**PO**^{Br}**-Ni** vs time. (Condition: [^{MeO}**PO**^{Br}**-Ni**] = 0.0118 M, [py] = 0.0236 M, [tBA] = 0.59 M, solvent: C_6D_6, V(total) = 0.5 mL, T = 40 ºC).

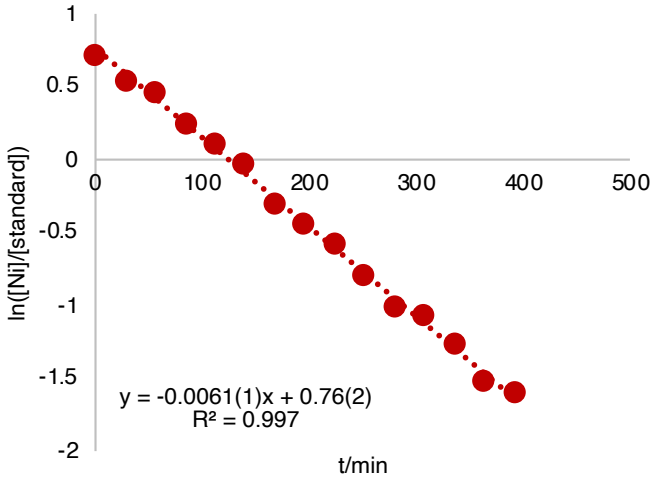

Figure S6.33. Log plot of relative concentration of ^{PhO}**PO**^{Br}**-Ni** vs time. (Condition: [^{PhO}**PO**^{Br}**-Ni**] = 0.0118 M, [py] = 0.0236 M, [tBA] = 0.59 M, solvent: C_6D_6, V(total) = 0.5 mL, T = 40 ºC).

7. Quantitative Kinetic Studies of Acrylate-Induced Reactions

7.1. Procedures: 0.0059 mmol of Ni catalyst prepared using the above procedure was dissolved in a C_6D_6 solution of pyridine (2 equiv.) and transferred to a J-Young tube. The solution was frozen in the coldwell pre-cooled by a liquid nitrogen bath, and a set amount of methyl acrylate (MA) was added via syringe (Total volume=0.50 ml). The resulting mixture was warmed up to thawing temperature and shaken vigorously prior to transferring to pre-heated NMR probe for acquisition of spectra at 25 °C. NMR monitoring of tBA insertion were performed by monitoring ^{1}H and ^{31}P{^{1}H} NMR spectra.

Note: a large excess of tBA and a small amount of pyridine were added to make sure their concentrations remain similar during monitoring (*pseudo*-1st order conditions).

7.2. Original kinetic plots:

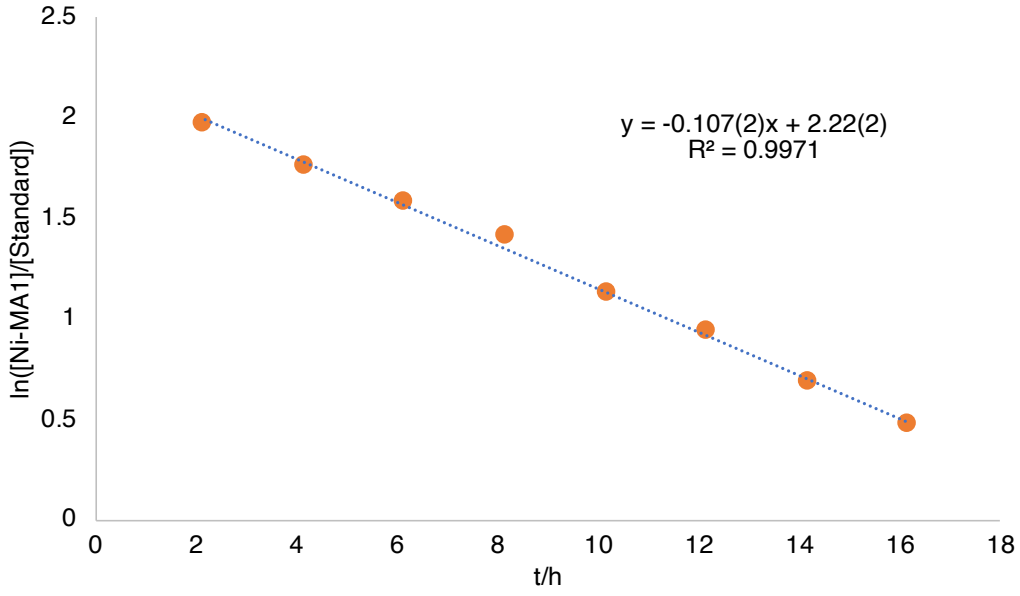

Figure S6.34. Log plot of relative concentration of ^{PhO}**PO**^{Br}**-Ni**^{Si}**CCO**^{M} vs time (Condition: [^{PhO}**PO**^{Br}**-Ni**] = 0.0118 M, [py] = 0, [MA] = 0.177 M, solvent: C_6D_6, V(total) = 0.5 mL, T = 25 °C).

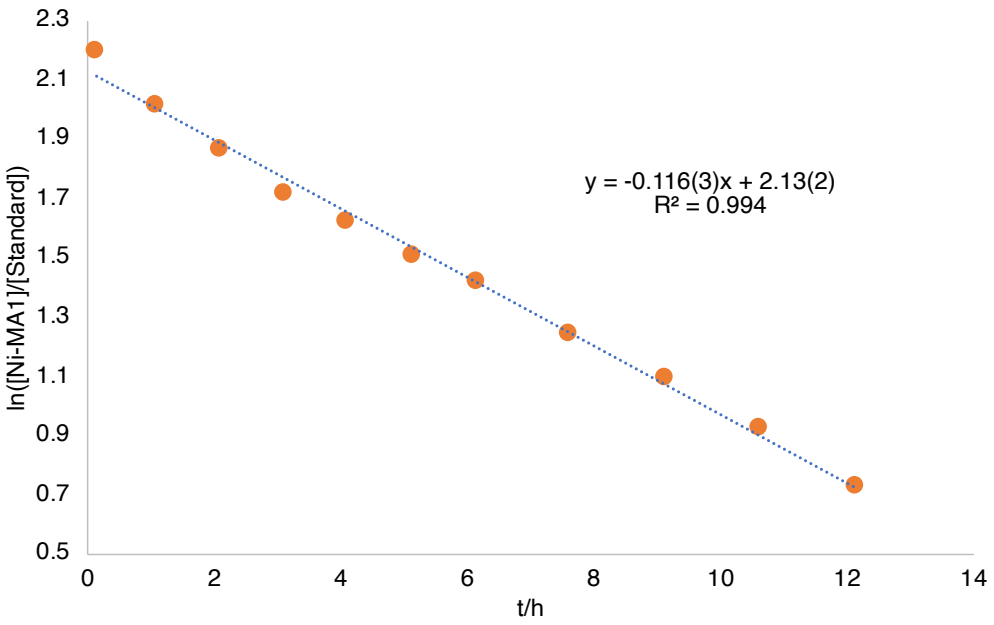

Figure S6.35. Log plot of relative concentration of ^{PhO}**PO**^{Br}**-Ni**^{Si}**CCO**^{M} vs time (Condition: [^{PhO}**PO**^{Br}**-Ni**] = 0.0118 M, [py] = 0, [MA] = 0.59 M, solvent: C_6D_6, V(total) = 0.5 mL, T = 25 ºC).

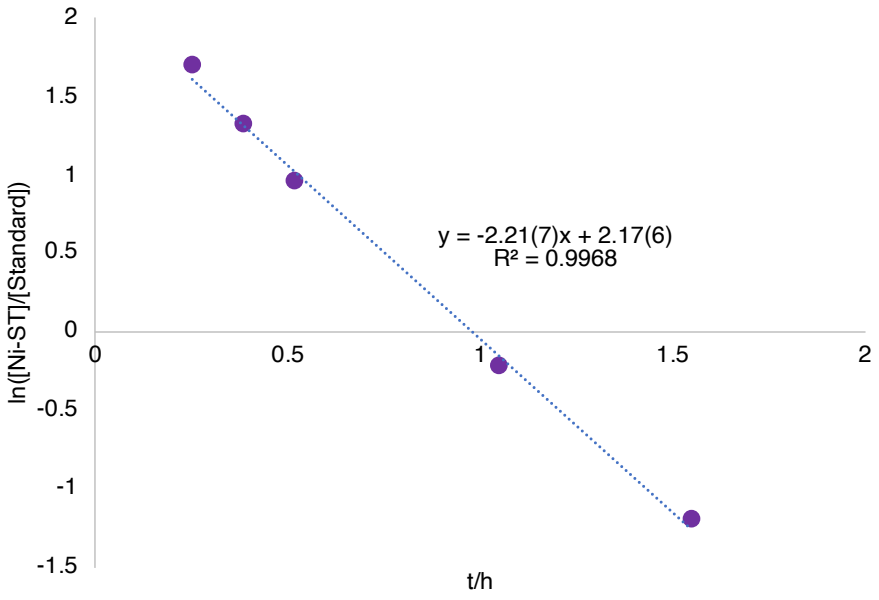

Figure S6.36. Log plot of relative concentration of ^{PhO}**PO**^{Br}**-Ni** vs time (Condition: [^{PhO}**PO**^{Br}**-Ni**] = 0.0118 M, [py] = 0.0039 M, [MA] = 0.59 M, solvent: C_6D_6, V(total) = 0.5 mL, T = 25 ºC).

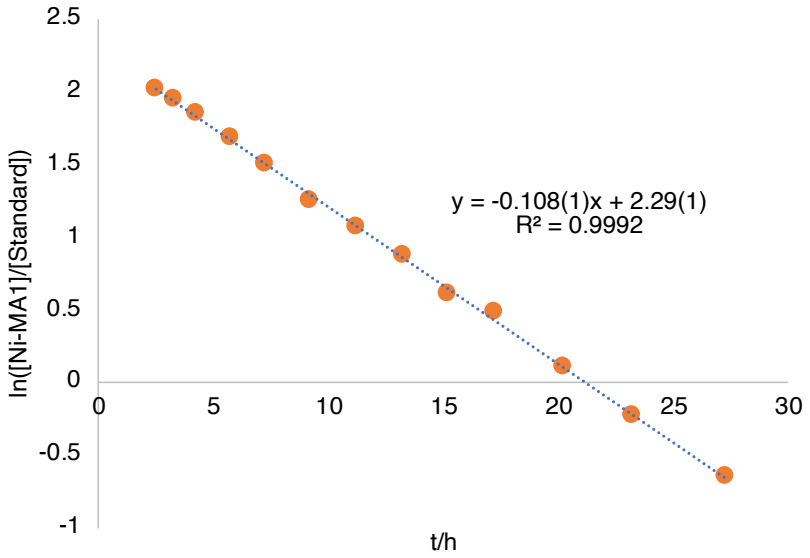

Figure S6.37. Log plot of relative concentration of ^{PhO}**PO**^{Br}**-Ni**^{Si}**CCO**^{M} vs time (Condition: [^{PhO}**PO**^{Br}**-Ni**] = 0.0118 M, [py] = 0.0039 M, [MA] = 0.59 M, solvent: C_6D_6, V(total) = 0.5 mL, T = 25 ºC).

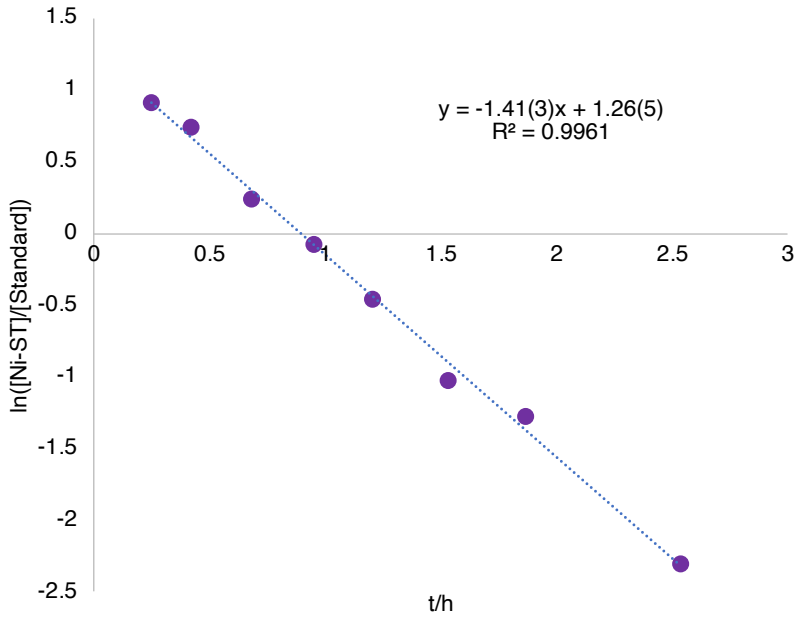

Figure S6.38. Log plot of relative concentration of ^{PhO}**PO**^{Br}**-Ni** vs time (Condition: [^{PhO}**PO**^{Br}**-Ni**] = 0.0118 M, [py] = 0.0059 M, [MA] = 0.59 M, solvent: C_6D_6, V(total) = 0.5 mL, T = 25 ºC).

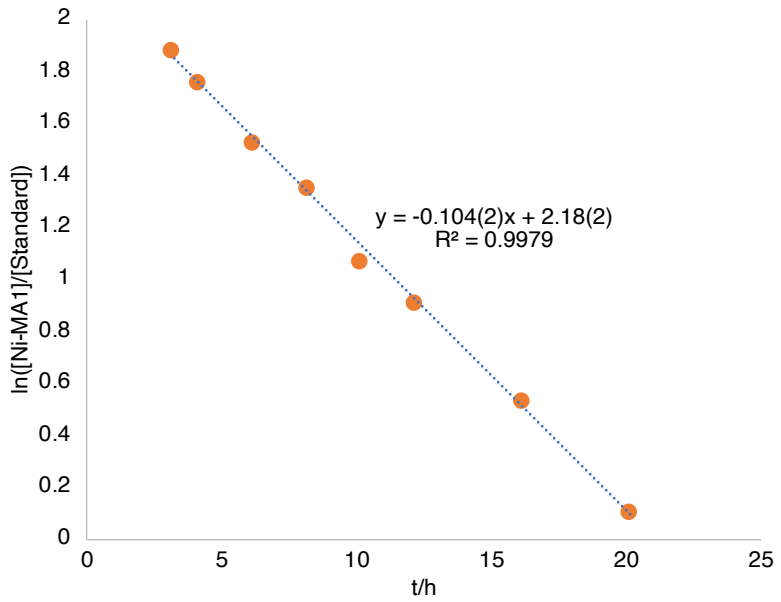

Figure S6.39. Log plot of relative concentration of ^{PhO}**PO**^{Br}**-Ni**^{Si}**CCO**^{M} vs time (Condition: [^{PhO}**PO**^{Br}**-Ni**] = 0.0118 M, [py] = 0.0059 M, [MA] = 0.59 M, solvent: C_6D_6, V(total) = 0.5 mL, T = 25 ºC).

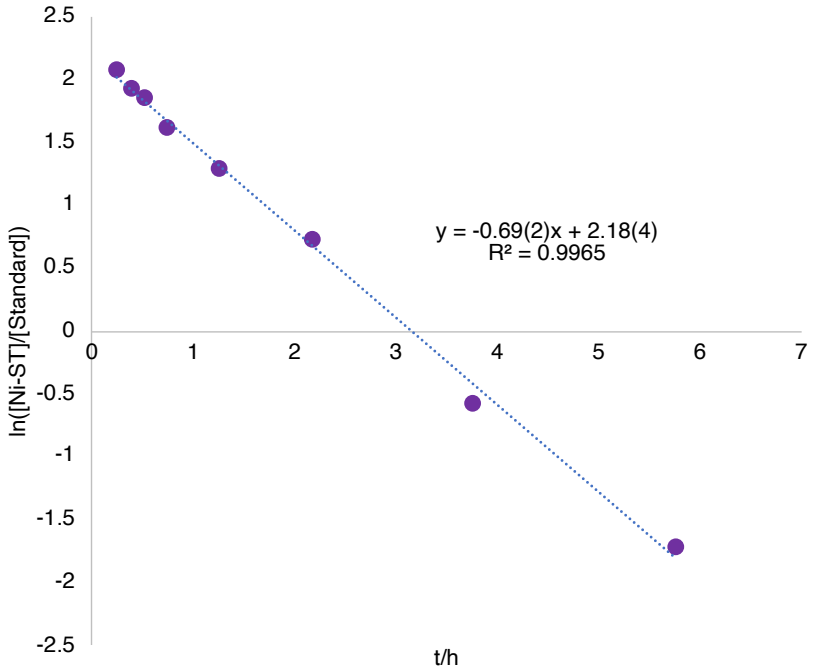

Figure S6.40. Log plot of relative concentration of ^{PhO}**PO**^{Br}**-Ni** vs time (Condition: [^{PhO}**PO**^{Br}**-Ni**] = 0.0118 M, [py] = 0.0118 M, [MA] = 0.59 M, solvent: C_6D_6, V(total) = 0.5 mL, T = 25 ºC).

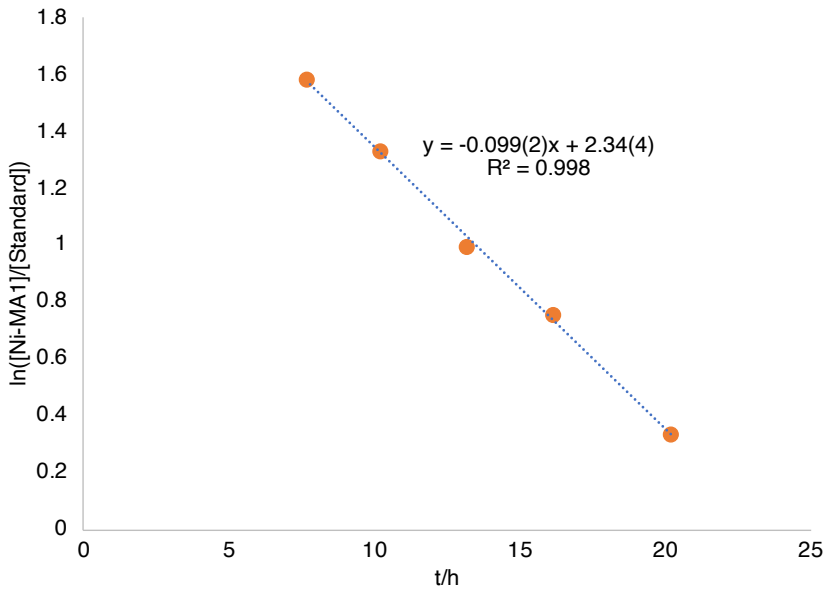

Figure S6.41. Log plot of relative concentration of ^{PhO}**PO**^{Br}**-Ni**^{Si}**CCO**^{M} vs time (Condition: [^{PhO}**PO**^{Br}**-Ni**] = 0.0118 M, [py] = 0.0118 M, [MA] = 0.59 M, solvent: C_6D_6, V(total) = 0.5 mL, T = 25 ºC).

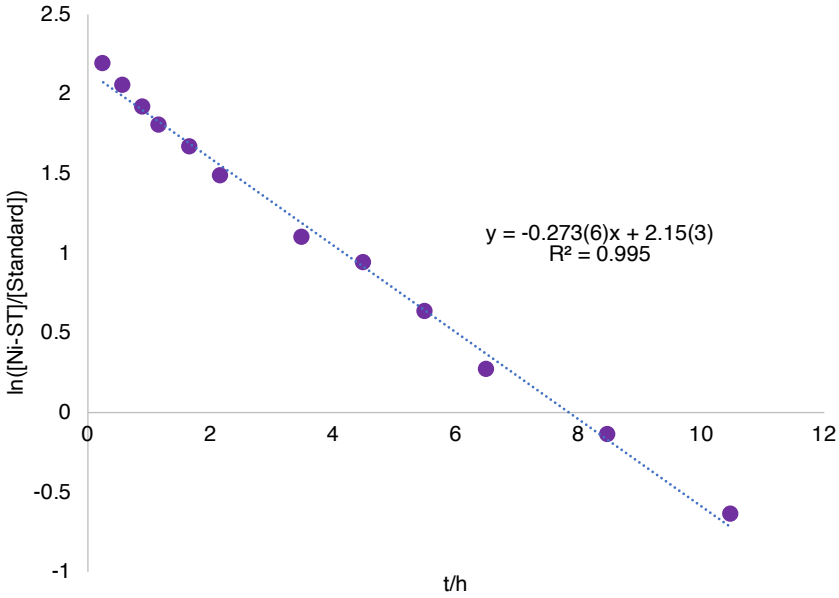

Figure S6.42. Log plot of relative concentration of ^{PhO}**PO**^{Br}**-Ni** vs time (Condition: [^{PhO}**PO**^{Br}**-Ni**] = 0.0118 M, [py] = 0.0236 M, [MA] = 0.59 M, solvent: C_6D_6, V(total) = 0.5 mL, T = 25 ºC).

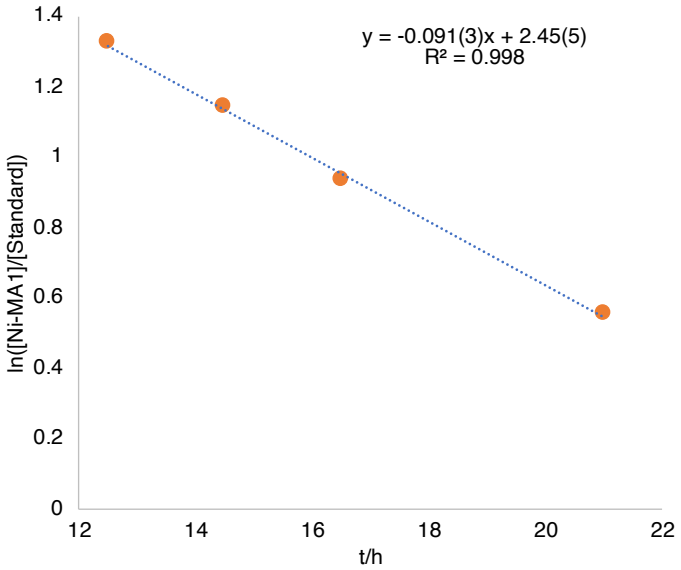

Figure S6.43. Log plot of relative concentration of ^{PhO}**PO**^{Br}**-Ni**^{Si}**CCO**^{M} vs time (Condition: [^{PhO}**PO**^{Br}**-Ni**] = 0.0118 M, [py] = 0.0236 M, [MA] = 0.59 M, solvent: C_6D_6, V(total) = 0.5 mL, T = 25 ºC).

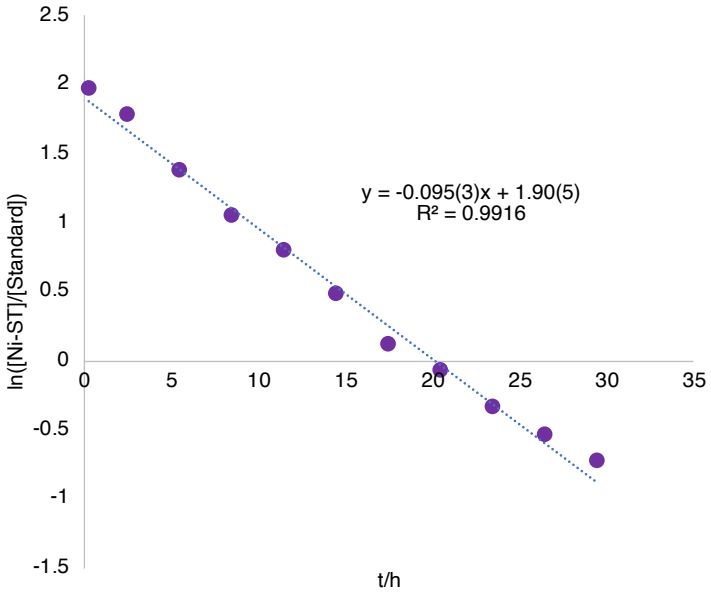

Figure S6.44. Log plot of relative concentration of ^{PhO}**PO**^{Br}**-Ni** vs time (Condition: [^{PhO}**PO**^{Br}**-Ni**] = 0.0118 M, [py] = 0.059 M, [MA] = 0.59 M, solvent: C_6D_6, V(total) = 0.5 mL, T = 25 ºC).

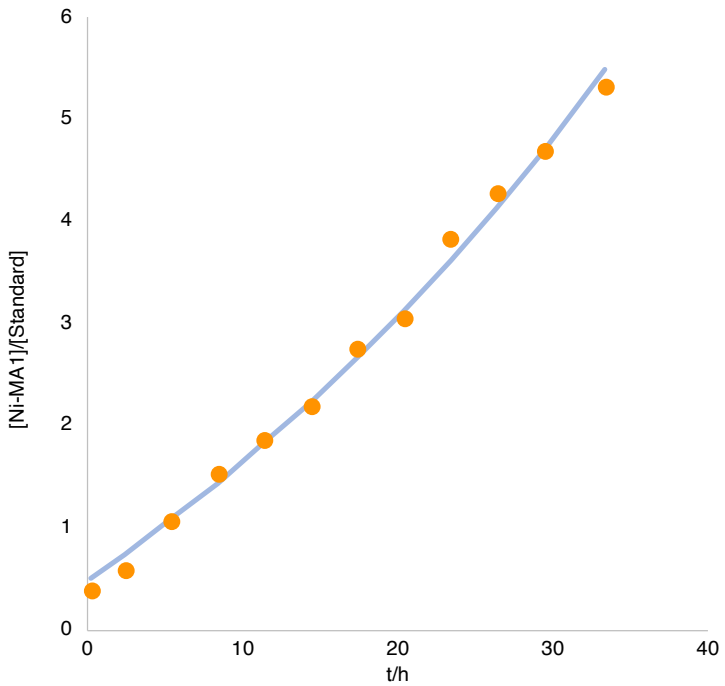

Figure S6.45. Plot of relative concentration of ^{PhO}**PO**^{Br}**-Ni**^{Si}**CCO**^{M} vs time (Condition: [^{PhO}**PO**^{Br}**-Ni**] = 0.0118 M, [py] = 0.059 M, [MA] = 0.59 M, solvent: C_6D_6, V(total) = 0.5 mL, T = 25 °C. Red spots: experimental data, blue line: fitted curve.)

- p=-0.02, SSR=0.153, k_2=0.0742 (See below for methods)

Methods for Figure S6.45. Pseudo-1st order rate constant of β-H elimination can be obtained based on changes of [**Ni-ST**] and [**Ni-MA1**] over time, which is shown below.

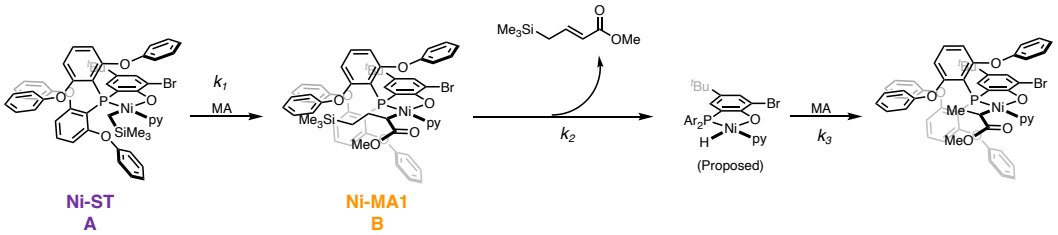

$$\frac{d[A]}{dt} = -k_1 \cdot [A] \quad \textbf{(i)}$$

$$[A] = [A]_0 \cdot e^{-k_1 t} \quad \textbf{(ii)}$$

$$\frac{d[B]}{dt} = k_1 \cdot [A] - k_2 \cdot [B] \quad \textbf{(iii)}$$

Based on (ii) and (iii), $k_2 \cdot [B] + \frac{d[B]}{dt} = k_1 \cdot [A]_0 \cdot e^{-k_1 t}$ **(iv) ->**

$k_2 \cdot e^{k_2 t} \cdot [B] + e^{k_2 t} \cdot \frac{d[B]}{dt} = k_1 \cdot [A]_0 \cdot e^{k_2 t} \cdot e^{-k_1 t}$ **(v) ->**

$\frac{d}{dt}(e^{k_2 t} \cdot [B]) = k_1 \cdot [A]_0 \cdot e^{(k_2 - k_1)t}$ **(vi) ->**

$e^{k_2 t} \cdot [B] = \frac{k_1}{k_2 - k_1} \cdot [A]_0 \cdot e^{(k_2 - k_1)t}$+C **(vii) ->**

$[B] = \frac{k_1}{k_2 - k_1} \cdot [A]_0 \cdot e^{-k_1 t}$+C$\cdot\ e^{k_2 t}$ **(viii)**

t=0, [B]=0, ∴ C=$-\frac{k_1}{k_2 - k_1} \cdot [A]_0$ **(ix)**

Based on (viii) and (ix), $[B] = \frac{k_1}{k_2 - k_1} \cdot [A]_0 \cdot (e^{-k_1 t} - e^{k_2 t})$ **(x)**

(viii)/(iii) -> $\frac{[B]}{[A]} = \frac{k_1}{k_2 - k_1} \cdot (1 - e^{-(k_2 - k_1)t})$ **(xi)**

If p=$k_2 - k_1$, $\frac{[B]}{[A]} = \frac{k_1}{p} \cdot (1 - e^{-pt})$ **(xii)**

[B]/[A] can be obtained from spectra, thereby p is solved via minimizing the difference of calculated curve (y axis: [B]/[A], x axis: time) and curve generated from exp in excel ("solver" add-on).

7.3. Analysis of β-H elimination

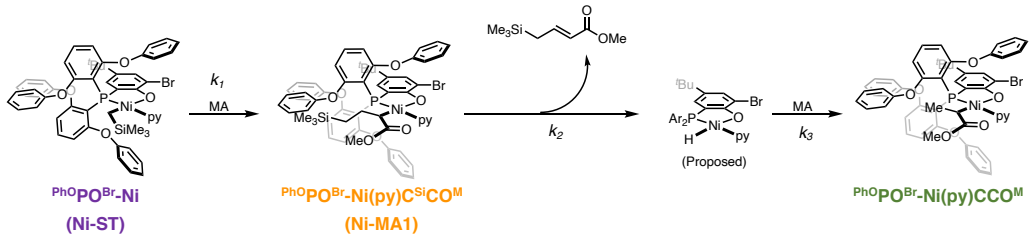

Table S6.6 *Pseudo*-1st order constants of the β-H elimination step (k_2) under different pyridine and acrylate concentrations.

Entry	[MA]/[Ni]	[py]/[Ni]	$k_{2\text{-obs}}$ (elimination)/h
1	15	0	0.107(2)
2	50	0	0.116(3)
3	50	0.33	0.108(1)
4	50	0.5	0.104(2)
5	50	1	0.099(2)
6	50	2	0.091(3)
7	50	5	0.0742

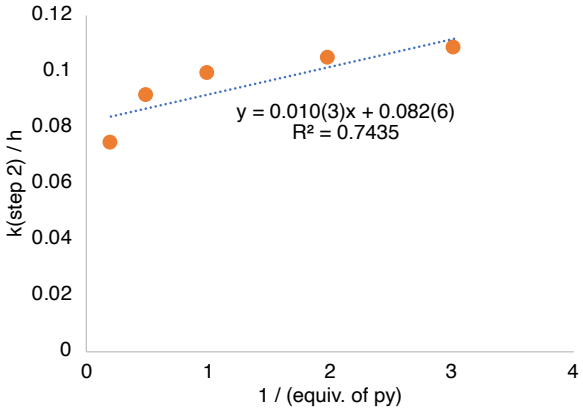

Figure S6.46. Plot of *pseudo*-1st order rate constant of β-H elimination after MA insertion vs 1 / (equivalents of pyridine added) (Conditions: [**PhOPOBr-Ni**] = 0.0118 M, [py] = 0.0039-0.059 M, [MA] = 0.59 M, solvent: C_6D_6, V(total) = 0.5 mL, T = 25 ºC).

As shown in the figure, a simple linear relationship in NOT observed between *pseudo*-1st order rate constant of the β-H elimination step (k_2) and equivalents of pyridine. This suggests a kinetic profile more complex than the pathway featuring a fast dissociative pre-equilibrium (See section S8 for rationale and other possibilities).

8. Discussion of pathways of β-H elimination

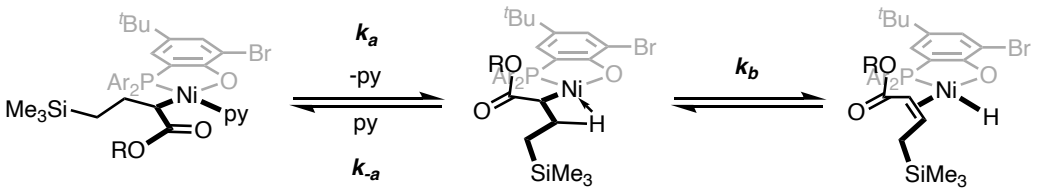

Case 1: Fast dissociation equilibrium (but K_a<<1, step a) followed by slow β-H transfer (step b)

$$\text{Rate} = \frac{k_b K_a}{[py]}\,[\text{Ni-CCO-py}]$$

$$k(\text{elimination}) = \frac{k_b K_a}{[py]}$$

This scenario is not consistent with Figure S6.46, as a simple linear relationship in NOT observed between pseudo-1st order rate constant of the β-H elimination step (k2) and equivalents of pyridine, and not consistent with Figure 6.3e, as the line is expected to cross the origin.

Case 2: Slow exchange (concerted mechanism, step a) followed by fast β-H transfer (step b)

$$\text{Rate} = k_a \frac{k_b}{k_{-a}[py]+k_b}\,[\text{Ni-CCO-py}]$$

$$k(\text{elimination}) = k_a \frac{k_b}{k_{-a}[py]+k_b},$$

$$[py]=0,\ k(\text{elimination}) = k_a$$

$$1/k(\text{elimination}) = \frac{k_{-a}[py]+k_2}{k_a k_b}$$

This scenario is consistent with Figure 6.3e.

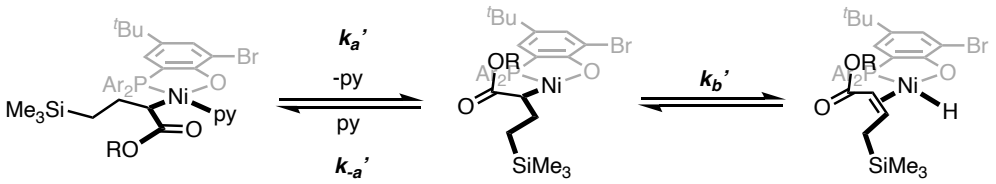

Case 3: Dissociative mechanism – slow pyridine dissociation followed by fast β-H transfer (step 2)

$$\text{Rate} = k_a' \frac{k_{b'}}{k_{-a'}[\text{py}]+k_{b'}} [\text{Ni-CCO-py}]$$

Similar to case 2, this case is also consistent with Figure 6.3e.

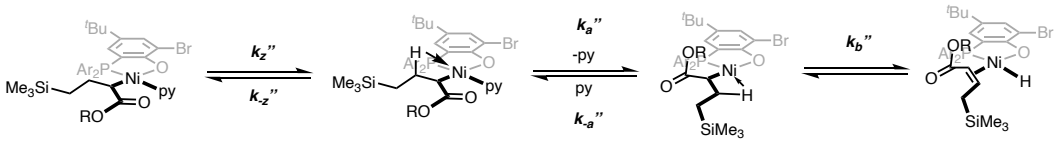

Case 4: Associative mechanism – slow coordination of fifth ligand followed by fast subsequent steps.

Rate = K [Ni-CCO-py] (K is a constant independent of pyridine concentration)

This scenario is not consistent with Table S6.6.

Case 5: Associative mechanism – fast coordination of fifth ligand follow by slow pyridine dissociation.

$$\text{Rate} = K_z''k_a''\frac{k_{b''}}{k_{-a''}[\text{py}]+k_{b''}} [\text{Ni-CCO-py}]$$

Similar as case 2, this case is also consistent with Figure 6.3e.

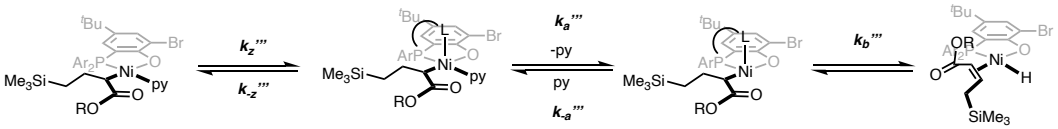

Case 6: Associative mechanism – slow coordination of fifth ligand followed by fast subsequent steps

Rate = K [Ni-CCO-py] (K is a constant independent of pyridine concentration)

This scenario is not consistent with Table S6.6.

Case 7: Associative mechanism – fast coordination of fifth ligand follow by slow pyridine dissociation.

$$\text{Rate} = K_z'''k_a'''\frac{k_b'''}{k_{-a}'''[\text{py}]+k_b'''}[\text{Ni-CCO-py}]$$

Similar as case 2, this case is also consistent with Figure 6.3e.

Overall, the linear relationship revealed by Figure 6.3e is consistent with case 2,3,4,5,7 in which pyridine dissociation is slow. This scenario implies that pyridine plays an important role in β-H elimination.

10. Crystallographic Information

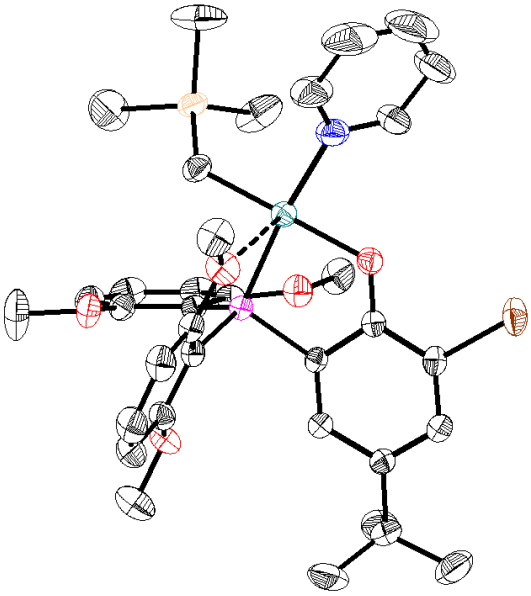

Figure S6.47. Solid-State Structure of ^{MeO}**PO**^{Br}**-Ni** (Green: Ni, Pink: P, Blue: N, Red: O, orange: Si, black: C). Ellipsoids are show at the 50% probability level. Hydrogen atoms and solvent molecules excluded for clarity.

Special Refinement Details for Ni0: Complex ^{MeO}**PO**^{Br}**-Ni** crystalizes in a P-1 space group with two full molecules in the asymmetric unit, as well as 3/8 THF molecule. A disorder was present in the 3/8 THF molecule and could not be modelled. The solvent mask (Olex® implementation of BYPASS/SQUEEZE) was used to suppress two sections of electron density likely corresponding to 1/4 THF molecule and 1/8 THF molecule. The void was calculated to be near 51 electrons per unit cell, which would be close to 3/8 THF molecule per asymmetric unit (Z=4).

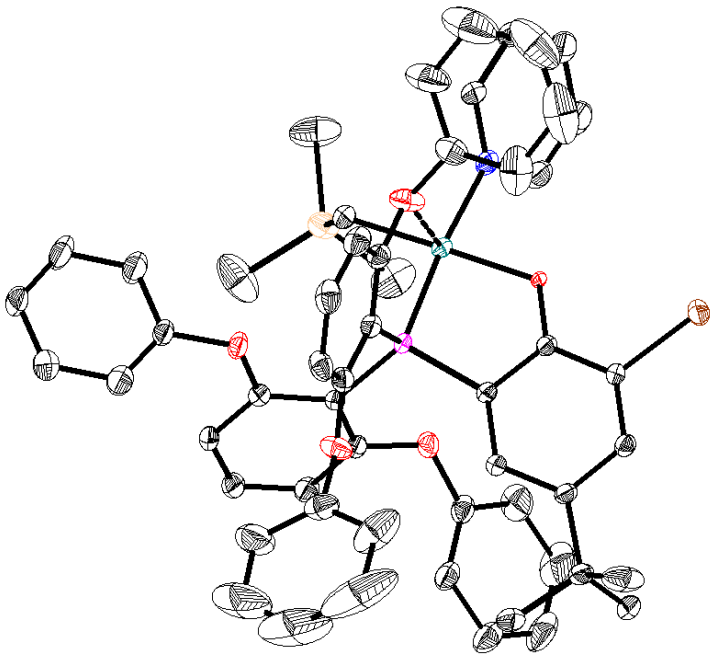

Figure S6.48. Solid-State Structure of ^{PhO}**PO**^{Br}**-Ni** (Green: Ni, Pink: P, Blue: N, Red: O, orange: Si, black: C). Ellipsoids are show at the 50% probability level. Hydrogen atoms and solvent molecules excluded for clarity.

Special Refinement Details for Ni0: Complex ^{PhO}**PO**^{Br}**-Ni** crystalizes in a $P2_1/n$ space group with one full molecule in the asymmetric unit, as well as one toluene molecule. A disorder was present in the one toluene molecule and could not be modelled. The solvent mask (Olex® implementation of BYPASS/SQUEEZE) was used to suppress one section of electron density likely corresponding to this one toluene molecule. The void was calculated to be near 184 electrons per unit cell, which would be close to one toluene molecule per asymmetric unit (Z=4).

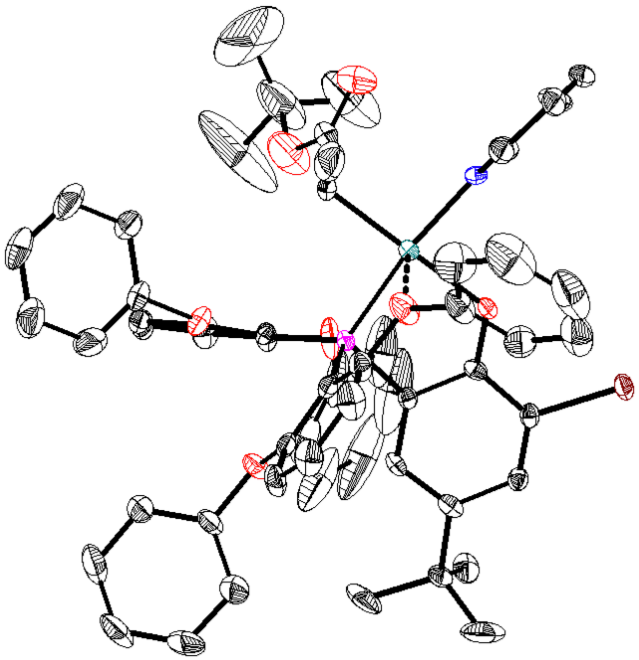

Figure S6.49. Solid-State Structure of ^{PhO}**PO**^{Br}**-NiCCO** (Green: Ni, Pink: P, Blue: N, Red: O, orange: Si, black: C). Ellipsoids are show at the 50% probability level. Hydrogen atoms and solvent molecules excluded for clarity.

Special Refinement Details for Ni0: Complex ^{PhO}**PO**^{Br}**-NiCCO** crystalizes in a $P2_1/n$ space group with one full molecule in the asymmetric unit, as well as half toluene molecule. One methyl group on t-butoxy moiety is modelled with two-site disorder with half occupancies for each. A disorder was present in the one and a half pentane molecules and could not be modelled. The solvent mask (Olex® implementation of BYPASS/SQUEEZE) was used to suppress one section of electron density likely corresponding to this half toluene molecule. The void was calculated to be near 108 electrons per unit cell, which would be close to half toluene molecule per asymmetric unit (Z=4).

Crystallographic Information

Table S6.7. Crystal and refinement data for complexes ^{MeO}**PO**^{Br}**-Ni**, ^{PhO}**PO**^{Br}**-Ni**, and ^{PhO}**PO**^{Br}**-NiCCO**.

	^{MeO}**PO**^{Br}**-Ni**	^{PhO}**PO**^{Br}**-Ni**	^{PhO}**PO**^{Br}**-NiCCO**
Empirical formula	$C_{35}H_{45}BrNNiO_5PSi$	$C_{55}H_{52}BrNNiO_5PSi$	$C_{58}H_{55}BrNiO_7P$
Formula weight	774.67	1089.82	1110.15
Temperature/K	100 K	100 K	100 K
Crystal system	Triclinic	Monoclinic	Monoclinic
Space group	P-1	$P2_1/n$	$P2_1/n$
a/Å	13.161(3)	13.733(2)	13.546(13)
b/Å	15.276(3)	17.573(2)	17.949(14)
c/Å	21.447(5)	22.824(3)	22.94(3)
α/°	102.207(10)	90	90
β/°	101.799(18)	103.207(12)	105.05(4)
γ/°	99.382(18)	90	90
Volume/Å^3	4028.4(16)	5363(1)	5386(9)
Z	4	4	4
ϱ_{calc}g/cm^3	1.277	1.350	1.369
μ/mm^{-1}	1.581	1.209	1.188
F(000)	1613	2280	2317
Radiation	MoKα (λ = 0.71073)	MoKα (λ = 0.71073)	MoKα (λ = 0.71073)
Reflections collected	128856	175043	75731
Independent reflections	26181	16282	16453
Goodness-of-fit on F^2	1.039	1.073	0.941
Final R indexes	R_1 = 4.00 %	R_1 = 4.02 %	R_1 = 10.31 %
[I>=2σ (I)]	R_2 = 10.00%	R_2 = 11.40 %	R_2 = 22.97 %

REFERENCES

(1) Osakada, K., *Organometallic Reactions and Polymerization*. Springer: 2014; Vol. 85.

(2) Chen, C., Designing catalysts for olefin polymerization and copolymerization: beyond electronic and steric tuning. *Nat. Rev. Chem.* **2018,** *2* (5), 6-14.

(3) Nakamura, A.; Ito, S.; Nozaki, K., Coordination− insertion copolymerization of fundamental polar monomers. *Chem. Rev.* **2009,** *109* (11), 5215-5244.

(4) Carrow, B. P.; Nozaki, K., Transition-metal-catalyzed functional polyolefin synthesis: effecting control through chelating ancillary ligand design and mechanistic insights. *Macromolecules* **2014,** *47* (8), 2541-2555.

(5) Chen, E. Y.-X., Coordination polymerization of polar vinyl monomers by single-site metal catalysts. *Chem. Rev.* **2009,** *109* (11), 5157-5214.

(6) Luckham, S. L. J.; Nozaki, K., Toward the Copolymerization of Propylene with Polar Comonomers. *Acc. Chem. Res.* **2020**.

(7) Baur, M.; Lin, F.; Morgen, T. O.; Odenwald, L.; Mecking, S., Polyethylene materials with in-chain ketones from nonalternating catalytic copolymerization. *Science* **2021,** *374* (6567), 604-607.

(8) Hustad, P. D., Frontiers in olefin polymerization: Reinventing the world's most common synthetic polymers. *Science* **2009,** *325* (5941), 704-707.

(9) Franssen, N. M.; Reek, J. N.; de Bruin, B., Synthesis of functional 'polyolefins': state of the art and remaining challenges. *Chem. Soc. Rev.* **2013,** *42* (13), 5809-5832.

(10) Tan, C.; Zou, C.; Chen, C., Material Properties of Functional Polyethylenes from Transition-Metal-Catalyzed Ethylene–Polar Monomer Copolymerization. *Macromolecules* **2022**.

(11) Boffa, L. S.; Novak, B. M., Copolymerization of polar monomers with olefins using transition-metal complexes. *Chem. Rev.* **2000,** *100* (4), 1479-1494.

(12) Zou, C.; Chen, C., Polar-functionalized, crosslinkable, self-healing, and photoresponsive polyolefins. *Angew. Chem. Int. Ed* **2020,** *59* (1), 395-402.

(13) Johnson, L. K.; Mecking, S.; Brookhart, M., Copolymerization of ethylene and propylene with functionalized vinyl monomers by palladium (II) catalysts. *J. Am. Chem. Soc.* **1996,** *118* (1), 267-268.

(14) Younkin, T. R.; Connor, E. F.; Henderson, J. I.; Friedrich, S. K.; Grubbs, R. H.; Bansleben, D. A., Neutral, single-component nickel (II) polyolefin catalysts that tolerate heteroatoms. *Science* **2000,** *287* (5452), 460-462.

(15) Guironnet, D.; Roesle, P.; Rünzi, T.; Göttker-Schnetmann, I.; Mecking, S., Insertion polymerization of acrylate. *J. Am. Chem. Soc.* **2009,** *131* (2), 422-423.

(16) Weng, W.; Shen, Z.; Jordan, R. F., Copolymerization of ethylene and vinyl fluoride by (phosphine-sulfonate) Pd (Me)(py) catalysts. *J. Am. Chem. Soc.* **2007,** *129* (50), 15450-15451.

(17) Tan, C.; Chen, C., Emerging palladium and nickel catalysts for copolymerization of olefins with polar monomers. *Angew. Chem.* **2019,** *131* (22), 7268-7276.

(18) Mu, H.; Zhou, G.; Hu, X.; Jian, Z., Recent advances in nickel mediated copolymerization of olefin with polar monomers. *Coord. Chem. Rev.* **2021,** *435*, 213802.

(19) Mu, H.; Pan, L.; Song, D.; Li, Y., Neutral nickel catalysts for olefin homo-and copolymerization: relationships between catalyst structures and catalytic properties. *Chem. Rev.* **2015,** *115* (22), 12091-12137.

(20) Johnson, L. K.; Killian, C. M.; Brookhart, M., New Pd (II)-and Ni (II)-based catalysts for polymerization of ethylene and. alpha.-olefins. *J. Am. Chem. Soc.* **1995,** *117* (23), 6414-6415.

(21) Liang, T.; Goudari, S. B.; Chen, C., A simple and versatile nickel platform for the generation of branched high molecular weight polyolefins. *Nat. Commun.* **2020,** *11* (1), 1-8.

(22) Xin, B. S.; Sato, N.; Tanna, A.; Oishi, Y.; Konishi, Y.; Shimizu, F., Nickel catalyzed copolymerization of ethylene and alkyl acrylates. *J. Am. Chem. Soc.* **2017,** *139* (10), 3611-3614.

(23) Nakano, R.; Nozaki, K., Copolymerization of propylene and polar monomers using Pd/IzQO catalysts. *J. Am. Chem. Soc.* **2015,** *137* (34), 10934-10937.

(24) Tao, W. j.; Nakano, R.; Ito, S.; Nozaki, K., Copolymerization of ethylene and polar monomers by using Ni/IzQO catalysts. *Angew. Chem. Int. Ed.* **2016,** *55* (8), 2835-2839.

(25) Carrow, B. P.; Nozaki, K., Synthesis of functional polyolefins using cationic bisphosphine monoxide–palladium complexes. *J. Am. Chem. Soc.* **2012,** *134* (21), 8802-8805.

(26) Zhang, W.; Waddell, P. M.; Tiedemann, M. A.; Padilla, C. E.; Mei, J.; Chen, L.; Carrow, B. P., Electron-rich metal cations enable synthesis of high molecular weight, linear functional polyethylenes. *J. Am. Chem. Soc.* **2018,** *140* (28), 8841-8850.

(27) Chen, M.; Chen, C., A Versatile Ligand Platform for Palladium - and Nickel - Catalyzed Ethylene Copolymerization with Polar Monomers. *Angew. Chem. Int. Ed.* **2018,** *57* (12), 3094-3098.

(28) Drent, E.; van Dijk, R.; van Ginkel, R.; van Oort, B.; Pugh, R. I., Palladium catalysed copolymerisation of ethene with alkylacrylates: polar comonomer built into the linear polymer chain. *Chem. Commun.* **2002,** (7), 744-745.

(29) Nakamura, A.; Anselment, T. M.; Claverie, J.; Goodall, B.; Jordan, R. F.; Mecking, S.; Rieger, B.; Sen, A.; Van Leeuwen, P. W.; Nozaki, K., Ortho-phosphinobenzenesulfonate: A superb ligand for palladium-catalyzed coordination–insertion copolymerization of polar vinyl monomers. *Acc. Chem. Res.* **2013,** *46* (7), 1438-1449.

(30) Chen, Z.; Brookhart, M., Exploring ethylene/polar vinyl monomer copolymerizations using Ni and Pd α-diimine catalysts. *Acc. Chem. Res.* **2018,** *51* (8), 1831-1839.

(31) Alberoni, C.; D'Alterio, M. C.; Balducci, G.; Immirzi, B.; Polentarutti, M.; Pellecchia, C.; Milani, B., Tunable "In-Chain" and "At the End of the Branches" Methyl Acrylate Incorporation in the Polyolefin Skeleton through Pd (II) Catalysis. *ACS Catal.* **2022,** *12* (6), 3430-3443.

(32) Ge, Y.; Li, S.; Wang, H.; Dai, S., Synthesis of Branched Polyethylene and Ethylene-MA Copolymers Using Unsymmetrical Iminopyridyl Nickel and Palladium Complexes. *Organometallics* **2021,** *40* (17), 3033-3041.

(33) Cui, L.; Jian, Z., A N-bridged strategy enables hemilabile phosphine–carbonyl palladium and nickel catalysts to mediate ethylene polymerization and copolymerization with polar vinyl monomers. *Polym. Chem* **2020,** *11* (38), 6187-6193.

(34) Xiong, S.; Hong, A.; Bailey, B. C.; Spinney, H. A.; Senecal, T. D.; Bailey, H.; Agapie, T., Highly Active and Thermally Robust Nickel Enolate Catalysts for the Synthesis of Ethylene-Acrylate Copolymers. *Angew. Chem. Int. Ed.* **2022**.

(35) Cao, L.; Cai, Z.; Li, M., Phosphinobenzenamine Nickel Catalyzed Efficient Copolymerization of Methyl Acrylate with Ethylene and Norbornene. *Macromolecules* **2022,** *55* (9), 3513-3521.

(36) Zhang, H.; Zou, C.; Zhao, H.; Cai, Z.; Chen, C., Hydrogen-Bonding-Induced Heterogenization of Nickel and Palladium Catalysts for Copolymerization of Ethylene with Polar Monomers. *Angew. Chem.* **2021**.

(37) Xiong, S.; Shoshani, M. M.; Zhang, X.; Spinney, H. A.; Nett, A. J.; Henderson, B. S.; Miller III, T. F.; Agapie, T., Efficient Copolymerization of Acrylate and Ethylene with Neutral P, O-Chelated Nickel Catalysts: Mechanistic Investigations of Monomer Insertion and Chelate Formation. *J. Am. Chem. Soc.* **2021,** *143* (17), 6516-6527.

(38) Xie, T.; McAuley, K. B.; Hsu, J. C.; Bacon, D. W., Gas phase ethylene polymerization: Production processes, polymer properties, and reactor modeling. *Ind. & Eng. Chem. Res.* **1994,** *33* (3), 449-479.

(39) Waltman, A. W.; Younkin, T. R.; Grubbs, R. H., Insights into the deactivation of neutral nickel ethylene polymerization catalysts in the presence of functionalized olefins. *Organometallics* **2004,** *23* (22), 5121-5123.

(40) Zhang, Y.; Mu, H.; Pan, L.; Wang, X.; Li, Y., Robust bulky [P, O] neutral nickel catalysts for copolymerization of ethylene with polar vinyl monomers. *ACS Catal.* **2018,** *8* (7), 5963-5976.

(41) Noda, S.; Nakamura, A.; Kochi, T.; Chung, L. W.; Morokuma, K.; Nozaki, K., Mechanistic studies on the formation of linear polyethylene chain catalyzed by palladium phosphine− sulfonate complexes: experiment and theoretical studies. *J. Am. Chem. Soc.* **2009,** *131* (39), 14088-14100.

(42) Mitsushige, Y.; Carrow, B. P.; Ito, S.; Nozaki, K., Ligand-controlled insertion regioselectivity accelerates copolymerisation of ethylene with methyl acrylate by cationic bisphosphine monoxide–palladium catalysts. *Chem. Sci.* **2016,** *7* (1), 737-744.

(43) Nakano, R.; Chung, L. W.; Watanabe, Y.; Okuno, Y.; Okumura, Y.; Ito, S.; Morokuma, K.; Nozaki, K., Elucidating the key role of phosphine− sulfonate ligands in palladium-catalyzed ethylene polymerization: Effect of ligand structure on the molecular weight and linearity of polyethylene. *ACS Catal.* **2016,** *6* (9), 6101-6113.

(44) Xiong, S.; Ghana, P.; Bailey, B. C.; Spinney, H. A.; Henderson, B. S.; Espinosa, M. R.; Agapie, T., Impact of Labile Ligands on Catalyst Initiation and Chain Propagation in Ni-Catalyzed Ethylene/Acrylate Copolymerization. *ACS Catal.* **2023,** *13* (7), 5000-5006.

(45) Shoshani, M. M.; Xiong, S.; Lawniczak, J. J.; Zhang, X.; Miller, T. F.; Agapie, T., Phosphine-Phenoxide Nickel Catalysts for Ethylene/Acrylate Copolymerization: Olefin Coordination and Complex Isomerization Studies Relevant to the Mechanism of Catalysis. *Organometallics* **2022**.

(46) Chen, Z.; Liu, W.; Daugulis, O.; Brookhart, M., Mechanistic studies of Pd (II)-catalyzed copolymerization of ethylene and vinylalkoxysilanes: Evidence for a β-silyl elimination chain transfer mechanism. *J. Am. Chem. Soc.* **2016,** *138* (49), 16120-16129.

(47) Leatherman, M. D.; Svejda, S. A.; Johnson, L. K.; Brookhart, M., Mechanistic studies of nickel (II) alkyl agostic cations and alkyl ethylene complexes: investigations of chain propagation and isomerization in (α-diimine) Ni (II)-catalyzed ethylene polymerization. *J. Am. Chem. Soc.* **2003,** *125* (10), 3068-3081.

(48) Shultz, L. H.; Brookhart, M., Measurement of the barrier to β-hydride elimination in a β-agostic palladium− ethyl complex: a model for the energetics of chain-walking in (α-diimine) PdR+ olefin polymerization catalysts. *Organometallics* **2001,** *20* (19), 3975-3982.

(49) Deng, L.; Woo, T. K.; Cavallo, L.; Margl, P. M.; Ziegler, T., The role of bulky substituents in Brookhart-type Ni (II) diimine catalyzed olefin polymerization: a combined density functional theory and molecular mechanics study. *J. Am. Chem. Soc.* **1997,** *119* (26), 6177-6186.

(50) Rappé, A.; Skiff, W.; Casewit, C., Modeling metal-catalyzed olefin polymerization. *Chem. Rev.* **2000,** *100* (4), 1435-1456.

(51) Britovsek, G. J.; Gibson, V. C.; Wass, D. F., The search for new-generation olefin polymerization catalysts: life beyond metallocenes. *Angew. Chem. Int. Ed.* **1999,** *38* (4), 428-447.

(52) Kenyon, P.; Wörner, M.; Mecking, S., Controlled polymerization in polar solvents to ultrahigh molecular weight polyethylene. *J. Am. Chem. Soc.* **2018,** *140* (21), 6685-6689.

(53) O'Reilly, M. E.; Dutta, S.; Veige, A. S., β-Alkyl elimination: fundamental principles and some applications. *Chem. Rev.* **2016,** *116* (14), 8105-8145.

(54) Liu, Q.; Wu, Y.; Yan, P.; Zhang, Y.; Xu, R., Polyisobutylene with high exo-olefin content via β-H elimination in the cationic polymerization of isobutylene with H2O/FeCl3/dialkyl ether initiating system. *Macromolecules* **2011,** *44* (7), 1866-1875.

(55) Xu, H.; Hu, C. T.; Wang, X.; Diao, T., Structural characterization of β-agostic bonds in Pd-catalyzed polymerization. *Organometallics* **2017,** *36* (21), 4099-4102.

(56) Xu, H.; White, P. B.; Hu, C.; Diao, T., Structure and Isotope Effects of the β-H Agostic (α-Diimine) Nickel Cation as a Polymerization Intermediate. *Angew. Chem. Int. Ed.* **2017,** *56* (6), 1535-1538.

(57) Grubbs, R. H.; Coates, G. W., α-Agostic interactions and olefin insertion in metallocene polymerization catalysts. *Acc. Chem. Res.* **1996,** *29* (2), 85-93.

(58) Chan, M. S.; Deng, L.; Ziegler, T., Density functional study of neutral salicylaldiminato nickel (II) complexes as olefin polymerization catalysts. *Organometallics* **2000,** *19* (14), 2741-2750.

(59) Chen, Z.; Leatherman, M. D.; Daugulis, O.; Brookhart, M., Nickel-catalyzed copolymerization of ethylene and vinyltrialkoxysilanes: catalytic production of cross-linkable polyethylene and elucidation of the chain-growth mechanism. *J. Am. Chem. Soc.* **2017,** *139* (44), 16013-16022.

(60) Friedberger, T.; Wucher, P.; Mecking, S., Mechanistic insights into polar monomer insertion polymerization from acrylamides. *J. Am. Chem. Soc.* **2012,** *134* (2), 1010-1018.

(61) Elia, C.; Elyashiv-Barad, S.; Sen, A.; López-Fernández, R.; Albéniz, A. C.; Espinet, P., Palladium-based system for the polymerization of acrylates. Scope and mechanism. *Organometallics* **2002,** *21* (20), 4249-4256.

(62) Neuwald, B.; Caporaso, L.; Cavallo, L.; Mecking, S., Concepts for stereoselective acrylate insertion. *J. Am.*

Chem. Soc. **2013,** *135* (3), 1026-1036.

(63) Guironnet, D.; Caporaso, L.; Neuwald, B.; Göttker-Schnetmann, I.; Cavallo, L.; Mecking, S., Mechanistic insights on acrylate insertion polymerization. *J. Am. Chem. Soc.* **2010,** *132* (12), 4418-4426.

(64) Berkefeld, A.; Drexler, M.; Möller, H. M.; Mecking, S., Mechanistic insights on the copolymerization of polar vinyl monomers with neutral Ni (II) catalysts. *J. Am. Chem. Soc.* **2009,** *131* (35), 12613-12622.

(65) Berkefeld, A.; Mecking, S., Deactivation pathways of neutral Ni (II) polymerization catalysts. *J. Am. Chem. Soc.* **2009,** *131* (4), 1565-1574.

(66) Rünzi, T.; Tritschler, U.; Roesle, P.; Göttker-Schnetmann, I.; Möller, H. M.; Caporaso, L.; Poater, A.; Cavallo, L.; Mecking, S., Activation and deactivation of neutral palladium (II) phosphinesulfonato polymerization catalysts. *Organometallics* **2012,** *31* (23), 8388-8406.

(67) Wucher, P.; Roesle, P.; Falivene, L.; Cavallo, L.; Caporaso, L.; Göttker-Schnetmann, I.; Mecking, S., Controlled acrylate insertion regioselectivity in diazaphospholidine-sulfonato palladium (II) complexes. *Organometallics* **2012,** *31* (24), 8505-8515.

(68) Guo, C.-Y.; Peulecke, N.; Basvani, K. R.; Kindermann, M. K.; Heinicke, J., 2-Phosphinophenolate Nickel Catalysts: Formation of Ethylene Copolymers with Isolated sec-Alkyl, Aryl, and Functionally Substituted Alkyl Groups. *Macromolecules* **2010,** *43* (3), 1416-1424.

(69) Heinicke, J.; Köhler, M.; Peulecke, N.; Keim, W., The impact of P substituents on the oligomerization of ethylene with nickel 2-diphenyl and 2-dicyclohexylphosphinophenolate phosphine catalysts. *J. Catal.* **2004,** *225* (1), 16-23.

(70) Zhang, Y.; Mu, H.; Wang, X.; Pan, L.; Li, Y., Elaborate tuning in ligand makes a big difference in catalytic performance: bulky nickel catalysts for (co) polymerization of ethylene with promising vinyl polar monomers. *ChemCatChem* **2019,** *11* (9), 2329-2340.

(71) Wang, X.-l.; Zhang, Y.-p.; Wang, F.; Pan, L.; Wang, B.; Li, Y.-s., Robust and Reactive Neutral Nickel Catalysts for Ethylene Polymerization and Copolymerization with a Challenging 1,1-Disubstituted Difunctional Polar Monomer. *ACS Catal.* **2021,** *11* (5), 2902-2911.

(72) Lin, F.; Morgen, T. O.; Mecking, S., Living Aqueous Microemulsion Polymerization of Ethylene with Robust Ni (II) Phosphinophenolato Catalysts. *J. Am. Chem. Soc.* **2021,** *143* (49), 20605-20608.

(73) Falivene, L.; Credendino, R.; Poater, A.; Petta, A.; Serra, L.; Oliva, R.; Scarano, V.; Cavallo, L., SambVca 2. A web tool for analyzing catalytic pockets with topographic steric maps. *Organometallics* **2016,** *35* (13), 2286-2293.

(74) Poater, A.; Cosenza, B.; Correa, A.; Giudice, S.; Ragone, F.; Scarano, V.; Cavallo, L., SambVca: A web application for the calculation of the buried volume of N-heterocyclic carbene ligands. Wiley Online Library: 2009.

(75) Baier, M. C.; Zuideveld, M. A.; Mecking, S., Post-metallocenes in the industrial production of polyolefins. *Angew. Chem. Int. Ed.* **2014,** *53* (37), 9722-9744.

(76) Lalwani, N.; Allen, D. W.; Horton, P. N.; Coles, S. J.; Cross, N. A.; Bricklebank, N., Methoxy-phenyl groups reduce the cytotoxicity and increase the aqueous solubility of phosphonium zwitterions and salts. *Polyhedron* **2019,** *158*, 515-523.

(77) Low, C. H.; Rosenberg, J. N.; Lopez, M. A.; Agapie, T., Oxidative coupling with Zr (IV) supported by a noninnocent anthracene-based ligand: Application to the catalytic cotrimerization of alkynes and nitriles to pyrimidines. *J. Am. Chem. Soc.* **2018,** *140* (38), 11906-11910.

(78) Palmer, W. N.; Zarate, C.; Chirik, P. J., Benzyltriboronates: building blocks for diastereoselective carbon–carbon bond formation. *J. Am. Chem. Soc.* **2017,** *139* (7), 2589-2592.

(79) Falivene, L.; Cao, Z.; Petta, A.; Serra, L.; Poater, A.; Oliva, R.; Scarano, V.; Cavallo, L., Towards the online computer-aided design of catalytic pockets. *Nat. Chem.* **2019,** *11* (10), 872-879.

(80) Ragone, F.; Poater, A.; Cavallo, L., Flexibility of N-heterocyclic carbene ligands in ruthenium complexes relevant to olefin metathesis and their impact in the first coordination sphere of the metal. *J. Am. Chem. Soc.* **2010,** *132* (12), 4249-4258.

CHAPTER 7

Interrogating Effects of Secondary Metal Additives in Ni-Catalyzed Olefin (Co)Polymerization

Chapter 7

CONTRIBUTIONS AND ACKNOWLEDGEMENTS

Shuoyan Xiong and Theodor Agapie conceived the presented idea. S.X. performed synthetic and mechanistic studies, polymerization studies and polymer characterization, and analyzed the catalysis data. Manar M. Shoshani performed single-crystal X-ray diffraction (scXRD) studies. Alex J. Nett, Heather S. Spinney, and Briana S. Henderson performed polymerization studies and polymer characterization. S.X. wrote the chapter.

We are grateful to Dow (TA) for funding. We thank Brad C. Bailey and Todd D. Senecal for insightful discussions. We thank Michael K. Takase and Lawrence Henling for assistance with X-ray crystallography, and David VanderVelde for assistance with NMR spectroscopy. We thank Hannah Bailey and Heidi Clements for assistance in collecting polymer characterization data (GPC, DSC, FT-IR). Support has been provided for the X-ray diffraction and NMR instrumentation via the Dow Next Generation Educator Fund.

Chapter 7

ABSTRACT

In this chapter we reported a class of *in situ* generated Ni-based multimetallic complexes based on a bisphosphine phenoxide ligand (POP). Several secondary metal (M_2) additives that are coordinated by the phosphine in POP inhibit olefin polymerization. Further isolation and characterization of relevant metallocycles revealed a deactivation pathway involving the ligand on M_2 (L^{M2}) bridging between two metals. For a variety of metal halides, alkyls and alkoxides, phosphine coordination drives M_2 to specific positions, which potentially enables facile formation of aforementioned metallocycles. On the other hand, $Al(O^iPr)_3$, as an secondary metal additive, is likely only coordinated by ether groups and promotes ethylene/acrylate copolymerization. Overall, these results reveal potential effects of ligands on M_2 (L^{M2}) on polymerization catalysis and the importance of M_2's position, both of which should be considered in future catalyst design.

Chapter 7

GENERAL INTRODUCTION

Incorporation of polar functionalities via coordination copolymerization can provide value-added polyolefins with precisely controlled physical and mechanical properties and potential degradability.[1-6] Conceptually inspired by multinuclear active sites in metalloenzymes, multimetallic catalysts have been pursued for this polymerization.[7-8] Over last two decades, a variety of symmetric bimetallic catalysts have been reported featuring enhanced activity, stability, molecular weight (Mw) or polar monomers incorporation compared to their monometallic counterparts (Figure 7.1a).[9-22] On the other hand, asymmetric multimetallic catalysts with two or more metal centers differing in both binding environments and roles in catalysis are much less explored in catalytic synthesis of polar polyolefins,[23-25] though several examples focused on ethylene homopolymerization have been reported.[26-34]

Previous mechanistic studies have identified polar monomer inserted species as the resting state of catalysis (Figure 7.1b).[35-41] It has been suggested that subsequent insertion is hindered by the preferential σ-coordination of heteroatoms to the active metal center M_1.[39, 41] Destabilization of this coordination can potentially promote further insertion, and thus is desirable. A specifically attractive strategy is introducing a *Lewis* acidic metal M_2 proximal to M_1 since the polar functionalities may prefer coordinating to M_2 instead of M_1 and thus inhibit the formation of aforementioned coordination (Figure 7.1c).[7-8]

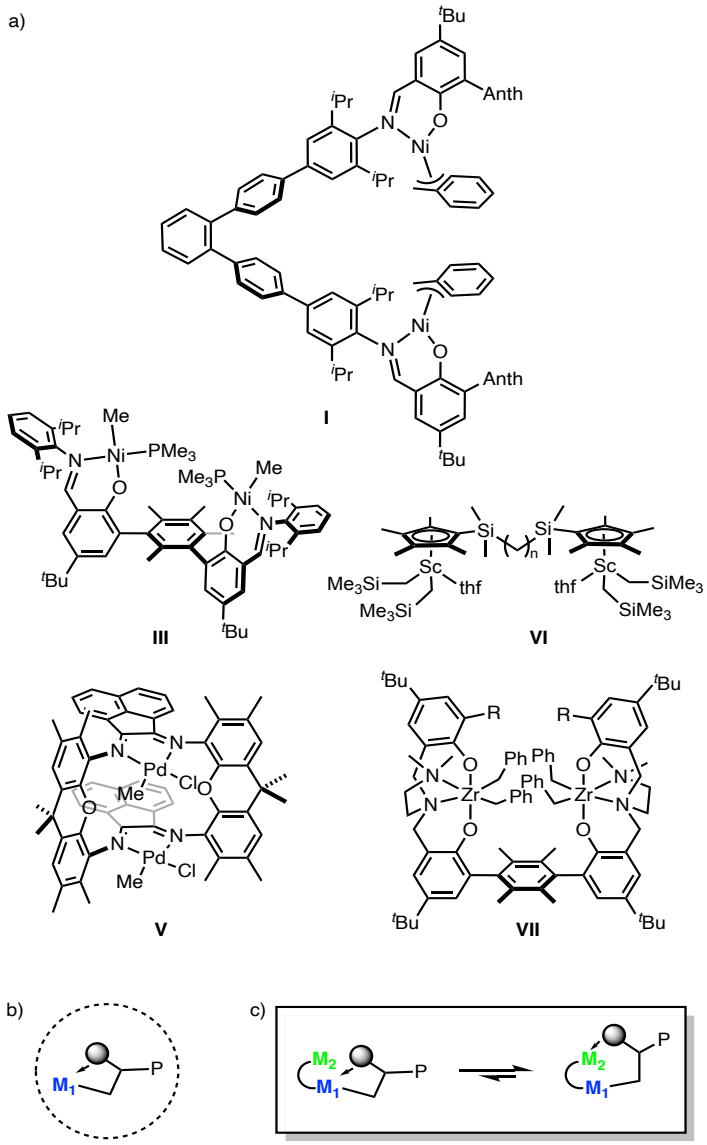

Figure 7.1. a) Examples of symmetric bimetallic catalysts for copolymerization involving polar monomers. b) Depiction of polar monomer inserted species. c) Depiction of potential cooperative effects of M_2 in polar monomer insertion. Grey spheres: polar groups.

This concept has been demonstrated, and alkali metal cations were employed as M_2 in most examples.[23-25] Specifically, Do group reported Pd-alkali catalysts that show enhancements in activity and copolymer Mw compared to the monopalladium counterpart.[23] The precise role of alkali ions remained unclear since they may not only

interact with polar monomers, but also increase M_1's electrophilicity. Potentially related to the latter, the secondary metal cation led to decreases in polymer Mw or polar monomer incorporation and increases in polymer dispersity in several other examples, which are undesirable for their material applications.[31-32, 42] In this regard, installing neutral *Lewis* acidic metal additives with X-type coordinating ligands ($\mathbf{L^{M2}}$) is attractive since the resulting multimetallic complexes would be overall neutral and change in electrophilicity of the active metal center (M_1) may be insignificant.

In general, we prefer nickel-based catalysts due to their relatively high efficiency and low cost of nickel.[9-10, 39-40, 43-45] Specifically, our previously reported Ni bisphosphine phenoxide catalyst **1** represents a suitable candidate for investigation of this approach. First, it showed state-of-art performance in activity, thermal stability and acrylate incorporation and thus further improvements are of practical relevance.[39, 46-48] Second, it features an additional phosphine moiety with four ether groups, which are suitable ligands for a variety of metals.

RESULTS AND DISCUSSION

Screening of Secondary Metal Additives

To figure out the binding affinity of **1**, we first screened several metal precursors with different X-type coordinating ligands ($\mathbf{L^{M2}}$) including $ZnMe_2$, $AlEt_3$, $ZnCl_2$, $Zn(OMe)_2$, $Al(O^iPr)_3$, KO^tBu. Reaction was performed in toluene, or THF if no reactivity was observed in toluene even at elevated temperatures. Among these

additives, several sets of new peaks were observed in ^{1}H and $^{31}P\{^{1}H\}$ NMR spectra with significant peak broadening upon addition of metal alkyls and most metal alkoxides, implying generation of multiple species (Figure 7.2, S2.1). Notably, addition of $ZnCl_2$ to **1** in toluene leads to one new set of broad doublets appeared in $^{31}P\{^{1}H\}$ NMR spectrum, indicating generation of one major compound. In the above cases, one of the most significant changes is shift of resonance for the free phosphine in **1**, potentially indicating its coordination to the secondary metal. In contrast, $Al(OiPr)_3$ only leads to minute changes in both ^{1}H and $^{31}P\{^{1}H\}$ NMR spectra (Figure 7.2, S7.2), implying a weak interaction. Resonances that shifted upon addition of $Al(OiPr)_3$ includes that for both phosphines in $^{31}P\{^{1}H\}$ NMR spectrum and for several protons including those on methoxy groups in ^{1}H NMR spectrum (Figure S7.2). This scenario is consistent with a weak interaction between aluminum and methoxy groups ortho to phosphine, instead of phosphine coordination which typically leads to significant changes in $^{31}P\{^{1}H\}$ NMR. Other possibilities of weak interactions cannot be ruled out.

Structure and Reactivity of Ni/Zn Heterobimetallics

As shown above, addition of $ZnCl_2$ leads to the generation of one major new species. Encouraged by this, we then conducted ethylene homopolymerization with a 1:5 1/$ZnCl_2$ mixture. Unexpectedly, negligible polymer production was observed, indicating severe activity suppression induced by $ZnCl_2$. To elucidate how it quenches polymerization, isolation and characterization of *in-situ* generated Ni/Zn heterobimetallics was pursued.

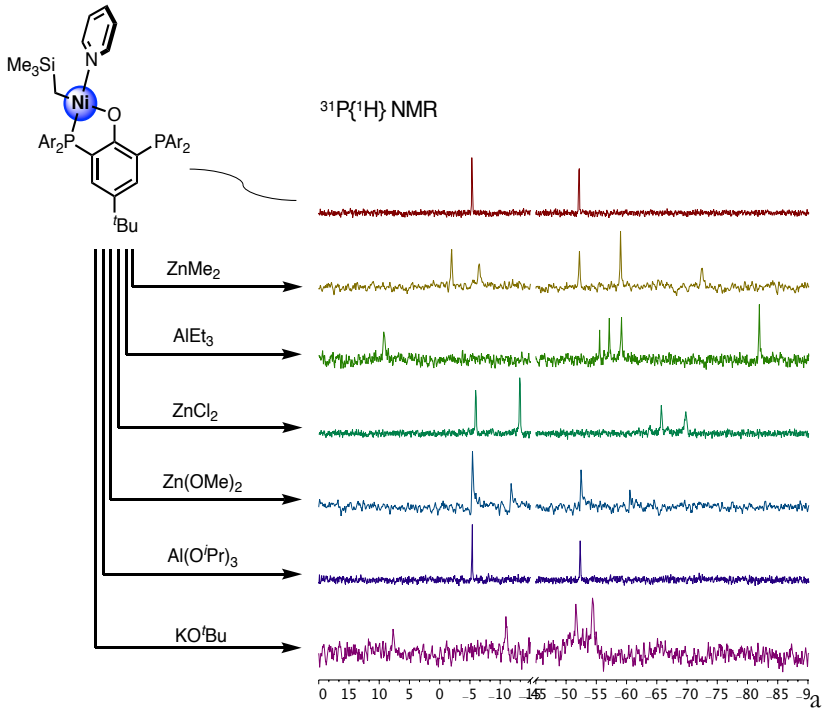

Figure 7.2. Reaction of **1** with several secondary metal additives featuring different metal centers and ligands on them (alkyls, chloride and alkoxides). See SI for details.

X-ray quality crystals were obtained from vapor diffusion of hexanes into a cold toluene solution of **1**/$ZnCl_2$. Solid-state characterization by single crystal X-ray diffraction (scXRD) confirmed the identity of a Ni/Zn heterobimetallic complex, **2** (Figure 7.3-4). It features a square planar nickel center and a tetrahedral zinc center, each coordinated by one phosphine and the central phenoxide. The scenario is consistent with the abovementioned NMR studies regarding phosphine coordination. The Ni(1)-O(1) distance in **2** is significantly elongated comparing to that in **1** (1.983(2) Å for **2** vs 1.926(3) Å for **1**), implying a weakened phenoxide coordination to nickel.

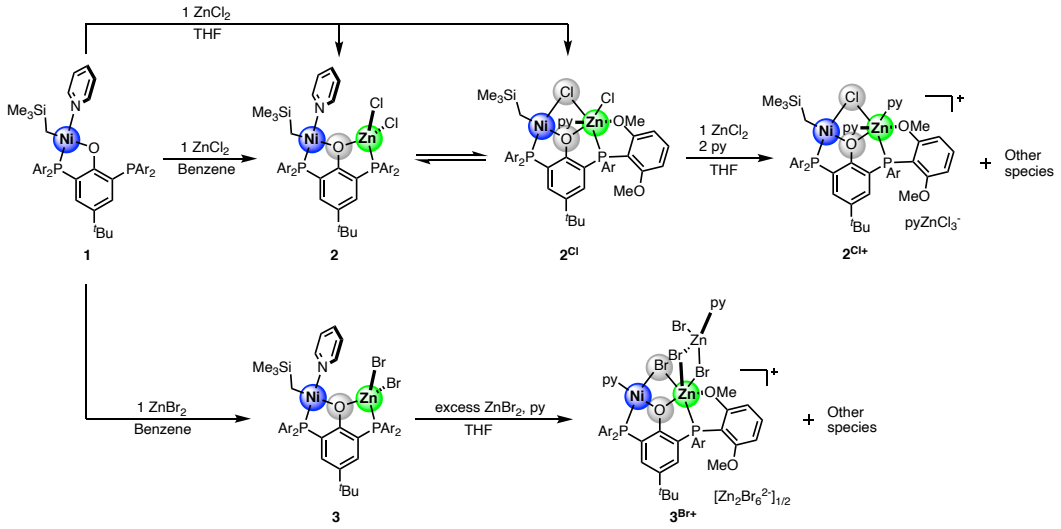

Figure 7.3. Preparation of Ni-Zn heterobimetallic compounds.

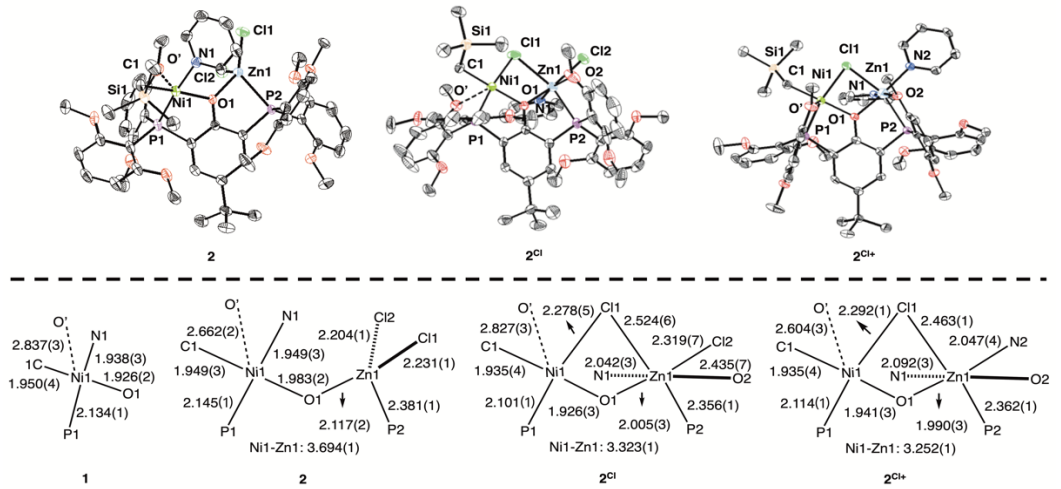

Figure 7.4. (Top) Solid-state structures of **2**, **2**^{Cl}, **2**$^{Cl+}$ and (bottom) selected bond distances (in Å, structure of **1** reported in ref 39). Solvent molecules, anions, and hydrogen atoms have been omitted for clarity. Check Experimental section 5 for more details.

In the NMR spectra of **2** (independent prepared or crystalized) in C_6D_6, one minor species was also observed (Figure AD7.5). Similarly, two new sets of doublets appeared if **1** and $ZnCl_2$ were mixed in THF (Figure AD7.2). One set is close to resonances of **2** and the other one is close to resonances of the above-mentioned minor species. Consistent with this, vapor diffusion of hexanes into THF solution of

an *in-situ* mixture of **1** and 1 equiv. of $ZnCl_2$ also led to crystallization of two species, **2** and a four-membered Ni/Zn metallocycles containing a bridged chloride (**2**^{Cl}, Figure 7.3-4). The latter is potentially generated from **2** via pyridine abstraction by zinc followed by chloride coordination to nickel. In **2**^{Cl}, the coordination geometry of zinc transferred from tetrahedral to octahedral. In addition, the Ni(1)-Zn(1) distance in **2**^{Cl} is significantly shorter than that in **2** (3.323(1) Å vs 3.693(1) Å), along with significant shorter Ni(1)-O(1) (1.926(3) Å vs 1.983(2) Å) and Zn(1)-O(1) distance (2.005(3) Å vs 2.116(2)), potentially due to the halide bridging in **2**.

Mimicking this stoichiometry in actual polymerization, we also examined the reaction of **2**/**2**^{Cl} and excess $ZnCl_2$. Notably, a cationic, chloride-bridged Ni/Zn heterobimetallic complex **2**$^{Cl+}$ was obtained in the presence of 2 equiv. of pyridine in THF and its identity was confirmed by ScXRD (Figure 7.3-4). The counterion is $pyZnCl_3^-$. This compound was likely generated from **2**^{Cl} via a terminal chloride abstraction by $ZnCl_2$. Compared to the Ni/Zn metallocycle in **2**^{Cl}, both bridged chloride and phenoxide in **2**$^{Cl+}$ is closer to zinc than in **2**^{Cl}, as evidenced by the elongated Ni(1)-O(1) and Ni(1)-Cl(1) distances and shortened Zn(1)-O(1), and Zn(1)-Cl(1) distances in **2**$^{Cl+}$. In addition, the Ni(1)-Zn(1) distance in **2**$^{Cl+}$ is 3.252(1) Å, shorter than that in **2**^{Cl} (3.323(1) Å). This distortion is potentially due to the generation of a more electrophilic zinc after chloride abstraction.

Overall, the generation of **2**^{Cl} and **2**$^{Cl+}$ revealed an underexplored role of ligands on the secondary metal of multimetallic olefin polymerization catalysts: bridging between two metals. Given the stability of the four-membered Ni-Cl-Zn-O metallocycle,

replacement of Ni-Cl bond by olefin coordination could be very challenging even in the presence of a large excess of ethylene. Indeed, negligible polymer generation was observed in ethylene polymerization by either **2/2**^{Cl} or **2**$^{Cl+}$. Though such four-membered metallocycle were isolated with $ZnCl_2$, similar process may happen with other additives featuring different metal centers or ligands on metal (**L**^{M2}). For example, reaction of 1 equiv. of 1 and $ZnBr_2$ in THF led to generation of two new species with resonances similar to **2** and the other isomer (possible **2**^{Cl}) mentioned above. The identity of major species is confirmed as **3** (Figure 7.3, S5.4), which is also inactive in ethylene polymerization. Further addition of excess $ZnBr_2$ led to the formation of bromide bridged species (Figure 7.3). In addition, this process can also happen during polymerization (Figure 7.5). After ethylene coordination or β-H elimination, a four-membered metallocycle could generate after replacement of corresponding olefins by **L**^{M2}. Formation of similar metallocycles may also happen with other ligand frameworks if two metals are in similar positions. For example, Tonks group have observed a metastable bromide-bridged NON-NiZn complex in ^{1}H NMR.[27] In general, the lack of open coordination site for olefin after formation of this metallocycle could inhibit further monomer coordination and migratory insertion, leading to activity, Mw suppression or catalyst deactivation.

To the best of our knowledge, these structures represent the first few crystallographically characterized examples of four-membered Ni/Zn metallocycles relevant to olefin polymerization. The additional phosphine donor proximal to nickel is the basis of ligand POP's unique ability to support and stabilize such metallocycles.

Coordination of this phosphine to M_2 drives M_2 proximal to nickel and thus make it possible for ligands on M_2 bridging between two metals.

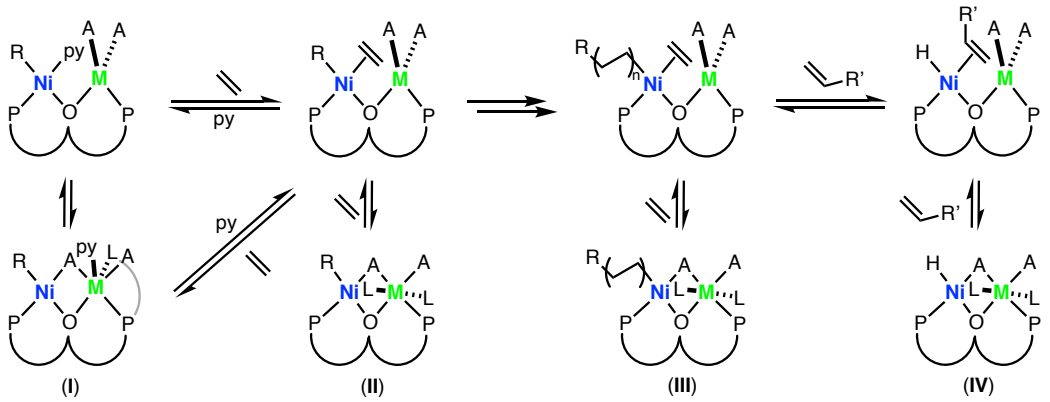

Figure 7.5. Potential metallocycle formation in four cases: (I) in the absence of ethylene/before ethylene coordination, (II)/(III) after ethylene coordination, and (IV) after β-H elimination. (L: pyridine or other ligands in the system, A: ligands on the second metal, R: alkyls/polymer chains on nickel, R': polar groups).

Ethylene/Acrylate Copolymerization by *In Situ* Mixtures of 1 and Al additives

To prevent the formation of abovementioned four-membered metallocycle, inhibition of phosphine coordination to M_2 may be a strategy for **1**. Notably, the weak interaction between **1** and $Al(O^iPr)_3$ implies the absence of phosphine coordination. Indeed, a 1:5 **1**/$Al(O^iPr)_3$ mixture was still active in ethylene polymerization and furthermore, an increase in activity was observed compared to **1** alone (~1100 kg/(mol*h) vs ~710 kg/(mol*h)) (Figure table S7.1).

Encouraged by this, we next investigated the performance of **1**/$Al(O^iPr)_3$ mixtures in ethylene/acrylate to evaluate effects of $Al(O^iPr)_3$ in the presence of polar monomers. This copolymerization is of increasing interest due to the wide applications of ester-functionalized polyolefins,[6, 49-52]

Table 7.1. Ethylene/tBA copolymerization.

Entry[a]	catalyst	[tBA]/M	Act.[b]	$M_w/10^3$	PDI	%Mol t-BA	Tm (ºC)
1	**1**	1000	550	54.3	2.1	2.1	110
2	**1** + 1 $Al(O^iPr)_3$	1000	940	51.1	2.3	2.2	111
3	**1** + 2 $Al(O^iPr)_3$	1000	990	51.6	2.3	2.1	110
4	**1** + 5 $Al(O^iPr)_3$	1000	1000	51.2	2.3	2.2	110
5	**1**	2000	290	34.8	2.3	4.8	97
6	**1** + 1 $Al(O^iPr)_3$	2000	510	39.8	2.4	4.6	99
7	**1** + 1 $AlEt_3$	1000	<10	N.D.	N.D.	N.D.	N.D.
8	**1** + 1 $Al(OEt)Et_2$	1000	480	56.1	2.4	2.1	111
9	**1** + 2 $Al(OEt)Et_2$	1000	290	52.6	2.2	2.2	110
10	**1** + 5 $Al(OEt)Et_2$	1000	90	48.0	2.4	2.3	109

[a] Unless specified, V(total) = 5 mL, [Ni] = 0.25 μmol, ethylene pressure = 400 psi, T = 90 ºC, toluene solvent. Polymerization runs were stopped at 1h or when ethylene uptake reached 80.13 psi (<1 h). Each entry represents an average of multiply replicated runs (see Table S7.2 for original data). [b] Act. = (kg/(mol·h)).

Compared to **1**, *in situ* generated Ni-Al heterobimetallic species prepared by mixing **1** and 1 equiv. of $Al(O^iPr)_3$ showed a ~60% increase in activity, along with a <10% decrease of Mw (Table 7.1, entry 1 vs 2). Notably, excess $Al(O^iPr)_3$ didn't show significant effect on the catalytic activity (comparing entry 2~4), potentially implying a saturation. Under higher tBA loading (entry 5 vs entry 6), an 80% increase in activity was observed with 1 equiv. of $Al(O^iPr)_3$. Consequently, tBA incorporation reached 4.6% with a catalytic activity of 510 kg/(mol·h). Comparing entry 1 vs 6, tBA incorporation increases by 120% while catalyst activity remains similar. This is of immediate practical relevance given that an increase in acrylate incorporation typically cooccurs with a decrease in catalyst activity.

Other Al additives were also examined to evaluate the effect of $\mathbf{L^{M2}}$. Opposite to $Al(O^iPr)_3$, addition of $AlEt_3$ quenched ethylene/tBA copolymerization (Table 7.1, entry 7). This is potentially related to the generation of multiple metal alkyl species as implied by *in-situ* NMR studies (Figure AD7.1). $Al(OEt)Et_2$, an additive featuring both alkoxide and alkyl ligands, also showed detrimental effects on ethylene/tBA copolymerization (Table 7.1, entry 1, 8~10). It's notable that higher equivalents of $Al(OEt)Et_2$ led to more severe activity suppression.

The above results are consistent with the proposal that inhibition of phosphine coordination to M_2 could prevent activity suppression in polymerization induced by metallocycle formation. The difference between effects of $Al(O^iPr)_3$, $Al(OEt)Et_2$, and $AlEt_3$ clearly demonstrated the influence of $\mathbf{L^{M2}}$ on polymerization. However, the origin of $Al(O^iPr)_3$'s promoting effect on catalysis remain unclear. Possibilities include aforementioned cooperative effect of $Al(O^iPr)_3$ after acrylate insertion, or increase in steric hindrance induced by $Al(O^iPr)_3$.

CONCLUSION

In summary, we have demonstrated coordination chemistry and polymerization behavior of a new class of Ni-based multimetallic catalyst system based on our previous reported mononickel complex **1**. $ZnCl_2$, $ZnBr_2$, and $AlEt_3$, which are coordinated by the additional phosphine in **1**, inhibit polymerization. On the other hand, $Al(O^iPr)_3$, which is likely only coordinated by ether groups, promotes both

ethylene polymerization and ethylene/tBA copolymerization. Further isolation and characterization of several stable metallocycles revealed a deactivation pathway involving a ligand on M_2 bridging between two metals. These results highlight a strategy that may promote catalysis: introducing a secondary metal additive that won't form stable metallocycle with the mononickel complex.

It has been a long-standing interest on the role of proximal secondary metal centers in olefin polymerization catalysis. Our results herein indicate that the ligand on the secondary metal (e.g. halides) can also strongly affect catalyst behavior, a topic underexplored in this field. This effect is especially important when two metal centers are in close proximity that allows the formation of multimetallic metallocycles. However, the secondary metal needs to stay close to nickel to affect the catalysis. Circumventing or addressing this conflict should be taken into account in designing multimetallic catalysts for polar polyolefin synthesis.

Chapter 7

EXPERIMENTAL SECTION

General Considerations

All air- and water-sensitive compounds were manipulated under N_2 or Ar using standard Schlenk or glovebox techniques. The solvents for air- and moisture-sensitive reactions were dried over sodium benzophenone ketyl or calcium hydride or by the method of Grubbs.[53] Deuterated solvents were purchased from Cambridge Isotopes Lab, Inc.; C_6D_6, and THF-d8 was dried over a purple suspension with Na/benzophenone ketyl and vacuum transferred; Ethylene (99.999%) for ethylene homopolymerization was purchased from Matheson Tri-Gas and equipped with a PUR-Gas in-line trap to remove oxygen and moisture before use. Tert-butyl acrylate were dried over 4 Å sieves for greater than 72h, vacuum transferred, and passed over an activated alumina plug. Dimethoxybenzene, 1-methoxynaphthalene, and pyridine were dried over calcium hydride and vacuum-transferred or distilled prior to use. Secondary metal precursors were purchased from Sigma-Aldrich and used without further purification. Bis(dimethoxyphenyl)phosphine chloride,[54] 1,3-dibromo-5-(tert-butyl)-2-(methoxymethoxy)-benzene,[55] $Nipy_2(CH_2Si(CH_3)_3$,[56] and mononuclear catalyst **1**[39] were synthesized according to literature procedures. All ^1H, ^{13}C, and ^{31}P spectra of organic and organometallic compounds were recorded on Varian Mercury 300, Varian INOVA-400, or 500, or Bruker Cryoprobe 400 spectrometers. ^1H and ^{13}C chemical shifts are reported relative to residual solvent resonances.

Binding Studies with Secondary Metal Additives

Conditions for Figure 3.2: Unless specified, **1**: 4.9 mg, 0.005 mmol; secondary metal additive: 5 equiv., 0.025 mmol; V(total): 0.5 mL.

Reaction was performed in toluene, or THF if no reactivity was observed in toluene at elevated temperatures. The mixtures were stirred/rotated at room temperature for 20 min prior to spectra

collection unless specified. The $^{31}P\{^{1}H\}$ spectrum of **1** (top spectrum) was collected in toluene wand calibrated by an external standard.

a) $ZnMe_2$: 0.1 mL, 0.25 M, toluene solvent. The mixture was heated at 50 ºC for 20 min prior to spectrum collection.

b) $AlEt_3$: 0.1 mL, 0.25 M in toluene; toluene solvent.

c) $ZnCl_2$: 3.4 mg, 0.025 mmol; toluene solvent.

d) $Zn(OMe)_2$: 3.2 mg, 0.025 mmol; THF was used instead of toluene. The mixture was heated at 50 ºC for 20 min prior to spectrum collection.

e) $Al(O^iPr)_3$: 5.1 mg, 0.025 mmol; toluene solvent. The mixture was heated at 50 ºC for 20 min prior to spectrum collection.

f) KO^tBu: 2.8 mg, 0.025 mmol; THF was used instead of toluene.

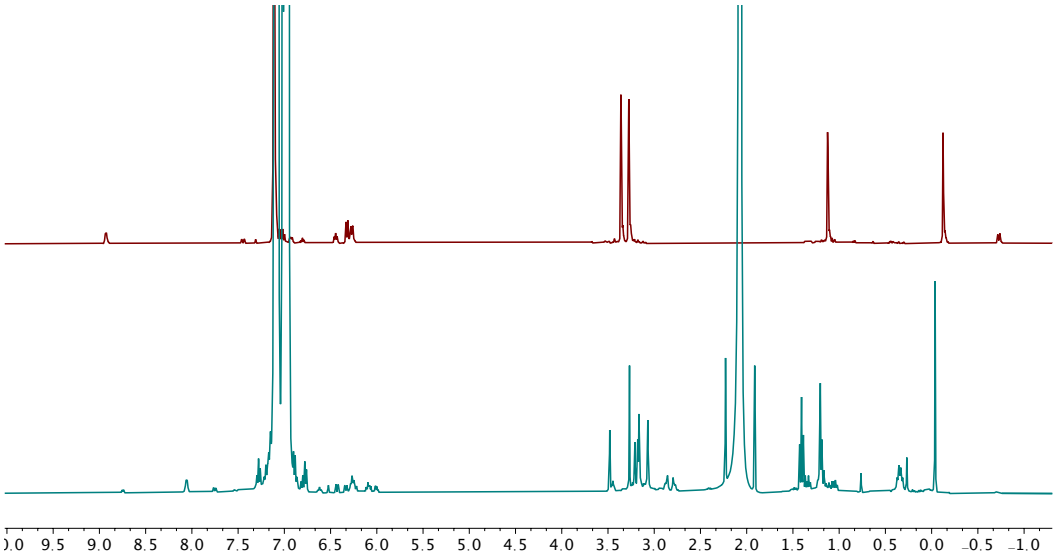

Figure S7.1: ^{1}H NMR spectra of: a) **1** (top) and b) **1** and 1 equiv. of $AlEt_3$ (bottom, $AlEt_3$: 0.03M in toluene) in C_6D_6.

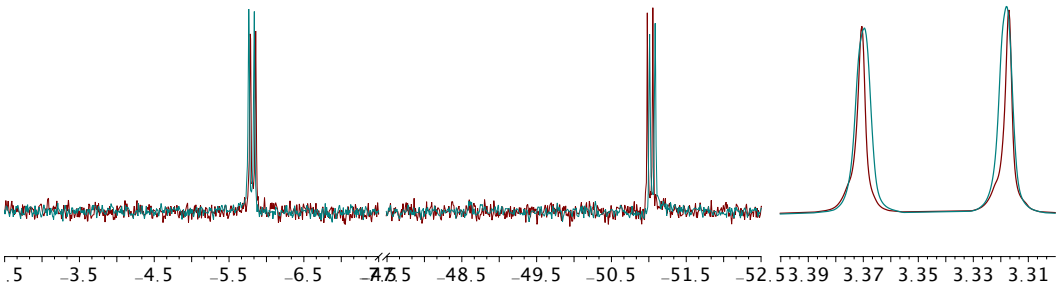

Figure S7.2: $^{31}P\{^{1}H\}$ NMR spectra (left) and ^{1}H NMR spectra (right, only the resonances for methoxy groups) of **1** (red) and **1** + 1 equiv. of $Al(O^{i}Pr)_3$ (green, condition: **1**: 5.8 mg, 0.0059 mmol; $Al(O^{i}Pr)_3$: 1.2 mg, 0.0059 mmol; tol-d8: 0.5 mL; temperature: 70 ºC).

Synthesis of Ni/Zn Compounds

2/2^{Cl}: In the glove box, to a solution of **1** (29.6 mg, 0.03 mmol) in THF (5 mL) was added a suspension of 1 equiv. of $ZnCl_2$ (4.1 mg, 0.03 mmol) in THF (0.5 mL). The mixture was stirred for 30 min under room temperature, forming a red-orange solution. ^{1}H and $^{31}P\{^{1}H\}$ NMR spectra of the reaction mixture indicate the generation of two new species (10% C_6D_6 was added for the ^{1}H NMR experiment). $^{31}P\{^{1}H\}$ NMR (121 MHz, C_6D_6): δ -5.99 (d, $^{4}J_{PP}$ = 12.1 Hz), -13.28 (d, $^{4}J_{PP}$ = 12.1 Hz), -65.80 (d, $^{4}J_{PP}$ = 12.1 Hz), -69.86 (d, $^{4}J_{PP}$ = 12.1 Hz). Mixture of orange and red crystals were obtained via vapor diffusion of hexanes into THF solution of an *in-situ* mixture of **1** and 1 equiv. of $ZnCl_2$ and identified as **2** and **2^{Cl}**.

Independent synthesis of **2** (with a small amount of the other isomer, potentially **2^{Cl}**): In the glove box, to a solution of **1** (29.6 mg, 0.03 mmol) in THF (1.5 mL) was added a suspension of 0.9 equiv. of $ZnCl_2$ (3.7 mg, 0.027 mmol) in THF (0.5 mL). The mixture was stirred for 20 min under room temperature, forming a red-orange solution. To this solution was added just thawed pentane (18 mL), allowing the formation of a yellow suspension. Solids were collected via vacuum filtration, yielding **2** as orange powders (21.8 mg, 65%). ^{1}H NMR (400 MHz, C_6D_6): δ 8.84-8.82 (m, 2H, PyH), 7.62-7.59 (m, 1H, PhH), 7.49−7.47 (m, 1H, PhH), 7.48−7.45 (m, 1H, PhH), 7.24−7.20 (m, 1H, PhH), 7.06−7.04 (m, 4H, PhH), 6.96−6.94 (m, 1H, PyH),

6.65−6.63 (m, 2H, PyH), 6.39−6.37 (m, 4H, PhH), 6.26−6.24 (m, 4H, PhH), 3.57 (s, 12H, OCH_3), 3.47 (s, 12H, OCH_3), 1.10 (s, 9H, $C(CH_3)_3$), 0.26 (s, 9H, $Si(CH_3)_3$), -0.39−-0.42 (d, $^3J_{HP}$ =10.3 Hz, 2H, $NiCH_2Si$) (Note: resonances assigned to the other isomer: δ 6.20−6.19 (m, 4H, PhH), 6.12−6.10 (m, 4H, PhH), 3.33 (s, 12H, OCH_3), 3.28 (s, 12H, OCH_3), 1.15 (s, 9H, $C(CH_3)_3$), 0.36 (s, 9H, $Si(CH_3)_3$); Other resonances correspond to this isomer are overlapped with resonances of the major isomer). $^{13}C\{^1H\}$ NMR (101 MHz, C_6D_6): 163.48 (broad s, 4C, Ar-C), 161.73 (broad s, 4C, Ar-C), 152.03 (m, 4C, Ar-C), 136.65 (m, 1C, Ar-C), 131.85 (m, 6C, Ar-C), 131.15 (s, 4C, Ar-C), 124.57 (s, 2C, Ar-C), 104.38 (m, 10C, Ar-C), 56.07 (s, 4C, OCH_3), 55.51 (s, 4C, OCH_3), 34.06 (s, 1C, $C(CH_3)_3$), 31.94 (s, 9C, $C(CH_3)_3$), 2.09 (s, 9C, $SiMe_3$), -14.58 (d, $^2J_{CP}$ = 30.5 Hz, 1C, $NiCH_2Si$) (Note: resonances assigned to the other isomer: δ 161.58 (broad s, 4C, Ar-C), 137.92 (m, 1C, Ar-C), 108.85-108.14 (m, Ar-C), 56.00 (s, 4C, OCH_3), 55.16 (s, 4C, OCH_3), 34.21 (s, 1C, $C(CH_3)_3$), 32.03 (s, 9C, $C(CH_3)_3$), 2.98 (s, 9C, $SiMe_3$). Other resonances corresponded to this isomer are overlapped with resonances of the major isomer); $^{31}P\{^1H\}$ NMR (121 MHz, C_6D_6): δ -5.62 (d, $^4J_{PP}$ = 10.1 Hz, 1P), -62.37 (d, $^4J_{PP}$ = 10.1 Hz, 1P). Anal. Calcd(%) for $C_{51}H_{63}Cl_2NNiO_9P_2Si$: C: 54.74, H: 5.67, N: 1.25; found: C: 55.72, H: 6.03, N: 1.86.

2^{Cl+} was obtained as red crystals via vapor diffusion of hexanes into THF solution of an *in-situ* mixture of **1** and 2 equiv. of $ZnCl_2$, or an *in-situ* mixture of **2/2^{Cl}** and 2 equiv. of $ZnCl_2$, in the presence of excess (2~5 equiv.) of pyridine. The resulting red crystals are poorly soluble in THF.

3: In the glove box, to a solution of **1** (29.6 mg, 0.03 mmol) in THF (1.5 mL) was added a suspension of 1 equiv. of $ZnBr_2$ (6.8 mg, 0.03 mmol) in THF (1.0 mL). The mixture was stirred for 30 min under room temperature, forming a red-orange solution. $^{31}P\{^1H\}$ NMR spectrum of this reaction mixture indicate the generation of two new species assigned to **3**

and possibly the bromide bridged analogue of **2Cl**. $^{31}P\{^1H\}$ NMR (121 MHz, C_6D_6): δ -5.78 (d, $^4J_{PP}$ = 12.4 Hz), -9.62 (d, $^4J_{PP}$ = 12.4 Hz), -63.42 (d, $^4J_{PP}$ = 12.4 Hz), -66.33 (broad d). To prepare **3** in high purity (>95%), a solution of **1** (29.6 mg, 0.03 mmol) in THF (2 mL) was mixed with 0.8 equiv. of $ZnBr_2$ (5.4 mg, 0.024 mmol) in THF (2 mL). The mixture was stirred for 30 min under room temperature. After removal of volatiles, unreacted **1** was washed away by diethyl ether and desired products were collected via vacuum filtration (31.1 mg, 74%). ^1H NMR (400 MHz, C_6D_6): δ 8.79-8.77 (m, 2H, PyH), 7.66−7.62 (dd, $^3J_{HP}$ = 10.8 Hz, $^4J_{HH}$ = 2.5 Hz, 1H, PhH), 7.52−7.49 (dd, $^3J_{HP}$ = 9.3 Hz, $^4J_{HH}$ = 2.5 Hz, 1H, PhH), 7.12−7.11 (m, 1H, PyH), 7.04−7.00 (m, 4H, PhH), 6.63−6.60 (m, 2H, PyH), 6.39−6.36 (dd, $^3J_{HH}$ = 8.3 Hz, $^4J_{HH}$ = 3.6 Hz, 4H, PhH), 6.29−6.26 (dd, $^3J_{HH}$ = 8.3 Hz, $^4J_{HH}$ = 3.6 Hz, 4H, PhH), 3.58 (s, 12H, OCH_3), 3.49 (s, 12H, OCH_3), 1.13 (s, 9H, $C(CH_3)_3$), 0.26 (s, 9H, $Si(CH_3)_3$), -0.40−-0.43 (d, $^3J_{HP}$ = 10.1 Hz, 2H, $NiCH_2Si$); $^{13}C\{^1H\}$ NMR (101 MHz, C_6D_6): 163.45 (s, 2C, Ar-C), 163.42 (s, 2C, Ar-C), 161.72 (s, 4C, Ar-C), 152.07 (m, 4C, Ar-C), 136.80 (m, 1C, Ar-C), 131.97 (m, 6C, Ar-C), 131.20 (s, 4C, Ar-C), 124.70 (s, 2C, Ar-C), 104.35 (m, 10C, Ar-C), 56.11 (s, 4C, OCH_3), 55.58 (s, 4C, OCH_3), 34.13 (s, 1C, $C(CH_3)_3$), 32.00 (s, 9C, $C(CH_3)_3$), 2.13 (s, 9C, $SiMe_3$), -14.26 (d, $^2J_{CP}$ = 30.5 Hz, 1C, $NiCH_2Si$); $^{31}P\{^1H\}$ NMR (121 MHz, C_6D_6): δ -5.80 (d, $^4J_{PP}$ = 10.3 Hz, 1P), -63.39 (d, $^4J_{PP}$ = 10.3 Hz, 1P). Anal. Calcd(%) for $C_{51}H_{63}Br_2NNiO_9P_2Si$: C: 50.71, H: 5.26, N: 1.16; found: C: 52.43, H: 5.18, N: 0.99.

Supplemental information for olefin copolymerization

General procedure for Fisher-Porter type reactor runs for preparation of polyethylene.

This high-pressure setup consists of a 3 oz Andrews glass pressure reaction vessel equipped with Swagelok valves and a gauge. For all ethylene homopolymerization, this setup was brought into the glove box with a magnetic stir bar and charged with a toluene mixture (5 mL) of the desired amounts of the nickel complex and the secondary metal additive (if applicable). The

setup was brought out of the box and clamped firmly over a hot plate which was preheated to desired temperature. The solution was stirred vigorously (1200 rpm). A nylon core hose equipped with quick connect adaptors was purged with ethylene for 1 minute and the pressure was set to 15 psi. The hose was connected to the setup and the setup was filled with ethylene. The pressure was increased to 100 psi. After the desired time (15 min), the ethylene hose was disconnected, the setup was vented and the reaction mixture was quenched with acidified methanol (3 times the reaction volume, 15 mL) to precipitate the polymer, which was collected as a white solid by filtration over a fine frit. All of the precipitates were dried under vacuum over at least 24 hours before the polymer masses were recorded.

Ethylene homopolymerization results.

Table S7.1 Ethylene homopolymerization results.

Entry[a]	Catalyst + n (equiv.) additive	Act.(kg/(mol·h))
1	**1**	682
2	**1**	747
3	**1** + 5 $ZnCl_2$	52
4	**1** + 5 $ZnCl_2$	17
5	**2/2^{Cl}**	<10
6	**2/2^{Cl}**	<10
7	**2^{Cl+}**	<10
8	**2^{Cl+}**	<10
9	**1** + 5 $ZnBr_2$	<10
10	**1** + 5 $ZnBr_2$	<10
11	**3**	<10
12	**3**	<10
13	**1** + 5 $Al(O^iPr)_3$	1322
14	**1** + 5 $Al(O^iPr)_3$	910
15	**1** + 5 $AlEt_3$	<10
16	**1** + 5 $AlEt_3$	<10

[a]Unless specified, V(total) = 5 mL, [Ni] = 4 μmol, pressure = 100 psi, T = 70 ºC, toluene solvent, time = 15 min.
[b]Act.=(kg/(mol·h)).

General procedure for for preparation of polyethylene and ethylene/tBA copolymers.

Polyolefin catalysis screening was performed in a high throughput parallel polymerization reactor (PPR) system. The PPR system was comprised of an array of 48 single cell (6 x 8 matrix) reactors in an inert atmosphere glovebox. Each cell was equipped with a glass insert with an internal working liquid volume of approximately 5 mL. Each cell had independent controls for pressure and was continuously stirred at 800 rpm. Catalysts were prepared in toluene. All liquids (i.e., solvent, tBA, and catalyst solutions) were added via robotic syringes. Gaseous reagents (i.e., ethylene) were added via a gas injection port. Prior to each run, the reactors were heated to 50 °C, purged with ethylene, and vented.

All desired cells were injected with tBA followed with a portion of toluene (This step was skipped for ethylene homopolymerization). The reactors were heated to the run temperature and then pressured to the appropriate psig with ethylene. Catalyst were then added to the cells. Each catalyst addition was chased with a small amount of toluene so that after the final addition, a total reaction volume of 5 mL was reached. Upon addition of the catalyst, the PPR software began monitoring the pressure of each cell. The desired pressure (within approximately 2-6 psig) was maintained by the supplemental addition of ethylene gas by opening the valve at the set point minus 1 psi and closing it when the pressure reached 2 psi higher. The pressure of each cell was monitored during and after the quench to ensure that no further ethylene consumption happens. The shorter the "Quench Time" (the duration between catalyst addition and oxygen quench), the more active the catalyst. All drops in pressure were cumulatively recorded as "Uptake" or "Conversion" of the ethylene for the duration of the run. After 1h, each reaction was then quenched by addition of 1% oxygen in nitrogen for 30 seconds at 40 psi higher than the reactor pressure. After all the reactors were quenched they were allowed to cool to about 60 °C. They were then vented and the tubes were

removed. The polymer samples were then dried in a centrifugal evaporator at 60 °C for 12 hours, weighed to determine polymer yield and submitted for IR (tBA incorporation) and GPC (molecular weight) analysis. NMR analysis were performed separately for microstructural analysis.

Original polymerization runs for ethylene/tBA copolymerization in high throughput parallel polymerization reactors (PPR)

Table S7.2. Ethylene/tBA copolymerization by in-situ mixture of **1** and aluminum additives (Original data for Table 1)

Entry[a]	Catalyst + n (equiv.) additive	[tBA]/[**1**]	Act. [b]	t (s)	Mw*10^{-3}	PDI	%Mol tBA	Tm (ºC)
1[c]	**1**	1000	659	2250	53.08	2.2	2.24	110
2[c]	**1**	1000	472	3601	53.98	2.2	1.99	111
3[c]	**1**	1000	514	3447	55.79	2.2	2.01	111
4[c]	**1** + 1 $Al(O^iPr)_3$	1000	954	1857	53.30	2.3	2.16	111
5[c]	**1** + 1 $Al(O^iPr)_3$	1000	981	1600	49.43	2.2	2.22	110
6[c]	**1** + 1 $Al(O^iPr)_3$	1000	923	1653	50.63	2.4	2.21	111
7[c]	**1** + 2 $Al(O^iPr)_3$	1000	977	1666	52.21	2.2	2.15	110
8[c]	**1** + 2 $Al(O^iPr)_3$	1000	1002	1480	52.23	2.3	2.11	111
9[c]	**1** + 2 $Al(O^iPr)_3$	1000	1037	1582	50.32	2.2	2.14	110
10[c]	**1** + 5 $Al(O^iPr)_3$	1000	1000	1569	50.05	2.3	2.16	110
11[c]	**1** + 5 $Al(O^iPr)_3$	1000	1015	1590	52.10	2.4	2.09	110
12[c]	**1** + 5 $Al(O^iPr)_3$	1000	1008	1628	51.42	2.4	2.32	110
13	**1** + 1 $Al(OEt)Et_2$	1000	476	3601	58.20	2.4	2.15	111
14[c]	**1** + 1 $Al(OEt)Et_2$	1000	500	3369	54.57	2.2	2.06	111
15[c]	**1** + 1 $Al(OEt)Et_2$	1000	458	3523	55.38	2.5	2.07	111
16	**1** + 2 $Al(OEt)Et_2$	1000	324	3601	52.64	2.2	2.27	110
17	**1** + 2 $Al(OEt)Et_2$	1000	272	3602	53.64	2.2	2.12	111
18	**1** + 2 $Al(OEt)Et_2$	1000	252	3601	51.56	2.3	2.27	110
19	**1** + 5 $Al(OEt)Et_2$	1000	108	3600	45.07	2.2	2.42	109
20	**1** + 5 $Al(OEt)Et_2$	1000	100	3601	47.13	2.2	2.27	110
21	**1** + 5 $Al(OEt)Et_2$	1000	84	3600	48.81	2.6	2.31	109
22	**1** + 1 $AlEt_3$	1000	<10	3601	N.D.	N.D.	N.D.	N.D.
23	**1** + 1 $AlEt_3$	1000	<10	3601	N.D.	N.D.	N.D.	N.D.
24	**1** + 1 $AlEt_3$	1000	<10	3601	N.D.	N.D.	N.D.	N.D.
25	**1**	2000	280	3600	34.59	2.3	4.54	99
26	**1**	2000	268	3601	35.04	2.4	5.01	94
27	**1** + 1 $Al(O^iPr)_3$	2000	514	3309	41.30	2.4	4.42	99
28	**1** + 1 $Al(O^iPr)_3$	2000	515	3494	38.24	2.3	4.69	100

[a]Unless specified, V(total) = 5 mL, [Ni] = 0.25 μmol, ethylene pressure = 400 psi, T = 90 ºC, toluene solvent, time = 1 h. [b]Act. = (kg/(mol·h)). [c]Polymerization runs were stopped when ethylene uptake reached 80.13 psi (<1 h).

Crystallographic Information

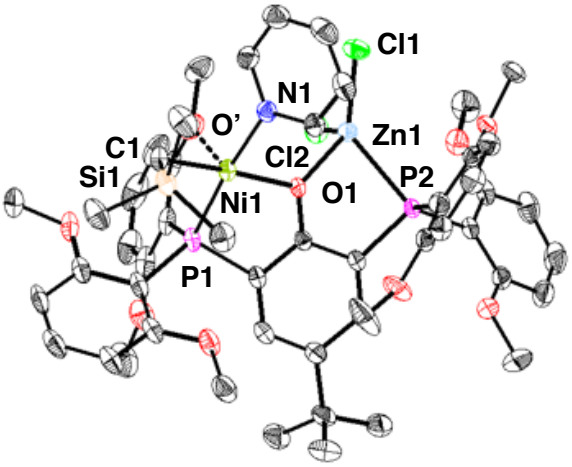

Figure S7.3. Solid-state structure of **2**. Ellipsoids are show at the 50% probability level. Hydrogen atoms and solvent molecules excluded for clarity.

Special Refinement Details for 2: Complex **2** crystalizes in a $P_{21/C}$ space group with the full molecule, half of a benzene molecule and two THF molecules in the asymmetric unit. A disordered THF molecule is observed and is refined isotropically to prevent NPDs.

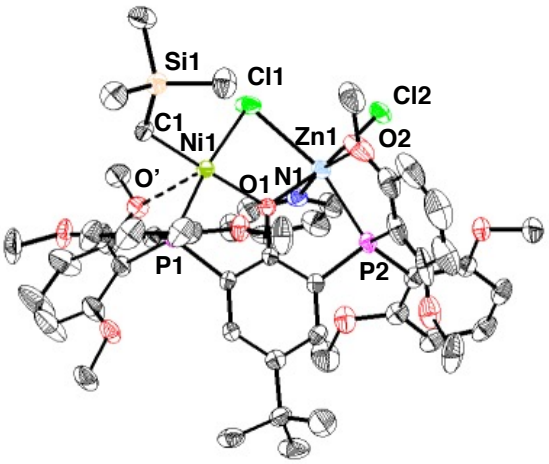

Figure S7.4. Solid-state structure of $\mathbf{2^{Cl}}$. Ellipsoids are show at the 50% probability level. Hydrogen atoms and solvent molecules excluded for clarity. Disordered dimethoxyphenyl and chlorides excluded for clarity.

Special Refinement Details for $\mathbf{2^{Cl}}$: Complex $\mathbf{2^{Cl}}$ crystalizes in a $P_{21/n}$ space group with the full molecule and one benzene molecule in the asymmetric unit. Two chlorides (Cl1 and Cl2) are modelled with two-site disorder with occupancies of 0.746 and 0.254. One of the dimethoxyphenyl group is also modelled with two-site disorder with occupancies of 0.746 and 0.254.

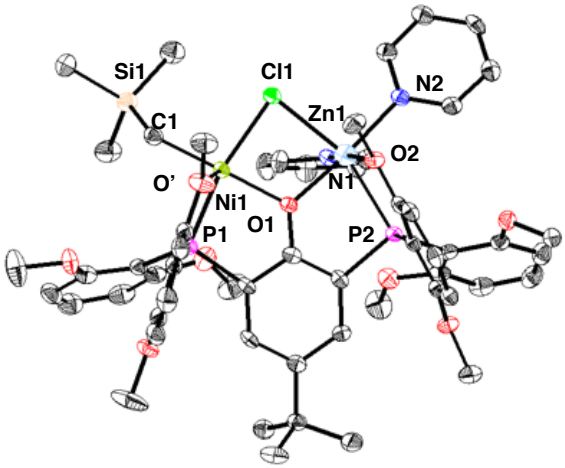

Figure S7.5. Solid-state structure of **2**$^{Cl+}$. Ellipsoids are show at the 50% probability level. Hydrogen atoms, solvent molecules, and the couterion excluded for clarity.

Special Refinement Details for 2^{Cl+}**:** Complex **2**$^{Cl+}$ crystalizes in a P-1 space group with the full molecule and one benzene molecule in the asymmetric unit.

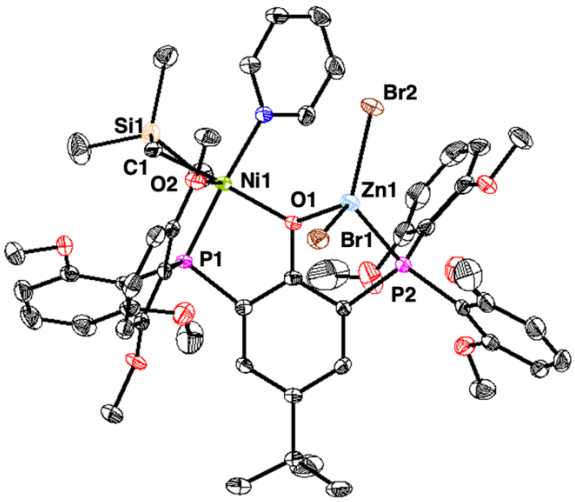

Figure S7.6. Solid-state structure of **3**. Ellipsoids are show at the 50% probability level. Hydrogen atoms and solvent molecules excluded for clarity.

Special Refinement Details for 2 Complex **3** crystalizes in a P-1 space group with the full molecule and one diethylether molecule in the asymmetric unit.

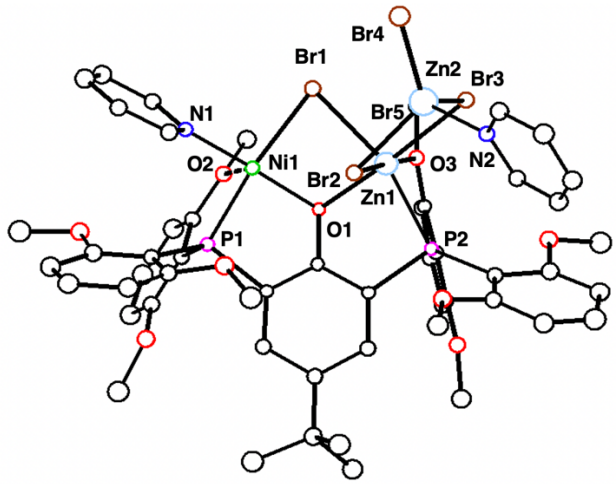

Figure S7.7. Solid-state structure of a bromide bridged Ni/Zn complex. Data quality is only sufficient for depicting the connectivity. Hydrogen atoms and solvent molecules excluded for clarity.

Table S7.3: Crystal and refinement data (part 1)

	2	**2^{Cl}**
Empirical formula	$C_{61.42}H_{79.99}Cl_2NNiO_{10.86}P_2SiZn$	$C_{57}H_{69}Cl_2NNiO_9P_2SiZn$
Formula weight	1290.98	1194.14
Temperature/K	100 K	100 K
Crystal system	Monoclinic	Monoclinic
Space group	$P_{21/C}$	$P_{21/n}$
a/Å	13.826(2)	12.897(3)
b/Å	17.674(2)	19.086(7)
c/Å	26.488(3)	23.021(6)
α/°	90	90
β/°	91.636(11)	90.746(16)
γ/°	90	90
Volume/Å^3	6470.2(15)	5666(3)
Z	4	4
ϱ_{calc}g/cm^3	1.325	1.403
μ/mm^{-1}	2.677	2.989
F(000)	2713	2504
Radiation	CuKα (λ = 1.54178)	CuKα (λ = 1.54178)
Reflections collected	136826	51336
Independent reflections	13826	11686
Goodness-of-fit on F^2	1.039	0.934
Final R indexes [I>=2σ (I)]	R_1 = 5.66 %	R_1 = 6.40 %
	R_2 = 15.73 %	R_2 = 17.76 %

Table S7.4: Crystal and refinement data (part 2)

	2^{Cl+}	**3**
Empirical formula	$C_{33.5}H_{39.5}Cl_{1.5}N_{1.5}Ni_{0.5}O_{4.50}PSi_{0.50}Zn$	$C_{55}H_{73}Br_2NNiO_{10}P_2SiZn$
Formula weight	745.80	1282.07
Temperature/K	100 K	100 K
Crystal system	Triclinic	Triclinic
Space group	P-1	P-1
a/Å	11.564(4)	12.358(13)
b/Å	13.159(3)	14.836(6)
c/Å	24.094(6)	17.474(11)
α/°	82.753(18)	93.63(2)
β/°	82.18(2)	99.68(3)
γ/°	74.389(16)	110.98(3)
Volume/Å^3	3482.9(16)	2922(4)
Z	4	2
ρ_{calc}g/cm^3	1.422	1.457
μ/mm^{-1}	3.581	3.668
F(000)	1548	1324
Radiation	CuKα (λ = 1.54178)	CuKα (λ = 1.54178)
Reflections collected	58754	92640
Independent reflections	13466	12436
Goodness-of-fit on F^2	1.084	1.495
Final R indexes [I>=2σ (I)]	R_1 = 6.38 %	R_1 = 3.83 %
	R_2 = 13.99 %	R_2 = 16.15 %

REFERENCES

(1) Franssen, N. M.; Reek, J. N.; de Bruin, B., Synthesis of functional 'polyolefins': state of the art and remaining challenges. *Chem. Soc. Rev.* **2013,** *42* (13), 5809-5832.

(2) Patrick, J. F.; Robb, M. J.; Sottos, N. R.; Moore, J. S.; White, S. R., Polymers with autonomous life-cycle control. *Nature* **2016,** *540* (7633), 363-370.

(3) Chen, C., Designing catalysts for olefin polymerization and copolymerization: beyond electronic and steric tuning. *Nat. Rev. Chem.* **2018,** *2* (5), 6-14.

(4) Zou, C.; Chen, C., Polar-functionalized, crosslinkable, self-healing, and photoresponsive polyolefins. *Angew. Chem. Int. Ed.* **2020,** *59* (1), 395-402.

(5) Baur, M.; Lin, F.; Morgen, T. O.; Odenwald, L.; Mecking, S., Polyethylene materials with in-chain ketones from nonalternating catalytic copolymerization. *Science* **2021,** *374* (6567), 604-607.

(6) Nakamura, A.; Ito, S.; Nozaki, K., Coordination− insertion copolymerization of fundamental polar monomers. *Chem. Rev.* **2009,** *109* (11), 5215-5244.

(7) Delferro, M.; Marks, T. J., Multinuclear olefin polymerization catalysts. *Chem. Rev.* **2011,** *111* (3), 2450-2485.

(8) Cai, Z.; Xiao, D.; Do, L. H., Cooperative Heterobimetallic Catalysts in Coordination Insertion Polymerization. *Comments Inorg. Chem.* **2019,** *39* (1), 27-50.

(9) Radlauer, M. R.; Day, M. W.; Agapie, T., Bimetallic effects on ethylene polymerization in the presence of amines: Inhibition of the deactivation by lewis bases. *J. Am. Chem. Soc.* **2012,** *134* (3), 1478-1481.

(10) Radlauer, M. R.; Buckley, A. K.; Henling, L. M.; Agapie, T., Bimetallic Coordination Insertion Polymerization of Unprotected Polar Monomers: Copolymerization of Amino Olefins and Ethylene by Dinickel Bisphenoxyiminato Catalysts. *J. Am. Chem. Soc.* **2013,** *135* (10), 3784-3787.

(11) Takano, S.; Takeuchi, D.; Osakada, K.; Akamatsu, N.; Shishido, A., Dipalladium catalyst for olefin polymerization: Introduction of acrylate units into the main chain of branched polyethylene. *Angew. Chem. Int. Ed.* **2014,** *53* (35), 9246-9250.

(12) Takeuchi, D.; Chiba, Y.; Takano, S.; Osakada, K., Double-Decker-Type Dinuclear Nickel Catalyst for Olefin Polymerization: Efficient Incorporation of Functional Co-monomers. *Angew. Chem. Int. Ed.* **2013,** *52* (48), 12536-12540.

(13) Chen, J.; Gao, Y.; Wang, B.; Lohr, T. L.; Marks, T. J., Scandium-Catalyzed Self-Assisted Polar Co-monomer Enchainment in Ethylene Polymerization. *Angew. Chem. Int. Ed.* **2017,** *56* (50), 15964-15968.

(14) Sampson, J.; Bruening, M.; Akhtar, M. N.; Jaseer, E. A.; Theravalappil, R.; Garcia, N.; Agapie, T., Copolymerization of Ethylene and Long-Chain Functional α-Olefins by Dinuclear Zirconium Catalysts. *Organometallics* **2021,** *40* (12), 1854-1858.

(15) Sujith, S.; Joe, D. J.; Na, S. J.; Park, Y.-W.; Chow, C.; Lee, B. Y., Ethylene/polar norbornene copolymerizations by bimetallic salicylaldimine-nickel catalysts. *Macromolecules* **2005,** *38* (24), 10027-10033.

(16) Takeuchi, D.; Chiba, Y.; Takano, S.; Kurihara, H.; Kobayashi, M.; Osakada, K., Ethylene polymerization catalyzed by dinickel complexes with a double-decker structure. *Polym. Chem* **2017,** *8* (34), 5112-5119.

(17) Takeuchi, D.; Iwasawa, T.; Osakada, K., Double-Decker-Type Dipalladium Catalysts for Copolymerization of Ethylene with Acrylic Anhydride. *Macromolecules* **2018,** *51* (14), 5048-5054.

(18) Chen, Z.; Yao, E.; Wang, J.; Gong, X.; Ma, Y., Ethylene (co) polymerization by binuclear nickel phenoxyiminato catalysts with cofacial orientation. *Macromolecules* **2016,** *49* (23), 8848-8854.

(19) Ji, G.; Chen, Z.; Wang, X.-Y.; Ning, X.-S.; Xu, C.-J.; Zhang, X.-M.; Tao, W.-J.; Li, J.-F.; Gao, Y.; Shen, Q., Direct copolymerization of ethylene with protic comonomers enabled by multinuclear Ni catalysts. *Nat. Commun.* **2021,** *12* (1), 1-9.

(20) Chen, S.-Y.; Pan, R.-C.; Liu, Y.; Lu, X.-B., Bulky o-Phenylene-Bridged Bimetallic α-Diimine Ni (II) and Pd

(II) Catalysts in Ethylene (Co) polymerization. *Organometallics* **2021,** *40* (22), 3703-3711.

(21) Suo, H.; Solan, G. A.; Ma, Y.; Sun, W.-H., Developments in compartmentalized bimetallic transition metal ethylene polymerization catalysts. *Coord. Chem. Rev.* **2018,** *372*, 101-116.

(22) Cheng, H.; Wang, H.; Li, Y.; Hu, Y.; Zhang, X.; Cai, Z., Structurally simple dinuclear nickel catalyzed olefin copolymerization with polar monomers. *J. Catal.* **2018,** *368*, 291-297.

(23) Cai, Z.; Do, L. H., Thermally Robust Heterobimetallic Palladium–Alkali Catalysts for Ethylene and Alkyl Acrylate Copolymerization. *Organometallics* **2018,** *37* (21), 3874-3882.

(24) Xiao, D.; Cai, Z.; Do, L. H., Accelerating ethylene polymerization using secondary metal ions in tetrahydrofuran. *Dalton Trans* **2019,** *48* (48), 17887-17897.

(25) Tahmouresilerd, B.; Xiao, D.; Do, L. H., Rigidifying Cation-Tunable Nickel Catalysts Increases Activity and Polar Monomer Incorporation in Ethylene and Methyl Acrylate Copolymerization. *Inorg. Chem.* **2021**.

(26) Chiu, H.-C.; Pearce, A. J.; Dunn, P. L.; Cramer, C. J.; Tonks, I. A., β-Oxo-δ-diimine Nickel Complexes: A Comparison of Tautomeric Active Species in Ethylene Polymerization Catalysis. *Organometallics* **2016,** *35* (12), 2076-2085.

(27) Chiu, H.-C.; Koley, A.; Dunn, P. L.; Hue, R. J.; Tonks, I. A., Ethylene polymerization catalyzed by bridging Ni/Zn heterobimetallics. *Dalton Trans* **2017,** *46* (17), 5513-5517.

(28) Smith, A. J.; Kalkman, E. D.; Gilbert, Z. W.; Tonks, I. A., ZnCl2 Capture Promotes Ethylene Polymerization by a Salicylaldiminato Ni Complex Bearing a Pendent 2, 2′-Bipyridine Group. *Organometallics* **2016,** *35* (15), 2429-2432.

(29) Tran, T. V.; Karas, L. J.; Wu, J. I.; Do, L. H., Elucidating secondary metal cation effects on nickel olefin polymerization catalysts. *ACS Catal.* **2020,** *10* (18), 10760-10772.

(30) Tran, T. V.; Nguyen, Y. H.; Do, L. H., Development of highly productive nickel–sodium phenoxyphosphine ethylene polymerization catalysts and their reaction temperature profiles. *Polym. Chem* **2019,** *10* (27), 3718-3721.

(31) Xiao, D.; Do, L. H., Triazolecarboxamidate Donors as Supporting Ligands for Nickel Olefin Polymerization Catalysts. *Organometallics* **2018,** *37* (2), 254-260.

(32) Xiao, D.; Do, L. H., In Situ Generated Heterometallic Nickel–Zinc Catalysts for Ethylene Polymerization. *Organometallics* **2018,** *37* (18), 3079-3085.

(33) Cai, Z.; Do, L. H., Customizing polyolefin morphology by selective pairing of alkali ions with nickel phenoxyimine-polyethylene glycol catalysts. *Organometallics* **2017,** *36* (24), 4691-4698.

(34) Cai, Z.; Xiao, D.; Do, L. H., Fine-tuning nickel phenoxyimine olefin polymerization catalysts: performance boosting by alkali cations. *J. Am. Chem. Soc.* **2015,** *137* (49), 15501-15510.

(35) Chen, Z.; Liu, W.; Daugulis, O.; Brookhart, M., Mechanistic studies of Pd (II)-catalyzed copolymerization of ethylene and vinylalkoxysilanes: Evidence for a β-silyl elimination chain transfer mechanism. *J. Am. Chem. Soc.* **2016,** *138* (49), 16120-16129.

(36) Rix, F. C.; Brookhart, M.; White, P. S., Mechanistic studies of the palladium (II)-catalyzed copolymerization of ethylene with carbon monoxide. *J. Am. Chem. Soc.* **1996,** *118* (20), 4746-4764.

(37) Mecking, S.; Johnson, L. K.; Wang, L.; Brookhart, M., Mechanistic studies of the palladium-catalyzed copolymerization of ethylene and α-olefins with methyl acrylate. *J. Am. Chem. Soc.* **1998,** *120* (5), 888-899.

(38) Berkefeld, A.; Drexler, M.; Möller, H. M.; Mecking, S., Mechanistic insights on the copolymerization of polar vinyl monomers with neutral Ni (II) catalysts. *J. Am. Chem. Soc.* **2009,** *131* (35), 12613-12622.

(39) Xiong, S.; Shoshani, M. M.; Zhang, X.; Spinney, H. A.; Nett, A. J.; Henderson, B. S.; Miller III, T. F.; Agapie, T., Efficient Copolymerization of Acrylate and Ethylene with Neutral P, O-Chelated Nickel Catalysts: Mechanistic Investigations of Monomer Insertion and Chelate Formation. *J. Am. Chem. Soc.* **2021,** *143* (17), 6516-6527.

(40) Shoshani, M. M.; Xiong, S.; Lawniczak, J. J.; Zhang, X.; Miller, T. F.; Agapie, T., Phosphine-Phenoxide Nickel Catalysts for Ethylene/Acrylate Copolymerization: Olefin Coordination and Complex Isomerization Studies Relevant to the Mechanism of Catalysis. *Organometallics* **2022**.

(41) Nakamura, A.; Anselment, T. M.; Claverie, J.; Goodall, B.; Jordan, R. F.; Mecking, S.; Rieger, B.; Sen, A.; Van Leeuwen, P. W.; Nozaki, K., Ortho-phosphinobenzenesulfonate: A superb ligand for palladium-catalyzed

coordination–insertion copolymerization of polar vinyl monomers. *Acc. Chem. Res.* **2013,** *46* (7), 1438-1449.

(42) Akita, S.; Nozaki, K., Copolymerization of ethylene and methyl acrylate by palladium catalysts bearing IzQO ligands containing methoxyethyl ether moieties and salt effects for polymerization. *Polymer Journal* **2021,** *53* (9), 1057-1060.

(43) Mu, H.; Pan, L.; Song, D.; Li, Y., Neutral nickel catalysts for olefin homo-and copolymerization: relationships between catalyst structures and catalytic properties. *Chem. Rev.* **2015,** *115* (22), 12091-12137.

(44) Xiong, S.; Hong, A.; Bailey, B. C.; Spinney, H. A.; Senecal, T. D.; Bailey, H.; Agapie, T., Highly Active and Thermally Robust Nickel Enolate Catalysts for the Synthesis of Ethylene-Acrylate Copolymers. *Angew. Chem. Int. Ed.* **2022**.

(45) Radlauer, M. R.; Day, M. W.; Agapie, T., Dinickel bisphenoxyiminato complexes for the polymerization of ethylene and α-olefins. *Organometallics* **2012,** *31* (6), 2231-2243.

(46) Xin, B. S.; Sato, N.; Tanna, A.; Oishi, Y.; Konishi, Y.; Shimizu, F., Nickel catalyzed copolymerization of ethylene and alkyl acrylates. *J. Am. Chem. Soc.* **2017,** *139* (10), 3611-3614.

(47) Zhang, Y.; Mu, H.; Pan, L.; Wang, X.; Li, Y., Robust bulky [P, O] neutral nickel catalysts for copolymerization of ethylene with polar vinyl monomers. *ACS Catal.* **2018,** *8* (7), 5963-5976.

(48) Zou, C.; Si, G.; Chen, C., A general strategy for heterogenizing olefin polymerization catalysts and the synthesis of polyolefins and composites. *Nat. Commun.* **2022,** *13* (1), 1-12.

(49) Tan, C.; Zou, C.; Chen, C., Material Properties of Functional Polyethylenes from Transition-Metal-Catalyzed Ethylene–Polar Monomer Copolymerization. *Macromolecules* **2022**.

(50) Talkowski, C. J., Ethylene-acid copolymer and ionomer blends having improved high temperature properties and processibility. Google Patents: 1996.

(51) Vaughn, W. L.; McKeand, J. T. J., Ionomers of ethylene/carboxylic acid copolymers. Google Patents: 1994.

(52) Zhang, L.; Brostowitz, N. R.; Cavicchi, K. A.; Weiss, R., Perspective: Ionomer research and applications. *Macromol. Rapid Commun.* **2014,** *8* (2), 81-99.

(53) Pangborn, A. B.; Giardello, M. A.; Grubbs, R. H.; Rosen, R. K.; Timmers, F. J., Safe and convenient procedure for solvent purification. *Organometallics* **1996,** *15* (5), 1518-1520.

(54) Neuwald, B.; Caporaso, L.; Cavallo, L.; Mecking, S., Concepts for stereoselective acrylate insertion. *J. Am. Chem. Soc.* **2013,** *135* (3), 1026-1036.

(55) Low, C. H.; Rosenberg, J. N.; Lopez, M. A.; Agapie, T., Oxidative coupling with Zr (IV) supported by a noninnocent anthracene-based ligand: Application to the catalytic cotrimerization of alkynes and nitriles to pyrimidines. *J. Am. Chem. Soc.* **2018,** *140* (38), 11906-11910.

(56) Palmer, W. N.; Zarate, C.; Chirik, P. J., Benzyltriboronates: building blocks for diastereoselective carbon–carbon bond formation. *J. Am. Chem. Soc.* **2017,** *139* (7), 2589-2592.

CHAPTER 8

Multimetallic Effects in Nickel-Catalyzed Ethylene/Acrylate Copolymerization

Chapter 8

CONTRIBUTIONS AND ACKNOWLEDGEMENTS

Shuoyan Xiong and Theodor Agapie conceived the presented idea. S.X. performed synthetic and mechanistic studies and polymer characterization and analyzed the catalysis data. Brad C. Bailey, Heather A. Spinney, and Briana S. Henderson performed polymerization studies and polymer characterization. S.X. wrote the chapter.

We are grateful to Dow for funding (T.A.). We thank Alex J. Nett and Todd D. Senecal for insightful discussions. We thank Hannah Bailey and Heidi Clements for GPC and tBA incorporation analysis. We thank Matthew R. Espinosa and Manar M. Shoshani for assistance with X-ray crystallography and David VanderVelde for assistance with NMR spectroscopy. Support has been provided for the X-ray diffraction and NMR instrumentation via the Dow Next Generation Educator Fund.

Chapter 8

ABSTRACT

Dinickel complexes (**X-Ni$_2$**) supported by a BINOL-based ligand (X) was reported for ethylene/acrylate copolymerization. Mechanistic studies revealed that monomer insertions on both Ni center are possible, while insertion into the second Ni center is slower than the first one. Further, two proximal phenoxide moieties in the framework allow for binding with Na cation with a 1:1 X-Ni$_2$:Na ratio. In ethylene/acrylate copolymerization, *in-situ* generated Ni$_2$Na species shows significant increase in activity but decrease in copolymer Mw and acrylate incorporation compared to X-Ni$_2$, which is consistent with results of mechanistic studies that Ni$_2$Na species features slower acrylate insertion and faster β-H elimination. Further, fast shuttling of Na cation between different complexes was observed, potentially allowing efficient synthesis of high Mw copolymers with high acrylate incorporation, or bimodal copolymers with good molecular level entanglement and minimal phase separation.

Chapter 8

GENERAL INTRODUCTION

Nature positions multiple metal centers in close proximity and proper orientation in many enzymes to achieve exceptional activity and selectivity.[1-3] Conceptually inspired by this, extensive efforts have been made toward developing abiotic multimetallic catalysts that exhibit similar beneficial properties.[3-9] Specifically, a variety of multimetallic catalysts have been developed for olefin (co)polymerization, CO_2/epoxide copolymerization, and lactide/lactone (co)polymerization, as catalyst efficiency and selectivity are also vital in these preparations.[9-20] Indeed, many examples show enhancements in catalyst activity, selectivity of monomer incorporation, polymer molecular weight (Mw) and microstructures compared to their mononuclear counterparts (Figure 8.1a).

In polymer synthesis, a significant challenge is coordination copolymerization of ethylene and polar monomers.[21-26] This copolymerization can provide value-added polyolefins with precisely controlled physical, mechanical properties and potential degradability.[25, 27-32] In this regard, a large number of transition metal catalysts have been developed for this preparation to date (Figure 8.1b).[26, 33-48] Among them, Ni catalysts are of special interest due to nickel's low oxophilicity and relative earth abundance.[26, 44, 49] Despite this progress, major issues exist in this preparation, including low catalyst activity, stability and copolymer Mw.[31, 50-63] This is generally credited to coordination of polar group to the metal center that outcompetes vinyl coordination, slows subsequent insertion and leads to catalyst deactivation.[42, 45, 64-73]

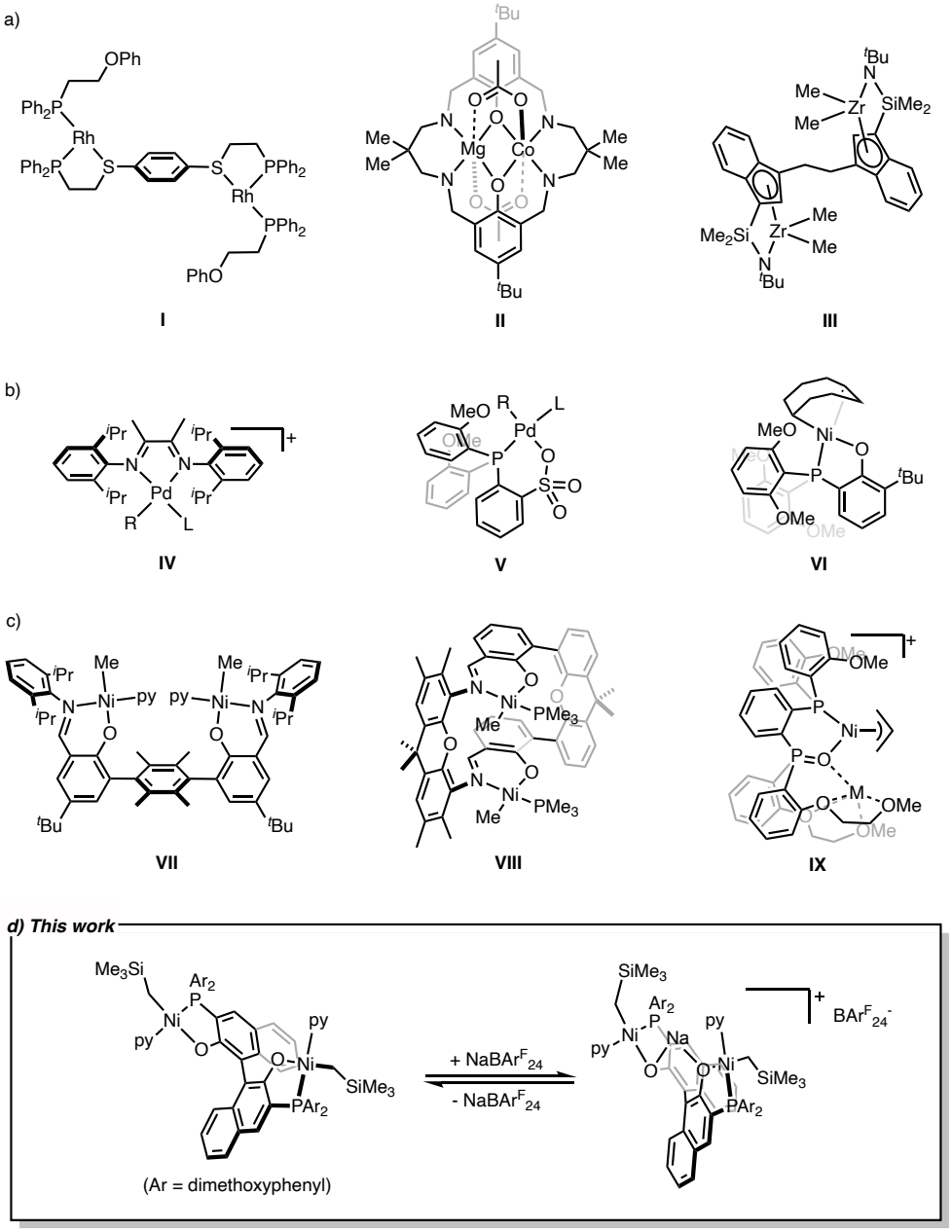

Figure 8.1. Examples of multimetallic polymerization catalysts (a), mononuclear (b) and multimetallic catalysts (c) for copolymerization of ethylene and polar monomers, and catalyst design in this work(d).

To address this, one strategy being of increasing interest is aforementioned catalyst design featuring multiple metal centers in close proximity, which have been proposed to disfavor aforementioned inhibitory coordination of polar groups.[9, 74] Ni-based

multimetallic complexes have thus been studied for the copolymerization of polar and nonpolar olefins, and the superiority of multimetallic catalysts over their monometallic analogues have been observed in some cases (Figure 8.1c).[51, 61, 75-90] Such favorable multimetallic effects have been explained by several mechanisms, such as metal-metal cooperativity or rigidity-induced inhibition of deactivation.[51, 74-76, 88] However, experimental mechanistic studies that support such rationale or elucidate the nature of monomer interactions with multimetallic catalysts or the role of each metal center in catalysis are far less frequently presented.

RESULTS AND DISCUSSION

Catalyst Design, Preparation and Characterization

In the design of a ligand for Ni-based multimetallic polymerization catalysts, a 1,1'-bi-2-naphthol moiety was chosen as a suitable backbone with restricted but still tunable rotations around the aryl-aryl bonds. In the presented work, two phosphine-phenoxide motifs were used as binding sites for nickel on naphthyl rings due to the reported polar group tolerance of P,O-Ni catalysts as well as the feasibility of experimental mechanistic studies with this type of single-component catalysts.[29, 35, 69, 91-96] Further, two proximal phenoxide moieties may act as binding sites for additional alkali metal cations, allowing further tuning of catalyst performance (Figure 8.1d).

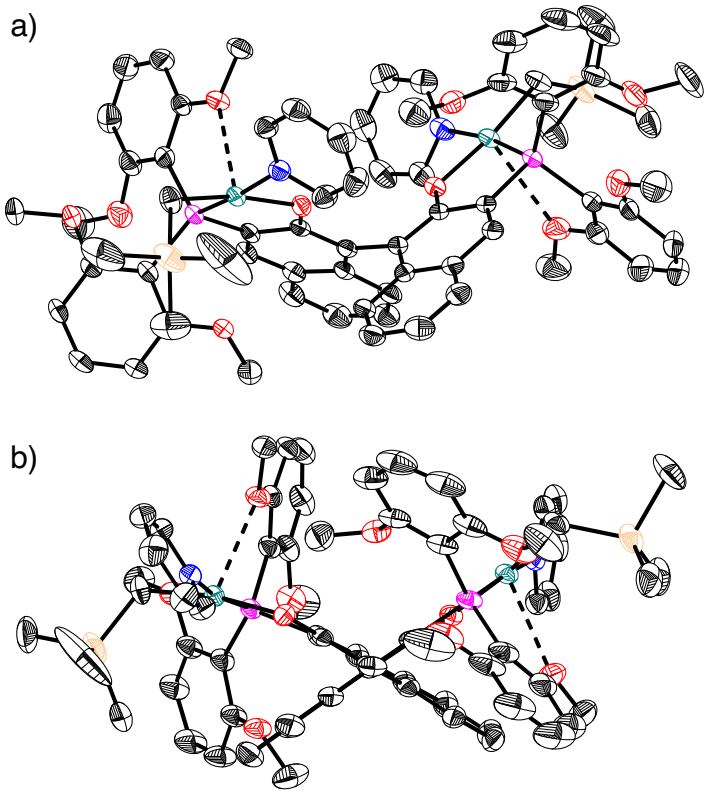

Figure 8.2. Solid-state structure of **X-Ni$_2$** in two views (Green: Ni, Pink: P, Blue: N, Red: O, orange: Si, black: C). Ellipsoids are shown in 50% probability. Hydrogen atoms and solvent molecules are excluded for clarity.

This ligand (**XH$_2$**) was synthesized by deprotonation of MOM-protected 1,1'-bi-2-naphthol with 2 equiv. of ^{n}BuLi, followed by addition of 2 equiv. of bis(dimethoxyphenyl)phosphine chloride and MOM deprotection. The nickel complex (**X-Ni$_2$**) was synthesized by reacting the dinaphthol with 2 equiv. of py$_2$Ni(CH$_2$SiMe$_3$)$_2$. Intermediates in which only 1 equiv. of Ni precursor reacts with **XH$_2$** was not observed. In ^{1}H NMR spectrum of **X-Ni$_2$**, the diasterotopic methylene (Ni-CH$_2$Si) signals are found at δ ~-0.6 and ~-1.0 ppm. Single-crystal X-ray diffraction (scXRD) further confirms the molecular structure of **X-Ni$_2$** (Figure 8.2). The distance between the two Ni centers is 7.727(1) A° and the dihedral angle between two naphthols

is 112~118°. The coordination environment around each Ni is similar to that in previous reported Ni phosphine phenoxide complexes. Notably, the distance between two phenoxide-O (4.275(3) Å) is significantly smaller than twice of the sum of van der Walls radius of Na and O atoms (~7.5 Å), implying further introduction of Na cation between two dinaphthols is possible (Figure 8.1d).

Na Binding Studies

0~2 equiv. of $NaBAr^F_{24}$ in THF was added to the C_6D_6 solution of X-Ni_2 and $^{31}P\{^1H\}$ spectra was employed to probe Na binding (Figure 8.3, and Figure S8.1-2). Addition of 0.25 equiv. of $NaBAr^F_{24}$ led to two broad resonances in $^{31}P\{^1H\}$ spectra with a ~3:1 ratio in 10 min. The major one (*A*) is close to the resonance of **X-Ni_2**. Two similar resonances with more significant line-broadening and a ~1:1 ratio was observed upon addition of 0.5 equiv. of $NaBAr^F_{24}$, implying faster shuttling of Na cation between different **X-Ni_2** molecules in this case. Notably, addition of 1 equiv. of $NaBAr^F_{24}$ led to disappearance of peak *A* and significant sharpening of peak *B*. Addition of excess $NaBAr^F_{24}$ (>1 equiv.) led to no change in chemical shifts and minimal changes in peak *B*'s broadness (Figure S8.2). Overall, the above scenario suggests fast binding of Na cation to **X-Ni_2** in a 1:1 ratio and *in-situ* generation of Ni_2Na species. Further, fast shuttling of Na cation exists between different **X-Ni_2** molecules may enable additional tuning of catalyst behavior.

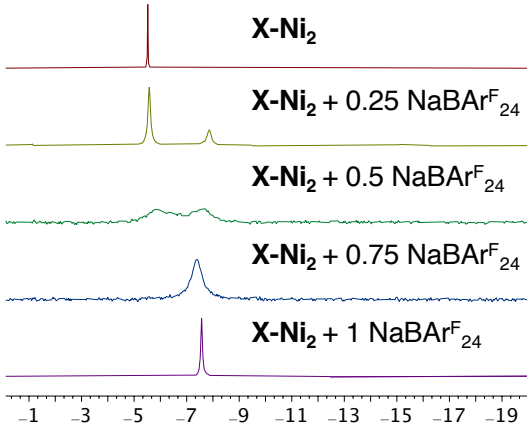

Figure 8.3. $^{31}P\{^{1}H\}$ NMR spectra of *in-situ* mixture of **X-Ni2** and 0~1 equiv. of $NaBAr^{F}_{24}$ (Referenced with an external standard, see Experimental section 3 for details).

Ethylene/Acrylate Copolymerization

Both **X-Ni$_2$** and *in-situ* generated Ni_2Na species are highly active in ethylene/acrylate copolymerization (Table 1). To the best of our knowledge, this represent first dinickel examples that are capable of copolymerizing ethylene and fundamental polar monomers with polar groups directly attach to the vinyl, allowing for further structure-performance studies. Increase in tBA concentration leads to increase in tBA incorporation and decrease in catalyst activity and copolymer Mw (Entry 1~3), consistent with the behavior of reported mononuclear Ni phosphine phenoxide catalysts.[35, 69, 91, 93-94] Notably, *in-situ* generated Ni_2Na species (**X-Ni$_2$** + 1 equiv. of $NaBAr^{F}_{24}$) features significantly increased activity and produced copolymers with decreased copolymer Mw and acrylate incorporation compared to **X-Ni$_2$** (Entry 1 vs 4, or 7 vs 8). Analysis of ethylene uptake curves of copolymerization reveals that both compounds remain highly active during catalysis and Ni_2Na species feature faster chain propagation compared to **X-Ni$_2$** (Figure S8.4). Addition of excess (>1 equiv.)

$NaBAr^F_{24}$ show minimal effect on ethylene copolymerization (Entry 4~6), consistent with 1:1 binding of Na cation with **X-Ni$_2$**. Compared to the difference observed in ethylene/acrylate copolymerization, addition of 1 equiv. of $NaBAr^F_{24}$ leads to a less significant increase in activity, but similar decrease in polymer Mw in ethylene polymerization (entry 9 vs 10). Overall, **X-Ni$_2$** and *in-situ* generated Ni_2Na species feature distinct performance in ethylene/acrylate copolymerization, while both are efficient catalysts for this preparation.

Table 8.1. Ethylene/acrylate copolymerization results.[a]

Entry	Catalyst	T_m/°C	[tBA][b]	Act. [c]	M_w[d]	PDI	%Mol tBA	T_m/°C
1	**X-Ni$_2$**	90	0.05	240	85.1	2.9	1.9	115
2	**X-Ni$_2$**	90	0.10	150	60.8	3.0	2.8	107
3	**X-Ni$_2$**	90	0.20	93	40.1	2.8	6.1	96
4	**X-Ni$_2$** + 1 $NaBAr^F_{24}$	90	0.05	820	31.7	2.6	0.7	120
5	**X-Ni$_2$** + 2 $NaBAr^F_{24}$	90	0.05	920	31.4	2.7	0.7	121
6	**X-Ni$_2$** + 5 $NaBAr^F_{24}$	90	0.05	870	33.9	2.4	0.8	120
7	**X-Ni$_2$**	110	0.05	170	53.2	3.7	2.0	115
8	**X-Ni$_2$** + 1 $NaBAr^F_{24}$	110	0.05	410	35.2	3.8	0.8	121
9[d]	**X-Ni$_2$**	90	0	$10*10^4$	31.2	4.9	-	128
10[d]	**X-Ni$_2$** + 1 $NaBAr^F_{24}$	90	0	$14*10^4$	10.7	4.3	-	122

[a] V = 5 mL, [Catalyst] = 0.05 mM, ethylene pressure = 400 psi, solvent: 95% toluene + 5% THF; each entry represents multiple replicated runs (see Experimental section S5 for detailed procedure). [b] Mol/L. [c] Activity in 1000 kg/(mol·h). [d] kg/mol.

Acrylate Insertion Studies

For catalysts featuring multiple metal centers in close proximity, one fascinating question is their role in catalysis. Based on catalyst structures and outcome in polymerization, it have been proposed that olefin insertion happens on multiple metal centers in some cases, while one or more metal center are inert from chain propagation in some other cases.[17, 51, 75-77, 82, 97-98] However, monomer insertion studies that directly reveals the nature of metal centers are far less presented. The dearth of multinickel examples promoting acrylate insertion is also notable. In this regard, the reactivity of **X-Ni$_2$** with tBA was studied. Addition of excess tBA leads to a color change from brown to dark red. Analysis of ^{1}H and ^{31}P{^{1}H} NMR confirms the consumption of tBA, disappearance of **X-Ni$_2$**, appearance of an intermdiate species featuring one -CH_2SiMe_3 group linked to Ni that disappears over time afterwards, and appearance of another species without the -CH_2SiMe_3 group (Experimental section 7). Resonances in the aromatic region indicate that pyridine coordination was observed in both new species, which are assigned to **X-NiNiCCO**, the intermediate mono-inserted species, and the latter is assigned to **X-(NiCCO)$_2$**, the double-inserted species (Figure 8.4).

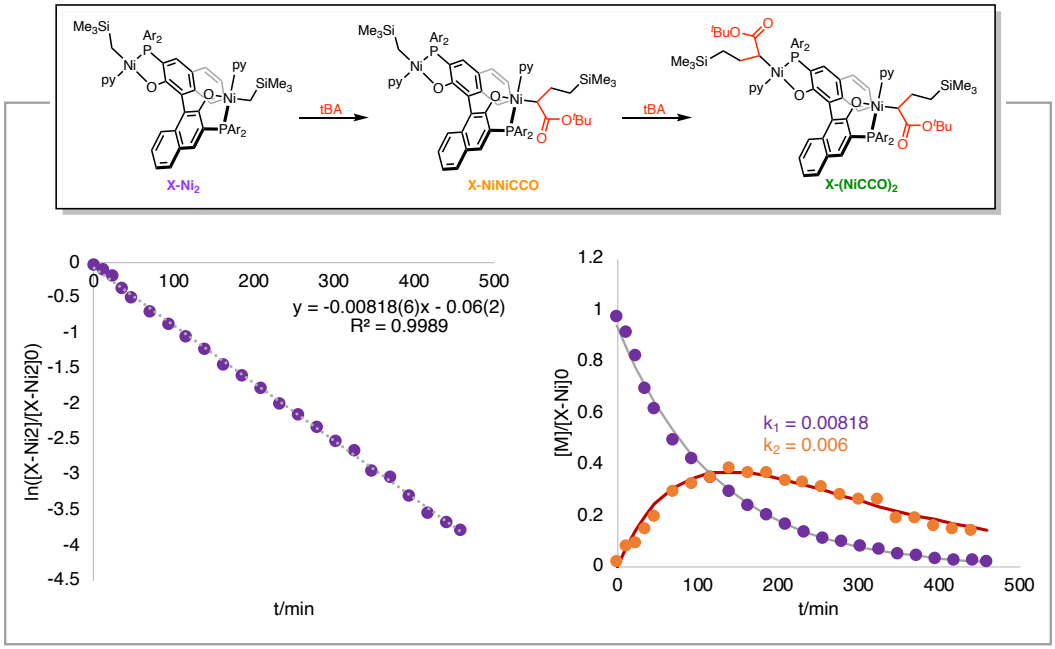

Figure 8.4. a) Insertion of tBA into **X-Ni₂**. b) Log plot of relative concentration of **X-Ni₂** vs time (Kinetics of the first insertion). c) Plot of relative concentration of **X-Ni₂** and **X-NiNiCCO** vs time and an approximation of second insertion kinetics with k_A/k_B = 1.364. (Condition: [**X-Ni₂**] = 0.01 M, [py] = 0.02 M, [tBA] = 0.5 M, solvent: C_6D_6, V(total) = 0.5 mL, T = 40 ºC).

Quantitative kinetic measurements were conducted with additional pyridine and a large excess of tBA (*Pseudo*-1st order conditions). A linear relationship was observed in the log plot of [**X-Ni₂**] over time (Figure 8.4d). Assuming tBA insertion into **X-Ni₂** follows the same mechanism as mononuclear Ni phosphine phenoxide complexes (d[Ni]/dt = (k_1*[tBA]/[py])*[Ni]),[69] the rate constant k_1 independant of pyridine and tBA concentrations was obtained (0.00037 min^{-1}). Under same assumptions, an estimation of k_2, rate constant of tBA insertion into X-NiNiCCO independant of pyridine and tBA concentrations, was achieved via non-linear approximation and a k_1/k_2 ratio of ~1.4 was obtained (Experimental section 8). This suggests that the first tBA

insertion into one Ni center, does affect the subsequent tBA insertion into another Ni center, though inhibitively.

Consistent with lower acrylate incorporation observed in copolymerization, acrylate insertion significantly slows upon addition of $NaBAr^{F}_{24}$ (Experimental section 9). It also notable that a new olefinic species was observed with resonances close to the internal olefin, t-butyl-4-(trimethylsilyl)-2-butenoate, discussed in chapter 6. This scenario indicates that $NaBAr^{F}_{24}$ also promote β-H elimination, consistent with the lower copolymer Mw comparing entry 1,2 vs 5,7 in table 1.

OUTLOOK

Efficient synthesis of polar functional polyolefin remains a significant challenge in polymer synthesis. Specifically, ethylene/acrylate copolymers are of high interest due to their wide applications. Despite extensive catalyst developments, a catalyst featuring high activity and ability to incorporate high levels of acrylate is still lacking. In this work, **X-Ni$_2$** is a moderately active catalyst produce high Mw copolymers with high acrylate incorporation, while *in-situ* generated Ni_2Na species are highly active catalyst with moderate Mw and acrylate incorporation. Fast exchange between these two species exists in solution, potentially occurring via Na shuttling. This phenomenon may provide a new strategy to address the above challenge. If copolymerization was conducted with **X-Ni$_2$** and <1 equiv. of $NaBAr^{F}_{24}$, two active species, **X-Ni$_2$** and *in-situ* generated Ni_2Na species, would present in catalysis, potentially allowing high

activity, copolymer Mw and acrylate incorporation together. Depending on the rate of the exchange, or Na shuttling, two type of copolymerization behaviors may be observed, while both are of interest. If Na shuttling is faster than growing of one polymer chain, then monodispersed ethylene/acrylate copolymers would be generated via a dynamic switched mechanism.[99] Under this scenario, generation of many polymer chains per catalyst is feasible together with chain growth control, which is not accessible with living copolymerization. A wide range of copolymers with different molecular weights and molecular distributions are also accessible. On the other hand, if Na shuttling is slower than growing of one polymer chain, bimodal copolymers would be produced. Nevertheless, this shuttling phenomenon may prevent cluttering of one species in solution and thus allow good molecular level entanglement and minimal phase separation in resulting copolymers.

CONCLUSION

In summary, dinickel complex (**X-Ni$_2$**) supported by a BINOL-based ligand (**X**) was reported for ethylene/acrylate copolymerization. In addition, two proximal phenoxide moieties in the framework allow binding with Na cation with a 1:1 X-Ni$_2$:Na ratio and consequent *in-situ* generation of a Ni$_2$Na species. **X-Ni$_2$** is moderately active in producing high Mw copolymers with high acrylate incorporation, while *in-situ* generated Ni$_2$Na species is highly active and produce copolymers with moderate Mw and acrylate incorporation, which is consistent with results of monomer insertion studies. Mechanistic studies also reveals that monomer insertions on both Ni center in

X-Ni$_2$ are possible, while insertion into the second Ni center is ~30% slower than the first one. The distinct copolymerization behaviors of **X-Ni$_2$** and *in-situ* generated Ni$_2$Na species are significant, especially given that they are both high-performance catalysts. Further, fast shuttling of Na cation between different complexes was observed, and thus efficient synthesis of high Mw copolymers with high acrylate incorporation, or bimodal copolymers with good molecular level entanglement and minimal phase separation may be feasible, depending on the rate of Na cation shuttling.

Chapter 8

EXPERIMENTAL SECTION

1 General Considerations

All air- and water-sensitive compounds were manipulated under N_2 or Ar using standard Schlenk or glovebox techniques. The solvents for air- and moisture-sensitive reactions were dried over sodium benzophenone/ketyl, calcium hydride, or by the method of Grubbs.[100] Deuterated solvents were purchased from Cambridge Isotopes Lab, Inc.; C_6D_6, was dried over a purple suspension with Na/benzophenone ketyl and vacuum transferred. t-Butyl acrylate was dried over 4 Å sieves for greater than 72h. (±)-1,1'-Bi-2-naphthol, 2.5 M ^{n}BuLi in hexanes were purchased from Sigma-Aldrich and used without further purification. Chloromethyl methyl ether solution,[101] 2,2'-Bis(methoxymethoxy)-1,1'-binaphthalene,[102] bis(dimethoxyphenyl)phosphine chloride,[103] and $py_2Ni(CH_2SiMe_3)_2$[104] were synthesized according to literature procedures. All ^{1}H, ^{13}C, and ^{31}P spectra of organic and organometallic compounds were recorded on Varian INOVA-400, or Bruker Cryoprobe 400 spectrometers. ^{1}H and ^{13}C chemical shifts are reported relative to residual solvent resonances.

2 Synthesis of Ligands and Transition Metal Complexes

Ligand ***BINOL-(POH)$_2$:*** A Schlenk flask fitted with a screw-in Teflon stopper was charged with a solution of 2,2'-bis(methoxymethoxy)-1,1'-binaphthalene (3.76 g, 10.0 mmol) in THF (40 mL) and cooled to -78 °C under nitrogen. A hexane solution of *n*-butyllithium (8.4 mL, 2.5 M, 21.0 mmol) was added dropwise via syringe. After stirring for an additional 30 min at -78 °C, the reaction was allow to warm up to 0 °C and stirred for an additional 4 h before cooled back to -78 °C. Next, a solution of bis(2,6-dimethoxyphenyl)phosphine chloride (6.82 g, 20.0 mmol) in THF (20 mL) was added dropwise via cannula. After complete addition, the reaction was allowed to warm up to room temperature and stirred for an additional 6 h, yielding a bright yellow solution. To this solution was added degassed MeOH (10 mL) and concentrated aqueous HCl (10 mL, degassed by three freeze-pump-thaw cycles with a liquid nitrogen bath prior to usage). After stirring for 12 h under room temperature, volatiles were removed under vacuum. In a N_2-filled glovebox (no exclusion of water), the resulting yellow residue was taken up in CH_2Cl_2 (20 mL), washed with saturated aqueous solutions of K_2CO_3 (3 x 10 mL) and NH_4Cl (3 x 10 mL), dried over $MgSO_4$, and filtered through Celite. The volatiles were removed under reduced pressure. In a glovebox (exclusion of water and oxygen), the resulting pale-yellow solid was dissolved in benzene and filtered through Celite. The volatile materials were removed once more under vacuum and the resulting mixture was washed by pentane (3 x 5 mL) and hexanes (3 x 5 mL) and the solid was collected via vacuum filtration, yielding **BINOL-(POH)$_2$** (3.80 g, 44% yield) as a yellow powder.

^{1}H NMR (400 MHz, C_6D_6): δ δ 8.33 (d, *J* = 9.7 Hz, 2H, ArH), 7.56 (d, *J* = 7.3 Hz, 2H, ArH), 7.33 (dd, *J* = 8.4, 1.2 Hz, 2H, ArH), 7.09-7.04 (m, 4H, ArH), 7.04 – 6.99 (m, 2H, ArH), 6.93 (ddd, *J* = 8.3, 6.8, 1.4 Hz, 2H, ArH), 6.60 (s, 2H, ArOH), 6.27 (dd, *J* = 2.8, 1.8 Hz, 4H, ArH),

6.25 (dd, *J* = 2.8, 1.8 Hz, 4H, ArH), 3.13 (s, 18H, -OCH_3); $^{13}C\{^1H\}$ NMR (101 MHz, C_6D_6): δ 162.96 (d, *J* = 8.6 Hz, 4C, ArC), 162.86 (d, *J* = 8.6 Hz, 4C, ArC), 155.51 (s, 1C, ArC), 155.42 (s, 1C, ArC), 134.98 (s, 2C, ArC), 134.27 (d, *J* = 27.9 Hz, 2C, ArC), 129.85 (d, *J* = 12.1 Hz, 4C, ArC), 134.61 (s, 2C, ArC), 129.47 (d, *J* = 2.8 Hz, 2C, ArC), 126.16 (s, 2C, ArC), 125.77 (s, 2C, ArC), 122.97 (s, 2C, ArC), 114.72 (d, *J* = 45.7 Hz, 2C, ArC), 114.02 (d, *J* = 48.0 Hz, 2C, ArC), 113.74 (s, 2C, ArC), 105.92 (d, *J* = 136.4 Hz, 2C, ArC), 104.85 (s, 4C, ArC), 104.67 (s, 4C, ArC), 55.74 (s, 12C, OCH_3), 55.62(s, 12C, OCH_3); $^{31}P\{^1H\}$ NMR (121 MHz, C_6D_6): δ -54.06 (s, 2P).

***BINOL-(PO-Ni)$_2$ (or X-Ni$_2$)*:** In the glove box, to a solution of $Py_2Ni(CH_2SiMe_3)_2$ (44 mg, 0.119 mmol) in benzene (4 ml) in a vial was added a solution of **BINOL-(POH)$_2$** (50.39 mg, 0.0563 mmol) in benzene (8 ml). The mixture was stirred for 2 h under room temperature, forming a red-brown solution. Volatile materials were removed under vacuum. The residue was extracted with pentane (3 x 5 mL), then washed by pentane (3 x 5 mL) and hexanes (3 x 5 mL) and the solid was collected via vacuum filtration, yielding the complex **X-Ni$_2$** (55 mg, 73%) as a brown solid.

^1H NMR (400 MHz, C_6D_6): δ 8.43 (dd, *J* = 4.8, 1.7 Hz, 4H, PhH), 8.31 (d, *J* = 12.0 Hz, 2H, PhH), 7.95 (dd, *J* = 8.6, 1.0 Hz, 2H, PhH), 7.74 (dd, *J* = 8.1, 1.5 Hz, 2H, PhH), 7.21 – 7.07 (m, 6H, PhH), 6.99 (ddd, *J* = 7.9, 6.5, 1.2 Hz, 2H, PhH), 6.60 – 6.52 (m, 2H, PhH), 6.34 (dd, *J* = 8.3, 3.5 Hz, 4H, PhH), 6.28 (dd, *J* = 8.3, 3.5 Hz, 4H, PhH), 6.17 (t, *J* = 7.0 Hz, 4H, PhH), 3.34 (s, 12H, -OCH_3), 3.19 (s, 12H, -OCH_3), -0.17 (s, 18H, -$Si(CH_3)_3$), -0.59 (t, *J* = 11.7 Hz, 2H, -C<u>H</u>H'$Si(CH_3)_3$), -0.96 (dd, *J* = 12.1, 7.0 Hz, 2H, -CH<u>H</u>'$Si(CH_3)_3$); $^{13}C\{^1H\}$ NMR (101 MHz, C_6D_6): δ 169.14 (d, *J* = 21.2 Hz, 4C, ArC), 162.02 (d, *J* = 29.5 Hz, 8C, ArC), 151.35 (s, 4C, ArC), 137.72 (s, 2C, ArC), 135.43 (s, 2C, ArC), 134.32 (d, *J* = 52.1 Hz, 2C, ArC), 130.46 (d, *J* = 38.3 Hz, 4C, ArC), 128.66 (d, *J* = 2.8 Hz, 2C, ArC), 128.49 (s, 2C, ArC), 127.94 (s, 2C, ArC), 126.47

(d, J = 8.3 Hz, 2C, ArC), 124.44 (s, 2C, ArC), 122.85 (s, 4C, ArC), 118.28 (s, 2C, ArC), 112.23 (d, J = 45.7 Hz, 2C, ArC), 111.60 (d, J = 48.0 Hz, 2C, ArC), 105.06 (d, J = 4.2 Hz, 4C, ArC), 104.81 (d, J = 4.2 Hz, 4C, ArC), 55.57 (s, 4C, OCH_3), 55.06 (s, 4C, OCH_3), 2.48 (s, 6C, $SiMe_3$), -18.73 (d, J = 30.0 Hz, 2C, $NiCH_2Si$); $^{31}P\{^1H\}$ NMR (121 MHz, C_6D_6): δ -5.52 (s, 2P).

3 Cation-Binding Studies

Procedures: 0.005 mmol of **X-Ni$_2$** prepared using the above procedure was dissolved in C_6D_6 (0.4 mL). To this solution was added a certain amount of THF solution of $NaBAr^F{}_{24}$ (0.05 M). The mixture was transferred to a J-Young tube with a capillary insert with $CDCl_3$ solution of $MePPh_3{}^+Br^-$ inside as an external standard. Spectra were collected every 10 min on a Bruker Cryoprobe 400 spectrometer until no further change was observed.

NMR spectra:

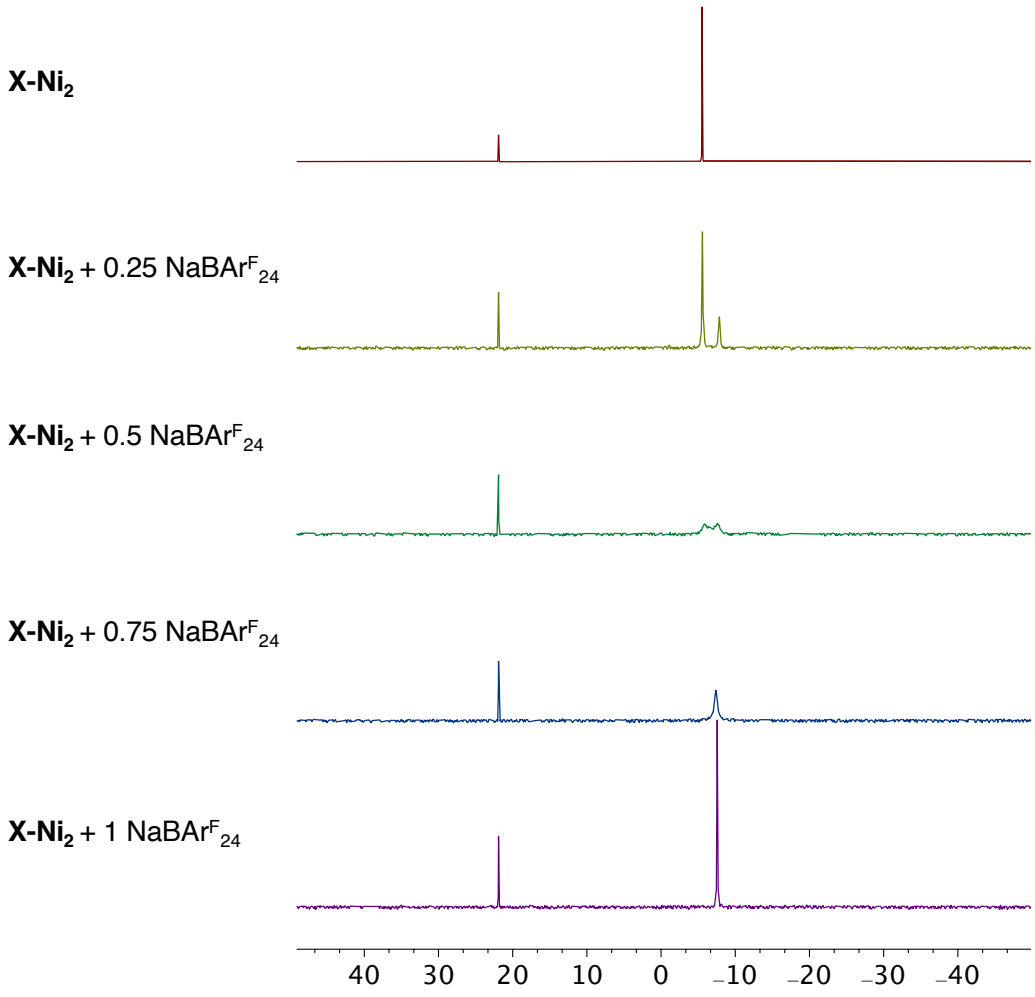

Figure S8.1. $^{31}P\{^{1}H\}$ NMR spectra of *in-situ* mixture of **X-Ni2** and 0~1 equiv. of $NaBAr^{F}_{24}$.

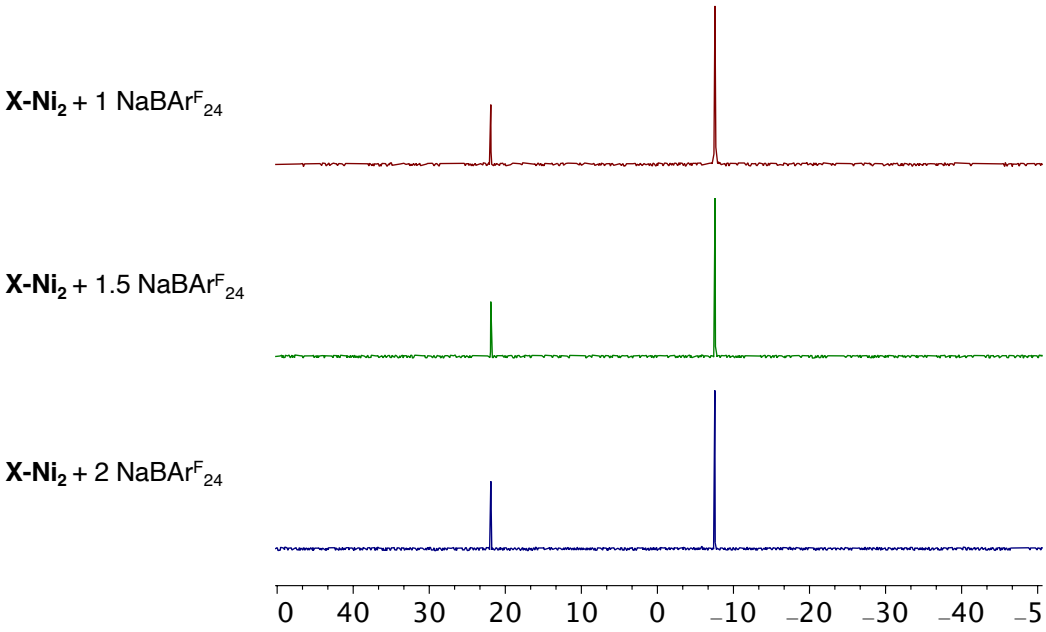

Figure S8.2. $^{31}P\{^{1}H\}$ NMR spectra of *in-situ* mixture of **X-Ni2** and 1~2 equiv. of $NaBAr^{F}_{24}$.

4 Crystallographic Information

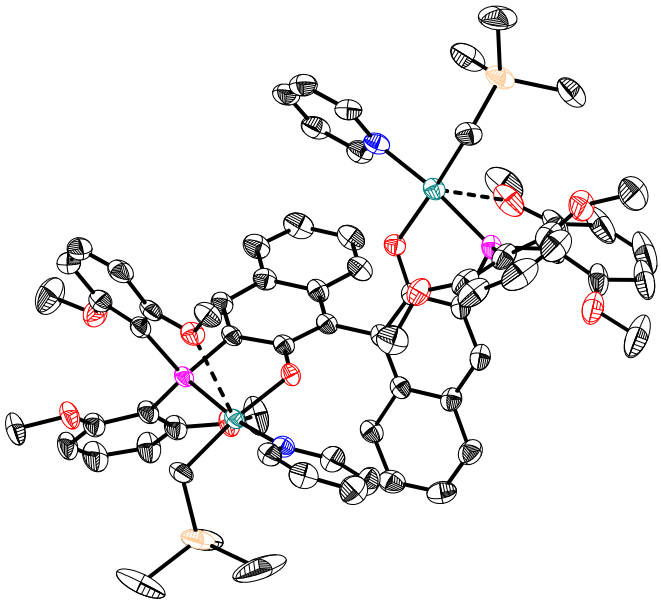

Figure S8.3. Solid-State Structure of **X-Ni$_2$** (Green: Ni, Pink: P, Blue: N, Red: O, orange: Si, black: C). Ellipsoids are show at the 50% probability level. Hydrogen atoms and solvent molecules excluded for clarity.

Special Refinement Details for X-Ni$_2$: Complex **X-Ni$_2$**. crystalizes in a P3$_2$21 space group with one full molecule in the asymmetric unit, as well as two and a half pentane molecules. A disorder was present in the one and a half pentane molecules and could not be modelled. The solvent mask (Olex® implementation of BYPASS/SQUEEZE) was used to suppress one section of electron density likely corresponding to these one and a half pentane molecules. The void was calculated to be near 542 electrons per unit cell, which would be close to one and a half pentane molecules per asymmetric unit (Z=8).

Crystallographic Information

Table S8.1. Crystal and refinement data for complexes **Ni0**, ^{R}**P*O^{Ar}-Ni**s, and ^{Ph}**P*O^{ArO}-Ni**.

	X-Ni$_2$
Empirical formula	$C_{70}H_{79}N_2O_{10}Si_2P_2Ni_2$
Formula weight	1343.89
Temperature/K	100 K
Crystal system	Trigonal
Space group	$P3_221$
a/Å	19.8368(14)
b/Å	19.8368(14)
c/Å	37.603(4)
α/°	90
β/°	90
γ/°	120
Volume/Å^3	12814(2)
Z	8
ρ_{calc}g/cm^3	1.393
μ/mm^{-1}	2.057
F(000)	5656
Radiation	CuKα (λ = 1.54178)
Reflections collected	248658
Independent reflections	16862
Goodness-of-fit on F^2	0.942
Final R indexes [I>=2σ (I)]	R_1 = 3.63%, R_2 = 10.89%

5 Procedures for Ethylene Homopolymerization and Ethylene/tBA Copolymerization

General procedure for high throughput parallel polymerization reactor (PPR) runs. Polyolefin catalysis screening was performed in a high throughput parallel polymerization reactor (PPR) system. The PPR system was comprised of an array of 48 single cell (6 x 8 matrix) reactors in an inert atmosphere glovebox. Each cell was equipped with a glass insert with an internal working liquid volume of approximately 5 mL. Each cell had independent controls for pressure and was continuously stirred at 800 rpm. Catalyst solutions (with $Ni(COD)_2$ if necessary) were prepared in toluene. All liquids (i.e., solvent, tBA, and catalyst solutions) were added via robotic syringes. Gaseous reagents (i.e., ethylene) were added via a gas injection port. Prior to each run, the reactors were heated to 50 °C, purged with ethylene, and vented.

All desired cells were injected with tBA followed with a portion of toluene (This step was skipped for ethylene homopolymerization). The reactors were heated to the run temperature and then pressured to the appropriate psig with ethylene. Catalyst solutions were then added to the cells. $NaBAr^{F}_{24}$ was then added as THF solution. Each catalyst addition was chased with a small amount of toluene so that after the final addition, a total reaction volume of 5 mL was reached (95% toluene + 5% THF). Upon addition of the catalyst, the PPR software began monitoring the pressure of each cell. The desired pressure (within approximately 2-6 psig) was maintained by the supplemental addition of ethylene gas by opening the valve at the set point minus 1 psi and closing it when the pressure reached 2 psi higher. All drops in pressure were cumulatively recorded as "Uptake" or "Conversion" of the ethylene for the duration of the run or until the uptake or conversion requested value was reached, whichever occurred first. Each reaction was then quenched by addition of 1% oxygen in nitrogen for 30 seconds at 40 psi higher than the reactor pressure. The pressure of each cell was monitored during and after

the quench to ensure that no further ethylene consumption happens. The shorter the "Quench Time" (the duration between catalyst addition and oxygen quench), the more active the catalyst. In order to prevent the formation of too much polymer in any given cell, the reaction was quenched upon reaching a predetermined uptake level of 80 psig. After all the reactors were quenched, they were allowed to cool to about 60 °C. They were then vented, and the tubes were removed. The polymer samples were then dried in a centrifugal evaporator at 60 °C for 12 hours, weighed to determine polymer yield and used in subsequent IR (tBA incorporation), GPC, DSC and NMR (copolymer microstructures) analysis.

Measurement of ethylene uptake curves. Upon addition of the catalyst, the PPR software began monitoring the pressure of each cell. The desired pressure (within approximately 2-6 psig) was maintained by the supplemental addition of ethylene gas by opening the valve at the set point minus 1 psi and closing it when the pressure reached 2 psi higher. For example, the pressure was maintained between approximately 399-402 psi if the original pressure was set to 400 psi. All drops in pressure were cumulatively recorded as "Uptake" or "Conversion" of the ethylene for the duration of the run. The unit of this "Uptake" is in psi and the uptake curves over time were used to analyze the real-time activity of catalysts and rates of chain propagation.

Procedure for gel permeation chromatography (GPC). High temperature GPC analysis was performed using a Dow Robot Assisted Delivery (RAD) system equipped with a Polymer Char infrared detector (IR5) and Agilent PLgel Mixed A columns. Decane (10 μL) was added to each sample for use as an internal flow marker. Samples were first diluted in 1,2,4-trichlorobenzene (TCB) stabilized with 300 ppm butylated hydroxyl toluene (BHT) at a concentration of 10 mg/mL and dissolved by stirring at 160°C for 120 minutes. Prior to injection the samples are further diluted with TCB stabilized with BHT to a concentration of 3 mg/mL. Samples (250 μL) are eluted through one PL-gel 20 μm (50 x 7.5 mm) guard column

followed by two PL-gel 20 μm (300 x 7.5 mm) Mixed-A columns maintained at 160 °C with TCB stabilized with BHT at a flowrate of 1.0 mL/min. The total run time was 24 minutes. To calibrate for molecular weight (MW) Agilent EasiCal polystyrene standards (PS-1 and PS-2) were diluted with 1.5 mL TCB stabilized with BHT and dissolved by stirring at 160 °C for 15 minutes. These standards are analyzed to create a 3rd order MW calibration curve. Molecular weight units are converted from polystyrene (PS) to polyethylene (PE) using a daily Q-factor calculated to be around 0.4 using the average of 5 Dowlex 2045 reference samples.

Procedure for Fourier-transform infrared spectroscopy (FTIR). The 10 mg/mL samples prepared for GPC analysis are also utilized to quantify tert-butyl acrylate (tBA) incorporation by Fourier Transform infrared spectroscopy (FTIR). A Dow robotic preparation station heated and stirred the samples at 160°C for 60 minutes then deposited 130 μL portions into stainless wells promoted on a silicon wafer. The TCB was evaporated off at 160°C under nitrogen purge. IR spectra were collected using a Nexus 6700 FT-IR equipped with a DTGS KBr detector from 4000-400 cm-1 utilizing 128 scans with a resolution of 4. Ratio of tBA (C=O: 1762-1704 cm−1) to ethylene (CH2: 736-709 cm−1) peak areas were calculated and fit to a linear calibration curve to determine total tBA.

Differential scanning calorimetry (DSC). Differential scanning calorimetry analyses was performed on solid polymer samples using a TA Instruments, Inc. Discovery Series or TA Instruments, Inc., DSC2500, programmed with the following method: Equilibrate at 175.00 °C; Isothermal for 3 minutes; Ramp 30.00 °C/min to 0.00 °C; Ramp 10.00 °C/min to 175.00 °C; Data was analyzed using TA Trios software.

NMR characterization. NMR spectra of ethylene/tBA copolymers were recorded on a Bruker 400 MHz using o-dichlorobenzene at 120 °C. ^{1}H NMR analysis of copolymers were done using a relaxation time (0.2 s), and an acquisition time (1.8 s) with the number of FID's

collected per sample (512). $^{13}C\{^{1}H\}$ NMR analysis of copolymers were done using 90° pulse of 17.2 μs, a relaxation time (22.0 s), an acquisition time (5.3 s), and inverse-gated decoupling with the number of FID's collected per sample (1536). Analysis of the spectra was based on literature.[35, 69]

6 Supplemental data for ethylene/tBA copolymerization

Ethylene uptake curves

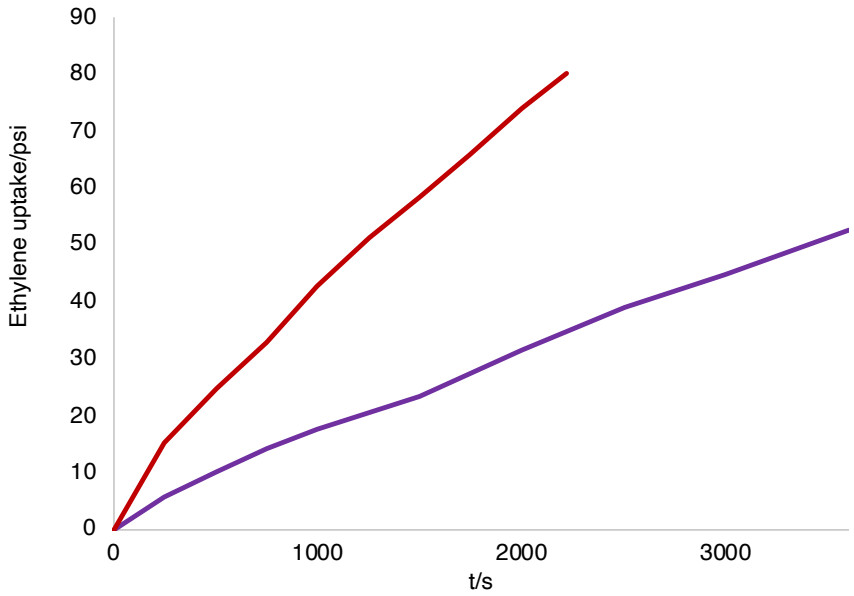

Figure S8.4. Ethylene uptake curves of ethylene/acrylate copolymerization by **X-Ni$_2$** and **X-Ni$_2$**+NaBAr$^F{}_{24}$ under otherwise identical conditions (V = 5 mL, [Catalyst] = 0.05 mM, ethylene pressure = 400 psi, solvent: 95% toluene + 5% THF).

7 Investigations of tBA insertion into X-Ni$_2$

Procedures: 0.005 mmol of **X-Ni$_2$** prepared using the above procedure was dissolved in C_6D_6 and transferred to a J-Young tube. The solution was frozen in the coldwell pre-cooled by a liquid nitrogen bath, and *t*-butyl acrylate (tBA) was added via syringe (Total volume=0.50 ml). The resulting mixture was warmed up to thawing temperature and shaken vigorously prior to transferring to pre-heated NMR probe for acquisition of spectra at 25 ºC. NMR monitoring of tBA insertion were performed by monitoring the ^{1}H and ^{31}P{^{1}H} NMR.

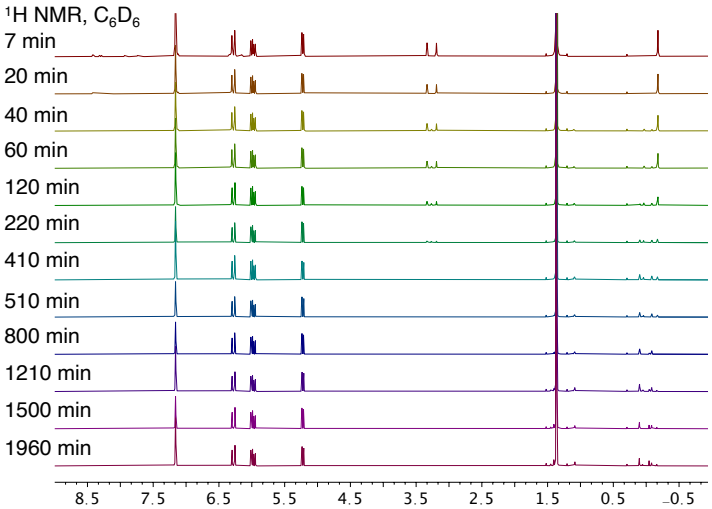

Figure S8.5. ^{1}H NMR monitoring of reaction of tBA with **X-Ni$_2$** (Condition: [**X-Ni$_2$**] = 0.01 M, [tBA] = 0.4 M, solvent: C_6D_6, V(total) = 0.5 mL, T = 25 ºC).

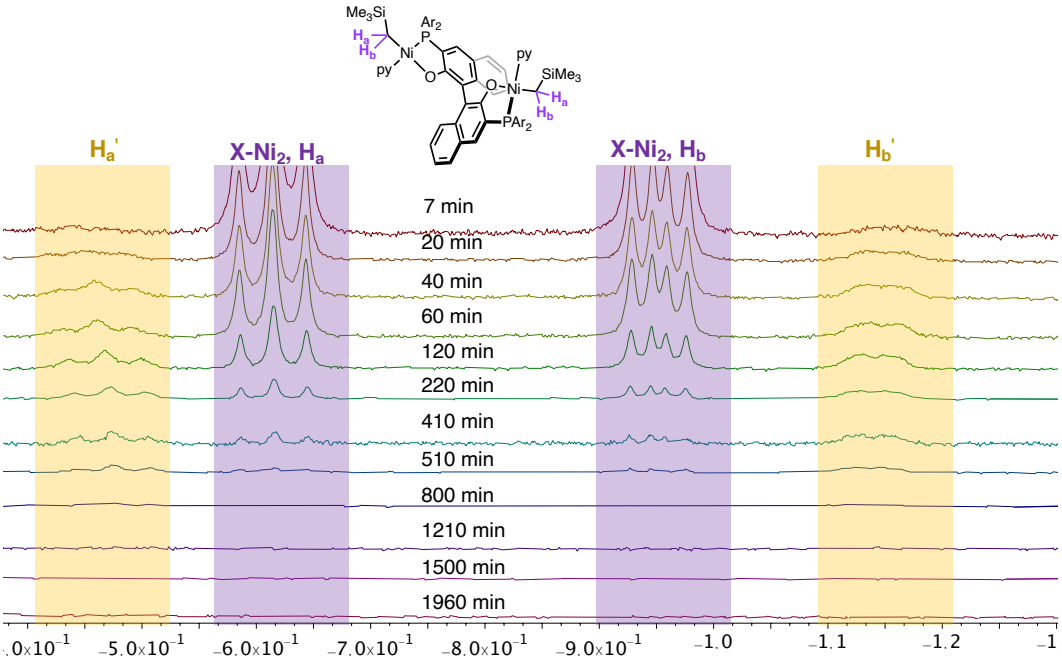

Figure S8.6. ^{1}H NMR monitoring of reaction of tBA with **X-Ni$_2$** (-NiCH$_2$Si- region, purple: **X-Ni$_2$**, yellow: new species, Condition: [**X-Ni$_2$**] = 0.01 M, [tBA] = 0.4 M, solvent: C_6D_6, V(total) = 0.5 mL, T = 25 ºC).

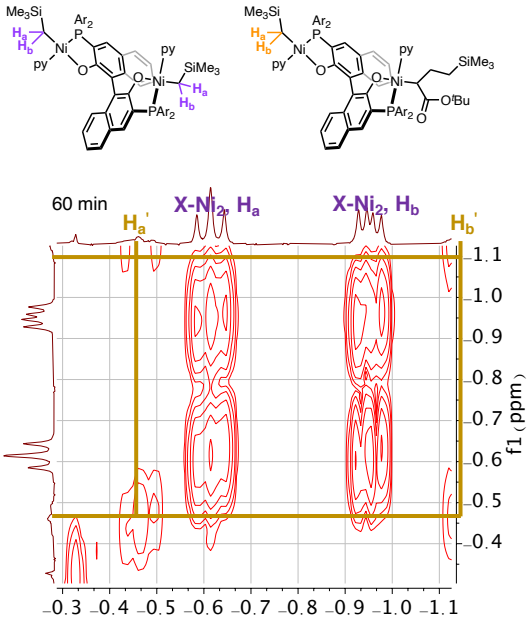

Figure S8.7. ^{1}H-^{1}H COSY NMR spectrum of -NiCH$_2$= Si- region (t 60 min). (Condition: [**X-Ni$_2$**] = 0.01 M, [tBA] = 0.4 M, solvent: C_6D_6, V(total) = 0.5 mL, T = 25 ºC).

As shown above, two new resonances appeared and disappeared overtime in the region of $NiCH_2SiR_3$ species. Based on this as well as the ^1H-^1H COSY NMR, these two resonances are tentatively assigned to monoinserted species, **X-NiNiCCO**. The disappearance of all $NiCH_2SiR_3$ species at the end implies that tBA inserts into both nickel centers in X-Ni_2.

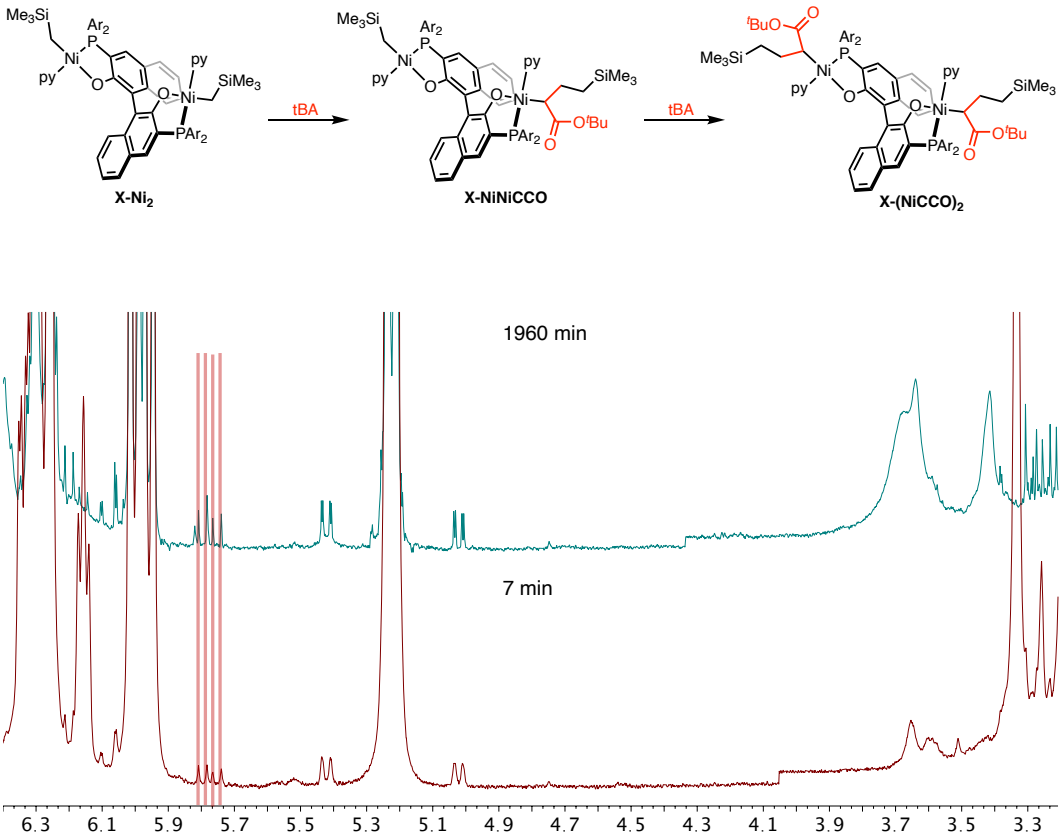

Figure S8.8. ^1H NMR spectrum of olefinic region (No appearance of new olefinic species). (Condition: [**X-Ni$_2$**] = 0.01 M, [tBA] = 0.4 M, solvent: C_6D_6, V(total) = 0.5 mL, T = 25 ºC).

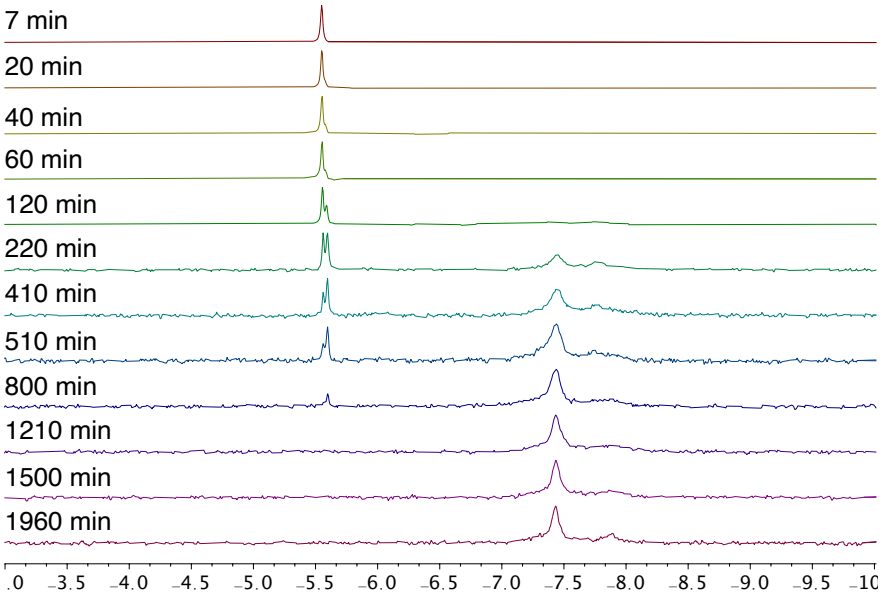

Figure S8.9. $^{31}P\{^{1}H\}$ NMR monitoring of reaction of tBA with **X-Ni$_2$**. (Condition: [**X-Ni$_2$**] = 0.01 M, [tBA] = 0.4 M, solvent: C_6D_6, V(total) = 0.5 mL, T = 25 ºC).

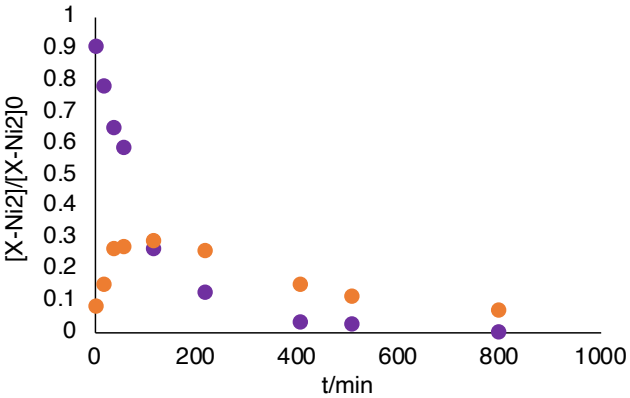

Figure S8.10. Plot of relative concentration of **X-Ni$_2$** (purple), and **X-NiNiCCO** (orange) vs time (Condition: [**X-Ni$_2$**] = 0.01 M, [tBA] = 0.4 M, solvent: C_6D_6, V(total) = 0.5 mL, T = 25 ºC).

8 Kinetic studies of tBA insertion into X-Ni$_2$

Procedures: 0.005 mmol of **X-Ni$_2$** prepared using the above procedure was dissolved in a C_6D_6 solution of pyridine (2 equiv.) and transferred to a J-Young tube. The solution was frozen in the coldwell pre-cooled by a liquid nitrogen bath, and 50 equiv. of *t*-butyl acrylate (tBA) was added via syringe (Total volume=0.50 ml). The resulting mixture was warmed up to thawing temperature and shaken vigorously prior to transferring to pre-heated NMR probe for acquisition of spectra at 40 ºC. NMR monitoring of tBA insertion were performed by monitoring ^{1}H NMR spectra.

Note: a large excess of tBA and a small amount of pyridine were added to make sure their concentrations remain similar during monitoring (*pseudo*-1st order conditions).

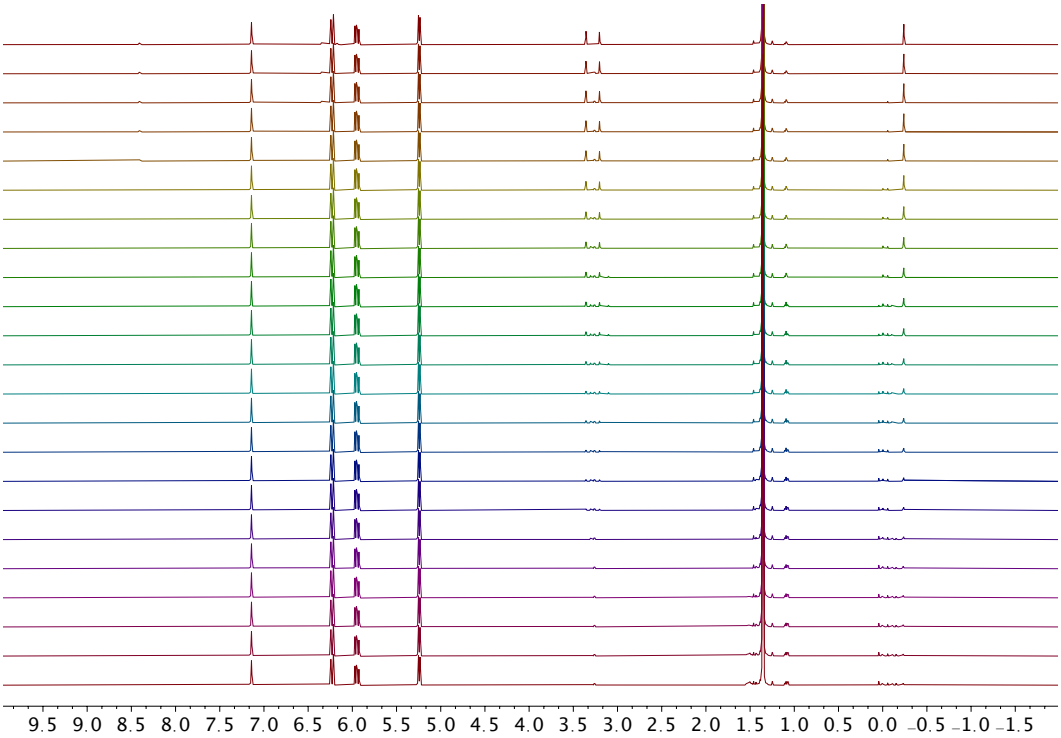

Figure S8.11. ^{31}P{^{1}H} NMR monitoring of reaction of tBA with **X-Ni$_2$**. Top five: spectra were collected every ~696s (11.6 min). Others: spectra were collected every ~1392s (23.2 min) (Condition: [**X-Ni$_2$**] = 0.01 M, [py] = 0.02 M, [tBA] = 0.5 M, solvent: C_6D_6, V(total) = 0.5 mL, T = 40 ºC)

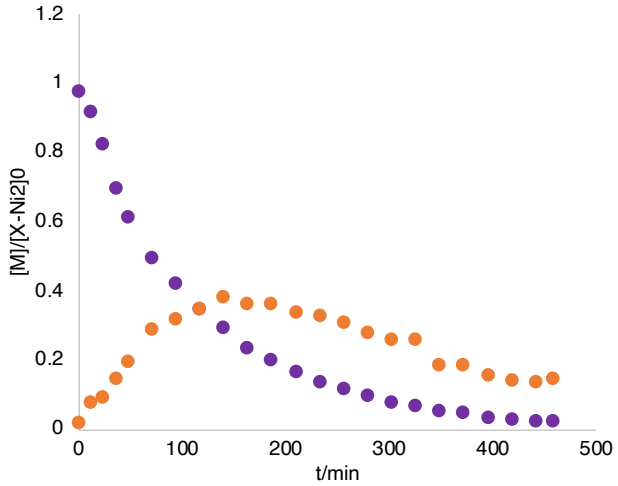

Figure S8.12. Plot of relative concentration of **X-Ni$_2$** (purple), and **X-NiNiCCO** (orange) vs time (Condition: [**X-Ni$_2$**] = 0.01 M, [py] = 0.02 M, [tBA] = 0.5 M, solvent: C_6D_6, V(total) = 0.5 mL, T = 40 ºC).

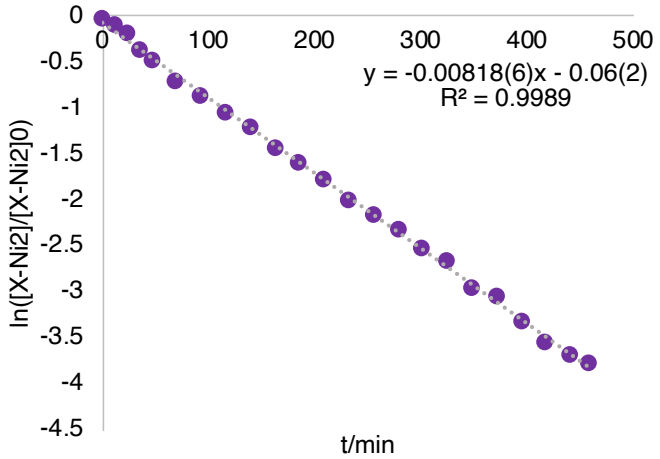

Figure S8.13. Log plot of relative concentration of **X-Ni$_2$** vs time. (Condition: [**X-Ni$_2$**] = 0.01 M, [py] = 0.02 M, [tBA] = 0.5 M, solvent: C_6D_6, V(total) = 0.5 mL, T = 40 ºC)

Assuming tBA insertion into X-Ni$_2$ follows a mechanism similar to that of mononuclear Ni phosphine phenoxide complexes (d[Ni]/dt = (k_1*[tBA]/[py])*[Ni], *the rate constant k_1 independent of pyridine and tBA concentrations* can be obtained (0.00037 min^{-1}).

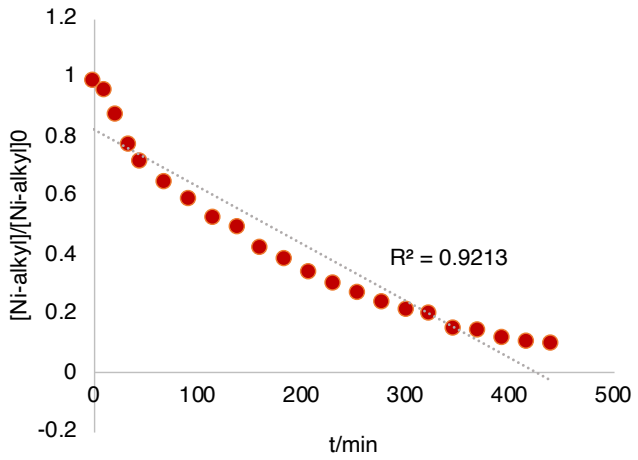

Figure S8.14. Log plot of relative concentration of nickel alkyls vs time (Note: each of **X-Ni$_2$** counts two alkyls and each **X-NiNiCCO** counts one alkyl. Condition: [**X-Ni$_2$**] = 0.01 M, [py] = 0.02 M, [tBA] = 0.5 M, solvent: C_6D_6, V(total) = 0.5 mL, T = 40 °C).

The decay of **[X-Ni$_2$]** follows a first order kinetics why the decay of nickel alkyls overall does not, indicates a difference in rates of first tBA insertion (tBA insertion into **X-Ni$_2$**) and second tBA insertion (tBA insertion into **X-NiNiCCOX-Ni$_2$**).

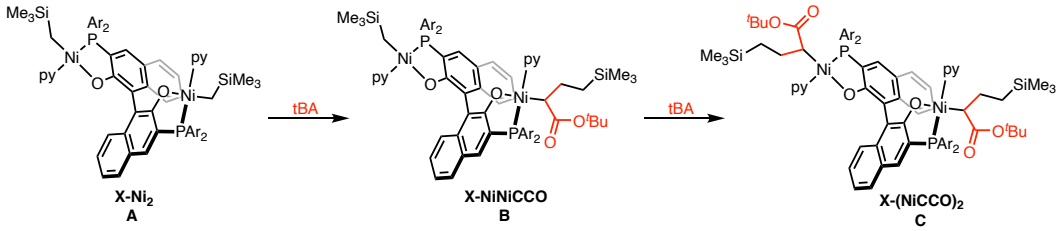

[**A**]=[**X-Ni$_2$**]/[**X-Ni$_2$**]$_0$

[**B**]=[**X-NiNiCCO**]/[**X-Ni$_2$**]$_0$

As shown above, concentration of [**A**] and [**B**] over time can be obtained from NMR monitoring, which allows determination of rate constant of first insertion (shown above) and estimation of rate constant of second insertion (shown below).

Based on figure S8.10, ln([**A**]) = -0.00818*t-0.06, [**A**]=[**X-Ni$_2$**]/[**X-Ni$_2$**]$_0$, k_a = 0.00818

Thus

$$[\mathbf{A}]_{cal} = e^{-0.00818t-0.06} \quad (1)$$

$$\frac{d[B]}{dt} = 0.00818t \cdot [A] - k_B \cdot [B] \quad \text{(ii)}$$

$$[B]_{cal} = \sum_{i=1}^{m} \left(\frac{d[B]}{dt}\right)_{t=t(i)} * ((t(i)-t(i-1))$$

$$= \sum_{i=1}^{m} (0.00818t \cdot [A]_{cal,t=t(i)} - k_2 \cdot [B]_{exp,t=t(i)}) * ((t(i)-t(i-1)) \quad \text{(iii)}$$

$[A]_{cal,t=t(i)}$ can be obtained from (i) and $[B]_{exp,t=t(i)}$ can be obtained from NMR monitoring. A set of $[B]_{cal}$ can be obtained based on a given number of k_2 ($k_{2\text{-}est}$). By minimizing the derivation between $[B]_{exp}$ and $[B]_{cal}$, k_2 may be solved.

Below shown $[B]_{cal}$ curves with k_A/k_B=1, 1.25, 1.5 and 1.75:

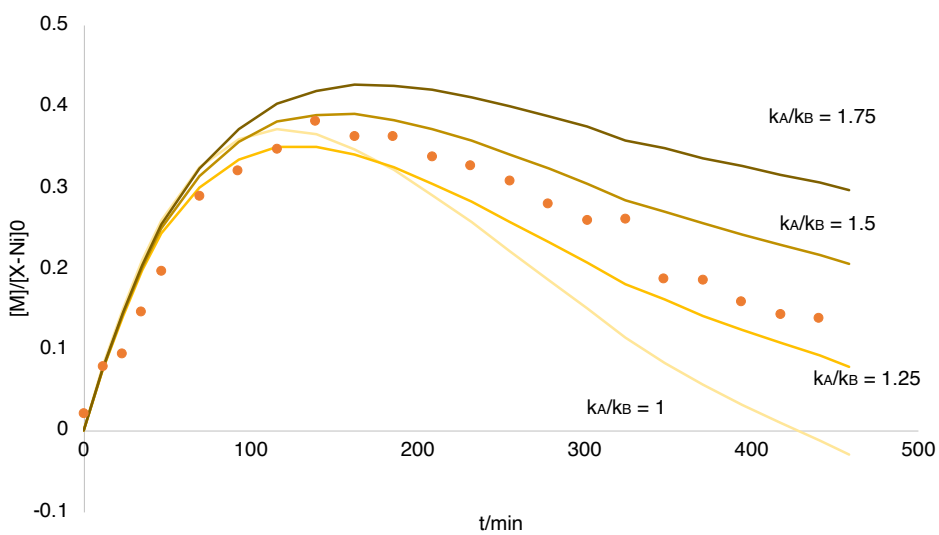

Figure S8.15. Plot of relative concentration **X-NiNiCCO** vs time and four sets of approximation with different k_A/k_B values (Condition: [**X-Ni$_2$**] = 0.01 M, [py] = 0.02 M, [tBA] = 0.5 M, solvent: C_6D_6, V(total) = 0.5 mL, T = 40 ºC).

Based on figure S8.12, k_A/k_B is between 1.25 and 1.50. By minimizing the SSR of $[B]_{exp}$ and $[B]_{cal}$ ($([B]_{exp}-[B]_{cal})^2$), an estimated value of k_A/k_B can be obtained (1.364). Assuming tBA insertion into **X-NiNiCCO** follows a mechanism similar to that of mononuclear Ni phosphine phenoxide complexes (d[Ni]/dt = (k*[tBA]/[py])*[Ni], *the rate constant k_2 independent of pyridine and tBA concentration* can be obtained ($k_B = k_2$*[tBA]/[py], k_2=0.00027 min^{-1}).

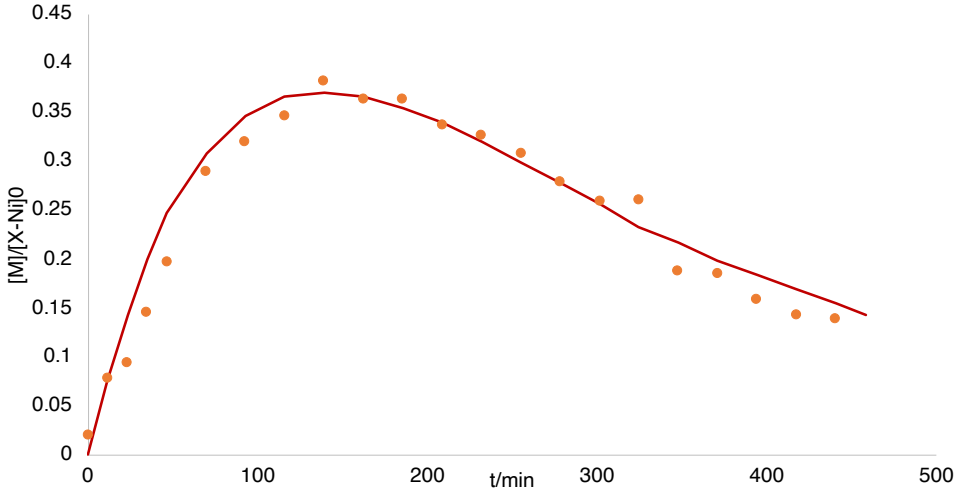

Figure S8.16. Plot of relative concentration **X-NiNiCCO** vs time an approximation with k_A/k_B = 1.364. (Condition: [**X-Ni$_2$**] = 0.01 M, [py] = 0.02 M, [tBA] = 0.5 M, solvent: C_6D_6, V(total) = 0.5 mL, T = 40 °C).

9 Investigations of tBA insertion into in-situ generated Ni_2Na species

Procedures: 0.005 mmol of **X-Ni$_2$** prepared using the above procedure was dissolved in of C_6D_6. To this solution was added THF solution (0.05 mL) of $NaBAr^F{}_{24}$ (1 equiv.). The mixture was transferred to a J-Young tube and frozen in the coldwell pre-cooled by a liquid nitrogen bath. *t*-Butyl acrylate (tBA) was added via syringe (Total volume=0.50 ml). The resulting mixture was warmed up to thawing temperature and shaken vigorously prior to transferring to pre-heated NMR probe for acquisition of spectra at 25 ºC. NMR monitoring of tBA insertion were performed by monitoring the ^{1}H and ^{31}P{^{1}H} NMR.

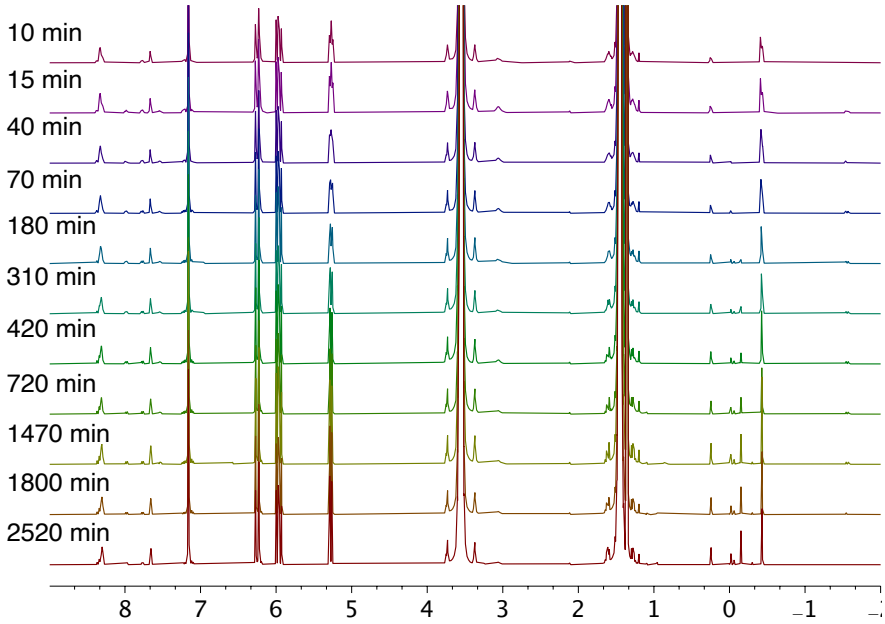

Figure S8.17. ^{1}H NMR monitoring of reaction of tBA with *in-situ* generated Ni_2Na species. (Condition: [**X-Ni$_2$**] = 0.01 M, [tBA] = 0.4 M, solvent: 10% THF-H8/90% C_6D_6, V(total) = 0.5 mL, T = 25 ºC).

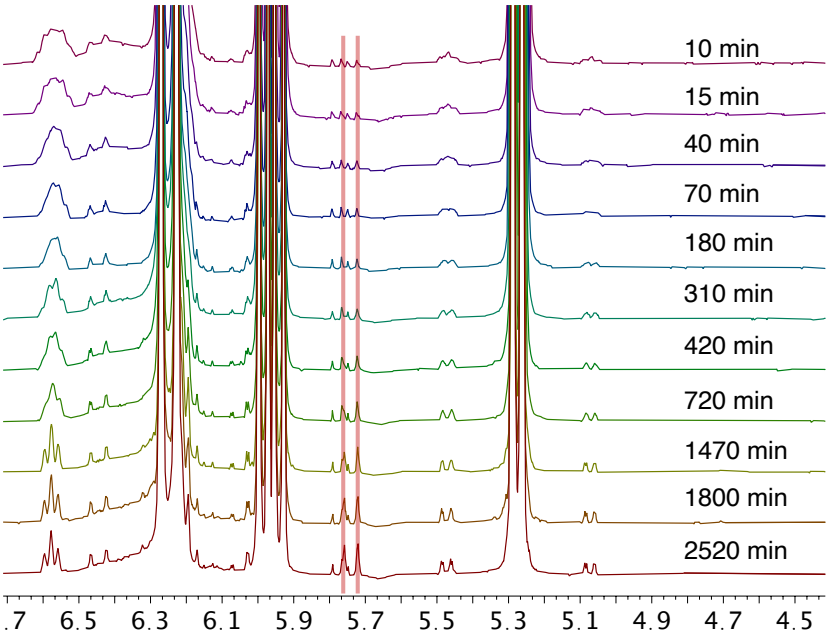

Figure S8.18. ^{1}H NMR monitoring of reaction of tBA with *in-situ* generated Ni_2Na species (Olefinic region, appearance of one new olefinic resonance, Condition: [**X-Ni$_2$**] = 0.01 M, [tBA] = 0.4 M, solvent: 10% THF-H8/90% C_6D_6, V(total) = 0.5 mL, T = 25 ºC).

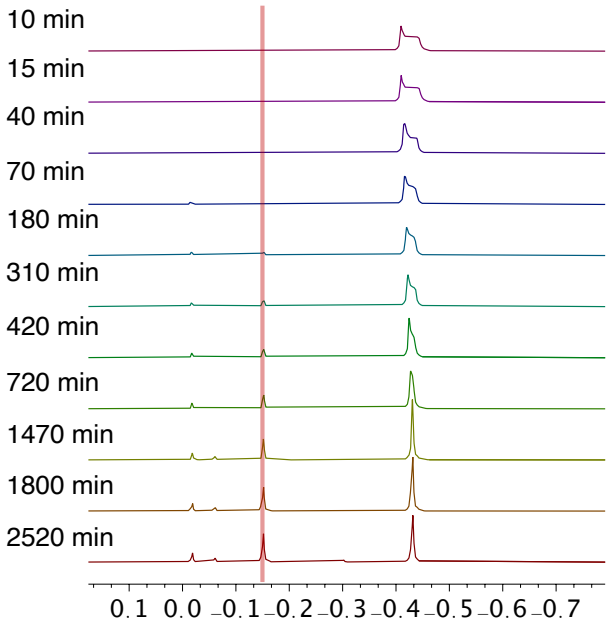

Figure S8.19. ^{1}H NMR monitoring of reaction of tBA with *in-situ* generated Ni_2Na species (-SiR_3 region, appearance of two new $SiMe_3$ resonance with one labelled in red, Condition: [**X-Ni$_2$**] = 0.01 M, [tBA] = 0.4 M, solvent: 10% THF-H8/90% C_6D_6, V(total) = 0.5 mL, T = 25 ºC).

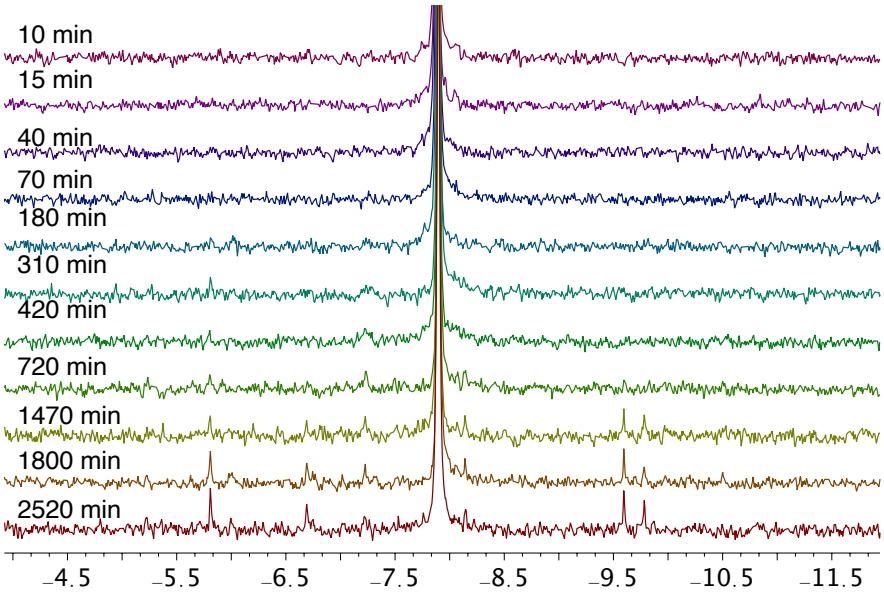

Figure S8.20. $^{31}P\{^{1}H\}$ NMR monitoring of reaction of tBA with *in-situ* generated Ni_2Na species (Condition: [**X-Ni$_2$**] = 0.01 M, [tBA] = 0.4 M, solvent: 10% THF-H8/90% C_6D_6, V(total) = 0.5 mL, T = 25 ºC).

REFERENCES

(1) Jedrzejas, M. J.; Setlow, P., Comparison of the binuclear metalloenzymes diphosphoglycerate-independent phosphoglycerate mutase and alkaline phosphatase: their mechanism of catalysis via a phosphoserine intermediate. *Chem. Rev.* **2001,** *101* (3), 607-618.

(2) Mitić, N.; Smith, S. J.; Neves, A.; Guddat, L. W.; Gahan, L. R.; Schenk, G., The catalytic mechanisms of binuclear metallohydrolases. *Chem. Rev.* **2006,** *106* (8), 3338-3363.

(3) Ghosh, A. C.; Duboc, C.; Gennari, M., Synergy between metals for small molecule activation: Enzymes and bio-inspired complexes. *Coord. Chem. Rev.* **2021,** *428*, 213606.

(4) Maity, R.; Birenheide, B. S.; Breher, F.; Sarkar, B., Cooperative Effects in Multimetallic Complexes Applied in Catalysis. *ChemCatChem* **2021,** *13* (10), 2337-2370.

(5) Buchwalter, P.; Rose, J.; Braunstein, P., Multimetallic catalysis based on heterometallic complexes and clusters. *Chem. Rev.* **2015,** *115* (1), 28-126.

(6) Shibasaki, M.; Kanai, M.; Matsunaga, S.; Kumagai, N., Recent progress in asymmetric bifunctional catalysis using multimetallic systems. *Acc. Chem. Res.* **2009,** *42* (8), 1117-1127.

(7) Powers, D. C.; Ritter, T., Bimetallic redox synergy in oxidative palladium catalysis. *Acc. Chem. Res.* **2012,** *45* (6), 840-850.

(8) Kattel, S.; Ramírez, P. J.; Chen, J. G.; Rodriguez, J. A.; Liu, P., Active sites for CO2 hydrogenation to methanol on Cu/ZnO catalysts. *Science* **2017,** *355* (6331), 1296-1299.

(9) Delferro, M.; Marks, T. J., Multinuclear olefin polymerization catalysts. *Chem. Rev.* **2011,** *111* (3), 2450-2485.

(10) Yoon, H. J.; Kuwabara, J.; Kim, J.-H.; Mirkin, C. A., Allosteric supramolecular triple-layer catalysts. *Science* **2010,** *330* (6000), 66-69.

(11) Deacy, A. C.; Kilpatrick, A. F.; Regoutz, A.; Williams, C. K., Understanding metal synergy in heterodinuclear catalysts for the copolymerization of CO 2 and epoxides. *Nat. Chem.* **2020**, 1-9.

(12) Kember, M. R.; Knight, P. D.; Reung, P. T.; Williams, C. K., Highly active dizinc catalyst for the copolymerization of carbon dioxide and cyclohexene oxide at one atmosphere pressure. *Angew. Chem.* **2009,** *121* (5), 949-951.

(13) Kember, M. R.; Jutz, F.; Buchard, A.; White, A. J.; Williams, C. K., Di-cobalt (ii) catalysts for the copolymerisation of CO 2 and cyclohexene oxide: support for a dinuclear mechanism? *Chem. Sci.* **2012,** *3* (4), 1245-1255.

(14) Thevenon, A.; Romain, C.; Bennington, M. S.; White, A. J.; Davidson, H. J.; Brooker, S.; Williams, C. K., Dizinc lactide polymerization catalysts: hyperactivity by control of ligand conformation and metallic cooperativity. *Angew. Chem. Int. Ed.* **2016,** *55* (30), 8680-8685.

(15) Li, L.; Metz, M. V.; Li, H.; Chen, M.-C.; Marks, T. J.; Liable-Sands, L.; Rheingold, A. L., Catalyst/cocatalyst nuclearity effects in single-site polymerization. Enhanced polyethylene branching and α-olefin comonomer enchainment in polymerizations mediated by binuclear catalysts and cocatalysts via a new enchainment pathway. *J. Am. Chem. Soc.* **2002,** *124* (43), 12725-12741.

(16) Li, H.; Marks, T. J., Nuclearity and cooperativity effects in binuclear catalysts and cocatalysts for olefin polymerization. *Proc. Natl. Acad. Sci. U. S. A.* **2006,** *103* (42), 15295-15302.

(17) Liu, S.; Motta, A.; Mouat, A. R.; Delferro, M.; Marks, T. J., Very large cooperative effects in heterobimetallic titanium-chromium catalysts for ethylene polymerization/copolymerization. *J. Am. Chem. Soc.* **2014,** *136* (29), 10460-10469.

(18) Kremer, A. B.; Mehrkhodavandi, P., Dinuclear catalysts for the ring opening polymerization of lactide. *Coord. Chem. Rev.* **2019,** *380*, 35-57.

(19) Gruszka, W.; Garden, J. A., Advances in heterometallic ring-opening (co) polymerisation catalysis. *Nat. Commun.* **2021,** *12* (1), 1-13.

(20) Garden, J. A.; Saini, P. K.; Williams, C. K., Greater than the sum of its parts: a heterodinuclear polymerization catalyst. *J. Am. Chem. Soc.* **2015,** *137* (48), 15078-15081.

(21) Chen, C., Designing catalysts for olefin polymerization and copolymerization: beyond electronic and steric tuning. *Nat. Rev. Chem.* **2018,** *2* (5), 6-14.

(22) Marks, T. J.; Chen, J.; Gao, Y., Early Transition Metal Catalysis for Olefin-Polar Monomer Copolymerization. *Angew. Chem. Int. Ed.* **2020**.

(23) Luckham, S. L. J.; Nozaki, K., Toward the Copolymerization of Propylene with Polar Comonomers. *Acc. Chem. Res.* **2020**.

(24) Chen, E. Y.-X., Coordination polymerization of polar vinyl monomers by single-site metal catalysts. *Chem. Rev.* **2009,** *109* (11), 5157-5214.

(25) Boffa, L. S.; Novak, B. M., Copolymerization of polar monomers with olefins using transition-metal complexes. *Chem. Rev.* **2000,** *100* (4), 1479-1494.

(26) Younkin, T. R.; Connor, E. F.; Henderson, J. I.; Friedrich, S. K.; Grubbs, R. H.; Bansleben, D. A., Neutral, single-component nickel (II) polyolefin catalysts that tolerate heteroatoms. *Science* **2000,** *287* (5452), 460-462.

(27) Franssen, N. M.; Reek, J. N.; de Bruin, B., Synthesis of functional 'polyolefins': state of the art and remaining challenges. *Chem. Soc. Rev.* **2013,** *42* (13), 5809-5832.

(28) Zou, C.; Chen, C., Polar-functionalized, crosslinkable, self-healing, and photoresponsive polyolefins. *Angew. Chem. Int. Ed* **2020,** *59* (1), 395-402.

(29) Baur, M.; Lin, F.; Morgen, T. O.; Odenwald, L.; Mecking, S., Polyethylene materials with in-chain ketones from nonalternating catalytic copolymerization. *Science* **2021,** *374* (6567), 604-607.

(30) Nakamura, A.; Ito, S.; Nozaki, K., Coordination− insertion copolymerization of fundamental polar monomers. *Chem. Rev.* **2009,** *109* (11), 5215-5244.

(31) Tan, C.; Zou, C.; Chen, C., Material Properties of Functional Polyethylenes from Transition-Metal-Catalyzed Ethylene–Polar Monomer Copolymerization. *Macromolecules* **2022**.

(32) Wang, K.; Amin, K.; An, Z.; Cai, Z.; Chen, H.; Chen, H.; Dong, Y.; Feng, X.; Fu, W.; Gu, J., Advanced functional polymer materials. *Mater. Chem. Front.* **2020,** *4* (7), 1803-1915.

(33) Johnson, L. K.; Killian, C. M.; Brookhart, M., New Pd (II)-and Ni (II)-based catalysts for polymerization of ethylene and. alpha.-olefins. *J. Am. Chem. Soc.* **1995,** *117* (23), 6414-6415.

(34) Liang, T.; Goudari, S. B.; Chen, C., A simple and versatile nickel platform for the generation of branched high molecular weight polyolefins. *Nat. Commun.* **2020,** *11* (1), 1-8.

(35) Xin, B. S.; Sato, N.; Tanna, A.; Oishi, Y.; Konishi, Y.; Shimizu, F., Nickel catalyzed copolymerization of ethylene and alkyl acrylates. *J. Am. Chem. Soc.* **2017,** *139* (10), 3611-3614.

(36) Nakano, R.; Nozaki, K., Copolymerization of propylene and polar monomers using Pd/IzQO catalysts. *J. Am. Chem. Soc.* **2015,** *137* (34), 10934-10937.

(37) Tao, W. j.; Nakano, R.; Ito, S.; Nozaki, K., Copolymerization of ethylene and polar monomers by using Ni/IzQO catalysts. *Angew. Chem. Int. Ed.* **2016,** *55* (8), 2835-2839.

(38) Carrow, B. P.; Nozaki, K., Synthesis of functional polyolefins using cationic bisphosphine monoxide–palladium complexes. *J. Am. Chem. Soc.* **2012,** *134* (21), 8802-8805.

(39) Zhang, W.; Waddell, P. M.; Tiedemann, M. A.; Padilla, C. E.; Mei, J.; Chen, L.; Carrow, B. P., Electron-rich metal cations enable synthesis of high molecular weight, linear functional polyethylenes. *J. Am. Chem. Soc.* **2018,** *140* (28), 8841-8850.

(40) Chen, M.; Chen, C., A Versatile Ligand Platform for Palladium-and Nickel-Catalyzed Ethylene Copolymerization with Polar Monomers. *Angew. Chem. Int. Ed.* **2018,** *57* (12), 3094-3098.

(41) Drent, E.; van Dijk, R.; van Ginkel, R.; van Oort, B.; Pugh, R. I., Palladium catalysed copolymerisation of ethene with alkylacrylates: polar comonomer built into the linear polymer chain. *Chem. Commun.* **2002,** (7), 744-745.

(42) Nakamura, A.; Anselment, T. M.; Claverie, J.; Goodall, B.; Jordan, R. F.; Mecking, S.; Rieger, B.; Sen, A.; Van Leeuwen, P. W.; Nozaki, K., Ortho-phosphinobenzenesulfonate: A superb ligand for palladium-catalyzed

coordination–insertion copolymerization of polar vinyl monomers. *Acc. Chem. Res.* **2013,** *46* (7), 1438-1449.

(43) Chen, Z.; Brookhart, M., Exploring ethylene/polar vinyl monomer copolymerizations using Ni and Pd α-diimine catalysts. *Acc. Chem. Res.* **2018,** *51* (8), 1831-1839.

(44) Mu, H.; Pan, L.; Song, D.; Li, Y., Neutral nickel catalysts for olefin homo-and copolymerization: relationships between catalyst structures and catalytic properties. *Chem. Rev.* **2015,** *115* (22), 12091-12137.

(45) Carrow, B. P.; Nozaki, K., Transition-metal-catalyzed functional polyolefin synthesis: effecting control through chelating ancillary ligand design and mechanistic insights. *Macromolecules* **2014,** *47* (8), 2541-2555.

(46) Alberoni, C.; D'Alterio, M. C.; Balducci, G.; Immirzi, B.; Polentarutti, M.; Pellecchia, C.; Milani, B., Tunable "In-Chain" and "At the End of the Branches" Methyl Acrylate Incorporation in the Polyolefin Skeleton through Pd (II) Catalysis. *ACS Catal.* **2022,** *12* (6), 3430-3443.

(47) Ge, Y.; Li, S.; Wang, H.; Dai, S., Synthesis of Branched Polyethylene and Ethylene-MA Copolymers Using Unsymmetrical Iminopyridyl Nickel and Palladium Complexes. *Organometallics* **2021,** *40* (17), 3033-3041.

(48) Cui, L.; Jian, Z., A N-bridged strategy enables hemilabile phosphine–carbonyl palladium and nickel catalysts to mediate ethylene polymerization and copolymerization with polar vinyl monomers. *Polym. Chem* **2020,** *11* (38), 6187-6193.

(49) Mu, H.; Zhou, G.; Hu, X.; Jian, Z., Recent advances in nickel mediated copolymerization of olefin with polar monomers. *Coor. Chem. Rev.* **2021,** *435*, 213802.

(50) Zhang, H.; Zou, C.; Zhao, H.; Cai, Z.; Chen, C., Hydrogen-Bonding-Induced Heterogenization of Nickel and Palladium Catalysts for Copolymerization of Ethylene with Polar Monomers. *Angew. Chem.* **2021**.

(51) Takeuchi, D.; Chiba, Y.; Takano, S.; Osakada, K., Double-Decker-Type Dinuclear Nickel Catalyst for Olefin Polymerization: Efficient Incorporation of Functional Co-monomers. *Angew. Chem. Int. Ed* **2013,** *52* (48), 12536-12540.

(52) Tan, C.; Chen, C., Emerging palladium and nickel catalysts for copolymerization of olefins with polar monomers. *Angew. Chem.* **2019,** *131* (22), 7268-7276.

(53) Rhinehart, J. L.; Brown, L. A.; Long, B. K., A robust Ni (II) α-diimine catalyst for high temperature ethylene polymerization. *J. Amer. Chem. Soc.* **2013,** *135* (44), 16316-16319.

(54) Dai, S.; Sui, X.; Chen, C., Highly Robust Palladium (II) α-Diimine Catalysts for Slow-Chain-Walking Polymerization of Ethylene and Copolymerization with Methyl Acrylate. *Angew. Chem. Int. Ed* **2015,** *54* (34), 9948-9953.

(55) Long, B. K.; Eagan, J. M.; Mulzer, M.; Coates, G. W., Semi-Crystalline Polar Polyethylene: Ester-Functionalized Linear Polyolefins Enabled by a Functional-Group-Tolerant, Cationic Nickel Catalyst. *Angew. Chem. Int. Ed* **2016,** *55* (25), 7106-7110.

(56) Fu, X.; Zhang, L.; Tanaka, R.; Shiono, T.; Cai, Z., Highly robust nickel catalysts containing anilinonaphthoquinone ligand for copolymerization of ethylene and polar monomers. *Macromolecules* **2017,** *50* (23), 9216-9221.

(57) Li, M.; Wang, X.; Luo, Y.; Chen, C., A Second-Coordination-Sphere Strategy to Modulate Nickel-and Palladium-Catalyzed Olefin Polymerization and Copolymerization. *Angew. Chem. Int. Ed.* **2017,** *56* (38), 11604-11609.

(58) Zhang, D.; Chen, C., Influence of Polyethylene Glycol Unit on Palladium-and Nickel-Catalyzed Ethylene Polymerization and Copolymerization. *Angew. Chem. Int. Ed.* **2017,** *56* (46), 14672-14676.

(59) Chen, M.; Chen, C., Rational design of high-performance phosphine sulfonate nickel catalysts for ethylene polymerization and copolymerization with polar monomers. *ACS Catal.* **2017,** *7* (2), 1308-1312.

(60) Wang, X.-l.; Zhang, Y.-p.; Wang, F.; Pan, L.; Wang, B.; Li, Y.-s., Robust and Reactive Neutral Nickel Catalysts for Ethylene Polymerization and Copolymerization with a Challenging 1, 1-Disubstituted Difunctional Polar Monomer. *ACS Catal.* **2021,** *11* (5), 2902-2911.

(61) Xiao, D.; Cai, Z.; Do, L. H., Accelerating ethylene polymerization using secondary metal ions in tetrahydrofuran. *Dalton Trans* **2019,** *48* (48), 17887-17897.

(62) Zhang, Y.; Wang, C.; Mecking, S.; Jian, Z., Ultrahighly Branched Main-Chain-Functionalized Polyethylenes via Inverted Insertion Selectivity. *Angew. Chem. Int. Ed.* **2020**.

(63) Yang, B.; Xiong, S.; Chen, C., Manipulation of polymer branching density in phosphine-sulfonate palladium and nickel catalyzed ethylene polymerization. *Polym. Chem* **2017,** *8* (40), 6272-6276.

(64) Rünzi, T.; Tritschler, U.; Roesle, P.; Göttker-Schnetmann, I.; Möller, H. M.; Caporaso, L.; Poater, A.; Cavallo, L.; Mecking, S., Activation and deactivation of neutral palladium (II) phosphinesulfonato polymerization catalysts. *Organometallics* **2012,** *31* (23), 8388-8406.

(65) Berkefeld, A.; Mecking, S., Deactivation pathways of neutral Ni (II) polymerization catalysts. *J. Am. Chem. Soc.* **2009,** *131* (4), 1565-1574.

(66) Friedberger, T.; Wucher, P.; Mecking, S., Mechanistic insights into polar monomer insertion polymerization from acrylamides. *J. Am. Chem. Soc.* **2012,** *134* (2), 1010-1018.

(67) Guironnet, D.; Caporaso, L.; Neuwald, B.; Göttker-Schnetmann, I.; Cavallo, L.; Mecking, S., Mechanistic insights on acrylate insertion polymerization. *J. Am. Chem. Soc.* **2010,** *132* (12), 4418-4426.

(68) Berkefeld, A.; Drexler, M.; Möller, H. M.; Mecking, S., Mechanistic insights on the copolymerization of polar vinyl monomers with neutral Ni (II) catalysts. *J. Am. Chem. Soc.* **2009,** *131* (35), 12613-12622.

(69) Xiong, S.; Shoshani, M. M.; Zhang, X.; Spinney, H. A.; Nett, A. J.; Henderson, B. S.; Miller III, T. F.; Agapie, T., Efficient Copolymerization of Acrylate and Ethylene with Neutral P, O-Chelated Nickel Catalysts: Mechanistic Investigations of Monomer Insertion and Chelate Formation. *J. Am. Chem. Soc.* **2021,** *143* (17), 6516-6527.

(70) Chen, Z.; Liu, W.; Daugulis, O.; Brookhart, M., Mechanistic studies of Pd (II)-catalyzed copolymerization of ethylene and vinylalkoxysilanes: Evidence for a β-silyl elimination chain transfer mechanism. *J. Am. Chem. Soc.* **2016,** *138* (49), 16120-16129.

(71) Rix, F. C.; Brookhart, M.; White, P. S., Mechanistic studies of the palladium (II)-catalyzed copolymerization of ethylene with carbon monoxide. *J. Am. Chem. Soc.* **1996,** *118* (20), 4746-4764.

(72) Mecking, S.; Johnson, L. K.; Wang, L.; Brookhart, M., Mechanistic studies of the palladium-catalyzed copolymerization of ethylene and α-olefins with methyl acrylate. *J. Am. Chem. Soc.* **1998,** *120* (5), 888-899.

(73) Shoshani, M. M.; Xiong, S.; Lawniczak, J. J.; Zhang, X.; Miller, T. F.; Agapie, T., Phosphine-Phenoxide Nickel Catalysts for Ethylene/Acrylate Copolymerization: Olefin Coordination and Complex Isomerization Studies Relevant to the Mechanism of Catalysis. *Organometallics* **2022**.

(74) Cai, Z.; Xiao, D.; Do, L. H., Cooperative Heterobimetallic Catalysts in Coordination Insertion Polymerization. *Comments Inorg. Chem.* **2019,** *39* (1), 27-50.

(75) Radlauer, M. R.; Day, M. W.; Agapie, T., Bimetallic effects on ethylene polymerization in the presence of amines: Inhibition of the deactivation by lewis bases. *J. Am. Chem. Soc.* **2012,** *134* (3), 1478-1481.

(76) Radlauer, M. R.; Buckley, A. K.; Henling, L. M.; Agapie, T., Bimetallic Coordination Insertion Polymerization of Unprotected Polar Monomers: Copolymerization of Amino Olefins and Ethylene by Dinickel Bisphenoxyiminato Catalysts. *J. Am. Chem. Soc.* **2013,** *135* (10), 3784-3787.

(77) Takano, S.; Takeuchi, D.; Osakada, K.; Akamatsu, N.; Shishido, A., Dipalladium catalyst for olefin polymerization: Introduction of acrylate units into the main chain of branched polyethylene. *Angew. Chem. Int. Ed.* **2014,** *53* (35), 9246-9250.

(78) Chen, J.; Gao, Y.; Wang, B.; Lohr, T. L.; Marks, T. J., Scandium-Catalyzed Self-Assisted Polar Co-monomer Enchainment in Ethylene Polymerization. *Angew. Chem. Int. Ed.* **2017,** *56* (50), 15964-15968.

(79) Sampson, J.; Bruening, M.; Akhtar, M. N.; Jaseer, E. A.; Theravalappil, R.; Garcia, N.; Agapie, T., Copolymerization of Ethylene and Long-Chain Functional α-Olefins by Dinuclear Zirconium Catalysts. *Organometallics* **2021,** *40* (12), 1854-1858.

(80) Sujith, S.; Joe, D. J.; Na, S. J.; Park, Y.-W.; Chow, C.; Lee, B. Y., Ethylene/polar norbornene copolymerizations by bimetallic salicylaldimine-nickel catalysts. *Macromolecules* **2005,** *38* (24), 10027-10033.

(81) Takeuchi, D.; Chiba, Y.; Takano, S.; Kurihara, H.; Kobayashi, M.; Osakada, K., Ethylene polymerization catalyzed by dinickel complexes with a double-decker structure. *Polym. Chem* **2017,** *8* (34), 5112-5119.

(82) Takeuchi, D.; Iwasawa, T.; Osakada, K., Double-Decker-Type Dipalladium Catalysts for Copolymerization of Ethylene with Acrylic Anhydride. *Macromolecules* **2018,** *51* (14), 5048-5054.

(83) Chen, Z.; Yao, E.; Wang, J.; Gong, X.; Ma, Y., Ethylene (co) polymerization by binuclear nickel

phenoxyiminato catalysts with cofacial orientation. *Macromolecules* **2016,** *49* (23), 8848-8854.

(84) Ji, G.; Chen, Z.; Wang, X.-Y.; Ning, X.-S.; Xu, C.-J.; Zhang, X.-M.; Tao, W.-J.; Li, J.-F.; Gao, Y.; Shen, Q., Direct copolymerization of ethylene with protic comonomers enabled by multinuclear Ni catalysts. *Nat. Commun.* **2021,** *12* (1), 1-9.

(85) Chen, S.-Y.; Pan, R.-C.; Liu, Y.; Lu, X.-B., Bulky o-Phenylene-Bridged Bimetallic α-Diimine Ni (II) and Pd (II) Catalysts in Ethylene (Co) polymerization. *Organometallics* **2021,** *40* (22), 3703-3711.

(86) Suo, H.; Solan, G. A.; Ma, Y.; Sun, W.-H., Developments in compartmentalized bimetallic transition metal ethylene polymerization catalysts. *Coord. Chem. Rev.* **2018,** *372*, 101-116.

(87) Cheng, H.; Wang, H.; Li, Y.; Hu, Y.; Zhang, X.; Cai, Z., Structurally simple dinuclear nickel catalyzed olefin copolymerization with polar monomers. *J. Catal.* **2018,** *368*, 291-297.

(88) Tahmouresilerd, B.; Xiao, D.; Do, L. H., Rigidifying Cation-Tunable Nickel Catalysts Increases Activity and Polar Monomer Incorporation in Ethylene and Methyl Acrylate Copolymerization. *Inorg. Chem.* **2021**.

(89) Na, Y.; Wang, X.; Lian, K.; Zhu, Y.; Li, W.; Luo, Y.; Chen, C., Dinuclear α-Diimine NiII and PdII Complexes that Catalyze Ethylene Polymerization and Copolymerization. *ChemCatChem* **2017,** *9* (6), 1062-1066.

(90) Khoshsefat, M.; Dechal, A.; Ahmadjo, S.; Mortazavi, S. M. M.; Zohuri, G.; Soares, J. B., Cooperative effect through different bridges in nickel catalysts for polymerization of ethylene. *Applied Organometallic Chemistry* **2019,** *33* (6), e4929.

(91) Zhang, Y.; Mu, H.; Pan, L.; Wang, X.; Li, Y., Robust bulky [P, O] neutral nickel catalysts for copolymerization of ethylene with polar vinyl monomers. *ACS Catal.* **2018,** *8* (7), 5963-5976.

(92) Zou, C.; Si, G.; Chen, C., A general strategy for heterogenizing olefin polymerization catalysts and the synthesis of polyolefins and composites. *Nat. Commun.* **2022,** *13* (1), 1-12.

(93) Zhang, Y.; Mu, H.; Wang, X.; Pan, L.; Li, Y., Elaborate tuning in ligand makes a big difference in catalytic performance: bulky nickel catalysts for (co) polymerization of ethylene with promising vinyl polar monomers. *ChemCatChem* **2019,** *11* (9), 2329-2340.

(94) Wang, X.-l.; Zhang, Y.-p.; Wang, F.; Pan, L.; Wang, B.; Li, Y.-s., Robust and Reactive Neutral Nickel Catalysts for Ethylene Polymerization and Copolymerization with a Challenging 1,1-Disubstituted Difunctional Polar Monomer. *ACS Catal.* **2021,** *11* (5), 2902-2911.

(95) Baur, M.; Mecking, S., Polyethylenes with Combined In-Chain and Side-Chain Functional Groups from Catalytic Terpolymerization of Carbon Monoxide and Acrylate. *ACS Macro Lett.* **2022,** *11* (10), 1207-1211.

(96) Voccia, M.; Odenwald, L.; Baur, M.; Lin, F.; Falivene, L.; Mecking, S.; Caporaso, L., Mechanistic Insights into Ni (II)-Catalyzed Nonalternating Ethylene–Carbon Monoxide Copolymerization. *J. Am. Chem. Soc.* **2022,** *144* (33), 15111-15117.

(97) Tran, T. V.; Karas, L. J.; Wu, J. I.; Do, L. H., Elucidating secondary metal cation effects on nickel olefin polymerization catalysts. *ACS Catal.* **2020,** *10* (18), 10760-10772.

(98) Invergo, A. M.; Liu, S.; Dicken, R. D.; Mouat, A. R.; Delferro, M.; Lohr, T. L.; Marks, T. J., How close is too close? Polymerization behavior and monomer-dependent reorganization of a bimetallic salphen organotitanium catalyst. *Organometallics* **2018,** *37* (15), 2429-2436.

(99) Tran, T. V.; Lee, E.; Nguyen, Y. H.; Nguyen, H. D.; Do, L. H., Customizing Polymers by Controlling Cation Switching Dynamics in Non-Living Polymerization. *J. Am. Chem. Soc.* **2022,** *144* (37), 17129-17139.

(100) Waltman, A. W.; Younkin, T. R.; Grubbs, R. H., Insights into the deactivation of neutral nickel ethylene polymerization catalysts in the presence of functionalized olefins. *Organometallics* **2004,** *23* (22), 5121-5123.

(101) Berliner, M. A.; Belecki, K., Simple, rapid procedure for the synthesis of chloromethyl methyl ether and other chloro alkyl ethers1. *The Journal of Organic Chemistry* **2005,** *70* (23), 9618-9621.

(102) Cox, P. J.; Wang, W.; Snieckus, V., Expedient route to 3-and 3, 3'-substituted 1, 1'-bi-2-naphthols by directed ortho metalation and suzuki cross coupling methods. *Tetrahedron Lett.* **1992,** *33* (17), 2253-2256.

(103) Neuwald, B.; Caporaso, L.; Cavallo, L.; Mecking, S., Concepts for stereoselective acrylate insertion. *J. Am. Chem. Soc.* **2013,** *135* (3), 1026-1036.

(104) Palmer, W. N.; Zarate, C.; Chirik, P. J., Benzyltriboronates: building blocks for diastereoselective carbon–

carbon bond formation. *J. Am. Chem. Soc.* **2017,** *139* (7), 2589-2592.

APPENDIX A

P,N-Chelated Ni Complexes: Ligand Dearomatization and Metal-Ligand Aryl Exchange

CONTRIBUTIONS AND ACKNOWLEDGEMENTS

Shuoyan Xiong and Theodor Agapie conceived the presented idea. S.X. performed synthetic studies and analyzed the catalysis data. Brad C. Bailey, Heather A. Spinney, and Briana S. Henderson performed catalysis studies. S.X. wrote the chapter.

We are grateful to Dow for funding (T.A.). We thank Alex J. Nett for insightful discussions. We thank Hannah Bailey and Heidi Clements for helping analyzing catalytic data. We thank Linh Nguyen Vuong Le, Matthew R. Espinosa and Michael K. Takase for assistance with X-ray crystallography and David VanderVelde for assistance with NMR spectroscopy. Support has been provided for the X-ray diffraction and NMR instrumentation via the Dow Next Generation Educator Fund.

Appendix A

ABSTRACT

2-(Diarylphosphinomethyl)pyridine (**PC^{H}N**) and 2-(diarylphosphinoamino)pyridine (**PN^{H}N**) was prepared and their coordination chemistry with Ni^{II} was investigated. Neutral Ni(L)R complexes supported by anionic P,N ligands feature a partially dearomatized pyridyl ring and a weaker pyridine-N coordination compared to reported neutral P,N-Ni complexes. The nature of the bridging group (-CH_2- vs -NH_2-) between phosphine and pyridine was found to affect isomerization occurring during metalation and reactivity of resulting Ni complexes with ethylene. Specifically, a metal-ligand aryl exchange was observed in reaction of (PEt_3)NiPhCl with deprotonated 2-(diarylphosphinoamino)pyridine. Though not able to produce polyethylene, **PNN**-based catalysts indeed consumed ethylene under polymerization conditions.

GENERAL INTRODUCTION

Nickel phosphine complexes are widely utilized as catalysts in organic reactions and olefin polymerizations.[1-5] Specifically, P,O-chelated nickel complexes, with the "P" being diaryl phosphine and the "O" being sulfonate, phenoxide or enolate, are popular catalysts for coordination copolymerization of ethylene and polar monomers.[6-25] These complexes typically feature a neutral phosphine as a strong "L"-type donor and an anionic "O" as a weak "X"-type donor (Figure AA.1a). Both the ligand asymmetry and the overall neutral structure are important for catalysts' high activity and tolerance toward polar groups.[7, 12, 26-28]

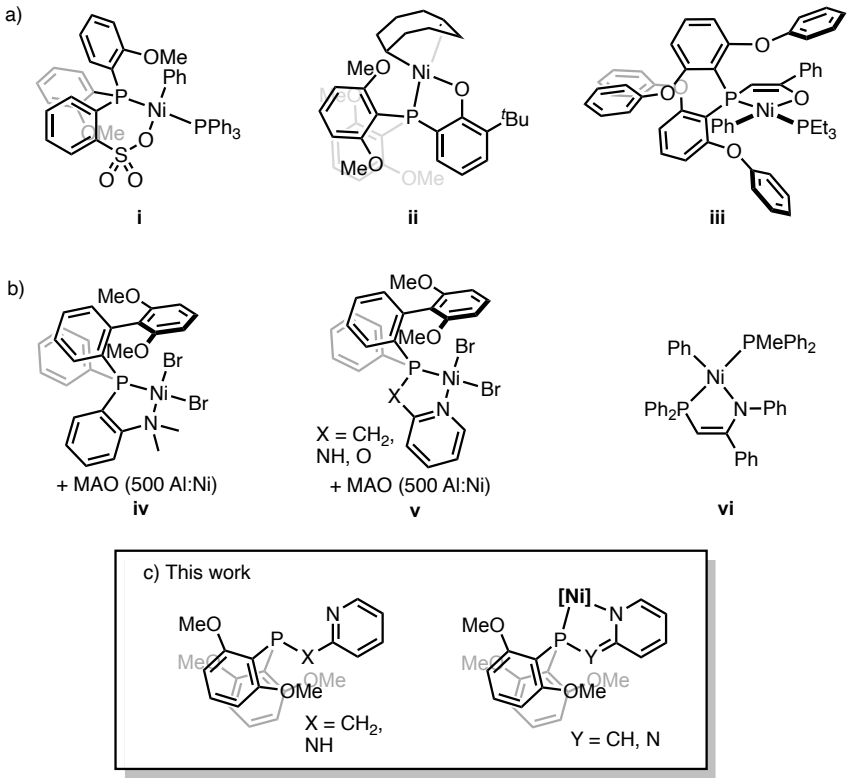

Figure AA.1. a) Examples of reported P,O-Ni complexes; b) examples of P,N-Ni complexes; c) P,N ligands in this work (left) and prepared coordination mode (right).

Though demonstrating promising in polar polyolefin synthesis, their activities are still below practical threshold.[3, 6] Parallel to steric or electronic tuning of reported P,O-ligands, another direction is to develop new ligands that feature potentially similar steric and electronic profile of reported P,O-ligands. P,N-type ligands is a potential choice (Figure AA.1b). However, metalation of neutral phosphine-amine ligands leads to cationic nickel complexes, which are prone to polar group-induced deactivation and thus show low activity in copolymerization with polar monomers.[29-31] The nickel center in neutral complexes supported by phosphine-amino ligands are less electrophilic, however, they are not an active catalysts for the conversion of ethylene to oligomers or polymers, potentially due to the significantly stronger coordination of amino-N to nickel compared to analogous "O" coordination in high-performance PO-Ni complexes.[32-35]

We envisaged that a weak N-coordination in neutral P,N-Ni complexes may be essential for activity in coordination polymerization, which could be achieved via partially delocalization of electron on the anionic "N"-donor.[36] Two ligands, 2-(diarylphosphinomethyl)pyridine (**PC^{H}N**) and 2-(diarylphosphinoamino)pyridine (**PN^{H}N**) were prepared (Figure AA.1c). Deprotonation of them leads to anionic ligands (**PCN** and **PNN**) with partially dearomatized pyridine ring and delocalized electron. Subsequent salt metathesis generates corresponding neutral P,N-chelated nickel complexes. Notably, metal-phosphine aryl exchange was observed in reaction of **PCN** with the nickel precursor, tmedaNiPhCl. Though not able to produce

polyethylene, **PNN**-based catalysts indeed consumed ethylene under polymerization conditions, consistent with our proposal.

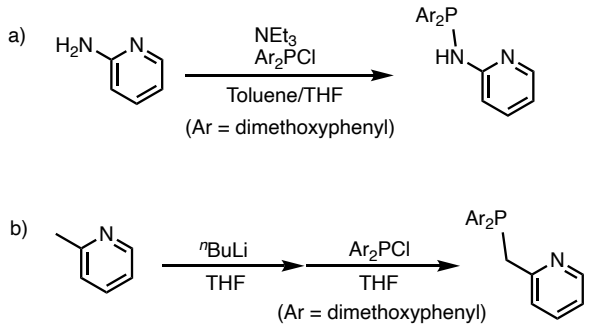

Figure AA.2. Preparation of **PN^{H}N** (a) and **PC^{H}N** (b).

RESULTS AND DISCUSSION

Preparation of P,N ligands

2-(diarylphosphinoamino)pyridine (**PN^{H}N**) was prepared by reacting 2-aminopyridine and bis(dimethoxyphenyl)phosphine chloride in the presence of triethylamine (Figure AA.2a). In $^{31}P\{^1H\}$ NMR of **PN^{H}N**, a sharp singlet around 0 ppm was observed. Preparation of 2-(diarylphosphinomethyl)pyridine (**PC^{H}N**) requires deprotonation of 2-methyl pyridine by ^{t}BuLi, and subsequent phosphine addition generates the desired proligand and LiCl (Figure AA.2b). A sharp singlet around -40 ppm was observed in $^{31}P\{^1H\}$ NMR of **PN^{H}N**, which is significantly differenct from **PC^{H}N** that of but close to triaryl phosphine.

Preparation and characterization of PNN-Ni complexes

Reaction of **PN^{H}N** and $py_2Ni(CH_2SiMe_3)_2$ generated a neutral nickel dialkyl complexes (**PN^{H}N-NiC$^{Si}_2$**) quantitatively, which is characterized by ^1H, $^{31}P\{^1H\}$ NMR

spectra as well as single-crystal X-ray diffraction (scXRD) studies (Figure AA.3). In solution, generation of $SiMe_4$ was observed overtime at elevated temperatures (e.g. 40 °C), along with a new species featuring a singlet at ~60 ppm in $^{31}P\{^1H\}$ NMR spectrum. This scenario potentially indicates generation of a nickel monoalkyl complex via protonolysis. Partial decomposition that generated nickel black was also observed, which made further purification of this complex challenging. Vapor diffusion of hexanes into the crude mixture with a ~95% conversion of **PN^{H}N-NiC$^{Si}_2$** in toluene generated single crystals that allows structure determination. scXRD revealed a structure of neutral Ni(L)R type complex, **PNN-Ni(py)C^{Si}**, in which the pyridine is cis to pyridyl group in PN ligand and trans to phosphine (Figure AA.3). Most single-component Ni catalysts for coordination polymerization are also Ni(L)R-type complexes, and thus **PNN-Ni(py)C^{Si}** is an attractive target. However, preparation of **PNN-Ni(py)C^{Si}** in larger scale via crystallization was attempted but showed no success yet.

An alternative synthesis route toward neutral Ni(L)R compounds is deprotonation of by a base, followed by salt metathesis with $L_2NiPhCl$ (e.g. $(PEt_3)_2NiPhCl$). Several common bases, including ^{t}BuLi, $LiCH_2SiMe_3$, or NaHMDS, led to a suspension after deprotonation, and mixtures of several species after reaction with $(PEt_3)_2NiPhCl$. On the other hand, deprotonation by KHMDS in THF leads to generation of a homogenous, pale green solution, of which the $^{31}P\{^1H\}$ NMR spectra features a broad resonance around 20 ppm that is distinct from that of **PN^{H}N**. This is consistent with deprotonation of **PN^{H}N** and generation of **PNN-K** (Figure AA.3). Subsequent

reaction with (PEt_3)NiPhCl leads to generation of three sets of peaks in the $^{31}P\{^1H\}$ NMR spectra, one broad singlet around -20 ppm corresponding to free PEt_3 that can be removed under vacuum, and two sets of doublets. One set of doublets (A) features a relative small coupling constant of ~20Hz, and another one (B) features a large coupling constant of ~180Hz. Therefore, we proposed that A corresponds to one isomer of desired compound with (***cis*-PNN-Ni(P)Ph**, Figure AA.3), and B corresponds corresponding to one isomer of desired compound with PEt_3 and diarylaminophosphine trans to each other (***trans*-PNN-Ni(P)Ph**. The former isomer is the major isomer (83%). The identity of the major isomer was confirmed by scXRD studies of the single crystals obtained from concentrated ether solutions.

Analogous nickel phenyl complex, **PNN-Ni(py)Ph**, was prepared by salt metathesis of **PNN-K** and tmedaNiPhCl in the presence of pyridine (Figure AA.3). Though it's challenge to determine its exact structure in solution. Results of scXRD studies are more consistent with the assignment of trans-isomer that feature pyridine (ligand L) and diarylaminophosphino trans to each other. It's notable that such trans-isomer is the minor isomer for **PNN-Ni(P)Ph**. This difference is potentially attributed to the difference in electronic effects between PEt_3 and pyridine.

Notably, a dearomatized pyridyl ring was observed in all three Ni(L)R complexes, **PNN-Ni(py)C^{Si}**, **PNN-Ni(P)Ph**, and **PNN-Ni(py)Ph**. For example, the C2-C3 distance in the pyridyl ring of in **PNN-Ni(P)Ph** (1.431(5) Å) is significantly longer than bond distance of C3-C4 (1.374(5) Å). However, it is still shorter than aliphatic C-C bond distance (~1.5 Å), for example, the C-C bond distance in PEt_3. This scenario

indicates the existence of retained partial aromaticity, and potential electron delocalization. The Ni-N distance in aforementioned three neutral Ni(L)R complexes (e.g. 1.981(2)Å for **PNN-Ni(P)Ph**) is significantly longer than that in reported neutral PN-Ni complexes, for example, the neutral Ni(PMe_3)Ph complexes supported by diarylamido phosphine ligands (1.947(5) Å).[37] This is potentially resulted from electron delocalization and indicating a weakened N-coordination.

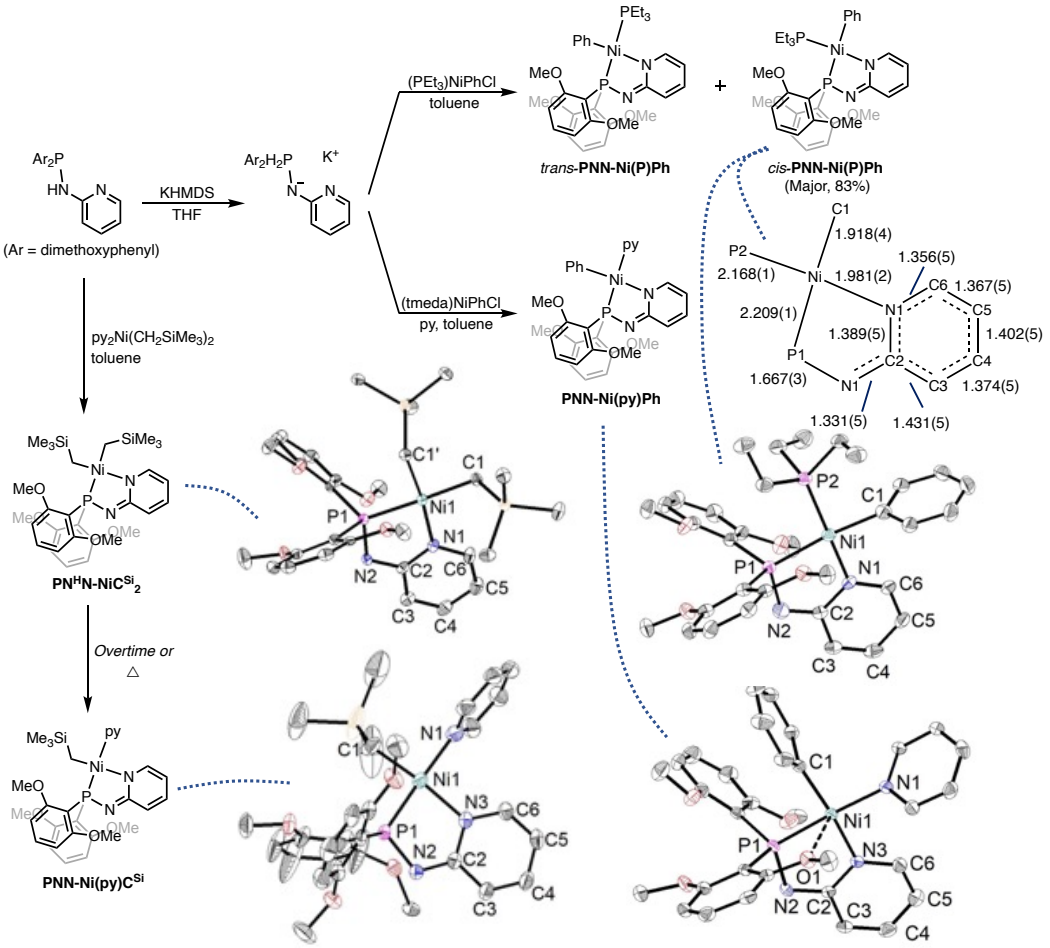

Figure AA.3. Synthesis and of **PN^{H}N-NiC$^{Si}_2$**, **PNN-Ni(py)C^{Si}**, and **PNN-Ni(P)Ph**, **PNN-Ni(py)Ph.** H-atoms are excluded for clarity.

Preparation and characterization of PCN-Ni complexes

Metalation of **PC^{H}N** proligand was achieved via a slightly different route. ^{t}BuLi was used for deprotonation and subsequent metathesis generated a set of doublets featuring relatively small coupling constants (~30Hz) in the $^{31}P\{^{1}H\}$ NMR spectrum, implying generation of a *cis*-isomer. The other isomer, trans-isomer that features a larger coupling constant, was not observed. In the ^{1}H NMR spectrum, two different sets of resonances was observed for two dimethoxyphenyl groups that originally linked to phosphine. This scenario is not consistent with proposed Ni(PEt$_3$)Ph compound in which two dimethoxyphenyl groups are chemically equivalent. scXRD studies of single crystals obtained from concentrated ether solutions revealed a structure of a square planar Ni complex with two phosphine cis to each other, **PCN-Ni(P)Ar^{O2}**. Notably, one dimethoxyphenyl group moved to nickel while the phenyl group originated linked to nickel in the precursor moved to the phosphine in the PN ligand (Figure AA.5). Due to limitations in the quality of single crystals, only connectivity data was obtained.

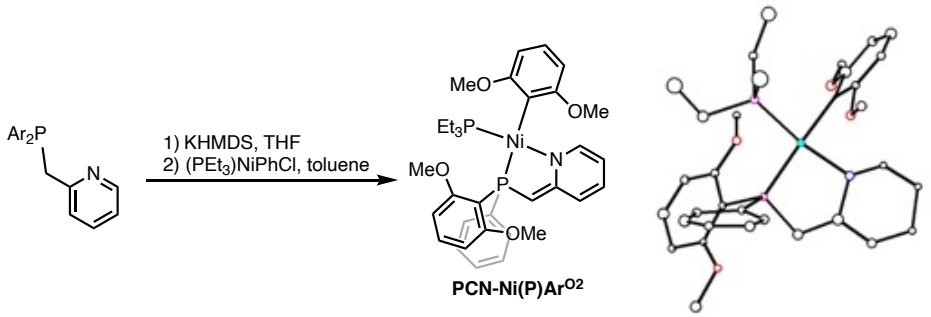

Figure AA.5. Synthesis and solid-state structures of **PCN-Ni(P)Ar^{O2}**. H-atoms are excluded for clarity.

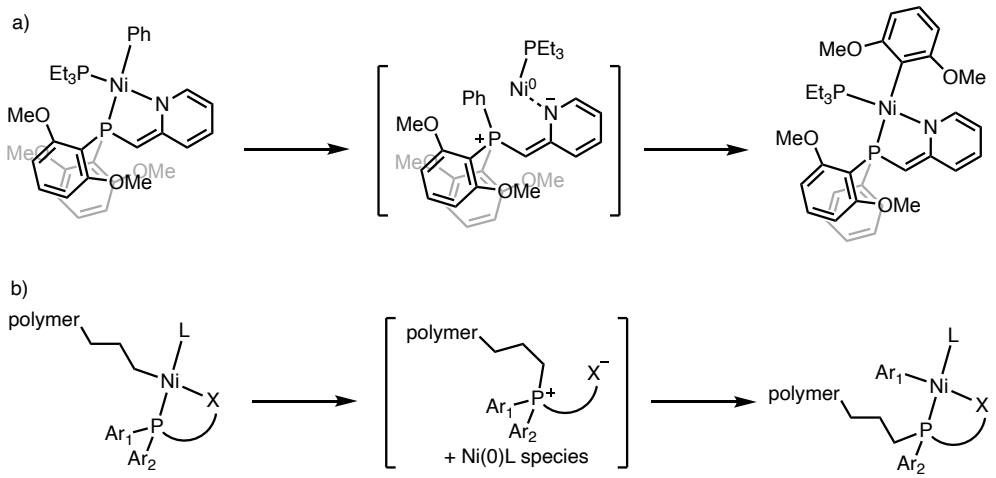

Figure AA.6. Potential pathways for metal-ligand aryl transfer with a **PCN-Ni** type complex (a) and for a generalized PO-Ni complex during catalysis (b).

The abovementioned aryl exchange between nickel and phosphine is rare. It's also notable that the aryl on nickel is actually cis to phosphine. One proposed mechanism is shown in Figure AA.6a: Steric repulsion between PEt_3 and bulky bis(dimethoxyphenyl)phosphino moiety promotes intramolecular reductive elimination that generates phosphonium phenoxide and Ni(0) species, and subsequent oxidative addition generates the sterically favored Ni(PEt_3)(dimethoxyphenyl) complexes. Considering the intermediate Ni(PEt_3)(Ph) species was not observed during the reaction, this proposed aryl exchange is faster than salt metathesis. Similar reductive elimination, or alkyl transfer from Ni(II) to phosphine, may also happen during catalysis as a catalyst deactivation pathway with other type of Ni phosphine complexes (Figure AA.6b). The resulting phosphonium may react with Ni(0) species again to regenerate Ni(II) species. However, the bulkier alkyl/aryl, initially bound to phosphine for steric shielding of the Ni center, is likely to transfer to Ni, leading to metal-phosphine carbyl exchange and generation of multiple active species. Previously,

Mecking has proposed a similar metal-phosphine carbyls exchange with phosphine-sulfonate Pd catalysts, while the Pd complex generated after exchange have not been isolated.[38] The isolation of **PCN-Ni(P)Ar^{O2}** provides a first Ni example, and a direct evidence of this exchange process with metal phosphine complexes.

Table AA.1. Reactivity of PN-Ni complexes with ethylene and tBA

Entry[a]	catalyst	T (ºC)	[tBA]/M	uptake/(psi*V_{re})
1	**PNN-Ni(P)Ph**	90	0	26
2	**PNN-Ni(py)Ph**	90	0	24
3	**PCN-Ni(P)Ar^{O2}**	90	0	7
4	**PNN-Ni(py)Ph**	70	0.05	33
5	**PNN-Ni(py)Ph**	90	0.05	27
6	**PNN-Ni(py)Ph**	110	0.05	12

[a] V(total)=5 mL, [Ni]=0.25 μmol, ethylene pressure=400 psi, toluene solvent, t=1 h, each entry represents three replicated runs.

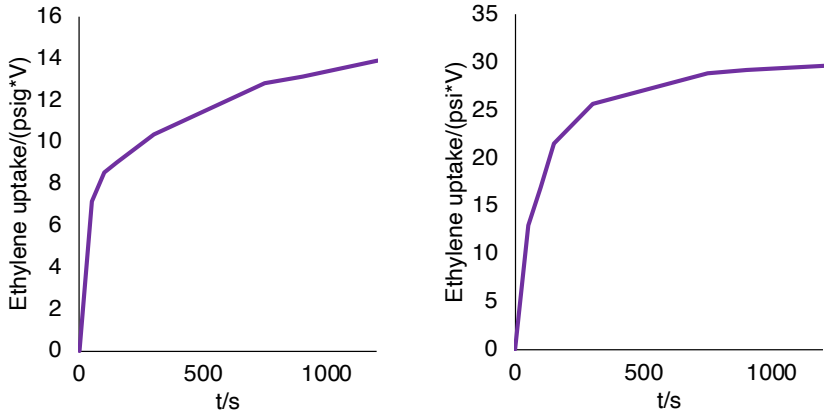

Figure AA.7. Ethylene uptake curves (first 20 min) of one ethylene polymerization under condition of entry 1(left) and 2(right), table AA.1.

Reactivity of PXN-Ni Complexes toward Ethylene

Encouraged by the weakened Ni-N distance and similarities between their structures and structures of P,O-Ni catalysts, three of the above Ni(L)R complexes, **PNN-**

Ni(P)Ph, **PNN-Ni(py)Ph**, and **PCN-Ni(P)Ar^{O2}** were also tested in ethylene polymerization and ethylene/tBA copolymerization. However, no polymer production was observed, while ethylene consumption was indeed observed (Table AA.1). The presence of tBA did not affect ethylene consumption, while higher reaction temperature leads to lower ethylene uptake. This scenario implies a temperature-dependent catalyst deactivation pathway. Further, ethylene uptake curves indicate ethylene consumption indeed happened at the early stage (c.a. first 60 s, Figure AA.7) but stopped quickly afterwards, implying fast catalyst decomposition. One rationale is the "N" coordination in these complexes is too weak to stabilize the active center. In addition, alkyl exchange from Ni to phosphine may be facile with these catalysts, given the observance of quantitative aryl exchange with PCN-supported Ni complexes.

CONCLUSION

Five neutral nickel complexes based on 2-(diarylphosphinomethyl)pyridine (**PC^{H}N**) and 2-(diarylphosphinoamino)pyridine (**PN^{H}N**) proligands were prepared and crystallographically characterized. Neutral Ni(L)R complexes supported by anionic P,N ligands feature a partially dearomatized pyridyl ring and a weaker pyridine-N coordination compared to reported neutral P,N-Ni complexes. Notably, a rarely observed metal-ligand aryl exchange was observed in reaction of (PEt_3)NiPhCl with deprotonated 2-(diarylphosphinoamino)pyridine, provides insights into catalysts deactivation and reactivation. Though being able to consume ethylene, these complexes

deactivates quickly under polymerization conditions and thus are not suitable for olefin polymerization catalysis.

Appendix A

EXPERIMENTAL SECTION

General Considerations

All air- and water-sensitive compounds were manipulated under N_2 or Ar using standard Schlenk or glovebox techniques. The solvents for air- and moisture-sensitive reactions were dried over sodium benzophenone ketyl or calcium hydride or by the method of Grubbs.[39] Deuterated solvents were purchased from Cambridge Isotopes Lab, Inc.; C_6D_6, and C_7D_8 was dried over a purple suspension with Na/benzophenone ketyl and vacuum transferred. Ethylene (99.999%) was purchased from Matheson Tri-Gas and used without further purification. 2-picoline was dried by stirring over CaH_2 for greater than 12 hours and distilling. 2-aminopyridine was purified by sublimation. PEt_3 was purchased from Sigma Aldrich and purified by distillation prior to use. t-butyl acrylate was dried over 3 Å sieves for greater than 72h, vacuum transferred, and passed over an activated alumina plug. Bis(dimethoxyphenyl)phosphine chloride,[40] $(Et_3P)_2NiPhCl$,[41] and tmedaNiPhCl[42] were synthesized according to literature procedures. All ^1H, ^{13}C, and ^{31}P spectra of organic and organometallic compounds were recorded on Varian INOVA-400, or 500, or Bruker Cryoprobe 400 spectrometers. ^1H and ^{13}C chemical shifts are reported relative to residual solvent resonances.

Synthesis of Ligands and Transition Metal Complexes

2-(bis(dimethoxyphenyl)phosphinomethyl)pyridine (PC^{H}N): In the glove box, to a thawing solution of 2-picoline (116 mg, 1.25 mmol) in THF (5 mL) was added a hexane solution of ^{n}BuLi (0.5 mL/2.5M, 1 equiv.). The yellow solution was stirred while warming to room temperature for 30 min. After stirring for additional 30 min, the mixture was cooled to -78 °C, and a THF solution (5 mL) of bis(dimethoxyphenyl)phosphine chloride (403 mg, 0.95 equiv.) was added. The mixture was then stirred while warming up to room temperature slowly for 2 h. Next, all volatiles were removed from solution which was triturated with n-pentane (3 x 5 mL). The resulting residue was washed by n-pentane (15 mL). The solids were collected via a filtration yielding spectroscopically pure **PC^{H}N** (351 mg, 71 % Yield).

^{1}H NMR (400 MHz, C_6D_6): δ 8.44 (d, *J*= 3.9 Hz, 1H, ArH), 7.21-7.18 (m, 1H, ArH), 7.06-6.95 (m, 3H, ArH), 6.52 (ddt, *J*= 7.3, 4.9, 1.2 Hz, 1H, ArH), 6.27 (dd, *J*= 8.3, 2.4 Hz, 4H, ArH), 4.51 (d, *J*= 2.3 Hz, 2H, -PCH$_2$-), 3.23 (s, 12H, -OCH$_3$). ^{13}C{^{1}H} NMR (101 MHz, C_6D_6): δ 162.54 (d, *J*= 8.2 Hz, 4C, Aryl-C), 161.62 (d, *J*= 11.7 Hz, 2C, Aryl-C), 148.84 (s, 1C, Aryl-C), 134.49 (s, 1C, Aryl-C), 128.97 (s, 2C, Aryl-C), 123.25 (d, *J*= 9.4 Hz, 1C, Aryl-C), 119.67 (s, 1C, Aryl-C), 116.92 (d, *J*= 116 Hz, 1C, Aryl-C), 104.41 (s, 4C, Aryl-C), 55.66 (s, 4C, -O<u>C</u>H$_3$), 36.22 (d, *J*= 16.2 Hz, 1C, -P<u>C</u>H$_2$-). ^{31}P{^{1}H} NMR (121 MHz, C_6D_6, 298 K): δ - 39.33 (s, 1P).

2-(bis(dimethoxyphenyl)phosphinoamino)pyridine (PN^{H}N): In the glove box, to a thawing toluene solution (10 mL) of 2-aminopyridine (109 mg, 1.16 mmol) was added a THF solution of bis(dimethoxyphenyl)phosphine chloride (387 mg, 0.98 equiv.). The mixture was then stirred while warming up to room temperature slowly for 2 h. All volatiles were removed from filtrate and the resulting solid was washed by n-pentane (15 mL) and Et_2O (5 mL), then dissolved in toluene (20 mL). Next, precipitates were removed via a filtration, and volatiles were removed once more, yielding spectroscopically pure **PN^{H}N** (361 mg, 78 % Yield).

^{1}H NMR (400 MHz, C_6D_6): δ 8.25 (broad d, 1H, ArH), 7.76-7.66 (m, 2H, ArH), 7.14-7.07 (m, 1H, ArH), 7.00 (t, *J*= 8.2 Hz, 2H, ArH), 6.37 (dd, *J*= 8.2 Hz, 5.4 Hz, 4H, ArH), 6.22 (d, *J*= 1.9 Hz, 1H, ArH), 3.30 (s, 12H, -OCH_3). ^{13}C{^{1}H} NMR (101 MHz, C_6D_6): δ 162.51 (d, *J*= 9.4 Hz, 4C, Aryl-C), 161.06 (d, *J*=30.5Hz, 2C, Aryl-C), 148.63 (s, 1C, Aryl-C), 136.88 (s, 1C, Aryl-C), 130.21 (s, 2C, Aryl-C), 117.83 (d, *J*=22.8 Hz, 1C, Aryl-C), 113.82 (s, 1C, Aryl-C), 109.20 (d, *J*=25.0 Hz, 1C), 104.89 (s, 4C, Aryl-C), 55.66 (s, 4C, -O<u>C</u>H_3). ^{31}P{^{1}H} NMR (121 MHz, C_6D_6, 298 K): δ - 0.81 (s, 1P).

PN^{H}N-NiC$^{Si}_2$: In the glove box, to a solution of pyNi(CH_2SiMe_3)$_2$ (23.8 mg, 0.06 mmol) in toluene (2 mL) was added a thawing solution of **PN^{H}N** (23.9 mg, 0.06 mmol) in toluene (2 mL). After stirring for 30 min, all volatiles were removed from solution which was triturated with n-pentane (3 x 5 mL). The resulting residue was washed by n-pentane (5 mL) and the solids were collected via a filtration yielding spectroscopically pure **PN^{H}N-NiC$^{Si}_2$** (31.6 mg, 84 % Yield).

^{1}H NMR (400 MHz, C_6D_6): δ 8.73 (d, *J*= 5.3 Hz, 1H, ArH), 7.00 (t, *J*= 8.3 Hz, 2H, ArH),6.78 (td, *J*= 6.9, 1.4 Hz, 1H, ArH), 6.36 (d, *J*= 6.7 Hz, 1H, ArH), 6.21 (dd, *J*= 8.3, 3.2 Hz, 4H, ArH), 6.14 (ddd, *J*= 7.1, 5.9, 1.3 Hz, 1H, ArH), 5.83-5.78 (m, 1H, Aryl-C), 3.20 (s, 12H, -OCH_3), 0.57 (s, 9H, -Si(CH_3)$_3$), 0.43 (d, *J* = 6.9 Hz, 2H, -NiC<u>H</u>$_2$-), 0.36 (s, 9H, -Si(CH_3)$_3$), 0.30 (d, *J* = 20.0 Hz, 2H, -NiC<u>H</u>$_2$-). ^{31}P{^{1}H} NMR (121 MHz, C_6D_6, 298 K): δ 42.85 (s, 1P).

PNN-Ni(P)Ph: In the glove box, to a precooled (-78 °C) solution of the ligand **PN^{H}N** (24mg, 0.06 mmol) in tetrahydrofuran (THF) (2 mL) was added a precooled (-78 °C) solution (2 mL) of KHMDS (13 mg, 1.05 equiv.) in THF. The mixture was then slowly warmed up to room temperature. After stirring for additional 30 min, all volatiles were removed from solution which was triturated with pentane (2 x 5 mL). The resulting residue was then dissolved in toluene (4 mL) and cooled to -78 °C. To this solution was added a toluene solution (2 mL)

of $(PEt_3)_2NiPhCl$ (24 mg, 0.99 equiv.). The mixture was then slowly warmed up to room temperature and stirred for additional 24 h. All volatiles were then removed from solution which was triturated with pentane (2 x 5 mL). The resulting residue was then washed with pentane (10 mL), hexanes (5 mL), and diethyl ether (3 mL), yielding spectroscopically pure **PNN-Ni(P)Ph** as yellow solids (25.7 mg, 66 % Yield).

The major isomer (*cis*-**PNN-Ni(P)Ph**). ^{1}H NMR (400 MHz, C_6D_6): δ 7.92 (ddd, *J*= 7.6, 3.9, 1.5 Hz, 2H, ArH), 7.20 (td, *J*= 7.6, 1.5 Hz, 2H, ArH), 7.03-6.91 (m, 4H, ArH), 6.82 (d, *J*= 8.6 Hz, 1H, ArH), 6.72-6.63 (m, 1H, ArH), 6.21 (dd, *J*= 8.3, 3.3 Hz, 4H, ArH), 5.56-5.48 (m, 1H, ArH), 3.28 (s, 12H, $-OCH_3$), 1.23-1.13 (m, 6H, $-PC\underline{H}_2-$), 0.64 (dt, *J*= 15.0, 7.6 Hz, 9H, $-PCH_2C\underline{H}_3$). $^{13}C\{^1H\}$ NMR (101 MHz, C_6D_6): δ 174.56 (d, *J*= 10.9 Hz, 4C, Aryl-C), 171.50 (dd, *J*=73.0, 45.4 Hz, 2C, Aryl-C), 161.89 (s, 1C, Aryl-C) 149.31 (d, *J*=6.3 Hz, 2C, Aryl-C) 137.06 (s, 2C, Aryl-C), 135.48 (d, *J*=3.8 Hz, 1C, Aryl-C), 129.48 (s, 1C, Aryl-C), 126.73 (dd, *J*=4.9, 2.6 Hz, 2C, Aryl-C), 122.51 (s, 1C, Aryl-C), 117.35 (d, *J*=44.9 Hz, 1C, Aryl-C), 115.74 (d, *J*=25.5 Hz, 1C), 105.13 (d, *J*=3.7Hz, 4C), 104.00 (s, 1C, Aryl-C), 55.90 (s, 4C, $-O\underline{C}H_3$), 16.46 (dd, *J*=27.2, 4.8 Hz, 3C, $-P\underline{C}H_2-$), 7.66 (d, *J*=3.3 Hz, 3C, $-PCH_2\underline{C}H_3$). δ $^{31}P\{^1H\}$ NMR (121 MHz, C_6D_6, 298 K): δ 60.20 (d, *J*= 44.4 Hz, 1P), 13.75 (d, *J*= 44.4 Hz, 1P).

The minor isomer (*trans*-**PNN-Ni(P)Ph**). *Resonances of the ArHs in trans-**PNN-Ni(P)Ph** were not included as they overlapped heavily with that in cis-**PNN-Ni(P)Ph**.* ^{1}H NMR (400 MHz, C_6D_6): δ 3.19 (s, 12H, $-OCH_3$), 1.02 (tdd, , *J*= 7.6, 5.5, 2.6 Hz, 6H, $-PC\underline{H}_2-$), 0.86 (dt, *J*= 15.0, 7.6 Hz, 9H, $-PCH_2C\underline{H}_3$). $^{13}C\{^1H\}$ NMR (101 MHz, C_6D_6): δ 55.69 (s, 4C, $-O\underline{C}H_3$), 14.71 (d, *J*=19.8 Hz, 3C, $-P\underline{C}H_2-$), 8.02 (s, 3C, $-PCH_2\underline{C}H_3$). $^{31}P\{^1H\}$ NMR (121 MHz, C_6D_6, 298 K): δ 61.44 (d, *J*= 273 Hz, 1P), 5.55 (d, *J*= 273 Hz, 1P).

PNN-Ni(py)Ph: In the glove box, to a precooled (-78 °C) solution of the ligand **PN^{H}N** (40mg, 0.1 mmol) in tetrahydrofuran (THF) (2 mL) was added a precooled (-78 °C) solution

(2 mL) of KHMDS (20.5 mg, 1.05 equiv.) in THF. The mixture was then slowly warmed up to room temperature. After stirring for additional 30 min, all volatiles were removed from solution which was triturated with pentane (2 x 5 mL). The resulting residue was then dissolved in toluene (6 mL) and added to a precooled (-78 °C) suspension of (tmeda)NiPhCl (27 mg, 0.95 equiv.) in toluene (4 mL). The mixture was then warmed up to room temperature and a small amount of pyridine (0.05 mL) was added and the resulting suspension was stirred for additional 24 h. All volatiles were then removed from solution which was triturated with pentane (2 x 5 mL). The resulting residue was then washed with pentane (10 mL), hexanes (10 mL), and diethyl ether (3 mL), yielding spectroscopically pure **PNN-Ni(py)Ph** as yellow solids (22.7 mg, 37 % Yield).

^{1}H NMR (400 MHz, C_6D_6): δ 8.62 (d, *J*= 5.3 Hz, 2H, ArH), 7.51 (d, *J*= 7.3 Hz, 2H, ArH), 7.11 (t, *J*= 8.2 Hz, 2H, ArH), 6.99 (d, *J*= 8.4 Hz, 2H, ArH), 6.95-6.84 (m, 1H, ArH), 6.75 (dd, *J*= 7.9, 6.8 Hz, 2H, ArH), 6.67-6.60 (m, 1H, ArH), 6.52 (dd, *J*= 7.8 Hz, 1H, ArH), 6.42 (dd, *J*= 6.2, 1.9 Hz, 1H, ArH), 6.33 (dd, *J*= 8.2, 3.7 Hz, 4H, ArH), 6.26 (d, *J*= 6.6 Hz, 2H, ArH), 5.71 (td, *J*= 6.2, 1.5 Hz, 1H, ArH), 3.28 (s, 12H, -OCH_3), 1.23-1.13 (m, 6H, -PC$\underline{H}_2$-), 0.64 (dt, *J*= 15.0, 7.6 Hz, 9H, -$PCH_2C\underline{H}_3$). ^{13}C{^{1}H} NMR (101 MHz, C_6D_6): δ 171.77 (s, 1C, Aryl-C), 161.39 (s, 4C, Aryl-C), 159.77 (dd, *J*=41.1 Hz, 2C, Aryl-C), 150.21 (s, 2C, Aryl-C), 145.22 (s, 1C, Aryl-C), 136.58 (s, 2C, Aryl-C), 135.44 (s, 1C, Aryl-C), 135.06 (s, 1C, Aryl-C), 129.55 (s, 2C, Aryl-C), 124.84 (s, 2C, Aryl-C), 123.83 (s, 2C, Aryl-C), 120.52 (s, 1C, Aryl-C), 115.97 (d, *J*=67.1 Hz, 1C, Aryl-C), 115.60 (d, *J*=25.6 Hz, 1C, Aryl-C), 104.89 (s, 4C, Aryl-C), 104.20 (s, 1C, Aryl-C), 55.83 (s, 4C, -O$\underline{C}H_3$-). ^{31}P{^{1}H} NMR (121 MHz, C_6D_6, 298 K): δ 64.97 (s, 1P).

PCN-Ni(P)Ar^{O2}: In the glove box, to a precooled (-78 °C) solution of the ligand **PN^{H}N** (40mg, 0.1 mmol) in tetrahydrofuran (THF) (2 mL) was added a precooled (-78 °C) solution (2 mL) of ^{t}BuLi (6.4 mg, 1.0 equiv., 0.1 mmol) in n-pentane. The mixture was then slowly

warmed up to room temperature. After stirring for additional 30 min, all volatiles were removed from solution which was triturated with pentane (2 x 5 mL). The resulting residue was then dissolved in toluene (4 mL) and cooled to -78 °C. To this solution was added a toluene solution (2 mL) of $(PEt_3)_2NiPhCl$ (39.2, 0.95 equiv.). The mixture was then slowly warmed up to room temperature and stirred for additional 24 h. All volatiles were then removed from solution which was triturated with pentane (2 x 5 mL). The resulting residue was then washed with pentane (10 mL) and hexanes (5 mL), yielding **PCN-Ni(P)Ar^{O2}** as red solids (15.0 mg, 46 % Yield).

^{1}H NMR (400 MHz, C_6D_6): δ δ 8.08-8.04 (m, 2H, ArH), 7.19-7.18 (m, 2H, ArH), 7.13-6.93 (m, 4H, ArH), 6.87 (d, *J*= 6.5 Hz, 1H, ArH), 6.46-6.33 (m, 6H, ArH), 5.29 (d, *J*= 4.4 Hz, 1H, -PC<u>H</u>=), 3.66 (s, 6H, -OCH_3), 3.50 (s, 6H, -OCH_3), 1.18 (td, *J*= 7.6, 4.5 Hz, 6H, ArH), 0.62 (dt, *J*= 14.7, 7.6 Hz, 9H, ArH). ^{31}P{^{1}H} NMR (121 MHz, C_6D_6, 298 K): δ 7.74 (d, *J*= 54.1Hz, 1P), -5.39 (d, *J*= 54.1 Hz, 1P).

Protonolysis of PN^{H}N-NiC$^{Si}_{2}$

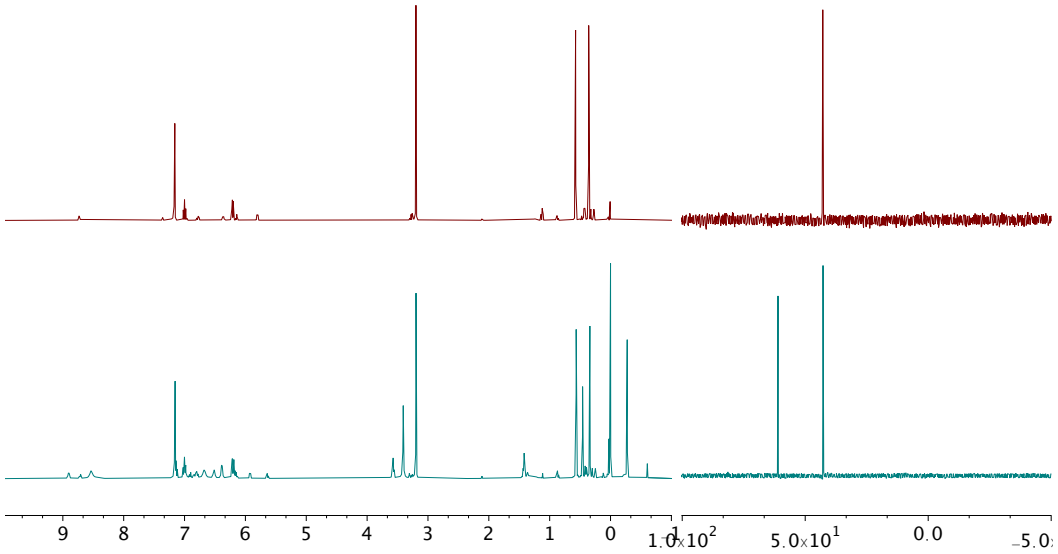

Figure SAA.1. ^{1}H (left) and ^{31}P{^{1}H} (right) NMR spectra of **PN^{H}N-NiC$^{Si}_{2}$** (top) and the mixture after being heated at 40 °C for 24 h.

Appendix A

Supplemental information for olefin copolymerization

General procedure for high throughput parallel polymerization reactor (PPR) runs.

Polyolefin catalysis screening was performed in a high throughput parallel polymerization reactor (PPR) system. The PPR system was comprised of an array of 48 single cell (6 x 8 matrix) reactors in an inert atmosphere glovebox. Each cell was equipped with a glass insert with an internal working liquid volume of approximately 5 mL. Each cell had independent controls for pressure and was continuously stirred at 800 rpm. Catalysts were prepared in toluene. All liquids (i.e., solvent, tBA, and catalyst solutions) were added via robotic syringes. Gaseous reagents (i.e., ethylene) were added via a gas injection port. Prior to each run, the reactors were heated to 50 °C, purged with ethylene, and vented.

All desired cells were injected with tBA followed with a portion of toluene (This step was skipped for ethylene homopolymerization). The reactors were heated to the run temperature and then pressured to the appropriate psig with ethylene. Catalyst were then added to the cells. Each catalyst addition was chased with a small amount of toluene so that after the final addition, a total reaction volume of 5 mL was reached. Upon addition of the catalyst, the PPR software began monitoring the pressure of each cell. The desired pressure (within approximately 2-6 psig) was maintained by the supplemental addition of ethylene gas by opening the valve at the set point minus 1 psi and closing it when the pressure reached 2 psi higher. The pressure of each cell was monitored during and after the quench to ensure that no further ethylene consumption happens. The shorter the "Quench Time" (the duration between catalyst addition and oxygen quench), the more active the catalyst. All drops in pressure were cumulatively recorded as "Uptake" or "Conversion" of the ethylene for the duration of the run. After 1h, each reaction was then quenched by addition of 1% oxygen in nitrogen for 30 seconds at 40 psi higher than the reactor pressure. After all the reactors were

quenched they were allowed to cool to about 60 °C. They were then vented and the tubes were removed. The polymer samples (if any) were then dried in a centrifugal evaporator at 60 °C for 12 hours, weighed to determine polymer yield.

Crystallographic Information

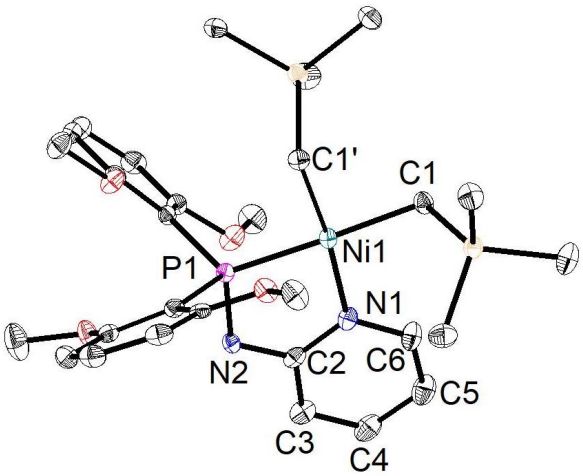

Figure SAA.2: Solid-State Structure of **PN^{H}N-NiC$^{Si}_{2}$**. Ellipsoids are show at the 50% probability level. Hydrogen atoms excluded for clarity.

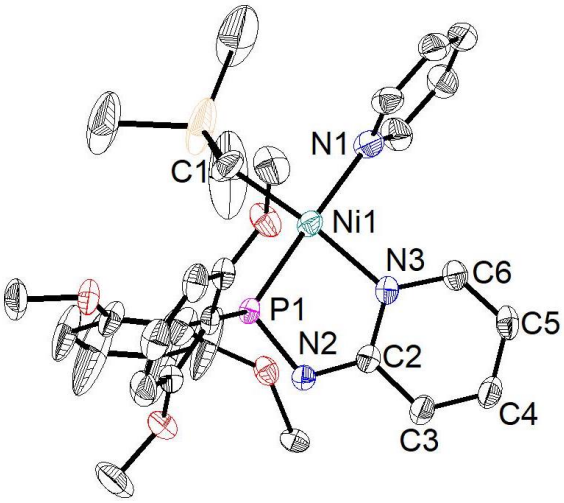

Figure SAA.3: Solid-State Structure of **PNN-Ni(py)C^{Si}**. Ellipsoids are show at the 50% probability level. Hydrogen atoms excluded for clarity.

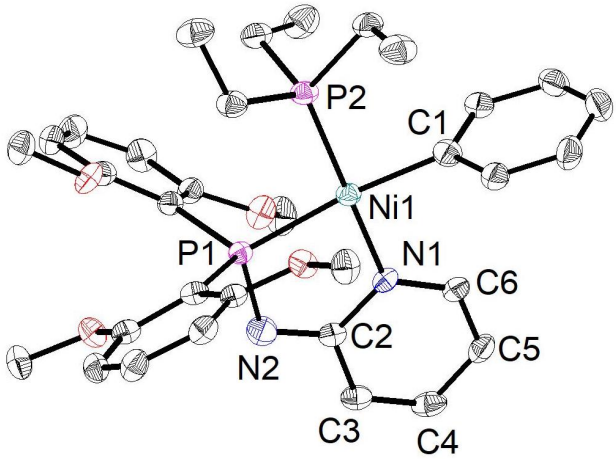

Figure SAA.4: Solid-State Structure of **PNN-Ni(P)Ph** (*cis*-isomer). Ellipsoids are show at the 50% probability level. Hydrogen atoms excluded for clarity.

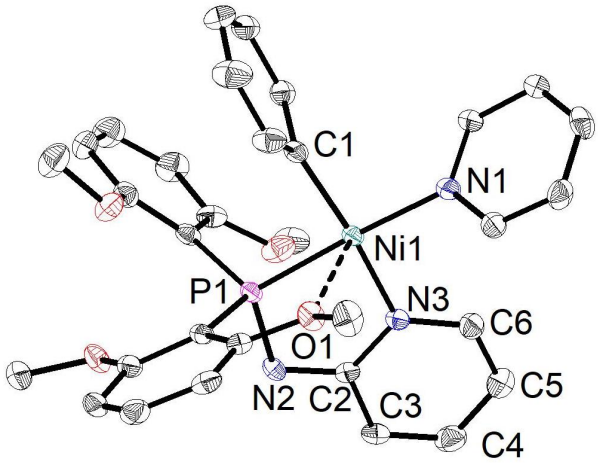

Figure SAA.5: Solid-State Structure of **PNN-Ni(py)Ph**. Ellipsoids are show at the 50% probability level. Hydrogen atoms excluded for clarity.

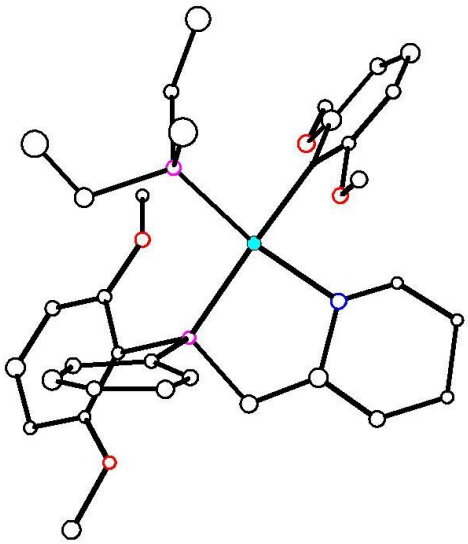

Figure SAA.6: Solid-State Structure of **PCN-Ni(P)Ar^{O2}**(connectivity).

REFERENCES

(1) Keim, W., Nickel: an element with wide application in industrial homogeneous catalysis. *Angewandte Chemie International Edition in English* **1990,** *29* (3), 235-244.

(2) Clevenger, A. L.; Stolley, R. M.; Aderibigbe, J.; Louie, J., Trends in the usage of bidentate phosphines as ligands in nickel catalysis. *Chem. Rev.* **2020,** *120* (13), 6124-6196.

(3) Mu, H.; Zhou, G.; Hu, X.; Jian, Z., Recent advances in nickel mediated copolymerization of olefin with polar monomers. *Coord. Chem. Rev.* **2021,** *435*, 213802.

(4) Grushin, V. V., Mixed phosphine− phosphine oxide ligands. *Chem. Rev.* **2004,** *104* (3), 1629-1662.

(5) Nair, P. P.; Philip, R. M.; Anilkumar, G., Nickel catalysts in Sonogashira coupling reactions. *Organic & Biomolecular Chemistry* **2021,** *19* (19), 4228-4242.

(6) Tan, C.; Chen, C., Emerging palladium and nickel catalysts for copolymerization of olefins with polar monomers. *Angew. Chem.* **2019,** *131* (22), 7268-7276.

(7) Mu, H.; Pan, L.; Song, D.; Li, Y., Neutral nickel catalysts for olefin homo-and copolymerization: relationships between catalyst structures and catalytic properties. *Chem. Rev.* **2015,** *115* (22), 12091-12137.

(8) Chen, M.; Chen, C., Rational design of high-performance phosphine sulfonate nickel catalysts for ethylene polymerization and copolymerization with polar monomers. *ACS Catal.* **2017,** *7* (2), 1308-1312.

(9) Xin, B. S.; Sato, N.; Tanna, A.; Oishi, Y.; Konishi, Y.; Shimizu, F., Nickel catalyzed copolymerization of ethylene and alkyl acrylates. *J. Am. Chem. Soc.* **2017,** *139* (10), 3611-3614.

(10) Xiong, S.; Hong, A.; Bailey, B. C.; Spinney, H. A.; Senecal, T. D.; Bailey, H.; Agapie, T., Highly Active and Thermally Robust Nickel Enolate Catalysts for the Synthesis of Ethylene-Acrylate Copolymers. *Angew. Chem. Int. Ed.* **2022**.

(11) Zhang, Y.; Mu, H.; Pan, L.; Wang, X.; Li, Y., Robust bulky [P, O] neutral nickel catalysts for copolymerization of ethylene with polar vinyl monomers. *ACS Catal.* **2018,** *8* (7), 5963-5976.

(12) Xiong, S.; Shoshani, M. M.; Zhang, X.; Spinney, H. A.; Nett, A. J.; Henderson, B. S.; Miller III, T. F.; Agapie, T., Efficient Copolymerization of Acrylate and Ethylene with Neutral P, O-Chelated Nickel Catalysts: Mechanistic Investigations of Monomer Insertion and Chelate Formation. *J. Am. Chem. Soc.* **2021,** *143* (17), 6516-6527.

(13) Wang, X.-l.; Zhang, Y.-p.; Wang, F.; Pan, L.; Wang, B.; Li, Y.-s., Robust and Reactive Neutral Nickel Catalysts for Ethylene Polymerization and Copolymerization with a Challenging 1,1-Disubstituted Difunctional Polar Monomer. *ACS Catal.* **2021,** *11* (5), 2902-2911.

(14) Zhang, Y.; Mu, H.; Wang, X.; Pan, L.; Li, Y., Elaborate tuning in ligand makes a big difference in catalytic performance: bulky nickel catalysts for (co) polymerization of ethylene with promising vinyl polar monomers. *ChemCatChem* **2019,** *11* (9), 2329-2340.

(15) Noda, S.; Kochi, T.; Nozaki, K., Synthesis of allylnickel complexes with phosphine sulfonate ligands and their application for olefin polymerization without activators. *Organometallics* **2009,** *28* (2), 656-658.

(16) Tan, C.; Qasim, M.; Pang, W.; Chen, C., Ligand–metal secondary interactions in phosphine–sulfonate palladium and nickel catalyzed ethylene (co) polymerization. *Polym. Chem* **2020,** *11* (2), 411-416.

(17) Xia, J.; Zhang, Y.; Zhang, J.; Jian, Z., High-performance neutral phosphine-sulfonate nickel (II) catalysts for efficient ethylene polymerization and copolymerization with polar monomers. *Organometallics* **2019,** *38* (5), 1118-1126.

(18) Liang, T.; Chen, C., Side-arm control in phosphine-sulfonate palladium-and nickel-catalyzed ethylene polymerization and copolymerization. *Organometallics* **2017,** *36* (12), 2338-2344.

(19) Yang, B.; Xiong, S.; Chen, C., Manipulation of polymer branching density in phosphine-sulfonate palladium and nickel catalyzed ethylene polymerization. *Polym. Chem* **2017,** *8* (40), 6272-6276.

(20) Wu, Z.; Chen, M.; Chen, C., Ethylene polymerization and copolymerization by palladium and nickel catalysts containing naphthalene-bridged phosphine–sulfonate ligands. *Organometallics* **2016,** *35* (10), 1472-1479.

(21) Ito, S.; Ota, Y.; Nozaki, K., Ethylene/allyl monomer cooligomerization by nickel/phosphine–sulfonate catalysts. *Dalton Trans* **2012,** *41* (45), 13807-13809.

(22) Baur, M.; Mecking, S., Polyethylenes with Combined In-Chain and Side-Chain Functional Groups from Catalytic Terpolymerization of Carbon Monoxide and Acrylate. *ACS Macro Lett.* **2022,** *11* (10), 1207-1211.

(23) Lin, F.; Morgen, T. O.; Mecking, S., Living Aqueous Microemulsion Polymerization of Ethylene with Robust Ni (II) Phosphinophenolato Catalysts. *J. Am. Chem. Soc.* **2021,** *143* (49), 20605-20608.

(24) Baur, M.; Lin, F.; Morgen, T. O.; Odenwald, L.; Mecking, S., Polyethylene materials with in-chain ketones from nonalternating catalytic copolymerization. *Science* **2021,** *374* (6567), 604-607.

(25) Zou, C.; Si, G.; Chen, C., A general strategy for heterogenizing olefin polymerization catalysts and the synthesis of polyolefins and composites. *Nat. Commun.* **2022,** *13* (1), 1-12.

(26) Chen, C., Designing catalysts for olefin polymerization and copolymerization: beyond electronic and steric tuning. *Nat. Rev. Chem.* **2018,** *2* (5), 6-14.

(27) Nakamura, A.; Anselment, T. M.; Claverie, J.; Goodall, B.; Jordan, R. F.; Mecking, S.; Rieger, B.; Sen, A.; Van Leeuwen, P. W.; Nozaki, K., Ortho-phosphinobenzenesulfonate: A superb ligand for palladium-catalyzed coordination–insertion copolymerization of polar vinyl monomers. *Acc. Chem. Res.* **2013,** *46* (7), 1438-1449.

(28) Shoshani, M. M.; Xiong, S.; Lawniczak, J. J.; Zhang, X.; Miller, T. F.; Agapie, T., Phosphine-Phenoxide Nickel Catalysts for Ethylene/Acrylate Copolymerization: Olefin Coordination and Complex Isomerization Studies Relevant to the Mechanism of Catalysis. *Organometallics* **2022**.

(29) Si, G.; Na, Y.; Chen, C., Ethylene (co) Oligomerization by Phosphine-Pyridine Based Palladium and Nickel Catalysts. *ChemCatChem* **2018,** *10* (22), 5135-5140.

(30) Cao, L.; Cai, Z.; Li, M., Phosphinobenzenamine Nickel Catalyzed Efficient Copolymerization of Methyl Acrylate with Ethylene and Norbornene. *Macromolecules* **2022,** *55* (9), 3513-3521.

(31) Chen, H.-P.; Liu, Y.-H.; Peng, S.-M.; Liu, S.-T., New Bulky Phosphino− Pyridine Ligands. Palladium and Nickel Complexes for the Catalytic Polymerization and Oligomerization of Ethylene. *Organometallics* **2003,** *22* (24), 4893-4899.

(32) Wang, H. Y.; Jin, G. X., Highly Active Neutral Nickel (ii) Complexes Bearing P, N-Chelate Ligands: Synthesis, Characterization and Their Application to Addition Polymerization of Norbornene. Wiley Online Library: 2005.

(33) Pietsch, J.; Braunstein, P.; Chauvin, Y., Nickel phenyl complexes with chelating κ 2-P, O ligands as catalysts for the oligomerization of ethylene into linear α-olefins. *New Journal of Chemistry* **1998,** *22* (5), 467-472.

(34) Braunstein, P.; Pietsch, J.; Chauvin, Y.; Mercier, S.; Saussine, L.; DeCian, A.; Fischer, J., Phenyl nickel complexes with a chelating P, N ligand. Structures of Ph 3 P [double bond, length half m-dash] CHC ([double bond, length half m-dash] NPh) Ph and [NiPh {Ph 2 PCH [horiz bar, double dot above] C)[horiz bar, double dot above] NPh) Ph}-{Ph 3 P [double bond, length half m-dash] CHC ([double bond, length half m-dash] NPh) Ph-N}]. *J. Chem. Soc., Dalton Trans.* **1996,** (17), 3571-3574.

(35) Braunstein, P.; Pietsch, J.; Chauvin, Y.; DeCian, A.; Fischer, J., Synthesis of nickel phenyl complexes with new chelating κ2-P, N ligands derived from α-iminoazatriphenylphosphoranes. *J. Organomet. Chem.* **1997,** *529* (1-2), 387-393.

(36) Takebayashi, S.; Iron, M. A.; Feller, M.; Rivada-Wheelaghan, O.; Leitus, G.; Diskin-Posner, Y.; Shimon, L. J.; Avram, L.; Carmieli, R.; Wolf, S. G., Iron-catalysed ring-opening metathesis polymerization of olefins and mechanistic studies. *Nat. Catal.* **2022**, 1-9.

(37) Liang, L.-C.; Lee, W.-Y.; Yin, C.-C., Nickel (II) complexes containing bidentate diarylamido phosphine ligands. *Organometallics* **2004,** *23* (14), 3538-3547.

(38) Rünzi, T.; Tritschler, U.; Roesle, P.; Göttker-Schnetmann, I.; Möller, H. M.; Caporaso, L.; Poater, A.; Cavallo, L.; Mecking, S., Activation and deactivation of neutral palladium (II) phosphinesulfonato polymerization catalysts. *Organometallics* **2012,** *31* (23), 8388-8406.

(39) Pangborn, A. B.; Giardello, M. A.; Grubbs, R. H.; Rosen, R. K.; Timmers, F. J., Safe and convenient procedure for solvent purification. *Organometallics* **1996,** *15* (5), 1518-1520.

(40) Neuwald, B.; Caporaso, L.; Cavallo, L.; Mecking, S., Concepts for stereoselective acrylate insertion. *J. Am.*

Chem. Soc. **2013,** *135* (3), 1026-1036.

(41) Tao, W. j.; Nakano, R.; Ito, S.; Nozaki, K., Copolymerization of ethylene and polar monomers by using Ni/IzQO catalysts. *Angew. Chem. Int. Ed.* **2016,** *55* (8), 2835-2839.

(42) Marshall, W. J.; Grushin, V. V., Activation of chlorobenzene with Ni(0) N,N-chelates A remarkably profound effect of a minuscule change in ligand structure. *Canadian Journal of Chemistry* **2005,** *83* (6-7), 640-645.

APPENDIX B

Nuclear Magnetic Resonance Spectra for Characterization of Isolated and in-situ Generated Compounds

Chapter 2

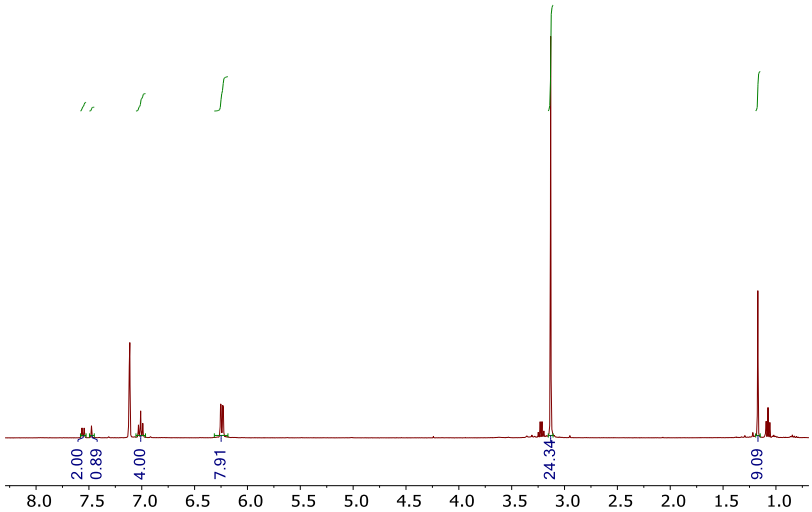

Figure AB2.1. ^{1}H NMR spectrum of **POPH** in C_6D_6.

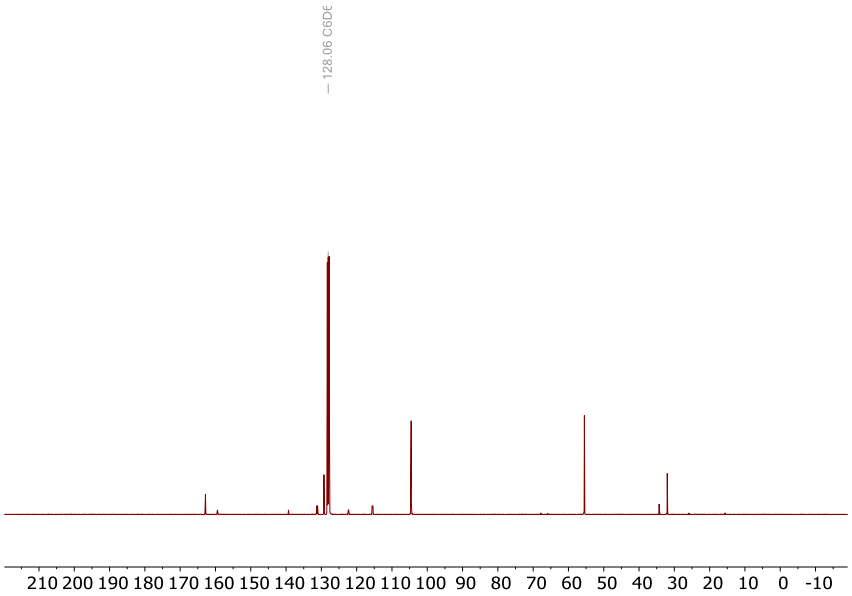

Figure AB2.2. ^{13}C{^{1}H} NMR of **POPH** in C_6D_6.

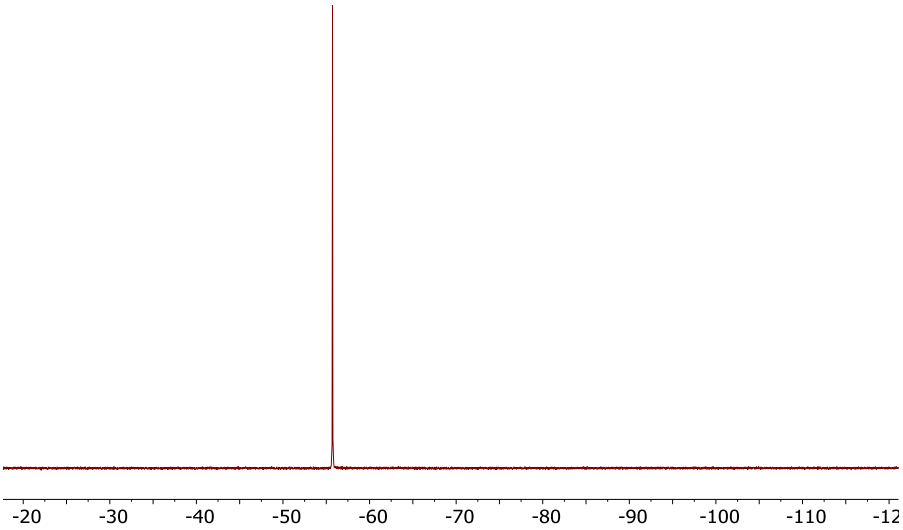

Figure AB2.3. $^{31}P\{^{1}H\}$ NMR spectrum of **POPH** in C_6D_6.

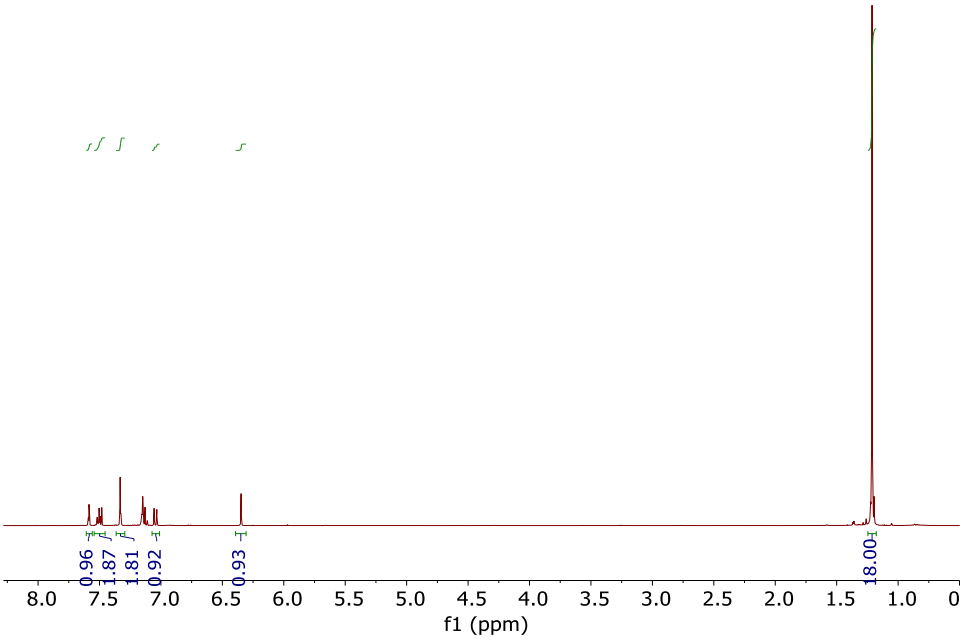

Figure AB2.4. ^{1}H NMR Spectrum of **D** in C_6D_6.

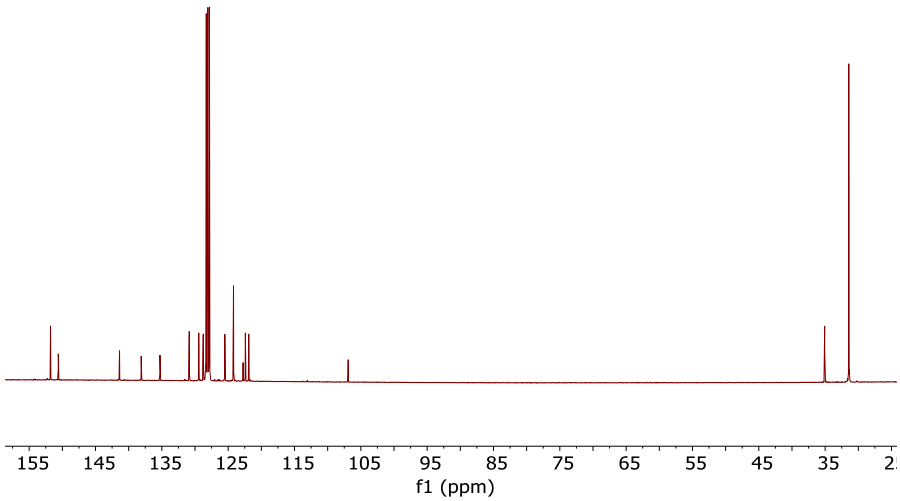

Figure AB2.5. $^{13}C\{^{1}H\}$ NMR Spectrum of **D** in C_6D_6.

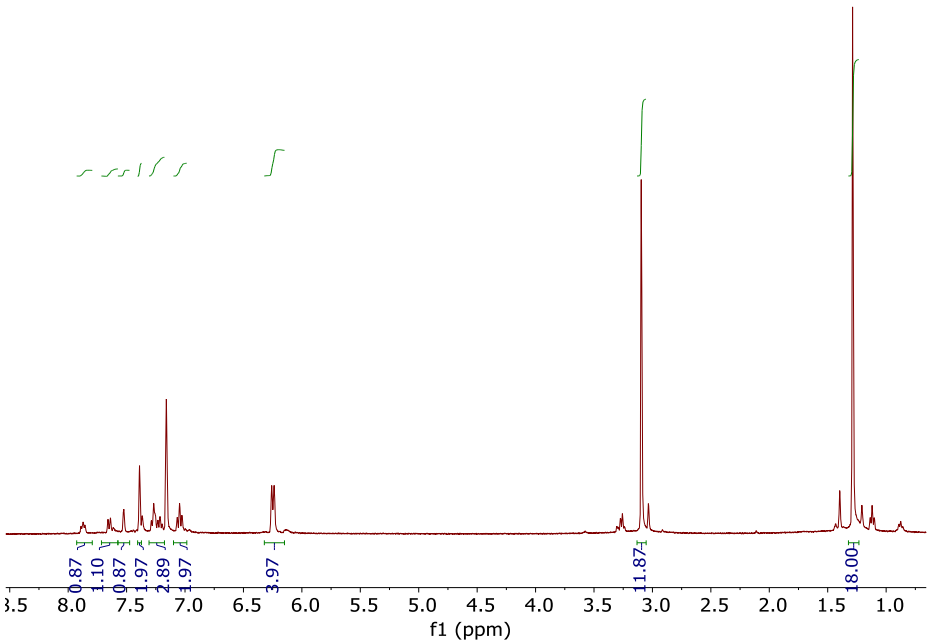

Figure AB2.6. ^{1}H NMR Spectrum of **PONapH** in C_6D_6.

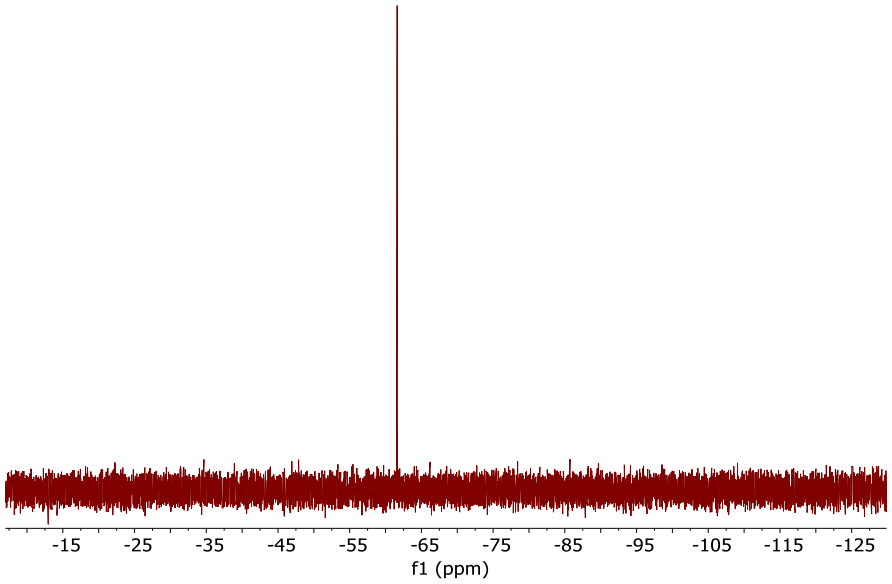

Figure AB2.7. $^{31}P\{^{1}H\}$ NMR spectrum of **PONapH** in C_6D_6.

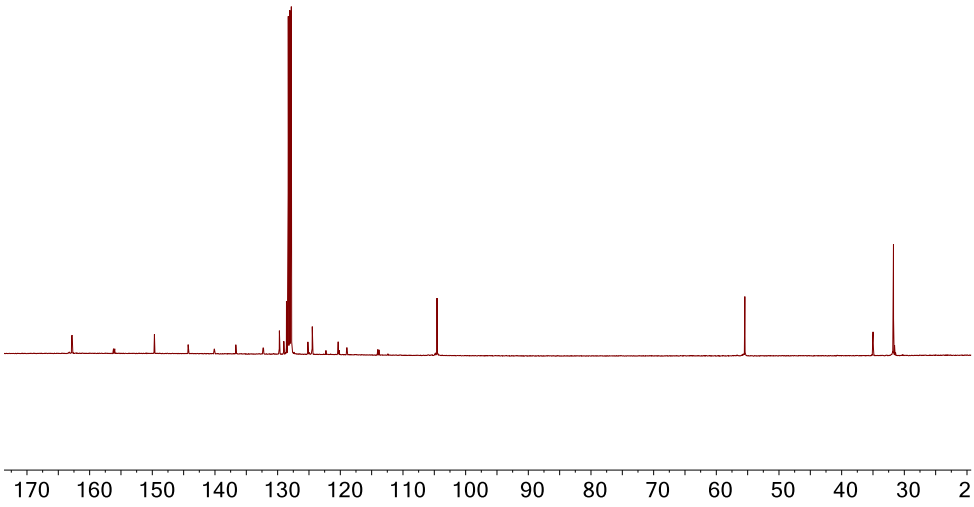

Figure AB2.8. $^{13}C\{^{1}H\}$ NMR spectrum of **PONapH** in C_6D_6.

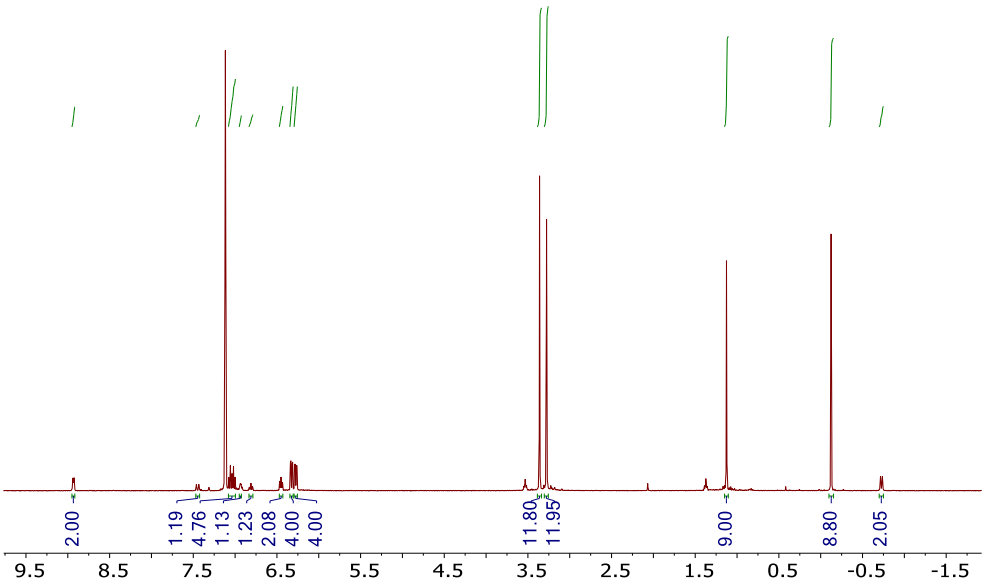

Figure AB2.9. ^{1}H NMR spectrum of **1** in C_6D_6.

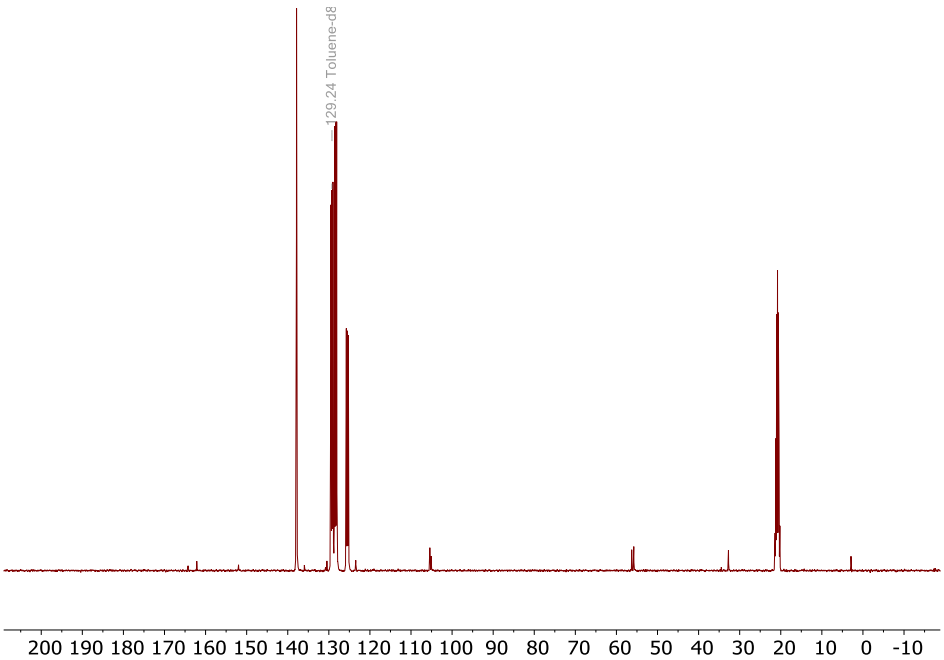

Figure AB2.10. $^{13}C\{^{1}H\}$ NMR spectrum of **1** in C_7D_8.

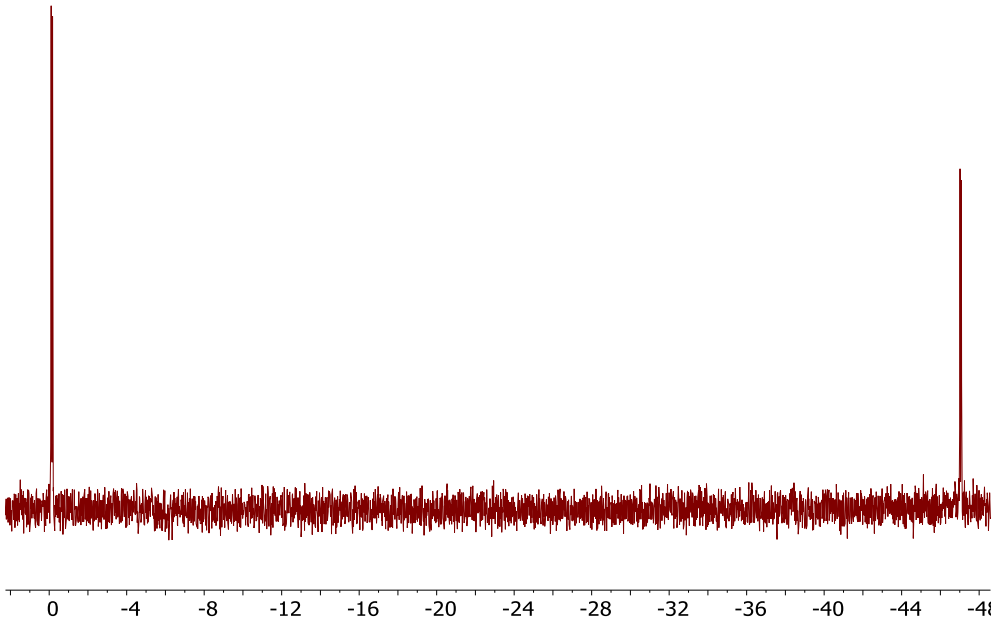

Figure AB2.11. $^{31}P\{^{1}H\}$ NMR spectrum of **1** in C_6D_6.

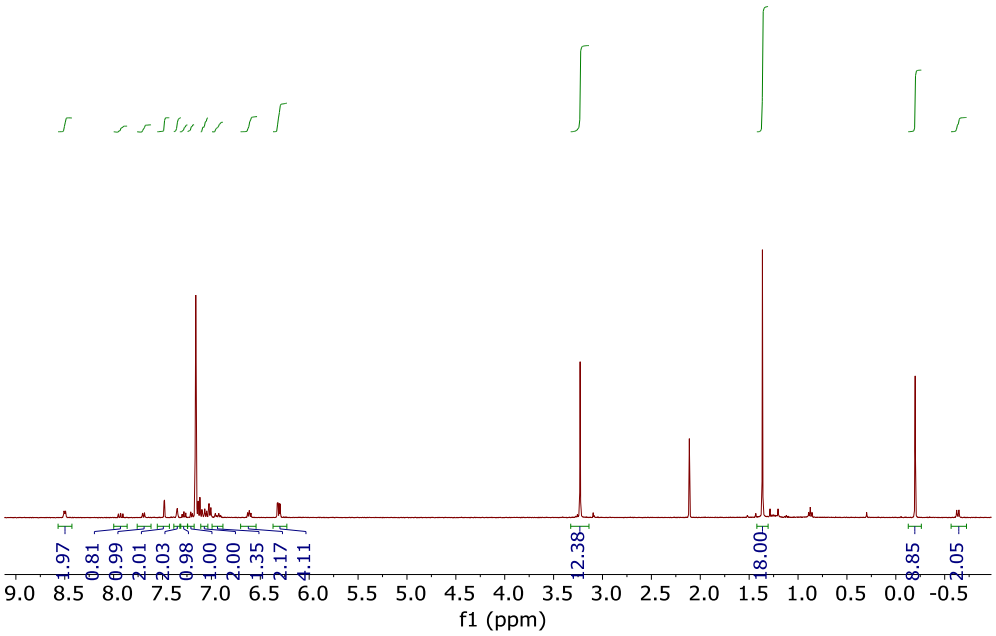

Figure AB2.12. ^{1}H NMR spectrum of **2** in C_6D_6.

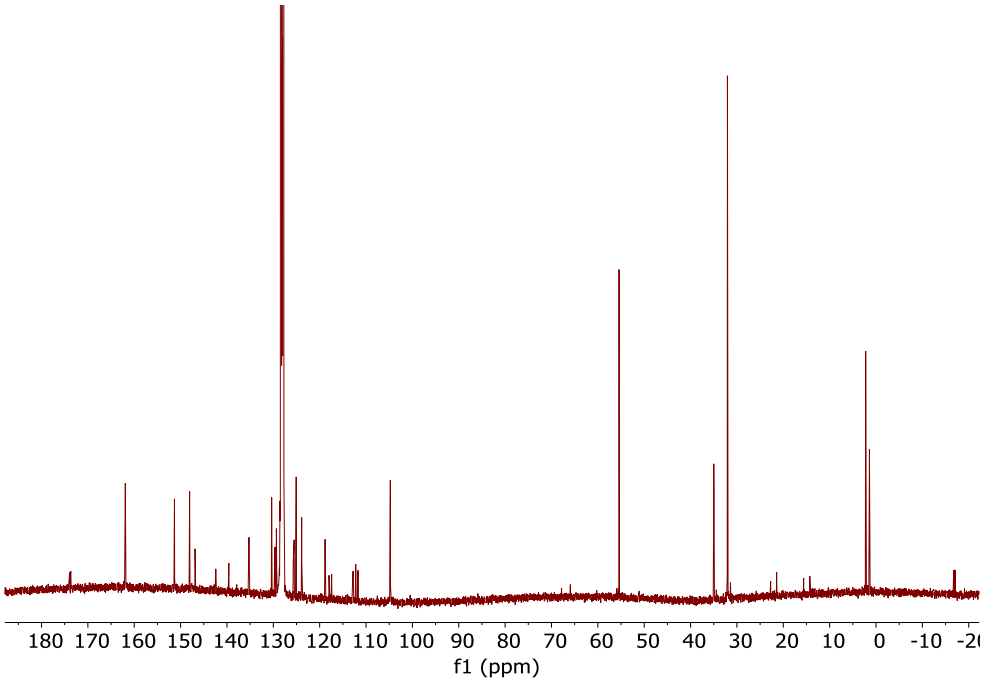

Figure AB2.13. $^{13}C\{^{1}H\}$ NMR spectrum of **2** in C_6D_6.

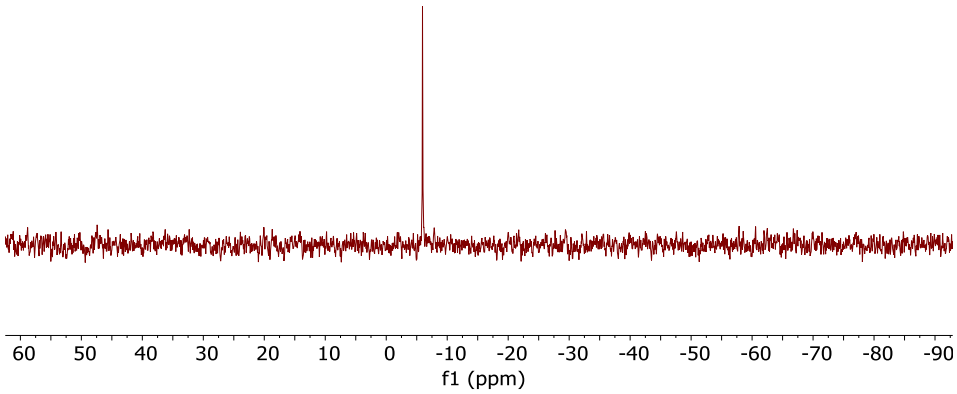

Figure AB2.14. $^{31}P\{^{1}H\}$ NMR spectrum of **2** in C_6D_6.

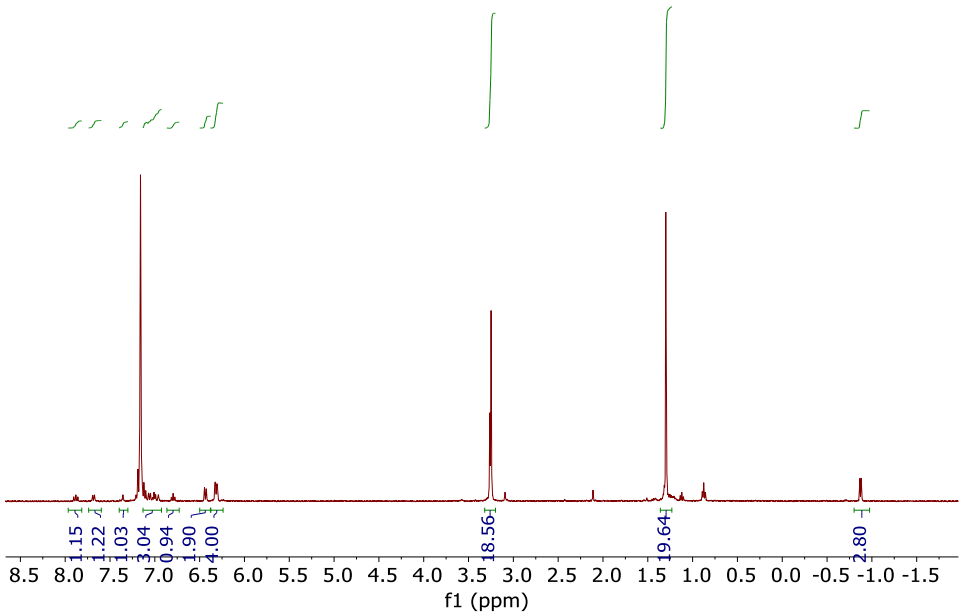

Figure AB2.15: ^{1}H NMR spectrum of **2-lut** in C_6D_6.

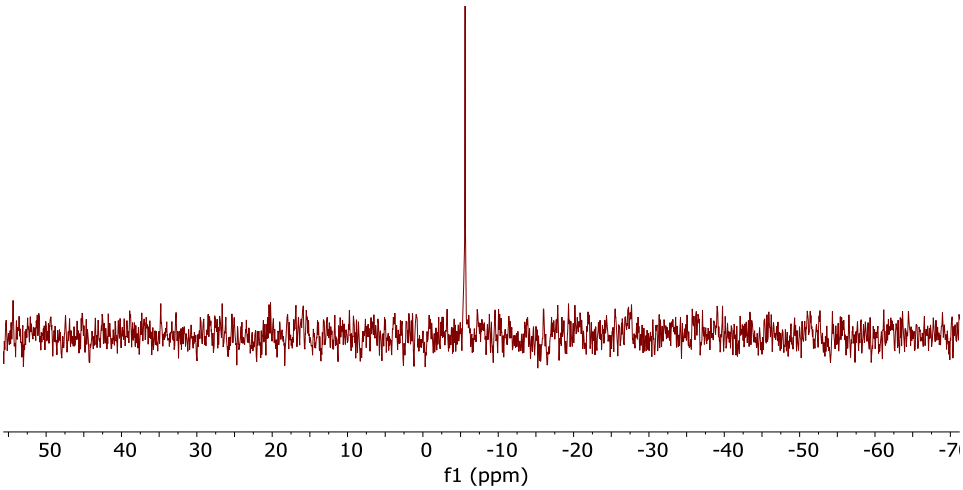

Figure AB2.16. ^{31}P{^{1}H} NMR spectrum of **2-lut** in C_6D_6.

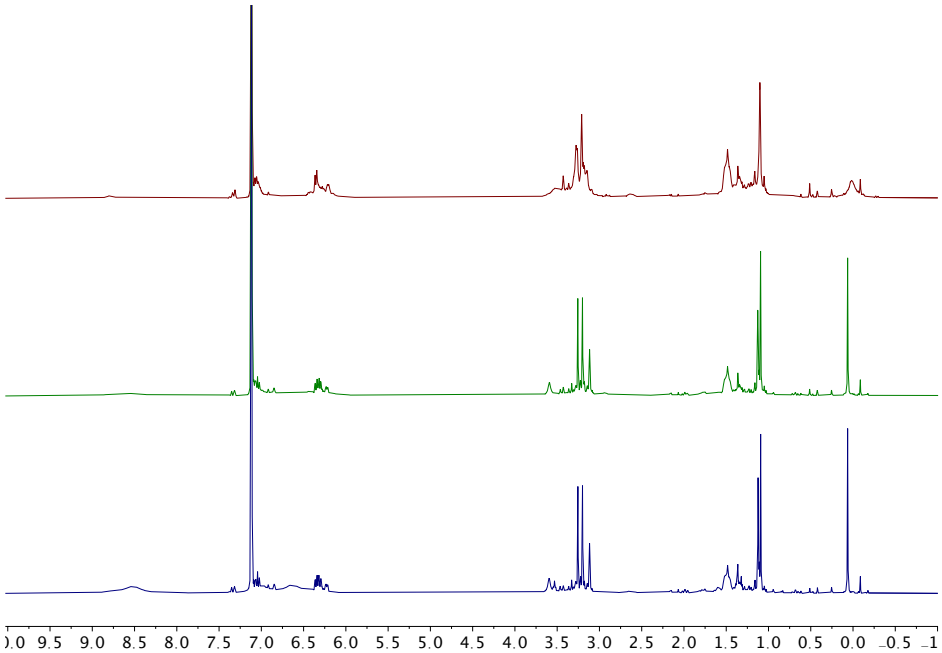

Figure AB2.17. ^{1}H NMR spectrum of **3** in C_6D_6 (top). ^{1}H NMR spectrum of **3** + 1 equiv. pyridine in C_6D_6 (middle). ^{1}H NMR spectrum of **3** + 5 equiv. pyridine in C_6D_6 (bottom).

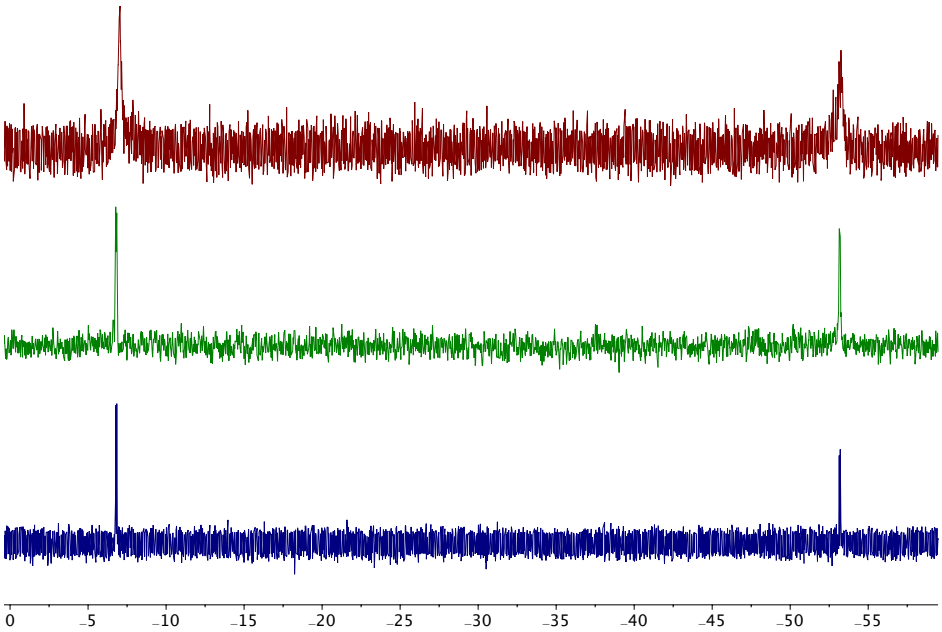

Figure AB2.18. ^{31}P{^{1}H} NMR spectrum of **3** in C_6D_6 (top). ^{31}P{^{1}H} NMR spectrum of **3** + 1 equiv. pyridine in C_6D_6 (middle). ^{31}P{^{1}H} NMR spectrum of **3** + 5 equiv. pyridine in C_6D_6 (bottom).

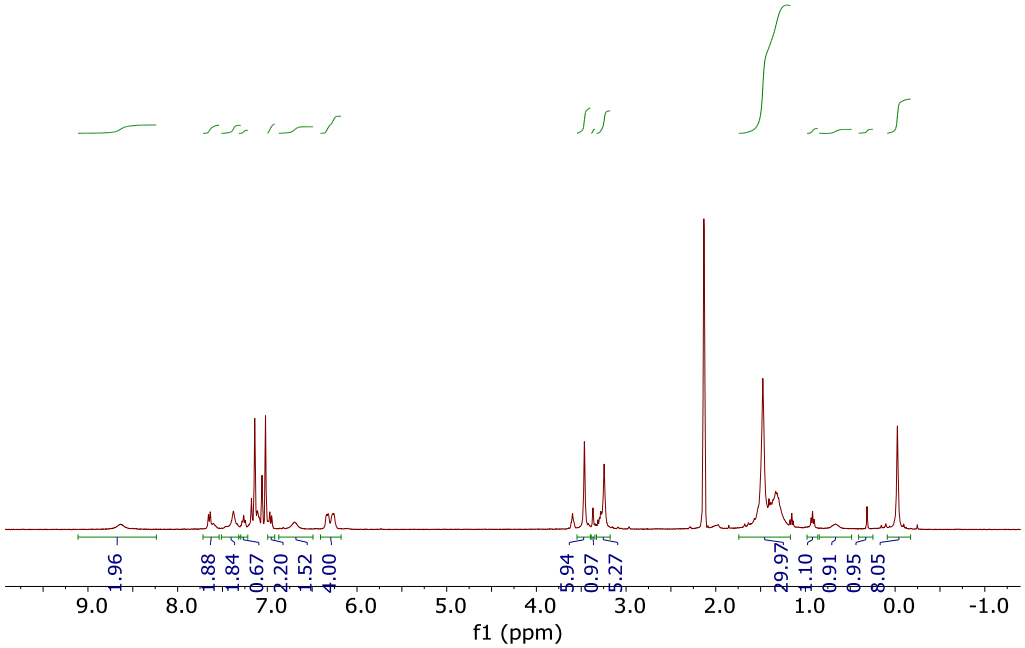

Figure AB2.19. ^{1}H NMR spectrum of **4** in C_6D_6.

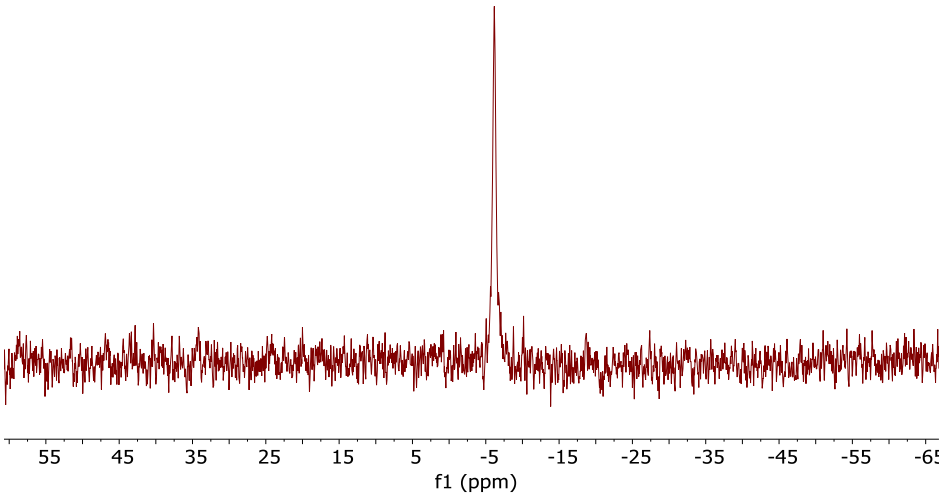

Figure AB2.20. $^{31}P\{^{1}H\}$ NMR spectrum of **4** in C_6D_6.

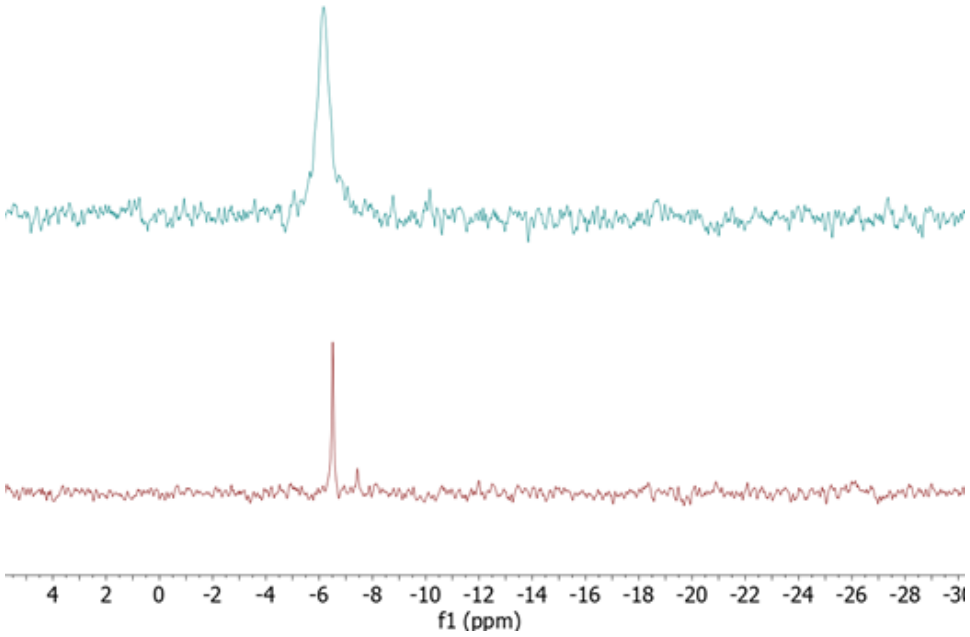

Figure AB2.21. $^{31}P\{^{1}H\}$ NMR spectrum of **4** in C_7D_8(top). $^{31}P\{^{1}H\}$ NMR spectrum **4** + 10 equivalents of pyridine in C_6D_6(bottom).

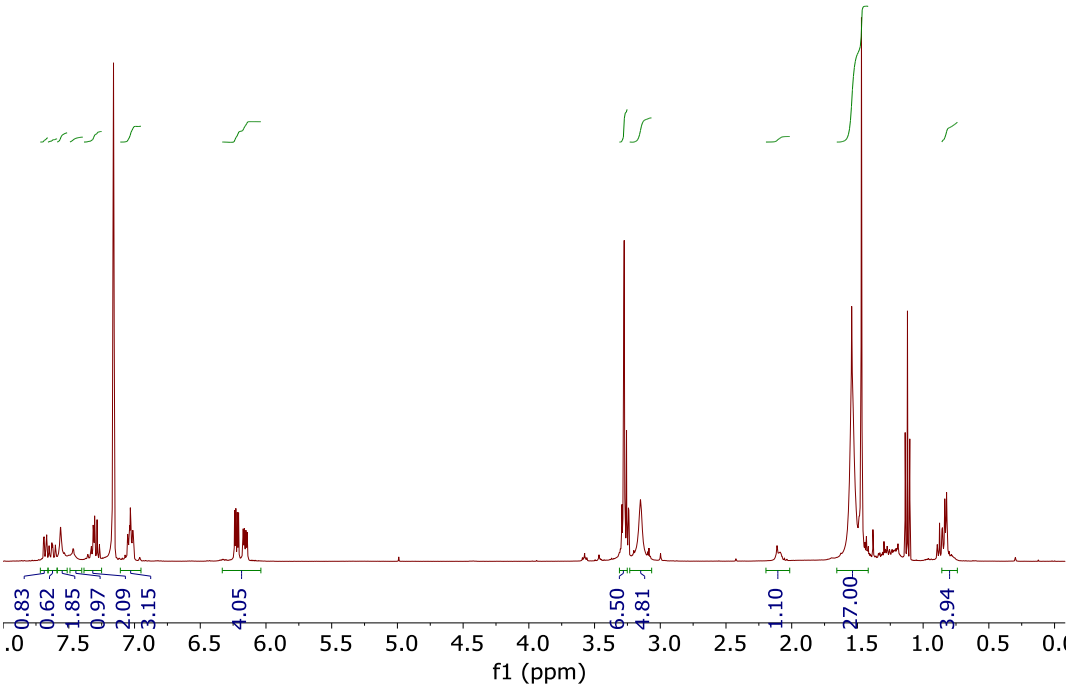

Figure AB2.22. ^{1}H NMR spectrum of **5** in C_6D_6

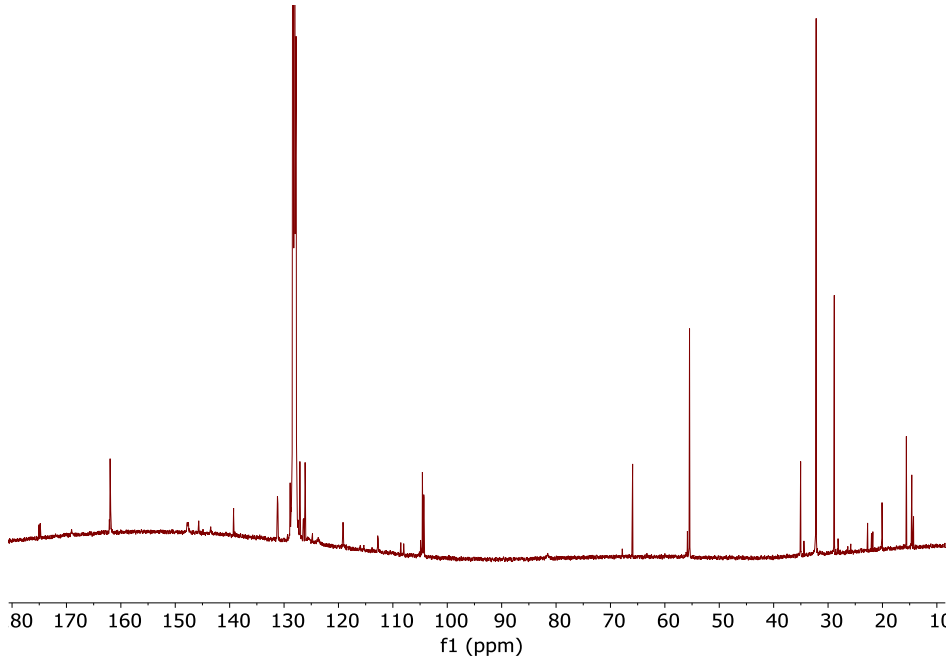

Figure AB2.23 $^{13}C\{^{1}H\}$ NMR spectrum of **5** in C_6D_6

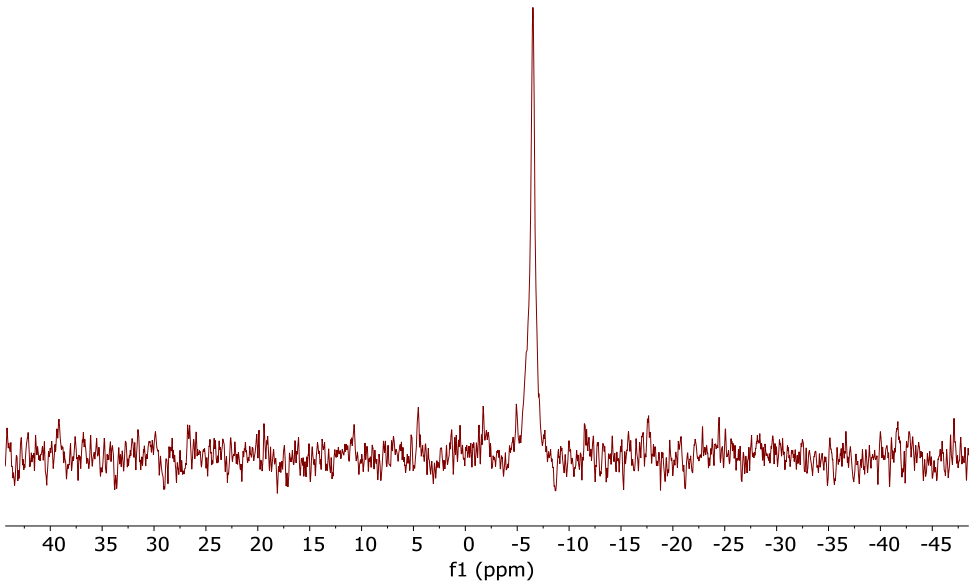

Figure AB2.24. $^{31}P\{^{1}H\}$ NMR spectrum of **5** in C_6D_6

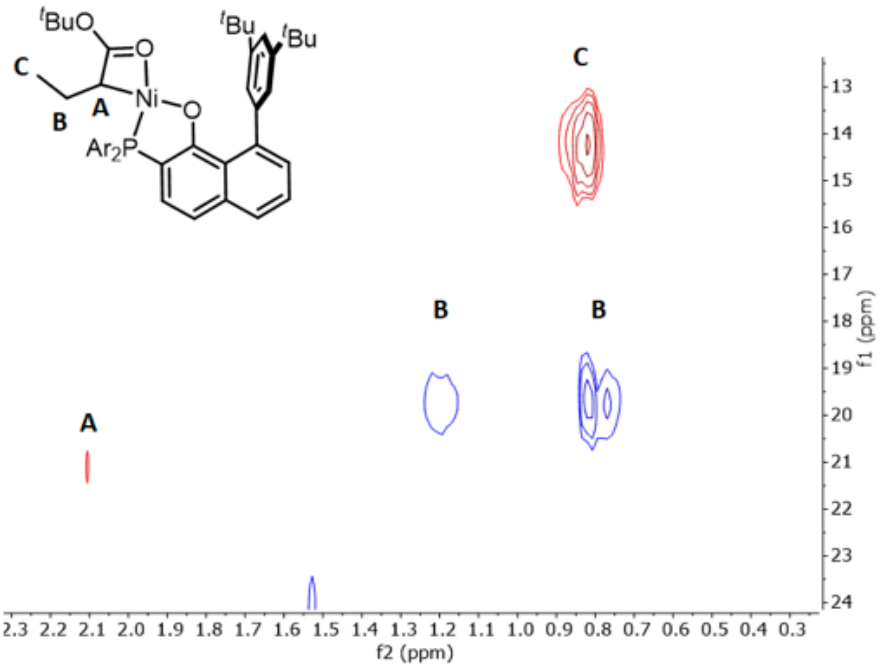

Figure AB2.25. $^{13}C\{^{1}H\}$-^{1}H HSQC NMR Spectrum of **5** in C_7D_8

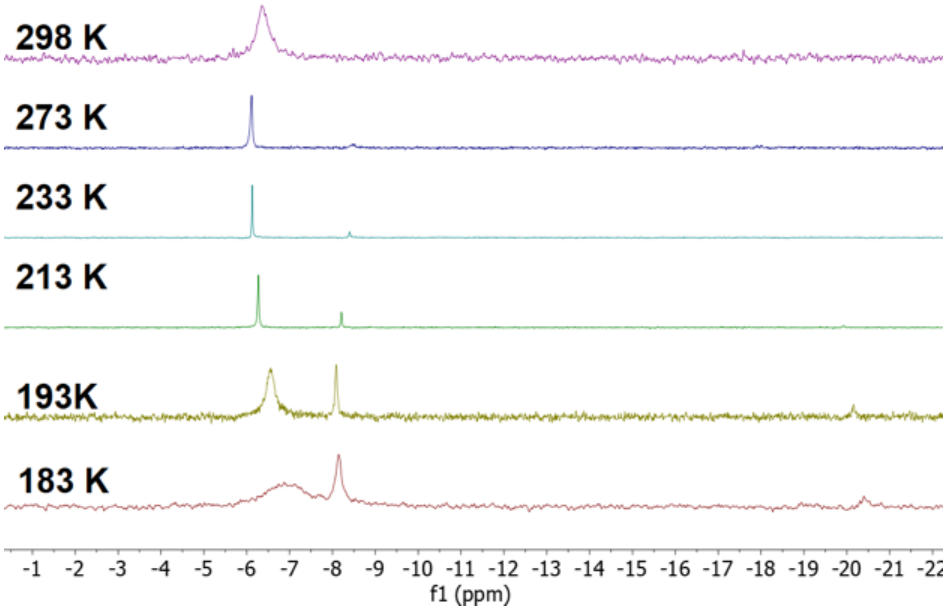

Figure AB2.26. $^{31}P\{^{1}H\}$ Variable-Temperature NMR Spectra of **5** in C_7D_8

Chapter 3

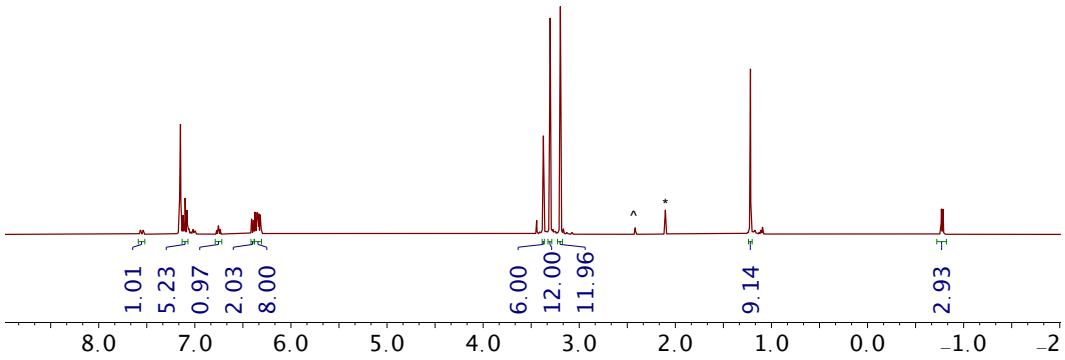

Figure AB3.1. ^{1}H NMR of **1lut-Me** in C_6D_6 (*: residue toluene, ^: residue free lutidine)

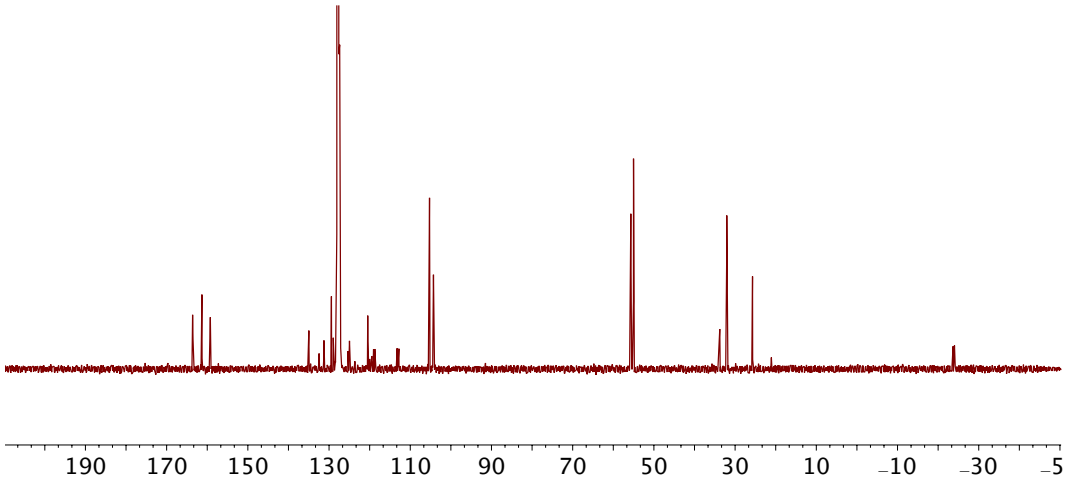

Figure AB3.2. ^{13}C{^{1}H} NMR of **1lut-Me** in C_6D_6.

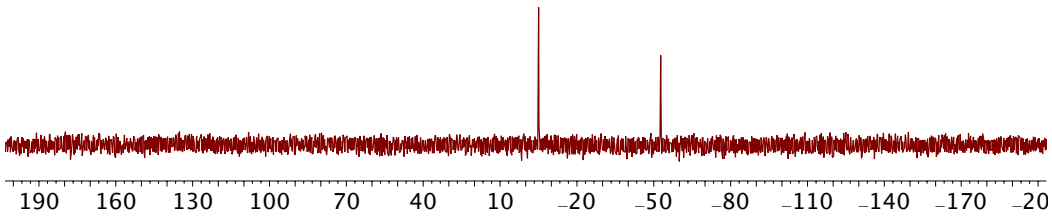

Figure AB3.3. ^{31}P{^{1}H} NMR of **1lut-Me** in C_6D_6.

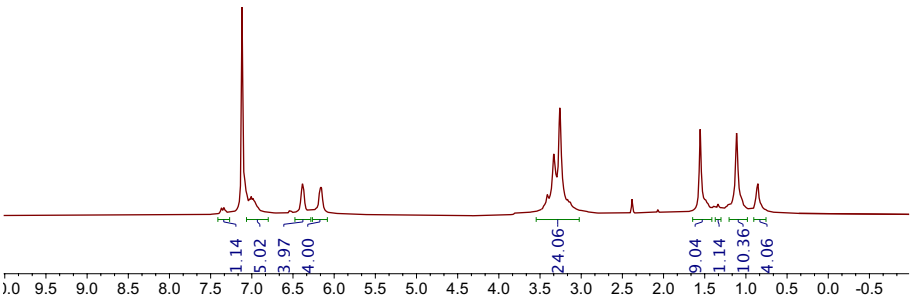

Figure AB3.4. ^{1}H NMR of **2-CCO** in C_6D_6.

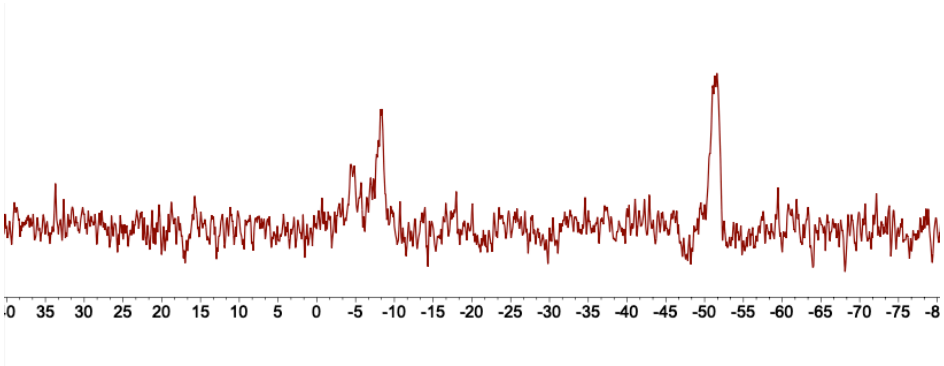

Figure AB3.5. ^{31}P{^{1}H} NMR NMR of **2-CCO** in C_6D_6.

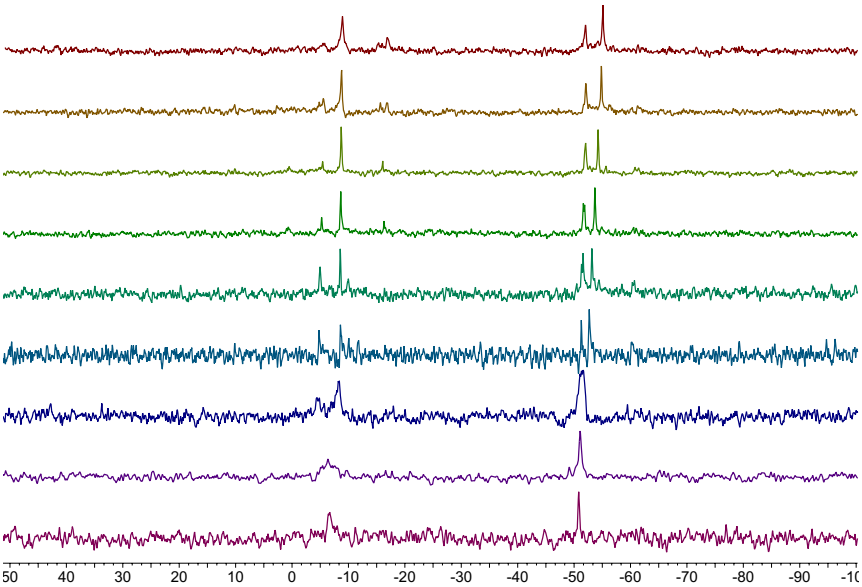

Figure AB3.6. ^{31}P{^{1}H} NMR of **1-CCO** in Tol-d8 at different temperatures (top to bottom: -90 °C, -60 °C, -40 °C, -20 °C, -0 °C, 25 °C, 40 °C, 60 °C).

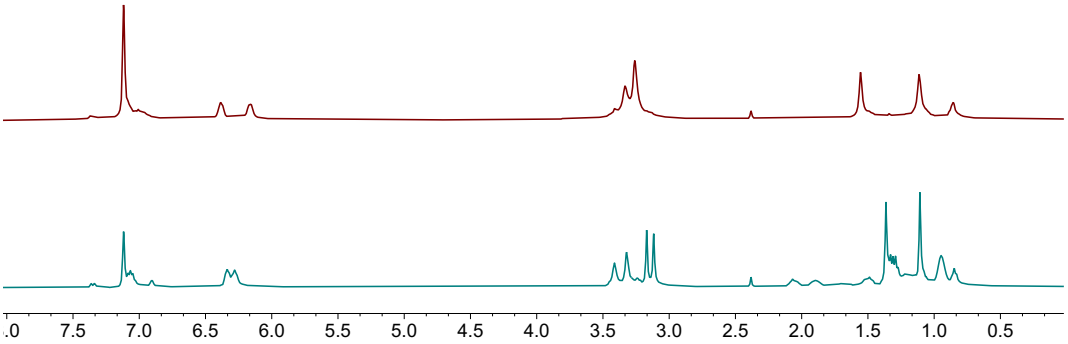

Figure AB3.7. ^{1}H NMR Spectra of conversion of **1-CCO** (top) to **1P-CCO** (bottom)upon ACdition of PEt_3.

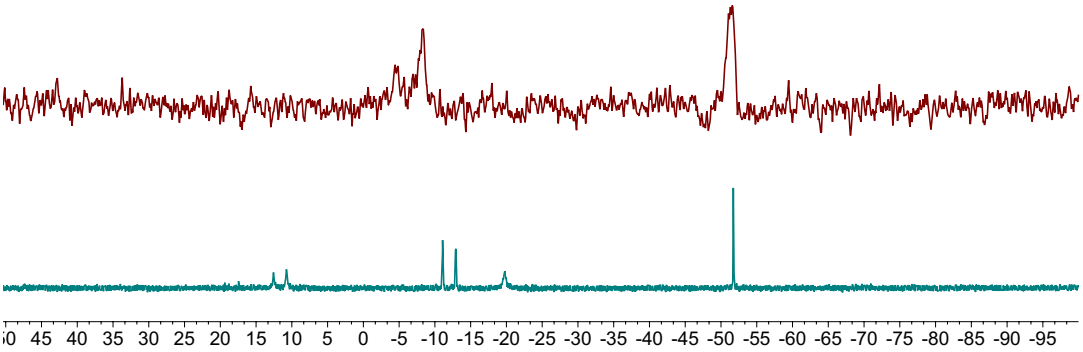

Figure AB3.8. ^{31}P{^{1}H} NMR Spectra of conversion of **1-CCO** (top) to **1P-CCO** (bottom)upon ACdition of PEt_3.

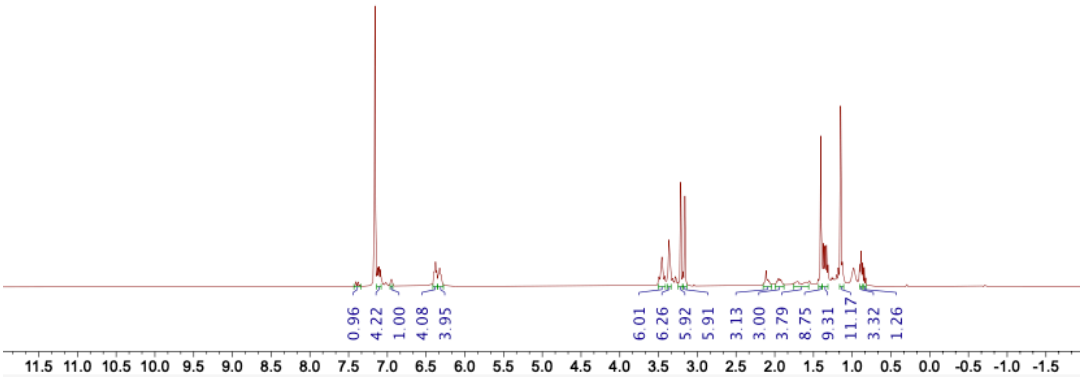

Figure AB3.9. ^{1}H NMR of **1P-CCO** in C_6D_6.

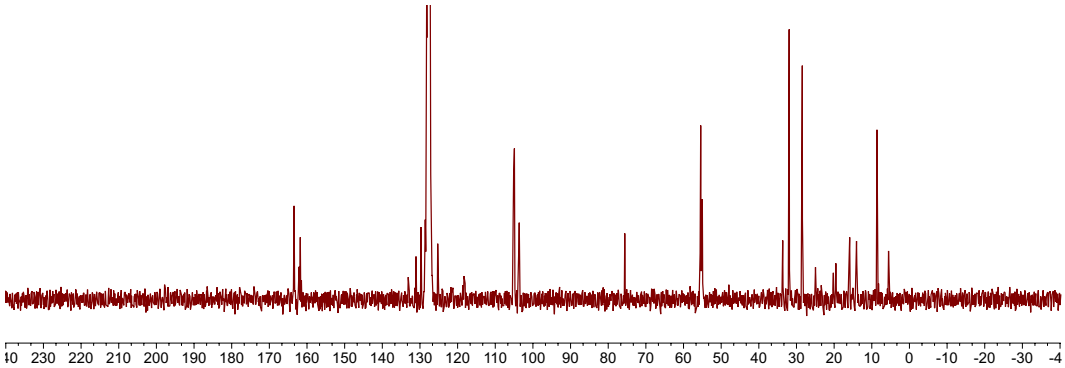

Figure AB3.10. $^{13}C\{^1H\}$ NMR of **1P-CCO** in C_6D_6.

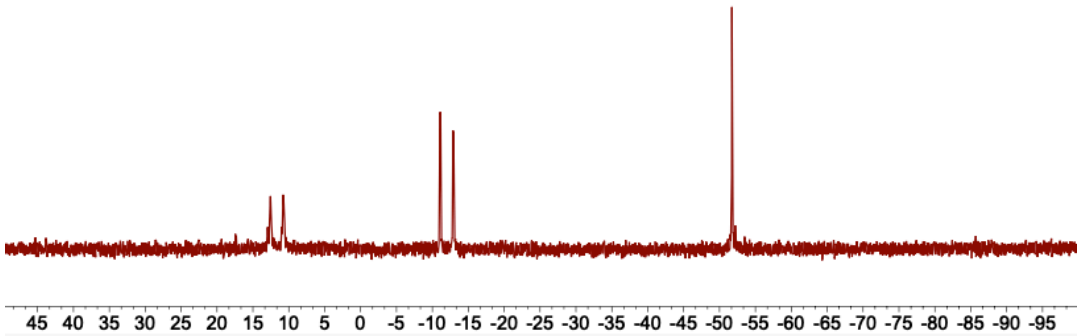

Figure AB3.11. $^{31}P\{^1H\}$ NMR of **1P-CCO** in C_6D_6.

Formation of **2et-CCO** from the ACdition of 4 atm. of ethylene to a solution of **2-CCO**

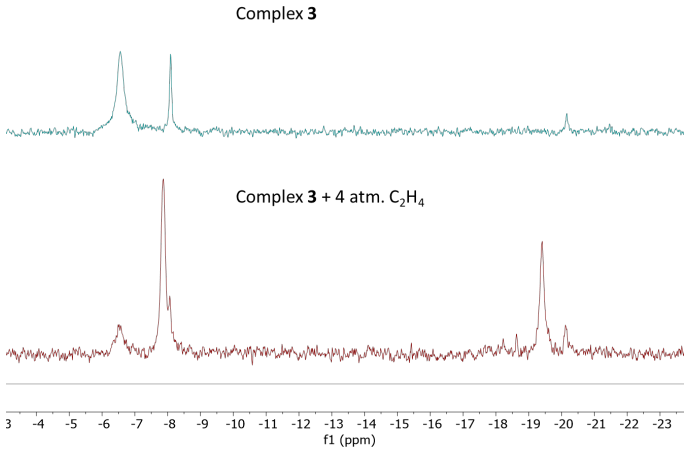

Figure AB3.12 $^{31}P\{^1H\}$ NMR spectra of **2-CCO** (top) and **2-CCO** + 4 atm. ethylene (bottom) (temperature: -80 °C, solvent: C_7D_8)

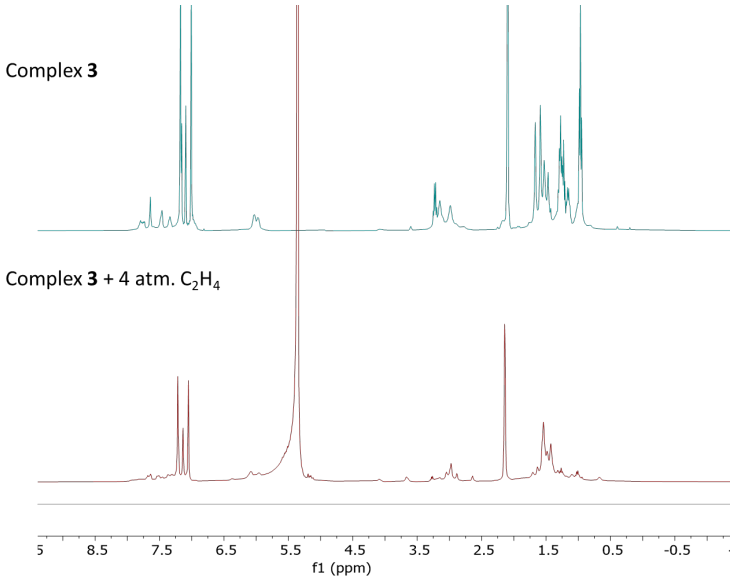

Figure AB3.13 ^{1}H NMR spectra of **2-CCO** (top) and **2-CCO** + 4 atm. ethylene (bottom) (temperature: -80 °C, solvent: C_7D_8)

^{31}P{^{1}H} NMR showing formation of **2hex-CCO** from **2-CCO** and 1-hexene

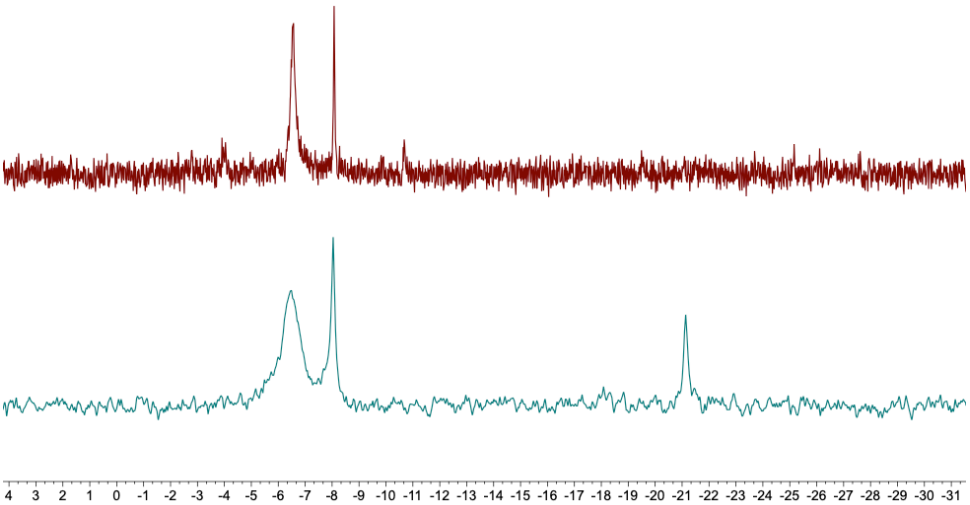

Figure AB3.14 ^{31}P{^{1}H} NMR spectra of **2-CCO** (top) and **2-CCO** + 200 equiv. of 1-hexene (bottom) (temperature: -80 °C, solvent: C_7D_8)

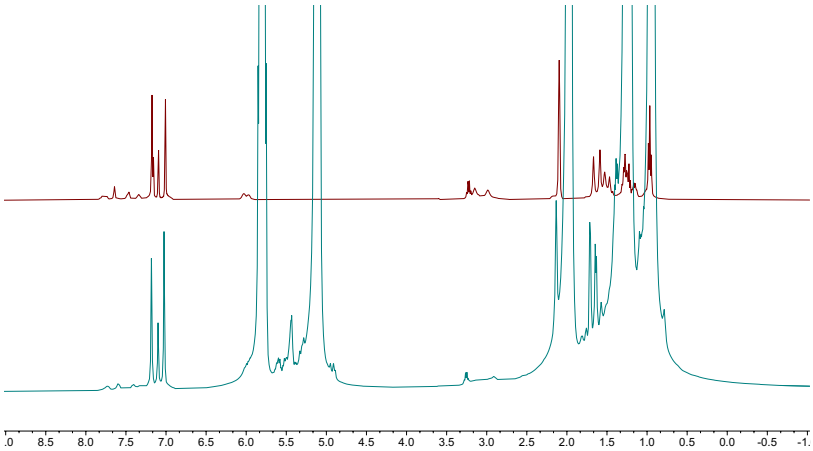

Figure AB3.15 ^{1}H NMR spectra of **2-CCO** (top) and **2-CCO** + 200 equiv. of 1-hexene (bottom) (temperature: -80 °C, solvent: C_7D_8)

Formation of **2et*-CCO** from the ACdition of 4 atm. of ^{13}C labelled ethylene to a solution of **2-CCO**

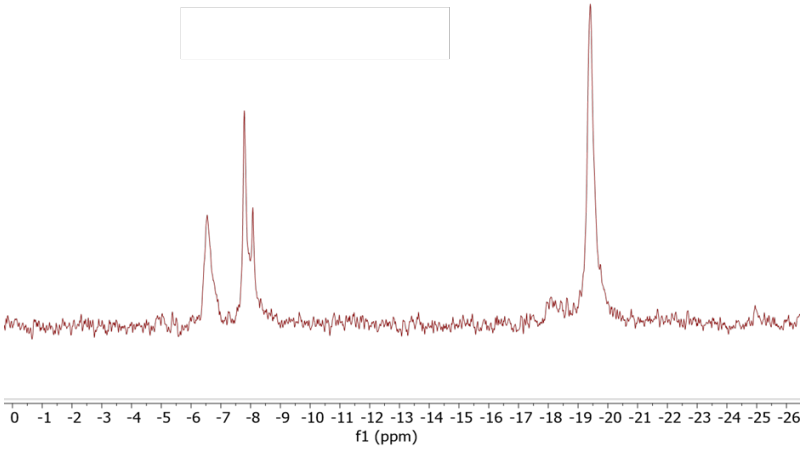

Figure AB3.16 ^{31}P{^{1}H} NMR spectrum of **2et*-CCO** (temperature: -90 °C, solvent: C_7D_8)

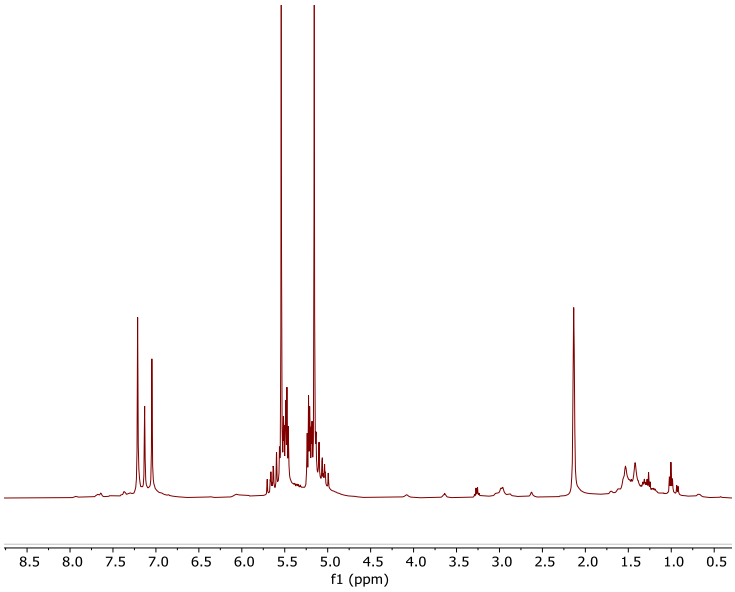

Figure AB3.17 ^{1}H NMR spectrum of **2et*-CCO** in the presence of 4 atm. ethylene (temperature: -90 °C, solvent: C_7D_8)

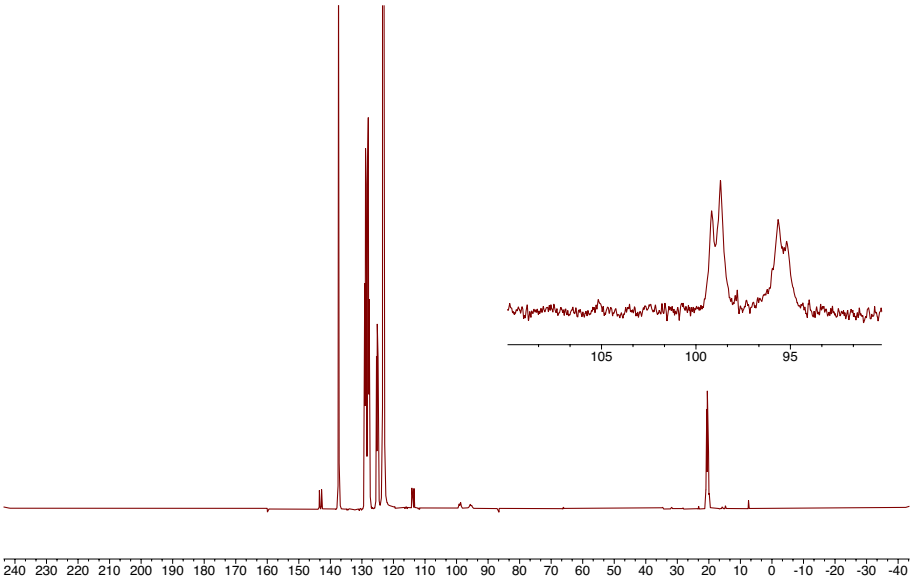

Figure AB3.18 ^{13}C{^{1}H} NMR spectrum of **2^{13}et-CCO** in the presence of 4 atm. ethylene (temperature: -90 °C, solvent: C_7D_8)

Formation of **2py-CCO** from the ACdition of pyridine to a mixture of **2-CCO** and **2et-CCO**

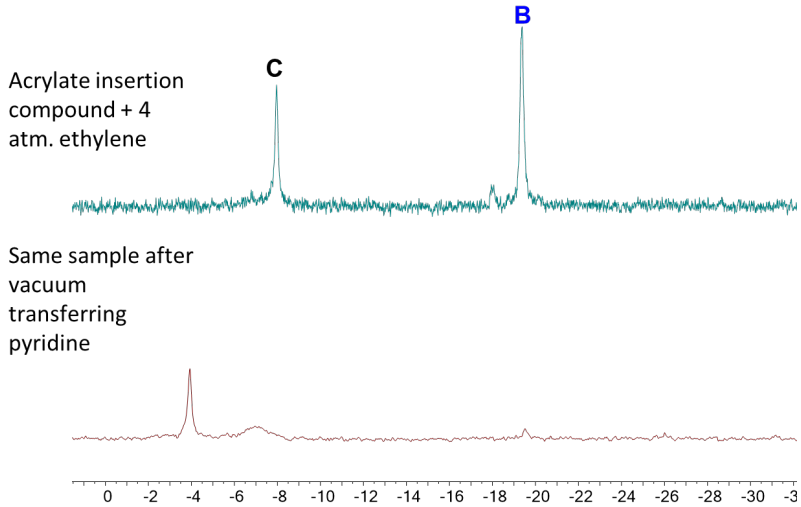

Figure AB3.19 $^{31}P\{^{1}H\}$ NMR spectra of (top) **2-CCO** (acrylate insertion compound, C) + **2et-CCO** (B) and (bottom) **2-CCO** + **2et-CCO** + **2py-CCO**. (Temperature: -90 °C, solvent: C_7D_8)

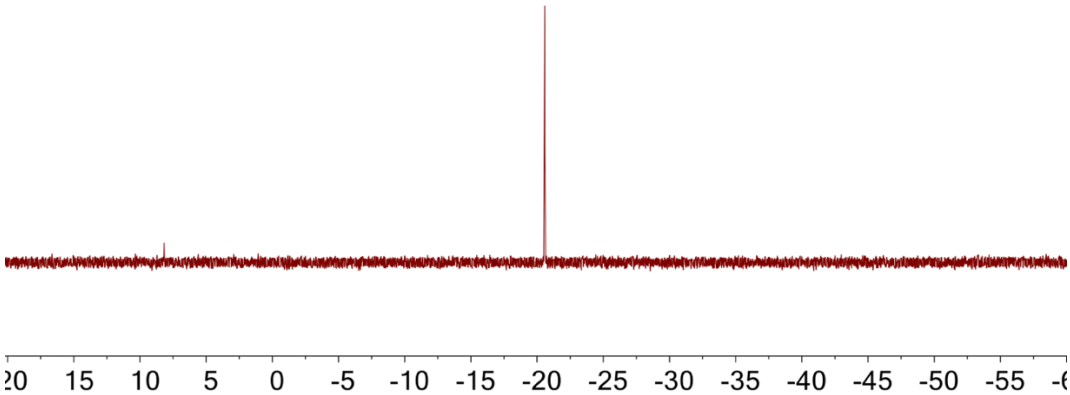

Figure AB3.20 $^{31}P\{^{1}H\}$ NMR spectra of **2-C_8H_{13}** (temperature: 25 °C, solvent: C_6D_6)

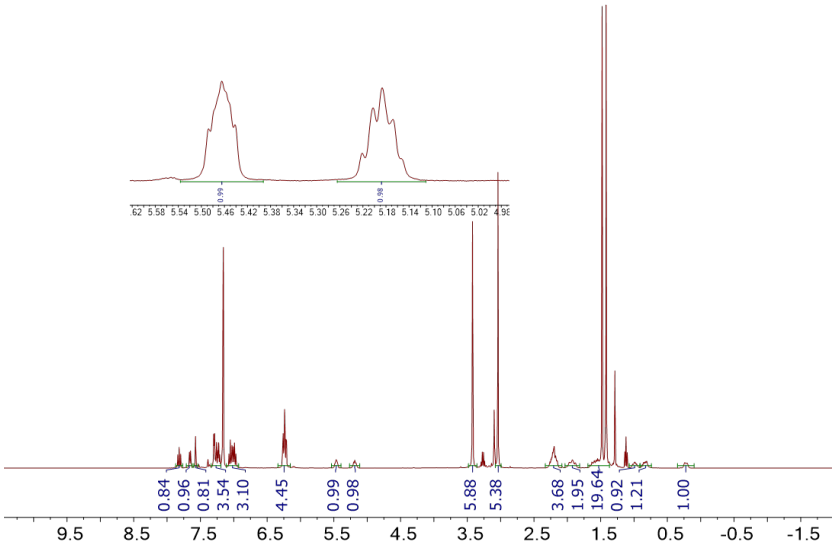

Figure AB3.21 ^{1}H NMR spectra of **2-C_8H_{13}** (temperature: 25 °C, solvent: C_6D_6)

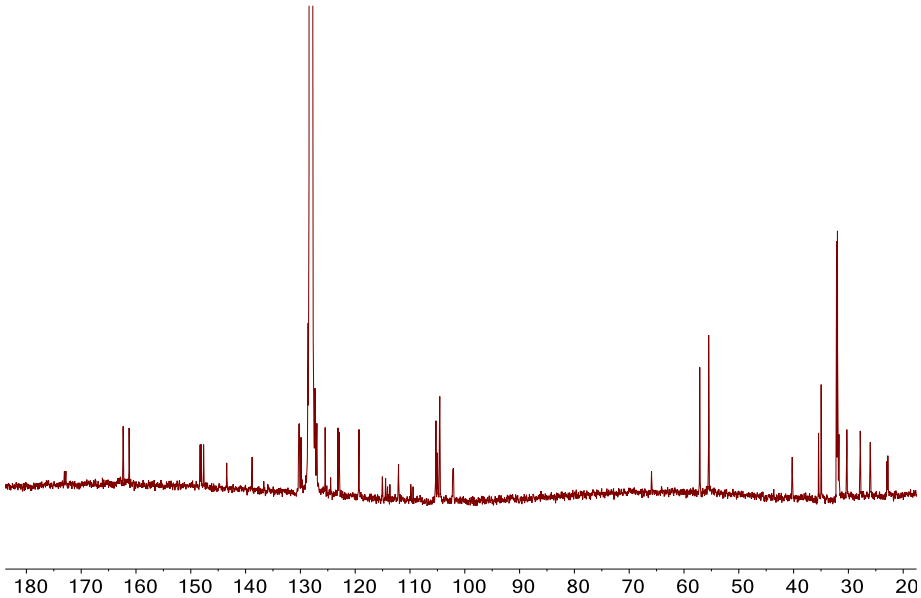

Figure AB3.22 ^{13}C{^{1}H} NMR spectra of **2-C_8H_{13}** (temperature: 25 °C, solvent: C_6D_6)

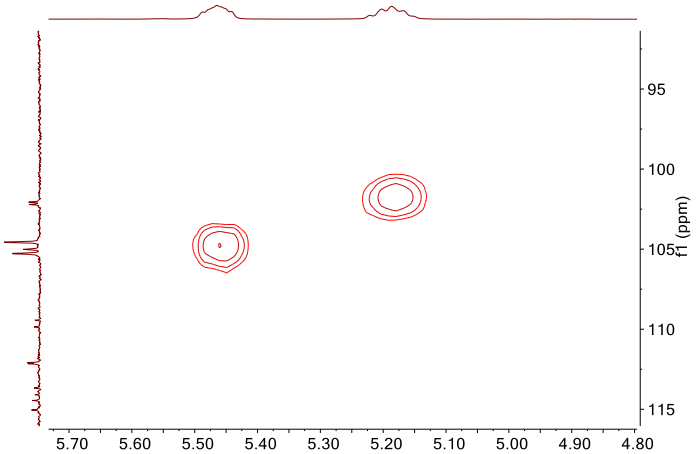

Figure AB3.23 $^{13}C\{^{1}H\}$-^{1}H HSQC NMR Spectrum of **2-C_8H_{13}** (temperature: 25 °C, solvent: C_6D_6)

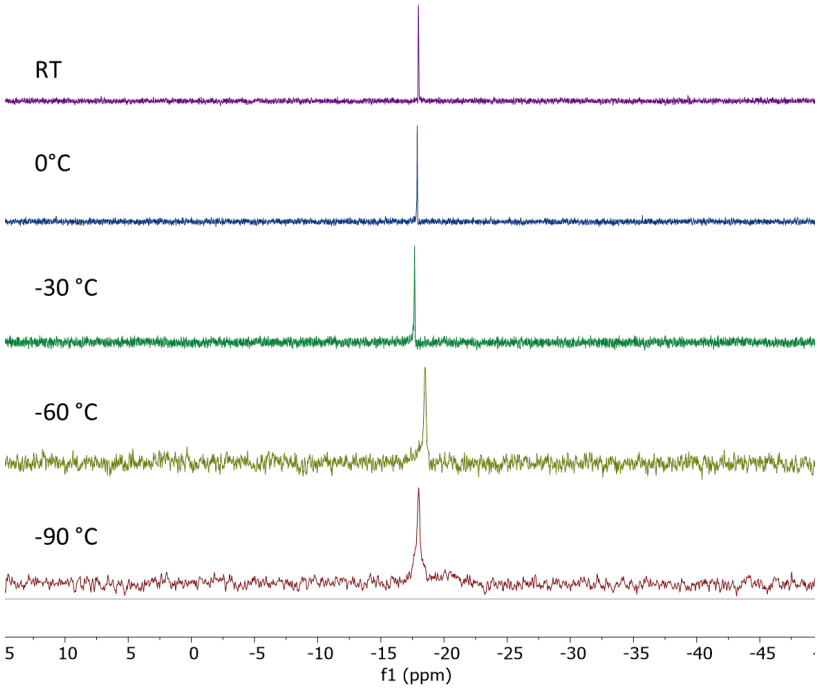

Figure AB3.24 $^{31}P\{^{1}H\}$ NMR Spectra of **2-C_8H_{13}** at different temperatures (solvent: C_7D_8).

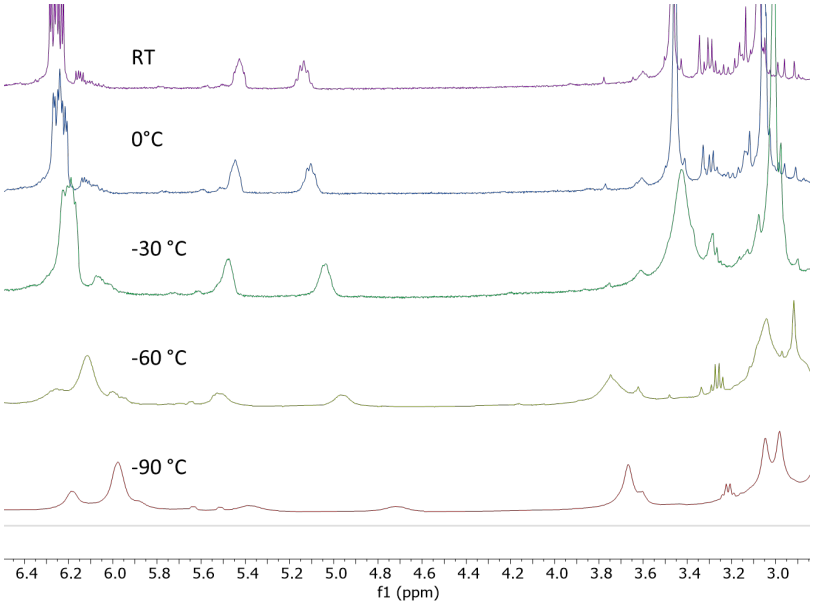

Figure AB3.25 ^{1}H NMR Spectra of **2-C$_8$H$_{13}$** at different temperatures (Olefinic region, solvent: C_7D_8).

^{31}P{^{1}H} NMR Spectrum of PONap-Ni-CCO + POP-Ni-CCO-Py

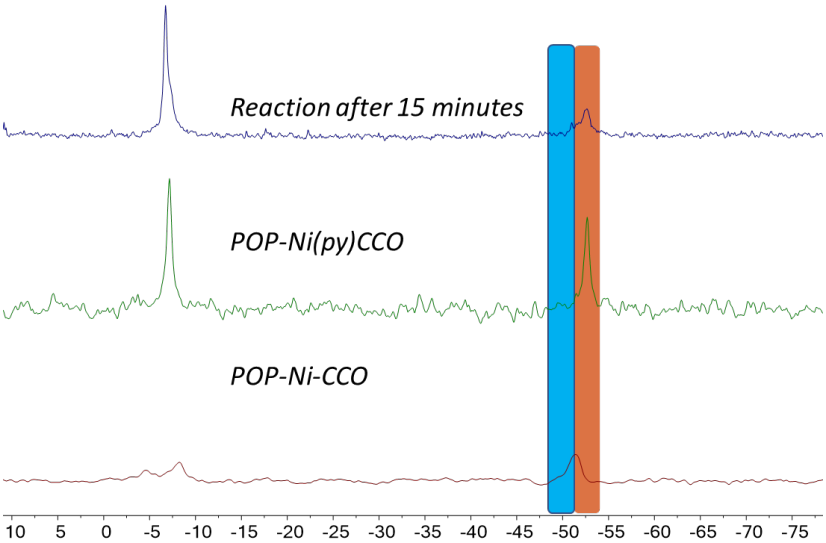

Figure AB3.26 ^{31}P{^{1}H} NMR of mixture of **1py-CCO** + **2-CCO** (top), **1py-CCO** (medium) and **1-CCO** (bottom) in C_6D_6

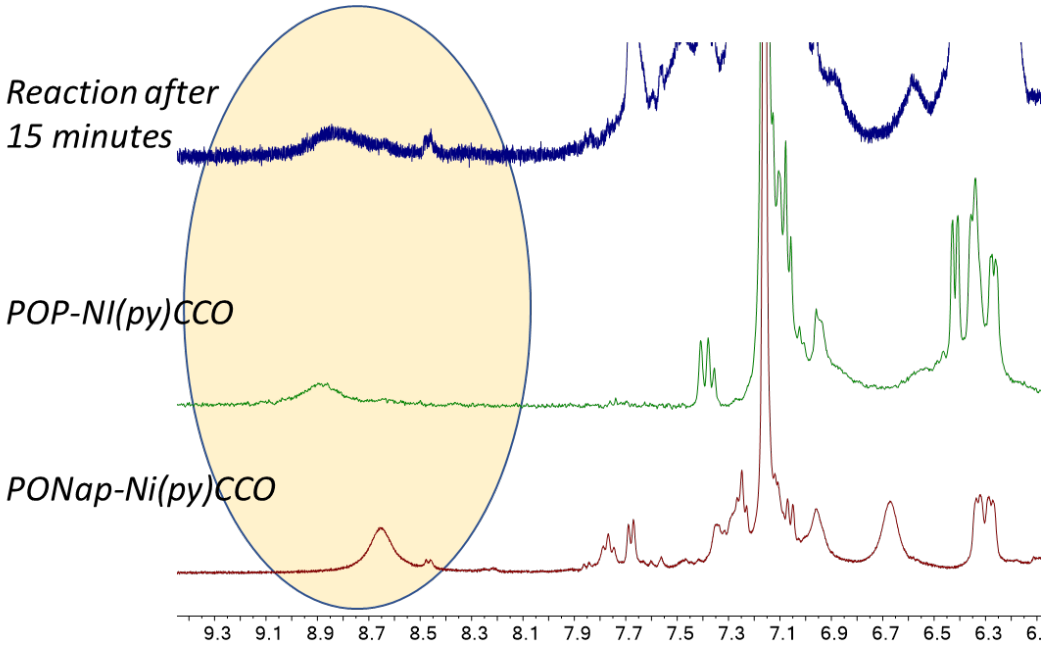

Figure AB3.27 $^{31}P\{^{1}H\}$ NMR of mixture of **1py-CCO** + **2-CCO** (top), **1py-CCO** (medium) and **2-CCO** (bottom) in C_6D_6

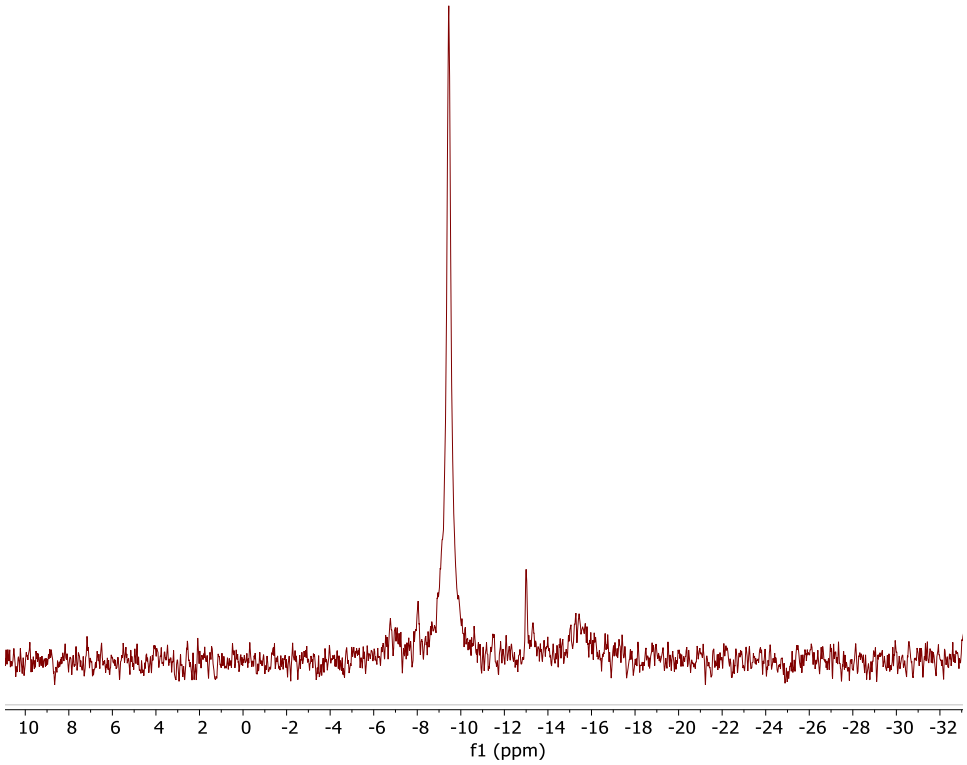

Figure AB3.28 $^{31}P\{^{1}H\}$ NMR spectrum of mixture of **2lut-CCO** at -90 °C in tol-d8.

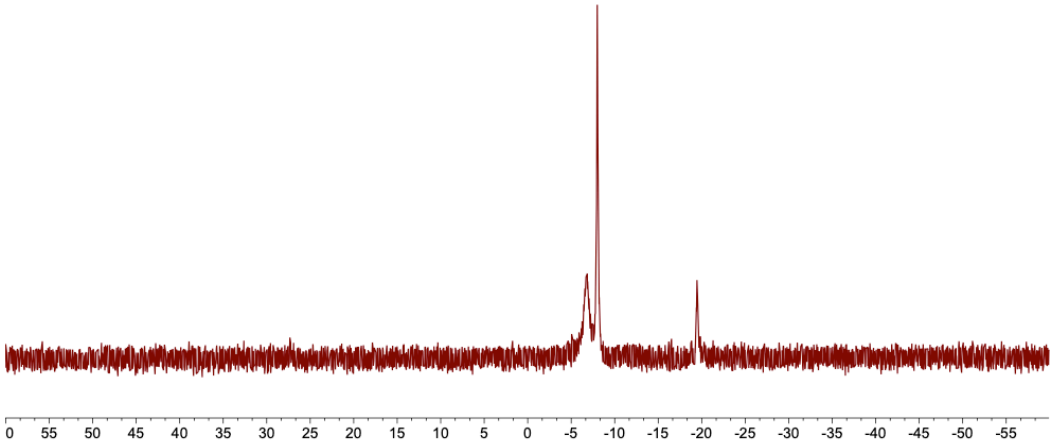

Figure AB3.28 $^{31}P\{^{1}H\}$ NMR spectrum of thermodynamic mixture of **2-CCO** and **2et-CCO** at -90 °C in tol-d8.

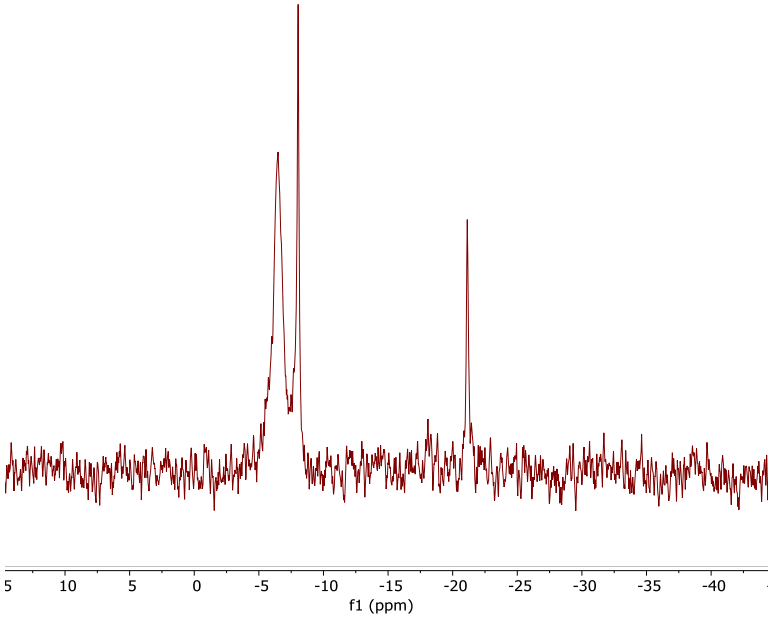

Figure AB3.29. $^{31}P\{^{1}H\}$ NMR spectrum of thermodynamic mixture of **2-CCO** and **2hex-CCO** at -90 °C in tol-d8.

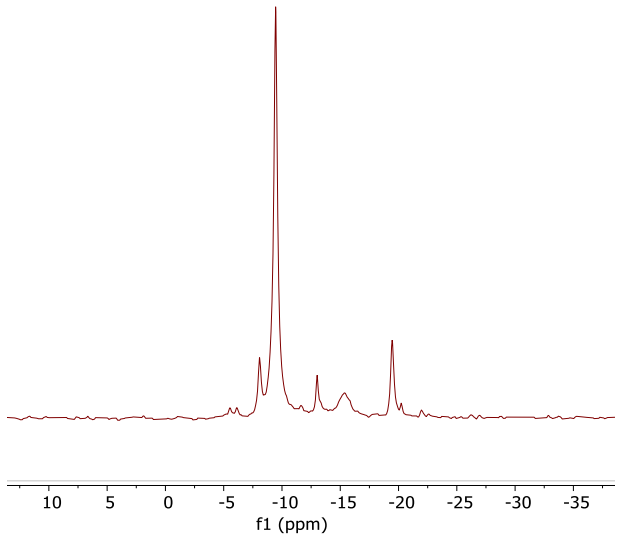

Figure AB3.30. $^{31}P\{^{1}H\}$ NMR spectrum of thermodynamic mixture of **2et-CCO** and **2lut-CCO** at -90 °C in tol-d8.

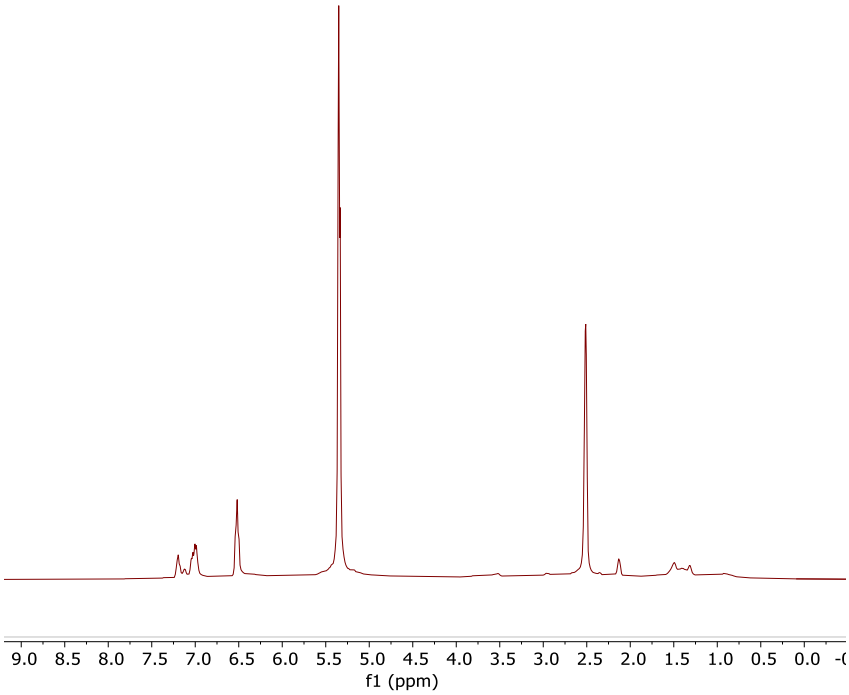

Figure AB3.31. ^{1}H NMR spectrum of thermodynamic mixture of **2-CCO** and **2et-CCO** at -90 °C in tol-d8.

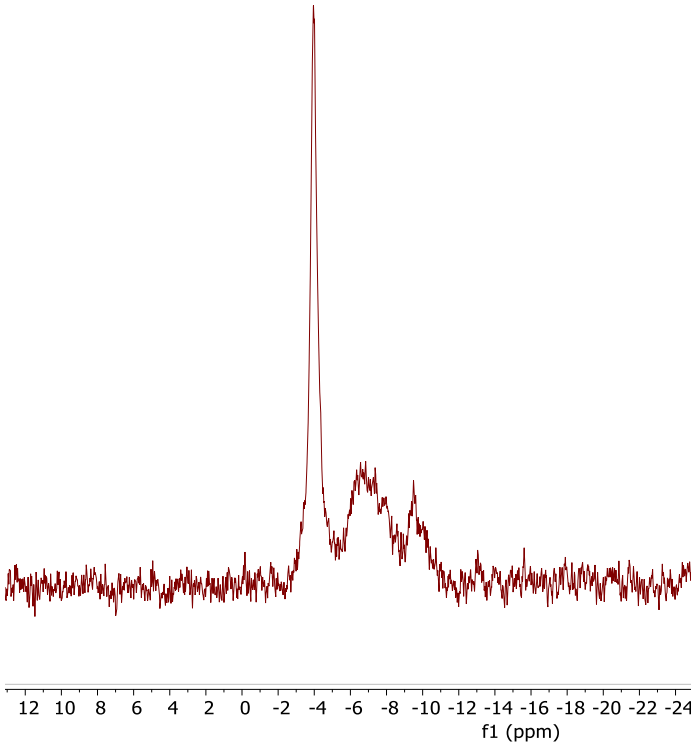

Figure AB3.32. $^{31}P\{^{1}H\}$ NMR spectrum of thermodynamic mixture of **2py-CCO** and **2lut-CCO** at -90 °C in tol-d8.

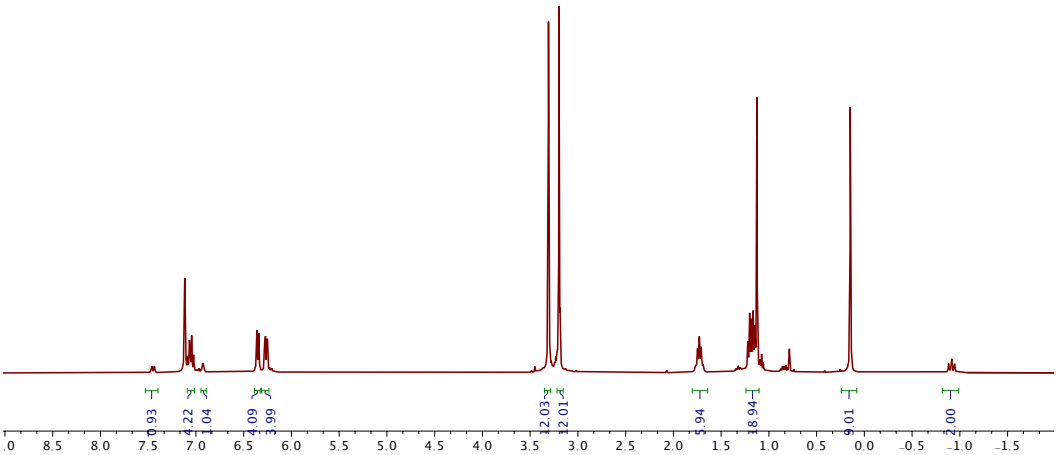

Figure AB3.33. ^{1}H NMR spectrum of **1P** in C_6D_6.

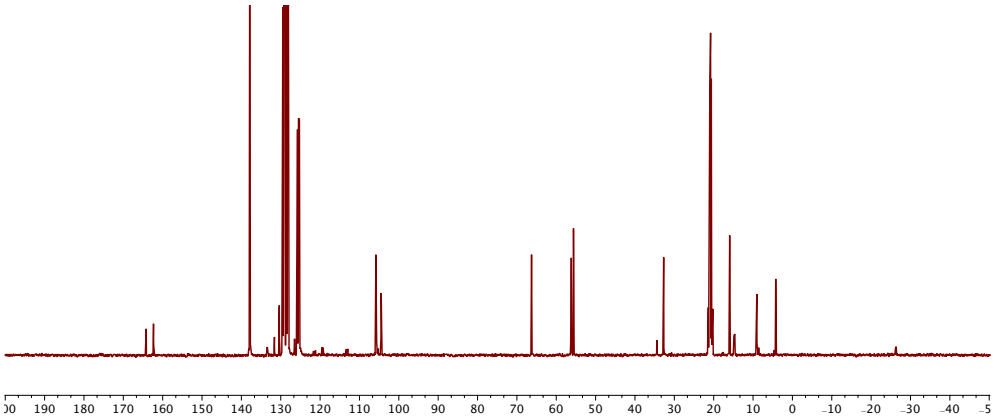

Figure AB3.34. $^{13}C\{^{1}H\}$ NMR spectrum of **1P** in tol-d8.

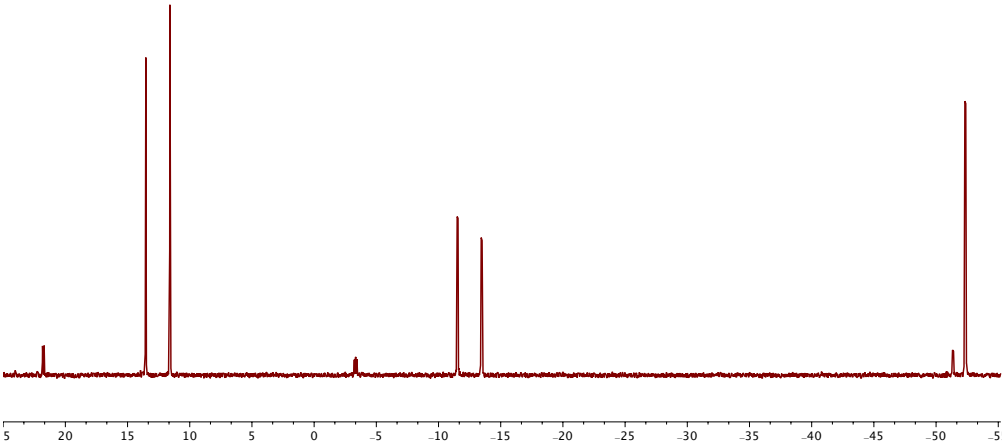

Figure AB3.35. $^{31}P\{^{1}H\}$ NMR spectrum of **1P** in tol-d8.

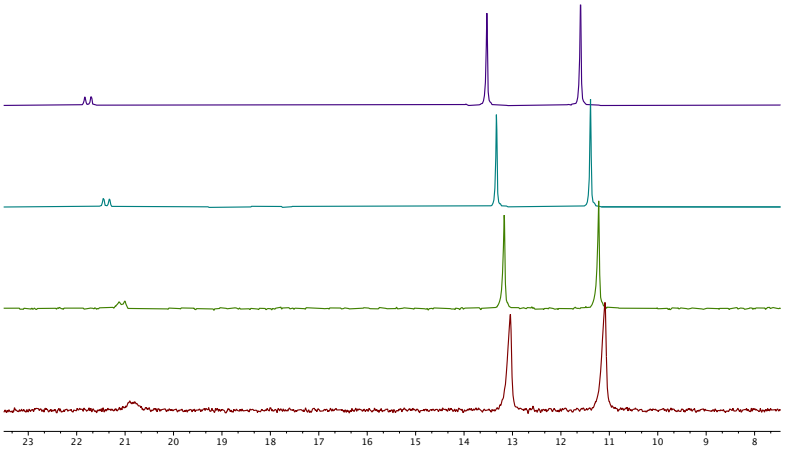

Figure AB3.36. $^{31}P\{^{1}H\}$ NMR spectrum of **1P** in tol-d8 at different temperatures (top to bottom: 25 °C, 50 °C, 70 °C, 90 °C)

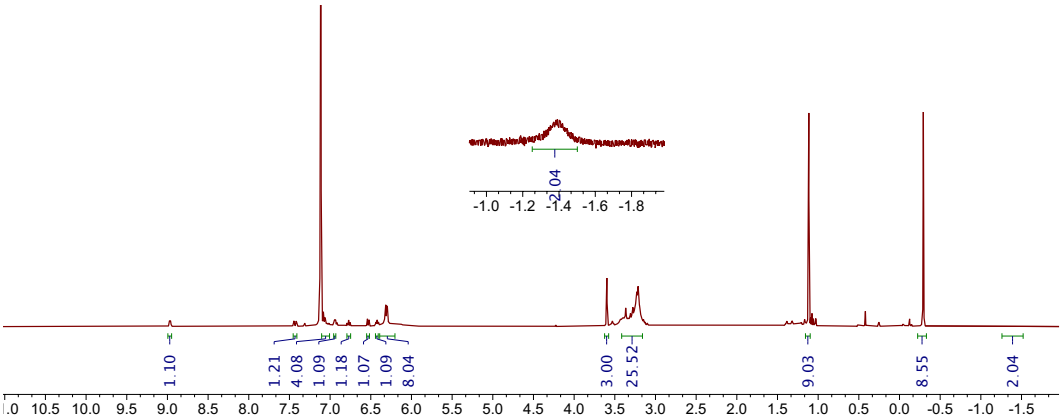

Figure AB3.37. ^{1}H NMR spectrum of **1pico** in C_6D_6.

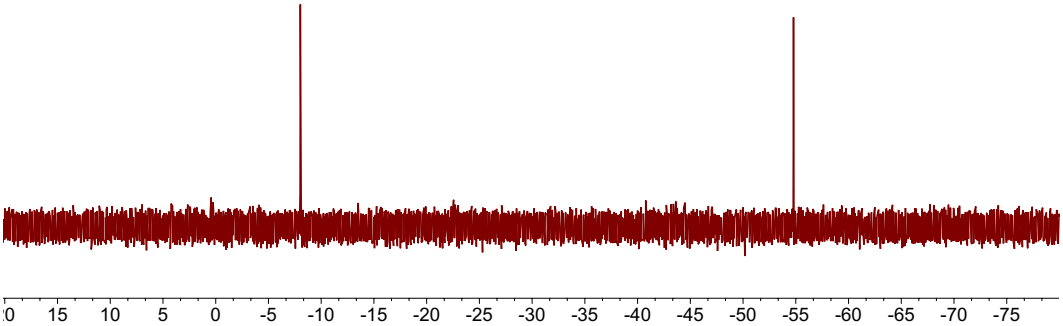

Figure AB3.38. ^{31}P{^{1}H} NMR spectrum of **1pico** in C_6D_6.

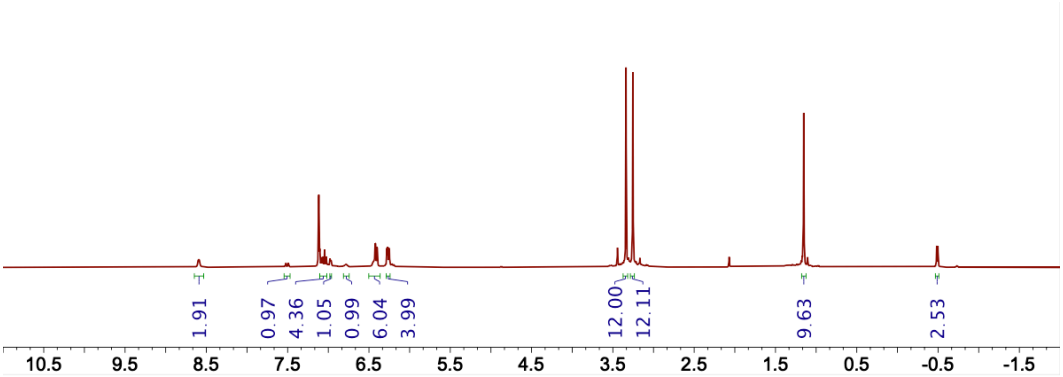

Figure AB3.39. ^{1}H NMR spectrum of **1py-Me** in C_6D_6.

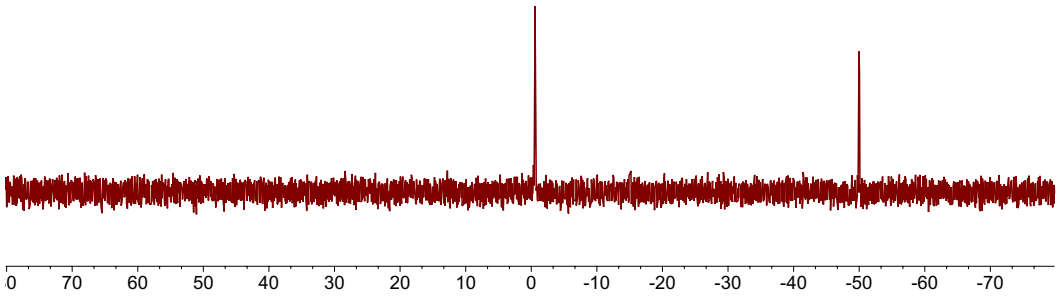

Figure AB3.40. $^{31}P\{^{1}H\}$ NMR spectrum of **1py-Me** in C_6D_6.

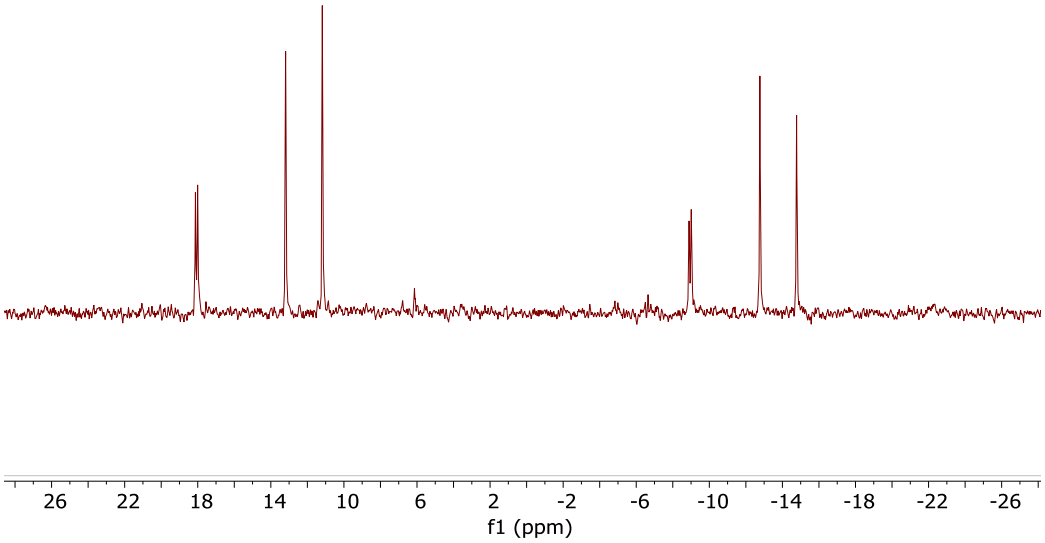

Figure AB3.41. $^{31}P\{^{1}H\}$ NMR spectrum **2P**.

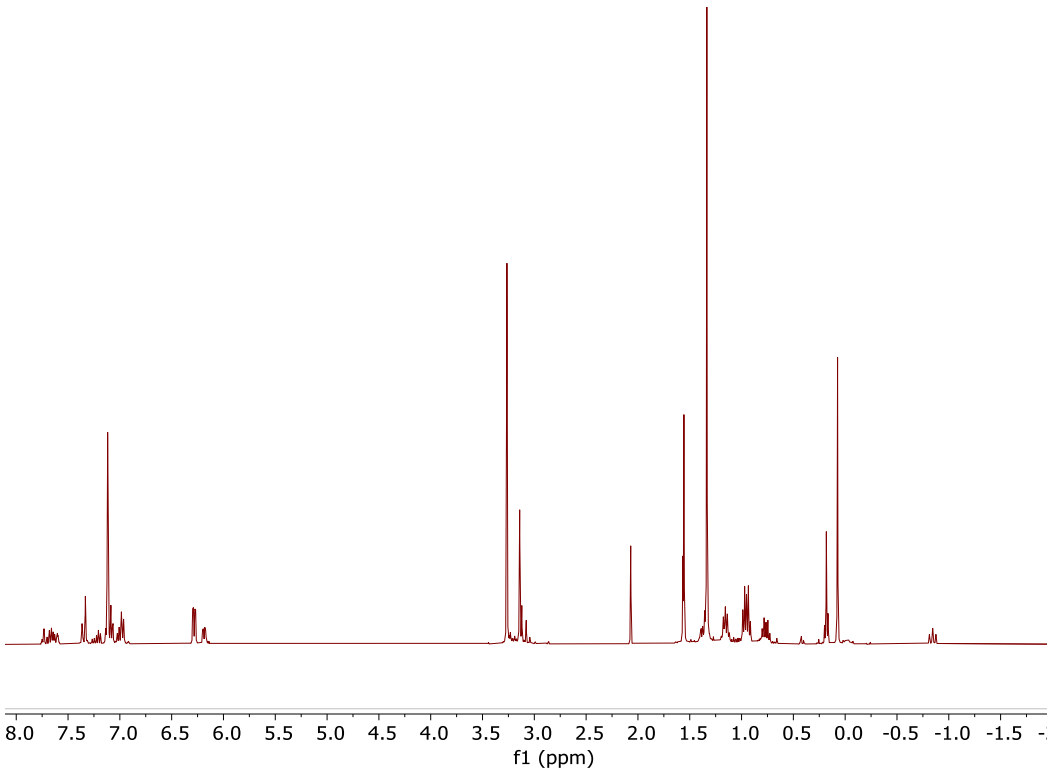

Figure AB3.42. $^{31}P\{^{1}H\}$ NMR spectrum **2P**.

Chapter 4

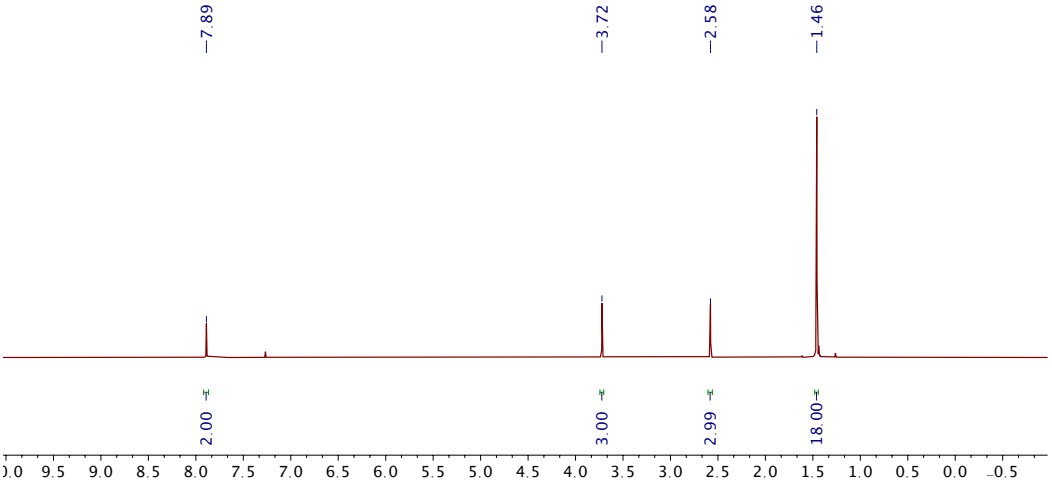

Figure AB4.1. ^{1}H NMR spectrum of 3', 5'-Di-tert-butyl-4'-methoxyacetophenone in $CDCl_3$.

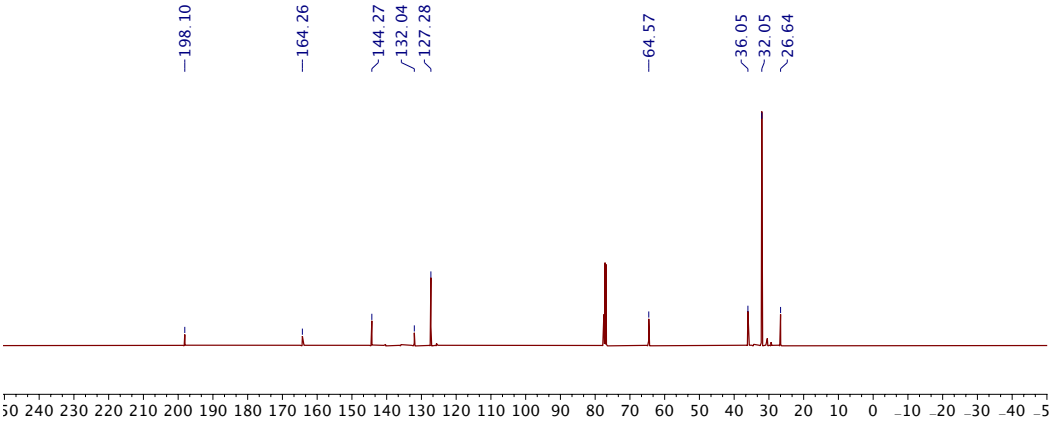

Figure AB4.2. ^{13}C{^{1}H} NMR spectrum of 3', 5'-Di-tert-butyl-4'-methoxyacetophenone in $CDCl_3$.

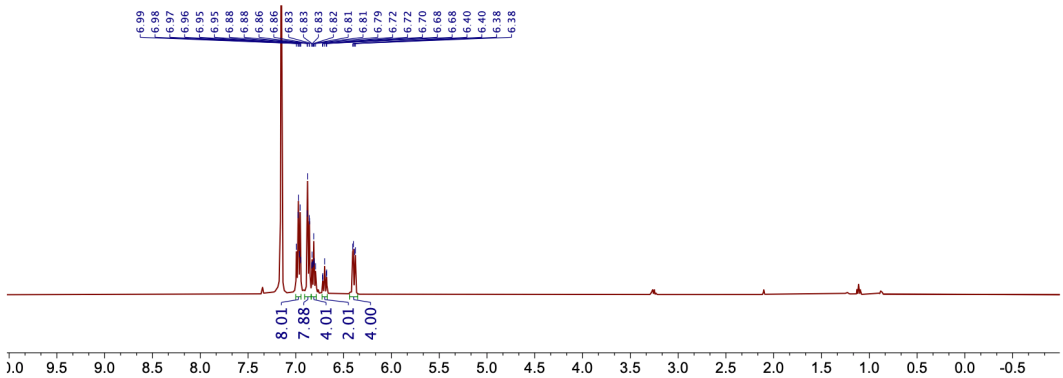

Figure AB4.3. ^{1}H NMR spectrum of bis(diphenoxyphenyl) phosphine chloride in C_6D_6.

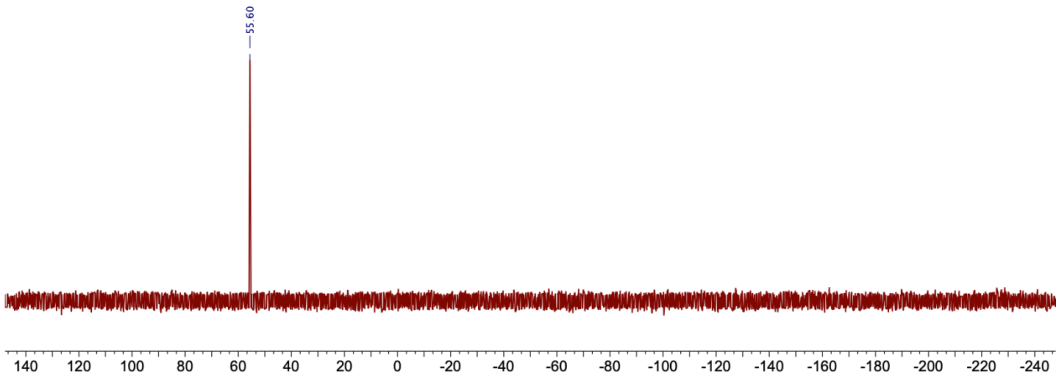

Figure AB4.4. $^{31}P\{^{1}H\}$ NMR spectrum of bis(diphenoxyphenyl) phosphine chloride in C_6D_6.

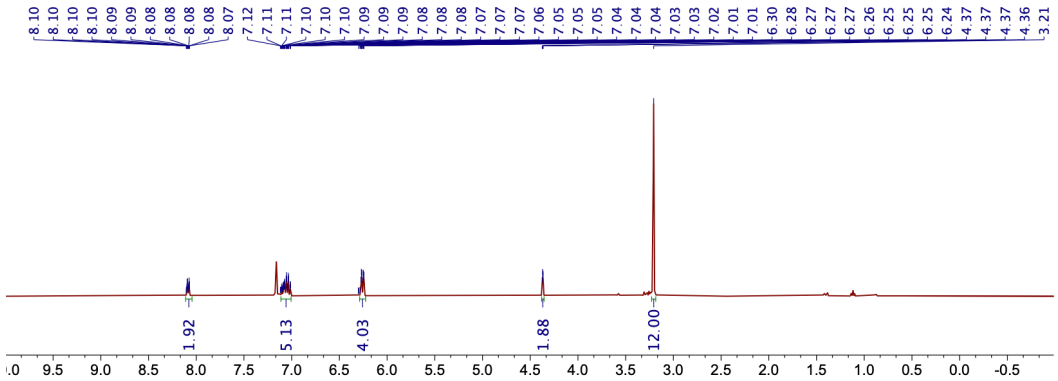

Figure AB4.5. ^{1}H NMR spectrum of ^{Me}**PO**^{Ph}**H** in C_6D_6.

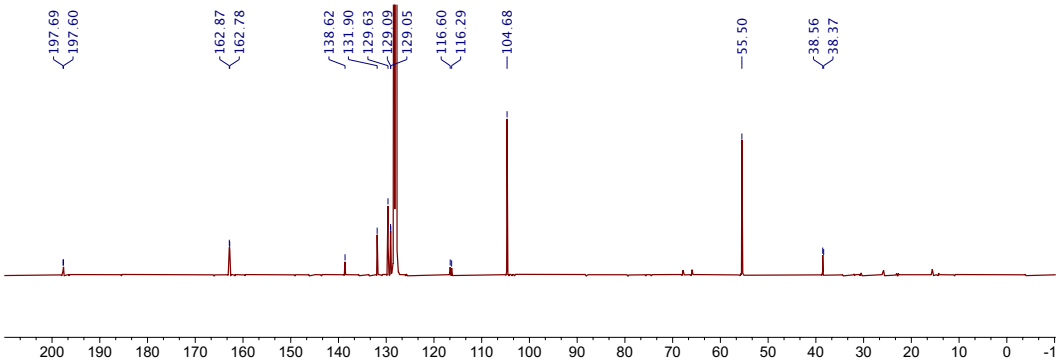

Figure AB4.6. $^{13}C\{^{1}H\}$ NMR spectrum of ^{Me}**PO**^{Ph}**H** in C_6D_6.

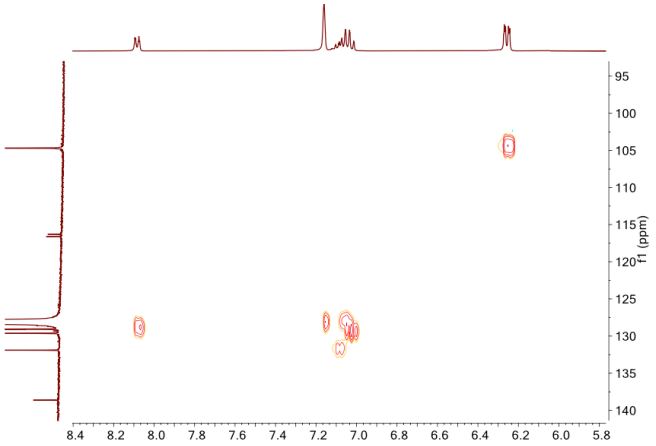

Figure AB4.7. ^{1}H-^{13}C HSQC NMR spectrum of ^{Me}**PO**^{Ph}**H** in C_6D_6.

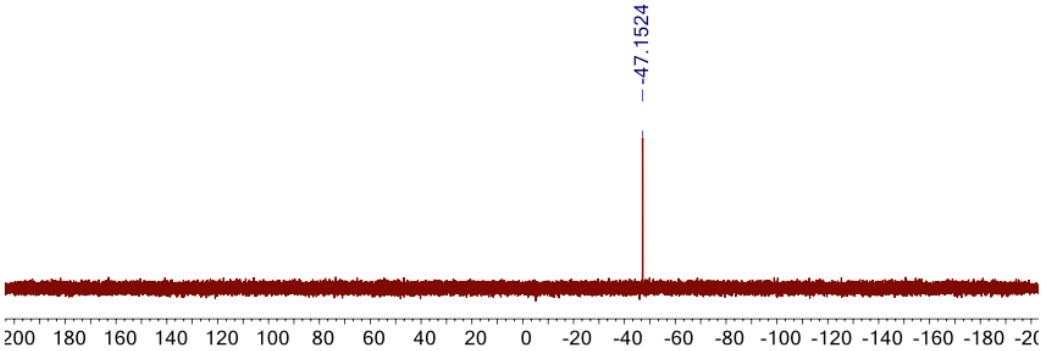

Figure AB4.8. ^{31}P{^{1}H} NMR spectrum of ^{Me}**PO**^{Ph}**H** in C_6D_6.

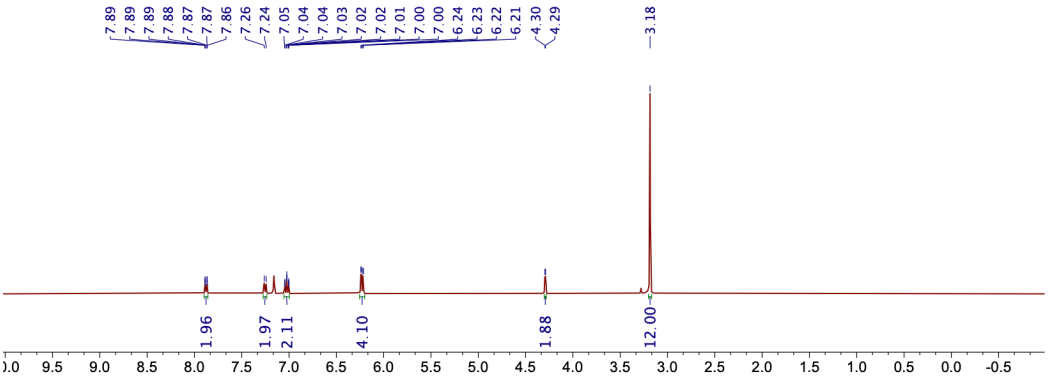

Figure AB4.9. ^{1}H NMR spectrum of ^{Me}**PO**^{PhCF3}**H** in C_6D_6.

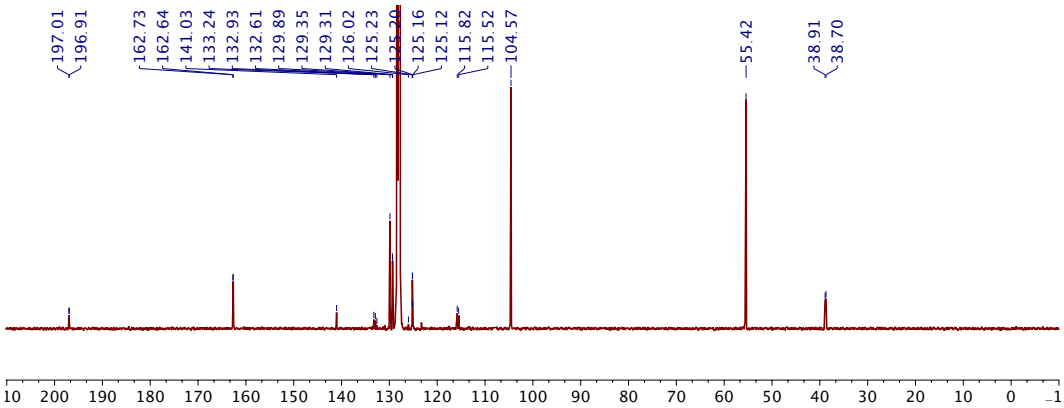

Figure AB4.10. $^{13}C\{^{1}H\}$ NMR spectrum of ^{Me}**PO**^{PhCF3}**H** in C_6D_6.

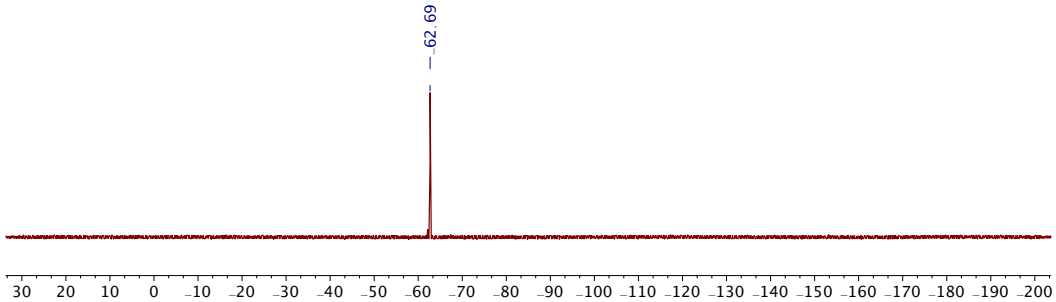

Figure AB4.11. ^{19}F NMR spectrum of ^{Me}**PO**^{PhCF3}**H** in C_6D_6

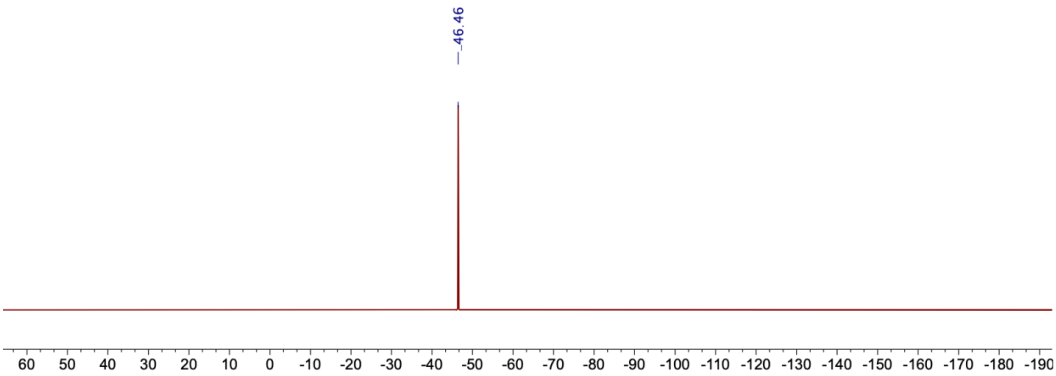

Figure AB4.12. $^{31}P\{^{1}H\}$ NMR spectrum of ^{Me}**PO**^{PhCF3}**H** in C_6D_6.

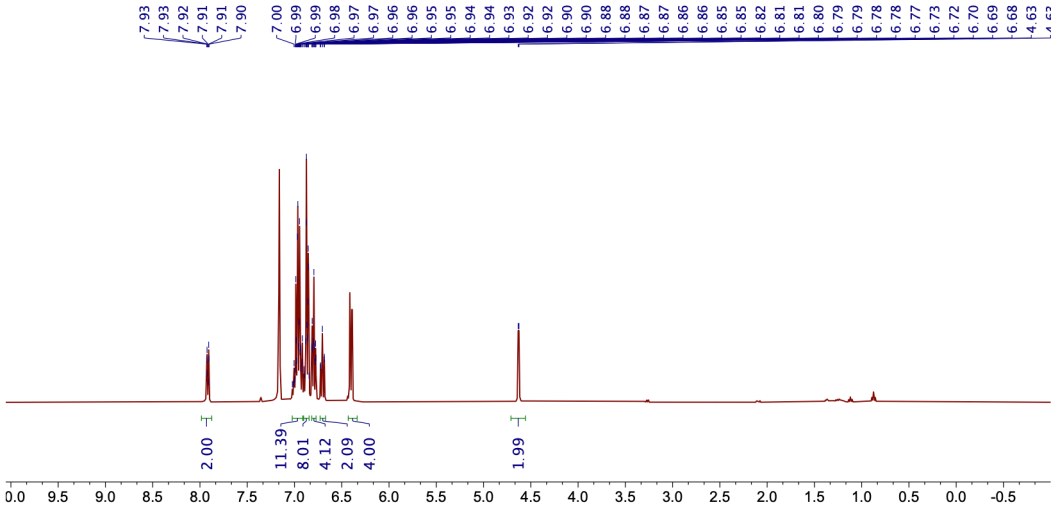

Figure AB4.13. ^{1}H NMR spectrum of ^{Ph}**PO**^{Ph}**H** in C_6D_6.

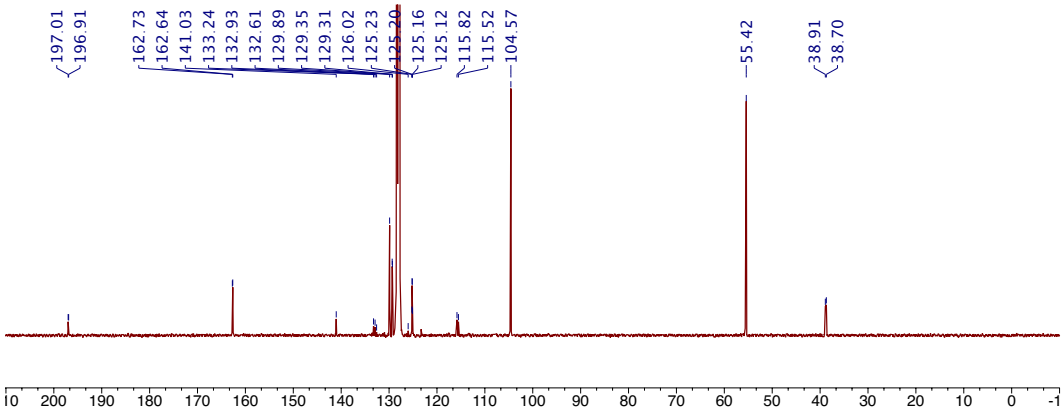

Figure AB4.14. ^{13}C{^{1}H} NMR spectrum of ^{Ph}**PO**^{Ph}**H** in C_6D_6.

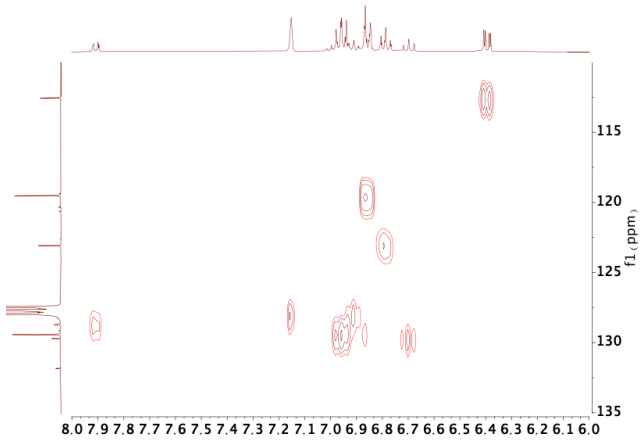

Figure AB4.15. ^{1}H-^{13}C HSQC NMR spectrum of ^{Ph}**PO**^{Ph}**H** in C_6D_6.

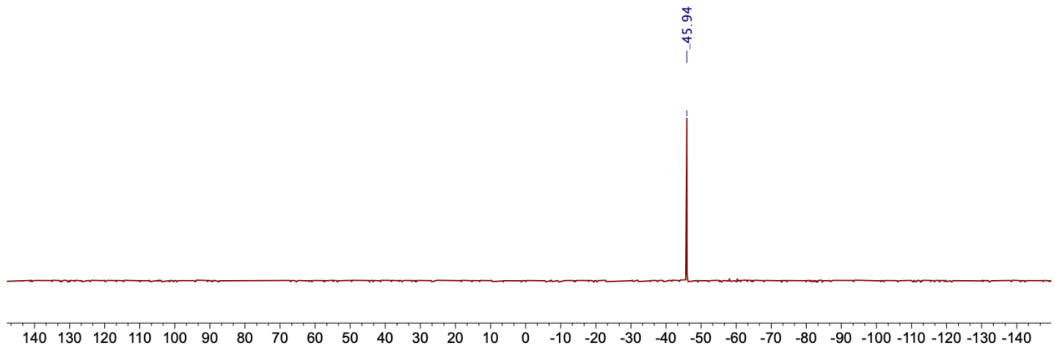

Figure AB4.16. $^{31}P\{^{1}H\}$ NMR spectrum of ^{Ph}**PO**^{Ph}**H** in C_6D_6.

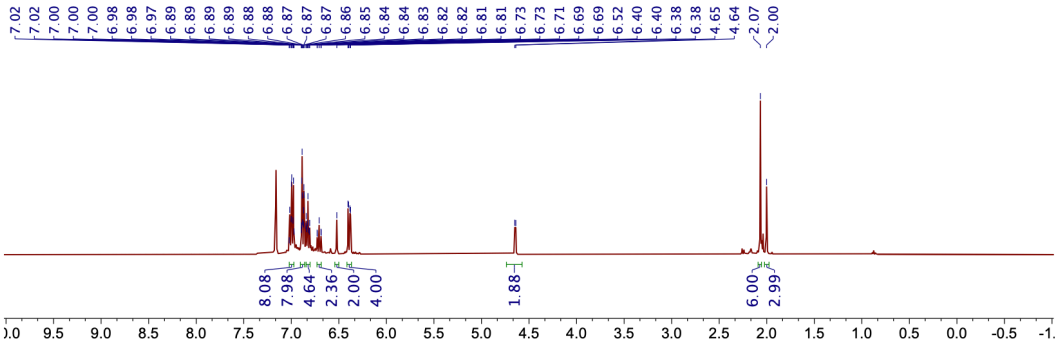

Figure AB4.17. ^{1}H NMR spectrum of ^{Ph}**PO**^{Mes}**H** in C_6D_6.

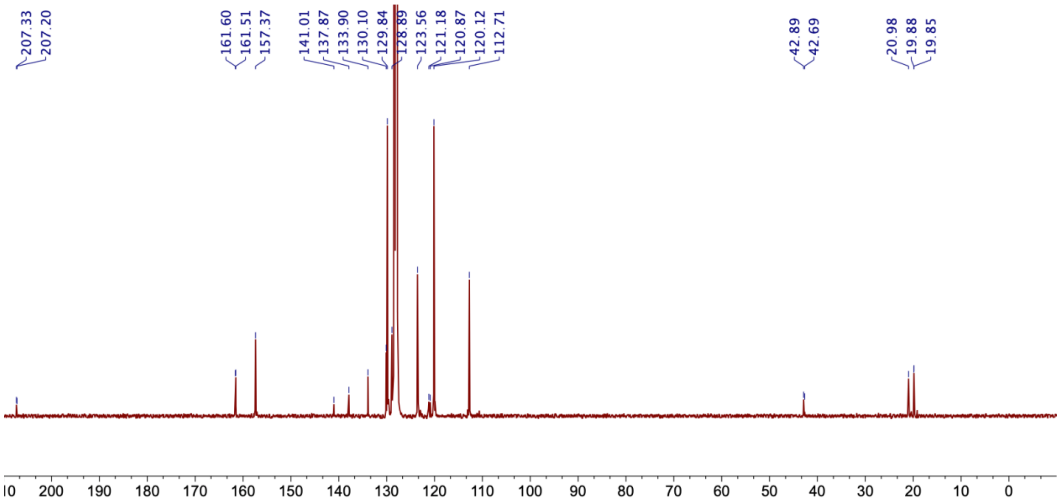

Figure AB4.18. $^{13}C\{^{1}H\}$ NMR spectrum of ^{Ph}**PO**^{Mes}**H** in C_6D_6.

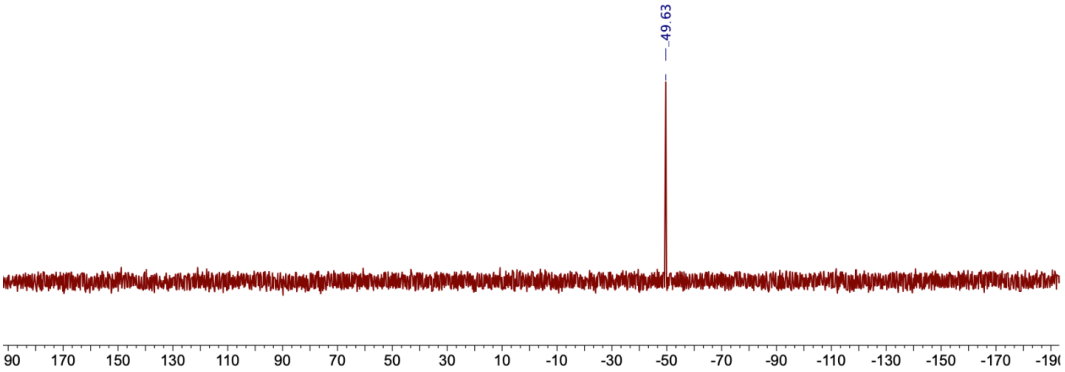

Figure AB4.19. $^{31}P\{^{1}H\}$ NMR spectrum of ^{Ph}**PO**^{Mes}**H** in C_6D_6.

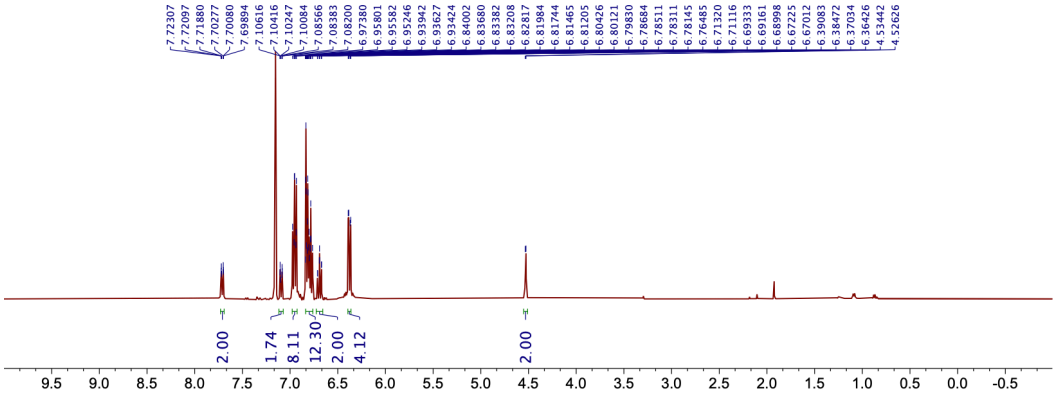

Figure AB4.20. ^{1}H NMR spectrum of ^{Ph}**PO**^{PhCF3}**H** in C_6D_6.

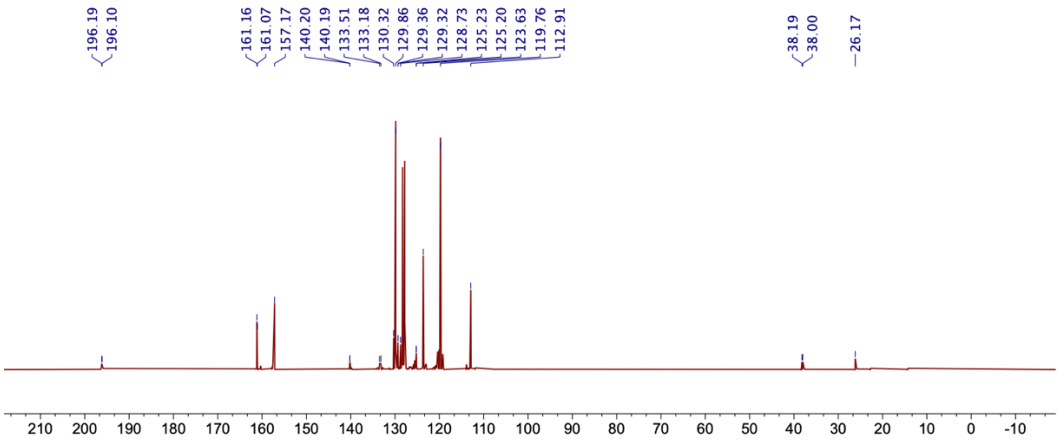

Figure AB4.21. $^{13}C\{^{1}H\}$ NMR spectrum of ^{Ph}**PO**^{PhCF3}**H** in C_6D_6.

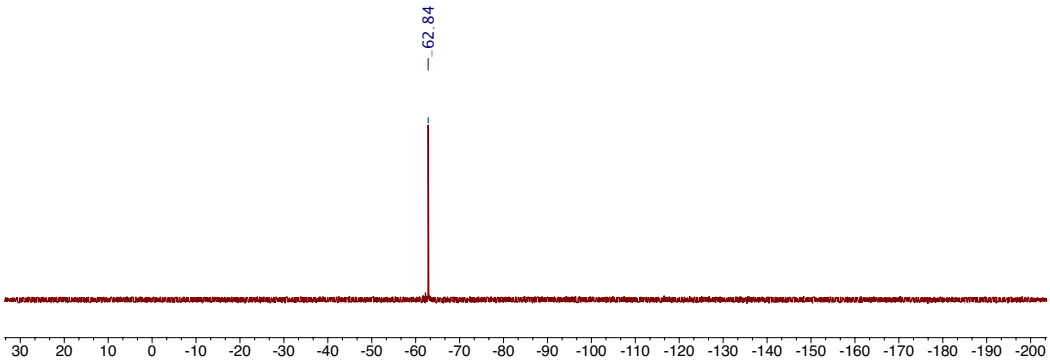

Figure AB4.22. ^{19}F NMR spectrum of ^{Ph}**PO**^{PhCF3}**H** in C_6D_6.

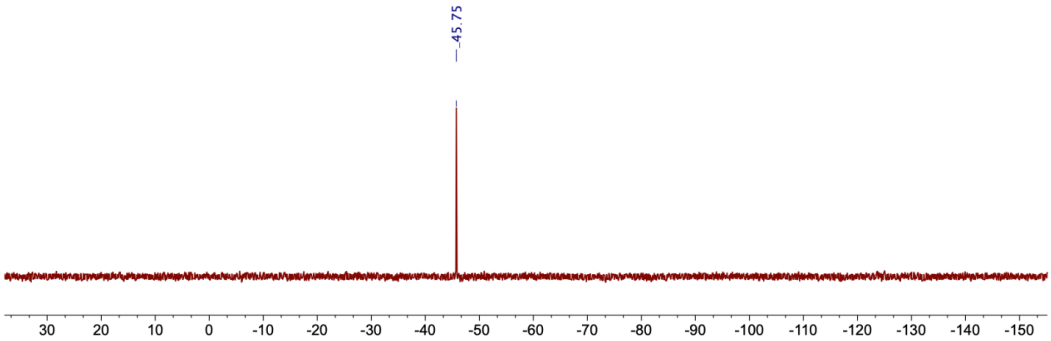

Figure AB4.23. ^{31}P{^{1}H} NMR spectrum of ^{Ph}**PO**^{PhCF3}**H** in C_6D_6.

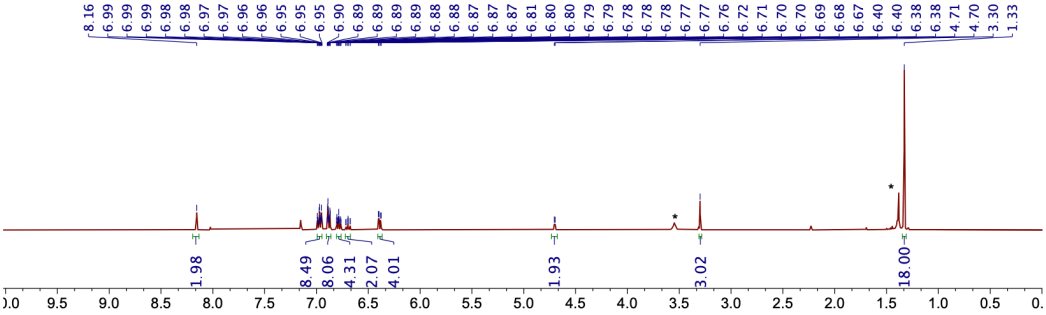

Figure AB4.24. ^{1}H NMR spectrum of ^{Ph}**PO**^{ArOMe}**H** in C_6D_6 (*: residual THF).

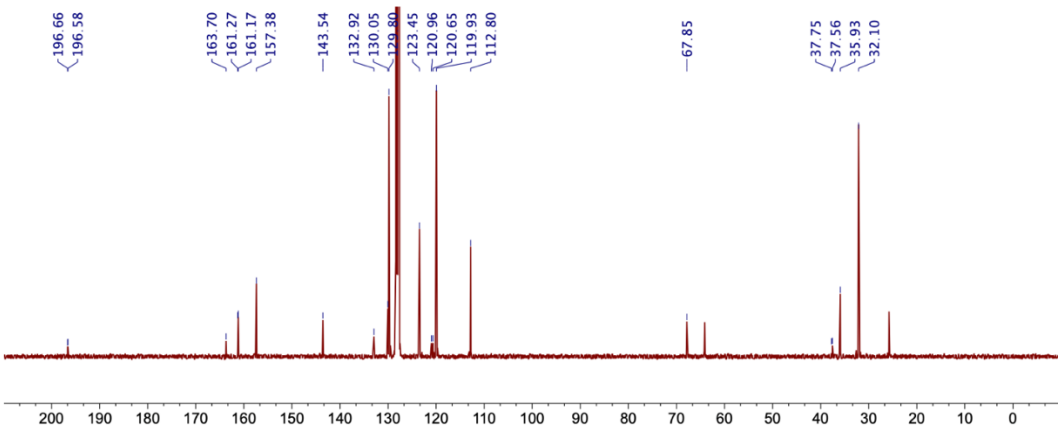

Figure AB4.25. $^{13}C\{^{1}H\}$ NMR spectrum of ^{Ph}**PO**^{ArOMe}**H** in C_6D_6 (*: residual THF).

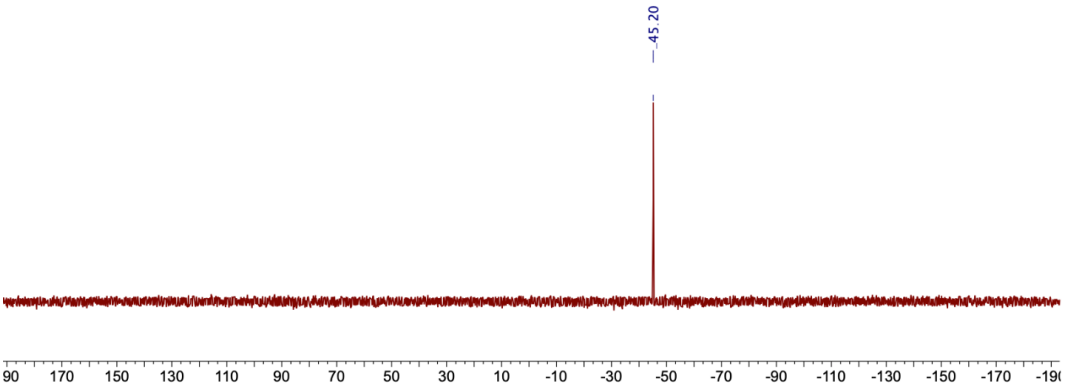

Figure AB4.26. $^{31}P\{^{1}H\}$ NMR spectrum of ^{Ph}**PO**^{ArOMe}**H** in C_6D_6.

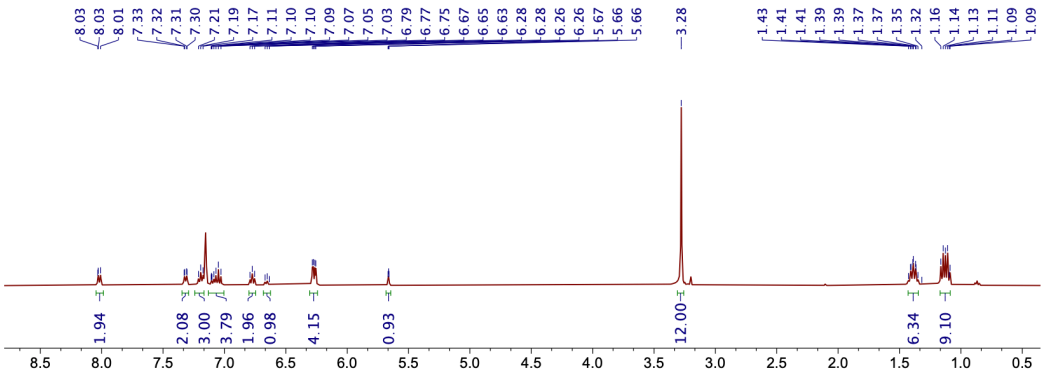

Figure AB4.27. ^{1}H NMR spectrum of ^{Me}**PO**^{Ph}**-Ni** in C_6D_6.

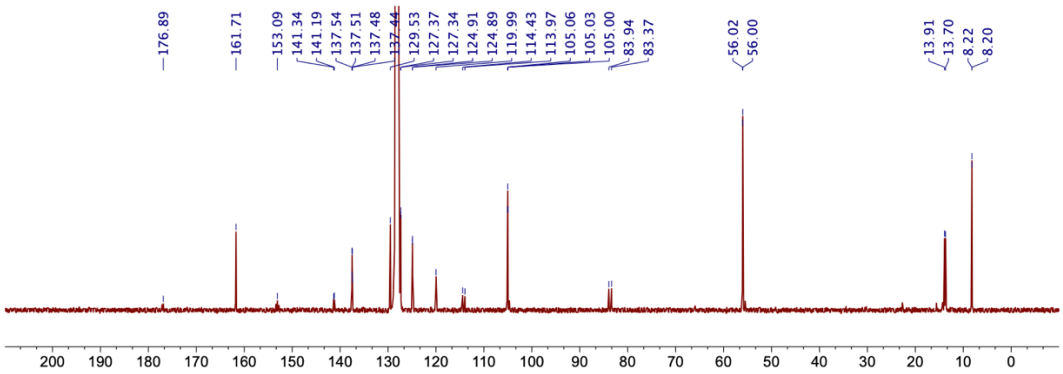

Figure AB4.28. $^{13}C\{^{1}H\}$ NMR spectrum of **$^{Me}PO^{Ph}$-Ni** in C_6D_6.

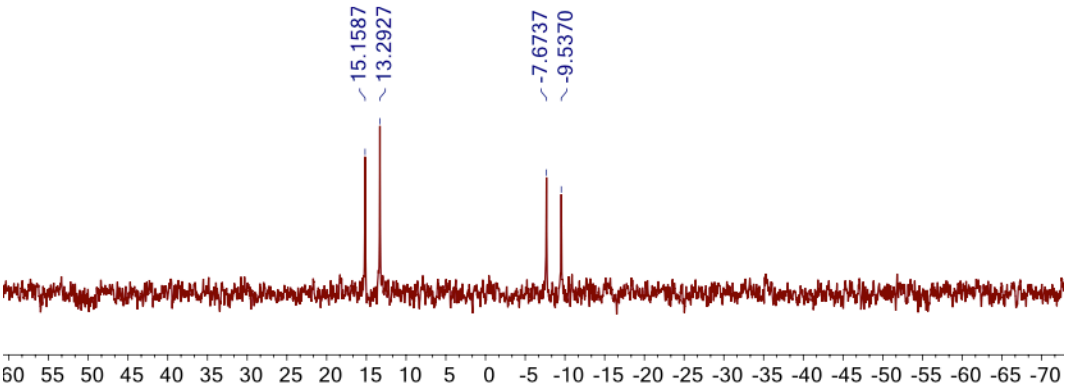

Figure AB4.29. $^{31}P\{^{1}H\}$ NMR spectrum of **$^{Me}PO^{Ph}$-Ni** in C_6D_6.

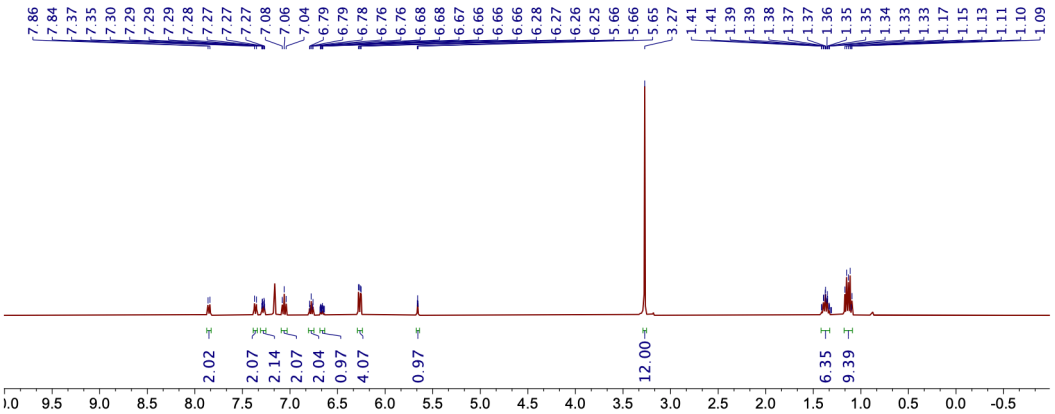

Figure AB4.30. ^{1}H NMR spectrum of **$^{Me}PO^{PhCF3}$-Ni** in C_6D_6.

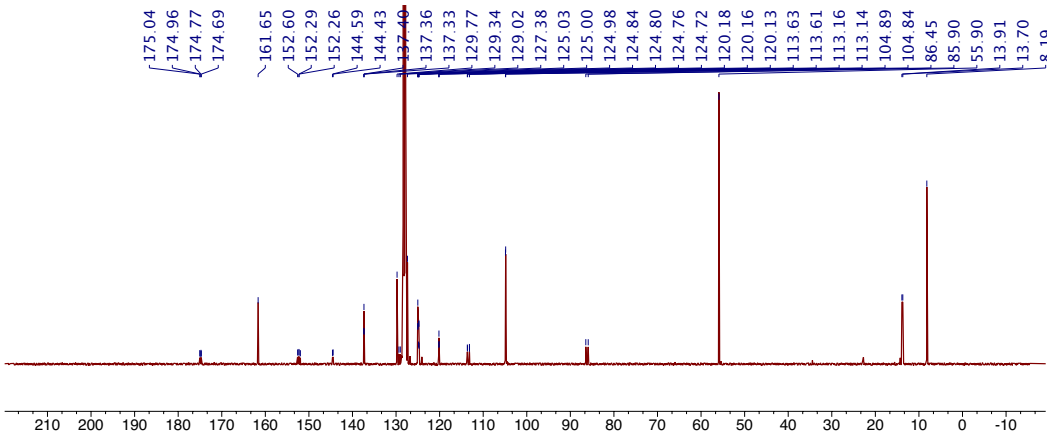

Figure AB4.31. $^{13}C\{^{1}H\}$ NMR spectrum of **^{Me}PO^{PhCF3}-Ni** in C_6D_6.

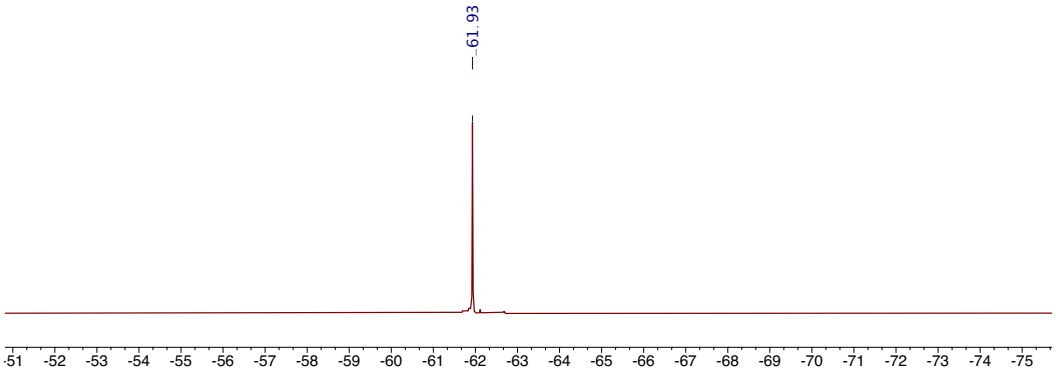

Figure AB4.32. ^{19}F NMR spectrum of **^{Me}PO^{PhCF3}-Ni** in C_6D_6.

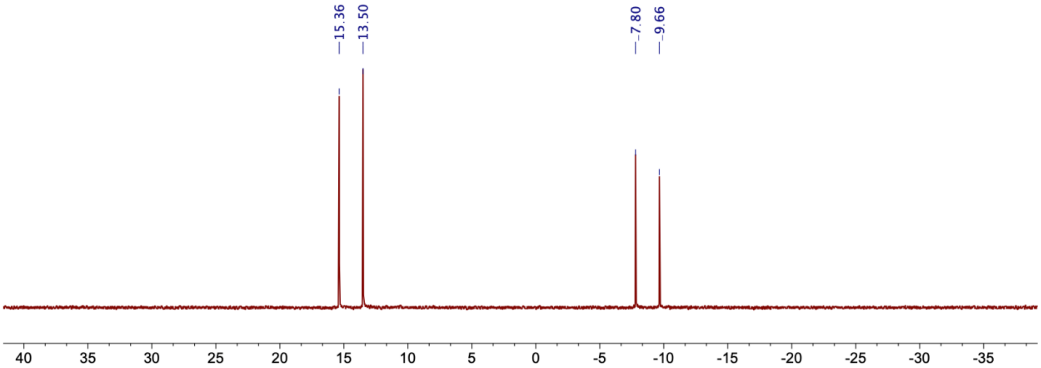

Figure AB4.33. $^{31}P\{^{1}H\}$ NMR spectrum of **^{Me}PO^{PhCF3}-Ni** in C_6D_6.

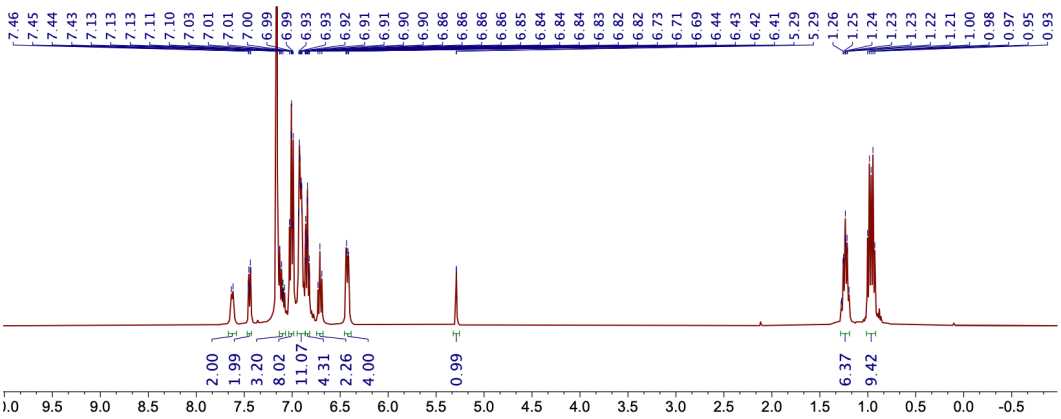

Figure AB4.34. ^{1}H NMR spectrum of ^{Ph}**PO**^{Ph}**-Ni** in C_6D_6.

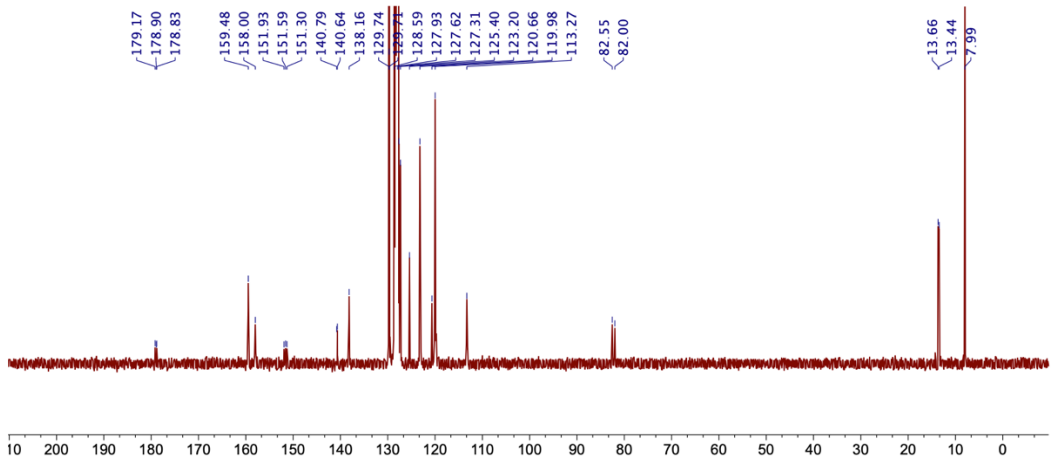

Figure AB4.35. ^{13}C{^{1}H} NMR spectrum of ^{Ph}**PO**^{Ph}**-Ni** in C_6D_6.

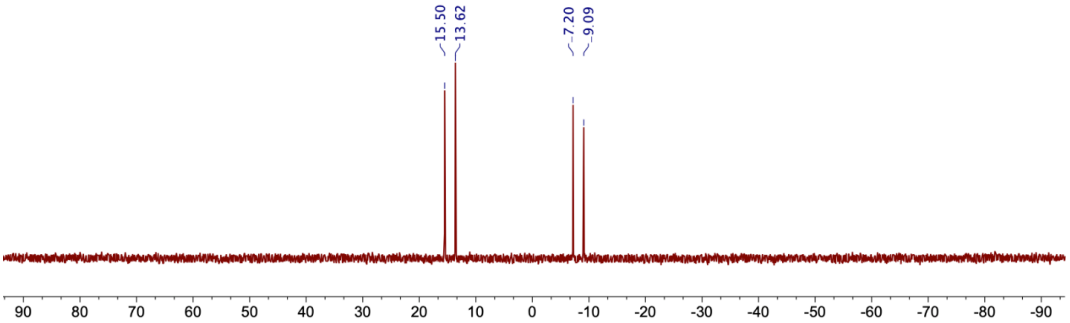

Figure AB4.36. ^{31}P{^{1}H} NMR spectrum of ^{Ph}**PO**^{Ph}**-Ni** in C_6D_6.

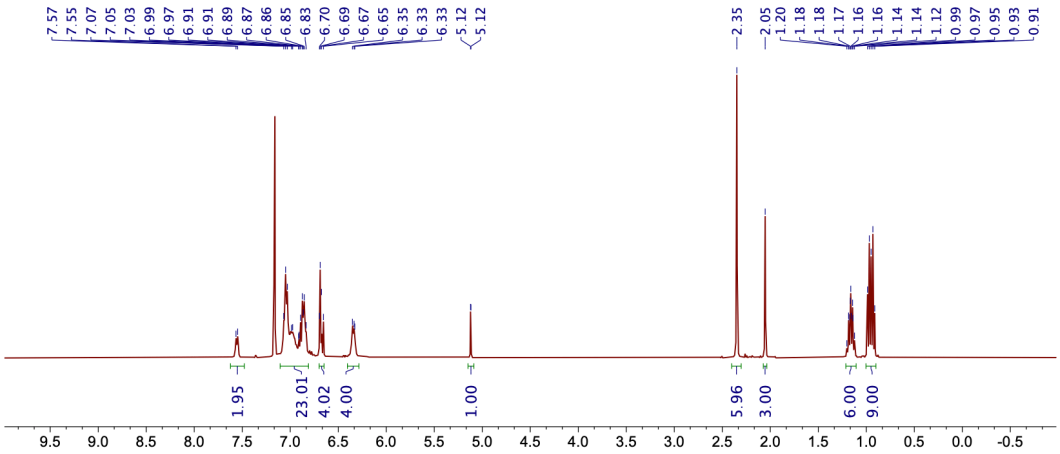

Figure AB4.37. ^{1}H NMR spectrum of **^{Ph}PO^{Mes}-Ni** in C_6D_6.

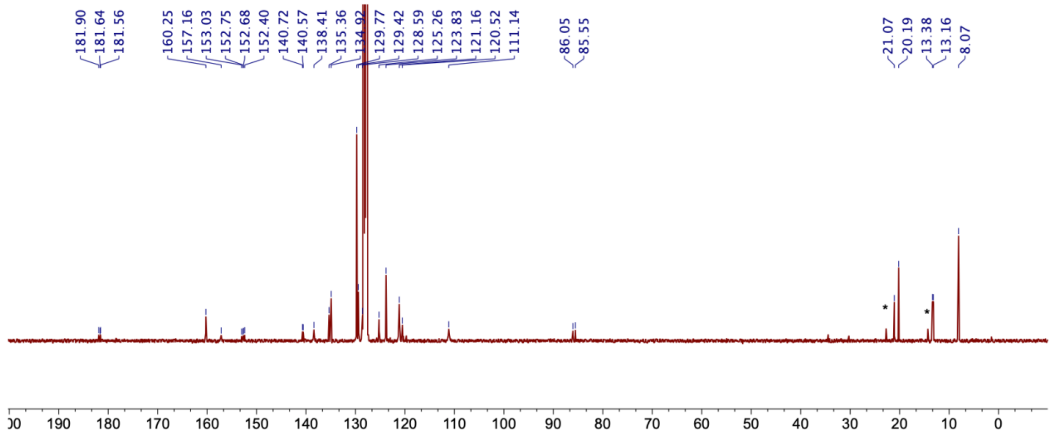

Figure AB4.38. ^{13}C{^{1}H} NMR spectrum of **^{Ph}PO^{Mes}-Ni** in C_6D_6 (*: hexenes).

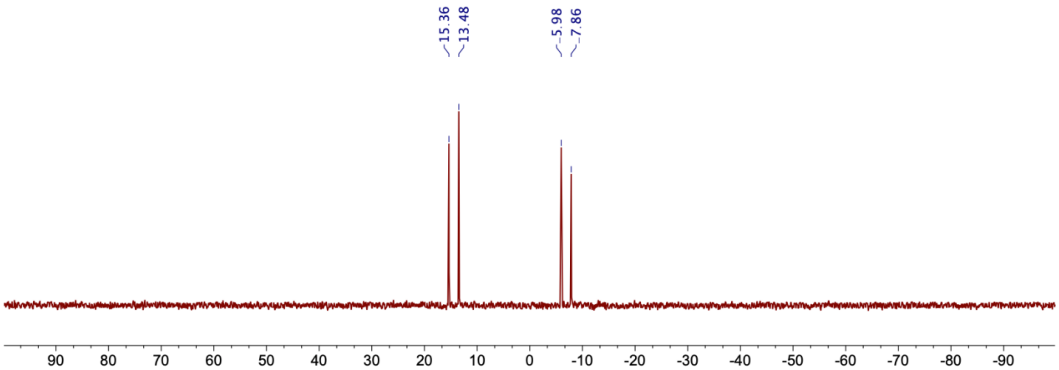

Figure AB4.39. ^{31}P{^{1}H} NMR spectrum of **^{Ph}PO^{Mes}-Ni** in C_6D_6.

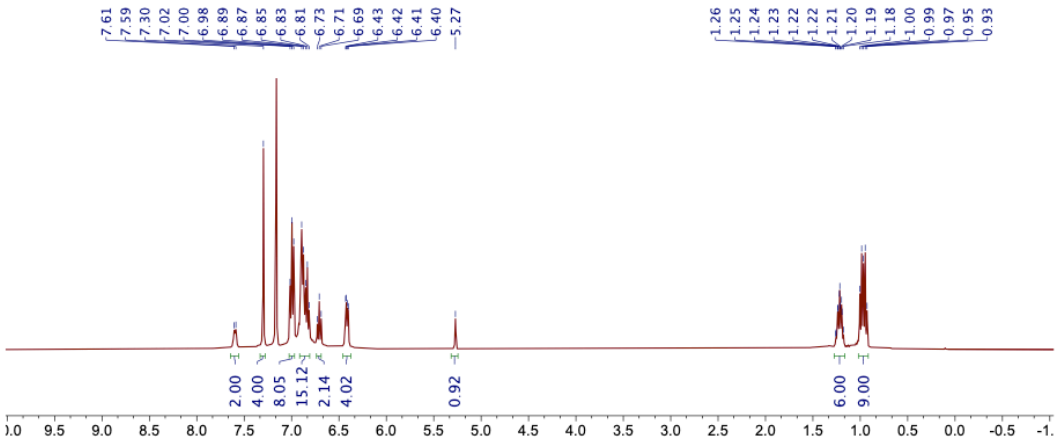

Figure AB4.40. ^{1}H NMR spectrum of **^{Ph}PO^{PhCF3}-Ni** in C_6D_6.

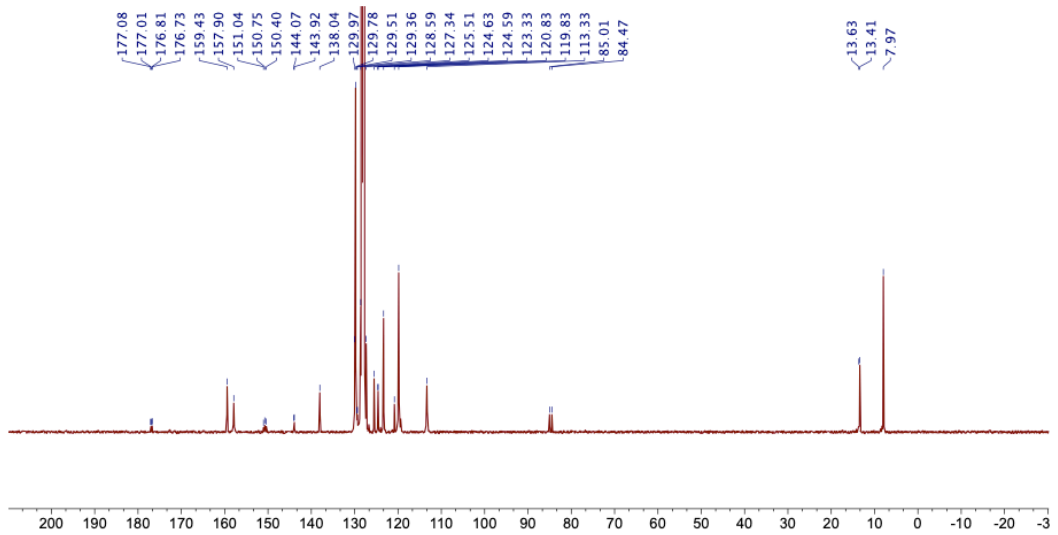

Figure AB4.41. ^{13}C{^{1}H} NMR spectrum of **^{Ph}PO^{PhCF3}-Ni** in C_6D_6.

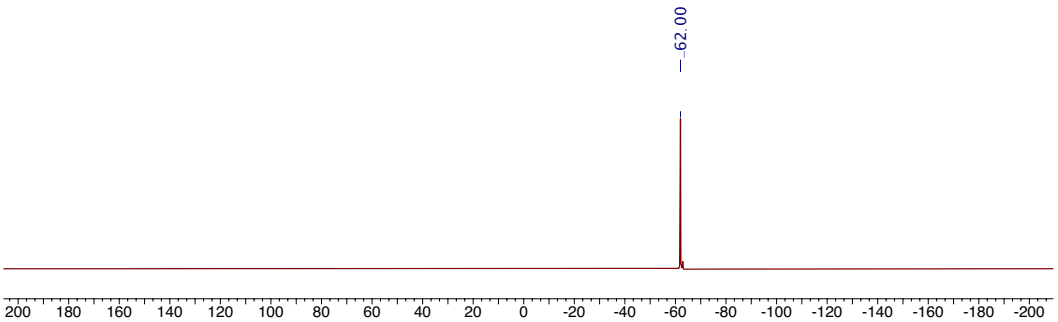

Figure AB4.42. ^{19}F NMR spectrum of **^{Ph}PO^{PhCF3}-Ni** in C_6D_6.

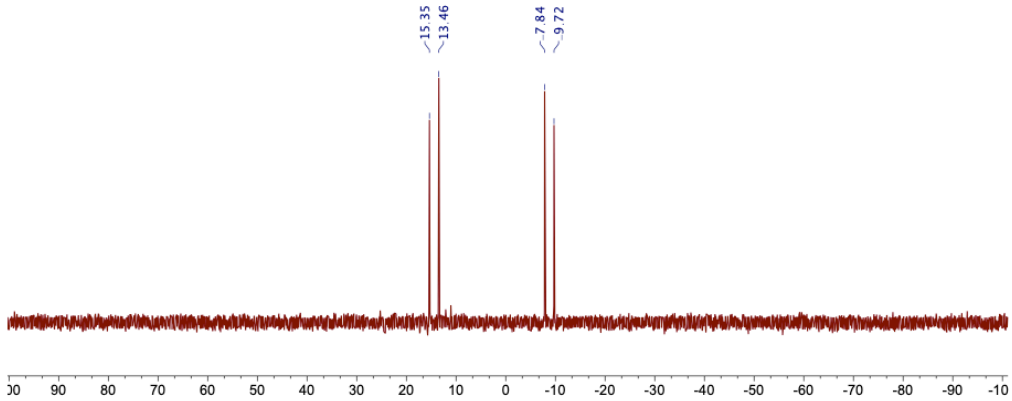

Figure AB4.43. $^{31}P\{^{1}H\}$ NMR spectrum of **$^{Ph}PO^{PhCF3}$-Ni** in C_6D_6.

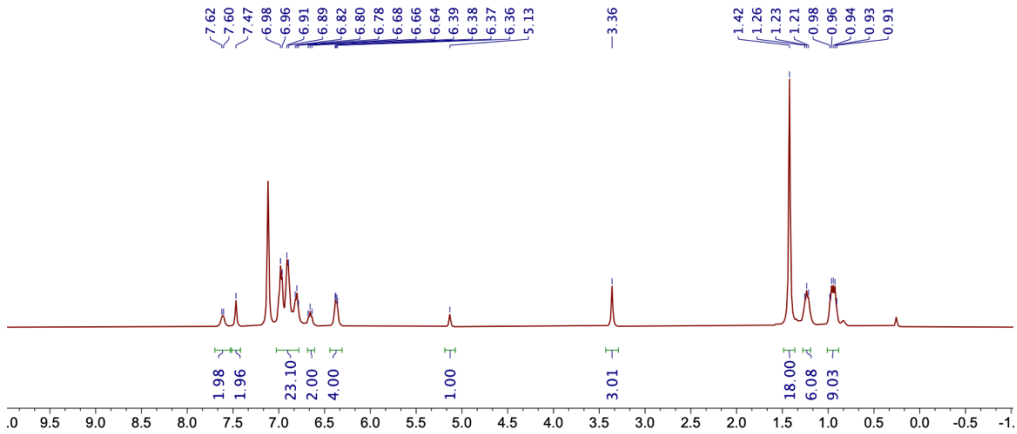

Figure AB4.44. ^{1}H NMR spectrum of **$^{Ph}PO^{ArOMe}$-Ni** in C_6D_6.

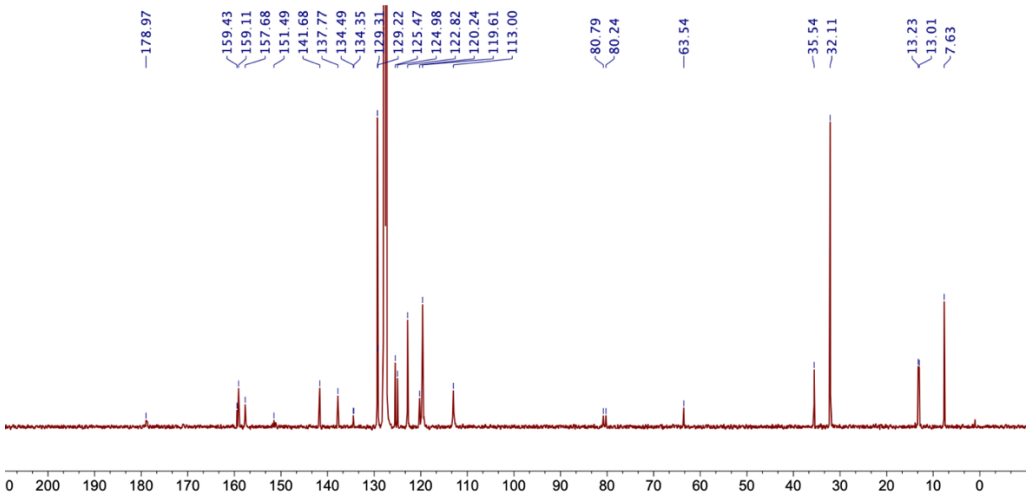

Figure AB4.45. $^{13}C\{^{1}H\}$ NMR spectrum of **$^{Ph}PO^{ArOMe}$-Ni** in C_6D_6.

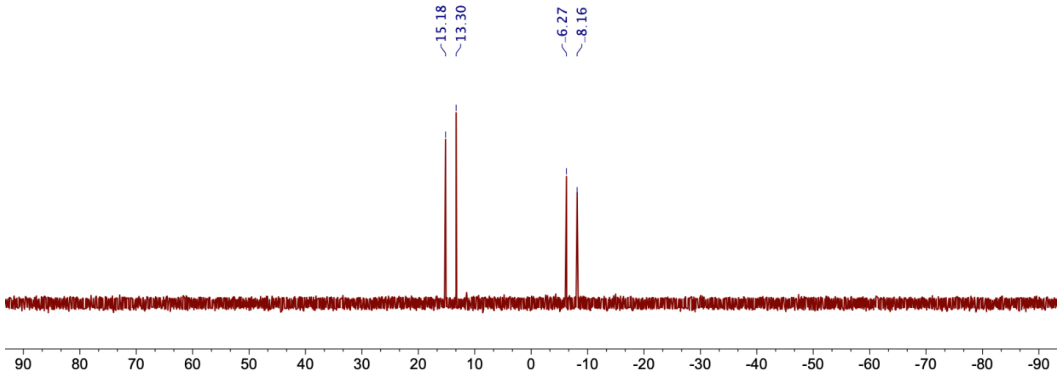

Figure AB4.46. $^{31}P\{^{1}H\}$ NMR spectrum of **^{Ph}PO^{ArOMe}-Ni** in C_6D_6.

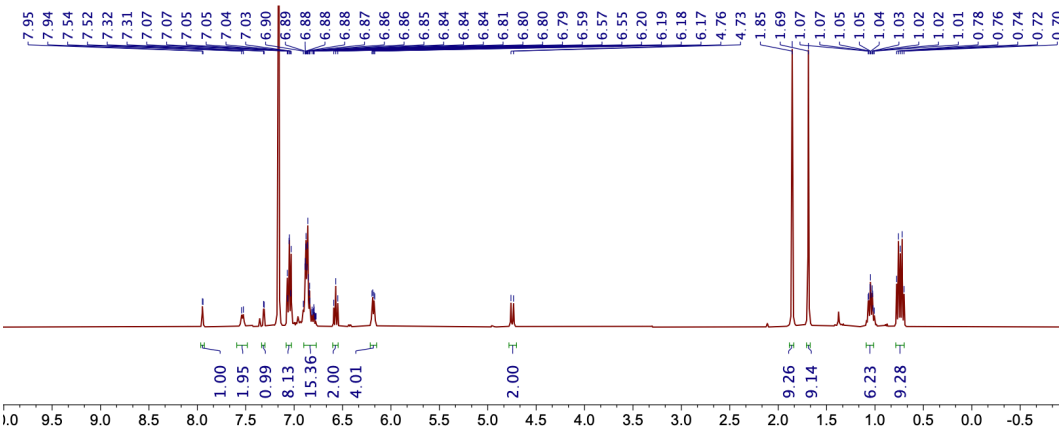

Figure AB4.47. ^{1}H NMR spectrum of **^{Ph}P*O^{ArO}-Ni** in C_6D_6.

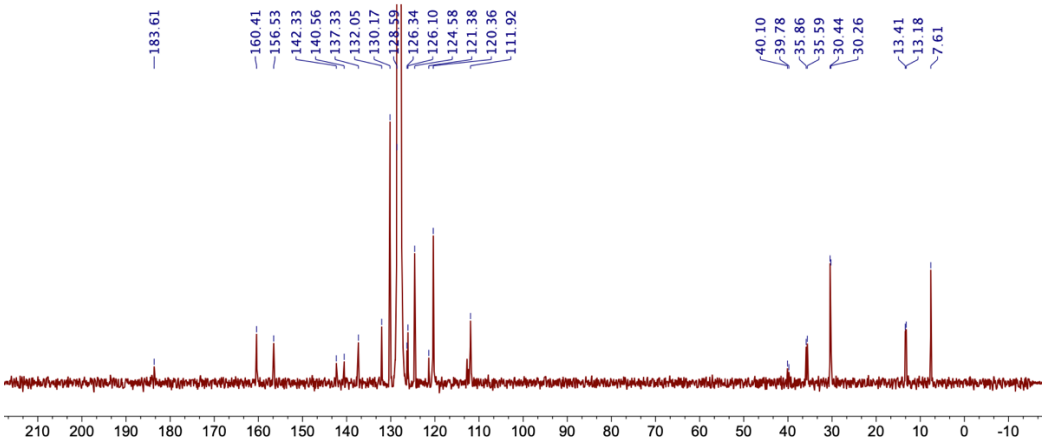

Figure AB4.48. $^{13}C\{^{1}H\}$ NMR spectrum of **^{Ph}P*O^{ArO}-Ni** in C_6D_6.

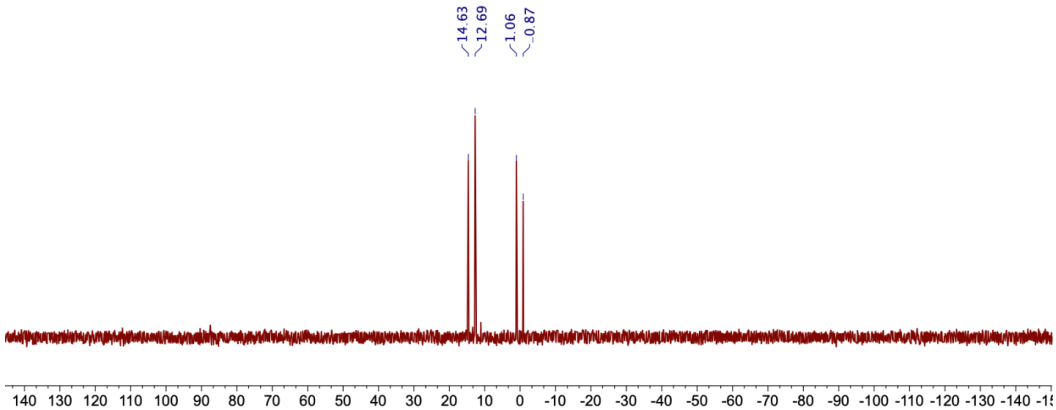

Figure AB4.49. $^{31}P\{^{1}H\}$ NMR spectrum of ^{Ph}**P*O^{ArO}-Ni** in C_6D_6

Chapter 5

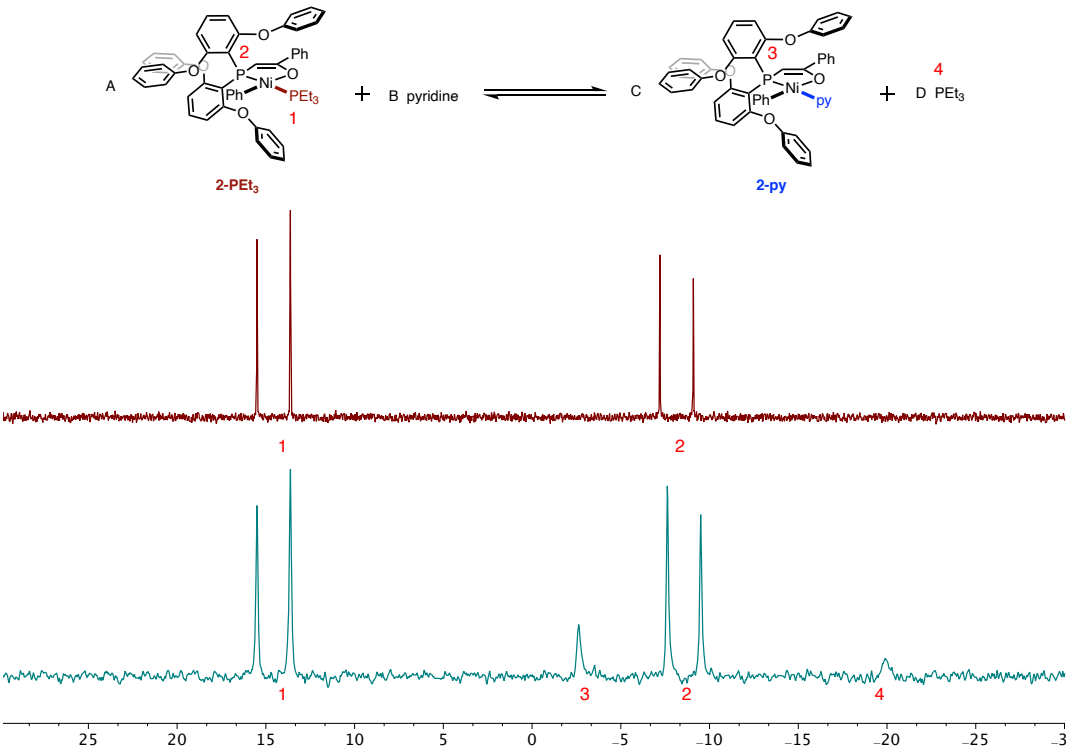

Figure AB5.1. Representative $^{31}P\{^{1}H\}$ NMR spectra for exchange studies. Top/Red spectrum: **2-PEt$_3$** (in C_6D_6); Bottom/Green spectrum: Mixtures upon addition of excess pyridine to **2-PEt$_3$** (Condition: **2-PEt$_3$**: 0.0059 mmol, pyridine: 5.9 mmol, no additional solvent, T: 25 °C)

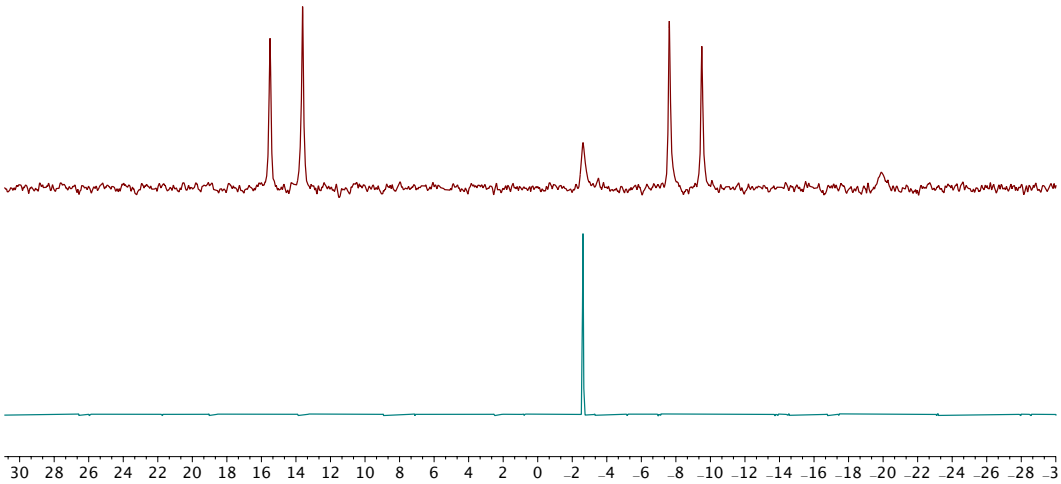

Figure AB5.2. Comparison of mixture generated in exchange studies (Top/Red spectrum, also shown as the bottom spectrum in Figure AB5.1) and independently synthesized **2-py** (bottom/Green spectrum, in C_6D_6).

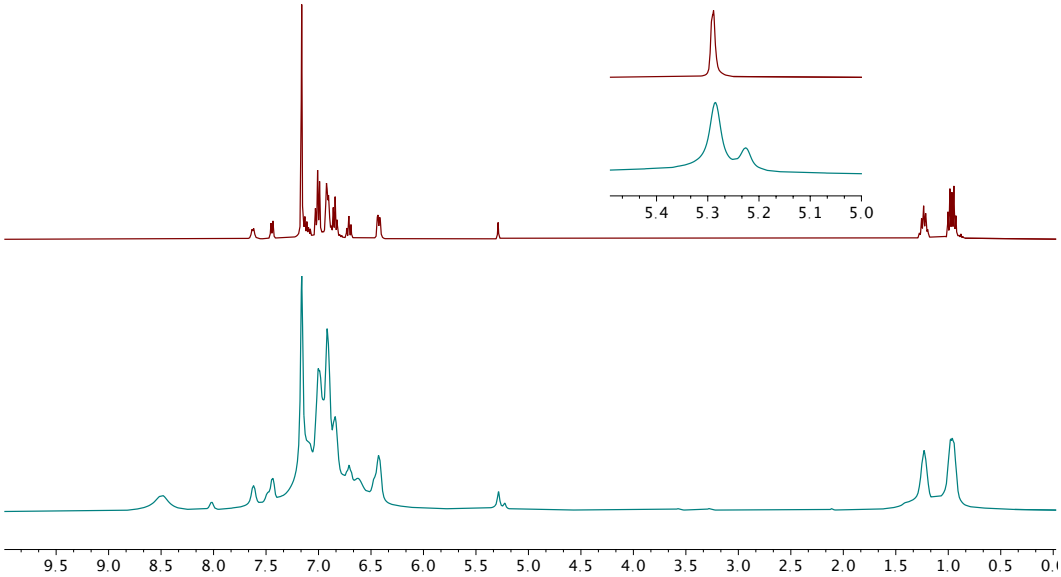

Figure AB5.3. Comparison of **2-PEt$_3$** (Top/Red spectrum, in C_6D_6) and mixture generated in exchange studies (Bottom/Green spectrum, condition: To the benzene solution of **2-PEt$_3$** was added 1500 equiv. of pyridine, the mixture was then stirred overnight, and volatiles were then removed.

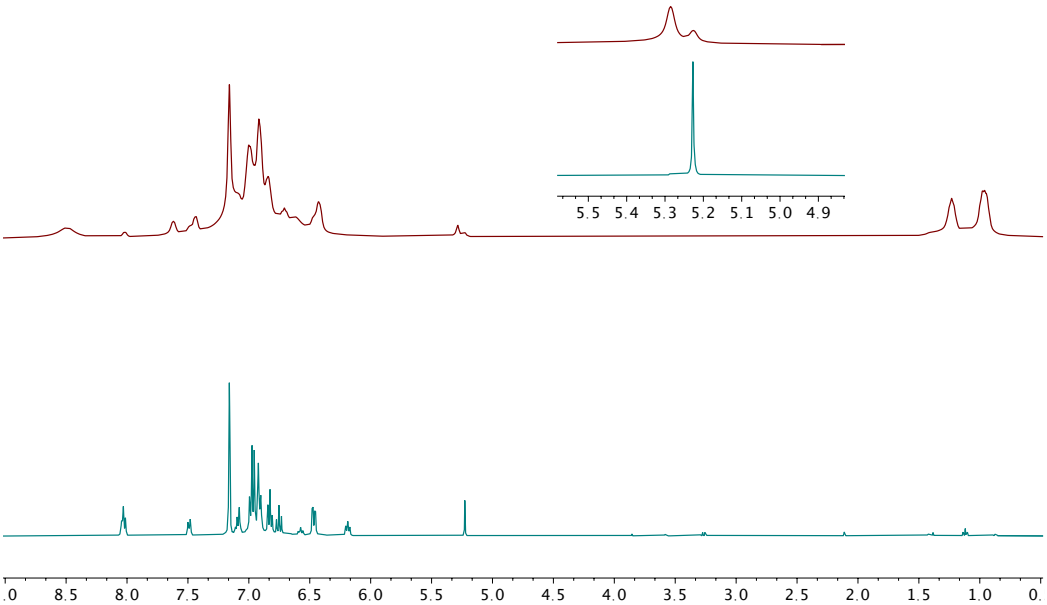

Figure AB5.4. Comparison of mixture generated in exchange studies (Top/Red spectrum, also shown as the bottom spectrum in Figure AB5.3) and **2-py** (Bottom/Green spectrum, in C_6D_6).

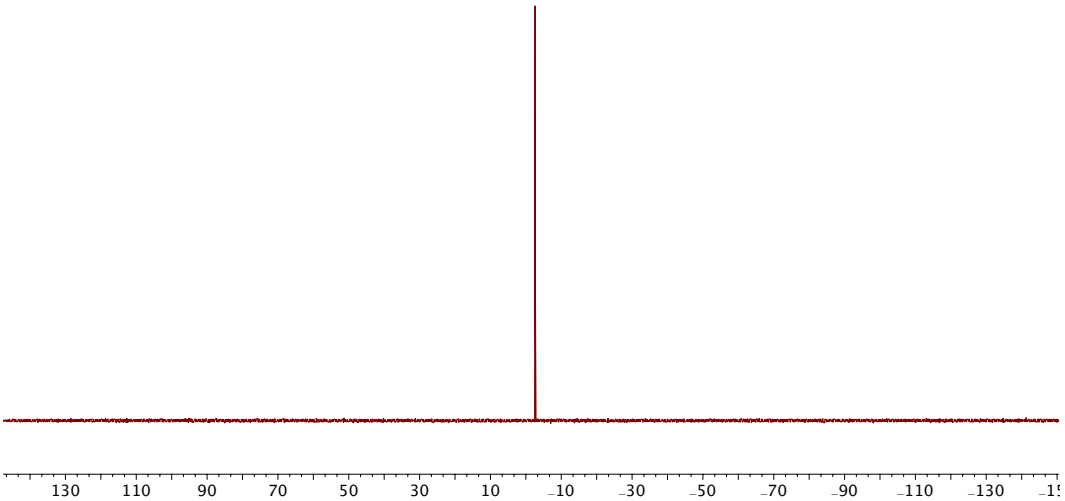

Figure AB5.5. $^{31}P\{^{1}H\}$ NMR spectrum of **2-py** in C_6D_6.

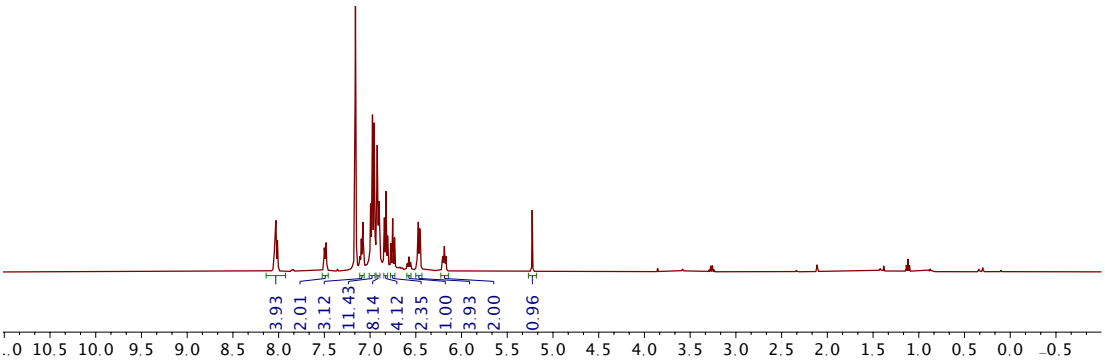

Figure AB5.6. ^{1}H NMR spectrum of **2-py** in C_6D_6.

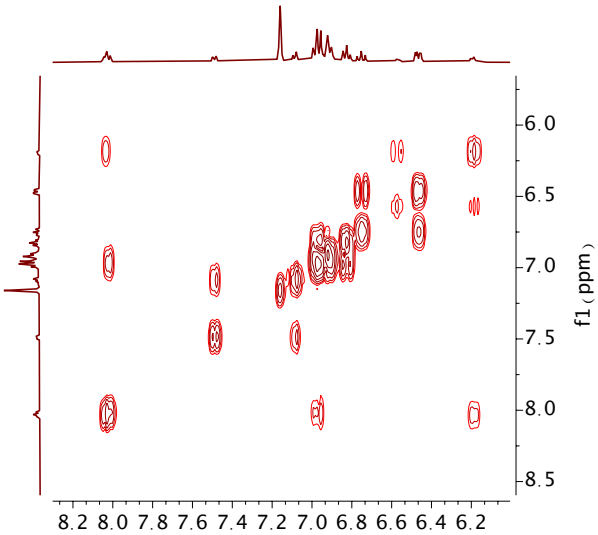

Figure AB5.7. ^{1}H-^{1}H COSY NMR spectrum of **2-py** in C_6D_6.

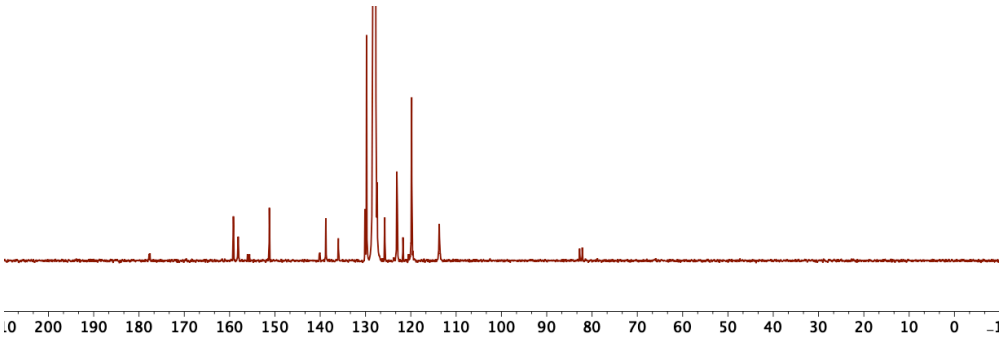

Figure AB5.8. ^{13}C{^{1}H} NMR spectrum of **2-py** in C_6D_6.

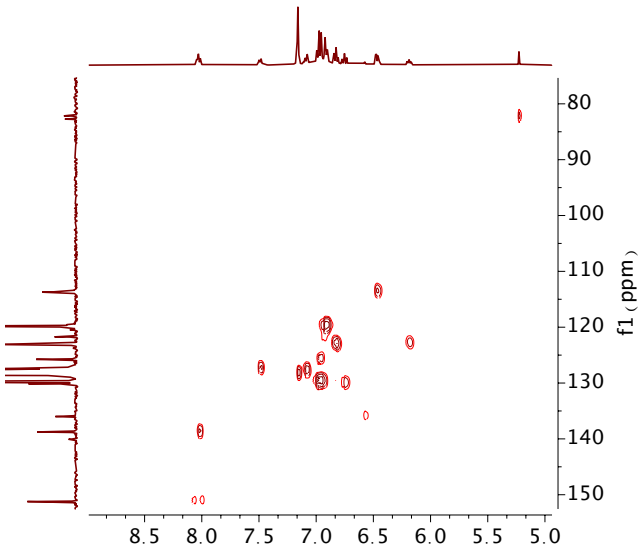

Figure AB5.9. ^{1}H-^{13}C HSQC NMR spectrum of **2-py** in C_6D_6.

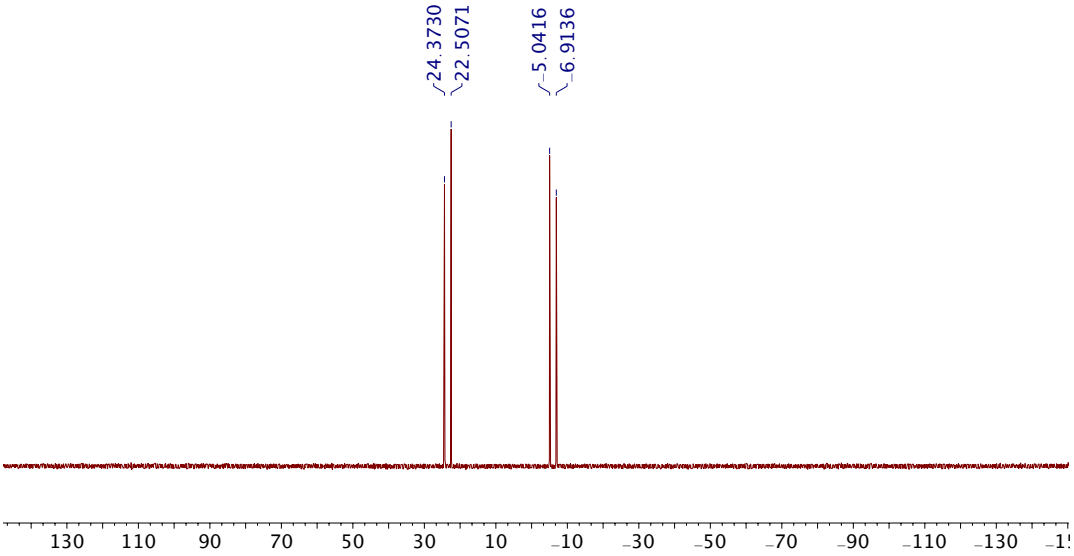

Figure AB5.10. $^{31}P\{^{1}H\}$ NMR spectrum of **2-PPh$_3$** in C_6D_6.

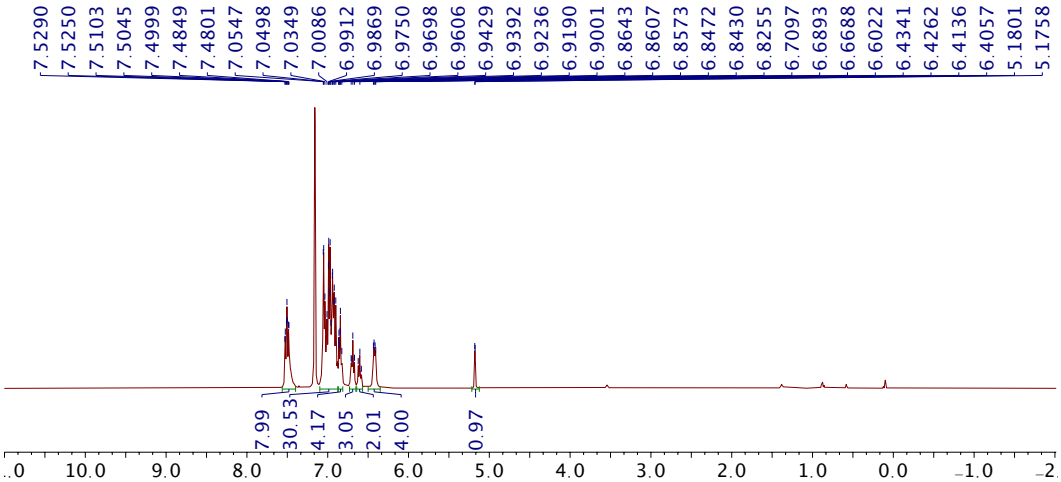

Figure AB5.11. ^{1}H NMR spectrum of **2-PPh$_3$** in C_6D_6.

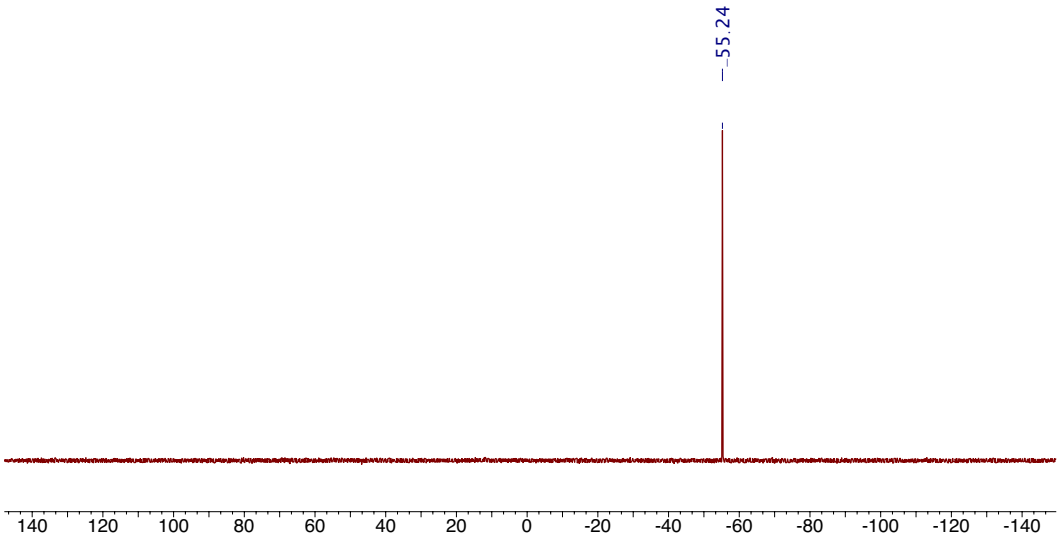

Figure AB5.12. ^{31}P{^{1}H} NMR spectrum of **^{MeO}POBrH** in C_6D_6.

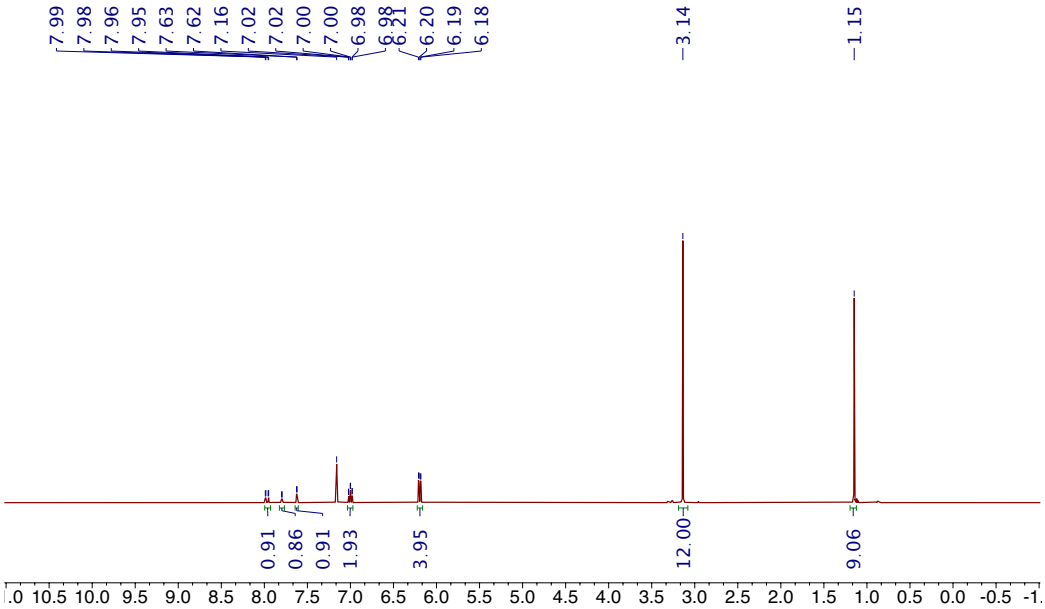

Figure AB5.13. ^{1}H NMR spectrum of ^{MeO}**POBrH** in C_6D_6.

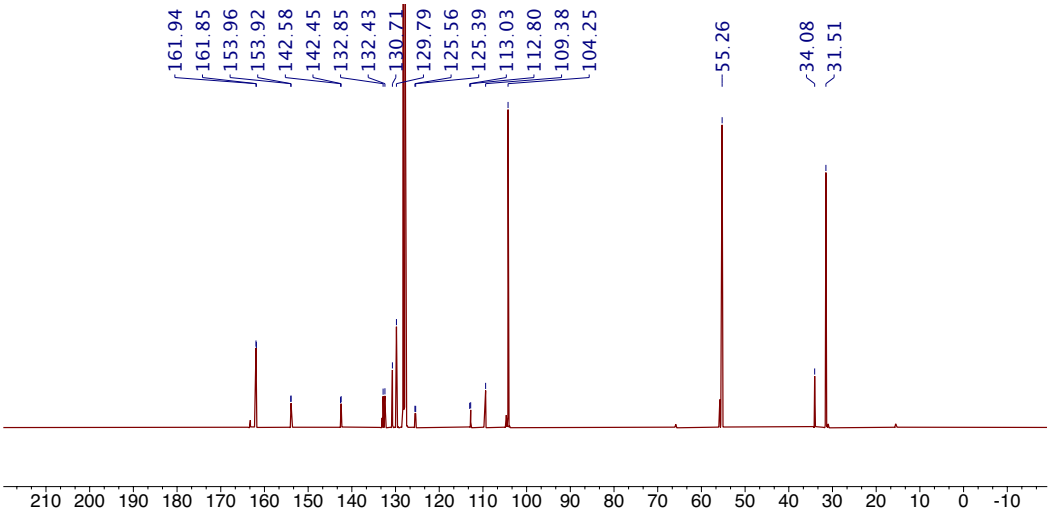

Figure AB5.14. ^{13}C{^{1}H} NMR spectrum of ^{MeO}**POBrH** in C_6D_6.

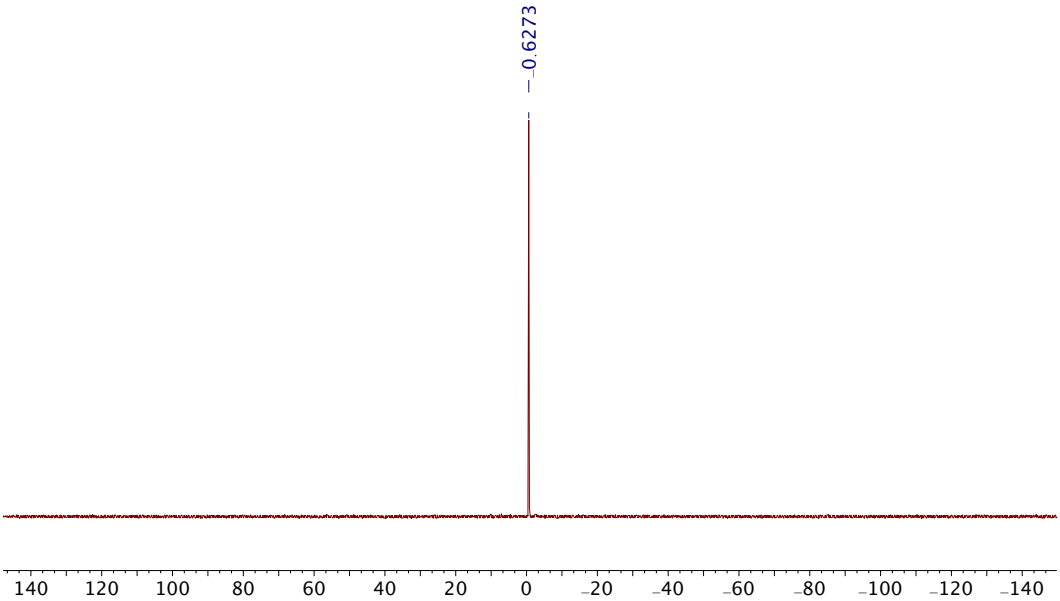

Figure AB5.15. $^{31}P\{^{1}H\}$ NMR spectrum of **1-py** in C_6D_6.

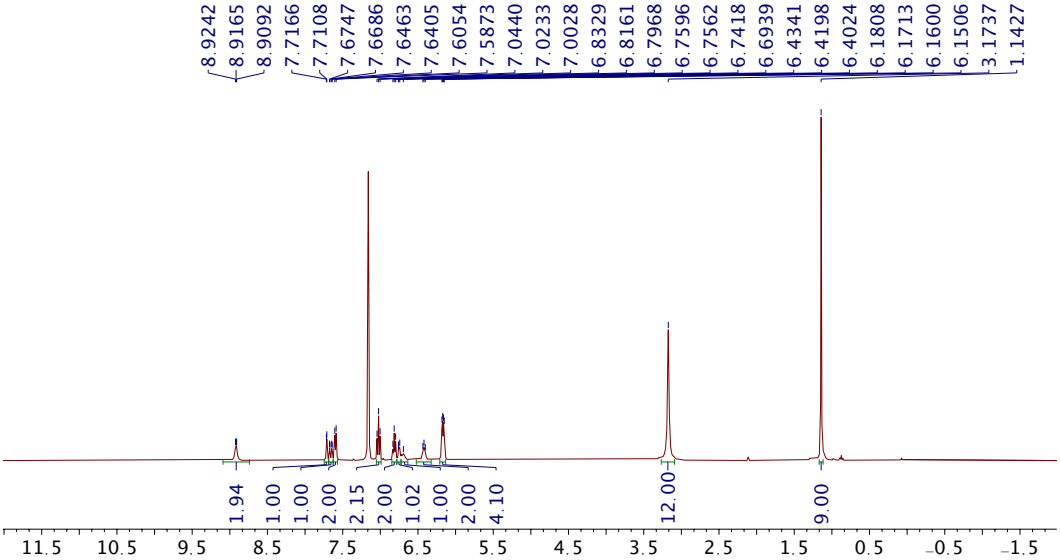

Figure AB5.16. ^{1}H NMR spectrum of **1-py** in C_6D_6.

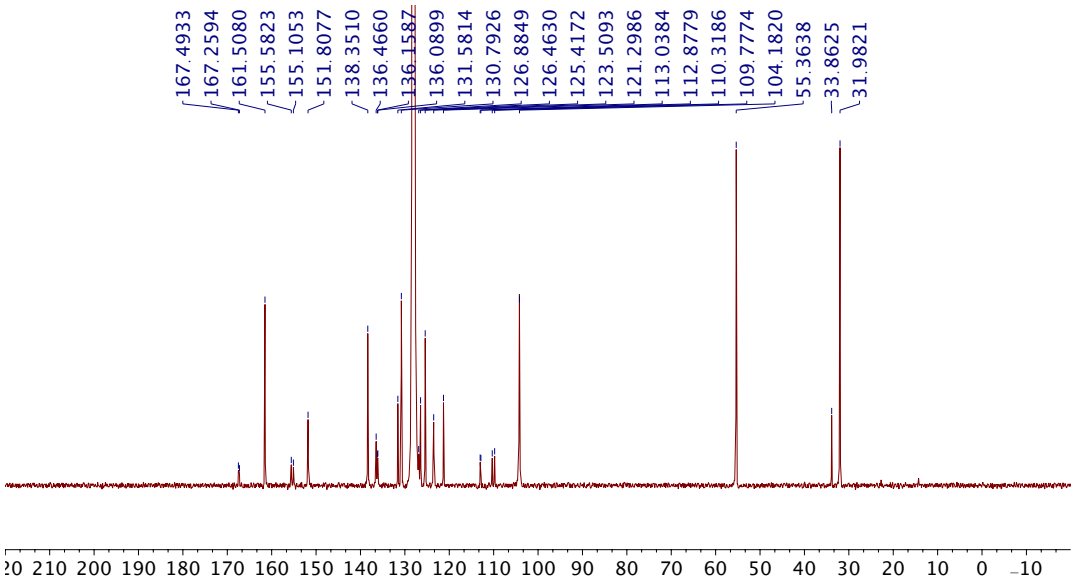

Figure AB5.17. $^{13}C\{^{1}H\}$ NMR spectrum of **1-py** in C_6D_6.

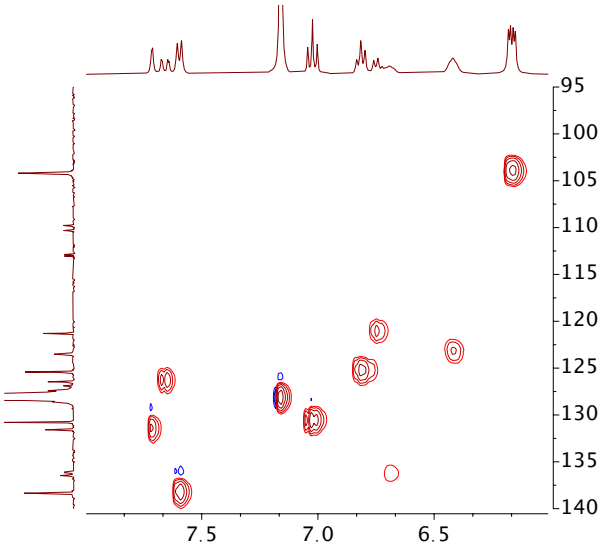

Figure AB5.18. ^{1}H-^{13}C HSQC NMR spectrum of **1-py** in C_6D_6.

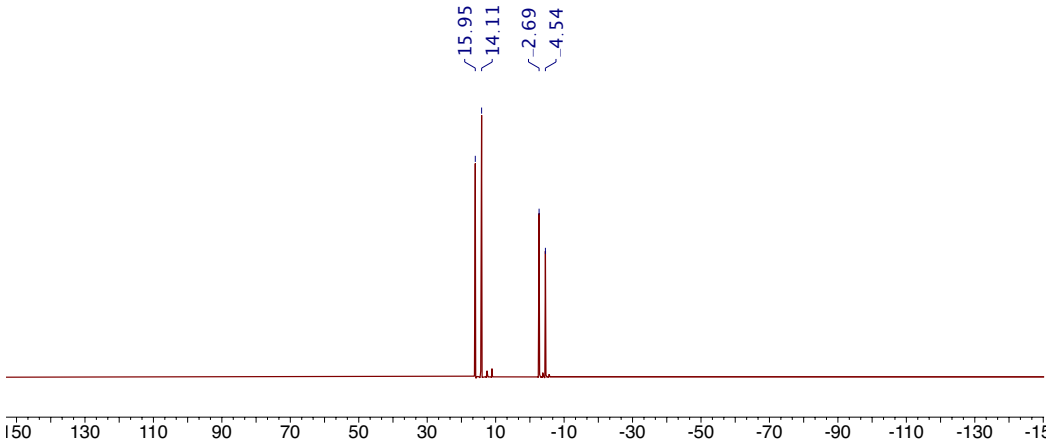

Figure AB5.19. $^{31}P\{^{1}H\}$ NMR spectrum of **1-PEt$_3$** in C_6D_6.

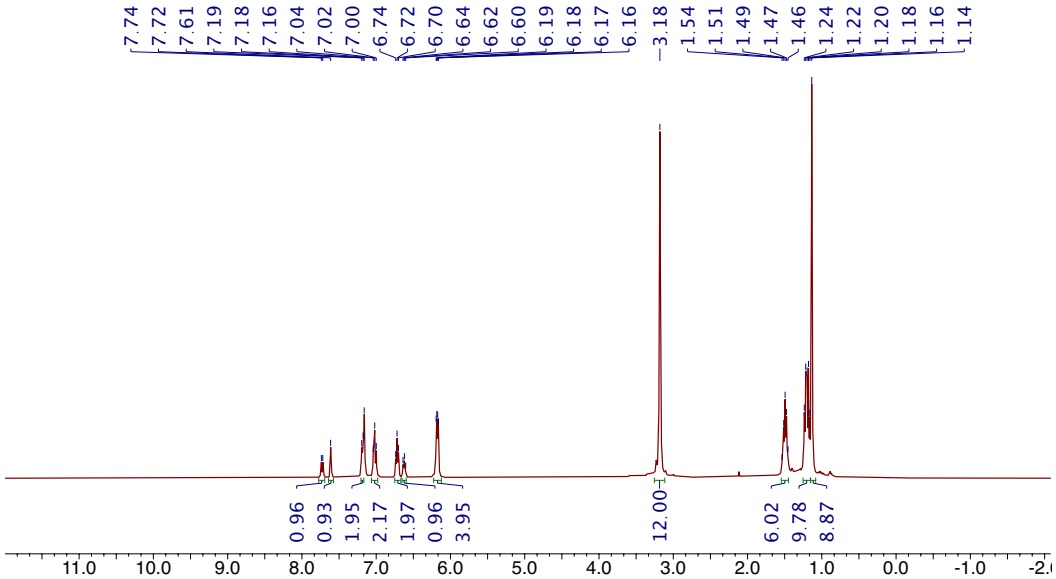

Figure AB5.20. ^{1}H NMR spectrum of **1-PEt$_3$** in C_6D_6.

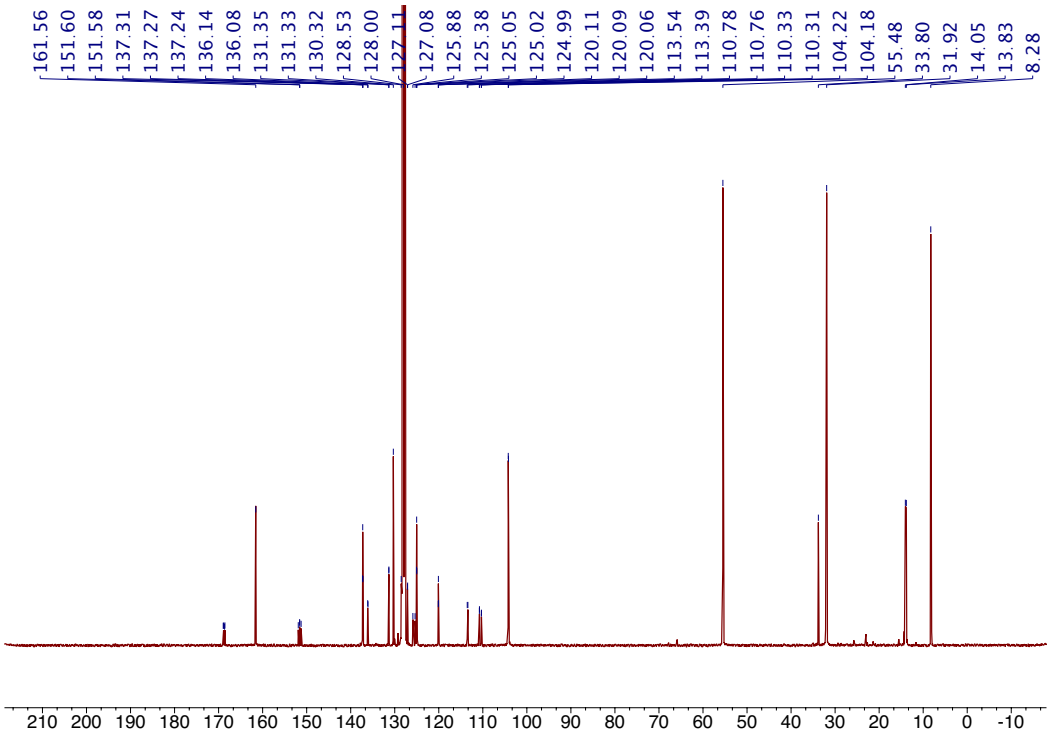

Figure AB5.21. $^{13}C\{^{1}H\}$ NMR spectrum of **1-PEt$_3$** in C_6D_6.

Chapter 6

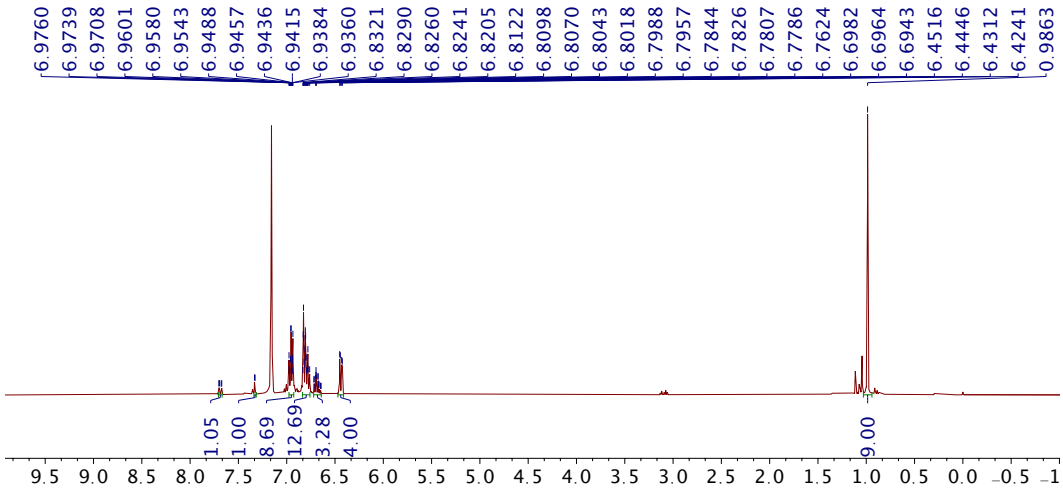

Figure AB6.1: ^{1}H NMR spectrum of ^{PhO}**POBrH** in C_6D_6.

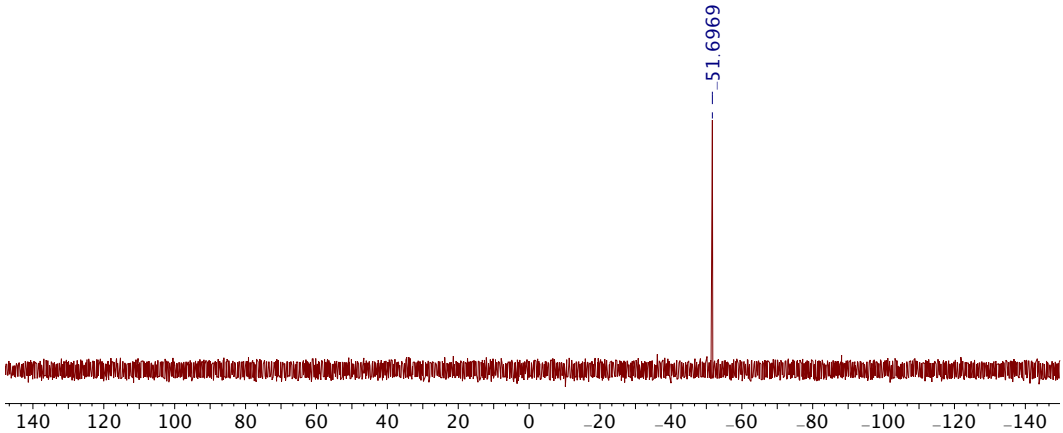

Figure AB6.2: ^{31}P{^{1}H} NMR spectrum of ^{PhO}**POBrH** in in C_6D_6.

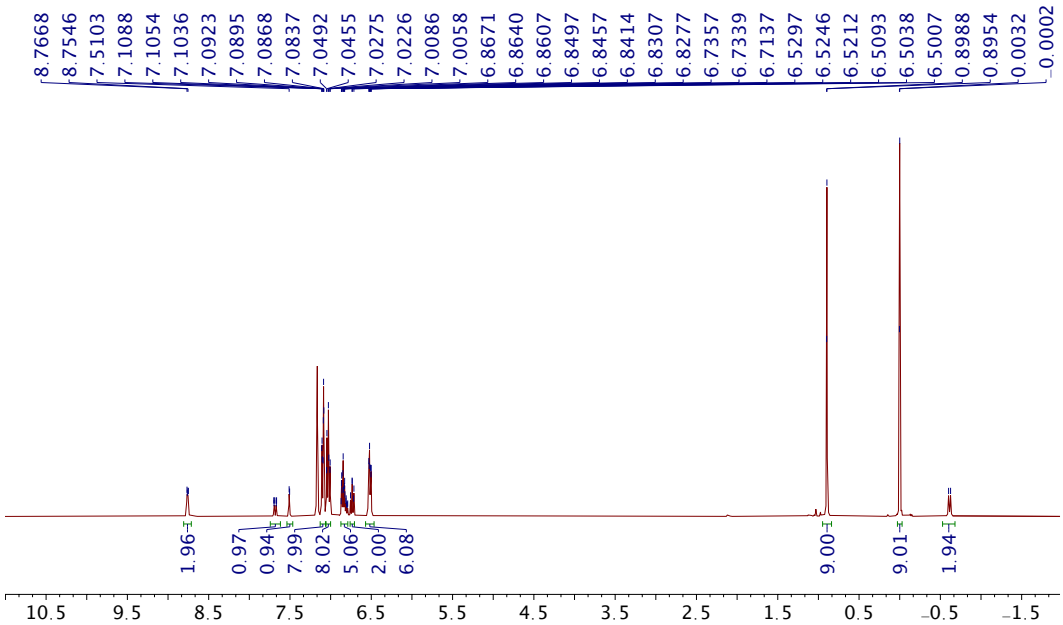

Figure AB6.3: ^{1}H NMR spectrum of ^{PhO}**POBr-Ni** in C_6D_6.

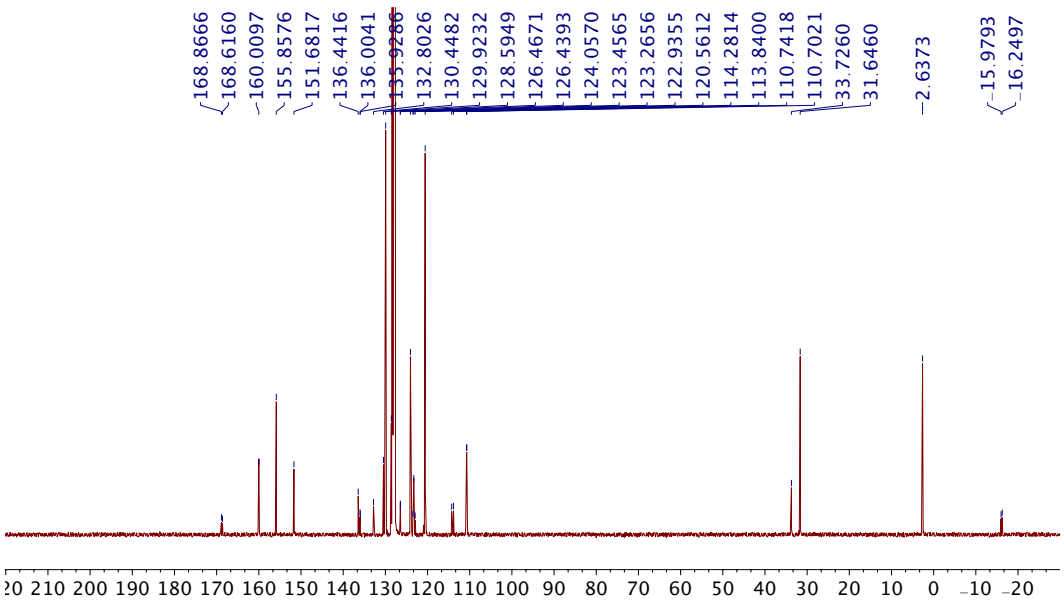

Figure AB6.4: ^{13}C{^{1}H} NMR spectrum of ^{PhO}**POBr-Ni** in C_6D_6.

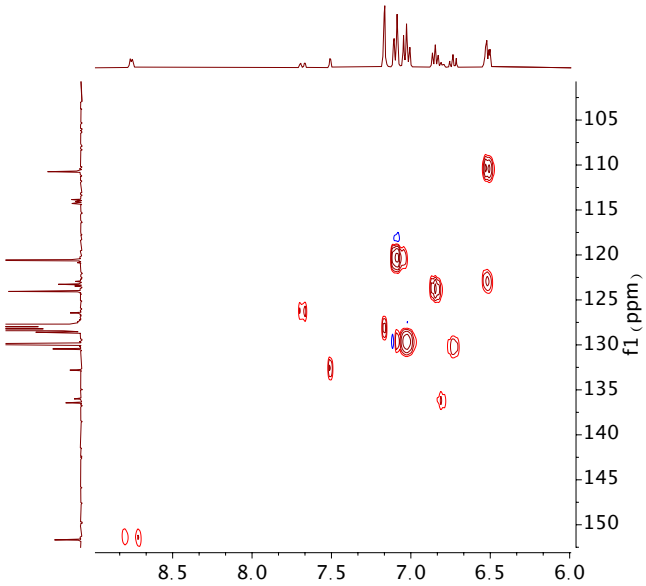

Figure AB6.5: ^{1}H-^{13}C{^{1}H} HSQC NMR spectrum of ^{PhO}**POBr-Ni** in C_6D_6.

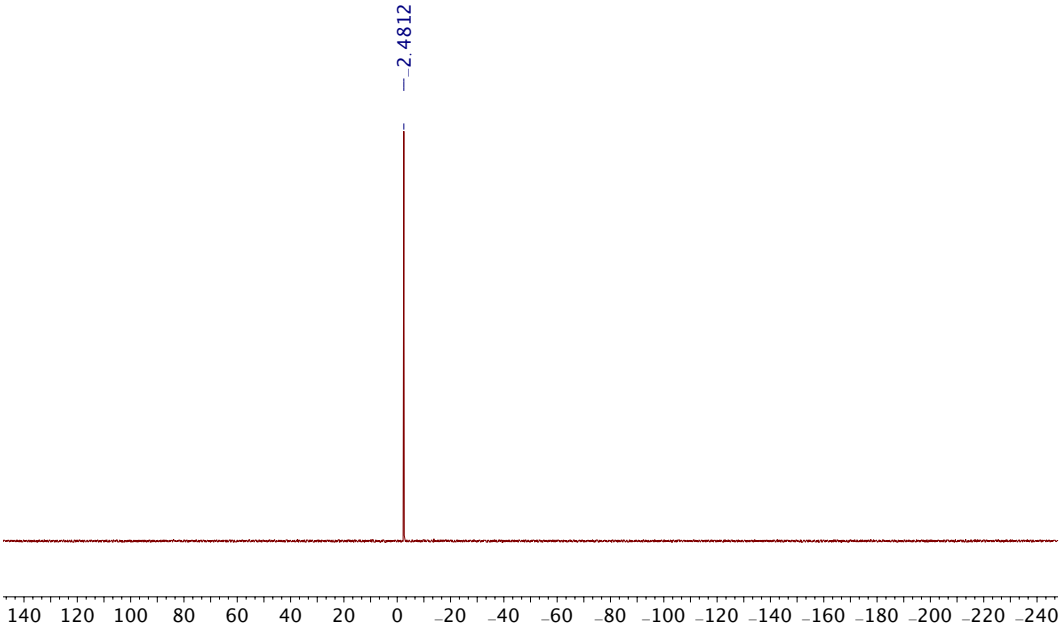

Figure AB6.6: ^{31}P{^{1}H} NMR spectrum of ^{PhO}**POBr-Ni** in in C_6D_6.

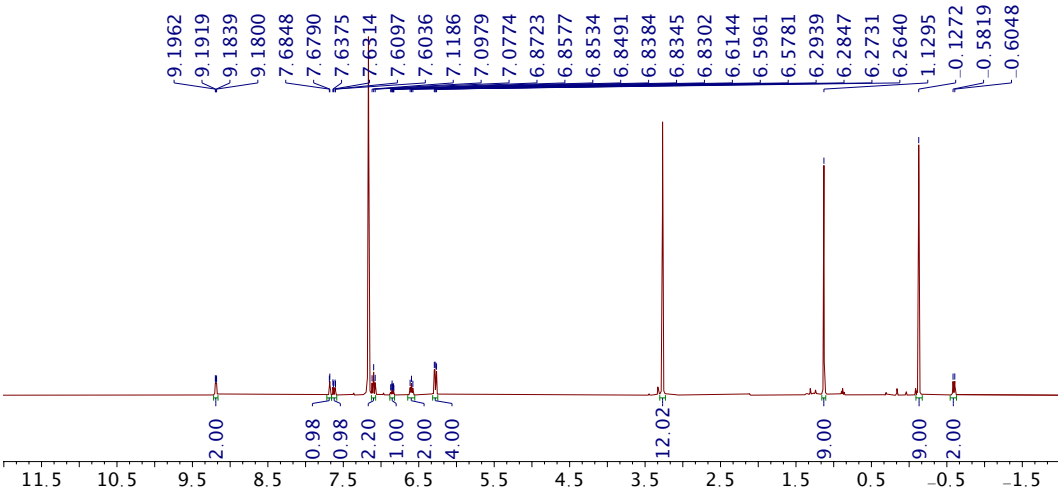

Figure AB6.7: ^{1}H NMR spectrum of ^{MeO}**POBr-Ni** in C_6D_6.

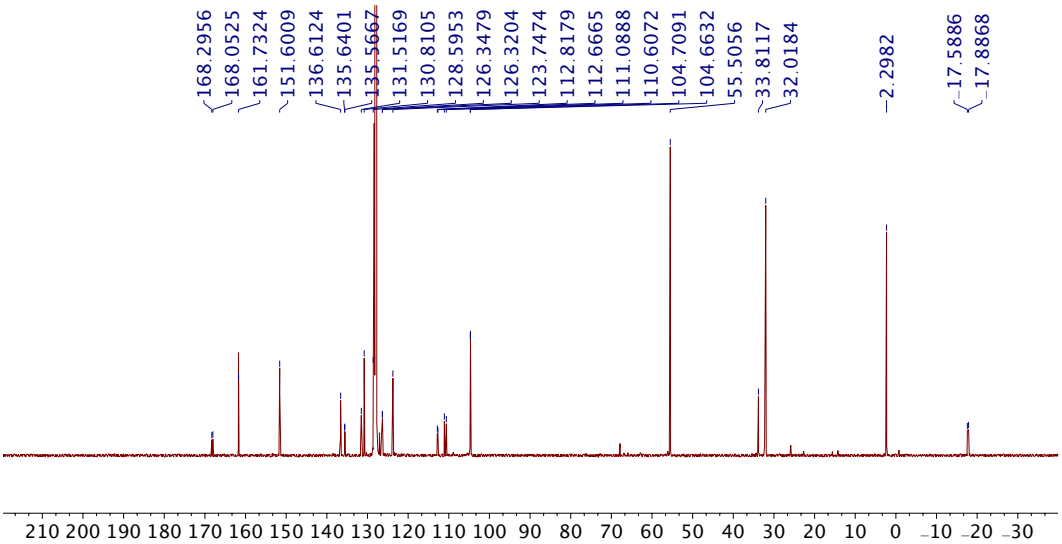

Figure AB6.8: ^{13}C{^{1}H} NMR spectrum of ^{MeO}**POBr-Ni** in C_6D_6.

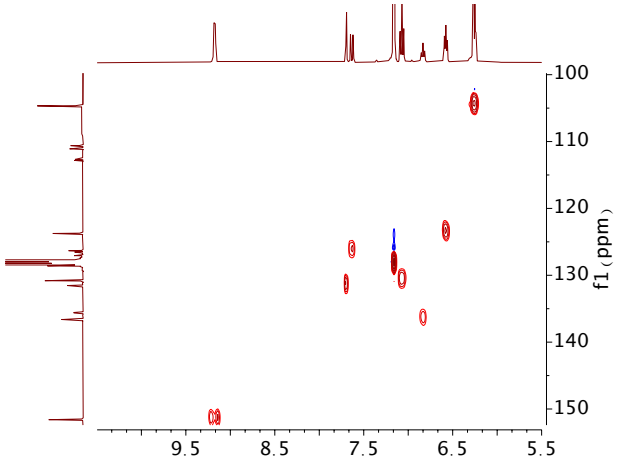

Figure AB6.9: ^{1}H-$^{13}C\{^{1}H\}$ HSQC NMR spectrum of ^{MeO}**POBr-Ni** in C_6D_6.

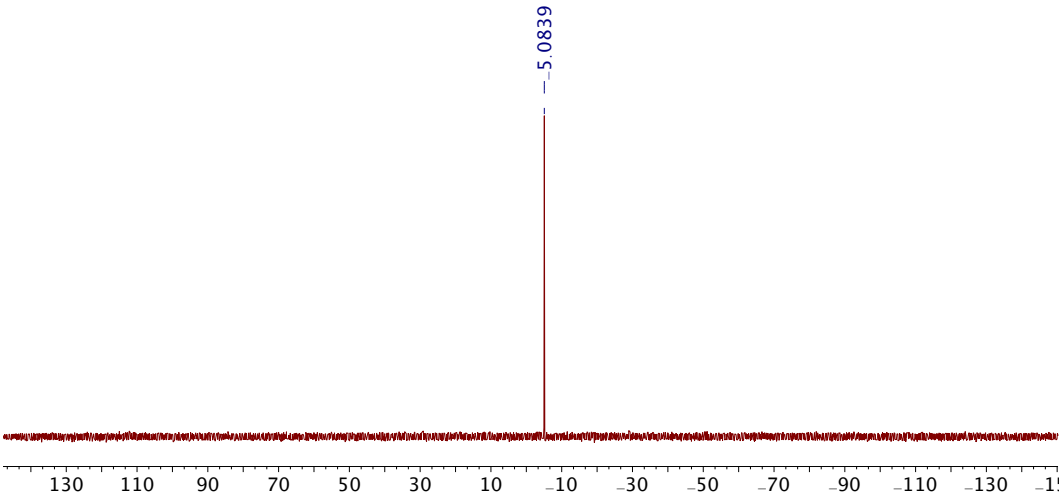

Figure AB6.10: $^{31}P\{^{1}H\}$ NMR spectrum of ^{MeO}**POBr-Ni** in in C_6D_6.

Chapter 7

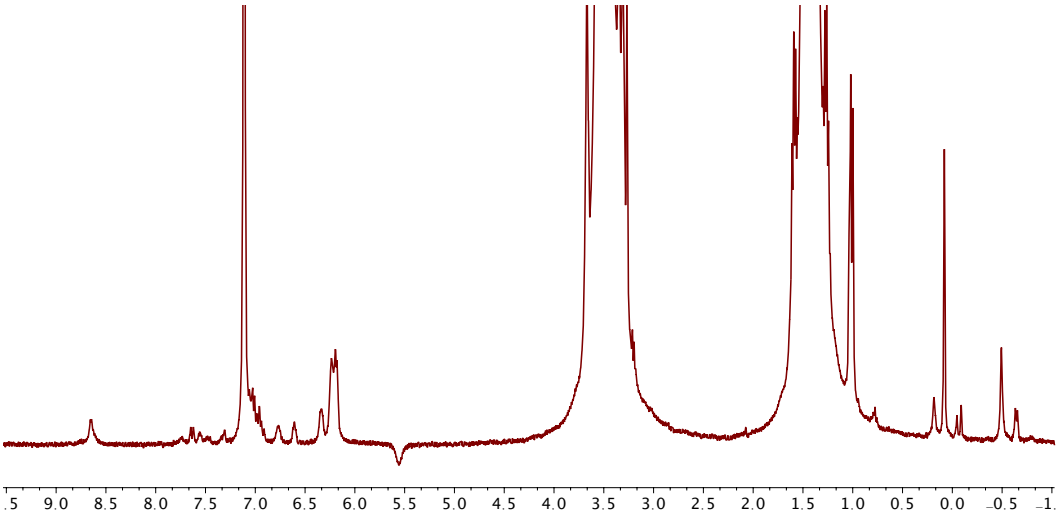

Figure AB7.1: ^{1}H NMR spectrum of **1** + 1 equiv. of $ZnCl_2$ in 10% C_6D_6/90% THF-H8.

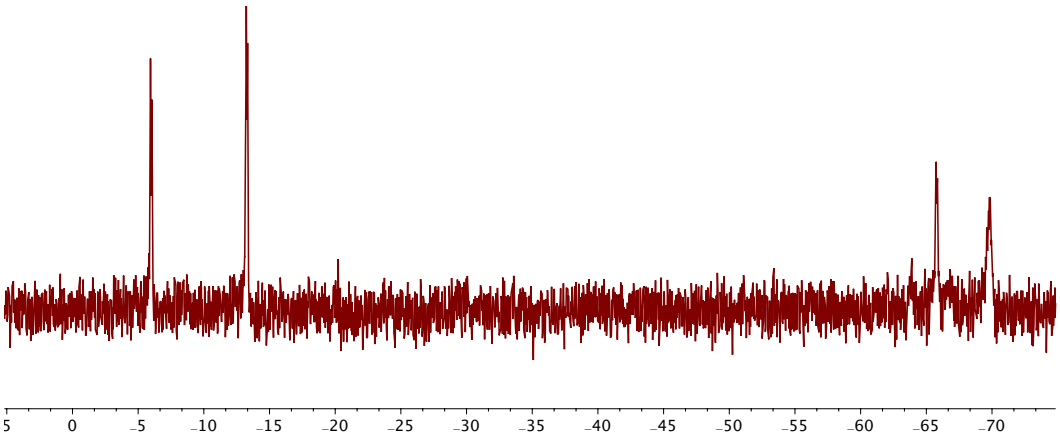

Figure AB7.2: ^{31}P{^{1}H} NMR spectrum of two isomers (crude mixture of **1** + 1 equiv. of $ZnCl_2$) in 10% C_6D_6/90% THF-H8.

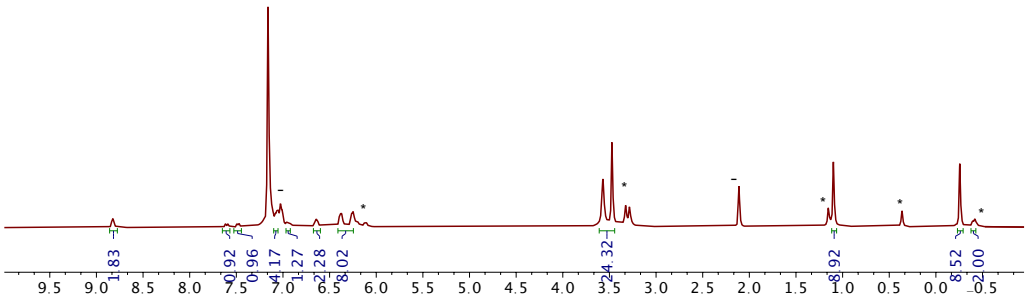

Figure AB7.3: ^{1}H NMR spectrum of **2** in in C_6D_6 (*: the other isomer, -: toluene, only resonances of **2** is integrated).

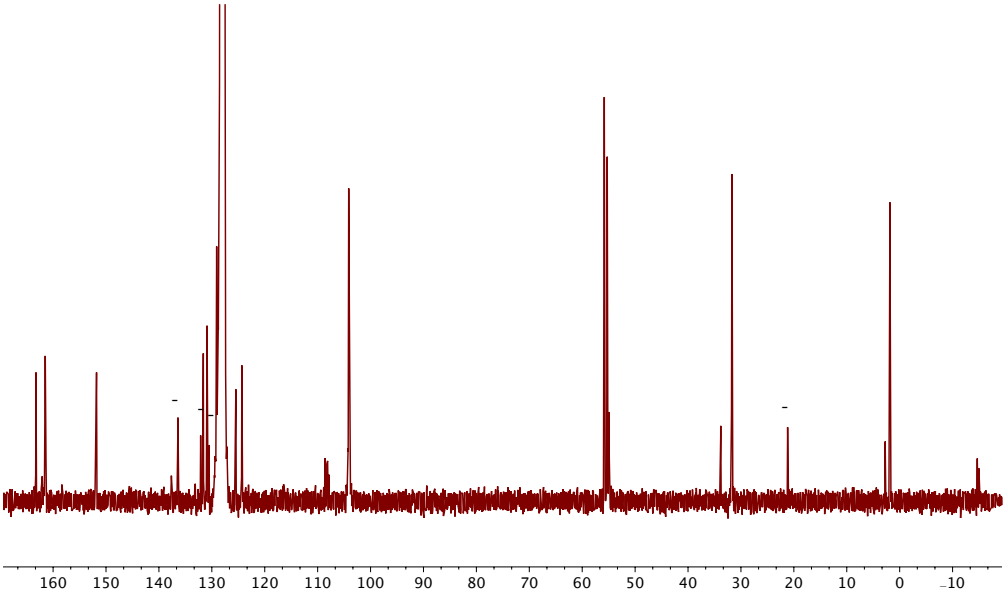

Figure AB7.4: ^{13}C{^{1}H} NMR spectrum of **2** in C_6D_6 (-: toluene).

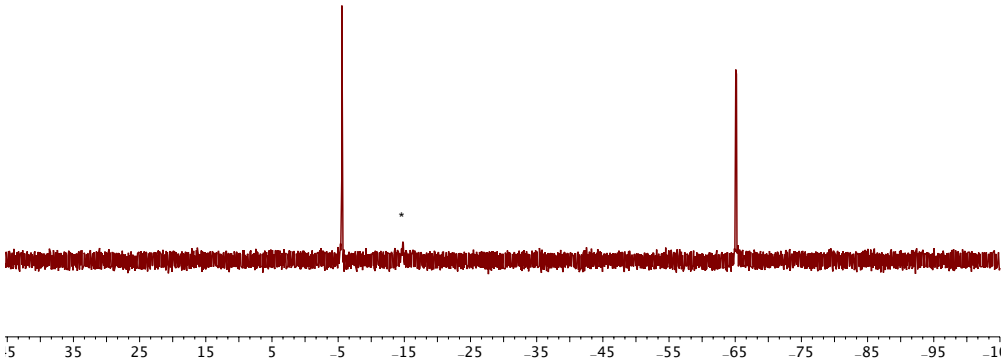

Figure AB7.5: ^{31}P{^{1}H} NMR spectrum of **2** in in C_6D_6 (*: the other isomer).

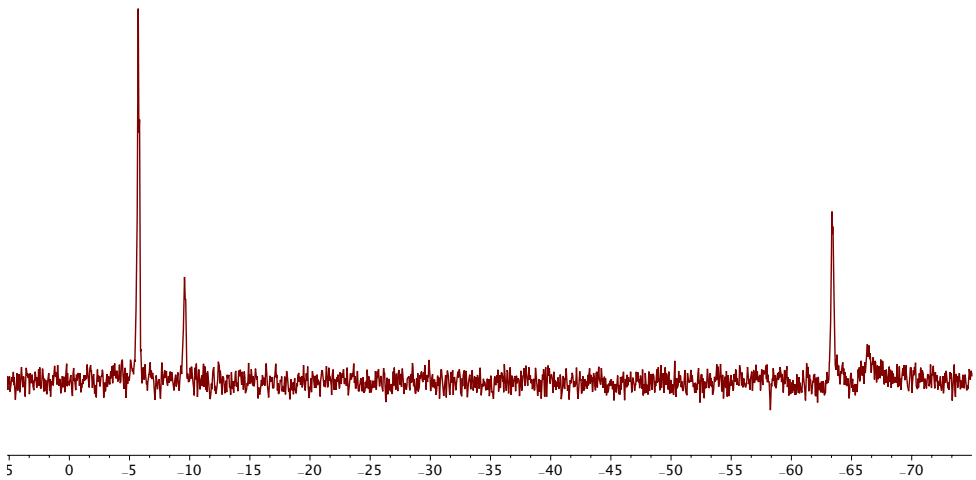

Figure AB7.6: $^{31}P\{^{1}H\}$ NMR spectrum of two isomers (crude mixture of **1** + 1 equiv. of $ZnBr_2$) in THF-H8.

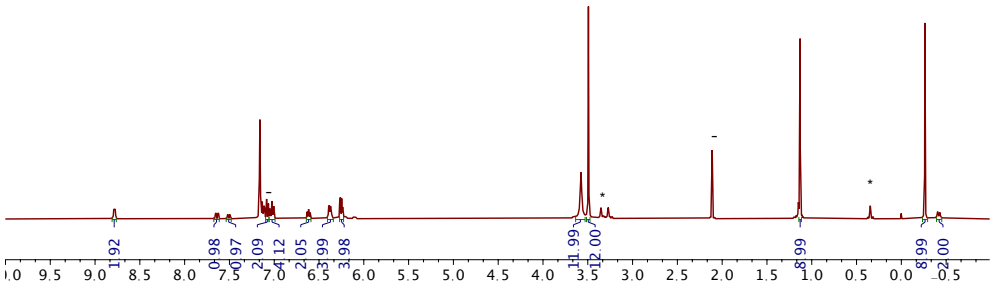

Figure AB7.7: ^{1}H NMR spectrum of **3** in C_6D_6 (*: the other isomer, -: toluene, only resonances of **3** is integrated).

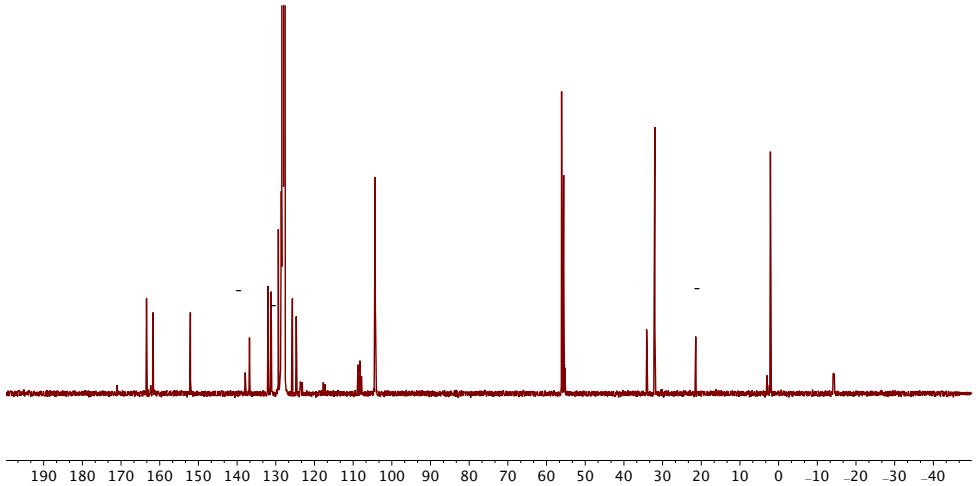

Figure AB7.8: $^{13}C\{^{1}H\}$ NMR spectrum of **3** in C_6D_6 (-: toluene).

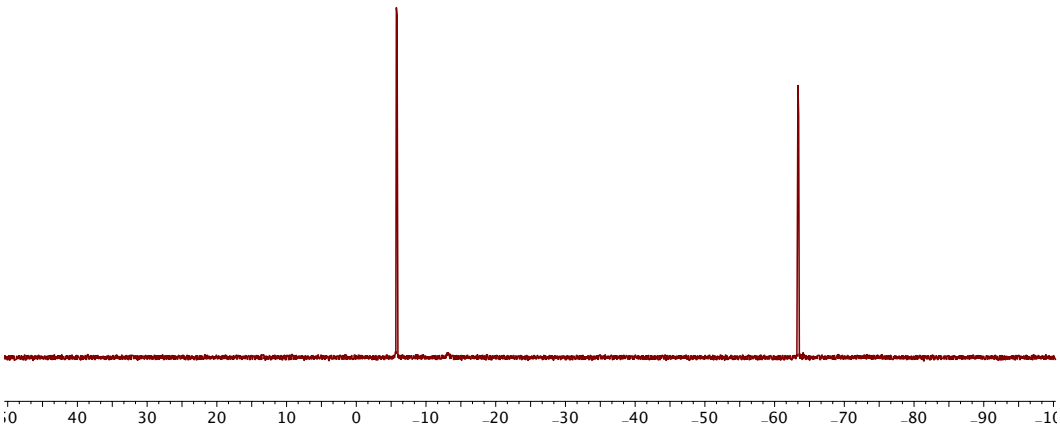

Figure AB7.9: $^{31}P\{^{1}H\}$ NMR spectrum of **3** in in C_6D_6.

Chapter 8

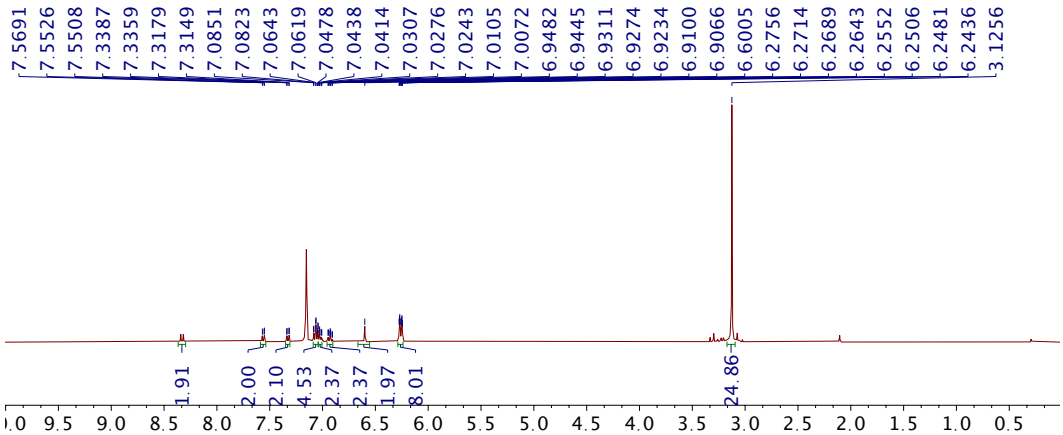

Figure AB8.1: ^{1}H NMR spectrum of **BINOL-(POH)$_2$** in C_6D_6.

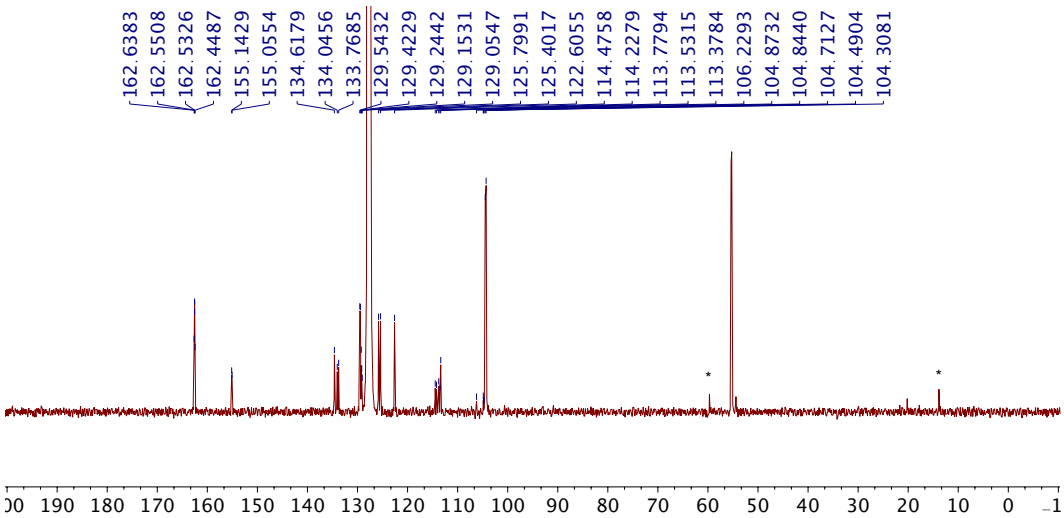

Figure AB8.2: ^{13}C{^{1}H} NMR spectrum of **BINOL-(POH)$_2$** in C_6D_6 (*: Et_2O).

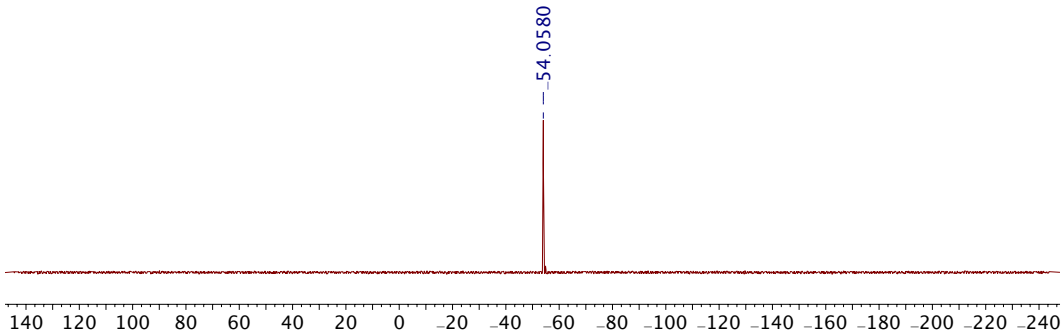

Figure AB8.3: ^{31}P{^{1}H} NMR spectrum of **BINOL-(POH)$_2$** in in C_6D_6.

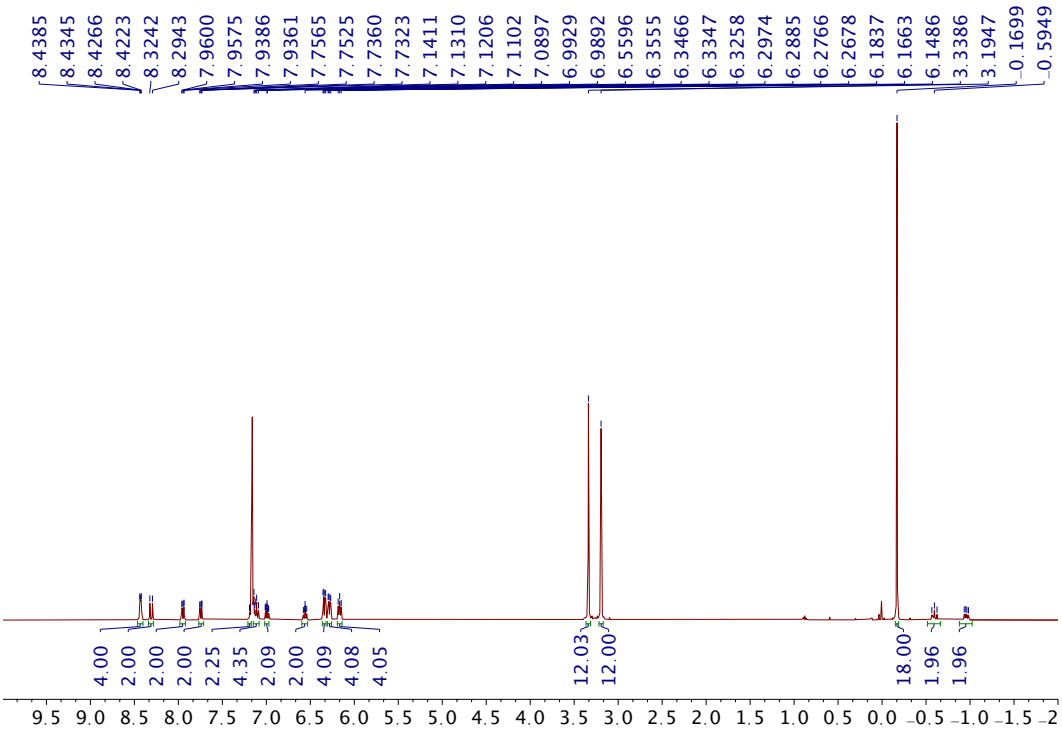

Figure AB8.4: ^{1}H NMR spectrum of **BINOL-(PO-Ni)$_2$** (**X-Ni$_2$**) in C_6D_6.

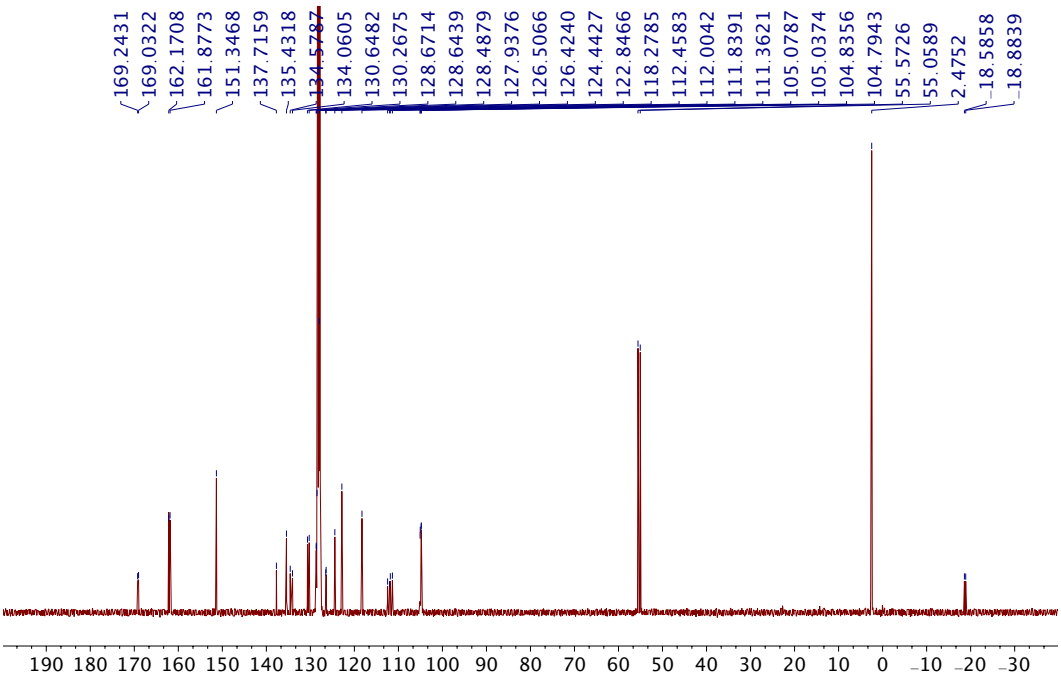

Figure AB8.5: ^{13}C{^{1}H} NMR spectrum of **BINOL-(PO-Ni)$_2$** (**X-Ni$_2$**) in C_6D_6.

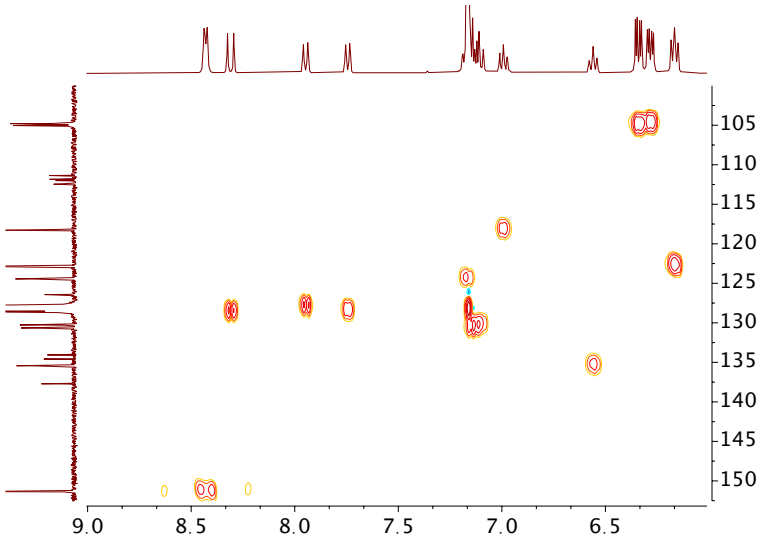

Figure AB8.6: ^{1}H-$^{13}C\{^{1}H\}$ HSQC NMR spectrum of **BINOL-(PO-Ni)$_2$** (**X-Ni$_2$**) in C_6D_6.

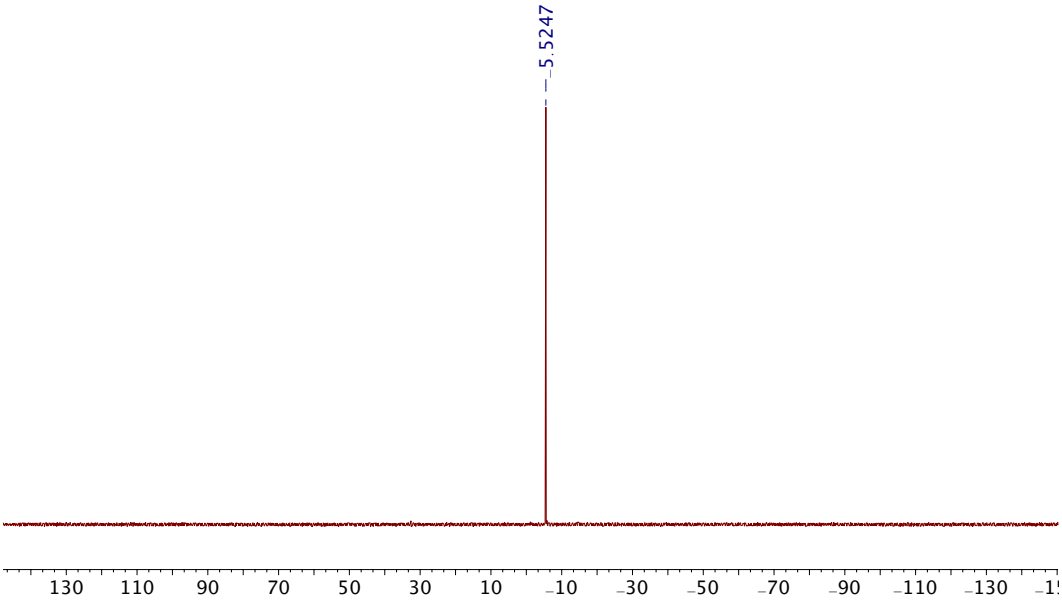

Figure AB8.7: $^{31}P\{^{1}H\}$ NMR spectrum of **BINOL-(PO-Ni)$_2$** (**X-Ni$_2$**) in in C_6D_6.

Appendix A

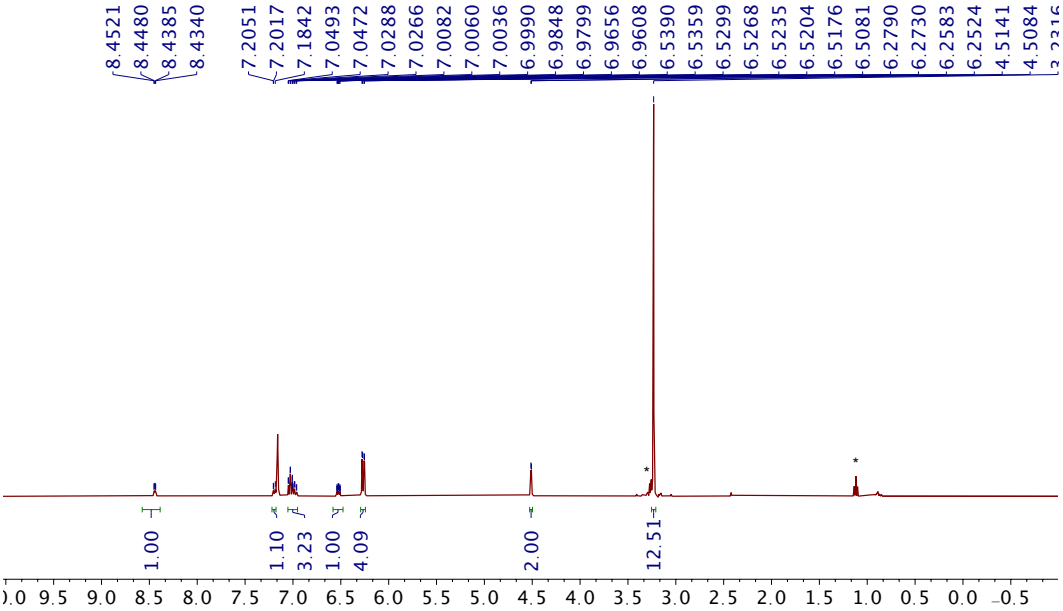

Figure AB.AA.1: ^{1}H NMR spectrum 2-(bis(dimethoxyphenyl)phosphinomethyl)pyridine (**PC^{H}N**) in C_6D_6 (*: THF).

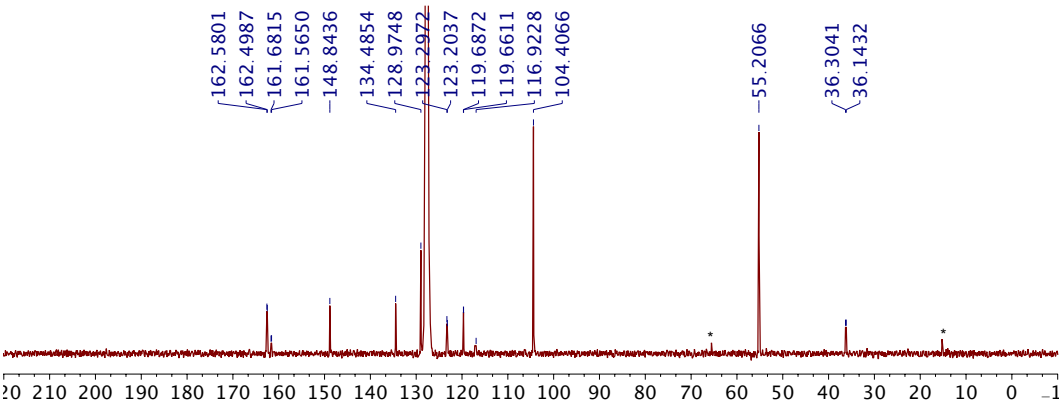

Figure AB.AA.2: ^{13}C{^{1}H} NMR spectrum of **PC^{H}N** in C_6D_6 (*: THF).

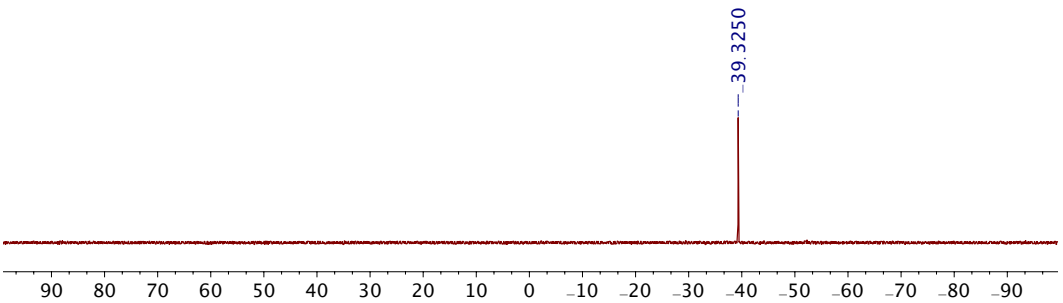

Figure AB.AA.3: ^{31}P{^{1}H} NMR spectrum of **PC^{H}N** in C_6D_6.

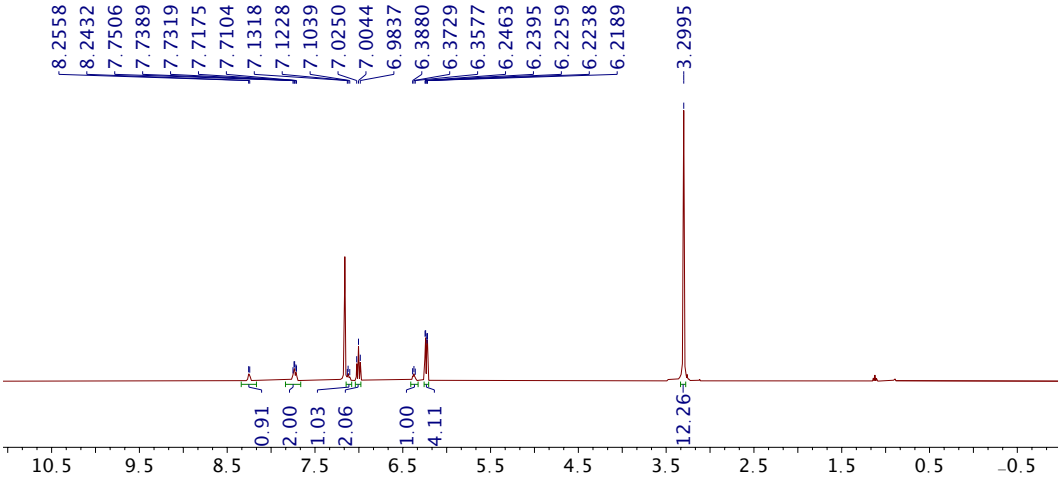

Figure AB.AA.4: ^{1}H NMR spectrum 2-(bis(dimethoxyphenyl)phosphinoamino)pyridine (**PN^{H}N**) in C_6D_6.

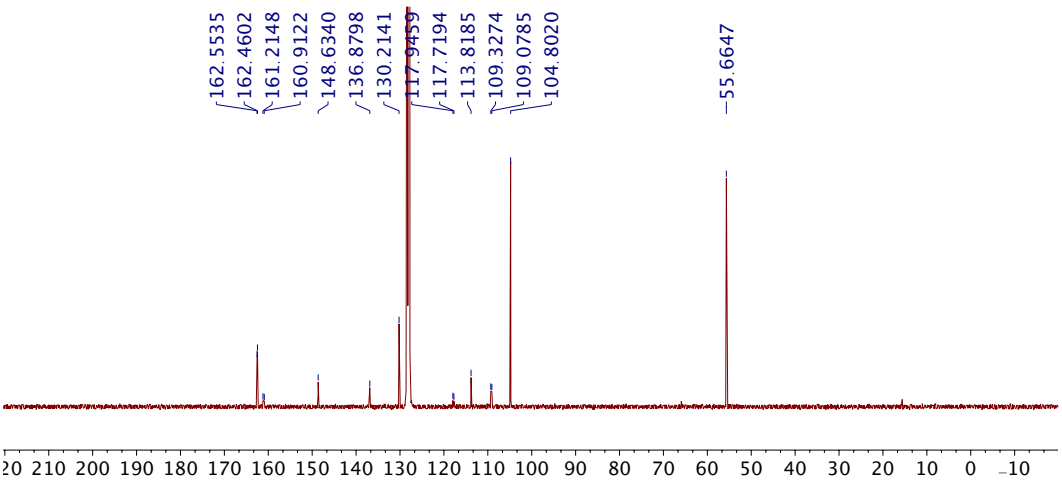

Figure AB.AA.5: ^{13}C{^{1}H} NMR spectrum of **PN^{H}N** in C_6D_6.

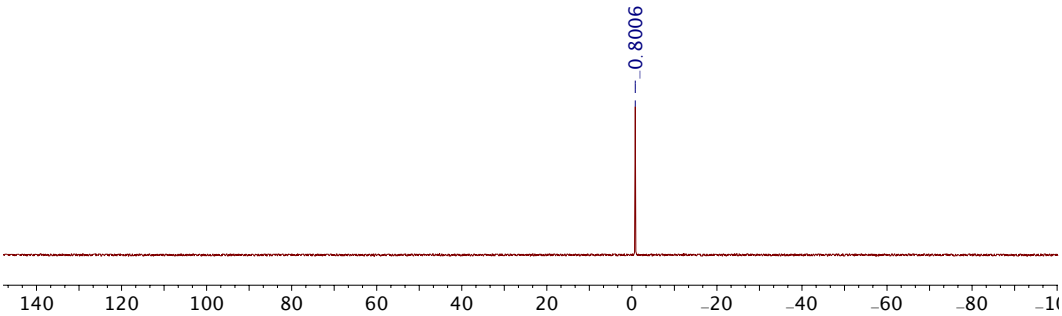

Figure AB.AA.6: ^{31}P{^{1}H} NMR spectrum of **PN^{H}N** in C_6D_6.

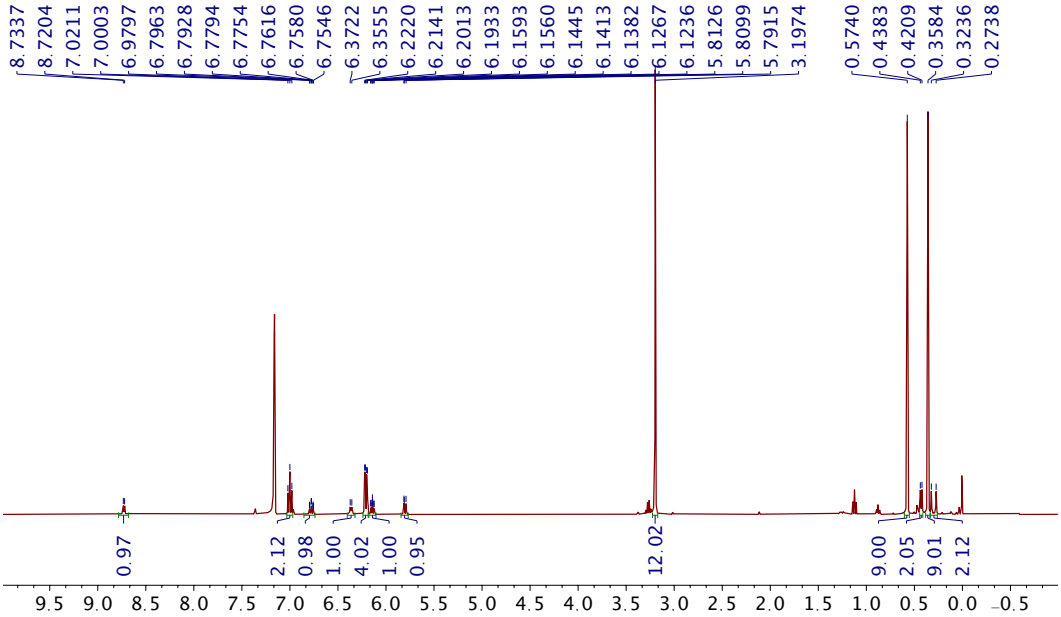

Figure AB.AA.7: ^{1}H NMR spectrum of **PN^{H}N-NiC^{Si}$_{2}$** in C_6D_6.

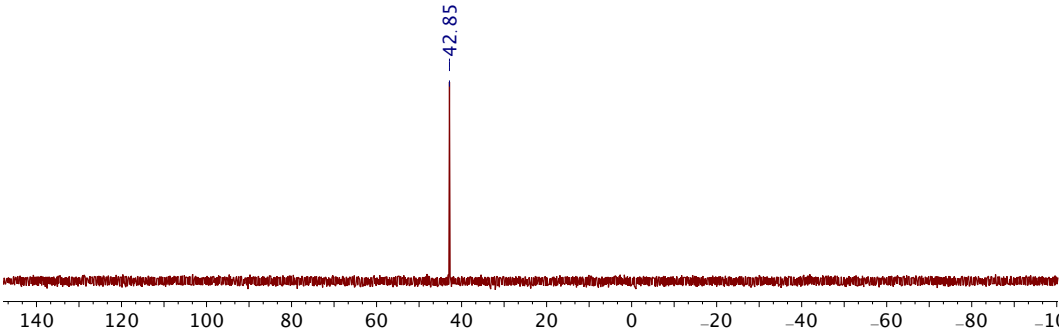

Figure AB.AA.9: ^{31}P{^{1}H} NMR spectrum of **PN^{H}N-NiC^{Si}$_{2}$** in C_6D_6.

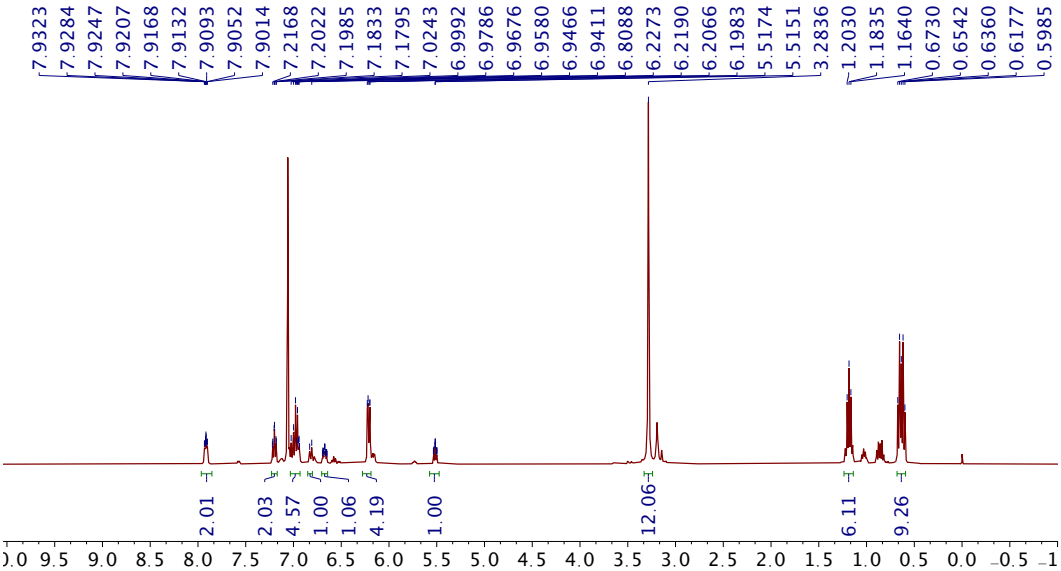

Figure AB.AA.10: ^{1}H NMR spectrum **PNN-Ni(P)Ph** in C_6D_6 (Integration of resonances of the minor isomer not included).

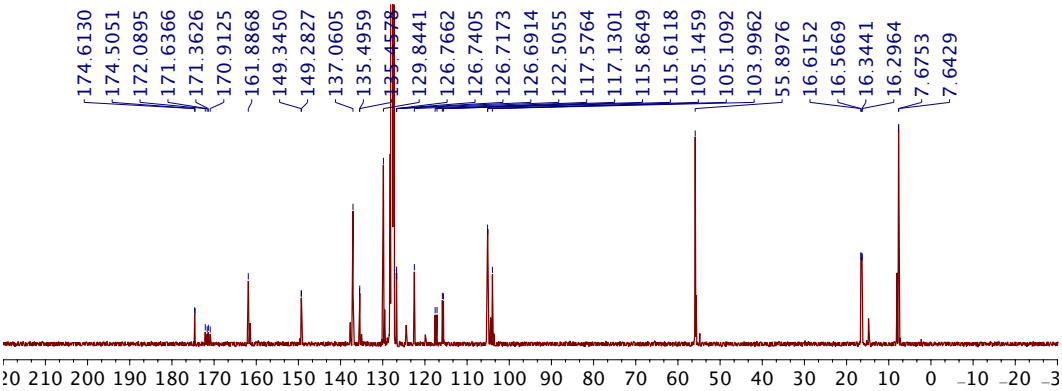

Figure AB.AA.11: ^{13}C{^{1}H} NMR spectrum of **PNN-Ni(P)Ph** in C_6D_6 (Resonances of the minor isomer not included).

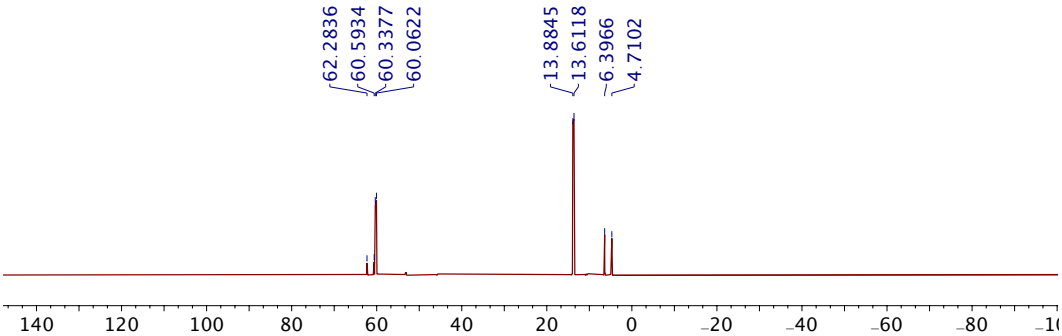

Figure AB.AA.12: ^{31}P{^{1}H} NMR spectrum of **PNN-Ni(P)Ph** in C_6D_6.

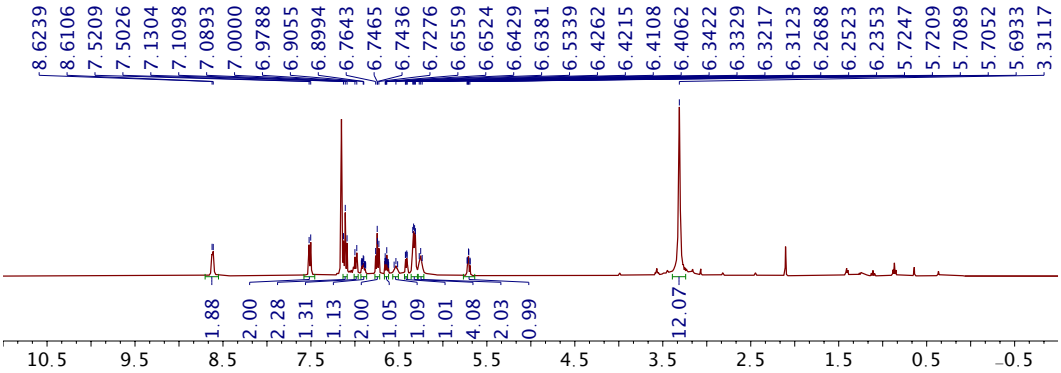

Figure AB.AA.13: ^{1}H NMR spectrum **PNN-Ni(py)Ph** in C_6D_6.

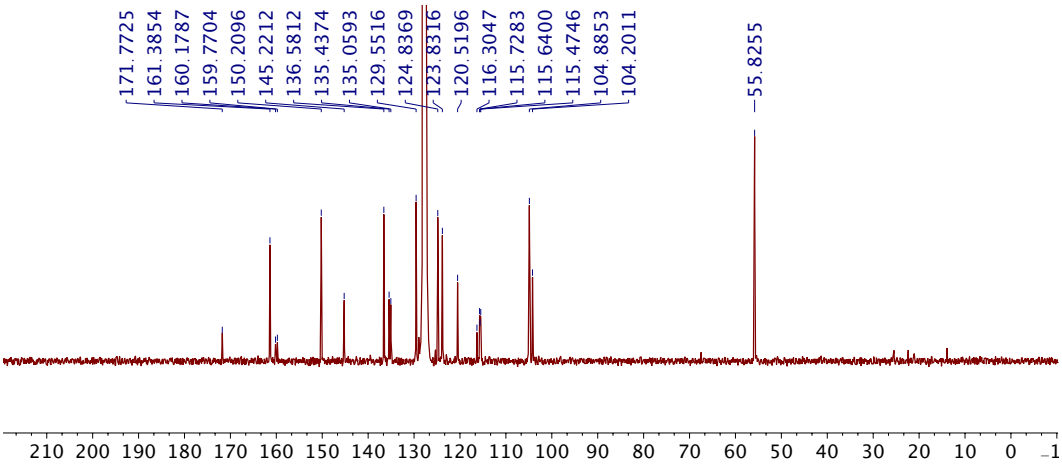

Figure AB.AA.14: ^{13}C{^{1}H} NMR spectrum of **PNN-Ni(py)Ph** in C_6D_6.

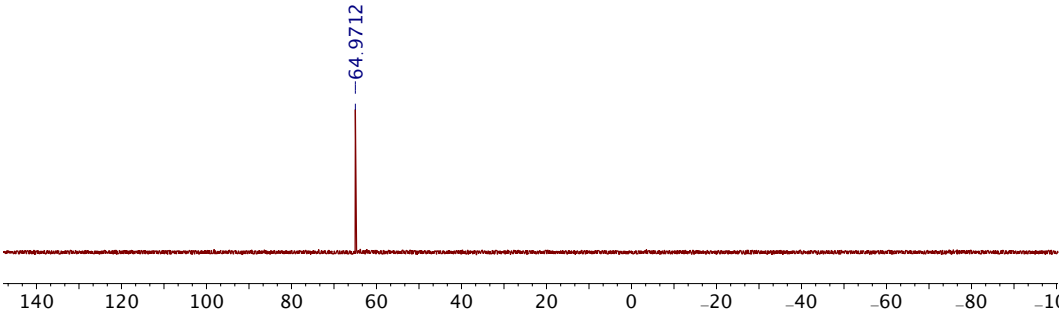

Figure AB.AA.15: ^{31}P{^{1}H} NMR spectrum of **PNN-Ni(py)Ph** in C_6D_6.

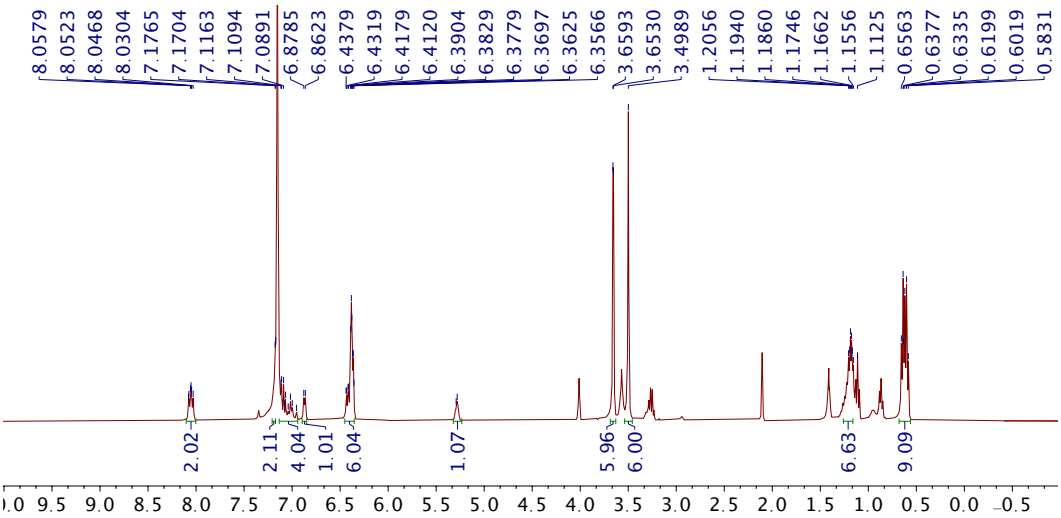

Figure AB.AA.16: ^{1}H NMR spectrum **PCN-Ni(P)Ar^{O2}** in C_6D_6.

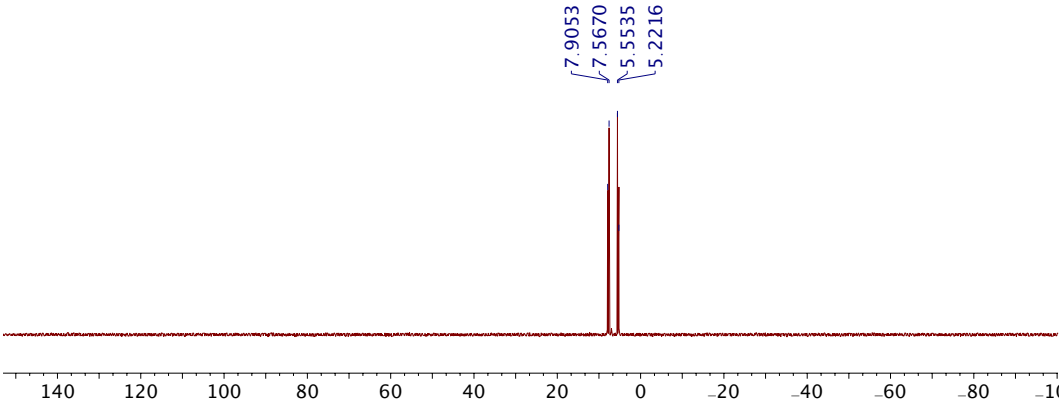

Figure AB.AA.18: ^{31}P{^{1}H} NMR spectrum of **PCN-Ni(P)Ar^{O2}** in C_6D_6.

APPENDIX C

Miscellaneous X-Ray Crystal Structures

Part 1 POP supported mono- and multimetallic complexes (Beyond nickel)

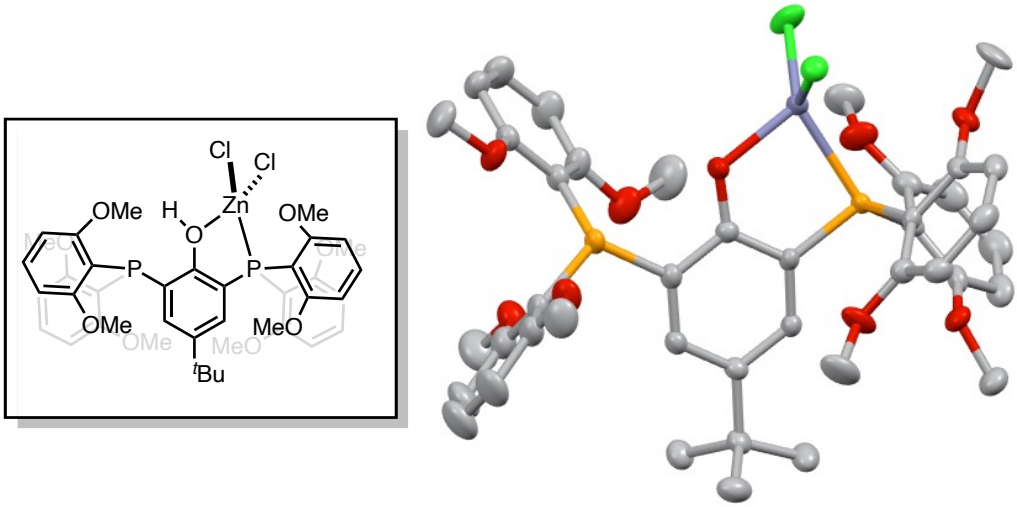

Figure AC.1. A Zn complex supported by POP ligands.

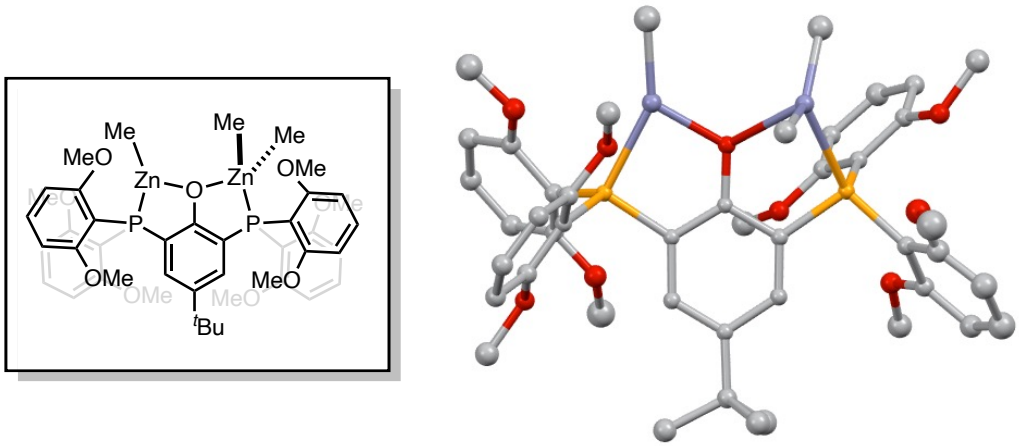

Figure AC.2. A dizinc complex supported by POP ligands (Connectivity only).

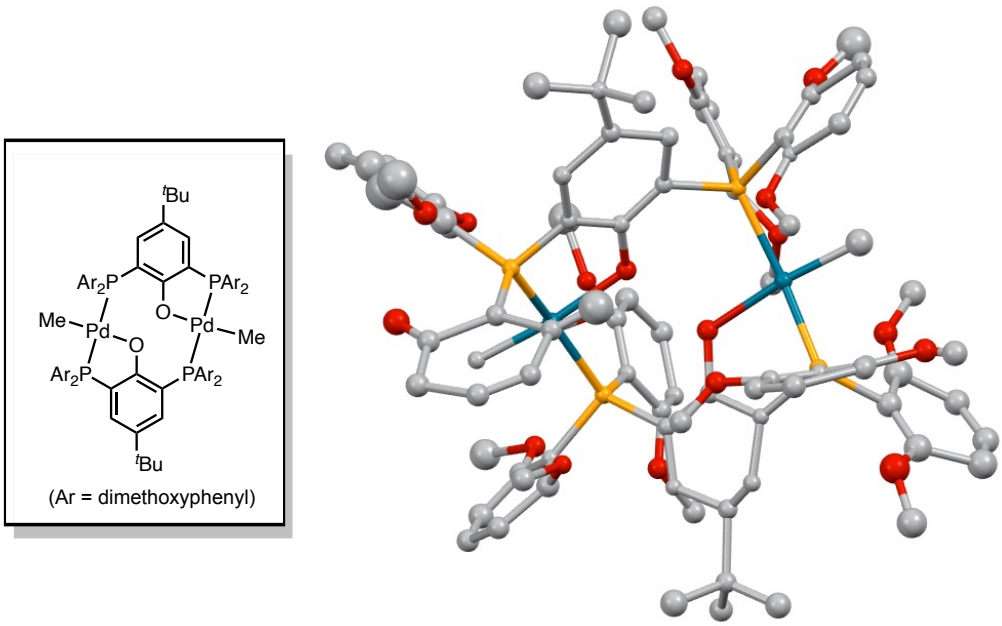

Figure AC.3. A dipalladium complex supported by two POP ligands (Connectivity only).

Part 2 Mononickel complexes supported by POP

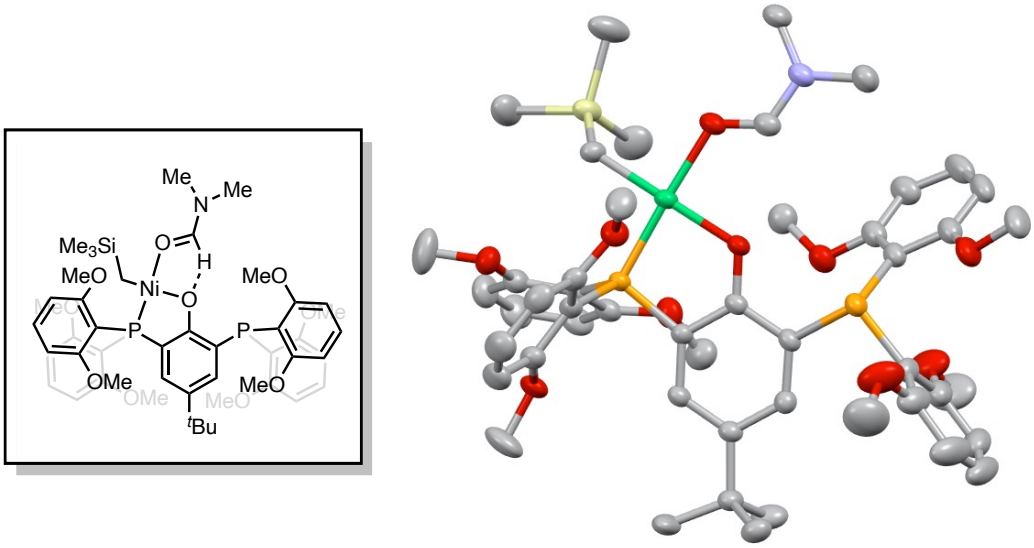

Figure AC.4. Structure of **POP-Ni(dmf)**.

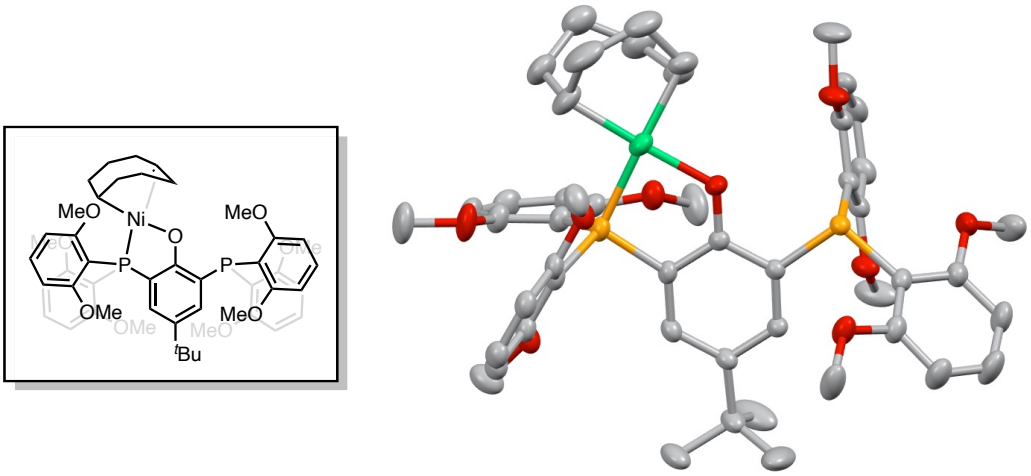

Figure AC.5. Structure of **POP-NiC$_8$H$_{13}$**.

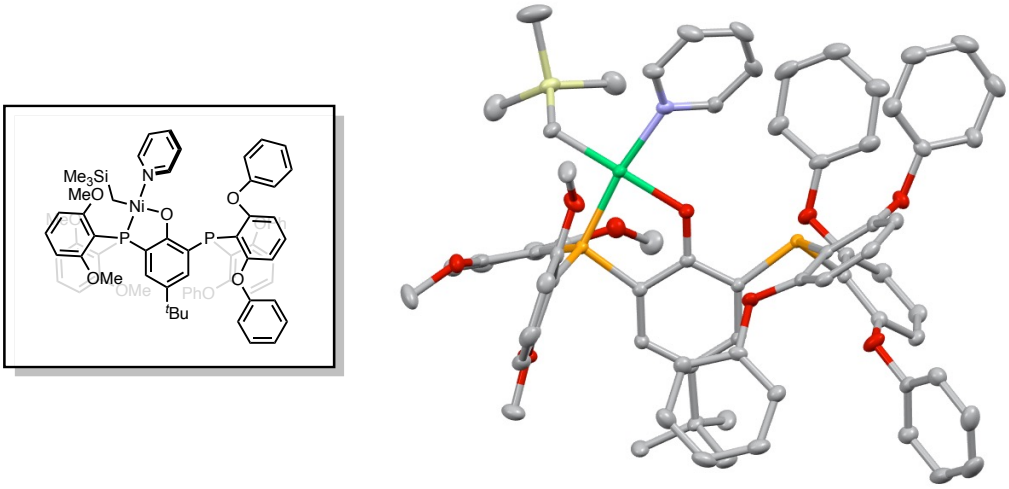

Figure AC.6. Structure of **POP^{PhO}-Ni**.

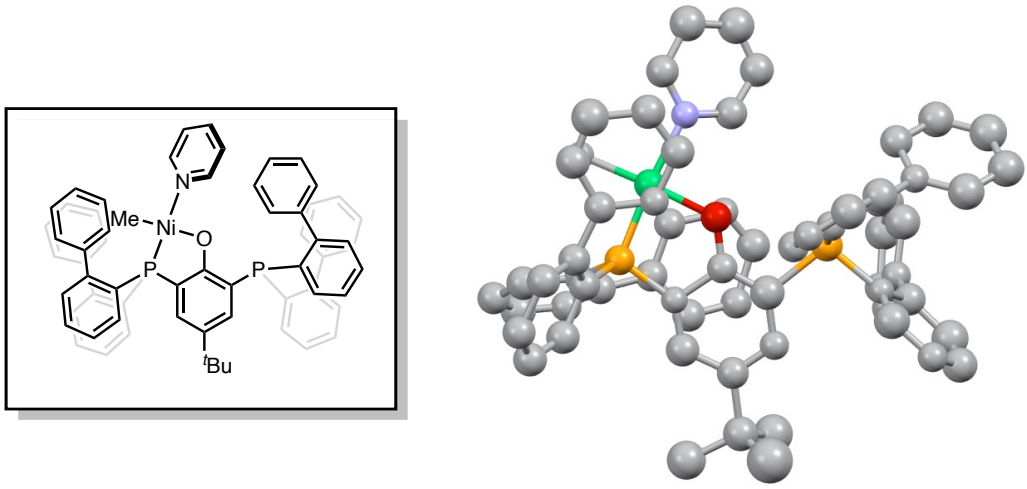

Figure AC.7. A Ni complex supported by the bis(bis(2-biphenyl)phosphine)phenoxide ligand.

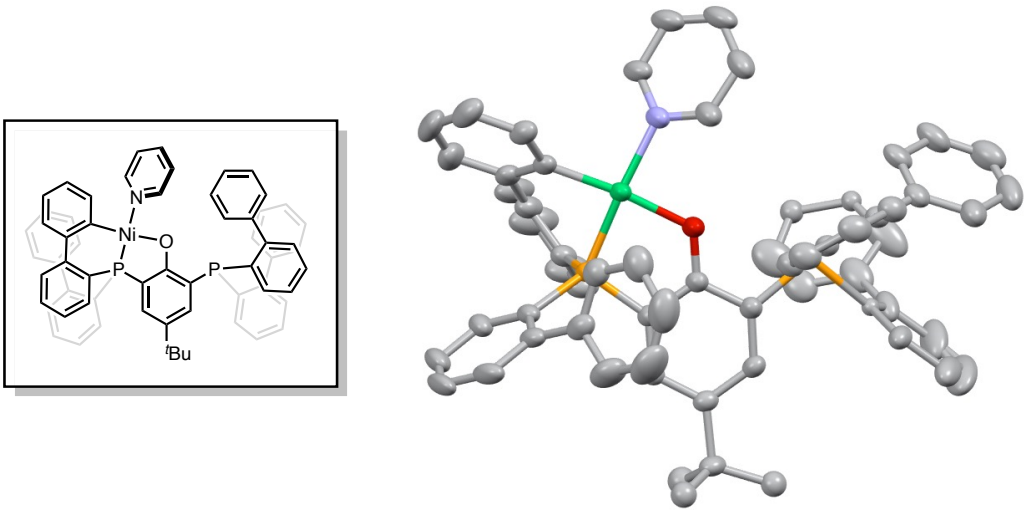

Figure AC.8. A pincer-like Ni complex supported by the bis(bis(2-biphenyl)phosphine)phenoxide ligand.

Part 3 Nickel-based multimetallic complexes supported by POP

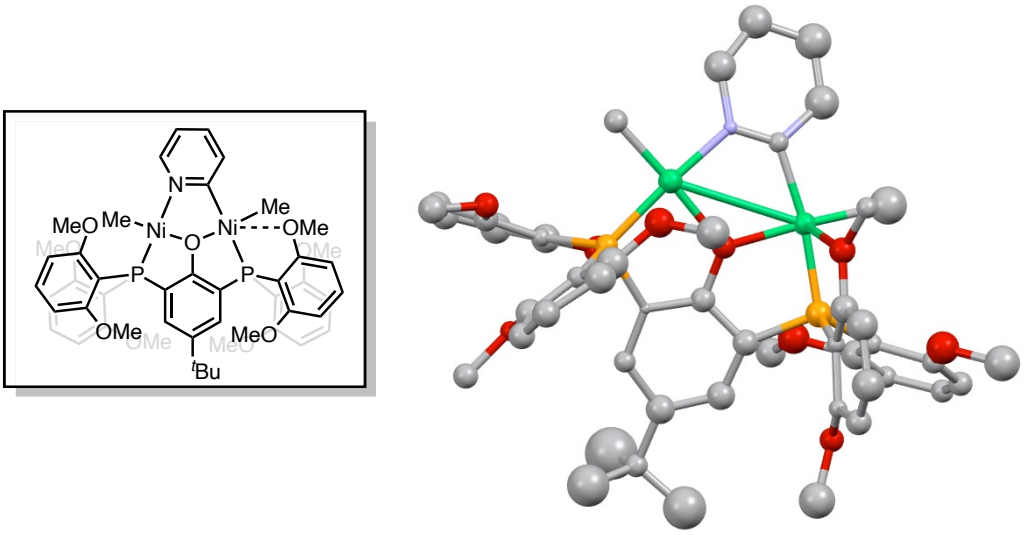

Figure AC.9. A dinickel complex with a bridged pyridine (Connectivity only).

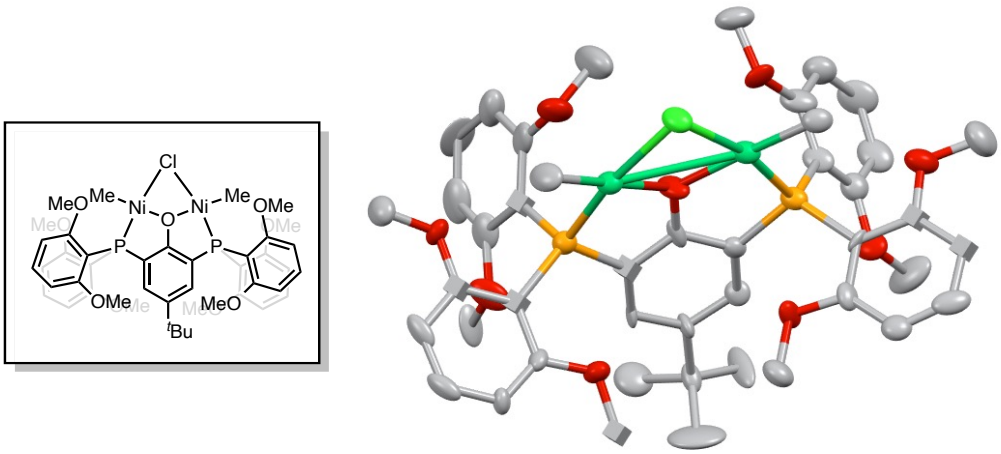

Figure AC.10. A symmetric dinickel complex with a bridged chloride (Connectivity only).

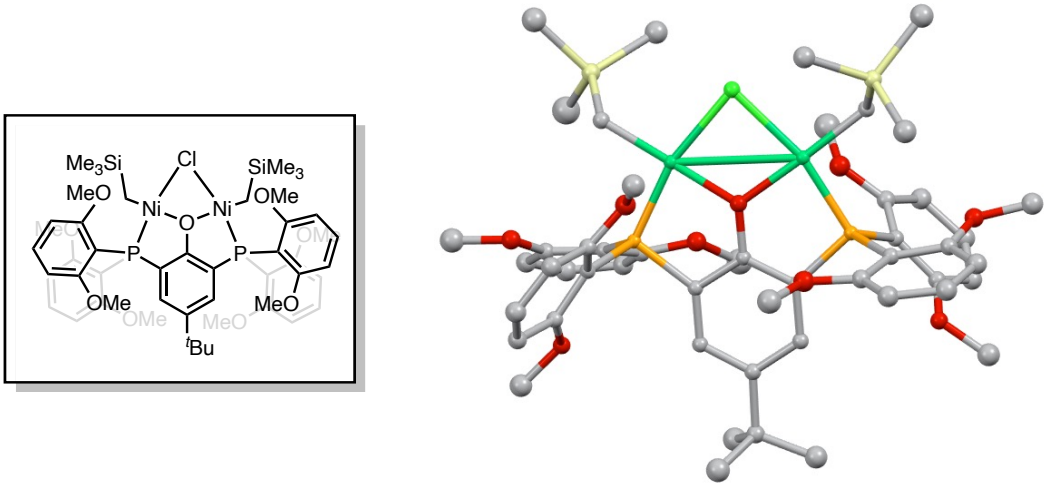

Figure AC.11. A dinickel complex with a bridged chloride (Connectivity only).

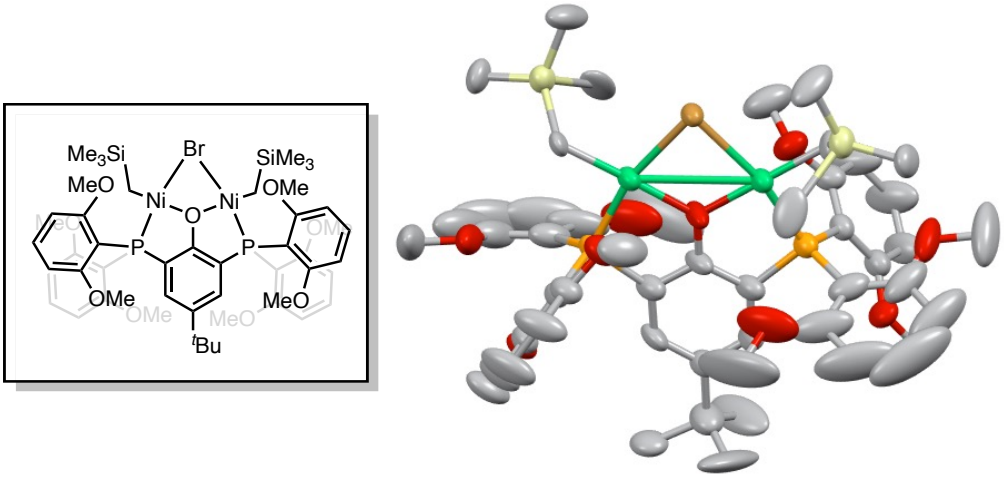

Figure AC.12. A dinickel complex with a bridged bromide.

Part 4 Structures relevant to catalyst decomposition

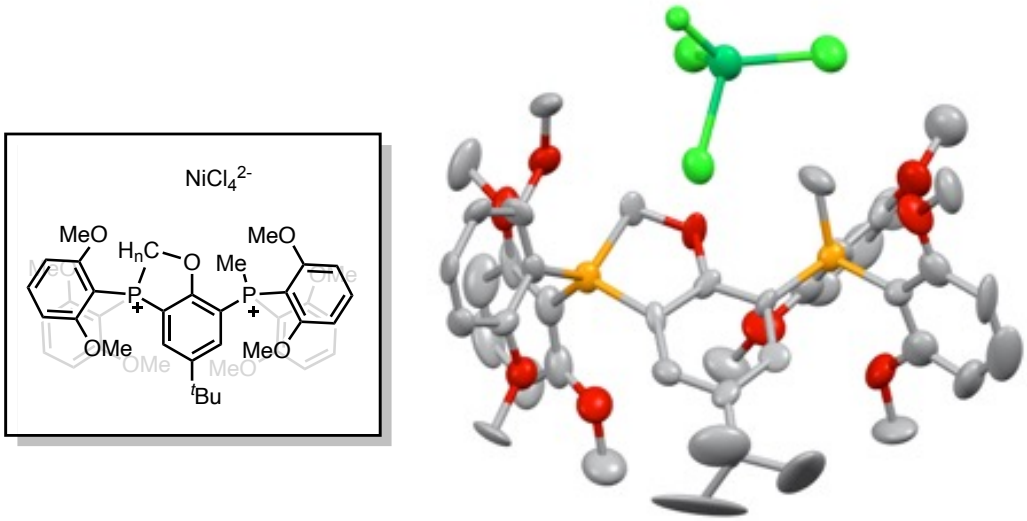

Figure AC.13. A diphosphonium-based compound with $NiCl_4^{2-}$ as the dianion.

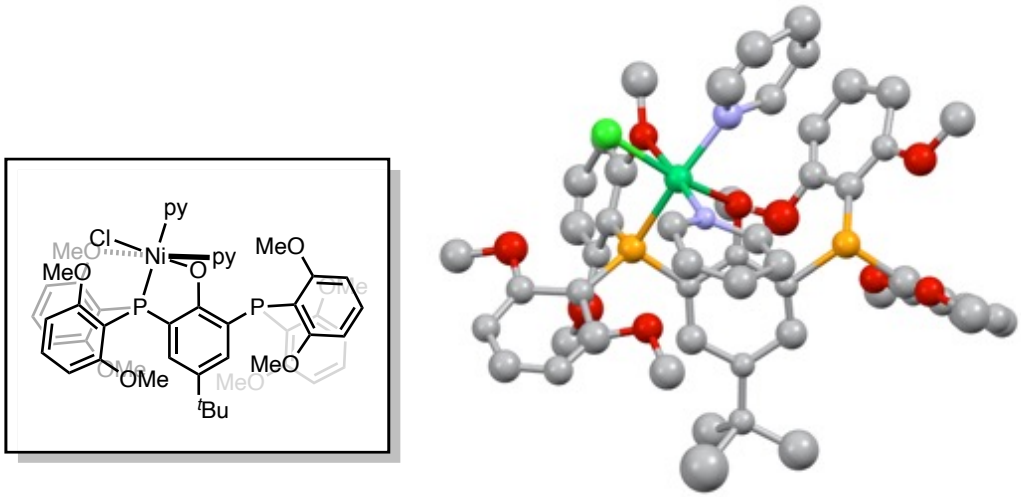

Figure AC.14. A NiCl-based compound with an octahedral Ni center.

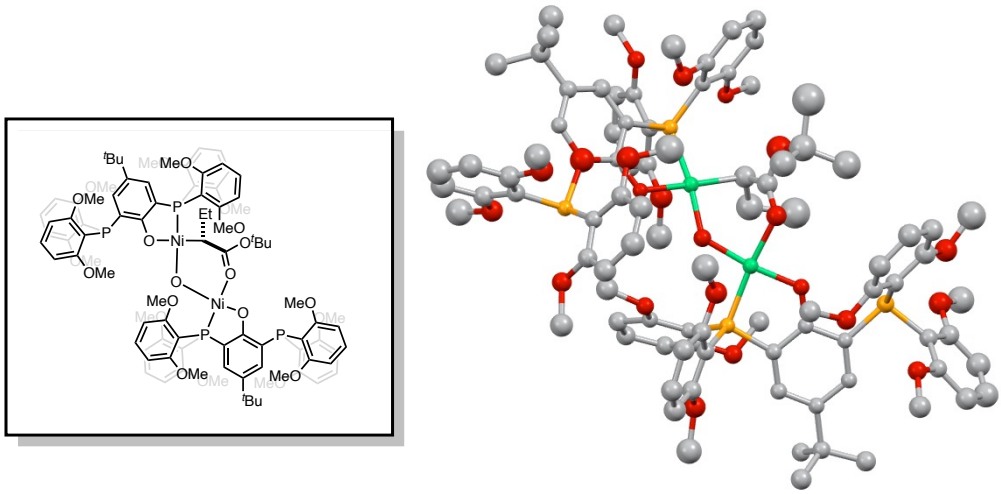

Figure AC.15. A dinickel compound generated after tBA insertion.

Part 5 Structures based on other PO ligands

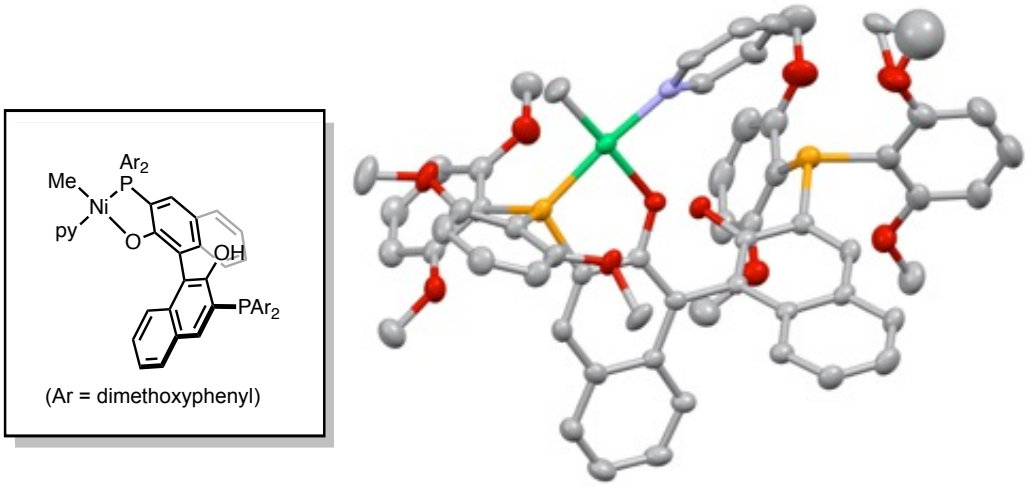

Figure AC.16. A mono-Ni compound based on the **XH$_2$** ligand.

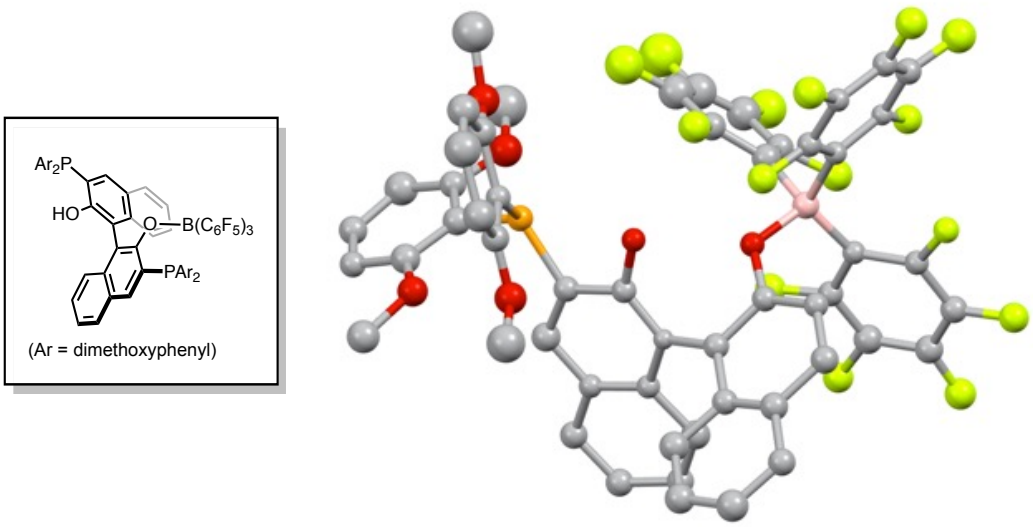

Figure AC.17. A $B(C_6F_5)_3$ adduct of the **XH$_2$** ligand.

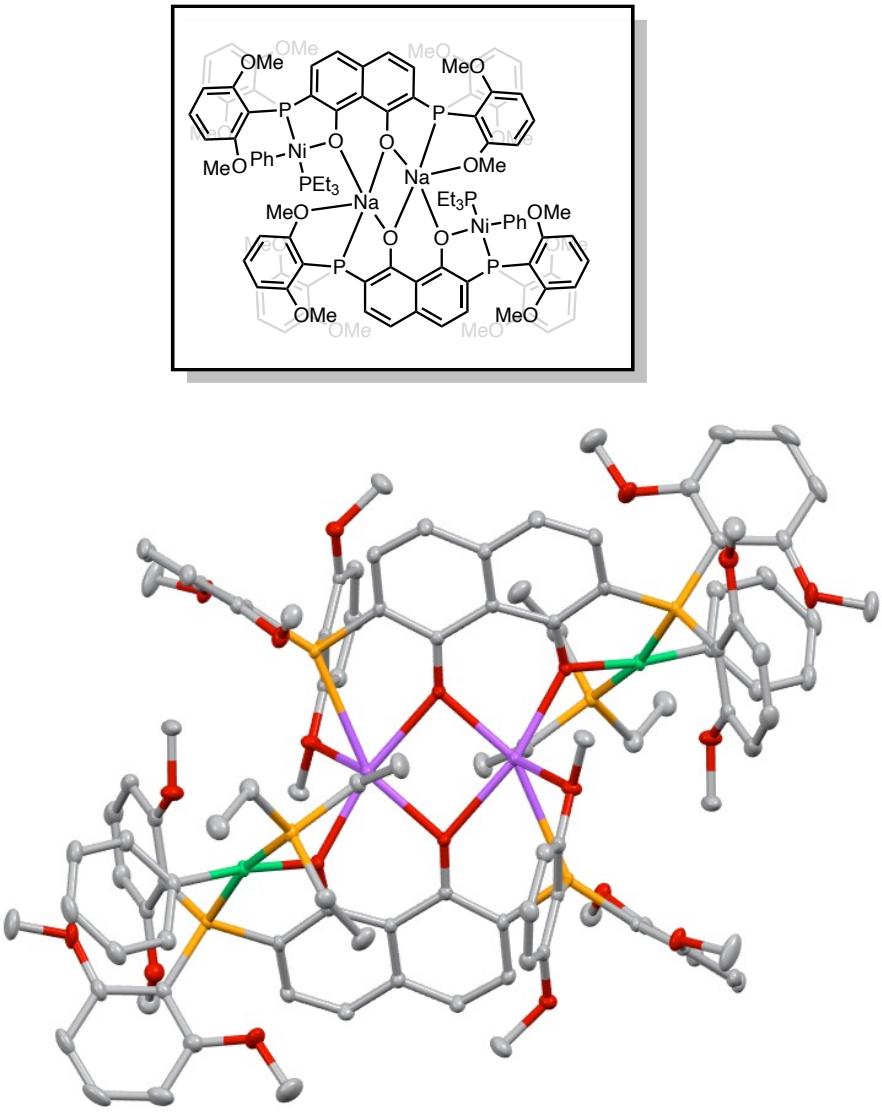

Figure AC.18. Structure of a Ni_2Na_2 complex based on the napdiol-based bisphosphine ligand.

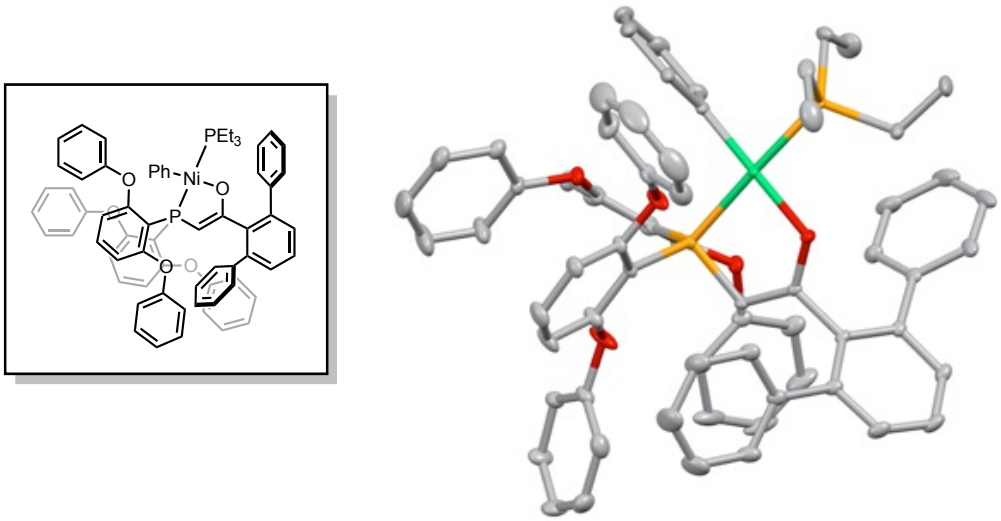

Figure AC.19. Structure of $^{Ph}PO^{terphenyl}$-Ni(PEt_3)Ph (with Alex Hong).

Part 6 Structures based on ligands beyond POs.

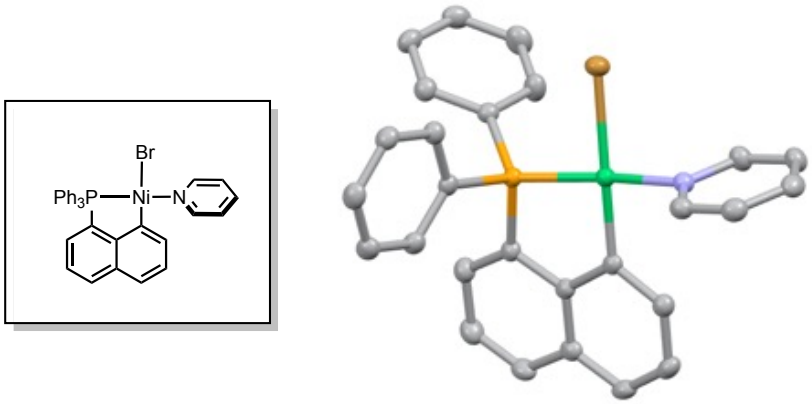

Figure AC.20. Structure of a P,C-Ni complex.

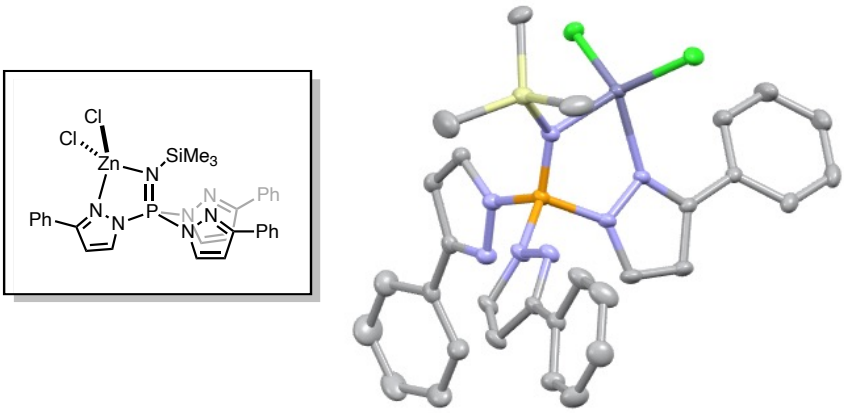

Figure AC.21. Structure of a N,N-Zn complex.

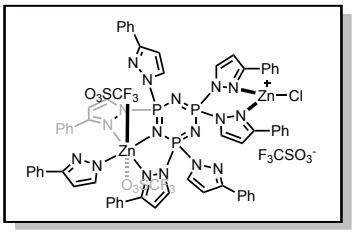

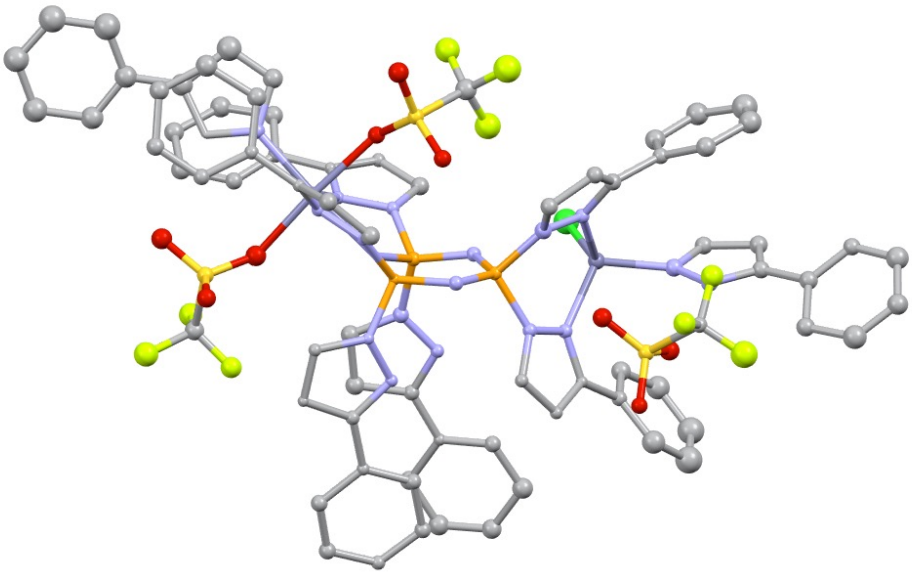

Figure AC.22. Structure of a dizinc complex featuring a P_3N_3 core.

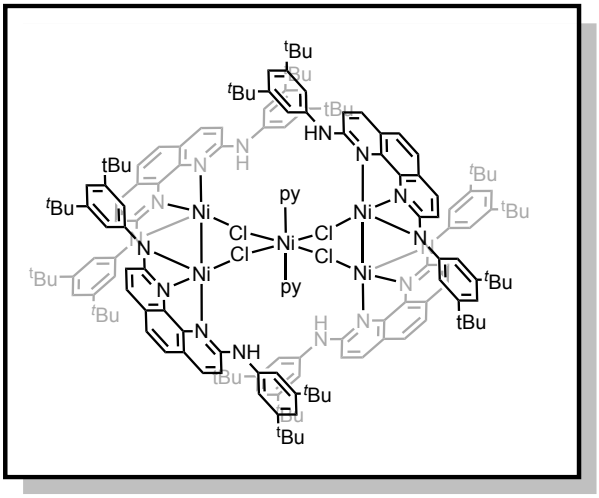

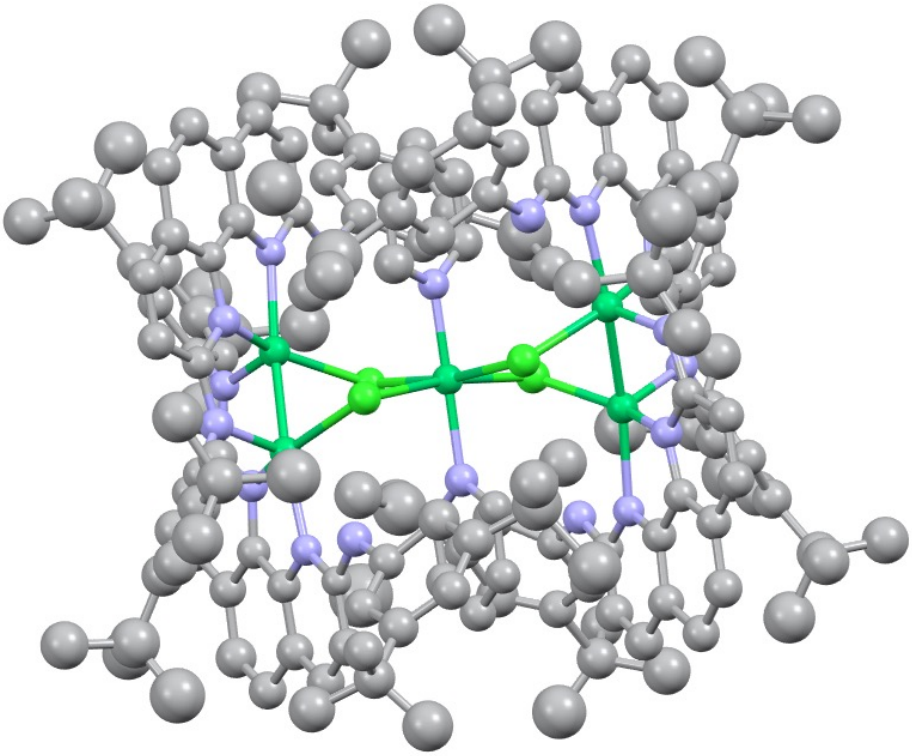

Figure AC.23. Structure of a Ni_5 cluster.

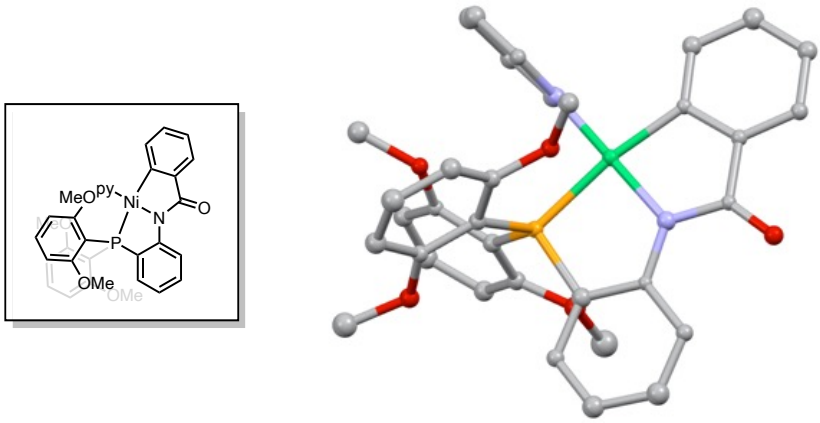

Figure AC.24. Structure of a pincer-type P,N-Ni complex.

ABOUT THE AUTHOR

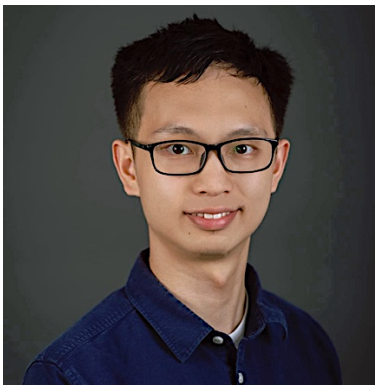

Shuoyan Xiong, or Sam, was born in Jiangxi, China. When he was seven-year-old, his family moved to Guangdong, where he finished elementary school and high school. While attending the University of Science and Technology of China (USTC), he found two loves: chemistry (now his career) and Yu (now his wife). His passion for polymer chemistry took him through Prof. Changle Chen's lab at USTC and Prof. Tobin J. Marks's lab at Northwestern University for undergraduate research. Fascinated by the efficiency and elaborateness of transition metal polymerization catalysts, he moved to Pasadena, CA for his Ph.D. studies in inorganic chemistry with Prof. Theodor Agapie at Caltech. Following graduation in 2023, he is heading to Bay area to postdoc in Prof. Jeffrey R. Long's lab at University of California, Berkeley.